Morphodynamics, Sedimentation and Sediment Dynamics of a Gravel Beach

by DANIEL D. BUSCOMBE


A Thesis submitted to the University of Plymouth in partial fulfilment for the degree of

Doctor of Philosophy

School of Geography

Faculty of Social Science & Business

Summary

Morphodynamics, Sedimentation and Sediment Dynamics of a Gravel Beach.

Daniel Buscombe, January 2008.

The morphodynamics of a gravel barrier beach in Devon, UK (Slapton Sands: tanβ 0.15 - 0.25, D_{50} 2 - 8mm), was studied with reference to its sedimentology. Three time scales were sampled for nearshore hydrodynamics, intertidal morphologies and sedimentologies. A series of surveys were carried out over individual tidal cycles (sampling every 5 - 10mins for between 6 and 9hrs); on consecutive low tides over half-lunar tidal cycles (1 - 2 cross-shore profiles sampled every 0.5 - 1m, on 2 spring - spring tidal cycles comprising 26 and 24 tides, respectively); and finally every 2 weeks at spring low tide, over 1 calendar year (13-17 profile lines surveyed and sampled for sediment over 3.25 - 4.25km).

In order to further our understanding of gravel beaches, sediment data needs to be collected at a resolution similar to that of the hydrodynamics. Innovative automatic sediment sizing techniques based on digital images of sediments were therefore developed, and software written, to allow the collection and analysis of high-resolution sediment data.

The gravel beach step and berm are accretionary features, tidally modulated, and evolve under different time scales. A new technique to determine bed mobility from the nearshore, using underwater video cameras, was devised. Nearshore sediment transport was suggested as being related to sub-incident wave frequencies.

No aspect of morphological change could be found to have a statistically significant association with sedimentological change, but dimensional-reduction techniques did satisfactorily detect association. The lack of co-variance and obvious patterns is stochastic noise, not parameterisation.

Over one year, the barrier underwent asymmetrical rotation over one year, highlighting the importance of alongshore sediment transport processes on this supposedly 'swash aligned' beach.

A statistical model based on the log-hyperbolic distribution of surface particle sizes was found to be a reasonable predictor of mean net sedimentation over individual tides. Its complicated parameter space could possibly map onto a simpler plane based on traditional moments. Sediment trend vector models based on sorting alone out-performed a traditional approach. Moments of a surface grain-size distribution appear to be inappropriate to characterise sedimentological change at time-scales greater than a semi-diurnal tidal cycle. Sub-surface sampling on the intertidal zone on diurnal and semi-lunar time-scales is useful in assessing the dynamics of the step, itself an important mechanism for onshore and offshore net volumetric transport.

TABLE OF CONTENTS

LIST OF TABLES

LIST OF FIGURES & PLATES

LIST OF SYMBOLS, SUBSCRIPTS & ABBREVIATIONS

Tab. 0.1 *Parameters*

Symbol	Description
Λ	absolute low-pass-filtered time series
Λ_F	fetch length
Ω	bed motion coefficient
Ω_{rr}	rounded and rescaled Ω
Φ	sorting coefficient
Π	steady state vector for Markov chain
Θ	angular frequency
Θ_m	generic model
Θ_w	wave direction (oceanographic convention)
α	significance level
α_I	image matrix at time t relative to its mean
α_{LH}	internal parameter in log-hyperbolic PDF
α_{LH0}	value of α_{LH} which corresponds to χ_{LH}=0
β	beach slope
β_I	image matrix at time $t+1$ relative to its mean
β_{LH}	internal parameter in log-hyperbolic PDF
χ^2	chi-squared distribution value
χ_{LH}	log-hyperbolic skewness
δ_{AR}	scaling coefficient in AR model
δ_{LH}	spread of log-hyperbolic distribution
δ_t	GSD variate

Continued on next page

Table 0.1 – continued from previous page

Symbol	Description
ε	energy
ϵ	fluid-controlled sedimentation
ϵ_w	spectral width
ϵ_s	surf scaling parameter
η	water surface elevation
γ	semi-variance
γ_o	Yule-Walker AR model
γ_p	spectral variogram precursor
γ_{LH}	'coarse-grade coefficient' log-hyperbolic distribution
ι	proportion of grain-size fraction
κ	grain-controlled sedimentation
λ	eigenvalue
λ_p	rate of occurrence in Poisson queue model
μ_{LH}	mean of log-hyperbolic distribution
μ_N	mean of log-normal distribution
μ_Y	mean of Y
ν	degrees of freedom
ν_{LH}	typical log grain size (log-hyperbolic model)
ω	phase shift (wave)
π_d	proportion of d relative to that previously
ϕ	phi grain-size scale
ϕ_{LH}	'fine-grade coefficient' log-hyperbolic distribution
ψ	psi grain-size scale
$\psi(t)$	temporal phase function of CEOF
φ_o	AR coefficients (order o)
ϖ	complexity of operations
ρ	density of seawater
ρ_e	irreducible random error
ρ_{LH}	ratio of χ_{LH} and ξ_{LH}
ϱ	eigenfunctions of covariance matrix
$\overline{\rho_P}$	mean waiting time in Poisson queue model
σ	generalised standard deviation/sorting
σ_A	standard deviation of A (input noise)

Continued on next page

Table 0.1 – continued from previous page

Symbol	Description
σ_N	spread of log-normal distribution
σ_X	standard deviation of X
τ_{kh}	internal parameter for kh
τ_{LH}	log-hyperbolic sorting
θ	Shields parameter
$\theta(x)$	spatial phase function of CEOF
ϑ	normalising factor in SVD
ξ	Iribarren number
ξ_{LH}	log-hyperbolic skewness
ζ	moment of auto-spectrum
$\otimes$	number of measurements
$\oslash$	chord length
$\wp$	Fourier coefficient 1
ℓ	Fourier coefficient 2
$\aleph$	arbitrary vector 1 (CCA)
∇	arbitrary vector 2 (CCA)
$\amalg$	canonical scores
$\hbar$	standard error
$\diamond$	internal parameter for the log-hyperbolic density function
$\perp$	norming (integral) constant
$\perp_0$	norming constant at initial conditions
$\in$	number of parameters
$\angle$	series of angles
A	(Gaussian) white noise
C	LUC calibration catalogue matrix
$\mathbf{C}$	orthogonal spatial eigenfunction matrix
CI	confidence interval
CR	correlation matrix
CV	covariance matrix
C_w	spectral taper correction factor
D	grain size percentile (suffixed)
D_{50}	median sediment size
D_a	probability matrix of arrival

Continued on next page

Table 0.1 – continued from previous page

Symbol	Description
D_{cr}	characteristic distance
D_f	fractal dimension
D_e	error in horizontal distance
D_p	probability matrix of departure
E	mathematical expectation
$\mathbf{E}$	orthogonal temporal eigenfunction matrix
F	2D Fourier transform (complex) of I
$\mathbf{F}$	F-distribution value
F^*	2D Fourier transform (complex) of I_d
$\hat{F}$	2D Fourier transform (complex) of I^2
F_c	complex conjugate of F
$\hat{F}_c$	complex conjugate of $\hat{F}$
G	gain function
GF	groupiness function
H_o	deep-water wave height
H_s	significant wave height
I	digital image (indexed by x and y)
I_d	indentity matrix
K	hydraulic conductivity
Kt	kurtosis (of GSD)
L	total number of lags
L_s	shallow water wave length
N	sample number
$\mathbf{N}$	Normal cumulative distribution function
N_{crit}	'quasi'-sample size
P	transition probability matrix
Q	Portmanteau sequence, beach volume
R	Run-up level
$\vec{R}$	resultant vector
R^2	squared correlation coefficient
$\overline{R_l}$	mean resultant length
R_u	Rayleigh test for non-uniformity
S	wave skewness

Continued on next page

Table 0.1 – continued from previous page

Symbol	Description
Sk	skewness (of GSD)
$\mathbf{T}$	Student's cumulative distribution function
T_o	deep-water wave period
T_s	significant wave period
Y	general time or spatial series
$\ddot{Y}$	reconstructed Y
$\tilde{Y}$	Hilbert transform of Y
X	grain-size array obtained from LUC procedure
$\mathbf{Z}$	Z-test score
$\emptyset$	vector of weights
a	tuning parameter for theoretical variogram model
a_u	acceleration in water velocity
$\mathbf{a}$	value in the LUC calibration catalogue
$\mathbf{b}$	value obtained from LUC procedure on digital image
c	celerity (group, wave)
$\mathbf{c}$	temporal eignefunction mode
$\mathbf{d}$	sensor depth
e	spatial eigenfunction mode
$\mathbf{f}$	frequency
$\mathbf{h}$	vectorial distance
h	local water depth
$\mathbf{k}$	local wave number
kh	empirical correction factor for H_s
$\mathbf{n}$	shoaling transformation coefficient
$\mathbf{p}$	data dimensionality
pv	percentile value
q	representative data dimensionality
$\vec{r}$	trend vector
r	(auto-/cross-) correlation coefficient
r_ϵ	vector of grain-controlled sedimentation
r_κ	vector of grain-controlled sedimentation
r_o	initial radius in a log-spiral function
r_s	radial vector in a log-spiral function

Continued on next page

Table 0.1 – continued from previous page

Symbol	Description
s	spectral density
s	grain size class
t	Student's t-distribution value
u	(cross-shore) current velocity
u_w	wind speed
u^*	wind stress
v	alongshore current velocity
w	beach width
xx	hypothetical variable
y	generalised row coordinate
z_r	z-transform of correlation coefficient

Tab. 0.2 *Subscripts*

Symbol	Description
1	relative to initial
C0	zero lag
CS	lag at which function does not increase in magnitude at further lag
LB	Ljung-Box (1978) correction
L	lower
U	row dimension of F
U	upper
V	column dimension of F
e	error
i	generic array index
i	over individual time increments
k	index of elements in m
kd	kernel density

Continued on next page

Table 0.2 – continued from previous page

Symbol	Description
lsnonneg	least-squares with non-negativity constraints
ls	least-squares
m	index of rows in C
m	relative to mean
md	measured
mi	measured & interpolated
n	index of columns in C
o	model order
orig	original
s	surface
ss	sub-surface
t	time
x	generalised column coordinate
x_o	interval in space between signal indexed at x
y	generalised row coordinate
y_o	interval in space between signal indexed at y
z	generalised elevation coordinate

Tab. 0.3 *Constants*

Symbol	Description
∞	infinity
π	ratio between circle's circumference and diameter
g	gravitational acceleration

Tab. 0.4 *Mathematical Operations*

Symbol	Description
$\|xx\|$	modulus of variable xx
$\overline{xx}$	generalisd mean of variable xx
Γ	kernel function
Δ	change
δ_m	Kronecker delta function
exp	exponent
$\Re$	real
$\Im$	imaginary
B	bandwidth for kernel density estimation
K_1	Bessel function, third kind, index 1
FT	Fourier transform
FFT	Fast Fourier Transform (algorithm)
T	matrix transpose
c	complex-conjugated, or complex-valued
$\mathbf{i}$	imaginary number
l	lag number
p	generalised probability density function, or probability
$\mathbf{w}$	Hann taper

Tab. 0.5 *Abbreviations*

Symbol	Description
2D	Two-Dimensional
3D	Three-Dimensional
Ac	Accuracy
ADV	Acoustic Döppler Velocimeter
AONB	Area of Outstanding Natural Beauty
AR	Autoregressive Process
BP	Before Present

Continued on next page

Table 0.5 – continued from previous page

Symbol	Description
CB+	GSTA rule Case B (Type 1)
CCA	Canonical Correlation Analysis
CCO	Channel Coastal Observatory
CD	Chart Datum
CEOF	Complex Empirical Orthogonal Function
DN	Digital Number
DOD	Depth of Disturbance
ECM	Electromagnetic Current Meter
EOF	Empirical Orthogonal Function
FB-	GSTA rule Case C (Type 2)
FSC	Field Studies Council
F & W	Folk & Ward (graphical grain size measures)
GCE	Generalised Cross Entropy
GCRS	Geological Conservation Review Site
GSD	Grain Size Distribution
GSTA	Grain Size Trend Analysis
H_0	null hypothesis
H_1	alternative hypothesis
HC	Heritage Coast
HT	High Tide
LSCB	Large Scale Coastal Behaviour
LUC	Look-Up Cataloguing
LW	Low Water
Ma	Millions of years ago
Md	median diameter
MB	Mega-Byte
MHWN	Mean High Water Neaps
MHWS	Mean High Water Springs
MSD	Morpho-Sedimentary-Dynamics
MSG	Mixed-Sand-Gravel
NLSWE	Non-Linear Shallow Water wave Equations
NNR	National Nature Reserve
NOAA	National Oceanic and Atmospheric Administration (USA)

Continued on next page

Table 0.5 – continued from previous page

Symbol	Description
O	Order (magnitude)
ODN	Ordnance Datum Newlyn
PSD	Power Spectral Density
PT	Pressure Transducer
RGB	Red-Green-Blue (digital image)
RMS	Root Mean Square
RTK-GPS	Real Time Kinematic Global Positionning System
Sp	Speed
SSSI	Site of Special Scientific Interest
SST	Total Sum of Squares variation
SVD	Singular Value Decomposition
TPM	Transition Probability Matrix
TR	Tidal Range
TTR	Tidal Translation Rate

ACKNOWLEDGEMENTS

This thesis is the product of a considerable amount of external assistance. First and foremost, I couldn't have had a better supervisor than Prof. Gerd Masselink, whose knowledge of, and incurable enthusiasm for, beaches is probably unsurpassable. I thank him particularly for two other things he has in spades, patience and energy, both of which I needed at more times than I can count during the last few years. Finally, I thank him for loads of ideas, and for giving me the chance in the first place. Tim Scott deserves special thanks for listening while I whittered away what must have seemed like an eternity, and who was a major steadying influence in the last year of this thesis, spooning out dollops of curry and Zen in almost equal measure. Also to Maria Campbell for being wonderful in every way. Dr Martin Austin was my technical guru, a good friend, and my collaborator for a considerable slab of the work. Thanks to George Graham for getting me into this (rather splendid) LaTeX typesetting. Thanks to my small army of field assistants, who were (in no particular order): Isabelle Emmanuelle, Amaia Ruiz de Alegria, Dave Dawson, Iain Fairley, Ian Ball, Sharief K, Katie S, Tom Deacon, Jon Tinker, George Graham, Dr Rich Charman, and Joshua Gibson. My office mates —Nadine Schafer, Amaia Ruiz de Alegria, Isabelle Emmanuelle, Alison Nock, Dae Dawson —are thanked heartily for putting up with my moods, and my mess. Rich Hartley was instrumental (forgive the pun!) in sorting out my kit requirements, and dealing with various breakages, spillages and misdemeanours. The British Society for Geomorphology gave me £300 to go to an international conference. Thanks to Ines Cifuentes of the American Geophysical Union who symapthesised with my predicament to help me to get to the AGU Fall Meeting. The Field Studies Council, Slapton Ley, were very tolerant of my waking and eating hours while I followed the rhythm of the tides, and provided me with excellent labs and cakes. Tom Deacon digitised and made available a lot of weather data for me. Thanks to SLNNR who gave me the opportunity to share my research with public and policy makers at their annual seminars, and let me set up survey base stations in their grounds. Chapter 2 benefitted from comments by Prof. Julian Orford, from Queens University, Belfast. Chapter 4 benefitted from some inspiration/advice from Dr Edith Gallagher from Franklin and Marshall College; Dr Dave Rubin and Dr Jonathan Warrick from the USGS; and Dr Peter Ruggiero from Oregon State University. Thanks also to Prof. Martin Kent, Dr Mark Davidson, Prof. Roland Gehrels and Dr Ken Kingston for some helpful chats along the way. Ken is also thanked for getting me started on Graphical User Interfaces, which helped with explaining (and hopefully exporting!) my digital grain size routines. Thanks my brother and my sister who put up with my, erm, foibles, and didn't mind *too much* when I drifted in and out of existence. Finally, a massive thank you to my mother Elizabeth, who couldn't have been more loving and supportive, and positive about 'that thing I do'.

AUTHOR'S DECLARATION

At no time during the registration for the degree of Doctor of Philosophy has the author been registered for any other University award without prior agreement of the Graduate Committee. This study was financed with the aid of a studentship form the Faculty of Social Science and Business.

A significant part of Chapter 5 was the result of a collaboration with Dr M.J. Austin of the University of Plymouth, which resulted in the joint publication detailed below (Austin & Buscombe). A lot of material from that publication has been reproduced in Chapter 5.

Relevant scientific seminars and conferences were regularly attended at which work was often presented; and several papers prepared for publication.

Publications:

Buscombe, D., and Masselink, G. [2006] Concepts in Gravel Beach Dynamics. *Earth Science Reviews* **79**, 33-52.

Buscombe, D., Austin, M.J., and Masselink, G. [2007] Field observations of step dynamics on a macrotidal gravel beach. In Kraus, N., and Rosati, J., (Eds) *Proceedings of Coastal Sediments 2007* (Volume 1), ASCE, USA.

Buscombe, D., and Masselink, G. [2007] The relationship between sediment properties and sedimentation patterns on a macrotidal gravel beach over a semi-lunar tidal cycle. *Eos Transactions American Geophysical Union Fall Meeting*, Abstract H53L-02.

Austin, M.J., and Buscombe, D. [2008] Morphological Change and Sediment Dynamics of the Beach Step on a Macrotidal Gravel Beach. *Marine Geology* **249**, 167-183. doi:10.1016/j.margeo.2007.11.008.

Masselink, G., Buscombe, D., Austin, M.J, O'Hare, T., Russell, P. [2008] Sediment Trend Models Fail to Reproduce Small Scale Sediment Transport Patterns on an Intertidal Beach. *Sedimentology* **55**, 667-687. doi: 10.1111/j.1365-3091.2007.00917.x.

Buscombe, D., and Masselink, G. [2008, in press] Grain Size Information from the Statistical Properties of Digital Images of Sediment. *Sedimentology*

Buscombe, D., Masselink, G., and Rubin, D.M. [2008, accepted] Granular Properties from Digital Images of Sediment: Implications for Coastal Sediment Transport Modelling. *International Conference on Coastal Engineering*, Hamburg, 2008.

Ruiz de Alegria, A., Masselink, G., Kingston, K., and Buscombe, D. [2008, accepted] Storm Impacts on a Gravel Beach Using the ARGUS video system. *International Conference on Coastal Engineering*, Hamburg, 2008.

Buscombe, D. [in review] Estimation of Grain Size Distributions and Associated Parameters from Digital Images of Sediment. *Sedimentary Geology*

Presentation and Conferences Attended:

Slapton Research Seminar, Field Studies Council, Slapton Ley, 4th December 2004. Talk entitled '*A tale of two storms*'.

Slapton Research Seminar, Field Studies Council, Slapton Ley, 18^{th} November 2006. Talk entitled '*A view from the beach*'

Slapton Research Seminar, Field Studies Council, Slapton Ley, 3^{rd} November 2006. Talk entitled '*A Year in the Life of Slapton Sands (Oct 2006-Oct 2007). But was it a typical year?*', with Tom Deacon from SLFSC.

Centre for Coastal Dynamics and Engineering (C-CoDE), University of Plymouth, 6^{th} December 2006. Talk entitled '*Field observations of morphological change and sediment dynamics from the nearshore of a gravel beach*'

Postgraduate Symposium, Faculty of Social Science and Business, University of Plymouth, 2^{nd}–3^{rd} March 2007. Talk entitled '*The Discrete- State Markov Chain: A General Tool for Categorical Data Analysis and Modelling*'.

3^{rd} Young Coastal Scientists and Engineers Conference (YCSEC) 2007, University of Plymouth, 20^{th} April 2007. Talk entitled '*Morpho-Sedimentary Co- Variation on a Macrotidal Gravel Beach: the Importance of Scale*'.

Others:

Buscombe, D., Masselink, G., Chadwick, A., Gehrels, R., and Austin, M. A Tale of Two Storms: Slapton Gravel Barrier Beach. Poster presentation at the Launch of the Centre for Coastal Dynamics and Engineering (C-Code), University of Plymouth, June 2005.

Buscombe, D. (ed.), The Quaternary Research Association Fourth International Postgraduate Symposium Abstract Book, School of Geography, University of Plymouth, UK, August 31st to September 2nd (2005)

Buscombe, D. A test for vertical order in sedimentary sequences. Poster presentation at The Quaternary Research Association Fourth International Postgraduate Symposium

Buscombe, D. Sediment Size from Digital Images Using Statistical 'Look Up Catalogues'. Poster presentation at the Young Coastal Scientists and Engineers Conference (YCSEC) 2006, University of Southampton May 2006 (awarded prize for best poster).

Buscombe, D., Masselink, G., Austin, M.J., Gehrels, W.R., Chadwick, A., Hartley, R., Ruiz de Alegria Arzaburu, A. Coastal Processes Research at Slapton Sands. Poster presentation for National Nature Reserve Information Centre, Slapton Ley.

Buscombe, D. The Discrete-State Markov Chain: A General Tool for Categorical Data Analysis and Modelling. Oral presentation at the 2007 PG Symposium, Faculty of Social Science and Business, University of Plymouth, 2-3rd March 2007.

Buscombe, D., Masselink, G. Optical remote sensing of nearshore sediment transport and sediment characteristics on a gravel beach. Poster presentation at the University of Plymouth's Research and Innovation Conference, 4th April 2007.

Buscombe, D., Masselink, G. Morpho-Sedimentary Co-Variation on a Macrotidal Gravel Beach: the Importance of Scale. Oral presentation at the Young Coastal Scientists and Engineers Conference (YCSEC) 2007, University of Plymouth April 2007

Buscombe, D., Masselink, G. (eds.), Field Visit Guide to Start Bay and Prawle Point, Young Coastal Scientists And Engineers Conference 2007, School of Geography, University of Plymouth.

Word count of main body of thesis: 68,364 (inc. 38 tables and 134 figures)

Signed ..... Date .....

1 INTRODUCTION

And they'll build systems dark and deep,
And systems broad and high;
But two or three will never agree
About the reason why.

Peter Pindar, The Three Wise Men of Gotham.

1.1 *Coastal Morphodynamics*

Coastal morphodynamics is defined as the *"mutual adjustment of topography and fluid dynamics involving sediment transport"* [Wright and Thom, 1977] in the coastal zone, an area which, on beaches, extends from wave closure depth on the continental shelf to the upper limit of the beachface. This definition crystallises two very important ideas: the first is that coastal morphologies develop and change in response to spatial gradients in sediment transport, which are driven by waves and tides, and associated currents. The second is that the amplitudes and length scales, and time scales of growth and decay of these features, are a complex function not only of the strength and duration of flows and the characteristics and supply of movable sediment, but also of mutual adjustments between flow fields and morphologies. These drive gradients in sediment transport and associated spatial patterns in sedimentation, in (often complicated) feedback loops [Cowell and Thom, 1994].

These feedback mechanisms may either damp/stabilise the development of coastal morphologies (termed negative feedback, leading to self-regulation), or cause growth/amplification of coastal topographies (termed positive feedback, leading to

instabilities and self-organisation; [King, 1970]). The former case may be exemplified by the recovery to equilibrium of a beach profile following a major storm, and the latter may be illustrated by the concentration of flow induced by a relatively small scour hole, which causes the hole to enlarge; or by the growth of sand ripples irrespective of a change in flow conditions [Austin et al., 2007]. At all scales coastal systems exhibit non-linear behaviour [Phillips, 1992; deVriend, 1997], thus the coastal science community is only just beginning to unravel the complexities of coastal evolution.

The ultimate goal of the science of coastal morphodynamics (hereafter, simply called 'morphodynamics') is the complete prediction of the motion of the interface between sediments and the sea, and associated changes in morphological features [Blondeaux, 2001]. There are competing views concerning the best method to acheive this ultimate goal: a 'top down' approach (which disaggregates observations into small scale processes using basic conservation principles) versus a 'bottom up' (integration of small scale processes through to larger scales) approach [deVriend, 1997]; or a deterministic approach versus a probabilistic approach. There is little guidance on the required, or acceptable, aggregation of scales [Terwindt and Wijnberg, 1991].

Terwindt and Battjes [1990] identify three approaches to the study of coastal behaviour:

The **geostatistical** approach which descriptively draws out trends from data sets.

The **phenomenological** approach which employs statistical analysis to parameterise processes which are considered relevant, including empirical relationships drawn without first principles.

The **modelling** approach which expresses fundamental relationships between flows and forms as a series of mathematical equations, from first principles.

Morphodynamics requires all three approaches to achieve its ultimate goal. This thesis will draw upon both geostatistical and phenomenological approaches to the study of coastal morphodynamics, with a strong emphasis on the collection of field data for subsequent analysis and interpretation. Morphodynamics relies strongly on field observations, since the collection and analysis of measurements and observations is crucial for the identification, classification and explanation of coastal features, and

change in these features. Theoretical research is then needed to formulate empirical and numerical models capable of predicting the behaviour of observed features. Field data, and insights from field experiments, are required at every stage in the process, from identification and definition of the problem at the appropriate spatial and temporal scales, to the validation and updating of these theoretical models. Coastal morphodynamics is thus strongly inter-disciplinary. Geomorphologists and oceanographers have traditionally carried out fieldwork and statistical data analysis in order to observe, measure, document and explain morphodynamic phenomena. Engineers and mathematicians are largely concerned with practical and theoretical advances, in the form of generalised numerical models, based on the insights obtained from the field data. Full-scale numerical models have been developed that attempt, in real time, to describe the physical processes involved in the interactions between flow fields and sediments, and thereby predict the time-evolution of observed morphologies at the correct length scales. Such models are complex and must be solved by advanced numerical techniques [Seminara, 1998; Blondeaux, 2001].

In general therefore, research which is essentially geomorphological in nature remains dominated by empirical case studies, and the theoretical study of morphodynamics is paralysed until appropriate field observations and measurements have revealed the dominant physical processes to parameterise, and likely patterns of sedimentation at the correct scaling. Occasionally, however, a pressing societal need requires a re-ordering of this template, where theoretical/numerical studies proceed at a pace before field observations have been documented. This may be compounded by a perceived or real logistical problem and/or technical limitation associated with field work and the collection of the required data to formalise the problem and formulate the solution. An example of this has been research conducted into coarse-grain/gravel beach morphodynamics in the past two decades.

Most gravel beaches are associated with mid-high latitude paraglacial or proglacial coasts of Europe and the Americas, which tend to be transgressive and sediment depleted [Orford et al., 2002]. Significant gravel accumulations also occur from river supply or reworked fluvial gravel fans associated with mountainous environments, which are usually regressive and sediment rich [Carter and Orford, 1988]. Gravel beaches occur in tectonically active areas at all latitudes [Dobkins and Folk, 1970], and are significant

locally where inner shelf deposits are reworked landwards [Hails, 1975] or where gravel-rich cliffs and platforms are eroding [Carter, 1998]. In the UK alone, over 900km of coastline is protected by coarse grain beaches [Fuller and Randall, 1988], often in populous areas.

Interest in developing quantitative prediction of gravel beach morphodynamics is increasing; gravel shores are perceived as especially important for shore protection, mineral extraction, and providing support for habitats. A gravel beach is a porous structure and hydraulically rough, which helps reduce wave energy and reduce the potential for coastal damage. This has prompted their extended use in aggregate mining and beach fills/nourishment as a sympathetic coastal defence, especially in Russia [Zenkovich and Schwartz, 1987], the UK [Mason and Coates, 2001] and the Pacific coast of the USA [Komar, 2007]. Gravel beaches often contain commercially exploitable minerals such as gold and diamonds [Komar, 1998], as well as serving as modern analogues for examining the reservoir potential of ancient sedimentary accumulations [Carter and Orford, 1984; Massari and Parea, 1988].

The societal importance of gravel beaches and gravel sediment transport, and the requirement of practical solutions, has meant that the study of gravel beaches has switched from qualitative statements of early observers [Palmer, 1834; Lewis, 1931] to highly mathematical treatments, largely without inductive studies derived from field measurement. For example, numerical solutions have been obtained for cross-shore sediment transport and profile evolution [Powell, 1990; Pedrozo Acuna et al., 2006]; gravel beach planform change [Brampton and Goldberg, 1991]; crest height [Lorang, 2002]; longshore gravel sediment transport [Van Wellen et al., 2000]; and swash flows/groundwater dynamics [Clarke and Damgaard, 2002; Lee et al., 2007], before these phenomena have been well documented [Ivamy and Kench, 2006]. This is uncommon in morphodynamics, and it means that there are few field data sets with which to validate these numerical models before practitioners begin to utilise them in project designs [the potential dangers of this are discussed by Cooper and Pilkey, 2004].

Particle sizes exhibit a wide (often bimodal) distribution in gravel bed environments. As stated previously, variable wave/tide conditions drive spatial/temporal changes in sediment transport gradients, resulting in spatial sedimentation patterns and (often complex) morphologies [Holman and Bowen, 1982]. The transport of heterogeneous

sediments involves a secondary process of preferential selection and deposition (sorting) according to the geometrical characteristics of those sediments. This results in the generation of patterns associated with a spatial/temporal rearrangement of grain size distributions (grading), and these features are particularly evident on gravel beaches. Some authors believe these sorting processes may have a morphodynamic role [Sherman et al., 1993; Rubin and Topping, 2001; Nicholson et al., 2003*a*; Gallagher and McMahan, 2006]. These claims have important implications (see Chapter 2) but are relatively new and remain unsubstantiated.

1.2 *Research Objectives*

The purpose of this study has been to gain a better understanding of morphological and sedimentological change on natural gravel beaches. Hydrodynamic, morphological, sediment transport and grain size distribution data has been obtained from a gravel beach at a range of spatial and temporal scales (Figure 1.1).

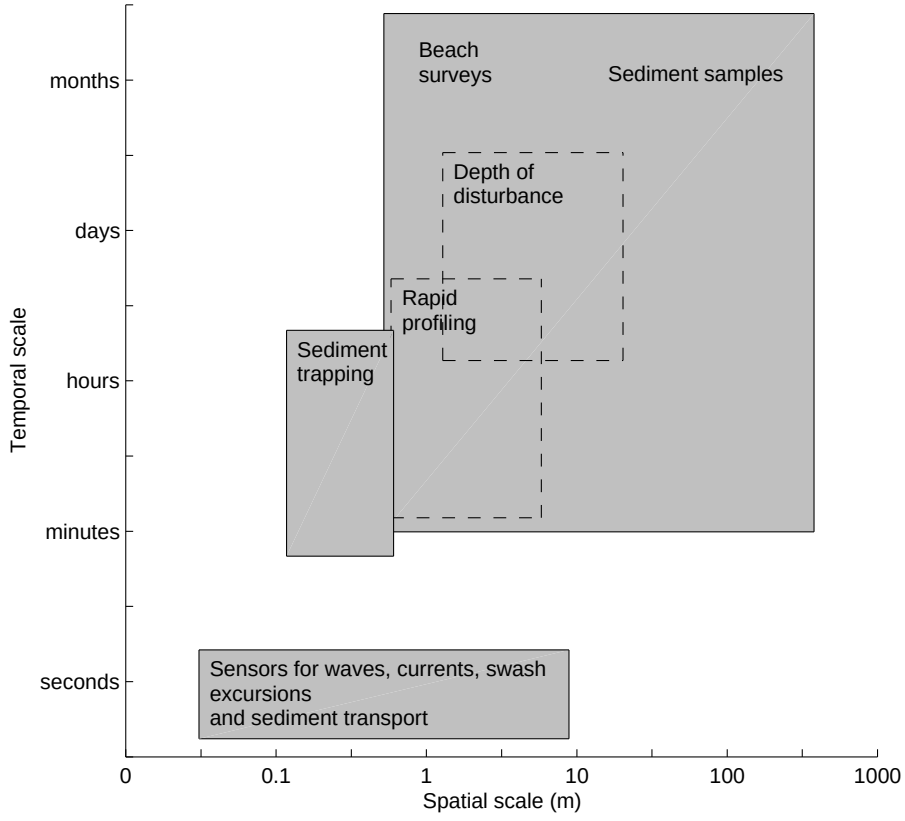

Fig. 1.1 *Scales associated with measurements in this study, modified from Terwindt and Wijnberg [1991].*

The specific objectives of this thesis are:

- to present an overview of the current understanding and possible future directions research related to gravel beach morphodynamics and sediment dynamics;
- to develop a methodology which enables the quantification of sediment characteristics at a resolution comparable with morphological and hydrodynamic measurements;
- to investigate morphological change and sediment dynamics on a gravel beach at a range of scales; and
- to propose a conceptual model for gravel beach morpho-sedimentary dynamics, which establishes a link between beachface sediments and morphological change.

1.3 *Thesis structure*

This study draws primarily upon field data collection, summarised in Table 1.1.

Tab. 1.1 *Field Data Collection Time Line*

Dataset	**Data Collection**	**Date**
S1	M[1]	October & November 2004
C1	Spilot[2]	April & May 2005
E1	M, S[3], H[4]	September 2005
E2	M, S, H, Vpilot[5], V[6]	June 2006
S2	M, S,	October 2006–October 2007
L	S	January, June, November 2006; February, May 2007
E3	M, S, H, V	April & May 2007

1=morphological (M) measurements/surveys; 2=digital sediment (S) technique pilot; 3=sediment samples; 4=hydrodynamic (H) data collection; 5=underwater video (V) pilot; 6=underwater video data collection

The field work detailed in Table 1.1 was in the first instance informed by an extensive literature review, and secondly by a series of pilot studies which tested field equipment and methods. Separating the work into a number of discrete campaigns, and subsequently analysing and assessing the data from those campaigns, was an essential part of the project since each data set informed the next direction of the research. Consequently a cycle of —fieldwork preparation, data collection, data analysis and algorithm development, synthesis and writing —continued throughout the research project.

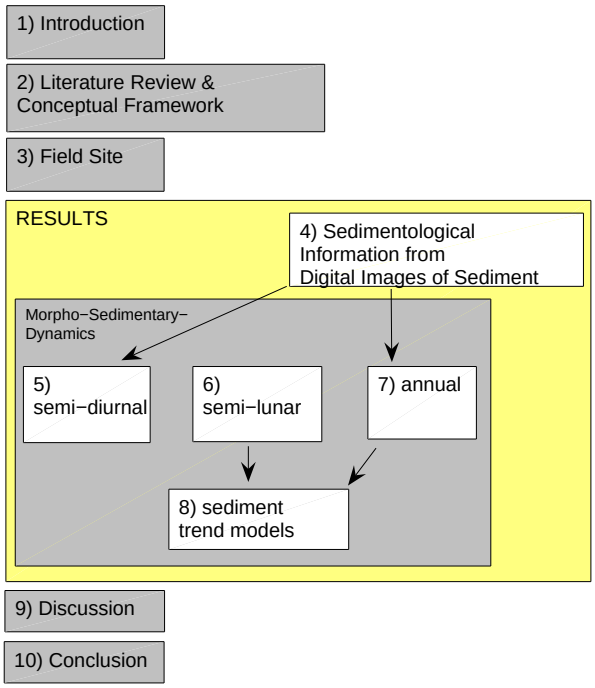

Fig. 1.2 *An outline of the thesis*

An outline of the thesis is summarised in Figure 1.2. Chapter 2 summarises the relevant literature, synthesising previous research into gravel beaches into a conceptual framework. Chapter 3 contains a description of the field study sites. There are five results chapters, each containing their own methods section which pertains almost exclusively to the data analysis in that chapter. These include Chapter 4 which documents the development of new methods without which the research would not have been possible; and Chapters 5 to 7 which address the same fundamental problem on a different scale. Chapter 5 looks at morphological and sedimentological change, as well as characterising some aspects of sediment transport in the nearshore, over small spatial scales at the time scale of the semi-diurnal tide. The topic of Chapter 6 is the morphological and sedimentological change over small spatial scales associated with the semi-lunar tide. Chapter 7 investigates the morpho-sedimentary changes over large spatial scales over one year. Each results chapter draws from measurements and insights obtained from various stages of the project. Chapter 8 investigates the utility and applicability of two distinct types of sedimentation modelling using distributional spatial

trends in grain size distributions. These insights are synthesised in Chapter 9, which also contains some reflection on the conceptual framework outlined in Chapter 2, as well as evaluating some of the general methodological issues raised by the research, before chapter 10 draws some conclusions.

2 GRAVEL BEACH DYNAMICS: LITERATURE REVIEW AND CONCEPTUAL FRAMEWORK

Whenever anyone mentions theory to a geomorphologist,
he instinctively reaches for his soil auger.

Richard Chorley, 'Geomorphology: Present Problems and Future Prospects', 1978.

2.1 *Introduction*

Various contemporary commentators have drawn attention to the discrepancy between recent advances made into the morphodynamics of sand beaches and the comparative lack of similar advances made into gravel beach dynamics [Van Wellen et al., 2000; Mason and Coates, 2001; Jennings and Shulmeister, 2002; Orford et al., 2002; Horn et al., 2003; Pontee et al., 2004]. Historically, our insights into shorter term gravel beach dynamics have lagged behind our understanding of littoral environments composed of sand, mainly because of the logistical problems associated with laboratory or field experimentation. It is important that this fact is redressed since it is well recognized that gravel beaches are one of the most efficient forms of coastal protection, with a remarkable degree of stability [Nicholls and Webber, 1988; Powell, 1988; Sherman, 1991]. Recently there has been some revival of interest in gravel beach dynamics, resulting in a spate of modelling efforts [Van Wellen et al., 2000; Clarke et al., 2004; Pedrozo Acuna et al., 2006; Lee et al., 2007]. Although swash-dominated, gravel beaches are scarcely mentioned in recent reviews of swash zone hydrodynamics and sediment transport [Butt and Russell, 2000; Elfrink and Baldock, 2002; Masselink and Puleo, 2006]. In order to restore the balance,

the intention of this chapter is to review shorter term, process-oriented gravel beach morphodynamics, exploring a number of features which may be peculiar to beaches composed of gravel-sized sediment. Further research will uncover a unifying theme common to all avenues of enquiry: the importance of spatial distributions in sediment size and shape, centred around the notion that the spatial heterogeneity of sediment properties are both an expression and a control on gravel beach morphodynamics.

2.2 *Nomenclature, Classification and Geographic Distribution*

The collective noun under the Udden-Wentworth classification scheme for sediment with a b-axis diameter of between 2 and 60 mm is 'gravel', which has physical connotations understood not only by coastal scientists and engineers, but geomorphologists, geologists and ecologists. The alternative term, 'shingle', is not as inter-disciplinary or international [Carter and Orford, 1993; Van Wellen et al., 2000; Orford et al., 2002]. A necessary distinction is made between gravel beaches so-classified and boulder beaches [Novak, 1972; Oak, 1984; Lorang, 2000; Johnston, 2001; Lorang, 2002], or beaches composed of coral gravel [Felton et al., 2000; Richmond and Morton, 2007].

Gravel beach sediments (Figure 2.1) have a characteristic size and shape heterogeneity [Zenkovich, 1967; King, 1972; Carter, 1998] since the physiographic context to the development of gravel beaches is glacial and mountain weathering. Therefore the geographic coverage is distinctly high-latitudinal, with long term sediment supply dominated by continental shelf reworking of gravels supplied by terrestrial weathering processes. Gravel beaches are particularly widespread on the wave-dominated coastlines of Northern Europe (especially Russia,the UK and Ireland), Canada, the USA, Japan, New Zealand, and Latin America. Orford et al. [2002] have recently provided a comprehensive review of the modern thinking behind the long-term, large-scale geomorphology of gravel beaches and barriers. Gravel beaches within large regional settings are the subjects of Isla and Bujalesky [2000] and Anthony [2002]. The structural sedimentology of gravel beaches, including the historical interpretation of internal beach structures/stratification (an enquiry which, incidentally, is almost wholly absent from the process-oriented gravel beach studies), is treated in detail by Bluck [1999]. To date, research on gravel beaches has been dominated by these longer term geomorphological

and sedimentological studies, but few studies have attempted to carry out detailed process measurements to elucidate gravel beach morphodynamics and sediment dynamics [Sherman, 1991; Ivamy and Kench, 2006; Austin and Masselink, 2006*a*]. This chapter reviews and discusses the dominant processes and concepts which can affect entire beach faces or sections of beach faces on larger features such as spits and barriers composed entirely of gravel sediment (Figure 2.1), in tidal settings which are affected directly by wave action. This primarily encompasses 'pure' gravel beaches, as defined by the classification scheme of Jennings and Shulmeister [2002], and includes cliffbacked and pocket beaches, as well as barrier and spit fontages, but not back beach deltas (which are formed and stranded by storms), lateral deltas formed by permanent barrier breach, and sheltered sections of spit heads.

Fig. 2.1 *Some images of gravel beaches in the UK and New Zealand, showing characteristic steepness and spatial segregation of sediment size.*

Pure gravel beaches are relatively narrow, very steep and reflective at all stages of the tide [Jennings and Shulmeister, 2002]. Whilst many of the concepts and processes

discussed here will be applicable to mixed sand and gravel (MSG) beaches or beach sections, the dynamics of such beaches are quite distinct [Kulkarni et al., 2004], and are the subject of review by Kirk [1980] and Mason and Coates [2001]. Studies into the fundamentals of gravel beach behaviour may be best carried out on pure gravel beaches, an 'end-member' in the coastal sedimentological continuum, without the complicating influence of varying concentrations of sand.

2.3 *Hydrodynamic & Hydraulic Forcing*

2.3.1 *Wave breaking*

The gravel beach morphodynamic system is forced at the boundary by ocean tides and offshore waves, which are in turn modified by large scale landform configurations (sub-and supra-tidal geology). Nearshore hydrodynamics (the combinatorial of waves and secondary waves, tides and associated currents) are modulated primarily by beach slopes, with a secondary control exerted by friction. Both are controlled, in turn, by grain size and sorting which allow steep slopes (Table 2.1) and a rapid attenuation of fluid momentum through friction (which includes permeability). Due to a high threshold of motion, and highly asymmetric wave action on the beachface, gravels have a greater tendency to move onshore compared with sands [Bagnold, 1940; Inman, 1949] forming steep slopes. The gravel beach is thus the classic narrow 'reflective' beach morphotype (Table 2.1) in the beach classification nomenclature [Carter and Orford, 1984, 1993; Jennings and Shulmeister, 2002].

Nearshore hydrodynamics on gravel beaches are dominated by the swash zone, where bores created by wave breaking travel and decay on the beachface in oscillatory phases termed uprush and backwash. Short wave bores induce highly asymmetrical swash motions at incident wave frequencies as waves break over steep slopes close to the shoreline. Very narrow surf zones support just one relatively uniform breaker line, quasi-perpendicular to the beach face [Baldock et al., 1997; Baldock and Holmes, 1999]. The rapidity of nearshore wave transformations dictate energy concentration at breakpoint, in close proximity to the shoreline, minimising the generation of broad-band infra-gravity oscillations, and maximising the importance of fluid motions at incident and subharmonic frequencies [Huntley and Bowen, 1975a; Mase, 1995; Miles and Russell,

Tab. 2.1 *Range of morphometric and morphodynamic values obtained from some pure gravel beach field studies/observations.*

Dataset	Tide	Slope (tan)	Md (mm)	ξ	Width (m)	Proc. Meas.
M82(site2)(JP)	micro	0.12	4.8	1.01*	26*	N
JS02(1)(NZ)	micro	0.14	4.7	2.27	51.63	N
JS02(2)(NZ)	micro	0.13	4.71	2.12	50.4	N
JS02(3)(NZ)	micro	0.23	5.23	3.79	23.89	N
JS02(4)(NZ)	micro	0.23	5.22	3.79	25.04	N
JS02(5)(NZ)	micro	0.10	4.79	1.58	38.4	N
JS02(6)(NZ)	micro	0.24	5.11	4	18.5	N
JS02(7)(NZ)	micro	0.20	4.98	3.26	28.01	N
L02 (US)	meso	0.22	593*	1.54*	45	Y (H,M,S)
HD06(NZ)	meso	0.11	50	0.83*	100-400	Y (H)
HL06 (UK)	macro	0.17	n/a	0.6-1.2	25	Y (H,M,G)
AM06 (UK)	macro	0.15	6	0.9-2	100	Y (H,M,G)

* indicates inferred or calculated values (where not explicitly stated). Md denotes median grain size; ξ Iribarren number; and for the process measurements H denotes hydrodynamics; M morphology; S sediment size; and G groundwater. M82 refers to Maejima [1982]; JS02 refers to Jennings and Shulmeister [2002]; L02 refers to Lorang [2002]; HD06 refers to Hartstein and Dickinson [2006]; HL06 refers to Horn and Li [2006] and AM06 refers to Austin and Masselink [2006*a*].

2004]. Significant wave grouping may remain at the shoreline [Ivamy and Kench, 2006], compounded by the interaction of successive swash events or the two phases of the same swash event (swash-backwash) which causes a downward shift in frequency from incident to sub-incident [Mase, 1995]. The lack of breakpoint variability, dictating a spatial concentration of energy, means that critical thresholds for sediment transport are almost always exceeded [Carter and Orford, 1993], although this may be limited to the surf and swash zones [Austin and Masselink, 2006*a*].

The tide is crucial to beach morphodynamics [Masselink and Short, 1993; Davidson et al., 1993]. The role of the tide is to advect the surf and swash zones across the intertidal beachface, therefore morphodynamic processes will differ depending on the stage of the tide and the local slope. The gravel beachface is typically convexo-planar in shape, so the swash and surf zone slope and associated morphodynamic processes, at any given point on the semi-diurnal tidal cycle, will change. For example, the local swash zone slope on the rising tide will be a compound function of the morphodynamics in operation on the corresponding time on the previous ebbing tide (assuming the same tidal range and identical wave setup). The local surf zone bed may inherit the slope from the passage of the previous swash zone. An additional control may be the rate of change

of the tide over the slope [tidal translation rate, Masselink and Short, 1993]. If and where the tidal frame dictates wave breaking over a shallow sand slope immediately seawards of the gravel bank, as on a 'mixed' beach, nearshore hydrodynamics are substantially different.

The interaction between the swash and surf zones on gravel beaches remain largely unstudied. Swash is asymmetrical [Hughes et al., 1997]: uprushes on sand beaches are typically shorter, faster, and more volumous [Masselink and Puleo, 2006]. This asymmetry is considered key in the amount of sediment transport and morphological change which occurs as a result of swash processes on the beachface. On gravel beaches, relatively high permeabilities may serve to enhance swash asymmetries, with important implications for beach change [Duncan, 1964; Masselink and Li, 2001; Austin and Masselink, 2006*a*]. Pre-and post-breaker energy fluxes may have interesting and important consequences for the spatial decay of energy with wave transformation distance, and turbulence, both locally-generated and the contribution advected from bore collapse [Puleo and Holland, 2001; Longo et al., 2002; Jackson et al., 2004; Butt et al., 2004; Pritchard and Hogg, 2005]. The potential importance of the advection of material convected by turbulent bore collapse into the swash zone, reported by numerous authors in recent years [and reviewed in Masselink and Puleo, 2006] appears particularly essential for swash-dominated gravel beach foreshores. The extent to which reflection is attenuated by the loss of fluid into highly permeable beach faces [Powell, 1990] is at present unknown, as are undertow and setup; and near-bed velocity profiles, which again are in need of much further scrutiny.

The nearshore hydrodynamic regime so-described allows bore theory [Peregrine, 1966] and the non-linear shallow water wave equations [NLSWE, or simply SWE; Shen and Meyer, 1963, reviewed in detail by Hughes, 1992, 1995; Peregrine and Williams, 2001], or the 'ballistic model' [Hughes and Baldock, 2004] to be particularly applicable. We may assume swash discretion (or uncurtailed individual events) with most validity on gravel foreshores where permeabilities (and therefore fluid loss) are high [Austin and Masselink, 2006*b*]. Although swash interaction has been shown to occur naturally [Austin and Masselink, 2006*b*], steep slopes and high permeabilities gratify the assumption that individual swashes are 'launched' up the foreshore slope [Hughes and Baldock, 2004]. When using the NLSWE, for the necessary formulations to hold, the fluid of the swash

tip must maintain very shallow depths [Peregrine and Williams, 2001]. Fluid loss through infiltration appears to be highest on the leading edge of the uprush during the latter stages of the uprush event [Horn et al., 2003], i.e. towards the top of the foreshore. Fluid exchanges on highly permeable substrates are possible to model using ballistic approaches [Clarke and Damgaard, 2002; Clarke et al., 2004; Shanehsazzadeh and Holmes, 2007]. For all of these reasons, a more complicated approach, such as employment of the Boussinesq equations [Pedrozo Acuna et al., 2006] may not be necessary to model swash motions. However, just like sand beach shorelines [Elfrink and Baldock, 2002; Masselink and Puleo, 2006], how swash zone hydrodynamics relate to sediment transport, sediment sorting and morphological change is much more problematical.

2.3.2 *Swash-groundwater hydraulic exchange & sediment transport*

A gravel beach is an unconfined aquifer which is affected primarily by tides, waves and terrestrial sources of water, and the permeability of the beachface, determined by grain size and sorting. The transmission of fluids through granular interstices, and swash flow modification as a result of differential groundwater responses over the varying sediments of a gravel foreshore, have interesting and under-studied implications for sediment transport and morphological change on gravel beaches [Masselink and Li, 2001; Austin and Masselink, 2006*b*].

Horn [2002] attributes the failure of various swash zone sediment transport models to the over-simplification of swash hydrodynamics with respect to swash groundwater flows (hydraulics). On a gravel beach, permeabilities and hydraulic conductivities are generally high [Horn et al., 2003]. Hydraulic conductivity shows a sensitive dependence on 1) sediment size (Figure 2.2), so the spatial distribution of surface sediment size, and 2) vertical size distributions, or the variation in sediment size with depth, are particularly significant on gravel beaches with respect to hydraulics. The qualitative behaviour and importance/magnitude of these features may be peculiar to gravel beaches, and their study may be more difficult in the field for three crucial reasons. Firstly, the magnitude of swash-groundwater exchanges is greater [Holmes et al., 2002; Horn et al., 2003]. Secondly, air encapsulation within groundwater sediment matrices, hitherto considered ineffectual for sand beaches, may be important for porous gravel

substrates [Horn, 2002]. Thirdly, the high seepage velocities under swash flows [reported by Holmes et al., 2002; Horn et al., 2003] implicates a non-Darcian flow regime, or a nonlinear groundwater (hydraulic) through-flow velocity dependence on hydrostatic pressure fields, explicating the sensitive nonlinear relationship between sediment size and hydraulic conductivity where permeability is high (a notion which has remained latent until very recently). Accordingly, instantaneous swash hydrodynamics and hydraulics (or simply their combinatorial, 'hydro-hydraulics') have taken on a new dimension and renewed impetus for gravel beach dynamics [Masselink and Li, 2001; Horn et al., 2003; Clarke et al., 2004; Isla and Bujalesky, 2005; Austin and Masselink, 2006*b*], where the hydrostatic forces of vertical water exchange are potentially so exacting.

Numerical models for gravel profile development [Powell, 1990; Clarke and Damgaard, 2002; Clarke et al., 2004; Pedrozo Acuna et al., 2006; Lee et al., 2007] acknowledge the importance of a rigorous groundwater module to account for infiltrational (percolation) effects over highly porous media. The next stage will be to allow for a range of sediment sizes, and spatial variability in sediment size, as will be needed in gravel beach sediment transport calculations. Derivation of mean boundary shear stress, used to describe the effect of bed roughness on swash flow characteristics, may be obscured by the nonlinear interaction of stress inherited from wave breaking, boundary layer development and micro-topographically induced acceleration and deceleration. Grain mobility, roughness to flow and infiltration may be inherently stochastic, dependent on the statistical distribution of sediment size and shape (facies) through time and space. The bulk (porosity, permeability, hydraulic conductivity) and transport-specific (sediment effective weight, surface tension and fluid cohesion, in/ex-filtration) parameters are potentially a complex function of size, shape, packing, orientation and vertical/horizontal gradation. Assessing the importance of groundwater dynamics in swash zone sediment transport may involve quantification of boundary layer development, the contribution of fluid exchanges to 'friction'; stabilisation/destabilisation [Turner and Masselink, 1998; Butt et al., 2001; Nielsen, 2002]; and measurement of the form of swash lens [Baldock et al., 2001; Horn et al., 2003; Baldock and Hughes, 2006]. It must be noted that 'friction' is a term employed loosely for roughness or 'skin friction', but in reality additionally encapsulates the instantaneous dissipation of potential energy associated with turbulent structures, and the loss of fluid mass, both of which may be more important in gravel

sediment transport and profile dynamics [Masselink and Li, 2001]. Separation of the relative frictional and infiltrational contributions to shear stress for sediment transport formulations will be more difficult for gravel beaches than for sand (and perhaps most difficult for mixed beaches).

On gravel beaches, permeability (which has a sensitive positive nonlinear relationship with sediment size) becomes more important in defining morphodynamic relationships. The best predictor of permeability, which is difficult to measure *in situ* [Horn, 2002], is sediment size and sorting (Figure 2.2).

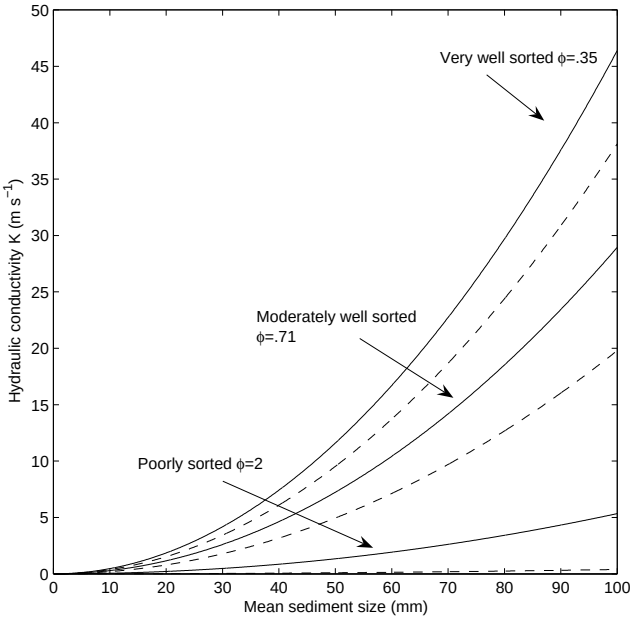

Fig. 2.2 *Nonlinear sensitivity of hydraulic conductivity K (m s^{-1} to size) to mean grain size (in mm) and sorting (in ϕ), derived from linear empirical formulae [Krumbein and Monk, 1943]. Horn [2002], however, notes that coarse and mixed size distributions may not show this dependence because flows may not strictly be Darcian.*

2.3.3 *Transport mode*

Saltation, traction-bedload and sheetflow dominate the nearshore of gravel beaches. Transport mode will be a direct function of swash hydrodynamics and hydraulics, but individual clast motion will be dictated by a number of micro-mechanical factors attributable to size and shape variation over a heterogeneous bed. Transport mode may have direct influence on the gross nature of sediment sorting, sediment transport and morphodynamic feedbacks. Gravel is large, so occupies a greater proportion of the volume of swash flows relative to sand. Sheet flow is therefore likely to be important in

gravel beach dynamics, especially on fluid-thin backwashes. Sheetflow is poorly defined, taken by some authors to mean any collision-dominated sediment slurry where fluid-momentum forces flow but sediment concentration is high [Savage, 1984]. Others define it in terms of the Shields parameter [e.g. Wilson, 1987 defines sheet flow as $\theta \geq 0.8$]; and others in particular reference to dispersive pressures which arise through grain collisions, resulting in inverse gradation or 'shear sorting' [dispersive pressures are greater on larger grains than small in the same horizon of flow, causing larger grains to migrate upwards, e.g. Bagnold, 1954; Inman et al., 1966; Clifton, 1969; Sallenger, 1979]. Finally, it may be defined in specific reference to hindered settling effects. Baldock et al. [2004] demonstrated that particle settling velocity may reduce to 10% of clear water settling velocity within sheet flow. At present the nature of sheet flow in the nearshore (e.g. contact stresses, pressure dispersion, inter-particle collision and hindered settling) is poorly understood [Seminara, 1998; Drake and Calantoni, 2001], especially for coarse sediments.

2.3.4 *Sorting & grading*

Gravel is not only larger, but usually varies over several orders of magnitude greater than that for beach sands. In consequence, gravel beach sediments are spatially differentiated in terms of both size and shape to a greater degree [Bluck, 1967]. Therefore textural zonation is more obvious on gravel beaches than sand beaches [Dobkins and Folk, 1970; Jones, 1971; Orford, 1975], forming mosaics of relatively fine and coarse sediment. The step, cusp horns, strands and berms are composed of larger sediment than foreshores, although a number of levels of textural zonation within this general case may be discernible as sediments are redistributed continually (the level at which sediment zonation becomes important in terms of the morphodynamics of the beach is conceptually interesting, and discussed later in this chapter). Sediments which are selectively entrained congregate as 'sediment structures' or 'assemblages' [Bluck, 1967; Dobkins and Folk, 1970; Jones, 1971; Bluck, 1999] whereby the difference between a sediment structure and a packing framework is the difference between a planimetric and an altimetric pattern (or horizontal and vertical grading) by virtue of their similarity in response to the prevalent hydro-hydraulic regime. In order to understand these processes, we require command over this notion of 'hydraulic equivalence'

[Rittenhouse, 1943]. This condition is manifest through a whole suite of 'emergent' sedimentary properties acquired through the mutual association of individual grains in a mixed population. In other words, individual grains acquire these properties only in context to 'background' populations of collections of grains. These emergent properties include packing arrangements (hence porosity, permeability and hydraulic conductivity); angle of pivot (hence relative flow protrusion, shadowing); shape-controlled imbrications and angular-interlocking; and angles of internal friction. Moss [1962, 1963] invoked the idea of particle rejection/acceptance to explain gradation phenomena through differential response to swash phase. Particles smaller than background size filter into the interstices of the large (a process known as kinetic sieving); and large particles override and outrun the small [called 'overpassing', e.g. Carr, 1969; King, 1972; Bird, 1996; Allan et al., 2006].

That different cross-shore size-shape zonations exist on gravel beaches (Figure 2.3) is verified by numerous authors [Flemming, 1964; Bluck, 1967; Orford, 1975; Williams and Caldwell, 1988; Petrov, 1989; Isla, 1993], although the relative importance of size and shape in sorting is yet to be resolved. Bluck [1967, 1999] postulated on the tendency of disc and blade-shaped particles to be preferentially transported upslope, acting like a hydrodynamic 'wing', and for spherical and roller shapes to be transported downslope [echoed by Wright et al., 1979; Williams and Caldwell, 1988; Petrov, 1989, but not supported by the findings of Carr, 1971; Jackson and Nordstrom, 1993; Allan et al., 2006]. It is not clear whether sorting by size, and sorting by shape, are achieved by two fundamentally different mechanisms; or what aspect of anisotropy is important ('shape' is, hydro-hydraulically, multi-faceted, [Winkelmolen, 1982; Illenberger, 1991; Le Roux, 2002], so varying measures of two-dimensional sphericity, aspect ratio and elongation, and the axially less dominant third dimension, or c-axis, may produce different responses to flow, individually, and as part of mixed beds).

A multi-size-fraction approach is required to model spatial sorting on coarse clastic beaches, such as taken by the sediment transport module of the numerical model developed by Lawrence et al. [2002] which includes a multiple size fraction sorting algorithm. The mean diameter of a sediment sample is more than a record of fluid power expenditure: it is a cumulative record of grain size filtering at successive positions along the sediment transport pathway. This is true both of sand and gravel beach sediments, but perhaps only on beaches composed of the larger clastic fractions does the material

being transported exert positive feedback control over subsequent transport events, and hence morphological change. If so, even multiple size fraction sediment transport and sorting formulae will not be enough to describe and account for observed changes in morphologies. This notion is developed further later in this chapter.

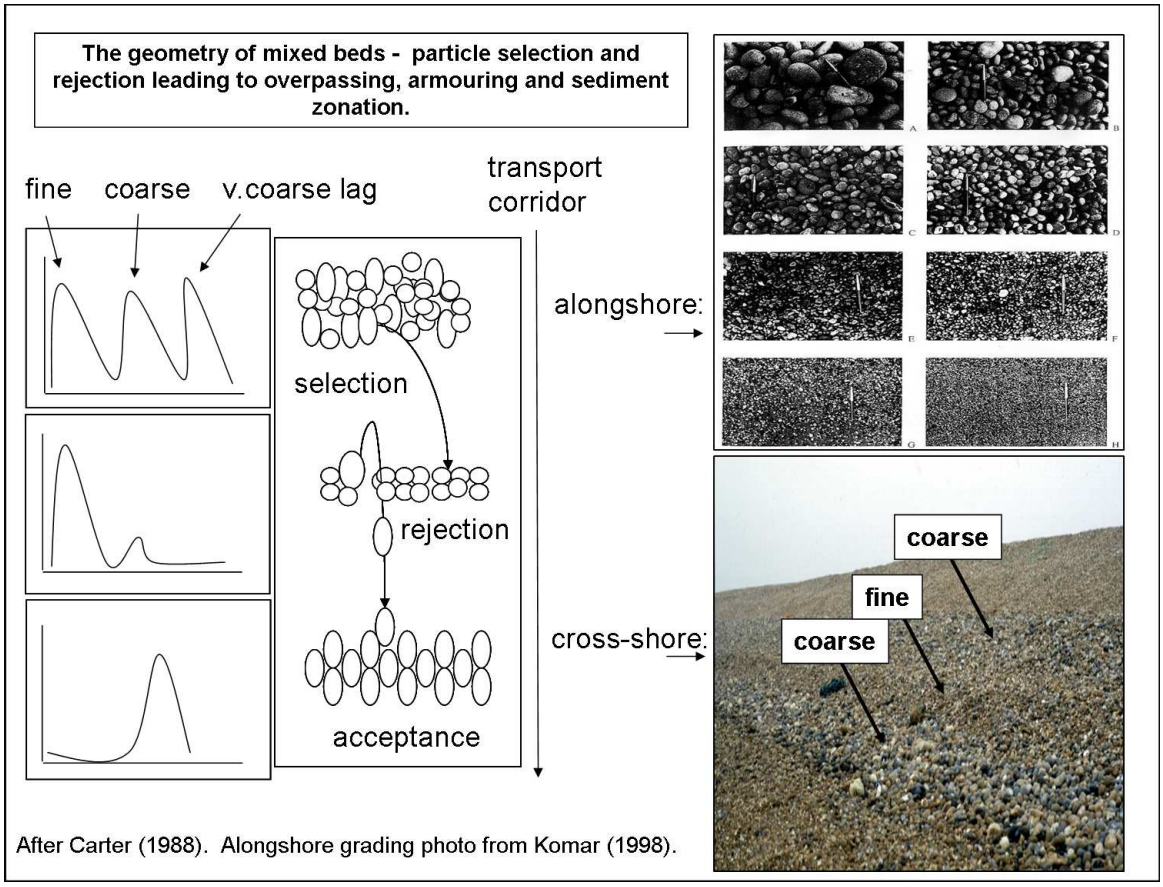

Fig. 2.3 *Diagrammatic portrayal of selective overpassing and armouring phenomena, expressed in terms of transport stresses on individual grains in mixed-size beds [after Carter, 1998], where overpassing occurs in the longshore [e.g. Bird, 1996] and armouring occurs in both long-and cross-shore directions [e.g. Isla, 1993].*

2.3.5 *Longshore sediment transport*

The principle of 'overpassing' (Figure 2.3) has been used to explain the existence of both cross shore and alongshore grading, the latter perfectly illustrated by gravel barriers such as Chesil Beach in the UK, and Hawke Bay Beach, New Zealand [Carr, 1969; King, 1972; Bird, 1996]. Overpassing is the process by which the large scale alongshore segregation of smaller and larger sediment occurs as a corollary of differential transport rates through acceptance or rejection into background material. A greater ratio between individual large grains and mixed beds increases the propensity for mobility since greater boundary layer flow projection is thought to concentrate fluid drag about the angle of pivot,

causing the preferential selection and transport of larger grains and proximal-distal coarsening. In contrast, a diminished ratio between individual and background sediment would perhaps impede transportation through hiding effects [and inverse-grading, see Isla, 1993]. Net or time-averaged grading may be viewed as a 'null point' argument [Cornaglia, 1877; Bowen, 1980], as reviewed by Miller and Ziegler [1958], and Horn [1992]: for every grain size there exists a unique alongshore position where the coarse/fine ratio grades perfectly alongshore.

Field measurements of longshore sediment transport on gravel beaches are difficult and often give statistically unreliable results [Lee and others., 2007]. Alongshore grading occurs within the swash, not as the result of longshore currents *sensu stricto*. The longshore movement of material in the swash of gravel beaches, aptly termed swash 'grazing' [Sherman and Nordstrom, 1985] is the subject of a comprehensive review by Van Wellen et al. [2000], who imply that 50–70% of longshore sediment transport of material occurs in the swash [also Allan et al., 2006]. This has importance not only in terms of overpassing and grading, but in the long term health of beach systems, sediment leakage, and planforms. Masselink and Puleo [2006] have recently suggested that the longshore component of cross-shore dominated swash flows may be more important than previously realised, although there are few published measurements of longshore sediment flux and hydrodynamics in the swash [Elfrink and Baldock, 2002]. Van Wellen et al. [2000] note the particular shortage of high quality field data on longshore sediment transport/volumetric changes on gravel beaches and spits, especially during storms [Chadwick et al., 2005], which has severely hampered progress in this area. According to Masselink and Puleo [2006], the same is also true of sand beaches.

2.4 *Morphological features*

2.4.1 *Berm*

The sediment volume contained under a particular beach surface is a function of present processes, as well as past surfaces which are a function of past processes [Sonu and Vanbeek, 1971; Caldwell and Williams, 1985]. Reflective beaches are typically two-dimensional, which should make it relatively straightforward to classify and characterise gravel beach profile shapes, however the morphodynamics of secondary

morphological features may prove to be more problematic. One reason for this is that it appears that absolute morphological changes appear larger on coarse grained beaches than on sand beaches over comparable timescales, even under low energy conditions [Van Wellen et al., 2000; Kulkarni et al., 2004; Austin and Masselink, 2006*a*; Horn and Li, 2006]. Another is that it appears grain size exerts some control over the development and morphometrics of these forms.

Austin and Masselink [2006*b*] show that watertable outcropping is highly dynamic on natural gravel foreshores, suggesting that infiltration at the swash limit contributes swash asymmetry, onshore sediment transport and berm formation. Berm building and onshore migration provides an additional mechanism for maintenance of beachface reflectivity. Grant [1948] and Duncan [1964] observed that larger foreshore sediments tend to move onshore, forming strand lines and berms, whilst fine material congregated further downslope. This seemed counter-intuitive since the velocity magnitude (and therefore flow competency) decreases landwards. Duncan [1964] explained it thus: toward the limit of each uprush, velocity is insufficient to retain sediment in transport because water volumes undergo increasing diminution through infiltration. Larger material stranded at the landwards extent of run-up lacks a mechanism for its removal since infiltrational losses have weakened backwash with respect to uprush, although some fine material is downcombed by backwash. In this way, a lens of sediment is pushed onshore over tidal cycles through cut-and-fill and berm building [Eriksen, 1970; Waddell, 1976; Horn et al., 2003; Austin and Masselink, 2006*b*; Weir et al., 2006]. Masselink and Li [2001] modelled the dependence of foreshore slope on swash infiltration, finding a critical sediment size of 1.5 mm beyond which infiltration-enhanced onshore flow asymmetry caused significant profile steepening.

2.4.2 *Step & foreshore*

The step is a relatively small and steep feature at the base of the foreshore, a submerged break of slope at the base of the swash zone which appears to adjust to nearshore hydrodynamic regime [Hughes and Cowell, 1987], characteristic of reflective sand and gravel beaches, and composed of sediment which is coarser than the sediment immediately landwards or seawards. Beach steps, which are relatively under-studied, have been reviewed by Bauer and Allen [1995]. The step is distinct from the scarp

[Sherman and Nordstrom, 1985] which is a subaerial (upper swash or tidally-stranded) feature. The steep seawards facing slope is of the order of 20° and 32° [Short, 1984; Larson and Sunamura, 1993]. Wave-breaking is thought to be forced and modulated by the step, a morphodynamic relationship possibly related to wave height [Sunamura, 1984], or surf similarity parameter. Bores develop, shoal, and collapse immediately following breaking over the relatively shallow (slip-)face of the step at the base of the foreshore [Austin and Masselink, 2006*b*]. Being permanently submerged, the step is technically not a feature of the swash zone, but initiation and maintenance is thought to have as much to do with swash processes as wave breaking, undergoing dimensional alteration in response to increases in wave height at breaking [therefore wave breaker type, Sunamura, 1984; Hughes and Cowell, 1987, and changes in swash regime; Larson and Sunamura, 1993]. As such, steps serve to highlight the importance of the interdependence of the pre-and post-breakpoint fluid motions on steep beach dynamics. Matsunaga and Honji [1980, 1983] demonstrated that supercritical flow conditions arrived at by strong backwashes curtailing strongly asymmetrical incident bores can create a hydraulic jump and associated backwash vortex, under various wave breaker types, that could be responsible for the formation of the step. Takeda and Sunamara [1983] and Larson and Sunamura [1993] developed these ideas into a dynamical model for step hydro-and sediment dynamics, postulating on the importance of the step in swash zone flows, slope development, sediment transport and sorting mechanisms. According to this interpretation, the step gradient is maintained by the upward stroke of a backwash vortex which impedes avalanching and allows for deposition on the crest. The coincidence of an unstable turbulent bore with an immediate antecedence of sediment entrained by a backwash vortex may cause advection of material onshore. This process may provide a mechanism for preferential slope building and supply the liberated coarse material for berms and cusp horns.

Step dynamics are likely to have consequence for swash zone sedimentation through convective-advective entrainment and transport on the uprush (see also the section on hydrodynamics and sediment transport) and foreshore adjustments. For example, a recent laboratory study [Lara et al., 2002] found that turbulence associated with breaking had a sensitive sediment-size dependency, where larger gravels induced an increase in the vertical velocity gradient and hence larger instantaneous shear stresses.

This finding would suggest that sediment would be convected at the step [where very coarse grains tend to concentrate, e.g. Short, 1984], to be advected by onshore-asymmetrical bores shoaling over the relatively flat step crest. Austin and Masselink [2006*a*] present a time-series of step dimensional adjustments on a gravel beach, showing the step to respond to wave height. The step may [Ivamy and Kench, 2006] or may not [Austin and Masselink, 2006*a*] migrate with the tide. Backwash vortices should be most energetic when resonance occurs between wave period and swash duration [Kemp, 1975]. Less clear is the requirement for backwash uprush interaction at the base of the foreshore to force supercriticality. Beach steps may thereby be central to our understanding of the modulation of foreshore adjustments in response to swash-swash interaction and frequency- downshifting [Kemp, 1975; Mase, 1988, 1995; Baldock et al., 1997; Holland and Puleo, 2001; Erikson et al., 2005]. Indeed, the role of the step appears crucial in gravel beach morphodynamics, being a dissipative feature perhaps analogous to a sand beach bar, and is discussed in detail later in this chapter.

Gravel beaches commonly support slopes in excess of 10 degrees [Longuet Higgins and Parkin, 1962; Williams and Caldwell, 1988; Austin and Masselink, 2006*a*]. The relative importance of nearshore hydrodynamics, sediment characteristics and beachface hydraulics, in the maintenance of reflectivity is unresolved. Hughes and Cowell [1987] emphasised the importance of the step in maintaining steep slopes, hypothesising that the morphodynamic adjustment of step dimensions to wave height acts in the same way, or has an analogous morphodynamic role as a dissipative surf zone. Step maintenance allows waves continue to shoal in deep water close to the shoreline; the energy of wave breaking forced by the step face is spatially concentrated, providing the conditions for step maintenance and for reflective conditions to persist. As stated previously, step height tends to increase with wave height, so surging breakers would flatten the step, and plunging breakers steepen the step face. As wave heights increase, the dominance of uncurtailed backwashes would provide the backwash strength required for interaction further downslope (i.e. at the base of the foreshore), vorticity generation and step building. Swash zone asymmetries therefore appear to satisfactorily resolve both the Matsunaga and Honji [1980] hypothesis for step formation and the Hughes and Cowell [1987] hypothesis for beach face reflectivity.

Bagnold [1940] famously stated that beach face angle depends only on the size of

grains, and was independent of wave height. Kemp [1975] also thought that there was no relationship between wave energy and beach face grading. Under the Hughes and Cowell [1987] hypothesis, foreshore slopes become less sensitive to incident wave energy since the step forces energetic breaking and bore collapse (as stated previously, the step is therefore the morphodynamic equivalent to a sand bar). The wave energy independence stated by Kemp [1975], therefore, is a direct result of dimensional alteration in response to an increase in wave energy, up to a certain threshold. It is unknown the extent to which beachface sediments interact with flows of the two swash phases, how this affects swash interaction modes, and therefore beachface morphodynamics.

2.4.3 *Cusps & Rhythmic Bedforms*

Cusps are small quasi-rhythmic crenulations formed at the shoreline by swash flows, composed of coarse horns and fine bays. They are a common ephemeral feature of steep beaches, signatory of a reflective morphodynamic state (Figure 2.4). Accordingly, cusps are a common occurrence on gravel beaches [Kuenen, 1948; Longuet Higgins and Parkin, 1962; Bluck, 1967; Williams, 1973; Bluck, 1999; Nolan et al., 1999; Sunamura and Aoki, 2000], but gravel cusps differ from sand cusps in that they are less of a coherent morphological form, and more of a collection of loose sediment structures, more obviously sorted by size, and often forming 'bands' of material down the foreshore (Figure 2.4).

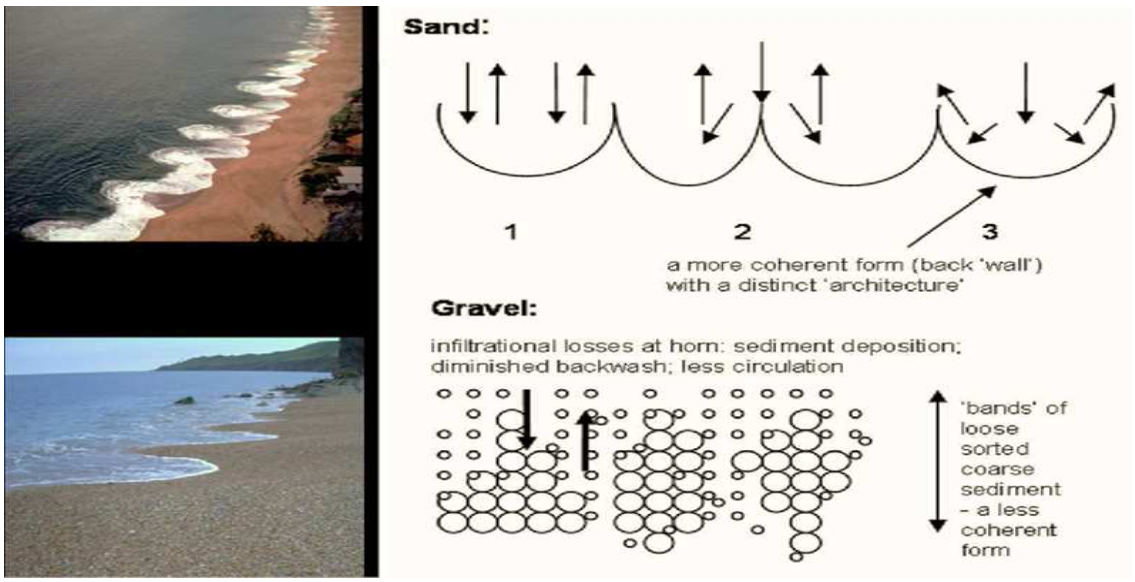

Fig. 2.4 *The processes of cusp formation on gravel beaches illustrate the role sediment may have in the morphodynamics of those beaches, building and maintaining morphology through feedback mechanisms to an extent never matched by sediments comprising sand beaches. Sand cusp photo courtesy of Dr. Peter Cowell.*

Bluck [1967, 1999] and Sherman et al. [1993] detail a wide range of potential couplings (facies) between shape and size and associated hydraulically equivalent sediment structures which may exist in relation to gravel cusps. Since the size variation of beach gravels is in general greater, the differentiation of coarse horns and fine bays is even more noticeable. Beach cusp formation hypotheses have been reviewed extensively elsewhere [Guza and Inman, 1975; Inman and Guza, 1982; Komar, 1998; Coco et al., 1999]. The developments and discussion of the two dominant models, namely the edge wave [hydrodynamic template, Huntley and Bowen, 1975a; Komar, 1998] and the swash-circulation/self-organisation [Werner and Fink, 1993; Masselink et al., 1997; Masselink and Pattiaratchi, 1998*a*, *b*; Coco et al., 1999, 2001; Masselink et al., 2004; Coco et al., 2004] hypotheses, have proceeded almost without reference to gravel cusps. Huntley and Bowen [1975a] attribute the formation of cusps on a gravel beach to zero-mode edge waves; however, the importance of wave reflection and associated standing wave forms on gravel beaches requires much greater scrutiny. Masselink et al. [2004] has shown that the assumption of edge waves during (or at least to initiate) cusp formation may not be convincing: energy within the edge wave band for a particular wave frequency may be the product of a whole suite of nearshore processes [Baldock et al., 1997], and the only satisfactory method of edge wave detection involves an array of sensors measuring both the cross-shore and long shore vertical structures of the water column. Masselink et al. [1997] state that cusp re-formation may be as much the product of antecedent morphology as hydrodynamics. One potentially interesting topic may be the formation and maintenance of cusps in the light of various swash-interaction modes and associated spectral [Mase, 1995] or frequency-distribution signature. It is clear that gravel cusps pose numerous interesting and unstudied avenues of enquiry, which may shed light on the nature of selective sorting at the shoreline.

2.4.4 *Storm Beach*

Swash-aligned gravel barrier beaches are thought to migrate onshore over time through a mechanism known as 'rollover' [Carter and Orford, 1993], whereby onshore sediment transport during storms throws material landwards to form a coarse storm-stranded lag, or storm beach. The relative altitude of this storm beach to spring high water level is remarkable, and can only be explained by storm-induced set-up superimposed upon a

high spring or high astronomical tide. The material is effectively lost from the active beach system, since it lacks a mechanism for removal (offshore transport) during calmer conditions. Elevated groundwater levels and bed fluidisation coincident with high energy plunging breakers is thought to cause seawards-directed transport, but the seemingly paradoxical nature of onshore storm sedimentation is far from resolved. Indeed, the mechanism for landwards sedimentation proposed by [Orford, 1977], invoking the formation of a breaker-bar to force wave-spilling at tidal extremities, remains the only interpretation forwarded thus far. Since analysis of high-magnitude storm events on gravel beaches is exceedingly rare [Sanders, 2000; Orford et al., 2003; Cooper et al., 2004], explanations are necessarily heuristic. The Orford [1977] hypothesis remains to be verified: indeed, the formation of a 'bar' (step) would require substantial resistance to planation [Orford et al., 2003]. The periodicity and nature of storm sedimentation may be studied using the internal structure of storm beach sedimentation/spill-over features [Orford et al., 1988; Bluck, 1999], which have good preservation potential, although the magnitude of associated beach sediment removal offshore, and the effect of this on the long-term health of the beach, is much more difficult to determine.

2.5 *Relationship between Morphology and Sediments*

2.5.1 *Morphodynamics in Heterogeneous Sedimentary Environments*

This chapter has reviewed gravel beach morphodynamics and it seems that in these environments sediment characteristics are, as least conceptually or based on qualitative observation, central to virtually all tenets of morphodynamics. Morphology [Longuet Higgins and Parkin, 1962; Austin and Masselink, 2006*a*], sediment transport [Kidson et al., 1958; Carr, 1971; Voulgaris et al., 1999; Lee and others., 2007], hydrodynamics and hydraulics [Huntley and Bowen, 1975a; Austin and Masselink, 2006*b*; Horn and Li, 2006] have either been shown or are considered conceptually to be grain size/sorting dependent. It therefore seems more than surprising that, to the authors' knowledge, the concurrent and co-located measurement of sedimentology and one or more of the above attributes, over short term and small (process) scales, in a process-based study with similar sample resolution, has never been attempted on pure gravel beaches. One reason for this may be that measurements of grain size distributions

are slow and laborious. It is currently not possible to quantify accurately grain attributes on a time scale even close to morphological and hydrodynamic measurements.

A handful of previous studies have alluded to the fact that sediment size and morphological change have a co-variability which may reinforce individual distinct morphological features, and sediment transport characteristics through those features, through feedback processes [Sherman et al., 1993; Tolman, 1994; Rubin and Topping, 2001; Gallagher and McMahan, 2006]. In other words, if grain size and morphological change have a correlated domain of joint variation (i.e. temporal structure) this would support the suggestion that sediment characteristics may reinforce the evolution of morphological features. Sensitivity to spatial variations in sediment size is another dominant theme, with respect to, for example, vertical velocity profiles, morphological (step, cusp, berm) and textural mosaic dimensions, kinetic sieving (acceptance), overpassing (rejection), and emergent sediment properties such as hydraulic conductivity and pivot angle. Larger sediment helps to dissipate and spatially concentrate energy at the step, forming a lag where infiltrational fluid losses are greatest.

The rest of this chapter develops the potential role of sediments in gravel beach morphodynamics into a conceptual framework. Carter and Orford [1993] state that the emergence of sorting patterns through selection, rejection and acceptance tend to create patterns which resist further movement. In other words, the formation of textural mosaics and morphologies would progressively have fewer configurational possibilities, which would limit further re-organisation. Therefore, gravel foreshores tend to become more organised, creating mosaics of sediment which have a distinct form [the sediment structures of Bluck, 1967, 1999], which are able to withstand and control transport [or limit work done –this notion is discussed in terms of 'entropy' by Carter and Orford, 1993 and briefly by Cowell et al., 1999], where sediments diffuse to eliminate work gradients. The wide range of size-shape structures reported in the literature [Bluck, 1967, 1999; Orford, 1975; Sherman et al., 1993] are interpreted as the product of this process, although it is far from clear which sediment assemblages represent periods of stability or order, and which assemblages are the cumulative product of periods of relative disorder, and indeed to what resolution one must measure. These claims are based almost wholly on qualitative observation, but require emplacement within a morphodynamic framework. Only an extensive data set of concurrent morpho-sedimentary measurements

will support, or otherwise, the veracity of these claims.

Gravel morphological features would perhaps appear to control the flux of energy and matter through themselves. In other words, gravel beach architectures may act as mechanisms themselves which recycle sediment selectively [Evans, 1939; Longuet Higgins and Parkin, 1962; Sherman et al., 1993; Bluck, 1999], so, effectively sorting may beget sorting. Sherman et al. [1993] cogently argues that sediment-structures, heterospatially but not stochastically arranged, have a distinctive form which 'survives' or 'consistently appears' as distinct, irrespective of location, due to their propensity to either migrate in response to changing conditions (through hydraulic equivalence) or withstand or indeed even control local process variations and dynamics either through flow diversion or constraint, or spatially differentiated hydro-hydraulic properties.

The perfect example of such a relationship is a gravel cusp (Figure 2.4). This potentially self-organised system is likely to be governed by internal (intrinsic) dynamics, and not exclusively by external hydrodynamic forcing: it remains dissipative (i.e. it requires continual energy transfer), but as it grows and becomes a more ordered, stable form. The formation of sediment structures may provide system memory, or templates for morphological change, as initial unpatterned (unordered) sediments form patterned (disordered) states. Time-lags between morphological adjustment (relatively long-term responses) and hydrodynamics (relatively short-term responses) in beach dynamics are common since sediment must be transported to invoke morphological change [Werner, 1999]. Energetics-type models [Bailard, 1981] treat sediment transport as 'work done' by a hydrodynamic machine: these sediment transport models may have to be adapted in light of the previous discussion, since sorting implies the storage of energy which cannot be used to do work. Sediment sorting may either be progressive (i.e. occurs upon deposition) or instantaneous (i.e. occurs on entrainment and transport). The former may be related to mixed bed sediment geometry and the processes of selection and rejection, and the latter may be more related to flow competence and power. The challenge will be in the separation of the signals from the two components which are acting in concert to sort sediment.

2.5.2 *Bedform Surrogacy*

On gravel beaches, why are coherent nearshore bedforms such as crescentic, longitudinal and transverse bars, and swash bars, absent? There may be several contributing factors. The hydrodynamic boundary conditions inhibit flow field instabilities [Dodd et al., 2003] associated with nearshore circulation, rips, shears and infra-gravity motions. Incident obliquity and longshore sediment flux, or bedload and sheetflow load dominance, obscures developing bedforms. Bedform initiation or maintenance requires low angles of internal friction. One might speculate that perhaps sorting forms graded sediment-structures, morphologies and mosaics of texture instead of bedforms. In other words, they draw physical resemblance to bedforms, or are bedform 'surrogates'. The explication of scale hierarchies between barely-perceptible and easily-perceptible sediment structures and packing frameworks, textural mosaics, and morphological features, could be named 'bedform surrogacy'.

Beaches must absorb enormous quantities of energy to maintain their structure and characteristics. Sedimentary and morphological reconfigurations and continual adjustments, through sediment transport, facilitate this energy dissipation. The features created are specific to available sediment size, and sediment size variation. For example, as reported earlier, as a dissipative feature forcing wave attenuation, the step may be analogous to a bar; and sand and gravel cusps may be morphodynamically equi-final. Size-sorting in discrete mixed beds is a function of relative transportability, whereas sediment sorting on bedforms is controlled by the passage and recycling of sediment through the bedforms. Both coherent bedforms and gravel mosaics and sediment structures share in common a certain rhythmicity. Considering gravel features as surrogates for quasi-regular and coherent nearshore bedforms may uncover analogies for bedform spatial dimensions and wavelengths; migration rates and propensity; alignment; local flow and transport mode modification; and stability fields. Potentially, this idea has implications for the relative contribution of form drag to total shear stress (usually produced by the pressure field associated with flow over bedforms, but which may equally have a gravel analogue in the form of coarse sediment patches), and skin friction, produced by individual grains. Accordingly, textural mosaics may yield information on vectorial dispersal and spatial energy gradients over larger areas [the use of grain size

characteristics is an approach common in coastal sedimentology, e.g. McLaren and Bowles, 1985; Gao and Collins, 1992 - see chapter 8]. Equally, sediment structures may be non-repeating in time or space. The ephemeral nature and migration rates of bedform surrogates may aid the quantification of sedimento-morphological relaxation and inertia. Sediments must be transported to invoke morphological change, so sediment transport leading to the spatial distribution of sedimentary variables may provide the system memory at the heart of many geophysical time lags. Textural mosaics, morphologies and hydro-hydraulics may be developing over discordant time-scales. Werner [1999] describes this phenomenon as 'slaving', where fast variables are 'slaved' to slow variables, for example in the long-term motion of grains slaved to the migration of bedforms.

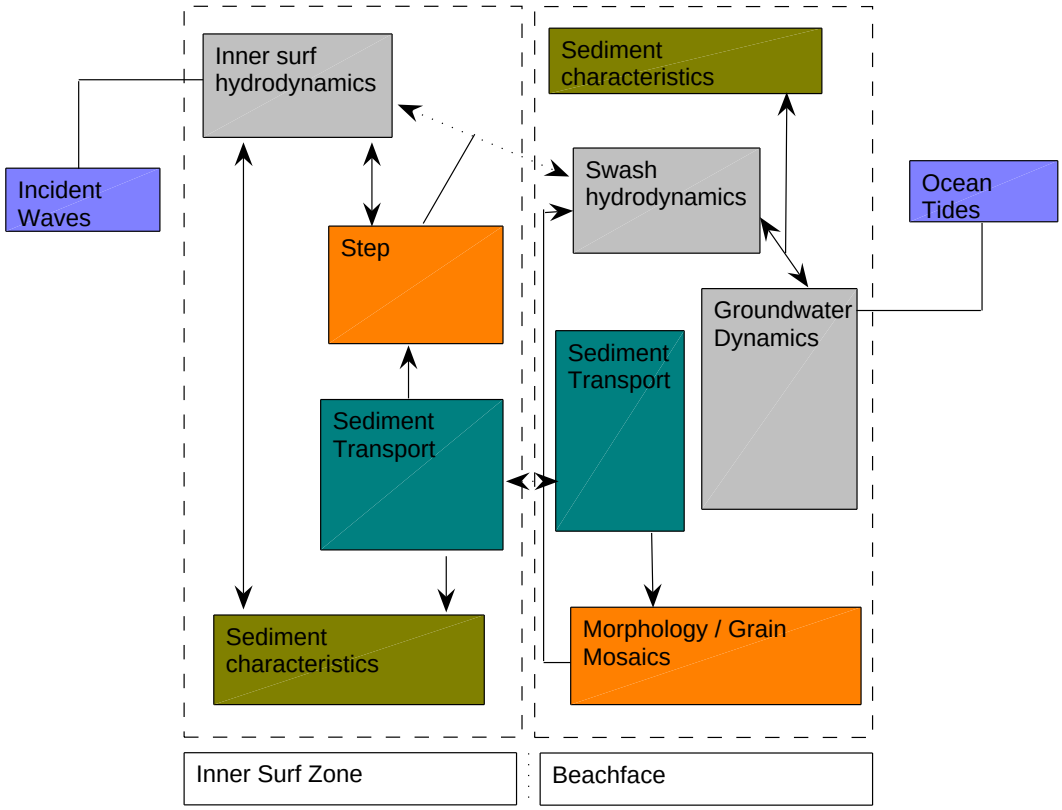

Fig. 2.5 *Conceptual morpho-sedimentary-dynamics diagram for the gravel beach face (modified from Masselink and Puleo (2006, their Fig. 1), which should be used as a guide to illustrate the conceptual differences between the two morpho-types).*

2.6 *Morpho-Sedimentary-Dynamics*

Gravel beaches have distinct dynamics, which may be explained not only through the mutual association between fluid flows and morphological change mediated through sediment transport, but extraneously on the particular controls sediment variations may exert on nearshore processes. It has become increasingly clear that the morphodynamic model first proposed by Wright and Thom [1977] can only partially explain gravel beach dynamics. Morphodynamics is a type of dyadic interaction, where a cluster of behaviours dominates the meaning of each member's behaviour. Morphodynamics is strongly non-linear, whereby synergistic qualities may appear which cannot be predicted from a knowledge of the properties of the individual components of a system. No single behaviour can be separated from the cluster for analysis without losing its meaning in the sequence. 'Morpho-sedimentary dynamics' (MSD) is defined as the mutual association and feedbacks in operation between flows (hydrodynamics and hydraulics), and forms (morphological architectures and textural mosaics), mediated through selective sediment transport mechanisms acting upon the mechanical, hydrodynamic and hydraulic properties of sediments. It represents a modification of the morphodynamic domain, applicable where textural differences are so great that traditional morphodynamics are incapable of accounting for the apparently complex time series of beach geometries and morphological behaviours. An MSD approach treats sediments, and the spatial heterogeneity of sediment characteristics, not as a boundary condition (along with, for example, tidal range, offshore wave height and physical obstructions) but as a fundamental and integral aspect which permeates through morphodynamics, which may act as both an expression and control on gravel beach behaviour (Figure 2.5). There are a number of extraneous interactions and feedbacks between system components, and more degrees of freedom (the number of parameters which may be independently varied). MSD therefore is about complexity, i.e. collective and emergent behaviour through nonlinear interactions, although at this stage we may only postulate upon how MSD may be implemented within approaches specifically adapted to account for these interactions, especially over larger temporal and spatial scales.

The dominant processes in gravel beach dynamics have been reviewed, highlighting some common themes which unify the various components of the gravel beach system,

the repercussions of which impart on how gravel beach dynamics might be understood conceptually. In particular, gravel beach dynamics are thought to be highly dependent on the temporal and spatial variation in grain size, and the continual adjustments made by an active beach step, both of which act not only as the expression of changing morphodynamic conditions, but also as a controlling influence. Morphodynamics, the notion that the exchanges on beaches between the hydrodynamics, sediment transport, and morphological change takes the form of reciprocal relationships which are mediated through feedback mechanisms (in such a way that they cannot be thought of or studied independently) is not a new one. Yet it appears that for the gravel beach, morphodynamics must be re-defined to describe conditions where variations in sediment size are thought to deserve parity, rather than as merely a sequent entity or boundary condition. 'Morpho-sedimentary-dynamics' is a phrase coined to intuit such cause and effect, detailing the co-evolution of morphology, hydro-hydraulics and sediment properties whilst acknowledging causative pluralism, feedbacks and multiplier effects. This is the recommended conceptual framework within which to crystallise thought and organise further research for the gravel beach. Essentially, it increases the minimum number of parameters needed to describe the state of the gravel beach as a physical system. Therefore, it is advised that simplicity will be most expedient in our future modelling efforts, if complexity is to be adequately encapsulated.

2.7 *Summary*

(i) Studies into the fundamentals of coarse grained beach behaviour may be best carried out on pure gravel beaches, an 'end-member' in the coastal sedimentological continuum, isolating the behaviour composed of one sedimentological class without the complicating influence of varying concentrations of sand.

(ii) On gravel beaches, permeability has an important role in defining morphodynamic relationships. The best proxy for permeability, which is difficult to measure *in situ*, is sediment size/sorting.

(iii) The mean diameter of a sediment sample on a gravel beach is more than a record of fluid power expenditure: it is a cumulative record of grain size filtering at successive positions along a sediment transport pathway.

(iv) Absolute morphological changes appear larger on coarse grained beaches than on sand beaches, even under low wave energy conditions.

(v) The dynamics of secondary morphological features may be controlled by fundamentally different morphodynamic relationships compared with sand beaches. The presence and dynamics of these features on a graded gravel beach may be as much a function of the variable sediment characteristics as forcing hydrodynamics.

(vi) It is currently not possible to accurately quantify granular attributes on a time-scale even close to morphological and hydrodynamic measurements, but this is required for the study of gravel beach morphodynamics to advance.

(vii) Various authors have suggested that sediment properties exert some control over subsequent beach evolution. These claims have been almost wholly subjective and require not only detailed and diligent verification by field measurements, but also emplacement within the morphodynamic conceptual framework.

(viii) The spatial segregation of sediments on gravel foreshores may draw more than physical resemblance to bedforms found on sandy beaches. Sorting patterns may be surrogates for bedforms, and further studies may uncover analogies for bedform attributes and the processes responsible. Sediments must be transported to invoke morphological change, so the development of spatial distribution of sedimentary

variables as bedform surrogates may be phase-lagged to instantaneous sedimentation gradients.

(ix) Spatial heterogeneity of sediment properties can be thought of conceptually as both an expression and a control on gravel beach morphodynamics, however, it has not thus far been convincingly demonstrated that morphological change leaves a parameterisable sedimentological trace on beaches of any composition.

3 FIELD SITE: SLAPTON SANDS

The Walrus and the Carpenter were walking close at hand:
They wept like anything to see such quantities of sand:
"If this were only cleared away", they said,"It would be grand!"
"If seven maids with seven mops swept it for half a year,
Do you suppose," the Walrus said, "That they could get it clear?"
"I doubt it," said the Carpenter, and shed a bitter tear.

Lewis Carroll (1832-1898). British poet. Through the Looking Glass.

3.1 *Geographic Setting & Geomorphological History*

Slapton Sands (Figures 3.1, 3.2 and 3.3, SX 826 441; [50° 16' 0 N, 3° 38' 60 W]) is an eastwards facing gravel barrier beach in Start Bay, Devon, UK. Curvilinear in plan, it extends continuously for c. 4.5km between headlands at Torcross to the south and Strete to the north. The central section of Slapton Sands fronts a freshwater lagoon, Slapton Ley, which is the largest freshwater lake in south-west England, and of considerable ecological importance [Barne et al., 1996]. The barrier beach is between 50 and 100m wide at high tide, widening northwards, and the barrier crest increases from 5.5m ODN (Ordnance Datum Newlyn, approximately 0.2m above mean sea level) at Torcross to 8m ODN at Pilchard Cove. Slapton Sands itself is a section of a much larger barrier system which occupies almost the entire coastal fringe of Start Bay, which in its contemporary form has segmented around rocky drainage interfluves or headlands [Hails, 1975]. Exposed on most low tides, there appears to be some exchange of material around these headlands between adjacent barrier beaches.

Start Bay is some 9km long, and 60km^2 in area [Hails, 1975b]. It is delimited in the

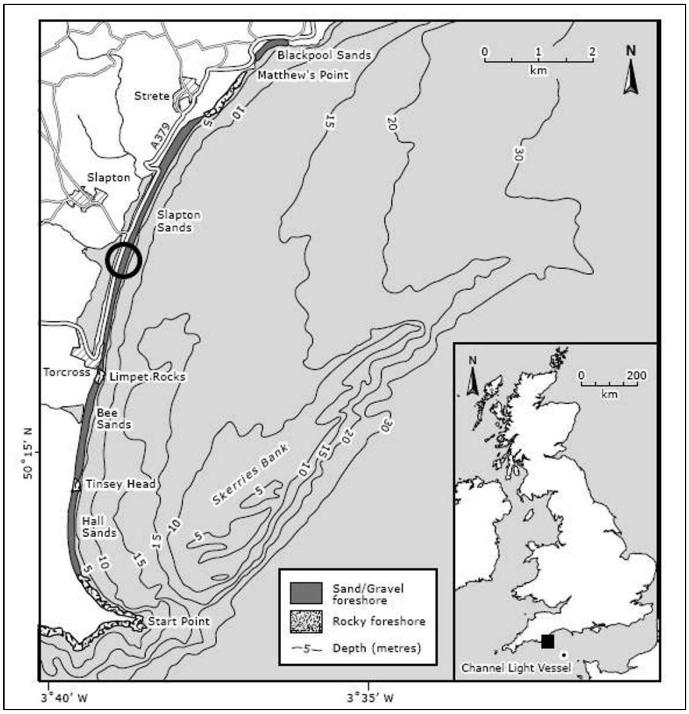

Fig. 3.1 *Location map of Slapton Sands within Start Bay (from Austin and Masselink [2006b]). Inset, position relative to the rest of the UK, and Channel Lightship wave buoy.*

Fig. 3.2 *Slapton Sands in the early spring of 2007, looking south from Strete.*

south by Start Point (SX 819 381; [50° 13' 0 N, 3° 43' 0 W]) and in the north by Berry Head (SX 941 562; [50° 23' 20 N, 3° 30' 44 W]) near the mouth of the river Dart. It is considered a closed sedimentary system [Hails, 1975; Halcrow Group, 2002], and present sea level has dictated a re-occupation of the ancestral Pleistocene cliffline, which has differed little in planform for 100,000 years [Hails, 1975; Morey, 1976, 1983]. This planform has been described as 'zeta-shaped' [Hails, 1975]: bays of a similar shape are common elsewhere, for example east Australia, and are thought to have adjusted to predominant refracted swell direction [Arber, 1940]. The geology of Start Bay is the Meadfoot series of the lower Devonian (400 Ma): to the south exposed outcrops are composed primarily of resistant schists (highly deformed and metamorphosed oceanic basalts); and towards the north the cliffs are composed of less resistant grits and slates.

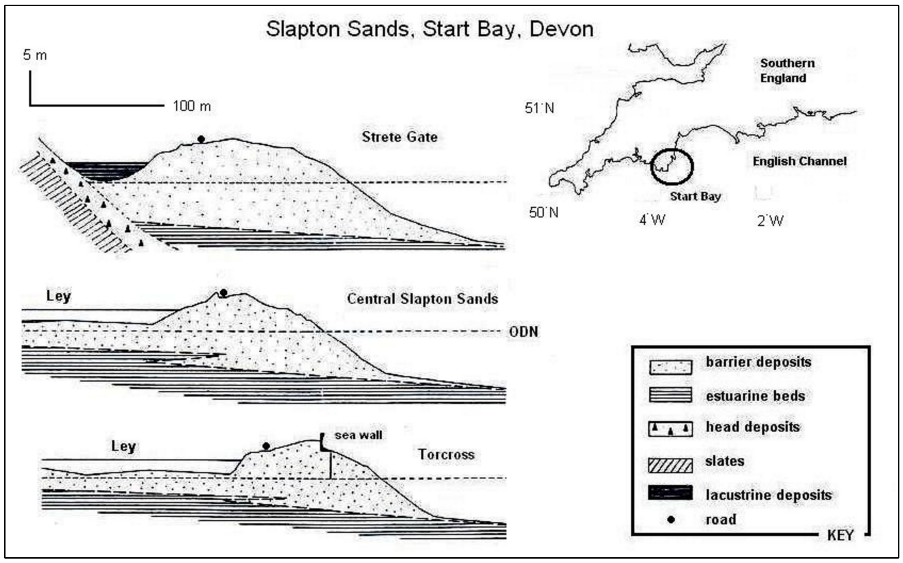

Fig. 3.3 *The stratigraphy in three cross sections through Slapton Sands, in the north (Strete Gate), central and southern (Torcross) sections (figure modified from Job, 1993).*

The beaches of Start Bay are nationally important and protected geomorphological features [Barne et al., 1996]. They are thought to have been formed by landward trangression of a gravel barrier during mid-late Holocene sea level rise, acquiring sediment from the floor of the English channel and Start Bay, eventually segmenting

around headlands, pushing landwards into previously shallow bays and river courses, which were locked and converted into freshwater lagoons. A detailed chronology and evolutionary history of the barrier-lagoonal systems in Start Bay may be found in Hails [1975] and Morey [1976, 1983]. This mechanism, termed 'barrier rollover', meant that the barrier deposits were able to keep up with the unprecedented rates in sea level rise between 8000 and 5000 BP. The most convincing evidence of the series of events just briefly summarised is that the barrier deposits of Start Bay (mostly chert flints and quartz, with minor proportions of slates, schists, grits and granites) have no local source: the most likely source is the floor of the English channel, from cretaceous (130 Ma) deposits 40km to the east [Gleason et al., 1975; Burt, 1993]. Some relict gravels on the floor of the Bay are angular and weathered little compared to contemporary barrier deposits, which provides further evidence of a landwards push [Burt, 1993]. Slapton Sands, it is believed, has occupied approximately the same position since 2–3000 BP [Morey, 1983].

In the south of subtidal Start Bay lies a banner bank called the 'Skerries', which is believed to be maintained in a closed sedimentary system by rectilinear tidal currents [Acton and Dyer, 1975], and which does not exchange sediment with the nearshore [Robinson, 1961; Hails, 1975], nor undergo appreciable dimensional alteration over the long term. It is thought that Skerries Bank is maintained by an anticlockwise tidal gyre, which forms because of a durational asymmetry between flood and ebb tides [Ferentinos and Collins, 1980]. Residual tidal currents are virtually negligible along the spine of the bank, which helps to maintain its position [Ferentinos and Collins, 1980]. It is unclear whether or not the bank pre-dates the barrier system of Start Bay [Hails, 1975], but its composition is coarse sand and shells, in contrast to the gravels of the barriers [McManus, 1975]. The seabed morphology of Start Bay is gentle in slope, and between 3 and 45m below mean sea level [Kelland and Hails, 1972; Hails et al., 1975]. The outer limit of the bay is marked by an ancient cliffline at -42m ODN, oriented approximately parallel to the contemporary shoreline planform [Hails et al., 1975]. Several bedrock-incised buried channels are apparent closer inshore, which extend the courses of modern day rivers and pre-date the barriers [Job, 1993]. They are not considered major features of the seabed with respect to hydrodynamics [Job, 1993].

Slapton Sands is actually a misnomer, being primarily composed of fine gravels and

granules with minor quantities of interstital coarse sand: up to 80% is quartz flint and quartzite, with small amounts of rhyolite, felsite and granite [Mottershead, 1986; Job, 1993]. This remaining 20% reflects the variable cliff and catchment lithologies. The gravel which makes up the modern Slapton Sands extends to 200-400m (increasing southwards) seawards of the low tide shoreline [Job, 1993], beyond which the Bay is composed primarily of medium-fine sands and muds rich in shell fragments [McManus, 1975]. Sediment sizes present on the barrier fall in the 1-64mm range, with most sediment between 2 and 16mm. For a gravel barrier in the UK, this is unusually well sorted and fine. The primary reason is that it is a closed sedimentary system, and presumably has been for some time. It is also probably because the barrier position has remained so steady, meaning that the gravels have been reworked by waves for more than 3000 years. There is little published data on abrasion rates for marine flints, although Latham et al. [1998] concluded that it would take 2300 years for a 90% reduction in volume for flints. It would therefore suggest that the sedimentary size range at Slapton was in the region 10-640mm some 2300 BP. Contemporary Slapton Sands is graded both cross-shore and alongshore, although this is highly variable. The thickness of the barrier deposits (Figure 3.3) varies between 5 and 11m, and in most places overlay brackish and marine muds [Chadwick et al., 2005]. The composition of gravels lain at depth are remarkably similar to modern day intertidal sediments in terms of shape, size and lithology [Kelland and Hails, 1972; Hails et al., 1975]. Central Slapton Sands is composed of some 11m depth of gravel, resting on marine muds whose surface lies at approximately -5m ODN [Mottershead, 1986]. It has been esimated that Slapton Sands has a total volume of 6.9 million cubic metres, some 69% of the total material comprising the beaches of Start Bay [Morey, 1983].

3.2 *Wave & Tide Climates*

The tidal regime is semi-diurnal and macrotidal, with a mean spring tidal range of 4.6m at Start Point [Carr et al., 1982]. Tidal levels for Slapton Sands are detailed in Table 3.1. The directional wave field is bi-modal, dominated by south-westerly Atlantic swell, which is attenuated by the large expanses of shallow water in Lannacombe and Start Bays, refracted by major headlands and subtidal shoals and banks [Holmes, 1975]. Higher

energy waves generated over smaller fetches to the east are less frequent [Holmes, 1975], but can be significant geomorphological agents, often causing a marked reduction in beach volumes [Job, 1993; Chadwick et al., 2005]. This is perhaps due to the headlands at either end of Slapton Sands being sufficiently spaced, and the barrier has sufficient central curvature (indentation), to disallow significant sheltering 'end effects' [e.g. Klein et al., 2002] therefore the beach is subject to some exposure. The strongest wave energy is thought to be at south-central portion of the Bay at Beesands, because of refraction effects caused by Skerries Bank [Holmes, 1975] on easterly storm waves, however these conclusions are at odds with HydraulicsResearch [1991] which stated that northeasterly waves undergo minimal modification.

There has been little published work on the wave climate of Start Bay, aside from the modelling efforts of Holmes [1975], HydraulicsResearch [1991] and Chadwick et al. [2005]. The shorelines of gravel beaches such as Slapton are commonly thought to be dominated by subharmonic energy [Wright and Short, 1984], and indeed subharmonic edge waves (a special case of reflected long wave trapped at the shoreline, with a period exactly twice that of the incident waves), which are historically given special importance by gravel beach researchers [e.g. Carter and Orford, 1984, 1993; Sherman et al., 1993], were first identified in the field at Slapton [Huntley and Bowen, 1975a]. Subharmonic edge waves are commonly associated with the formation of cusps [Wright and Short, 1984; Sherman et al., 1993], which are generally absent at Slapton. Austin [2005], through a series of detailed field experiments at Slapton, showed that subharmonic energy at the shoreline of subordinate importance to incident energy, thus challenging the commonly-held belief that subharmonic edge waves are an important component of the nearshore hydrodynamics of Slapton.

Tab. 3.1 *Tidal levels, from Burt [1993].*

Level	Elevation (m, ODN)
Once in 100 years tide level	3.15
Higest astronomical tide	2.85
Mean High Water Springs (MHWS)	2.2
Mean High Water Neaps (MHWN)	1.0

Primarily for the purposes of Chapter 7, three principal sources of secondary hydrodynamic data have been used (in addition to the nearshore wave data obtained as

part of individual monitoring campaigns-see chapters 5 and 6). The first, and longest, record was that of Met. Office station 62103 Channel Lightship, part of the UK Marine Automatic Weather Station network. Wind speed (knots), wind direction (in degrees), significant wave height (m) and mean wave period (s) data was available hourly since 12th May 2003. Significant wave height (hereafter, H_s) is defined as the average height of highest one third of waves in the measurement period. The second source of hydrodynamic data was the outputs from the WAVEWATCH III (WW III) model [Tolman, 1991, 2002g], a third generation wave model developed at NOAA (National Oceanic and Atmospheric Administration of the United States). This deep water ($\geq$15m) model outputs have been logged every 6 hours, from 19th January 2004, for a model node at Start Point at [50^{o}Lat., -3.75^{o}Long., Figure 3.4]. The data consist of wind speed (ms^{-1}) and direction (in degrees), H_s (m), T_{mean} (s), T_{peak} (s), and wave direction (^{o}N). The final hydrodynamic data source was an inshore Datawell Mk III directional waverider buoy within Start bay, in 10m water depth, located at approximately at [50.29^{o}Lat., -3.61^{o}Long., Figure 3.4]. Data is telemetered by radio link to a nearshore base station and then made available by the Channel Coastal Observatory (CCO). Data have been obtained every half hour, from 5th April 2007, consisting of H_s (m); maximum wave height (H_{max}, m); peak wave period (T_{peak} -wave period at which the highest wave energy is centred, s); zero-crossing wave period (T_z, s); mean wave direction (direction of the waves of period T_{peak} in degrees, measured clockwise from magnetic north); and wave spread (the distribution of energy around T_{peak}, in degrees. Low values indicate a narrow-banded sea and high values indicate a broad-banded sea).

Daily weather records have been collected by staff at Slapton Ley Field Studies Centre since the spring of 1960 [Ratsey, 1975; Burt and Horton, 2001]. A climatological station was designed and set up with the assistance of the Meteorological Office to measure a suite of meteorological variables at 9am each day by a Met. Office trained individual. This station is located to the north east of the Field Centre at an altitude of 32m (Figure 3.4) and is reasonably well exposed. Of primary interest to the present study, primarily chapter 7, were records of temperature, wind speed and wind direction, as indicators of 'storminess'. Annual means have been taken of daily weather records collected by FSC Slapton Ley, and these are charted in Figure 3.5. A linear least-squares fit through the wind speed data indicates a general decrease since 1960, and wind directions have shifted

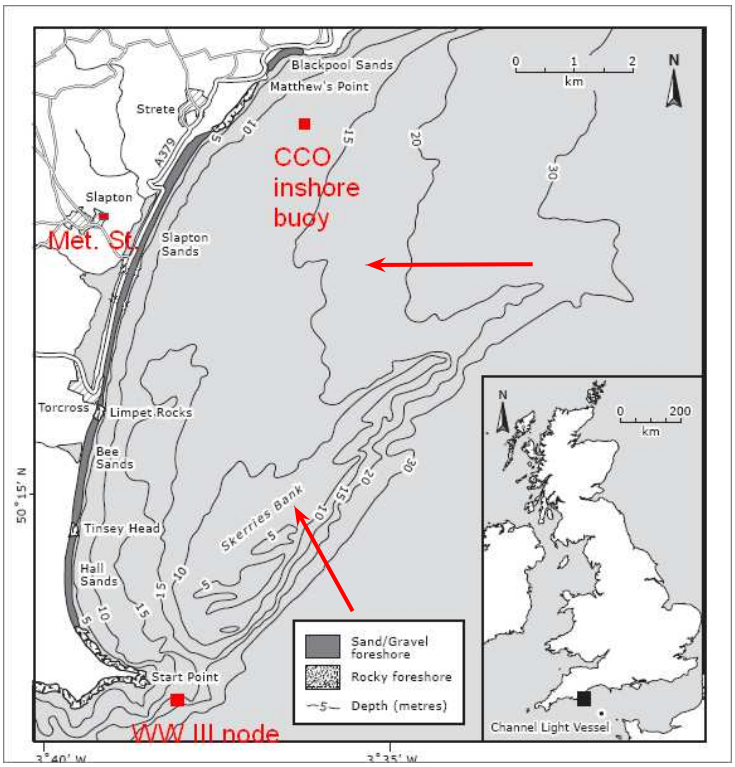

Fig. 3.4 *Map of Start Bay, with the positions of Slapton FSC metereological station, CCO inshore wave buoy, and nodal point for WW III model marked. The two arrows indicate the two prevailing wave directions.*

slightly to the south and west. Temperatures and rainfall are increasing.

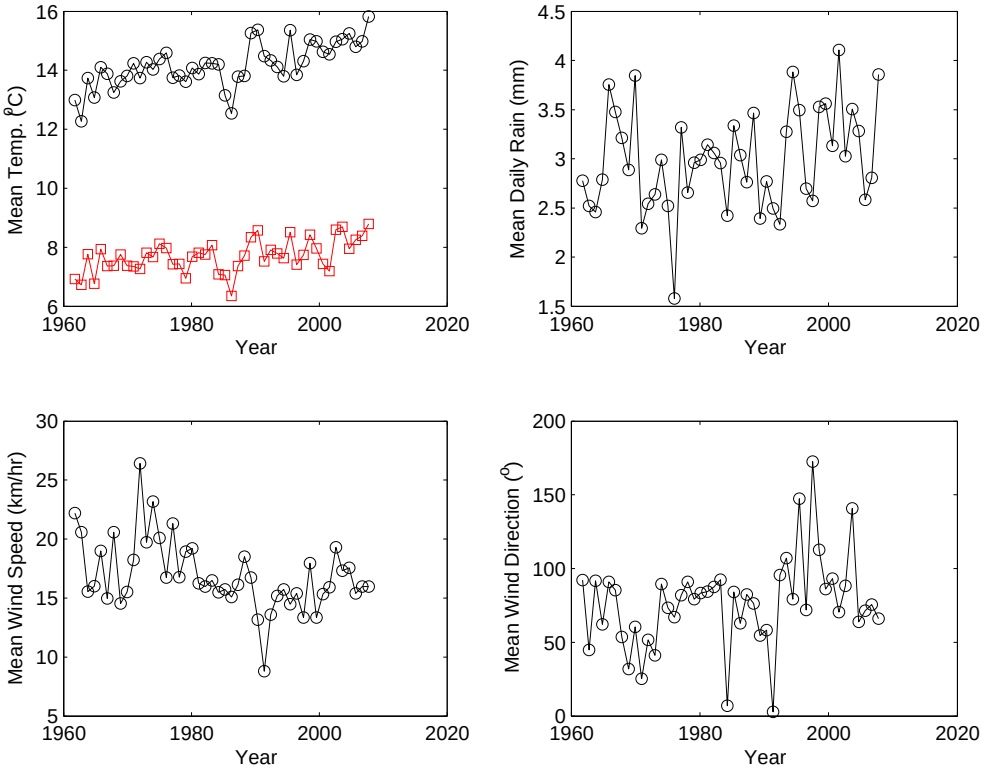

Fig. 3.5 *Annual means in,* ***clockwise from top left****: max. and min. temperature, rainfall, wind direction, and wind speed.*

3.3 *Contemporary Pressures & Management Issues*

It is predicted that sea levels will be some 0.5m higher than today by the year 2100 [IPCC, 2007], which will make extreme water levels more common, subject larger areas to more frequent (and more damaging) coastal flooding, and cause more frequent breaching and failure of coastal defences. Tide gauge measurements at Newlyn near Penzance in Cornwall show a 25cm rise in sea level since records began in 1915 [Gehrels, 2006], at a rate of 1.7mm/year [PSML, 2006]. The UK Climate Impact Programme predictions for the southwest for the year 2080 under a low-emission scenario are a relative sea level rise of 16cm (revised to 20cm by Chadwick et al. [2005] to take into account local isostatic readjustments). The central shorelines of Start Bay (Slapton Sands) experience perhaps the least wave energy, however it is here where the integrity of the barrier is perhaps most threatened, due to either an alongshore drift divergence [Chadwick et al., 2005] or because of the thinning influence of barrier curvature. Pethick [2001] calculated that

central Slapton Sands has suffered average annual retreat of 0.8m/year between 1972 and 1995, and that the barrier is decreasing in width by 15m per century. There is no evidence of contemporary sediment supply from offshore to sustain the barriers of Start Bay, although there is likely to be a long-term redistribution of sediment between individual barrier systems. For example, there is anecdotal and historical evidence for beaches at the extremes of the bay (towards Strete and towards South Hallsands) to be much more depleted or accreted than today, suggesting very long term beach rotations. Job [1993], for example, suggests that the net littoral pathway was southwards in the nineteenth century, the opposite of today, pointing to the very healthy beaches at South Hallsands during this time. Beach losses and crest cut back in the winters of 1995/6 and 2000/1 suggest a negative sediment budget, but this remains speculatory.

Figure 3.6 shows a map of Slapton from 1890 overlain onto a modern aerial photograph. Recessions in low tide shoreline are in evidence for the entire length of the barrier, and are marked onto this figure shaded in red. This shoreline recession wedge significantly thins northwards, and, at least qualitatively, supports the figure of 15m shoreline recession per century at Slapton, quoted by Pethick [2001], in response to barrier rollover under increasing sea-levels. Chadwick et al. [2005], who carried out a shoreline analysis for Slapton for the years 1999 to 2002 using a longshore sediment transport and one-contour shoreline model, stated that shoreline changes up to 45m could be possible at Slapton over a 4 year period. Job [1993] notes that the accumulation of material towards the north may have been a relatively recent phenomenon, and that there is map evidence which suggests the during the nineteenth century net drift may have been southerly (a theme elaborated upon in Chapter 7). At the present time the subject is uncertain, a lot of the evidence being anecdotal. A detailed historical analysis of shorelines within Start Bay warrants further study.

Eleven cross-shore lines have been surveyed by the Field Studies Council, Slapton Ley, between 1972 and 2003. The intervals in time are irregular, however, for eight of these profile lines a total of 32 surveys were carried out in these 31 years, so data from these were deemed to have sufficient temporal resolution to carry out an analysis of shoreline positions through the past three decades. The bearings of these profile lines range between 100 and 120 degrees relative to magnetic north, and the surveys were performed using a dumpy level. Twenty-three profiles from eight locations spaced approximately

Fig. 3.6 *Shoreline recession at Slapton between 1890 (map overlay) and the present day (aerial photo). The approximate recession in low tide shoreline is marked in red. Based on a figure prepared by Prof. Roland Gehrels, University of Plymouth.*

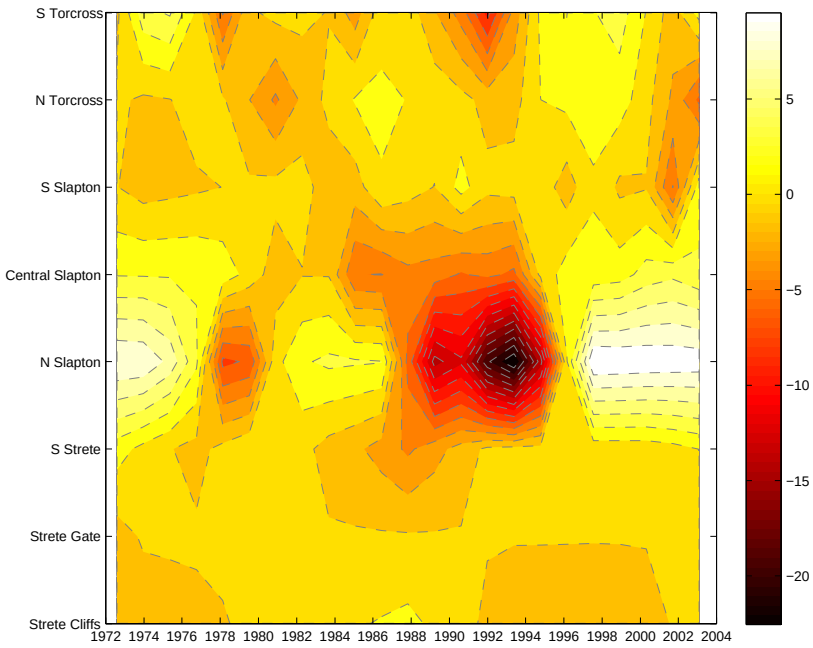

Fig. 3.7 *Net changes in shoreline for Slapton Sands between 1972 and 2003 based on profile records collected by Slapton Ley Field Studies Centre. Alongshore distance increases northwards down the page. Values contoured are for the horizontal distance from a datum on the barrier crest to the 1m ODN contour, relative to initial (1972), in metres. Dark values therefore represent relative shoreline recession, and the lightest areas represent relative shoreline advance.*

uniformly alongshore were selected (spanning August 1972 to February 2003) for a shoreline position analysis, here defined as 1m ODN (MHWN). Shoreline time-series for all eight locations were detrended and contoured, as seen in Figure 3.7 in metres accretion (positive values, light shading) and depletion (negative values, darker shading). What is immediately evident is the variability of the central portion of Slapton, where significant cut-backs up to 25m can occur. A cyclicity in the net change in shoreline for the entire beach over time can be seen in Figure 3.7 with a periodicity of approximately 15 years: during the 1970s and 1980s the shoreline was advanced relative to today, and during the 1990s the beach was relatively cut back. Central Slapton Sands contributes for the most part to this general trend, with net changes at Strete and Torcross being relatively insignificant.

Slapton Sands has been hit by several storms in the past few decades, most notably the damaging events of December-January 1978/9 and January 2001 [Burt, 1993; Chadwick et al., 2005]. As a result of the 2001 storms, the beach in the central portion of Slapton was lowered by more than 3 metres, and the barrier crest was both undercut

and overtopped. As a result, an important war memorial had to be resited, and a 250m section of road re-built (indeed, set back) which prompted the closure of that road, a vital local transport route, for more than 3 months. As a direct result of the inconvenience caused by the storm, especially to road users, a local interest group called the 'Slapton Line Partnership' was formed comprised of local councils and conservation bodies to make a decision on the future of the area with specific reference to the road. The decision is not straight forward, since the barriers natural response to storms and sea level rise is to transgress landwards [Pethick, 2001; Orford, 2001]. In addition, both the barrier and its hinterland are nationally protected (SSSI, AONB, NNR, HC, GCRS) natural features [Barne et al., 1996]. In 2002 the Slapton Line Partnership commisonned Atkins consultancy to carry out a scoping study, and later Scott Wilson consultancy to carry out a detailed study on the future of the barrier [ScottWilson, 2004; Chadwick et al., 2005]. In 2007, another consultancy (Royal Haskoning) reported its findings from another major study into the possible consequences of coastal breaching and flooding for Slapton Sands.

Eight cross-shore lines, spaced approximately 300m alongshore between Torcross and Strete, which were surveyed before and after a major storm which hit the barrier on 26–27th October 2004. The surveys were carried out on the 26th and 28th October, and again after a spring-spring tidal cycle on the 12th November, using an electronic total station. This data set was used to study both the behaviour of the beach in response to extreme storm conditions and the rates of its recovery, and also to draw comparisons between the changes measured fortnightly during 2006–2007 and the changes during a low-frequency, high-magnitude event.

The data collected surrounding the October 2004 storm is a good example of the profile response from an unusually severe storm. The storm that hit Slapton on the 27-28th October 2004 consisted of a coincident south easterly gale (maximum offshore H_s in excess of 5.5m) and high spring tide, resulting in a 0.75m storm surge, and overtopping waves. Gravel and debris deposited on the road immediately behind the beach frontage, both of which were closed for a short time, although overall no significant damage was caused. The storm induced crestal cut back, beach head erosion, and a new steeper post-storm beach profile. The measured profile changes are the subject of Figure 3.8. The magnitude of change during one storm event can be greater

than the net changes over an entire year, although the cross-shore location of change is crucially different, being confined to a narrower zone closer to the shoreline under normal wave conditions. As well as significant erosion (and some upper beach accretion due to over-washing), Figure 3.8 also shows that the beach can recover very quickly-the black dashed line representing the profile one spring tidal cycle after the storm shows that the beach had regained a lot of material after just two weeks of calm conditions.

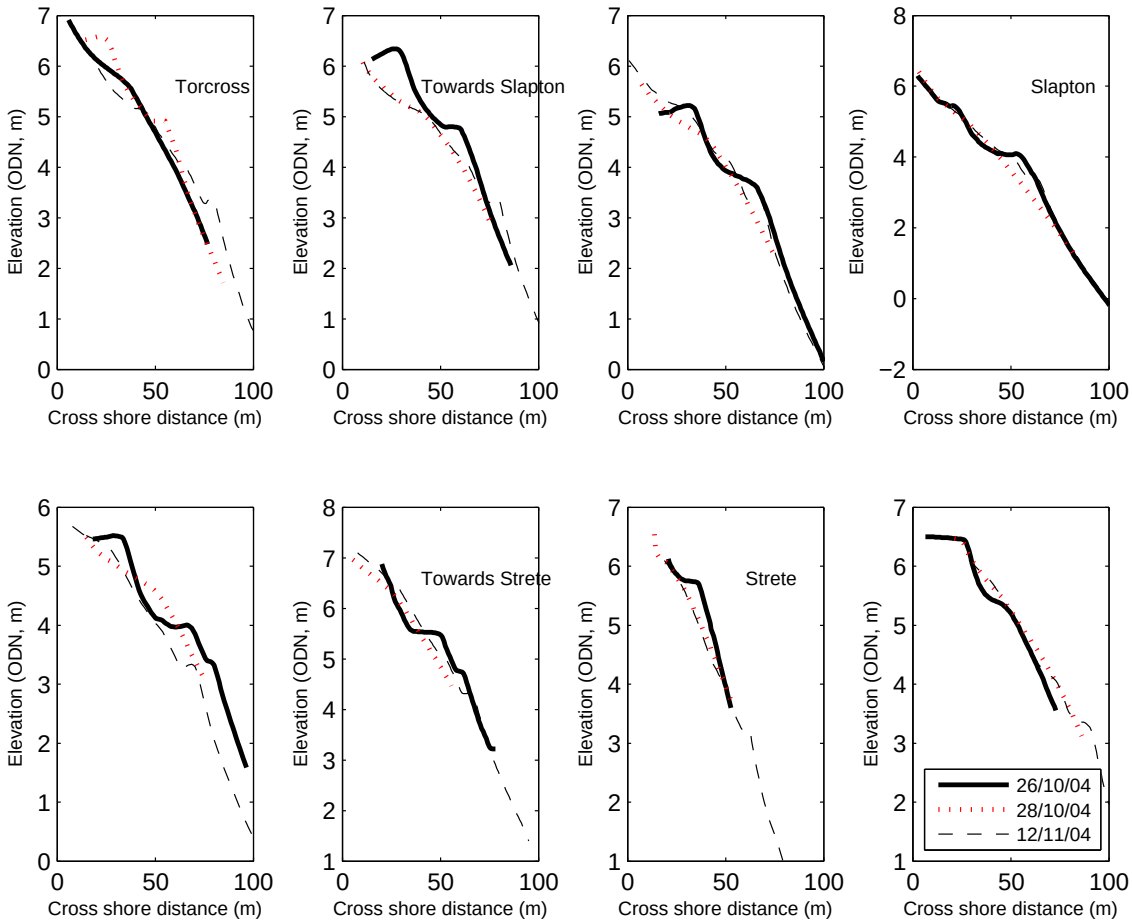

Fig. 3.8 *Profile change as a result of the October 2004 storm (increasing northwards from the left to right of each row). Measured profiles from 26th October (solid lines, prior to the storm); 28th October (dotted, immediately after the storm); and 12th November (dashed, after one spring-spring tidal cycle).*

These reports have all highlighted the need for (especially experimental/field work based) medium-short term morphodynamic studies at Slapton Sands, to complement a literature of more extensive and longer term geomorphological history of Start Bay [PosfordDuvivier, 1998; Orford, 2001; Pethick, 2001; Halcrow Group, 2002; ScottWilson, 2004]. These reports highlight the uncertainties surrounding morphological change and

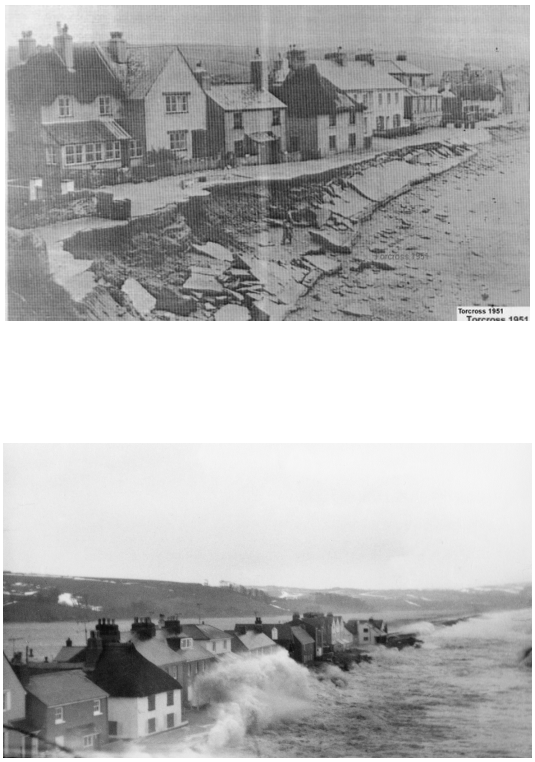

Fig. 3.9 *Storms hit Torcross in 1951 (**top**) and 1979 (**bottom**), causing considerable damage. (Photos courtesy of Slapton Ley Field Studies Council and South Hams District Council).*

sediment pathways, longshore drift and barrier plan shape, the behaviour of the beach during storms, as well as sediment storage and exchanges between the nearshore and offshore. Information on these will be required for a number of important coastal management decisions which will have to be made in the coming years [ScottWilson, 2004]. A good example of the need to understand the coastal morphodynamics of Slapton and similar beaches is provided by the response of the beach to a storm in October 2004. The storm which hit Start Bay on 27^{th} October 2004 saw the tide gauge at Newlyn register 6.422m CD, which has a return period of more than 1000 years based on records between 1915 and 1990 [Gehrels, 2006], much higher than those for the January 2001 event, which experienced similar wave heights. Yet the beach suffered minor damage in 2004 compared to 2001. The inconsistency of individual storm responses is thought to be attributable to different conditions of antecedence. Complex barrier responses as shown here make predicting the likely impacts of high magnitude, low frequency events on coastal areas a challenging task: coastal erosion/damage is not a simple linear function of energy or water levels, but a complex integral of the relative contribution of storm intensity, event sequencing, longshore superposition and conditions of antecedence. Prior to the storm of 2001, sub-aerial beach volumes were depleted owing to an energetic winter [Chadwick et al., 2005]. The event in 2004 was subsequent to relatively calm sustained accretionary conditions [Austin and Masselink, 2006*a*]. The antecedent state of the beach as well as the magnitude of the storm appears crucial in determining its impact. Storm directionality may also be important in determining the short term behaviour of a gravel barrier, but our insights into differential geometrical reponses of a barrier in response to these processes remains rudimentary.

Another illustration of the importance of a need to better understand coastal processes in Start Bay is provided by South Hallsands, one of the most notorious examples in the south west of coastal mis-management. An estimated 300,000m^3 of material was dredged from the foreshore here between 1897 and 1902 to provide aggregate for the construction of Plymouth dockyards. Between 1902 and 1917 the village was progressively destroyed in a series of storms, and it has never recovered. This demonstrates that exchanges in this location between the nearshore and offshore are limited, and there are no significant new sources of the sediment in the system. Lengthy discussions about this controversial disaster may be found in Robinson [1961] and Hails [1975b].

3.4 Morphodynamics of Slapton Sands

Slapton Sands is an ideal location for the scientific study of gravel beach morphodynamics. It is a pure gravel beach with very minor quantities of (undesirable) sand (Chapter 2). Nearshore wave conditions are energetic enough to drive significant morphological change over all scales of interest (Chapter 1), and the beach experiences a large range of sea states over a given year. Profiles are strongly two-dimensional, and so-called swash aligned. In addition, there is a long tradition of scientific studies at Slapton [Burt, 1994, for example Slapton Ley field studies centre have carried out discontinuous monitoring of various profile lines since 1972 [Chell, 2002], revealing the dynamic nature of profile adjustments], and renewed impetus into studying its dynamics in recent years, in part reflected by an Argus camera system installed in July 2005, a directional waverider buoy installed by the Channel Coastal Observatory (CCO) in April 2007, and recent initiation of a profile monitoring campaign by the CCO [Bradbury, 2001]. Most importantly, it is a beach perceived to be at risk, and knowledge of its dynamics is likely to inform management decisions made in the near future. SCOPAC [2007] stated that a detailed sediment budget is required for Slapton Sands, as are a profile monitoring campaign and a detailed study of the beach's sedimentology.

Sediment modification, loss or supply from in-situ weathering is thought to be negligible. For example, cliff recession is slow: analysis of cliff weathering rates just to the west of Start Point [Mottershead, 1983, 1989, 1998, 2000] suggest that weathering products are removed by solution. Fluvial and aeolian transport are not contributing significantly to the nearshore littoral sediment budget. Contemporary offshore and beach mining is absent, and the only beach replenishment that has taken place at Slapton Sands was the one-off creation of four 'bastions' in the central portion above MHWS in 2002 using material from Strete in the north. Hard artificial coastal structures are limited to Torcross, and impact minimally on the dynamics of the beach.

There are a handful of coastal process studies which have been carried out at Slapton and the remainding paragraphs of this chapter is devoted to briefly summarising their findings. In a sediment transport study, Carr [1974] provided evidence that relatively small pebbles travelled the maximum alongshore distances, in contrast with similar studies on Chesil Beach, Dorset, attributed to the phenomenon of overpassing [see

Chapter 2, and Carr, 1971]. Carr [1974] and Gleason et al. [1975] report tracer measurements indicating a weak net northerly drift. PosfordDuvivier [1998] calculated a net northward alongshore transport rate at Slapton of 61,500m^3/year, although these results were calculated using a sediment transport model which has not been validated for gravel sized sediment, prompting Chadwick et al. [2005] to re-evaluate alongshore transport direction and rates using the formula of Van Wellen et al. [2000] which had been validated for coarse grains. They also found net northwards movement for 1999-2002, in the region 25,000-75,000 m^3/year. In a cross shore sediment trapping study, Austin and Masselink [2006*a*] found that even low energy swash transported significant sediment volumes (up to 20 kg per unit metre beachface). As yet, no statistically significant correlations have been found between net sediment drift (as determined from tracer experiments) and wave parameters [Gleason et al., 1975; Carr et al., 1982]. Carr [1974] and Gleason et al. [1975] both report that Slapton is generally graded alongshore, fining northwards, but also that reversals in grading can occur over the short term. Indeed, Job [1993] argues that Slapton coarsens northwards. No studies have been able to shed light on whether the sediment budget for the beach as a whole is in balance.

Austin and Masselink [2006*a*] noted highly variable spectral widths, indicative of a highly variable wave field composition. Huntley and Bowen (1975) concluded that secondary wave generation associated with reflection may be significant, although Austin [2005] downplayed the significance of these standing wave forms. Both Austin and Masselink [2006*b*] and Horn and Li [2006] report measurements of groundwater responses to swash flows, concluding that groundwater dynamics were important factors in observed morphological changes. Austin and Masselink [2006*a*] found that the active beachface in the centre of Slapton Sands was reflective, with a mean slope of tanβ=0.2 and a mean grain size of approximately 6mm, moderately to well sorted, echoing Gleason et al. [1975], who also noted the limited extent of a storm beach, indicative of frequent inundation of the back beach, as well as a limited range in available grain sizes.

3.5 Summary

Slapton Sands is, despite its name, a pure gravel barrier beach thought to have been formed by Holocene marine transgression and to have remained in approximately the same position for 2-3000 years. It is well sorted and graded both cross shore and longshore, although this is highly variable. It is distinctly two-dimensional, however morphological changes can be substantial over several time scales of interest. It is unknown whether the beach has a positive or negative sediment budget, and the extent to which material is exchanged between nearshore and offshore under a range of conditions. It is possible beach rotation, and exchange between itself and neighbouring beaches within Start Bay, occurs on decadal to centennial time scales. The local hydrodynamics are poorly documented, however it is clear that wave fields are strongly bimodal with respect to direction, and highly variable over an average year. Due to a long term landwards transgression and an apparent accelerated rate in sea level rise, Slapton Sands is considered under threat from breaching and overtopping, although the effects of storms on the barrier are poorly studied, and depends critically on the ability of the system to maintain a sediment supply. The local importance of the beach cannot be understated. Slapton Sands is an ideal location for the study of gravel beach morphodynamics primarily because it is relatively devoid of human interference, and it contains barely significant quantities of sand.

4 SEDIMENTOLOGICAL INFORMATION FROM THE PROPERTIES OF DIGITAL IMAGES OF SEDIMENT.

The least movement is of importance to all nature. The entire ocean is affected by a pebble.

Blaise Pascal (1623-1662), French Scientist & Philosopher.

4.1 *Chapter Summary*

The autocorrelation technique for estimating grain-size from digital images of sand beds has been extended and validated for use on coarse sand (0.7mm) and gravel (up to ≈20mm). A number of aspects of the technique have been explored and some potential improvements suggested. Autocorrelation is just one suitable statistical method sensitive to the grain-size of sediment in digital images; four additional techniques are presented and their relative merits discussed. A collective suite of techniques applicable to the general problem of grain-size estimation from digital images of sediment might broaden the applicability to more sedimentary environments, as well as improve its accuracy. These are compared using a large data set from a gravel barrier beach in southern England. Based on over 180 samples, mean grain-size of sieved and imaged sediments correspond to within between 8 and 16%. Some theoretical aspects of the spatial arrangement of image intensity in digital images of natural sediments are addressed, including the fractal nature of sediments in images, which has potential implications for derivation of grain-size distributions from images of sand-sized material through segmentation and thresholding. These may also find application in further uncovering the

geometric structure of these beds, as well as in the simulation of sedimentation processes.

A new technique to estimate the grain-size distribution from a digital image of sediment is proposed, advancing the applicability of a suite of sedimentary 'look-up-catalogue' approaches originated by Rubin [2004]. The outputs of an automated procedure to estimate the grain-size distribution from digital images of sediment are examined with reference to the distributions obtained from manually sieving the corresponding sediment samples. Measures of grain-size obtained from the imaging procedure correlate very well with grain-size measures derived from the mass-frequency curve. Using the new distribution estimation technique, more realistic distributions are obtained than previous methods. The shape is not always mimicked exactly, however the percentiles obtained from the cumulative distribution compare well with those from sieved distributions, which allow for the first time computation of sorting and skewness which are accurate reflections of those measures obtained for sieved samples. Thus for the first time, it has been demonstrated that an automated technique based on the statistical properties of digital images of sediment is able to provide a realistic grain-size distribution. A realistic Grain Size Distribution (GSD) allows accurate estimates of GSD percentiles, which in turn allows the graphical parameters for sorting, skewness and kurtosis to be calculated. The values obtained for sorting and skewness were reasonable, which broadens the applicability of rapid, remote and automated quantification sand and gravel sediment for use in sediment trend and transport modelling, and detailed studies into spatial and temporal sedimentation in a number of sedimentary environments.

Indeed, it is now possible to measure grain-size nearly in real time in the field and in the laboratory, enabling enormous spatial and temporal coverage and resolution. Data collection can be very cheaply set up so as to be almost fully automated, and continuous. High resolution grain-size information may thus allow a new generation of sediment transport and morphological models with time-varying grain-size and associated/derived parameters, including temporally and spatially updatable shear stresses, friction, porosity, and transport efficiency terms. Work such as this promises to revolutionise field and laboratory studies where grain-size, and spatial/temporal variations of grain-size, respond or reflect the close kinematic coupling between bed composition and flow fields, which in turn drive both further changes in flows, and changes in landforms [Rubin and Topping, 2001; Gallagher et al., 2003].

4.2 Drivers for Research & Introduction

Grain-size information from natural environments is traditionally obtained using methods such as sieving, laser diffraction, and settling. The slow and labour-intensive nature of these methodologies has limited the spatial and temporal resolution with which one can collect grain-size data, which in turn has hindered our detailed understanding of sediment transport and geomorphological change. Indeed, studies of system dynamics, where grain-size is considered an important parameter, are fundamentally limited by the difficulty of sampling for sediment at the required frequency. One additional disadvantage is that sediment must be manually sampled, therefore physically removed from the environment under scrutiny, potentially altering subsequent system development. Only remote sensing methods can measure grain-size at a resolution comparable to measurements of hydraulic, hydrodynamic and morphological/topographical conditions.

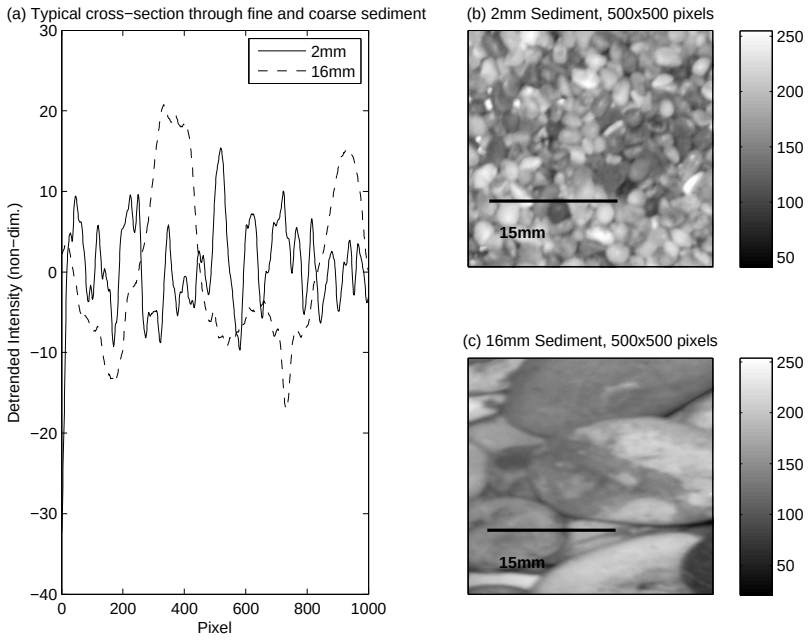

Fig. 4.1 *The nature of intensity variations in images of sediment: cross sectional profile through images of 2mm and 16mm sediment (panel a, solid and dashed line respectively); and magnified portions of the same images, with scale (panels b and c).*

The problem of deriving sediment size information from digital images of sediment has been approached using two different families of techniques. The first is based on edge detection and image segmentation principles [Butler et al., 2001; Sime and Ferguson, 2003; Graham et al., 2005]. Such techniques rely on marked image-intensity contrasts

between grains and gaps between grains (interstices), making thresholding possible to discriminate grains from the background intensity levels [Sime and Ferguson, 2003], to discern individual grains. These methods are thus far only suitable for instances where the overlapping of individual grains, or the apparent coalescence of adjacent grains due to indistinguishable similarities in colour and texture, are negligible. Such images are much more likely to be found in the larger sedimentary fractions, such as coarse gravels, cobbles and boulders, or surfaces composed of sand/clay and gravel mixtures, where one is able to apply thresholds to remove entire classes of grains. Images of coarse sands and fine sands are comprised of complicated objects that are difficult to segment: they have a much greater number of individual grains per image (Figure 4.1, b and c) so the potential for errors associated with grain overlap and grain coalescence, which have the effect of making the collections of grains appear larger than they really are, is significant.

The second approach is to treat grains within an image not as individual objects, but as a collection of 'textures'. With reference to Figure 4.1, sediments of varying sizes have recognisably different textures, for example the spatial arrangement of greyscale intensities is much more variable in images of smaller sediment (Figure 4.1). In such cases, accurate grain-size information of natural sediment surfaces may be derived through the statistical properties of those images, based on the notion that intensity values in any cross-section of digital images of sediment (Figure 4.1) are more similar over space in coarse sediments than in fine. Rubin [2004] showed that the autocorrelation function, used as a measure of two dimensional spatial (in-) dependence, could be sensitive to the size of grains within images of sand, and thus, given careful calibration, could be used to derive a rapid, yet accurate, measure of sediment size. This makes it possible to use remote sensing to measure grain-size nearly in real time in the field and in the laboratory, enabling enormous spatial and temporal coverage and resolution [Gallagher and McMahan, 2006; Rubin et al., 2006; Mustain et al., 2007; Ruggiero et al., 2007]. Data collection can be very cheaply set up so as to be almost fully automated, and continuous. Work such as this promises to revolutionize field and laboratory studies where grain-size respond or reflect the close kinematic coupling between bed composition and flow fields, which in turn could drive both further changes in flows, and changes in landforms [e.g. Rubin and Topping, 2001; Gallagher and McMahan, 2006]. High resolution grain-size information may thus allow a new

generation of sediment transport and morphological models with time-varying grain-size and associated/derived parameters, including temporally and spatially updatable shear stresses, friction, porosity, and transport efficiency terms.

The purpose of this chapter is to develop and validate a methodology which will give reliable and rapid estimates of grain-size distributions from digital images of sediment beds, using reliable and inexpensive methods. The present study relies on the numerical and computational methods employed for the estimation of grain-size distribution parameters to be sound, for although the present work does not solely rely on automated grain-size analysis using cameras, it does to a large extent. The objectives are therefore three-fold:

To develop and test a suite of statistical routines for grain-size estimation on use on coarse sand and gravel sized sediment,

To improve upon and validate existing algorithms for grain-size distribution estimation,

To explore the suite of techniques employed here in order to give them a sounder theoretical basis and make them more broadly applicable.

This contribution extends the statistical approach of Rubin [2004] in two ways. Firstly, by designing and validating a field image-collection methodology for use with gravel-sized sediment. Secondly, and more importantly, the general problem of obtaining an estimate of grain-size from an image of sand/gravel is put on a firmer theoretical basis by extending the theoretical/algorithmic work of Rubin (2004).

After a detailed introduction to the general problem of obtaining an estimate of grain-size from a digital image of sediment, termed 'look-up cataloguing' (LUC), four new numerical methods are introduced, three of which are prompted by the suggestion that the two-dimensional (Fast) Fourier transform (hereafter referred to as 2D-FFT) may be a viable alternative to the spatial autocorrelation routine to derive grain-size information from digital images of natural mixed beds [Rubin, 2004, p. 160]. The 2D-FFT algorithm has been applied to images for derivation of variograms, power spectra and fractal dimensions. The fourth numerical procedure is an autoregressive model, which quantifies serial correlation and thus is in the same family of methods as the autocorrelation function. It is found that similar results are achieved using a number

of different numerical techniques. Some example research applications are presented from a gravel beach, and the relative merits of different methods to obtain grain-size from images of sediment are evaluated. Theoretical considerations of the LUC approach, as well as the use of both statistical and segmentation methods in practice, are discussed before conclusions are drawn.

Several techniques have been utilised because they allow the nature of spatial variability of grey-level intensities within images of sediment to be explored theoretically. They may therefore provide a starting point to the rapid, automated and quantitative description of additional sedimentological traits such as grain orientation, shape, sorting, bimodality and mineralogy, which should be possible using the techniques presented in this paper for sizing. In addition, the use of these techniques may be useful in artificially modelling grain surfaces for use in sediment transport simulations and elsewhere. Researchers working in a wide range of environments are more accustomed to certain techniques than others, so the adoption of statistical sedimentological techniques is facilitated by exploring and suggesting a range of acceptable alternatives. Finally, since at present the primary advantage of LUC methods for sediment size is sample processing speed, a number of methods have been suggested who's speed or accuracy may depend on the software or (high-level) programming language used.

4.3 *The principles of Sedimentary 'Look up cataloguing'*

A standard red-green-blue (RGB) digital image is transformed into a 'greyscale' (intensity) image by eliminating the hue and saturation information, while retaining the luminance. The resulting two dimensional matrix is composed of 8 bit values which score shades of grey (intensity) in the visible spectrum on a 0:255 point scale. Figure 4.1 demonstrates the nature of variations in intensity between relatively fine and relatively coarse sediments. There are algorithms which are sensitive to either the serial correlation of numerical values represented by such images, or the nature of 'texture' within the images (i.e. statistical properties which tell us something about the two-dimensional distribution of grey levels within an image).

The numerical technique should operate on the information within the entire image or a large proportion of the image (two dimensions), not a single pixel line, to retain the

desired spatial arrangement of intensity within the image. This technique quantifies the size information obtained within the sediment image. Calibration images are taken of sediments which have been sieved into a number of size fractions, and the chosen numerical procedure is applied to each image to build up the catalogue. The number of observations must equal the number of observations in the calibration catalogue, so the calibration catalogue will consist of n observations multiplied by m calibration sizes. The procedure then involves 'looking up' the elements of the sample in the calibration catalogue, and, based upon their location, returning output values interpolated within the elements of the catalogue. The catalogue becomes a 'look up table', a data structure used to find solutions based on several pre-computed solutions. This general procedure may be termed sedimentary 'look up cataloguing' (LUC). Note that the use of several calibration catalogues is likely to enhance the accuracy of the estimated sizes: these calibration images must be based on sediment sizes derived from sieving, and not the outputs of previous LUC application to images of sediment, to avoid propagation errors. The calibration catalogue used may be similar to the (much simplified) table below, which contains typical values associated with the autocorrelation method:

sample	40*mm*	20*mm*	10*mm*	5*mm*	...	*m calibrationsizes*
0.9938	0.9966	0.9953	0.9958	***0.9950***	...	
0.9911	***0.9889***	0.9843	0.9859	0.9826	...	
0.9770	***0.9786***	0.9691	0.9720	0.9642	...	
0.9586	***0.9666***	0.9511	0.9546	0.9409	...	
0.9448	***0.9537***	0.9314	0.9338	0.9136	...	
0.9111	0.9403	***0.9108***	0.9106	0.8833	...	
0.8956	0.9269	***0.8901***	0.8854	0.8513	...	
0.8743	0.9136	***0.8692***	0.8590	0.8182	...	
0.8632	0.9005	***0.8486***	0.8319	0.7849	...	
0.8477	0.8876	***0.8283***	0.8044	0.7517	...	
⋮	⋮	⋮	⋮	⋮	⋱	
n lags						

The values highlighted in bold are those in the calibration (within brackets) which most closely match the sample (on the left) at every lag, so this simple example would have a grain-size array of $X = [5, 40, 40, 40, 40, 20, 20, 20, 20, 20]$ with mean value 26.5mm (note that in reality several more lags, and several more calibration sizes would be required, as would interpolation between sizes as explained below).

Fig. 4.2 *An example image taken of gravel sized sediment, taken at a known height using lights which cast uniformly on the bed.*

4.4 Numerical methods

The generalised problem and distribution estimation

The general linear equations for the problem of solving for the proportions of calibrated sizes that collectively give the best fit to a given sample's numerical signature are given by (modified from Rubin [2004]):

$$\begin{aligned}
\mathbf{a}_{(1,1)}\iota_1 + \mathbf{a}_{(1,2)}\iota_2 + \ldots \mathbf{a}_{(1,m)}\iota_m &= \mathbf{b}_1 \\
\mathbf{a}_{(2,1)}\iota_1 + \mathbf{a}_{(2,2)}\iota_2 + \ldots \mathbf{a}_{(2,m)}\iota_m &= \mathbf{b}_2 \\
&\vdots \\
\mathbf{a}_{(n,1)}\iota_1 + \mathbf{a}_{(n,2)}\iota_2 + \ldots \mathbf{a}_{(n,m)}\iota_m &= \mathbf{b}_n
\end{aligned}$$

where $\iota_1 \ldots \iota_m$ are the proportion of size fraction 1:m in the sample, $\mathbf{a}_{n,1} \ldots \mathbf{a}_{n,m}$ are the numerical signature values for lags 1:n of the calibration samples 1:m, and $\mathbf{b}_1 \ldots \mathbf{b}_n$ are the observed numerical values for lags 1:n in the current sample. This linear problem is therefore defined simply, where $\mathbf{a}$ is the sample array (a column vector with n components) and C is the $m \times n$ calibration catalogue, by:

$$\mathbf{b}(n) = \sum_{k=1}^{m} C(n,k) \times X(n) \tag{4.1}$$

where the vector solution $X = \iota_1 : \iota_n$ is the one that minimises the sum of squared errors between C and $\mathbf{b}$ ($(\mathbf{b} - CX)^T \times (\mathbf{b} - CX)$, where T denotes matrix transpose). This solution is the array of grain-sizes generated from the image. In this way, intermediate solutions which fall between two pre-computed values may be sought through interpolation. Sediments composed of mixed sizes are thus solved easily, for example using a measure of central tendency (mean or median) of X, an array consisting of weighted proportions of several sizes. For example, $X = [23, 30, 7, 20, 24, 14, 26, 29, 38, 25]$ has a mean value of 23.6mm, and a median value of 24.5mm. Note that the set of simultaneous equations above may be calculated in a least-squares sense with or without non-negativity constraints. The latter case can be found using an (iterative) optimisation routine [Lawson and Hanson, 1974] which Rubin [2004] uses to find the grain-size 'distribution', a vector solution which minimises $(\mathbf{b} - CX)^T \times (\mathbf{b} - CX)$ such that $\iota \geq 0$.

A third way is the simple matrix division of the sample array, $\mathbf{b}$ (a column vector with n components), into the calibration catalogue C ($m \times n$ matrix): the resulting equation $\mathbf{b} \times X = C$ may be computed by Gaussian elimination, where the solution X again is the array of sediment sizes (mm), by minimising $norm(\mathbf{b} \times X - C)$. Note that if several calibration catalogues are used, the linear problem is set for each one, so a single vector solution for each catalogue is obtained. A suitable averaging procedure should then be applied to obtain a single estimate of sediment size for each sample image.

For example, distributions were obtained from the imaged sample in Figure 4.2 using the autocorrelation algorithm detailed in Rubin [2004], and calculated using both 'least-squares' and 'least-squares with non-negativity' methods. The outputs may be seen in Figure 4.3 (dashed and dotted line, respectively), compared to the measured distribution for that sample as determined by dry mechanical sieving (solid line) at 1/4 ϕ. To ensure a fair comparison, the sieves used were identical to the fractions represented by the calibration catalogue used for the computations. This sample is typical of the behaviour exhibited by the two respective distribution-estimation methods on digital images of sediment: the least-squares method tends to produce a unimodal, well sorted distribution; and the least-squares with non-negativity method produce statistical artifacts such as a 'blocky', multimodal distribution. Often the reality lies somewhere between the two, as in Figure 4.3. While estimates of median size (D_{50}) closely match the real sample, derived measures such as sorting and skewness are often

wildly inaccurate using these distribution estimation methods.

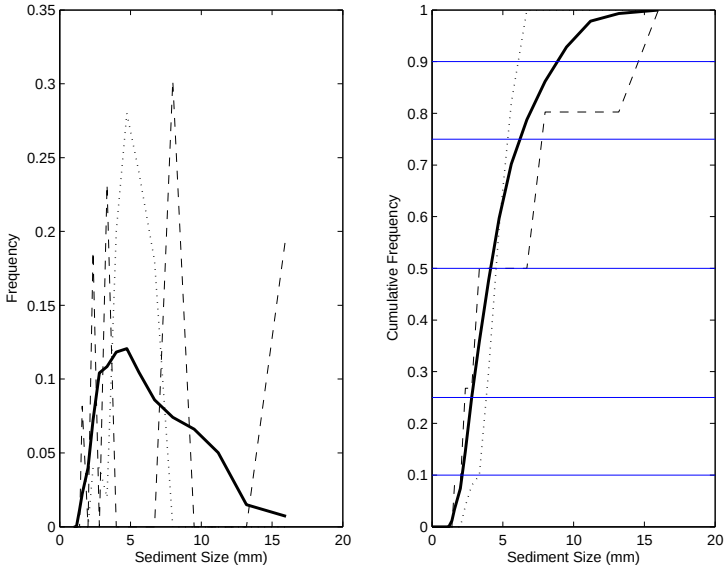

Fig. 4.3 *A Comparison of GSDs and cumulative GSDs obtained from sieving (solid line), and imaging the same sample (Figure 4.2). Dotted lines indicate the GSD derived using a linear least-squares and histogram approach; and dashed lines indicate the distribution obtained from a linear least-squares with non-negativity constraints approach. Horizontal lines indicate commonly used percentiles (10, 25, 50, 75 and 90).*

A very different class of approach is to arrive at the vector solution X using a least-squares approach, then to use X to compute a smooth probability density function (PDF) using a non-parametric kernel density estimation routine (otherwise known as a Parzen method), which takes the form:

$$p(\iota) = \frac{1}{NB} \sum_{i=1}^{N} \Gamma \left(\frac{\iota - \iota_i}{B} \right) \tag{4.2}$$

with kernel Γ, bandwidth B, and number of points N. The centre of the kernel is placed over every data point, and the influence of the datum is spread about its neighbourhood, depending on the shape of the kernel. The contribution of each datum is then summed to an overall estimate, thus removing the dependence on the end points of the bins. The kernel can take on several forms (similar to wavelets or digital filters). The bandwidth (or 'scaling factor') controls how far the probability mass is spread around a datum, thereby controlling the smoothness of the probability density estimate. In other words, replace each observation ι_i by a copy of the function Γ, shifted so that it is centred at ι_i, and scaled by a factor B. Kernel estimation is conducted using non-negativity constraints by provided a bounded support where only positive values can be recorded.

A lot of research has focussed on the optimal value for the bandwidth parameter [Sheather and Jones, 1991] since the quality of a kernel estimate generally depends less on the shape of the Γ than on the value of its bandwidth. In numerical trials it was found that the 'generalised cross entropy (GCE)' method of Botev [2006] to be most reliable, closely followed by the (computationally much simpler) 'rule-of-thumb' formula suggested by Bowman and Azzalini [1997]:

$$B = \left(\frac{4}{3N}\right)^{1/5} \sigma_X \tag{4.3}$$

where σ_X is the standard deviation of the histogram of X. Trials using different kernels on sample images in this study deemed a 'normal' or 'Gaussian' kernel to be suitable, given by [Bowman and Azzalini, 1997], given by:

$$\Gamma(\iota) = \frac{1}{\sigma_X \sqrt{2\pi}} \exp^{-\iota^2/2\sigma_X^2} \tag{4.4}$$

A non-parametric approach such as this is important because restricting an estimator to a certain parametric family can potentially miss significant features in the data. Thus, a kernel density estimate can be more effective than a parametric curve fit when the distribution is multimodal. The distribution estimated by the kernel density method may be seen in Figure 4.4 (dashed line) with reference to the sieved sample (solid line). The shapes closely agree, as do the percentiles in the cumulative distribution. Accordingly, the derived parameters from the distribution estimated by the kernel method are in better agreement with those derived from the sieved distribution, as detailed in Table 4.1, which shades the value in closest agreement with the actual value for each parameter. On this occasion, the kernel method performs better for size, sorting and kurtosis (but not for skewness, because it underestimates the coarse tail). Note that this sample was chosen at random: some fits are considerably better than this, and others marginally worse (see Figure 4.14 for a comparison of all samples used in this study).

4.4.1 *Autoregressive Techniques*

The autocorrelation function (r), and the Yule-Walker AR model (γ_o), may be classified broadly as 'autoregressive' statistics. This class of statistic is designed to uncover the nature and extent of serial correlation in data, or the tendency for successive values to be

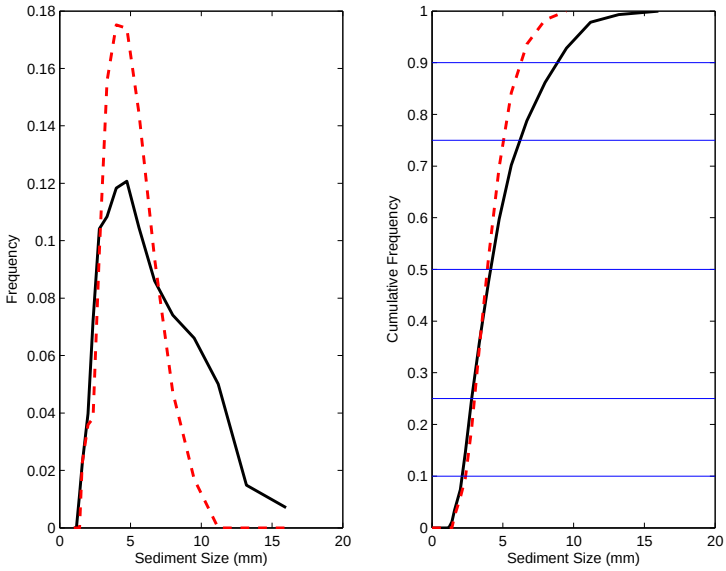

Fig. 4.4 *A Comparison of GSDs and cumulative GSDs obtained from sieving (solid line), and imaging the same sample (Figure 4.2). Dashed lines indicate the distribution obtained using a kernel density estimation approach on the linear least-squares solution vector. Horizontal lines indicate commonly used percentiles (10, 25, 50, 75 and 90).*

Tab. 4.1 *The parameters obtained from the sieving and imaging of the sample in Figure 4.2. D_{orig} denotes the sieved GSD; $D_{lsnonneg}$ denotes the least-squares with non-negativity GSD; D_{ls} denotes the least-squares GSD; and D_{kd} denotes the GSD obtained using the kernel density method. Shaded values represent those closest to reality (i.e. D_{orig})*

Parameter	$\mathbf{D}_{orig}$	$\mathbf{D}_{lsnonneg}$	$\mathbf{D}_{ls}$	$\mathbf{D}_{kd}$
$D_5(mm)$	1.64	1.41	2.39	1.86
$D_{10}(mm)$	2.15	2.046	3.36	2.331
$D_{16}(mm)$	2.39	2.07	3.45	2.60
$D_{25}(mm)$	2.793	2.331	3.825	3.007
$D_{50}(mm)$	4.91	3.398	4.53	3.89
$D_{75}(mm)$	6.24	7.775	5.32	5.07
$D_{84}(mm)$	7.60	13.77	5.69	5.7
$D_{90}(mm)$	8.90	14.6	6.09	6.3
$D_{95}(mm)$	10.1	15.26	6.22	7.18
D_{90}/D_{10}	2.9	3.79	1.58	2.7
D_{75}/D_{25}	2.23	3.33	1.39	1.69
$D_{90} - D_{10}(mm)$	4.09	5.72	1.95	3.99
$D_{75} - D_{25}(mm)$	3.45	5.44	1.49	2.06
Graphical sorting[1]	0.569	0.4350	0.7634	0.67
Graphical skewness[2]	0.2948	0.192	-0.2178	-0.0642
Graphical kurtosis[3]	0.598	1.1686	0.1293	0.289

Folk and Ward [1957] graphical measures, 1= $(\phi_{84} - \phi_{16})/4 + (\phi_{95} - \phi_5)/6.6$;
2= $(\phi_{16} + \phi_{84}) - 2(\phi_{50})/2(\phi_{84} - \phi_{16}) + (\phi_5 + \phi_{95}) - 2(\phi_{50})/2(\phi_{95} - \phi_5)$;
3=$(\phi_{95} - \phi_5)/(2.44(\phi_{75} - \phi_{25}))$

similar.

Kent et al. [2006] define spatial autocorrelation r as "... the tendency for random variables to co-vary as a function of their locations in space." Positive spatial autocorrelation is the tendency for objects closer together to be more similar than objects further apart. Taking image intensity as a random (spatial) variable, the extent to which information within images is independent may be quantified using an autocorrelation function. If values separated by a lag of l are similar, the array will have an autocorrelation coefficient r $\rightarrow$ 1, signifying serial dependence/correlation (Figure 4.5). If r $\rightarrow$ 0, the sequence is random or serially uncorrelated, and if the signal is periodic, so will the autocorrelation function be if the signal's period is covered by the number of lags over which the function is computed. For images of natural beds, pixel patches covering larger grains are more similar for a longer distance than pixel patches covering smaller grains. The spatial autocorrelation between an image and a copy at offset is given by [Davis, 1986]:

$$r = \frac{\left[\sum \left(I(x_i) - I(\bar{x})\right)\left(I(y_i) - I(\bar{y})\right)\right]}{\left[\left(\sqrt{\sum \left(I(x_i) - I(\bar{x})\right)^2}\right)\left(\sqrt{\sum \left(I(y_i) - I(\bar{y})\right)^2}\right)\right]} \tag{4.5}$$

where $I(x_i)$ and $I(y_i)$ are the greyscale intensities of each individual pixel in the corresponding positions in the two images, and $I(\bar{x})$ and $I(\bar{y})$ are the mean intensities.

Spatial autocorrelation as a function of incremental offset distance (lag) produces a curve: a correlogram. If the correlogram slope is relatively shallow, there is more similarity between consecutive values (Figure 4.5, panels a and b). Rubin [2004]'s method for calculation of the autocorrelation sequence was used with a modification, being one pre-processing step which rescales the image values to lie between 0 and 100 (rather than 0 and 255) and round these values to the nearest integer. This was found to enhance the differentiation between sizes by removing some short-wavelength noise in the images, thus removing the tendency for the correlogram to fluctuate around zero at larger offsets.

The Portmanteau statistic (also called the Q or Box-Pierce test) is a test for higher order serial correlation in residuals from a regression [Brockwell and Davis, n.d.], and is conventionally used to separate homoscedastic from heteroscedastic signals by testing for autocorrelation in the residuals from that regression. The regression is a 'self regression' of localised values in a sequence, testing the ability to predict the next few values in that

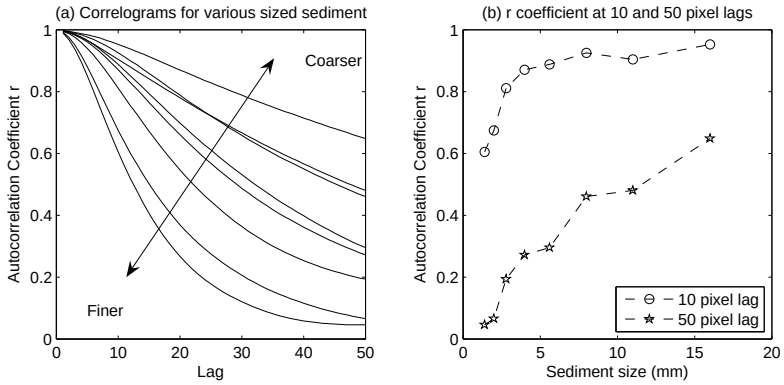

Fig. 4.5 *The autocorrelation (r) technique. Panel a (**left**)-correlograms for various sized sediments; panel b (**right**)-r coefficients associated with the 10^{th} and 50^{th} lags of the correlogram, for different sediment sizes.*

sequence. The residuals are the discrepancies between those values and the prediction, and instead of testing at each discrete lag, it tests over a number of lags (Figure 4.6). The statistic is given by:

$$Q_{LB} = \left[N(N+2) \sum_{l=1}^{L} \frac{r^2(l)}{N-l} \right] \tag{4.6}$$

where $r^2(l)$ is the squared autocorrelation coefficient at lag l (the coefficient is squared so the negative and positives do not cancel each other out), L is the number of lags (defined by the operator), and N is the sample size (number of pixels within the image). This definition is the standard Box-Pierce [Box and Pierce, 1970] test with the Ljung-Box [Ljung and Box, 1978] correction which adjusts the statistic by its asymptotic variance, bypassing problems associated with (potentially) small sample size. Q_{LB} at lags 1:L gives a sequence which increases in value as residuals in the input series become more independent, until a sill is reached where increasing lag does not produce a commensurate increase in independence (Figure 4.6). Here, the statistic is not used in its classical 'hypothesis testing' sense, rather as a signal generator which is sensitive to the degree of serial correlation in an image. If one takes the first derivative of an image, and vectorise it (stack successive columns of the image on top of one another to form an

array), it becomes suitable for analysis using the Portmanteau statistic. The first derivative is a proxy of the frequency of the image's singularity fronts, where the largest changes in intensity occur [Grazzini et al., 2007], i.e. at grain boundaries, thus enhancing the differences between the grains and gaps. Because the method tests for higher-order serial correlation, it requires far fewer offset lags than autocorrelation, thus aiding computational efficiency. Trials showed that the natural logarithm of sample size is an appropriate lag with which to calculate the Portmanteau sequence (Q_{LB}), so for the subaerial images used in this study, of dimensions 2048 × 1536, L=log(2048 × 1536)=15.

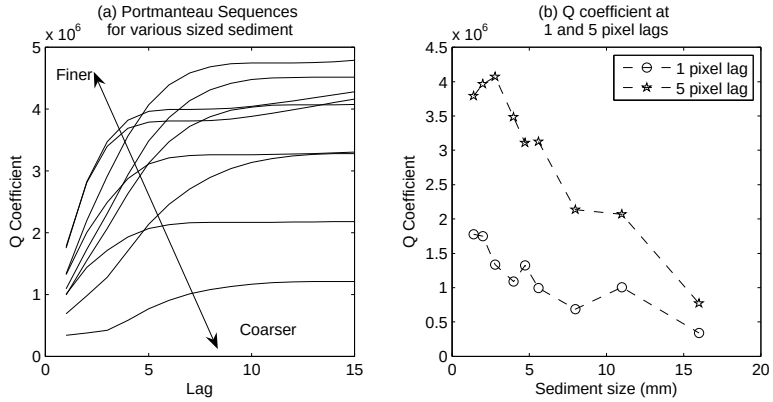

Fig. 4.6 *Portmanteau technique. Panel a (**left**)-portmanteau sequences for various sized sediments; and panel b (**right**)-Q coefficient at 1 and 5 pixel lags, as a function of sediment size.*

The Portmanteau sequence (Q_{LB}) may be interpreted as the degree to which values in any moving window can explain successive values beyond that window. This ability scores relatively low, is enhanced in highly autocorrelated signals, and therefore is typical of larger sediments (Figure 4.6). There is a strong linear relationship between values at sequence lag and sediment size (Figure 4.6).

The evolution of an autoregressive (AR) process can be described by a weighted sum of its previous values and a (white noise) error term. Forecasting is possible since at any point the value is linearly 'regressed' on previous values of itself to locally predict the next few values in the sequence [Brockwell and Davis, n.d.]. The size of that moving

window depends on the order of the model. The general form of an AR model is:

$$Y_t = \delta_{AR} + \varphi_1 Y_{t-1} + \varphi_2 Y_{t-2} + \ldots + \varphi_o Y_{t-o} + A_t \tag{4.7}$$

where Y_t is the time or spatial series, A_t is white noise, φ_o are the autoregressive coefficients, and $\delta_{AR} = (1 - \sum_{i=1}^{o} \varphi_i)\mu_Y$, with μ_Y as the mean and o as the (user defined) model order [Brockwell and Davis, n.d.].

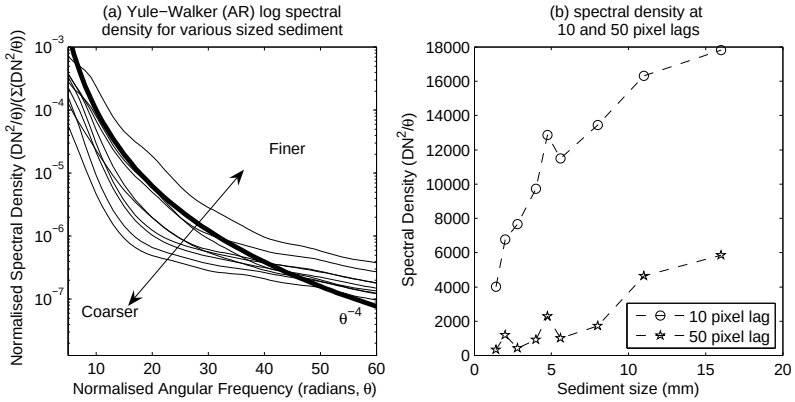

Fig. 4.7 *The AR-PSD technique. Panel a (**left**)-power spectral densities, in units of image intensity-squared per normalised angular frequency in radians (normalised so it sums to unity), for various sized sediments, calculated using an AR-model (γ_o), order 20. The sediment takes the general form θ^{-4}, shown as a heavy line; panel b (**right**)-spectral density associated with the 10^{th} and 50^{th} freqencies, for different sediment sizes.*

Power spectral density (PSD) is estimated using the Yule-Walker method, which, using a moving window, fits an autoregressive model to each successive portion of signal by minimising errors associated with extrapolation (in a simple least-squares sense; [Priestly, 1994]). The natural log transform of the PSD is sensitive to the size of grains in digital images (Figure 4.7). The Yule-Walker equation can be expressed as:

$$\gamma_o = \sum_{i=1}^{o} \varphi_k r_{y-i} + \sigma_A^2 + \delta_o \tag{4.8}$$

where r_y is the autocorrelation function of the input signal, φ_i are the autoregressive coefficients, σ_A is the standard deviation of the input error (noise), δ_o is the Kronecker delta function, and where o is the (user defined) order of the model, at any point

dictating how many previous values have an effect on the regression from the current window of values [Box and Jenkins, 1976]. Since the last part of the equation is ≥ 0 only when o=0, the Yule-Walker equation is usually solved as y+1 simultaneous equations of the form [Priestly, 1994]:

$$\begin{pmatrix} -\gamma_1 \\ -\gamma_2 \\ \vdots \\ -\gamma_y \end{pmatrix} = \begin{pmatrix} \gamma_0 & \gamma_1 & \cdots & \gamma_{y-1} & \varphi_1 \\ \gamma_1 & \gamma_0 & \cdots & \gamma_{y-2} & \varphi_2 \\ \vdots & \vdots & \ddots & \vdots & \vdots \\ \gamma_{y-1} & \gamma_{y-2} & \cdots & \gamma_0 & \varphi_y \end{pmatrix} \begin{pmatrix} \varphi_1 \\ \varphi_2 \\ \vdots \\ \varphi_y \end{pmatrix}$$

The Yule-Walker model is used as a parametric spectral estimation method, solved using Levinson-Durbin recursion [Kay, 1998] instead of a periodogram (calculated using a Fourier transform, thus decomposing the data into a regular trigonometrical series) because it produces a smoother power spectral density, and because order specification allows greater computational flexibility. In this study, the order of the autoregressive model used for images of natural sediments is o=20. The spectral density units are the squared magnitude of the frequency response of this model order [Kay, 1998].

The AR model (γ_o) signature may be interpreted thus: for images of natural sediments, pixel patches covering larger grains are more similar for a longer distance than pixel patches covering smaller grains, therefore power spectral density for any given frequency will generally be higher for images of smaller sediment, because there is more variance associated with that frequency (Figure 4.7). There is a strong correlation between percentiles of power spectral slope and sediment size (Figure 4.7).

4.4.2 *2D-FT Techniques*

'Texture' may be thought of as repetition of a basic structural pattern. In image processing these repetitive basic elements are known as 'texels', and it has been shown that 'texture' may be quantified statistically by using frequency transforms [Tuceryan and Jain, 1998]. These uncover the nature and separation of repeating patterns and texture within that image, represented in a space whose coordinate system has an interpretation closely related to characteristics of texture. Because the contents of the entire image are mapped as energies at all frequencies and orientations, angular and

radial bins in the Fourier domain detect and characterise image texture directionality and the rapidity of fluctuation [Davis, 1986]. Operating in the non-spatial domain, each Fourier coefficient depends on all pixel locations, thus enhancing the computational efficiency (without compromising the validity) of traditionally spatial operations such as the calculation of the variogram. In images of natural sediments, textural patterns are scale-dependent phenomena, requiring appropriate statistical techniques such as fractals. The type of Fourier transform applied on the images in this study is for an aperiodic, discrete signal, with a continuous spectrum given by the Fourier pair:

$$F(U,V) = \sum_{x=-\infty}^{\infty} \sum_{y=-\infty}^{\infty} I[x,y] \exp^{-j2\pi(U_x x_o + V_y y_o)} \tag{4.9}$$

$$I[x,y] = \frac{1}{UV} \int_0^U \int_0^V F(U,V) \exp^{j2\pi(U_x x_o + V_y y_o)} \tag{4.10}$$

where x_o and y_o are intervals in space between signal in the x and y directions. U and V are reciprocals of x_o and y_o ($U = 1/x_o$ and $V = 1/y_o$) and represent both sample rates in 2 directions, and also the period of the spectrum $F(U,V)$.

Semivariance is a measure of squared difference in DN (intensity) value between a pair of pixels located at a distance or lag, given by the classic equation in the spatial domain [Davis, 1986]:

$$\gamma(\mathbf{h}) = \frac{\left[E\left\{\left(I(x)+\mathbf{h}\right)_i, I(x_i)\right\}^2\right]}{2} \tag{4.11}$$

where the numerator is the mathematical expectation E of the quadratic increments of pixel pair $\{(I(x+\mathbf{h}))_i, I(x_i)\}$ values separated by distance $\mathbf{h}$, a vectorial function which varies with the modulus and angle of $\mathbf{h}$ between pixels $I(x+\mathbf{h})$ and I(x) [Gringarten and Deutsch, 2001]. Image detrending is a necessary pre-operation. Semivariance (γ) can be thought of as related to an inverse measure of spatial autocorrelation at specified location vector, at a certain lag in a given direction. A plot of semivariance (γ) as a function of lag distance is called a (semi-) variogram (Figure 4.8). The variogram has been used by researchers, for example, in the field of remote sensing to characterise textural properties of satellite imagery [Lark, 1996; Chica Olmo and Abarca Hernandez, 2000]. The use of the variogram for use on images of sediment is valid with respect to Tobler's Law [Kent et al., 2006] because the correlogram is positive for all lag distances.

Semivariance magnitude is binned at all frequencies and orientations. The variogram computation is performed using the algorithm detailed in Marcotte [1996], which uses a spectral rather than (traditional) spatial domain approach. This affords greater computational speed and efficiency, which is crucial in image processing where files are large and memory is at a premium. The complexity of operations is dictated by the number of pairs at all lags, ϖ, given by $\varpi = (2x-1) \times (2y-1) \times \log_2(2y-1)$ for an FT approach, and $\varpi = \frac{(x \times y)^2}{2}$ for a spatial approach, where $x \times y$ are the dimensions of the image. For example on a standard digital image of 1536×2048 pixels, this equates to 145 680 000 and 4 947 800 000 000 individual operations for spectral and spatial approaches respectively (the frequency approach is 'simpler', in terms of operations, by a factor of 3.4×10^4), with identical outputs. To avoid excessive mathematics here the variogram of a two-dimensional image using a spectral approach is defined by first defining a precursor, γ_p:

$$\gamma_p = \left[\frac{\widehat{F_c} \times F^* \times \widehat{F} - 2 \times F_c \times F}{N-2} \right] \tag{4.12}$$

where $\widehat{F_c}$ is the complex conjugate of $\widehat{F}$ and F_c is the complex conjugate of F; and where F, F^*, and $\widehat{F}$, are defined as the two-dimensional Fourier transforms of I, I^2, and I_d, respectively; I is an image of dimensions $x \times y$, I_d is an 'indicator' matrix of zeros of dimensions $x \times y$, and N is the number of pairs at all lags. The semivariance γ is then given by the two-dimensional inverse Fourier transform of γ_p, shifted so the zero frequency component is at the centre of the spectrum [Marcotte, 1996].

Images of larger grains have smaller mean semivariance values for a given lag than images of relatively small grains (Figure 4.8). Coarser sizes yield smaller semivariance values because the light-shadow pattern is larger, therefore the image's singularity fronts, where the largest changes in intensity occur, are larger. Images of smaller sediments yield larger semivariance values because the image intensities vary less as a vector function of lag than as a function of individual pixel values.

Modelling applications are facilitated if the theoretical variogram model of an image surface is known. As previously explained, semivariance quantifies the sum of squares differences between data separated by lag l. Semivariance between zero lag l_{C0}, and the lag at which semivariance does not increase with commensurate increase in lag (l_{CS}, the

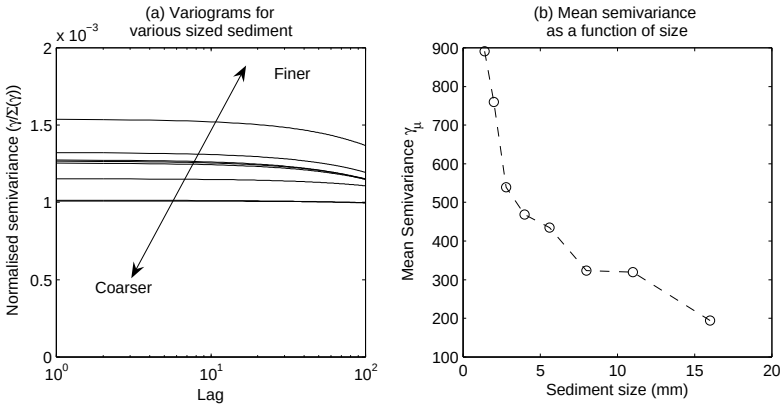

Fig. 4.8 *The variogram technique. Panel a (**left**)-semivariance (γ) sequences for various sized sediments, normalised so they sum to unity; and panel b (**right**)-mean semivariance (γ) as a function of sediment size.*

sill) may be classified using models with known mathematical properties, such as the spherical or exponential models [Gringarten and Deutsch, 2001]. It was found that digital images of natural sediments corresponded well with a spherical (also called 'circular') model which is given by:

$$\gamma_l = l_{C0} + l_{CS}(1.5(l/a) - 0.5(l/a)^3) \; 0 \leq l \leq a$$
$$0 \; if \; l = 0;$$
$$l_{C0} + l_{CS} \; otherwise$$

where a is a tuning parameter required for model fit. Figure 4.9 shows circular model fit (and associated values of a) to the empirical spatial semivariograms for different sized images of sediment (calibration images for 1, 2, 4.75, 11.2 and 16mm sediment, respectively). Note that for relatively large sediment ($\geq$ 4mm), the spherical model is cubic (i.e the second term, l/a^3, becomes dominant) where $l/a \approx 1$. In contrast, for relatively fine sediment ($\leq$ 4mm), the two terms (linear and cubic) are equally dominant since $l/a \neq 1$, meaning a composite linear least-squares fit is required.

Some natural surfaces have a quasi linear log-log power spectra, in units of distribution of power per unit frequency. Images of natural sediments are such surfaces, and ordinary

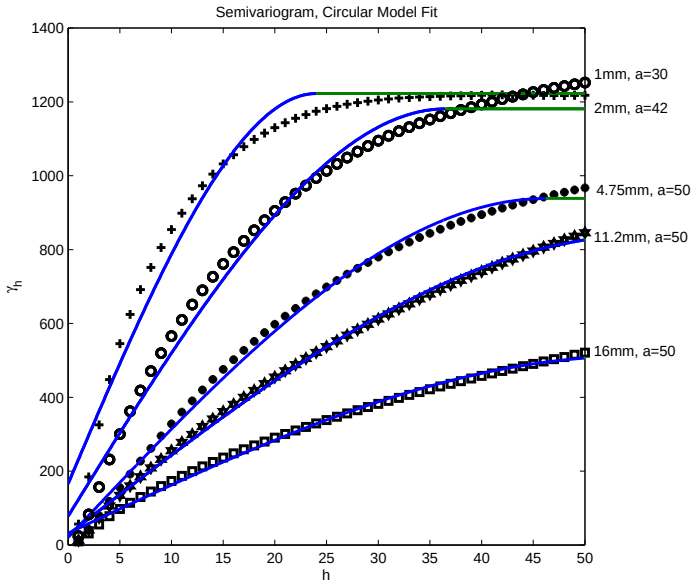

Fig. 4.9 *A theoretical circular model (solid lines) fitted to empirical semivariograms derived from digital images of various sized sediments (black markers).*

2D-FT power spectral estimation, when a log-log (magnitude-frequency) transform is applied, is sensitive to the size of sediments within images (Figure 4.10). The zero-frequency component of the image is shifted to the centre of the spectrum, and a two-dimensional discrete Fourier transform is carried out on the detrended zero shifted image. A linear least-squares polynomial is fit to the data in the log-log plot of the phase magnitude and frequency, which finds the average slope (Figure 4.10).

When spectral slopes are quasi linear, Voss [1988] demonstrated that the Hausdorff-Besicovitch or 'fractal' dimension (D_f) can be calculated from the log-log transform of the image's power spectrum. In such cases the fractal dimension has been shown to be an appropriate spectral estimator of texture [Chaudhuri and Sarkar, 1995]. The fractal dimension of the surface is given by 2 plus the slope of a regression line through the data [Smith et al., 1990; Bartlett, 1992]. Fractal surfaces have a dimension greater than the topological dimension of an image, which equals 2. Plotting the log of the magnitude in all directions against the log of the corresponding frequency [Richardson plot: Mandelbrot, 1983] yields a linear relationship from which the fractal (Hausdorff-Besicovitch) dimension is derived by the relationship:

$$D_f = 2 + \log(\frac{\Delta s}{\Delta \mathbf{f}}) \tag{4.13}$$

where s is the spectral density and $\mathbf{f}$ is frequency [Whalley and Orford, 1989]. The slope

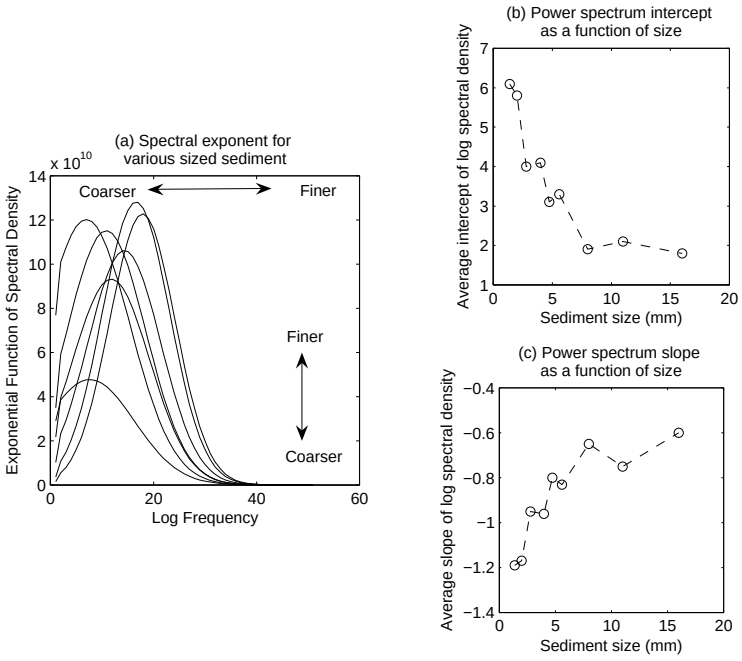

Fig. 4.10 *Panel a (**left**)-power spectral exponents for various sized sediments, in units of image intensity-squared per normalised angular frequency in radians, derived using ordinary 2D-FT (s) for various sediment sizes; panel b (**top right**)-mean log power spectral (s) slope as a function of sediment size; and panel c (**bottom right**)-log power spectral (s) intercept as a function of sediment size.*

($\Delta s/\Delta \mathbf{f}$, always negative), fractal dimension (D_f) and intercept of the spectrum are highly correlated to grain-size (Figure 4.10) : the higher the fractal dimension (D_f), the more variable or 'rugged' the grain surface, and the smaller the grain-size. The power spectrum is the Fourier transform of the autocorrelation function [Blackman and Tukey, 1958]. The fractal output may be interpreted thus: images of smaller grains have smaller scale invariance, or less self similarity in image intensity through the image, than images of larger grains. The variation of texture within the image, detected and quantified by its Fourier transform (F), has a scale dependency which may be characterised by its fractal dimension (D_f). Like the PSD estimation using the Yule-Walker (γ_o) technique, images of smaller sediment has larger energy associated with smaller frequencies than images of larger sediment (Figure 4.7).

4.5 *Field Methods and Calibration*

4.5.1 *Image Collection Guidelines*

With reference to Figure 4.11, the general procedure begins with a large sample of the parent material, which is manually sieved into size fractions (preferably at $\phi/4$). Samples

for calibration in the gravel size range have been collected according to the recommendations of Gale and Hoare [1992] for coarse clastic sampling, where ≥2 kg of material is believed sufficient for well sorted material up to 20mm diameter, where the largest stone is ≤5% of the total mass.

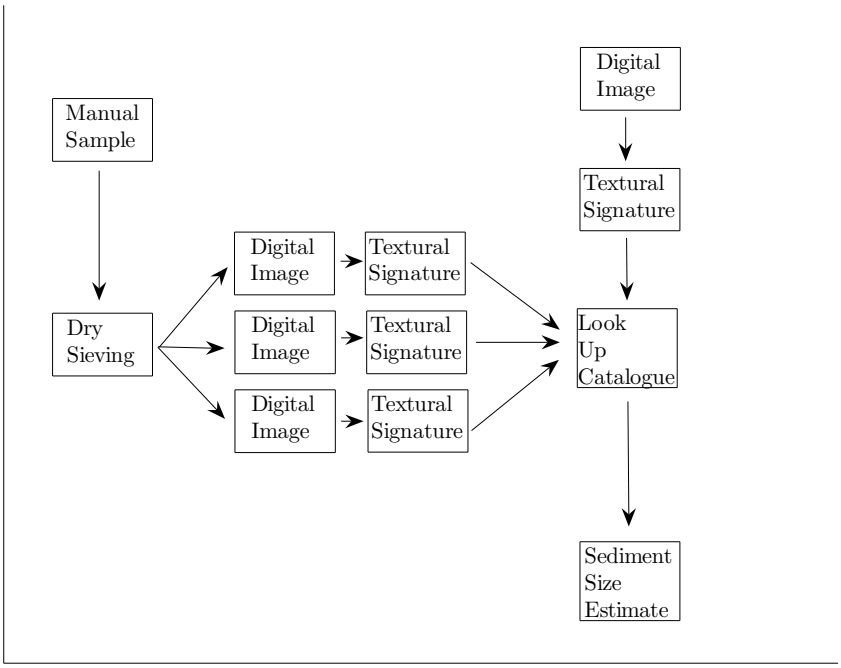

Fig. 4.11 *Schematic diagram of the stages involved in the 'look-up cataloguing' procedure.*

A digital image is then taken of each fraction, and a statistical procedure which is sensitive to the size of sediment on the greyscale complement of the image is then applied to the image. In this way a calibration 'catalogue' of numerical values for each sediment size is obtained. The collection of that image is crucial to the technique, and in the field, images of sediment are taken and then analysed using the same statistical technique used previously to create the calibration catalogue (Figure 4.11). Calibration and sample images have sufficient grains to have variation in colour and mineralogy, and images of grains have sufficient resolution so that the smallest grain in the image is larger than one pixel, in order to prevent aliasing problems (the largest grain-size likely to be encountered is smaller than the largest size catalogued by calibration to avoid numerical errors caused by linear extrapolation). Calibration ensures transferability to a range of sizes, shapes, lithologies and packing configurations and is carried out whenever

any of these changes significantly. The calibration is carried out again if camera type or settings are changed, or if sediment sizes fall out of the range of the sizes used for calibration. In general, this approach is designed to be site specific for the rapid quantification of sediment size across local space and/or time.

For coarse sand-gravel beds, a method has been designed which ensures that images are taken at a constant height above the surface. Using an off-the-shelf digital camera with 3.2 mega pixels, it was found that as a rule of thumb images should be taken at a height in centimetres equal to the largest likely encountered grain in millimetres. The camera's focal plane is parallel to the object (surface) plane, and the camera's settings are manually adjusted so the focal plane rests the same distance above the ground as the camera (in some cameras an automatic adjustment may be made). The problem of non-optimal exterior lighting suffered by thresholding techniques is overcome by incorporating lights into the camera's housing [Rubin et al., 2006; Barnard et al., 2007]. A constant illumination angle and magnitude should be maintained by ensuring the only light source is from the camera flash, thereby ensuring shadows are at a constant angle and shading magnitude, removing false intra grain edge noise and not biasing the statistic used. Items and markers are not placed inside the image. The camera's field of view was known, so the area represented by each image was also known, and this was held constant. Note that results are unaffected by variation caused by lens distortion, since the same distortion is within the calibration catalogue if the same camera and camera settings are used for both calibration and sampling. Images are inspected by eye for over-or under-exposure, or using a simple algorithm which flags images above and below thresholds of image 'noise' associated with exposure problems. The spatial heterogeneity of gravel sized sediment is likely to be greater than sand, and spatial averages of sediment size are strongly recommended [see Barnard et al., 2007]. The camera settings used in this study are detailed in Table 4.2.

The footprint of the image, in millimetres per pixel, may be found by:

$$p_{mm} = \frac{1}{\left(\frac{r}{f/r^2}\right)} \tag{4.14}$$

where f is the file size in bytes, and r is the resolution in dots-per-inch (dpi). Using this formula, the image collection technique outlined above with a resolution of

Tab. 4.2 *The same camera settings, detailed here, were used for all the images taken in this study*

Parameter	Value
area photographed	100 × 130mm
pixels	2048 × 1536
pixels per mm	15.54
exposure	1/60 seconds
focal length	17.4mm
flash	Yes
aperture	f/4.8

0.0788mm/pixel, which is, in terms of pixels per millimetre, equivalent to 12.68 times the required resolution the size of grains under scrutiny (≈1-20mm).

4.5.2 *LUC Size Outputs and Size Outputs from Sieving*

The size outputs from the traditional (three-dimensional) sieving method and the (two-dimensional) look-up catalogue technique are not directly comparable, which must be factored into sieve size - image size comparisons when differences exist. Imaged output cannot be directly compared to sieve data because a correction factor must first be applied, which requires both the intermediate and smallest axis diameter [Graham et al., 2005]. No image analysis routine can gratify the latter, and procedures based on the statistical attributes of whole images of course cannot provide either measure. A two-dimensional image may under represent larger grains whose primary axes are hidden; the image measures of size include the effects of overlapping imbricated grains. The image method is non-intrusive, therefore the spatial arrangement and packing configurations of all grains remain, and are destroyed by manual sampling. Sieved data output is usually mass-frequency rather than number-frequency. Conversion factors exist but require that all grains have the same shape. Sampling should also be carried out with care, for the contribution of subsurface particles to the sieved samples but not the imaged sediment may account for a certain amount of discrepancy. This is due to both human error, and the availability of adequate volume of material at point upon the surface. Sieving generally produces sizes which are underestimates of the sample, caused by intra-sieve sediment variability on the mesh, the aperture size of which is necessarily a 'lower bound'. Therefore larger clasts contribute weight to the proportion of the sample on the sieve which is then all counted as the lower bound size. This inherent

problem is due to the logarithmic spacing of sediment sizes: the problem is therefore neglible for sand and smaller gravels, but a potential problem for larger gravel sizes, as size spacing increases with sieve size [Ferguson and Paola, 1997]. As a consequence, the imaged size is consistently larger than the sieve data mean size, because large clasts resting on sieve meshes contribute weight and therefore relative proportionality, whereas in contrast all clasts within an image contribute to the size.

The numerical errors associated with the linear interpolation were found to be negligible. For example, unconstrained solution errors $[norm(\mathbf{b}X - C) - \mathbf{b}]$ or $[(\mathbf{b} - CX)^T \times (\mathbf{b} - CX) - \mathbf{b}]$, where C is the calibration catalogue, $\mathbf{b}$ is the vector input, and X is the output solution, were typically ≤ 0.0003 for the autocorrelation technique, which equates to a maximum 0.03% error at zero lag (and less than 0.01% elsewhere). Using the least-squares solution with non-negativity constraints, solution errors $[((\mathbf{b} - CX)^T \times (\mathbf{b} - CX) \geq 0) - \mathbf{b}]$, were typically less than 0.03, or a maximum of 3% at zero lag (and less than 1% elsewhere).

Rubin [2004]'s size 'distribution' of length m, which assigns a proportional weighting to each 'size' represented by the calibration, may yield an additional measure of size which is calculated as the sum of the product of each element of the 'distribution', $d_1 \ldots d_m$, and the corresponding size in millimetres, $D_1 \ldots D_k$, given as:

$$D_{GSD} = \sum_{m=1}^{k} d_k D_k \tag{4.15}$$

for example, $[0.25, 0.6, 0.15, 0]$, corresponding to sizes $[40, 20, 10, 5]$mm, yielding a 'distribution size' D_{GSD} of $[(0.25 \times 40) + (0.6 \times 20) + (0.15 \times 10) + (0 \times 5)] = 23.5$mm. The distribution may also be the solution to $\mathbf{b} \times X = C$ by Gaussian elimination, if the solutions are normalised so they sum to one. The size associated with the 'mode' of the distribution is 20mm. Of course, the more calibration images the better the size approximation, so sieving at $\phi/4$ and taking an image of each fraction is recommended.

Trials have shown that in practice there is little difference between the size values found using the two size measures, however on closer inspection there may be more tendency for the latter 'distribution' size to be more stable. This is because each value of the 'distribution' represents the proportion of non-negative least-squares variance, and the explained similarity attributable by the corresponding size fraction in the calibration

catalogue, therefore the size measure proposed above only accounts for the frequency of the size classes present in the image, and not those absent. By contrast, the grain-size array (X, from which the mean or median size is found) could contain negative elements, which is physically impossible (which is why a size distribution may not be obtained in this way by histogram binning obtained values into size classes). An additional (potential, and minor) problem with the ordinary least-squares method is as follows: because sizes may be found by linear interpolation at offset/frequencies which are not within the original calibration catalogue, there may be discrepancies associated with logarithmically spaced size classes. Using the ϕ scale sieve mesh diameters in the gravel range for calibration, the larger the sediment the greater the potential errors caused by linearly interpolating over logarithmically spaced classes.

4.6 *Validation*

A total of 181 samples were collected manually from Slapton, and two images taken of each before they were sieved into 17 classes in the $\phi/4$ size range between 1mm and 16mm. The graphical (Folk and Ward) mean of each sample was compared to the 'distribution mean size' derived from images of those samples. The images (1536 $\times$ 2048 pixels, 100 $\times$ 130 cm) used in this study were collected with a Pentax® Optio S30 3.2 mega pixel digital camera. Barnard et al. (2007) have recently shown that better size estimates are obtained if the size outputs from several images are averaged. In a similar vein, better size estimates were obtained by averaging over the values obtained from two different images and methods.

The results are summarised in Figure 4.12: close agreement is found even without averaging over several images (R^2=0.82-0.86, mean absolute deviation less than 1mm). The dashed lines indicate ±1mm from the sieved sizes (solid line)-the majority of samples lie less than 1mm from the solid line. These results are improved upon if averages from different techniques are taken (R^2=0.88-0.92). Accuracy was determined as the mean percentage deviation in imaged mean size from sieved mean size. Relative accuracy was determined as the ratio of accuracy achieved by a given method (or combination of methods) and that achieved by autocorrelation. Similarly, relative speed was judged as the ratio of the time taken for a computation (using Matlab® version 7,

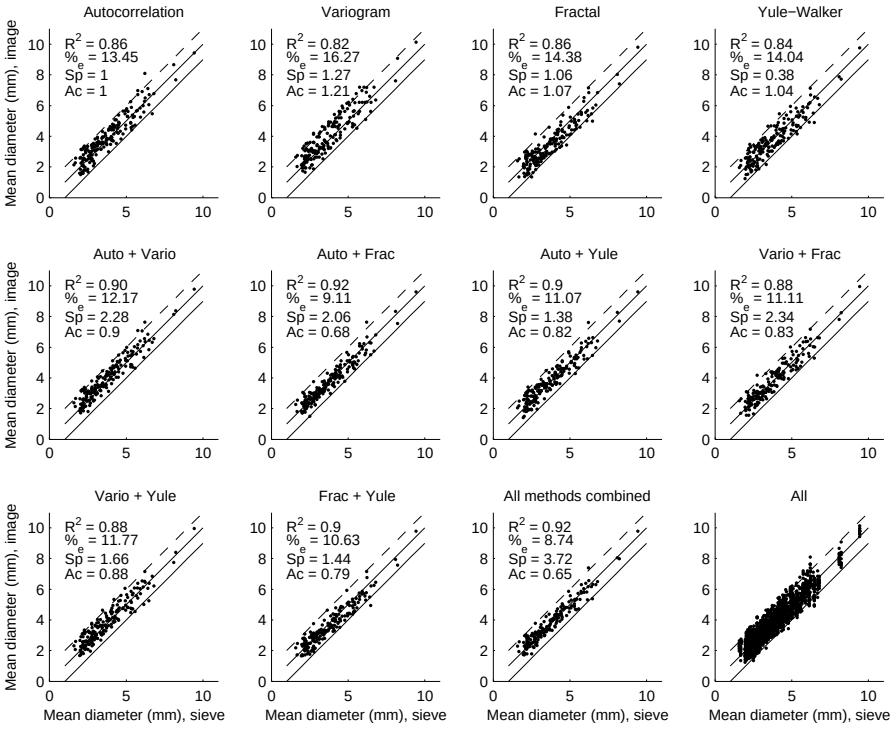

Fig. 4.12 *Comparison between average grain-size (mm) determined from 181 samples imaged twice, and the graphical mean size (mm) determined by traditional sieving for that sample. Dashed lines indicate +1 and-1mm departure in size. All values are Folk and Ward [1957] graphic mean.*

with a $\geq$2GHz dual processor) of a given method or combination of methods relative to the autocorrelation routine. Regression coefficients, accuracy, relative accuracy, and relative speed for each technique are scribed into the top left of the sub-panels in Figure 4.12. A schematic summarising the trade-off between relative speed and relative accuracy for the methods used in this chapter may be seen in Figure 4.13.

A further fifty-four sediment samples were collected from a range of sedimentary sub-environments on a gravel beach, and subsequently dried; imaged, and sieved at $\phi/4$ between 16mm and 1mm. Calibration catalogues were compiled for the autocorrelation and Yule-Walker techniques with images of sieved sediment in the corresponding sizes. Sieved distributions were analysed for various graphical measures of size, sorting, skewness and kurtosis, using graphical methods. Images were analysed using a variety of methods to obtain a GSD, and the same measures of size, sorting, skewness and kurtosis were obtained for each image.

In a series of trials it was found that optimal distribution fit was obtained by averaging the distributions obtained from the kernel method from histograms obtained, using both

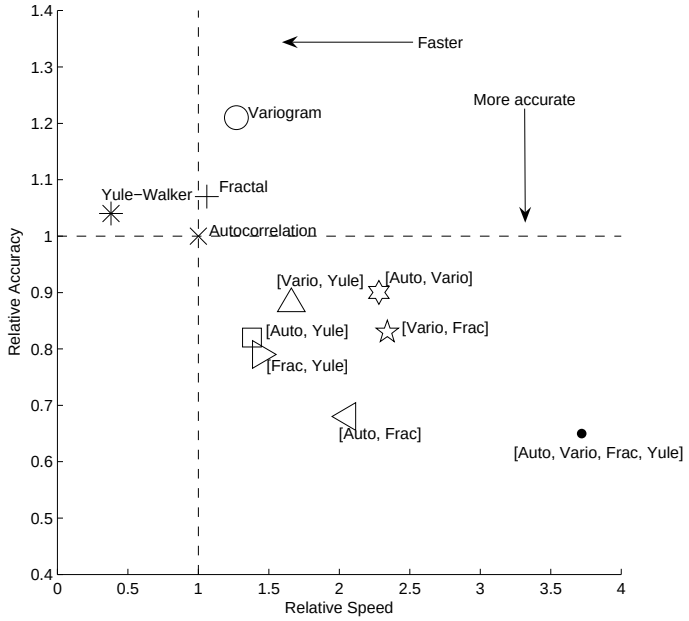

Fig. 4.13 *A schematic summarising the accuracy and speed of the techniques used in this study, based on 181 samples and relative to those obtained by the autocorrelation method. Speed increases right to left of the plot, and accuracy increases top to bottom.*

the autocorrelation and autoregressive techniques. Although this effectively doubles computation time, an 2MB image of 2048×1536 pixels will be processed in 1 min 40 sec. on a $\geq$ 1GHz processor, so batch processing images is still remarkably quick, and the averaging can significantly enhance estimated GSD precision.

The cumulative distributions obtained for each sieved sample were compared to those obtained by kernel density estimation on single images of the corresponding sample, using the 'hybrid' method explained above. Figure 4.14 shows that the cumulative distributions obtained are in close agreement (note that it is the cumulative distribution which is more important than the frequency distribution, since the primary aim of this exercise is to find close agreement in the percentiles for calculation of accurate graphical parameters).

Each derived parameter from image and sieving methods were analysed for dependence. Table 4.3 lists correlation coefficients (r) and squared correlation coefficients (R^2) for each parameter set, as well as the slope and intercept values of the linear least-squares best fit through the data. The statistical significance of the correlation coefficients were determined using a **t**-test to examine:

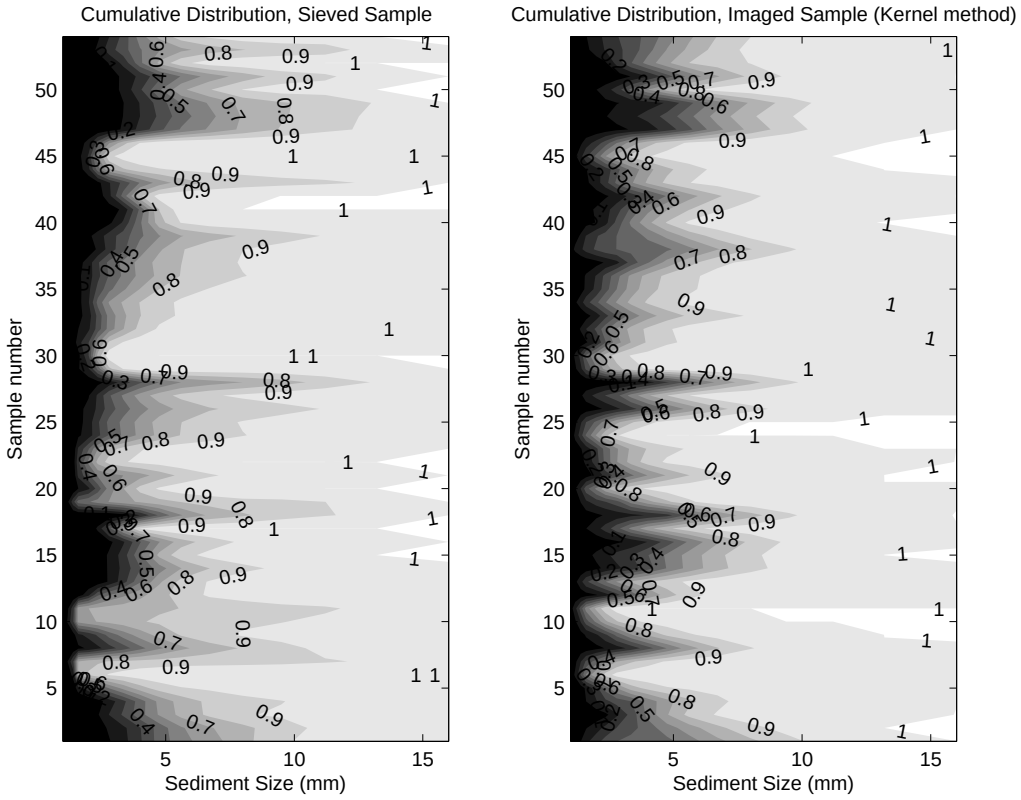

Fig. 4.14 *A Comparison of cumulative GSDs obtained from sieving (**left panel**), and imaging using the kernel density method (**right**), for all 54 samples. Values on the colourmaps represent contours for 'proportion finer' the corresponding size indicated by the bottom axes.*

$$H_0 : r = 0$$

$$H_1 : r \neq 0$$

That is, whether the observed sample correlation is significantly different from zero. A **t** test for significance of r is given by:

$$\mathbf{t} = \frac{r\sqrt{N-2}}{\sqrt{1-r^2}} \tag{4.16}$$

which has N-2 degrees of freedom, and which was tested at the α=0.05 (5%) level. With v_1=52, this means a critical value for **t** of 2.69. The results may be seen in Table 4.3: statistically significant dependencies were found for 20 out of 26 parameters tested.

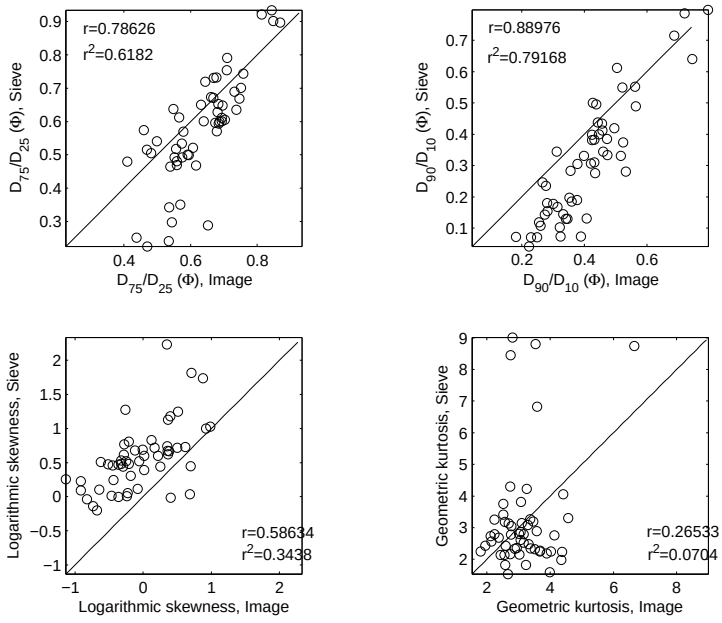

Fig. 4.15 *Measures of sorting, skewness and kurtosis.* ***Clockwise from top left****:* $D_{75}/D_{25}(\phi)$*;* $D_{90}/D_{10}(\phi)$*; Geometric kurtosis; and Logarithmic skewness.*

In addition, a one-way analysis of variance was carried out to determine the equivalency of each of the derived parameters obtained from the imaging and sieving methods. **F** was tested at the α=0.05 (5%) level with v_1=53 and v_2=53 (a critical value for **F** of 1.57). The results of this analysis may also be seen in Table 4.3: out of those 26 parameters tested, 22 had statistically significant equivalency in their means.

Table 4.3 shows that in general estimates for size and sorting are far better than those for skewness and kurtosis (indeed there are no significant relationships found for

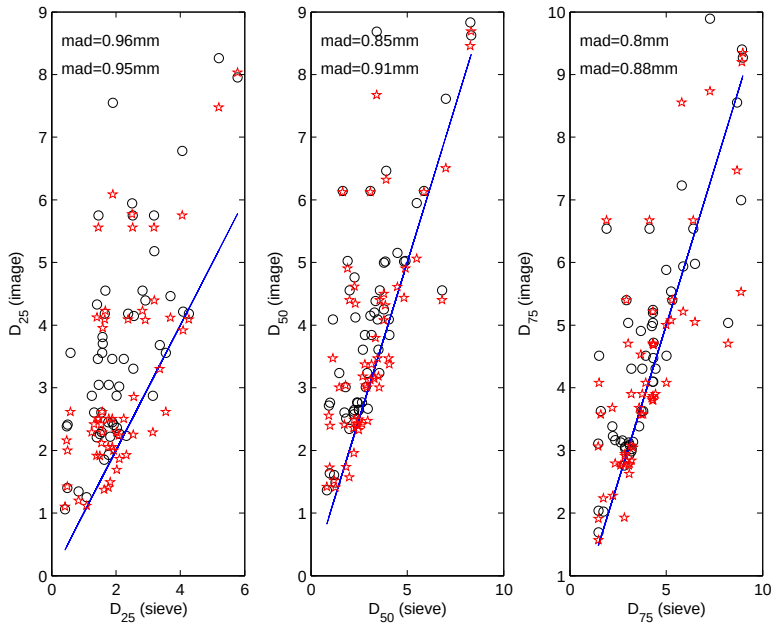

Fig. 4.16 *GSD percentiles of kernel image method compared to corresponding sieved distributions.* ***From left to right:*** *25^{th}, 50^{th} and 75^{th} percentiles for autocorrelation (circles) and Yule-Walker (stars) techniques. All values in mm.*

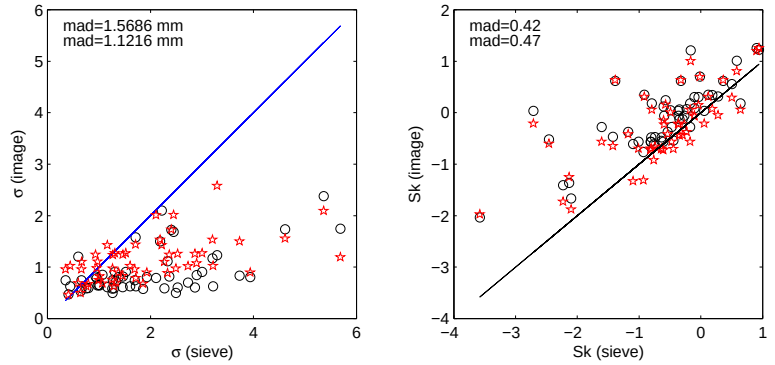

Fig. 4.17 *Geometric sorting (ϕ,* ***left****) and skewness (****right****) for the kernel image GSDs, compared to corresponding sieved distribution measures. Autocorrelation techniques shown as circles and Yule-Walker technique as stars.*

Tab. 4.3 ***F*** *(ratio between variation within and variance between samples); SST (total sum of squares variation); significance (T=true, F=false) at* α *=0.05 level; slope and intercept are the values for a linear equation through the data. Parameters shaded in black have significant correlation coefficients.*

	Parameter	F	SST	signif (F)	r	R^2	t(r)	signif(r)	slope	intercept
Arithmetic	mean	66.53	224.56	T	0.83	0.70	11.11	T	0.71	0.99
moments	sorting	31.73	32.79	T	0.17	0.03	1.31	F	0.21	1.67
	skewness	10.63	14.29	T	0.50	0.25	4.22	T	0.31	0.04
	kurtosis	89.59	90.56	T	0.10	0.01	0.74	F	0.03	3.12
Geometric	mean	36.82	202.46	T	0.90	0.81	15.29	T	0.75	0.67
moments	sorting	2.17	2.54	T	0.38	0.14	2.96	T	0.61	0.69
	skewness	10.20	15.55	T	0.58	0.34	5.21	T	0.62	-0.62
	kurtosis	156.45	168.30	T	0.26	0.07	1.98	F	0.58	1.39
Logarithmic	mean	4.28	15.67	T	0.85	0.72	11.75	T	0.81	-0.25
moments	sorting	1.42	1.75	F	0.42	0.18	3.41	T	0.63	0.30
Logarithmic	mean	41.15	226.80	T	0.90	0.81	15.31	T	0.77	0.58
Graphical	sorting	2.52	3.08	T	0.42	0.18	3.38	T	0.69	0.57
	skewness	1.12	1.15	F	0.16	0.02	1.21	F	0.17	-0.21
	kurtosis	6.87	7.06	T	-0.16	0.02	-1.20	F	-0.41	1.47
Graphical	mean	4.65	17.23	T	0.85	0.72	11.85	T	0.83	-0.21
	sorting	1.66	2.16	T	0.47	0.22	3.91	T	0.73	0.24
Percentiles	D10 (mm)	9.92	121.03	T	0.95	0.91	24.12	T	0.85	-0.20
	D50 (mm)	65.51	254.29	T	0.86	0.74	12.24	T	0.75	1.04
	D90 (mm)	245.22	401.64	T	0.62	0.38	5.75	T	0.52	3.21
	D10 (ϕ)	8.64	13.27	T	0.59	0.34	5.27	T	0.58	-1.10
	D50 (ϕ)	5.97	17.79	T	0.81	0.66	10.14	T	0.76	-0.47
	D90 (ϕ)	2.96	25.20	T	0.93	0.88	19.75	T	1.03	0.43
Ratios	(D90 / D10) (ϕ)	0.39	1.9	F	0.88	0.79	14.05	T	1.27	-0.21
and Ranges	(D90-D10) (ϕ)	12.18	15.82	T	0.47	0.22	3.93	T	0.77	0.59
	(D75 / D25) (ϕ)	0.54	1.42	F	0.78	0.61	9.17	T	1.21	-0.18
	(D75-D25) (ϕ)	8.07	8.95	T	0.31	0.09	2.38	F	0.53	0.54

kurtosis). These trends are underlined by Figure 4.15, which plots some of the better co-variations for given parameters on the 54 samples tested in this study. Note that the non-dimensionality of skewness and kurtosis dictates that logarithmic skewness and kurtosis have the same values as Geometric skewness and kurtosis. Simialrly, logarithmic graphical and graphical skewness and kurtosis are identical. Further comparisons are shown in Figures 4.16 and 4.17.

Following Sime and Ferguson [2003] and Graham et al. [2005], the performance of the 10^{th}, 50^{th} and 90^{th} percentiles estimated from the image distributions was assessed using mean error, mean-square error and irreducible random error, defined below where pv_{GSD} and pv_{LUC} denote the percentile value for the sieved and imaged distribution (in ψ units, or-ϕ), respectively, and N is the sample size (number of images multiplied by the number of percentiles tested):

$$\rho_e = 1/N \sum (pv_{GSD} - pv_{LUC})$$
$$\overline{e}^2 = 1/N \sum (pv_{GSD} - pv_{LUC})^2$$
$$e^2 = \overline{e}^2 - \rho_e^2$$

which yielded values of 0.2097, 0.1940, and 0.15 ψ respectively. The irreducible error is greater than the values quoted by Graham et al. [2005] (0.0691-0.089 ψ), but smaller than those quoted by Sime and Ferguson [2003] (0.253-0.26 ψ), in their studies utilising image object detection algorithms on much larger gravels.

The best available commercial package for the estimation of grain-size distributions from digital images of sediment is the 'Digital Gravelometer'© detailed by Graham et al. [2005]. The package uses sophisticated image processing to segment grains out of an image, and returns the grain-size distribution based on the area of pixels represented by each segmented grain in a calibrated image. Calibration is required of the user for each image so it is not a completely automated procedure. However, once images are loaded and calibrated (one-by-one), actual processing time is comparable to the automated statistically-based techniques described in this chapter (0.75-1.5 minutes per image). As a final validative procedure, ten samples were taken at random from the data-set, and the grain-size distributions obtained by the three methods (sieving, automated imaging using look-up catalogues, and the 'Digital Gravelometer'©) were

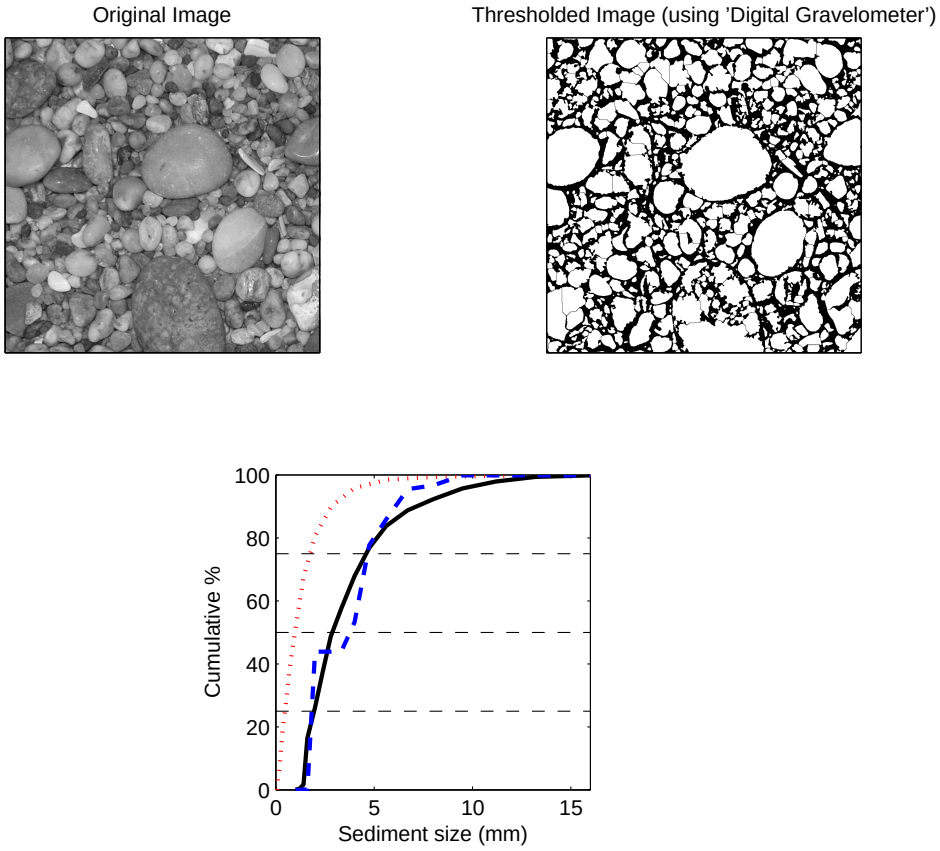

Fig. 4.18 *An example comparison between the distributions obtained from sieving (bottom panel, solid black line), the look-up catalogue imaging method (dashed blue line), and the current 'best available' commercial package (Digital Gravelometer©, Graham et al. [2005]) for grain-size estimation from digital images of sediment (dotted red line). The image used may be seen in the top left panel, and the corresponding thresholded image using the Digital Gravelometer© is shown in the top right panel.*

compared using three percentiles (25, 50 and 75) and two parameters ($D_{75} - D_{25}$ and D_{75}/D_{25}). The 'Digital Gravelometer'© was used under a 21-day trial licence agreement and the image collection and analysis guidelines detailed in the program's documentation (see http://www.sedimetrics.com/index.html) were closely followed. An example output is seen in Figure 4.18: note that the segmentation procedure has tended to split individual grains up into several smaller grains. This is typical of the routine on these fine gravels: it is very difficult to segment small grains which vary in colour and shape using automated segmentation principles such as these. The consequence for this study is that grain-size distributions and estimates of mean size are always finer than reality, an observation which motivated the development of the new suite of techniques detailed in this chapter. The look-up catalogue out-perfomed the Digital Gravelometer© on these images, having a closer value to reality on 44 out of 50 comparisons (Table 4.4). On images such as those used in this study, the best available commercial package performed poorly, consistently producing under-estimates of the distributions and associated parameters and percentiles.

Tab. 4.4 *Ten sieved samples chosen at random from a much larger data set were compared to automated image analysis of digital stills of those samples (LUC image processing, 'Digital Gravelometer'©). Five parameters were compared for the ten samples using the three methods: the value closest to reality (sieved) is shaded in black. The LUC method came closest 44 times out of 50 comparsions.*

Sample	$\mathbf{D}_{25}(mm)$	$\mathbf{D}_{50}(mm)$	$\mathbf{D}_{75}(mm)$	$\mathbf{D}_{75} - D_{25}(mm)$	$\mathbf{D}_{75}/D_{25}$
1	1.41 (**1.70**, 0.52)	1.56 (2.20, **0.96**)	2.00 (2.89, **1.61**)	0.59 (1.18, **1.08**)	1.42 (**1.69**, 3.09)
2	1.85 (**1.95**, 0.47)	2.84 (**3.54**, 0.96)	4.54 (**4.68**, 1.75)	2.68 (**2.72**, 1.28)	2.44 (**2.39**, 3.73)
3	1.95 (**2.45**, 0.42)	2.65 (**2.89**, 0.91)	3.34 (**3.78**, 1.81)	1.38 (1.33, **1.38**)	1.70 (**1.54**, 4.29)
4	4.56 (**2.65**, 0.41)	8.09 (**5.67**, 0.89)	9.45 (**8.57**, 1.68)	4.89 (**5.91**, 1.26)	2.07 (**3.22**, 4.07)
5	3.65 (**3.04**, 0.48)	5.86 (**4.69**, 1.01)	8.76 (**8.72**, 1.79)	5.10 (**5.68**, 1.31)	2.39 (**2.86**, 3.66)
6	4.21 (**1.81**, 0.51)	7.24 (**4.46**, 1.02)	8.91 (**6.07**, 1.71)	4.70 (**4.26**, 1.21)	2.11 (**3.35**, 3.37)
7	3.17 (**2.37**, 0.47)	4.86 (**4.09**, 0.98)	7.07 (**7.19**, 1.79)	3.89 (**4.81**, 1.32)	2.22 (**3.03**, 3.81)
8	2.62 (**3.92**, 0.56)	5.23 (**5.09**, 1.02)	8.53 (**8.05**, 1.69)	5.91 (**4.13**, 1.13)	3.25 (2.05, **3.00**)
9	4.09 (**2.65**, 0.62)	6.46 (**4.84**, 1.14)	8.61 (**8.66**, 1.91)	4.51 (**6.01**, 1.28)	2.10 (3.25, **3.06**)
10	3.06 (**2.51**, 0.49)	4.98 (**4.17**, 0.99)	6.80 (**6.52**, 1.75)	3.74 (**4.00**, 1.25)	2.22 (**2.59**, 3.52)

4.7 *Discussion*

Currently the major disadvantage of an LUC approach to grain-size from digital images is that it is not transferable between sites unless a calibration is performed which accounts for potentially significant variations in size range, colour/mineralogy, etc. The

techniques outlined in this paper potentially allow the quicker construction of a more robust calibration catalogue when so desired. Thresholding-segmentation techniques will still be an attractive option for sedimentologists working in areas where repeat-surveying is not required, and/or where few samples ($\leq$100) from that environment are needed.

However, a key point is that unless a threshold-segmentation method perfectly identifies the perimeters of each individual grain, it will disaggregate some, and aggregate others. Measures of mean/median size from the resulting size-mass distribution are still a function of the random false aggregation or disaggregation of grains within the image, but if the effects aggregation and disaggregation are equal, the mean size is a good approximation of the truth. Segmentation-thresholding techniques currently work less well for sand sized sediment as opposed to gravel perhaps because grain aggregation becomes more common than disaggregation, thus mean/median sizes are usually over-estimates. The fact that images of natural sediment beds have fractal scaling is a potentially important finding for developments in segmentation-thresholding of individual grains. The sum length of perimeter in an image of natural grains is related to some power of the average area (that power being the grain's fractal dimension), so relatively small reductions in area cause disproportionately large increases in sum perimeter length. That the length of perimeter which must be successfully segmented in an image of natural grains increases as some power of grain area (thus diameter holding shape constant), and because current thresholding techniques are not perfect, collectively mean that the number of misidentifications increases disproportionately with reducing grain-size. The above implies that there may be some practical lower limits to the size of material successfully identified by application of segmentation-threshold methods, and that lower limit is considerably higher than that currently for an LUC approach.

It is important to remember that grain-size derived from sieving and from an LUC method are unlikely to be equivalent because of the two-dimensional nature of the image, so better calibrations may be made by point-counts of grain in images (e.g. Barnard et al., 2007). A test was performed to see whether the fractal nature of images is dependent on the method employed to calculate the fractal dimension. Remembering that D_f is inversely proportional to sediment size (in mm), it was suspected that fractal dimensions found for coarser sediments using 2D-FT were over-estimated (larger) because of the 'hiding' of portions of the larger grains within the three-dimensional fabric of the

sediment bed, both within mixed beds and calibration images, using the 2D-FT (F) method. This causes larger sediments to plot in fractal space as finer than they are in reality. Using this method, coarser sediments should differentiate from finer sediments by more shallow slopes: spectral densities associated with coarser sediments are therefore either higher at low frequencies, or lower at high frequencies, than they ought to be. This may be because spectral densities are measured in units of squared intensity, whereas in reality the importance of absolute intensity magnitude is of subordinate relevance to relative intensity magnitude across local space as a function of frequency. In addition, spectra contain directional information which may complicate the estimation of fractal dimension. A fractal estimation technique was sought which is less sensitive to absolute magnitude of image intensity at varying frequencies, more sensitive to the general shape of the intensity trace through images of sediment, and non-directional.

The classic approach is to calculate D_f by 'chord fitting' by measuring the length of data with different sized chords, based on the notion that the distance measured will depend on the size of the chord used [Mandelbrot, 1983 cites the classic case of measuring the length of the UK coastline with different sized rulers]. This, where $\otimes$ is the number of times a measurement is taken (or the number of 'rulers' used) and $\oslash$ is the length of chord used to measure the distance (or the ruler length), may be expressed as:

$$D_f = \frac{\log \otimes}{\log(1/\oslash)} \tag{4.17}$$

Morphological opening, using kernel operators (structure functions) of differing lengths, was applied to images representing different sized sediments. A linear structure function applied to an image preserves regions which have a similar shape to that function, whilst destroying regions which do not [Radhakrishnan and Dinesh, 2006]. As the length of that function increases, less image detail is preserved after the operation. Figure 4.19 (panels *a*, *b* and *c*) shows the progressive loss of detail (smoothing) when structure functions of increasing length (5, 50, and 100 pixels respectively) are applied to an image of 1.4mm sediment. The details of the sediment are progressively missed, tantamount to 'removing objects' from the data stream, and analogous to the lengthening of the ruler with which the 'distance' covered by the data is measured. Figure 4.19, panel *d*, shows this effect on a short (400 pixel) section of data, with the same 5, 50, and 100 pixel structure functions. Sections of images of finer sediment contain more detail than

corresponding sections of images of coarser sediments: the effect of removing objects by morphological opening is therefore discordant, and a function of sediment size within the image (Figure 4.19, panel *e*). There is therefore an inverse relationship between sediment size and slope of the number of objects removed with increasing structure function length. This is because coarser sediments are more similar for a longer distance, therefore there are more pixel regions of similar shape to that function, so increasing structure function length removes fewer objects (Figure 4.19, panel *e*).

Fractal dimensions for this linear relationship were derived using equation 4.17, by dividing the slope of the log regression line through the data ($\log \otimes$) by the reciprocal of the log-ratio between the original image and the image after application of 100 structure functions of increasing length ($1/\oslash$). These are shown in Figure 4.19, panel *f*, and provide circumstantial support to the notion that fractal dimensions calculated using a 2D-FT method, whilst still showing the inverse trend with sediment size consistent with theory, are over estimated. This may be because spectral approaches are more sensitive to the hiding of primary axes of coarse sediments within the three-dimensional fabric of the bed, or because spectra contain directional information which may complicate estimation of D_f [Outcalt and Melton, 1992]. It may also be the reason why differentiation of sediment size on a log-log power spectral frequency plot is more difficult. The use of the classic chord-fitting approach is more intuitive in a fractal sense because as detail is successively removed, data 'length' must decrease as the ruler size increases, therefore very coarse sediments, which are more similar for a longer distance, must have a fractal dimension with a much smaller increment, a notion which resonates powerfully with spatial autocorrelation. Thus, although the spectral techniques used in this study performed well in terms of sediment size accuracy (see Figure 4.12), care may need to be taken when applying to certain sedimentological research applications. Now a linear relationship has been established between fractal dimension and sediment size within a digital image, it should possible to generate random autocorrelated surfaces with the same statistical properties, for use in sediment transport modelling and sedimentation simulations.

As previously shown, the sedimentary LUC technique depends on solving an under-determined system of equations. Conversely, where there are more equations than unknowns the system is said to be over-determined, and no exact solution can be found.

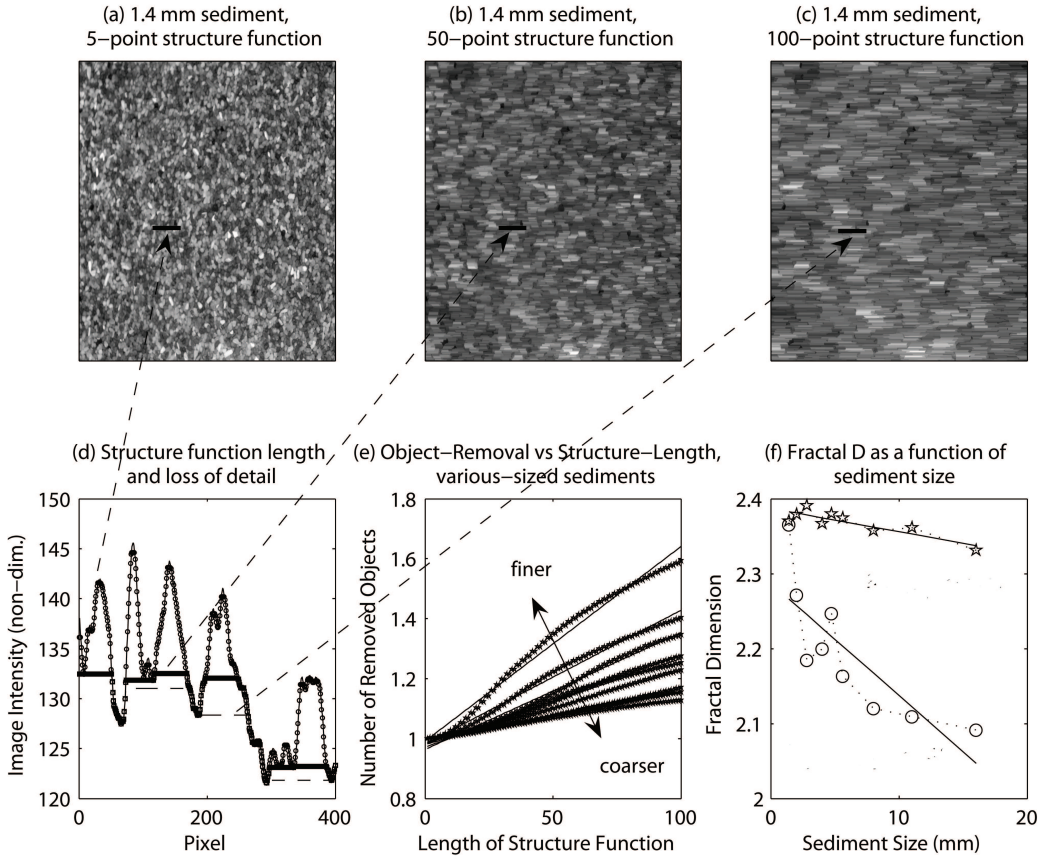

Fig. 4.19 *The Fractal Nature of Images of Sediment. Panels a to c: 1.4mm sediment after application of morphological opening operations (5, 50 and 100 pixel linear structure functions, respectively). Panels d and e: associated loss of detail in the resulting intensity-trace, and the relationship between structure function length and loss of detail for various sized sediments. Panel f: comparison between fractal dimensions estimated using the 2D-FT and chord-fitting methods.*

Graphically speaking, any method for obtaining the solution using the least-squares principle says that one should take the line through the data which minimisies the sum of squared errors, but the solution may not lie exactly on an interpolated line through the points representing the real solution. If one should plot calibration values $\mathbf{a}_n$, plus the lines representing the least-squares 'solution' ι_m both as a function of computed signature $\mathbf{b}_n$, one can tell if the system of linear equations are under-determined (thus a solution is possible) if the calibration values lie on the solution lines, and see a trace of the knowns versus unknowns through the linear system. This is illustrated in Figure 4.20 for the same sample image solved using Gaussian elimination for outputs of four different methods, and for four different sediment sizes.

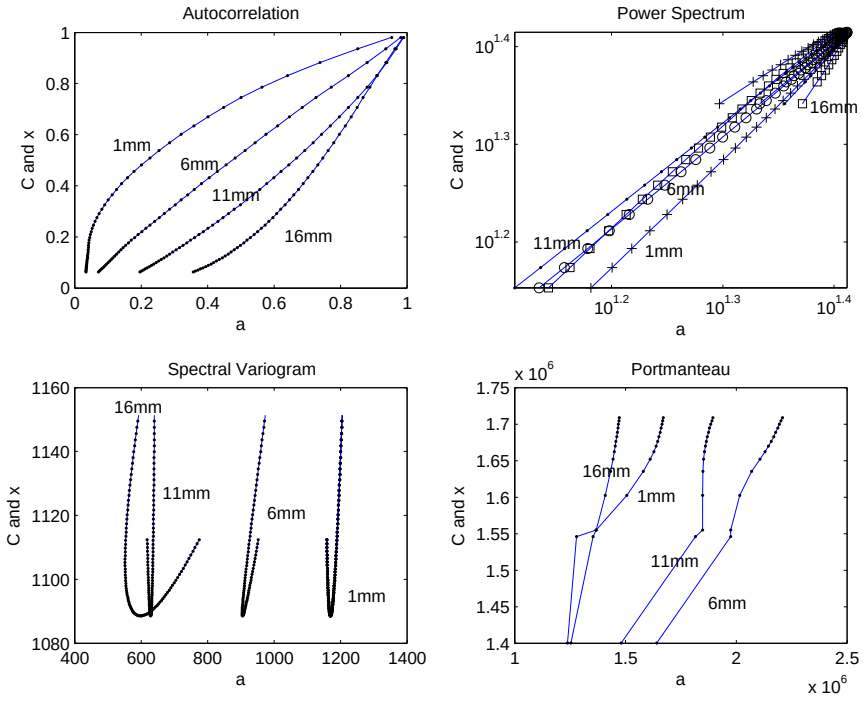

Fig. 4.20 *The linear system of equations in sedimentary LUC is under-determined, thus a solution is always found. Coefficients are marked by black dots, and their solutions marked as blue lines. Four methods are shown, for four different sample sizes in the calibration catalogue.*

4.8 Summary

(i) This study extends the image collection methodology proposed by Rubin [2004] and Rubin et al. [2006] for use on larger sediment sizes (coarse sand to pebbles). Importantly then, sizing from images is now possible in the full range from fine sands to very coarse gravels. The algorithms of Rubin [2004] have been improved, and a method proposed and validated for use on coarse grained sediment.

(ii) Four new numerical methods are introduced: the 2D-FT algorithm has been applied to images for derivation of variograms, power spectra and fractal dimensions, and the remaining numerical procedure is an autoregressive model. These techniques have been evaluated.

(iii) Rubin [2004]'s method has been used here for calculation of the autocorrelation sequence with a modification to enhance the differentiation between sizes by removing some short wavelength noise in the images, thus removing the tendency for the correlogram to fluctuate around zero at larger offsets.

(iv) It was found that the power spectral density of a digital image of sediment takes the general form θ^{-4}, where θ is normalised angular frequency in radians. The Fourier analysis of an image can detect and characterise image texture directionality, which may have implications in later studies for quantifying sediment shape and orientation.

(v) The fractal dimension of an image is a sensitive indicator of the size of particles in that image. Fractal dimensions found for coarser sediments using 2D-FT were over-estimated perhaps because of the 'hiding' of portions of the larger grains within the fabric of the sediment bed. A classic chord-fitting approach using morphological structure functions was more suitable. When using spectral techniques, care may need to be taken when applying to certain sedimentological research applications.

(vi) Digital images of natural sediments corresponded well with a spherical semivariogram model. For relatively large sediment ($\geq$ 4mm), the spherical model is cubic and for relatively fine sediment ($\leq$ 4mm), a composite linear least-squares

fit is required. This information could be useful for simple grain surface simulations in sediment transport modelling.

(vii) A better size estimate was obtained by averaging over the values obtained from two or more methods. The trade-off between method accuracy and method speed is discussed and quantified. The procedure was validated by comparing the 'distribution mean size' obtained from the image routine with mean size as determined by manually sieving at $\phi/4$, for 181 sieved and imaged samples.

(viii) A new technique has been proposed for the estimation of the GSD from a digital image of sediment. This method, based on non-parametric kernel density estimation, has been shown here to give more realistic estimates of GSDs of coarse sand-gravel sediments, as compared to sieving, than previously published methods [Rubin, 2004]. In turn, derived graphical percentiles from the cumulative distribution have allowed better approximations to sorting and skewness. Statistically significant dependencies were found for 20 out of 26 parameters tested, using 54 sediment samples. The percentile errors are better or at least comparable to previous published studies using different image processing techniques on larger grain-sizes. This new technique performed better than previous distribution estimation techniques, and better than the best commercially available package for grain-size distribution estimation from digital images of sediment, as compared to sieving.

(ix) Despite the theoretical difficulties in comparing GSDs obtained from two-dimensional images with GSDs obtained from sieving [see Sime and Ferguson, 2003 and Graham et al., 2005 for a discussion], these results are very encouraging. Estimates obtained using graphical methods for mean and sorting are good, and those obtained for skewness are adequate for most sedimentological purposes. Kurtosis cannot be quantified well, however this is a relatively unused parameter in sedimentology since it is very sensitive to small variations in a GSD.

5 MORPHO-SEDIMENTARY DYNAMICS OVER THE SEMI-DIURNAL TIDAL CYCLE

Good grief! The real waves look and act nothing like the neat ones that endlessly roll down the wave channel or march across the blackboard in orderly equations ...
should we slink back inside our reliable equations and brood over the inconsistencies of nature?
Never! Instead we must become outdoor wave researchers. It means being wet, salty, cold - and confused.

Willard Bascom, 1980. Waves and Beaches.

5.1 *Introduction*

Reflective beaches such as those composed of gravel are typically two-dimensional, but dominated by ephemeral secondary morphological features. Absolute morphological change appears to be larger on coarse grained beaches than on sand beaches over comparable timescales, even under low energy conditions [Van Wellen et al., 2000; Kulkarni et al., 2004; Austin and Masselink, 2006*a*; Horn and Li, 2006]. The step and berm (Figure 5.1) are common features on such reflective beaches [Bauer and Allen, 1995], and dominate the morphodynamics of those beaches. However, it is unclear the extent to which secondary morphological features have signature sedimentological responses, and if so, whether these exert some feedback-control over the development and morphometrics of these forms.

The dynamics of berms are relatively well documented, and it appears that on gravel beaches their development is explained, at least partially under good supply conditions and a range of sediment sizes, by a combination of highly asymmetric (onshore directed) swash motions, in turn partly influenced by significant infiltration at the landward extremities of swash cycles. This has been invoked to explain a lens of sediment pushed

onshore over tidal cycles through cut-and-fill berm building [Eriksen, 1970; Waddell, 1976; Horn et al., 2003; Austin and Masselink, 2006*b*; Weir et al., 2006], and is elaborated upon further in chapter 2.

The presence of the step imposes a steep hydrodynamic gradient across the nearshore which controls wave breaking. In chapter 2, the beach step has been considered analogous to a breakpoint bar common to sand beaches, which would imply it was a region of on/offshore sediment convergence. As well as controlling wave breaking, the importance of the step lies in the fact that it is a beach protective feature, locally steepening the active beachface and thus maintaining reflectivity during high waves [Hughes and Cowell, 1987]. It is able to do this because it is remarkably responsive to the semi-diurnal tidal cycle [Miller and Ziegler, 1958; Strahler, 1966]. Finally, because of the presence of the step, the beachface is more hazardous for bathers at high tide.

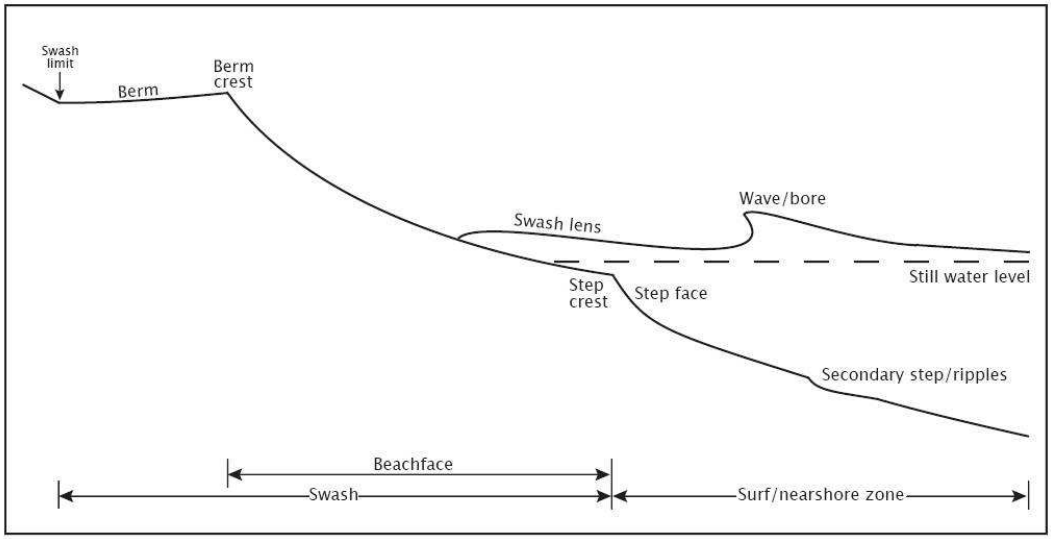

Fig. 5.1 *Schematic of the nearshore region on a pure gravel beach such as Slapton, including terminology used here and elsewhere.*

The lack of previous studies into beach step dynamics belittles its importance, and belies the fact that it is an interesting case study for coarse-grain beach

morpho-sedimentary-dynamics. This chapter reports on a series of detailed field experiments measuring hydrodynamic forcing, morphological and sedimentological change, and sediment transport. The formation of the beach step has provided an interesting problem for past researchers, and several theories have arisen which attempt to explain its formation; these can be separated into two groups: (1) those associated with sediment convergence (accretionary evolution); and (2) those linked to the formation of a backwash vortex. Miller and Ziegler [1958] and Strahler [1966] argue that the step is an accretionary feature formed by the convergence of sediment at the foreshore base (i.e. the incoming wave deposits sediment at the step upon breaking, and the backwash draws sediment down-slope). This also accounts for some of the observed coarsening of the sediments at the step, since wave breaking will remove finer fractions preferentially, leaving only the coarse fraction. The alternative explanation for step formation is the backwash vortex [Matsunaga and Honji, 1980, 1983; Takeda and Sunamara, 1983]. Flow separation during the backwash creates supercritical flow and vortex formation, whereby seawards flow at the base of the step sustains the step face through avalanching. The flow of water up the step face maintains fine sediments in suspension, which are subsequently removed by wave-induced currents, leaving the coarse fraction at the step. Larson and Sunamura [1993] indicated the importance of phase coupling between incident waves and swash motions to backwash vortex formation thereby suggesting a dependence on wave breaker type [Kemp, 1975; Bauer and Allen, 1995]. While there have been a number of previous studies that examine the beach step, many of them do so in isolation without consideration of the morphodynamics of the beachface as a whole. For example, the formation and/or migration of a beach step suggests considerable sediment transport, however a parallel process on most coarse-grained beaches, which also transports a large volume of sediment, is berm formation.

Berms principally develop due to asymmetric swash processes stranding sediments around the runup limit [Duncan, 1964]; however, these sediments must be sourced from lower on the beachface and if the source was simply the lower-swash or breakpoint region, a large trough would develop over a tidal cycle. In the field this does not occur, as sediment is transported onshore from depths of several metres to replenish the beachface [Austin and Masselink, 2006*a*], meaning that it must pass through the step

region. Several areas of ambiguity remain, for example how reponsive the step and berm are to the tidal cycle, and how sensitive they are to variations in wave breaker type [Larson and Sunamura, 1993], for example Sunamura [1984]; Hughes and Cowell [1987] suggest that step dimensions increase linearly with wave height. This is partly because there are few field studies of step dynamics.

A dominant influence on the morphodynamics of macrotidal beaches is the tidal state. Variations in water depth result in the horizontal translation of the swash, breaker and shoaling wave zones across the nearshore in phase with the tide. If it is assumed that the step is maintained roughly at the breakpoint, it should be expected that as the breakpoint migrates with the tide the step should migrate similarly [Bauer and Allen, 1995]. However, the above presupposes that the step has a very short relaxation time when it is well acknowledged that there is frequently a significant lag between geomorphic process and resultant morphological change. For example, in a nearshore context, Austin et al. [2007] recently showed that ebb tide adjustments to wave ripples on a sandy beach significantly lagged the falling tidal level. Thus, there exists the possibility that although the morpho-sedimentary dynamics of the step are likely to be influenced by the tidal state, relaxation times are also likely to be important.

The limited amount of work which has quantified transport of gravel-sized sediment in coastal environments has been shown transport to be a highly irregular function of instantaneous fluid forcing and mechanistic properties of the bed. Heathershaw and Thorne [1985] demonstrated that the majority of gravel sediment transport under tidal currents occurs as short duration, turbulent and particular events, un-related to time-averaged flow parameters. Further work by Thorne [1986]; Williams [1990]; Hardisty et al. [1996], and others (generally in deeper water), demonstrated the role particle inertia and the various mechanical properties of the bed may have to play on the (therefore highly nonlinear) response of natural gravel sediments to nearshore flow velocity. What is clear from this work is that gravel sediment transport is dependent on both deterministic (e.g. oscillatory and mean flow velocities), and probabilistic phenomena (e.g. bed configurations, sediment properties, turbulence), but little work has been carried out to quantify sediment transport in the nearshore until now because of the measurement difficulties associated with such work. Recently researchers have emphasised the role of fluid accelerations, and associated horizontal pressure gradients,

on coarse particle transport [Drake and Calantoni, 2001; Hoefel and Elgar, 2003; Stive et al., 2005].

The principal aim of this chapter is to describe the morpho-sedimentary evolution of the beachface over a tidal cycle on a macrotidal gravel beach, and investigate whether the morphological response can be traced through temporal and spatial variations in the hydrodynamics, sediment transport and sediment characteristics. Specifically, to test if the step and berm are co-evolutionary and whether periods of morphological change and sediment transport correlate to changes in the hydrodynamic forcing. First, the hydrodynamics during the field survey are investigated, followed by an examination of the morphological and sedimentological changes to the beachface and finally an analysis of sediment transport across the foreshore.

5.2 *Sites, Times and Methods*

5.2.1 *Sampling framework*

A series of detailed field surveys have been carried out on the beachface as it evolved around high tide (varying, up to +/- 6 hrs). The experiments were in each instance, conducted within a wider morpho-sedimentary monitoring campaign of Slapton over a spring-spring tidal cycle (see chapter 6). Detailed measurements have been made of hydrodynamic forcing, morphological and sedimentological change. Although in total nine experiments were carried out, this chapter utilises hydrodynamic and morphological data from five of these surveys which were deemed to have adequate temporal (10 minutes or less) and spatial (1m or less) morphological sampling resolution - namely those on the 27/09/05; 10/06/06; 25/04/07; 26/04/07 and 02/05/07. Additionally, sedimentological information at the same resolution as morphological information is available for the surveys on 27/09/05; 25/04/07; 26/04/07 and 02/05/07. A summary of the times, sites and environmental conditions for each experiment run may be seen in Table 5.1.

The main field experiment was carried out in September 2005, which included detailed measurements of sediment transport as well as hydrodynamics, sedimentology and morphological change. This experimental run will be the main focus of the chapter, and the other 3–4 runs will be used to provide context, and corroboration, to the main

experiment's findings. The observations from the other four experimental runs contribute qualitatively to the discussions and ideas presented in this chapter.

The sampling framework of the experiments was determined by the morphological response of the beachface. Previous field observations at Slapton [Austin, 2005; Austin and Masselink, 2006*a*] indicated that the step was most active in the hours immediately either side of high water, and was frequently absent around low water, instead replaced by a series of two or more shallower-sided subtidal ripple features (similar to those described on Chesil by Hart and Plint [1989], but within closure depth, i.e. not relict features). With one of the aims of the exercise being to monitor step-berm coupling, it was decided to deploy the instruments from mid-tide onwards (≈5 hours before high water), before the step had formed. Data collection continued during the falling tide, until such a time when beachface morphological change was negligible and the step had been destroyed, become insignificant or migrated seaward of the rig. Therefore data collection was maximised over the high tide period when morphological change was greatest and, being higher in the tidal frame, more important to the supply of sediment to the upper beach, thus maintaining the convexity so crucial to the protection of the beach's hinterland.

Tab. 5.1 *Experiment times, locations, and conditions. N refers to the number of sediment samples collected during the experimental run. H_s, T_s, Θ_w, and TR refer to significant wave height, period, direction and tidal range respectively.*

Run	location	tan β	duration (mins, rel. HT)	D_{50} (mm) (N)	H_s (m)	T_s (s)	Θ_w	TR (m)
27/09/05	Slapton	0.23	-180:180	9 (333)	0.5-0.4	7-10	236	1.25
10/10/06	Slapton	0.25	-390:150	6 (5)	0.4-0.6	9-11	89	3.51
25/04/07	Strete	0.158	-180:170	2.47 (140)	0.1-0.15	8-9	266	1.58
26/04/07	Strete	0.161	-290:180	2.52 (188)	0.1-0.15	7	15	1.67
02/05/07	Strete	0.157	-300:80	4.27 (152)	0.25-0.4	4-6	73	3.85

5.2.2 *Hydrodynamics and Morphology*

During the main field survey two instruments rigs were deployed in a cross-shore transect across the intertidal beachface. Rig 1, consisted of a Druck® pressure transducer (PT) and 2D Valeport® miniature discus head current meter (ECM), and measured water depth h and cross-shore u and alongshore v flow velocity 3cm above the bed around the mid-step position. Rig 2 was located at the base of the step and measured the velocity

0.1, 0.25 and 0.4m above the bed with a vertical array of two 3D Nortek® Vector velocimeters (ADV) and an ECM, and water depth with a PT. An underwater video camera was also mounted at Rig 2, positioned to observe the bed under the current meters, to provide an indication of sediment transport. A further PT was mounted on the seabed below the LW level to monitor the tide and wave conditions input to the beachface. The swash excursion was monitored with a resistance run-up wire which was calibrated *in situ*, mounted 2cm above the bed and extending from the step to landward of the high tide berm. The PTs, ECMs and run-up wire were centrally logged by a shore-based computer at 16Hz and the ADVs logged to internal memory at 32Hz. Images from the underwater camera were digitised directly to a computer at 25Hz. The remaining experimental runs had the seaward PT to record inshore hydrodynamic conditions as well as a single ECM mounted just seawards of the breakers. An additional video camera recorded the entire experiment from an oblique position just beyond the berm crest.

The following standard hydrodynamic parameters were obtained from each 5 minute segment of pressure data for each of the experimental runs. From top to bottom: significant wave height (H_s); spectral wave period (T_s); and spectral width (ϵ_w, Cartwright and LonguetHiggins [1956]):

$$H_s = 4\sigma_\eta \tag{5.1}$$

$$T_s = \zeta_0/\zeta_1 \tag{5.2}$$

$$\epsilon_w = \frac{(\zeta_0\zeta_4) - \zeta_2^2}{\zeta_0\zeta_4} \tag{5.3}$$

where η is the detrended water surface elevation, and ζ plus subscript denote the moments of the auto-spectrum of the detrended wave trace. H_s was corrected for attenuation losses by multiplying by a gain factor G, constructed using the empirical correction factor of [Hunt, 1979]:

$$G = \frac{\cosh(kh)}{\cosh(kd)} \tag{5.4}$$

where h, $\mathbf{d}$, and $\mathbf{k}$ are local water depth, sensor depth and local wave number, respectively, where the latter is given by $\mathbf{k} = kh/\mathbf{h}$, and where kh is given by:

$$kh = \left(\tau_{kh}^2 + \frac{\tau_{kh}}{(1 + 0.666\tau_{kh} + 0.355\tau_{kh}^2 + 0.161\tau_{kh}^3 + 0.0632\tau_{kh}^4 + 0.0218\tau_{kh}^5 + 0.00654\tau_{kh}^6)} \right)^{0.5} \tag{5.5}$$

where $\tau_{kh} = (4\pi^2 h)/(gT_s^2)$. The time series were Hann tapered to reduce leakage of spectral density from large to adjacent peaks [Hegge and Masselink, 1996] using:

$$\mathbf{w}(i) = 0.5 \left(1 - \cos \frac{2\pi i}{N-1} \right) \tag{5.6}$$

for $i = 1, 2, \ldots, N$. To account for taper-induced spectral variance loss, a correction factor was applied to the estimates given by:

$$C_w = \frac{N}{\sum_{i=1}^{N} \mathbf{w}(i)^2} \tag{5.7}$$

The groupiness function was computed according to List [1991], where the detrended time series is high and low pass filtered (cut off = 0.05Hz), a modulus taken, and multiplied by $\pi/2$ to yield Λ_t. The groupiness factor is then given by:

$$GF = \sqrt{2}\sigma_\Lambda / \overline{\Lambda_t} \tag{5.8}$$

where σ_Λ and $\overline{\Lambda_t}$ are the standard deviation and mean of Λ_t, respectively. Groupiness increases as GF $\rightarrow$ 1.

The hydrodynamic parameters were averaged over each consecutive 5-min period of the high tide and used to computed the following two morphodynamic indices:

$$\epsilon_s = \frac{4\pi^2 H_s}{gT_s^2 \tan^2 \beta} \tag{5.9}$$

$$\xi = \frac{\tan \beta}{\sqrt{H_s / L_s}} \tag{5.10}$$

where ϵ_s is the surf scaling parameter (Guza and Inman, 1975) and ξ is a shallow water form of the Iribarren number (Battjes, 1974). L_s is the shallow water wave length, g is gravitational constant and $\tan \beta$ is the beach gradient across the 'active' region of the beachface (between the R2% and R80% run-up limits). The tidal translation rate TTR

was obtained from the run-up data, and calculated as the cross-shore excursion of the R2% run-up limit between consecutive 5min periods; as such it averages out fluctuations caused by the tide, incident wave energy and breaker type.

$$TTR = \frac{\delta x R_{2\%}}{\delta t} \tag{5.11}$$

For all of the experimental runs, the beach profile was surveyed at low tide along a single shore-normal transect using a Trimble electronic total station. Morphological measurements with a higher temporal resolution were carried out during tidal inundation using a rapid profiling method similar to that of Sallenger and Richmond [1984]; Nordstrom and Jackson [1990]; Kulkarni et al. [2004]. This method is ideally suited to obtaining accurate bed-level data from under water and has been used previously on coarse beaches with consistently good results [Austin and Masselink, 2006*a*]; it has an estimated accuracy of 1 cm. Fibreglass rods (diameter 8mm) were inserted into the beachface and the exposed length of the rod above the gravel surface was measured at 5min intervals using a specially designed ruler. These rapid profile measurements were conducted from the spring high tide berm to seaward of the step (up to wading water depth).

5.2.3 *Sedimentology*

Two methods of sediment sampling for size were carried out for this study to optimise temporal and spatial resolution within the experimental set-up. A 10 m transect was established 2 m longshore of the morphological transect, and the sediments sampled every 10-min for the entire experiment. Subaqueous sediments from the step face and lower swash regions were grab-sampled, dried, and sieved at 1/4 ϕ intervals. Intermittently-submerged sediments in the upper swash were photographed every 5-min whilst subaerial, and analysed for size using the image analysis method outlined in chapter 4 (i.e. using averages from the autocorrelation and autoregressive techniques).

Sediment size and morphological change relative to the standard deviation was found to be the most meaningful comparison, and due to the noisy nature of the sediment size record, only the gross morpho-sedimentary trends could be considered. As a pre-analysis tool the morphological and sediment size data sets were deconstructed using empirical orthogonal functions (EOFs) in order to separate the dominant signals from the

fluctuations, about which we could have less certainty.

EOFs, also known as Principal Components, were used to decompose morphological and sedimentological data sets into their constituent 'modes' of behaviour, in order to investigate the characteristics of spatial and temporal variability. EOFs have had widespread usage in coastal disciplines, for example to investigate large scale coastal behaviour [Wijnberg and Terwindt, 1995; Larson et al., 2003], shoreline variability [Clarke et al., 1984; Miller and Dean, 2007], beach profile variability [Winant et al., 1975; Aubrey and Ross, 1985; Houser and Greenwood, 2005], and sediments [Medina et al., 1994; Liu et al., 2000]. The appeal of EOF analysis is the ability to simplify and tease structure out of data without using a model or abstracted principles (hence 'empirical'), i.e. decomposition is achieved by using the data itself to select the constituent functions, which differs markedly from Fourier and even Wavelet techniques. EOFs decompose a data set into a number of uncorrelated (orthogonal) variables or modes, each of which accounts for a proportion of the total variance within the original data set. The modes, or eigenfunctions, are scaled by an associated set of eigenvalues, and are ranked monotonically according to the percentage of the variance in the data they explain (displayed as a 'scree plot', Davis [1986]). Usually, most of the total variance in a data set consisting of $\mathbf{p}$ modes can be represented by a relatively small number of q modes [Swan and Sandilands, 1995] - it is said that the dimensionality of the data can be reduced from $\mathbf{p}$ to q. This is very useful for noisy natural systems because variation associated with low rank modes can be simply removed to reveal the cleaner data underneath, and in turn features not previously visible.

In this study, the morphological and sedimentological data sets analysed using EOFs consisted of matrices of observations over space (x, rows) organised in time (t, columns). Resulting eigenfunctions were therefore either temporal modes denoted $\mathbf{c}_q(t)$, or spatial modes denoted $e_q(x)$ (following Miller and Dean [2007]). The generic data $Y(x,t)$ is represented by a series of linear combinations of these space and time functions, for a non-square matrix, as:

$$\ddot{Y}(x,t) = \sum_{q=1}^{N} \vartheta_q \mathbf{c}_q(t) e_q(x) \tag{5.12}$$

for eigenfunctions *k:N*, N here being the smaller of the number spatial and temporal

samples, and where normalising factor is given by $\vartheta_q = \sqrt{\lambda_k N_x N_t}$, and where λ_q is the eigenvalue associated with the q^{th} eigenfunction [Miller and Dean, 2007]. In this study the EOFs were calculated using a singular value decomposition (SVD) algorithm on $Y_{x,t}$ to yield two orthogonal matrices, **C** and **E**, which contain the spatial eigenfunctions and temporal expansion coefficients, respectively. The problem may be stated thus:

$$\ddot{Y}(x,t) = \mathbf{E}\lambda\mathbf{C}^T \tag{5.13}$$

where λ are the eigenvalues of $Y_{x,t}$ [Swan and Sandilands, 1995] and T denotes matrix transpose. The temporal eigenfunctions are then calculated as the Hadamard product (multiplication of two matrices, element by element) of **E** and λ [Swan and Sandilands, 1995], and the variance associated with each mode (expressed as a percentage) is calculated as:

$$L = \left(\frac{\lambda^2/N - 1}{\sum \lambda^2/N - 1} \right) \times 100 \tag{5.14}$$

Eigenfunctions are purely mathematical constructs, therefore non-dimensional, and cannot be expressed with any physical magnitude. However, multiplication of the spatial eigenmodes and the temporal expansion coefficients yields the original data. Errors between original and reconstructed data sets, given by $\mathbf{e}_Y = \sqrt{\left(\left| \ddot{Y}_{x,t} - Y_{x,t} \right| \right)^2}$ should tend to zero [Davis, 1986].

5.2.4 *Sediment Transport*

The size of gravel clasts and nature of gravel sediment transport precludes the use of optical and acoustic backscatter sensors to quantify sediment flux in the nearshore, which occurs almost exclusively as bedload and sheetflow. Instead, the underwater video was used as a measurement tool to quantify the magnitude of sediment transport [Williams, 1990; Stive et al., 2005]. The underwater video collected as part of the September 2005 experiment was de-compiled into individual frames, each representing 1/25th second, and converted to greyscale. The individual images were filtered for so-called 'heavy tail' or 'impulse' noise, and speckle (electrical) noise, using a relaxed-median filter [Hamza et al., 1999]. Other sources of noise, for example motion-blur and non-uniform illumination, were filtered using a complex-valued,

log-Gabor wavelet filter described by Kovesi [1999]. This is an advanced multiscale denoising algorithm based on complex-valued log-Gabor wavelets. Compared to real-valued wavelets, the benefit of using complex wavelets is that it approximates the amplitude and the phase of the signal at various scales. This algorithm has shown to be particularly efficient for removing non-uniform patches of illumination, especially in underwater imagery [Arnold Bos et al., 2005], because it preserves edges, and it may be used in a completely automated manner, because it determines the amount of noise at each scale within the image. Operating in the frequency domain, it is very fast. Some images of the rig and video data collected may be seen in Figure 5.2. The greyscale image was cropped to the region of interest for sediment transport/bed mobility calculations. A two-dimensional correlation was applied between pixels in consecutive high-resolution greyscale images separated in time by 1/25s. This algorithm provided a relative measure of correlation between consecutive frames of a moving bed, the reciprocal of which proved useful as a dimensionless 'bed motion coefficient', sensitive to changes in bed 'texture' or gross (non-directional) bed mobility, and given by:

$$\Omega = 1/\left(\frac{\sum_m \sum_n \alpha_I \beta_I}{\sqrt{[\sum_m \sum_n \alpha_I^2] - [\sum_m \sum_b \beta_I^2]}}\right) \tag{5.15}$$

where $\alpha_I = I_{mn}^t - \overline{I}^t$, $\beta_I = I_{mn}^{t+1} - \overline{I}^{t+1}$, and where t is time, m and n are dimensions of image I and the overbar denotes the mean. The numerator is the spatial covariance between successive images, so Ω is an inverse measure of change, and by implication transport, which is why the reciprocal is used. The denominator is shown as the difference between the spatial variance of successive images. Ω lies between 0 and 1, and is very sensitive to changes in texture' between consecutive frames, and when other sources of change are removed by filtering, it becomes a sensitive indicator of gross bed mobility. In this way it is a similar process to that of Holland et al. [2001], which tracked image 'texture' to quantify swash flows from video imagery. High values of Ω indicate poorer correlation, therefore most change, and most sediment transport. Remaining differences between frames associated with electrical/optical noise after extensive filtering were minimal ($\leq$0.0001). Subsequently, the time series of Ω was resampled to 4Hz to correspond to the hydrodynamic time series.

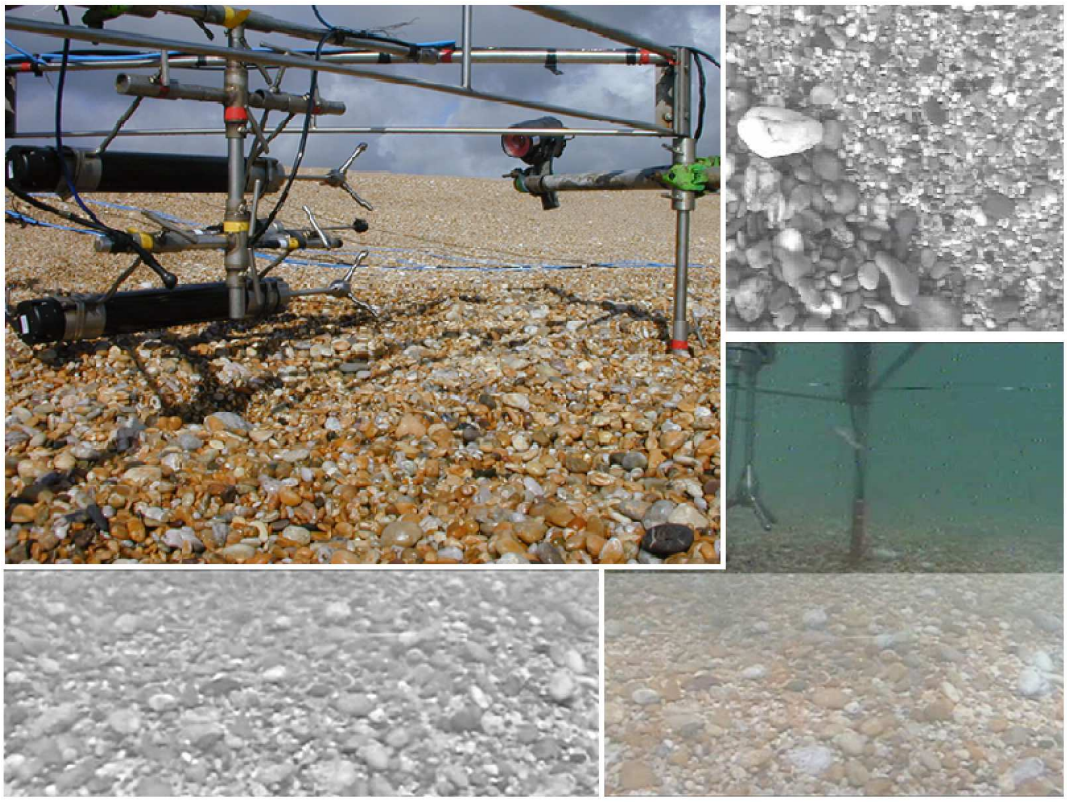

Fig. 5.2 *Underwater video photography was used during all of the experimental runs detailed in this chapter. The cameras were mounted either obliquely or face-down, and some images from these cameras are shown here.*

5.3 Results

The principal field survey was conducted over a single high tide on 27 September 2005 in the centre of Slapton Sands. During the experiment, the beach had a typical convexo-linear fairweather-type profile, with an intertidal gradient tanβ of 0.23, composed of moderately coarse and well-sorted sediments with a median size across the active beachface of D_{50} = 6mm, and the tide range was 1.25m.

Over the period of the field experiment, the water-level h in the region of the step varied by 0.75m, wave height H_s decreased from 0.6 to 0.5m and the time series of the spectrally-derived wave period T_s indicates that longer period waves were present during the second half of the survey (Figure 5.3). Between 10:00 and 12:00, the wave skewness S, calculated using the method of Elgar and Guza [1985], changes from positive ($S \approx$ 0.5) to negative ($S \approx$ -0.5). Subsequently, an inflection occurs and S is approximately zero until 15:00 when the waves are negatively skewed (suggesting reflection from the beachface). The evolution of the inshore wave spectra demonstrates that the wave field is composed of 5s and 12s waves, with the longer period waves becoming more prominent with time.

The overall semi-diurnal tidal curve (measured at PT3), TTR, ϵ_s and ξ are plotted in Figure 5.4 and highlight changes in the beach morphodynamics occurring during the tide. The tidal curve is slightly asymmetric, with a more gradual change in depth during the rising tide compared to during the falling tide. During the initial 1.5 hr of high tide, wave breaking is close to the plunging/surging transition (ξ = 1); wave breaking then moves rapidly into the fully surging regime (ξ 1.5) until 16:00 when ξ decreases. The beachface is predicted to be reflective ($\epsilon_s \leq$ 2.5), but after 11:30 ϵ decreases to $\approx$ 0.5, indicating strongly reflective conditions, until 16:00 when reflectivity begins to decrease.

5.3.1 Morphological and sedimentological change

The evolution of the intertidal beach profile along the main transect during the survey period is shown in Figure 5.5. Four distinct cross-shore regions can be identified across the beach profile, from seawards: the nearshore (x = 57.5 to 60m); beach step (x = 55.5 to 57.5 m); mid-swash (x = 54 to 55m); and berm (x = 50.5 to 53.5m). The berm and step appear principally to be accretionary features, whilst the nearshore is erosionary,

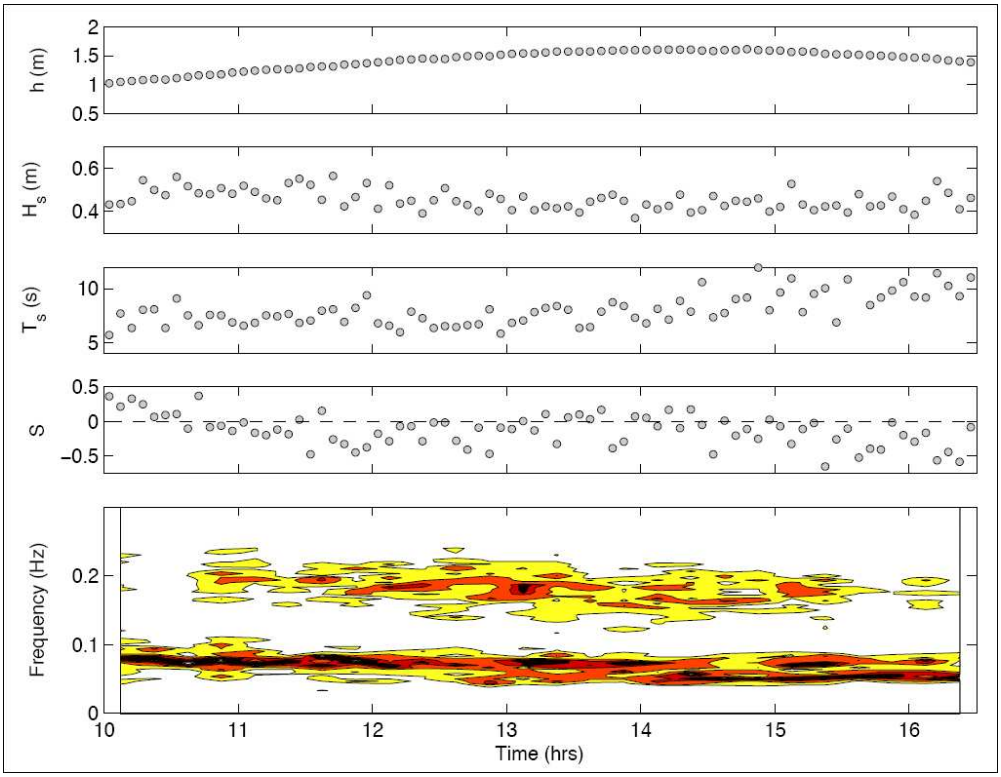

Fig. 5.3 *Hydrodynamic conditions encountered during the 27/09/05 field experiment - local water depth h; signifcant wave height H_s; significant wave period T_s; and wave skewness S. The contour plot in the lower panel represents the temporal evolution of the inshore wave spectrum. The spectra are normalised by their total variance, such that the contour plot shows the change in spectral shape, and not total energy content.*

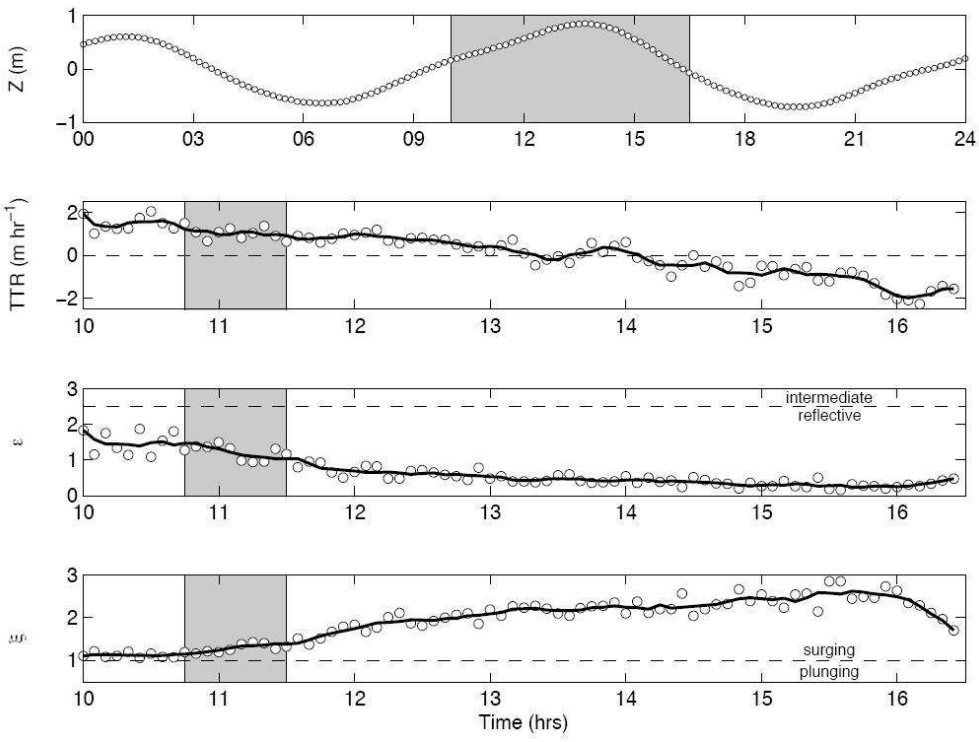

Fig. 5.4 *Time series of tidal elevation and morphodynamic indices for breaker conditions - tidal elevation h (where the shaded region is the experimental period), tidal translation rate TTR, surf scaling parameter ϵ_s and Iribarren number ξ. The horizontal lines in the middle and lower plots separate morphodynamic domains: intermediate versus reflective conditions in the middle panel [Guza and Inman, 1975]; and plunging versus surging breakers in the lower panel [Battjes, 1974]. The morphodynamic time series have been smoothed using a 5-point moving average indicated by the solid line. The shaded region indicates the period when ξ initially begins to increase and breaker type becomes predominantly surging.*

and little change in sediment volume occurs in the mid-swash region. To quantify the morphological response, the changes in sediment volume, relative to the start volume, were computed across each region (Figure 5.6, upper panel). Four distinct periods of morphological adjustment can be identified: (1) Phase I is associated with the initial tidal inundation of the beachface and displays moderate volumetric change; (2) Phase II corresponds to the rapid erosion of the nearshore region and strong growth of the step and berm; (3) during Phase III, there is continued berm growth but the lower-beachface is in near-equilibrium with the forcing; and (4) Phase IIa reciprocates Phase II during the ebb tide. During tidal inundation the beachface does not conserve mass; there is a net increase of 1.4 m^2 in sediment volume across each unit metre of beachface (Figure 5.6, lower panel). This sediment must either be sourced from the nearshore region or is the result of longshore transport.

Grouped variable scatter plots of the step and berm morphological facets plainly differentiate between the two systems (Figure 5.7). The coupled step nearshore mid-swash systems clearly display hysteresis loops, the distribution of which are strongly related to the phases of morphological change identifed in Figure 5.6 and hence the tidal translation. In contrast, the berm system displays no hysteresis, and is clearly un-coupled, at least at this time-scale, from the nearshore and mid-swash regions.

Figure 5.8 shows the original change in morphology and sediment size (relative at each time step to the standard deviation of sediment sizes across space), respectively. The morphological and sediment size data were re-mapped as a 'cleaner' trend with which to draw inference using the number of EOFs required to explain $\geq$90% of the variance in the morphology and sedimentology, 2 and 4 EOFs, respectively (Figure 5.8). The errors between the original and reconstructed data associated with these reconstructions are negligible. The region of foreshore from the berm face to the step crest (50-56m) became generally coarser throughout the experiment (Figure 5.8), whereas the region just seaward of the step became finer (56-58m). The main morphological trends are again seen, with the *in-situ* growth of a berm and step. The sedimentological trends are also clearer, with bands of relatively coarse and fine sediments showing some spatio-temporal persistence.

Figure 5.9 plots the percentage of explained variance attributable to each EOF. It demonstrates that over 90% of morphological and sedimentological change can be

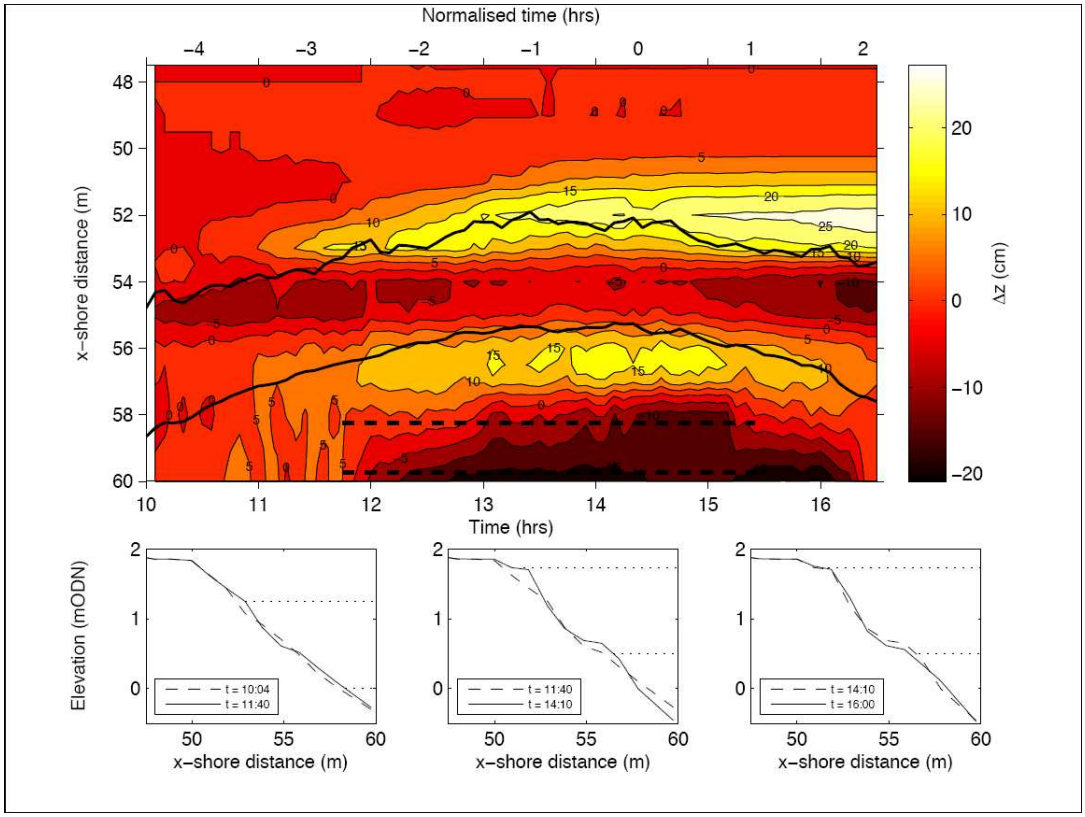

Fig. 5.5 *Morphological evolution of the main transect at cross-shore grid resolution of 0.5m (**upper panel**). The shading represents the residual bed-level change relative to the first profile and the contours show elevation change at 5cm intervals. Temporal profile change during selected periods (**lower panels**). The thick solid lines in the upper panel represent the R2% and R80% run-up limits and the dashed lines the cross-shore position and duration of deployment of the instrument rigs. Time normalised relative to high tide is shown on the upper axis. In the lower panels, the dotted lines indicate the maximum extent of the swash zone during that interval.*

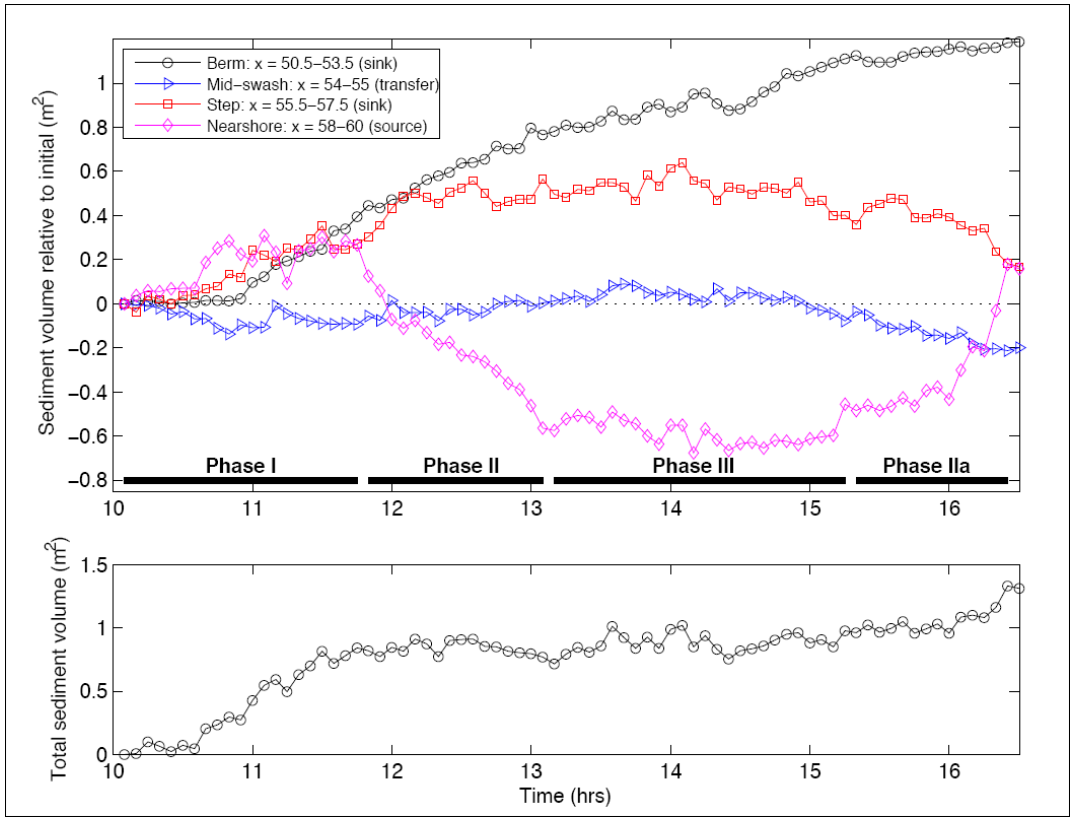

Fig. 5.6 *Volumetric beach change.* ***Upper panel*** *- variation in the sediment volume over the survey period at four cross-shore locations on the beachface.* ***Lower panel*** *- total change in beachface sediment volume during tidal inundation.*

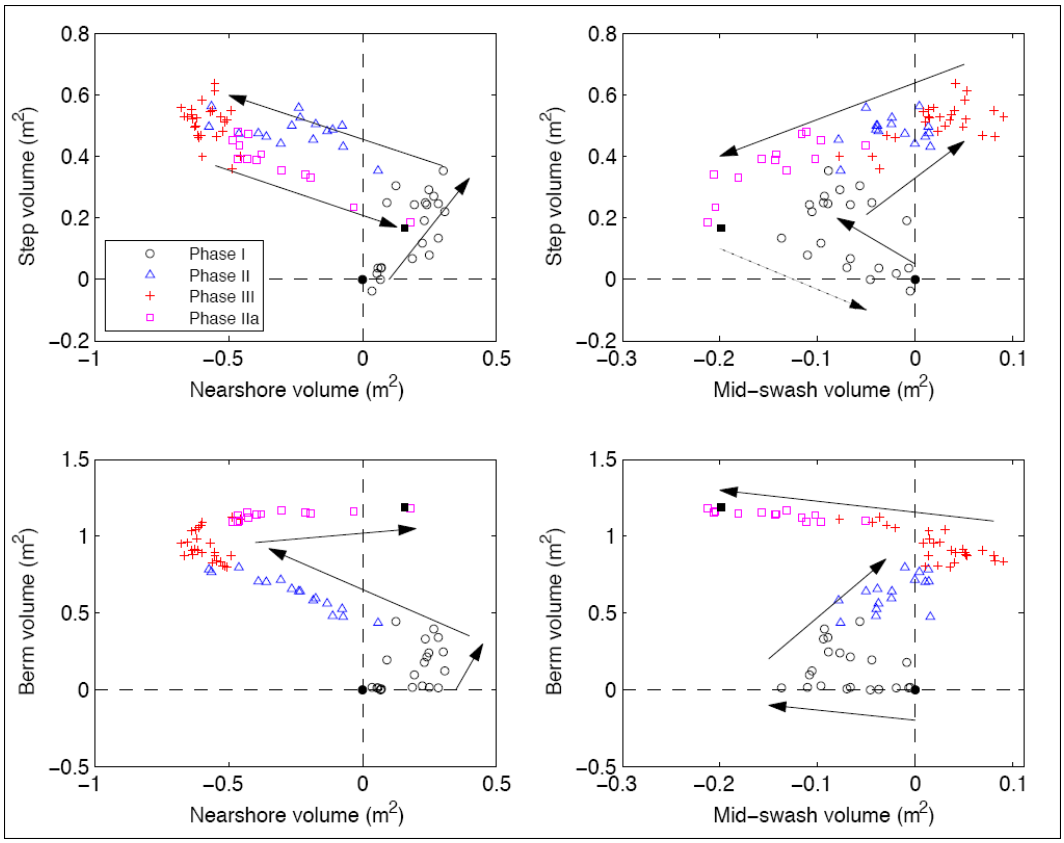

Fig. 5.7 *Grouped variable scatter plots of the different morphological facets.* ***Upper panels*** *- evolution of the beach step compared with the nearshore and mid-swash regions.* ***Lower panels*** *- berm evolution compared with the nearshore and mid-swash. The different marker types reflect the phases of morphological change identified in Figure 5.6 and the solid circles and squares indicate the start and end points of the sampling period, respectively. Arrows indicate the progression of the morphological change. Sediment volume is measured per unit width of beachface.*

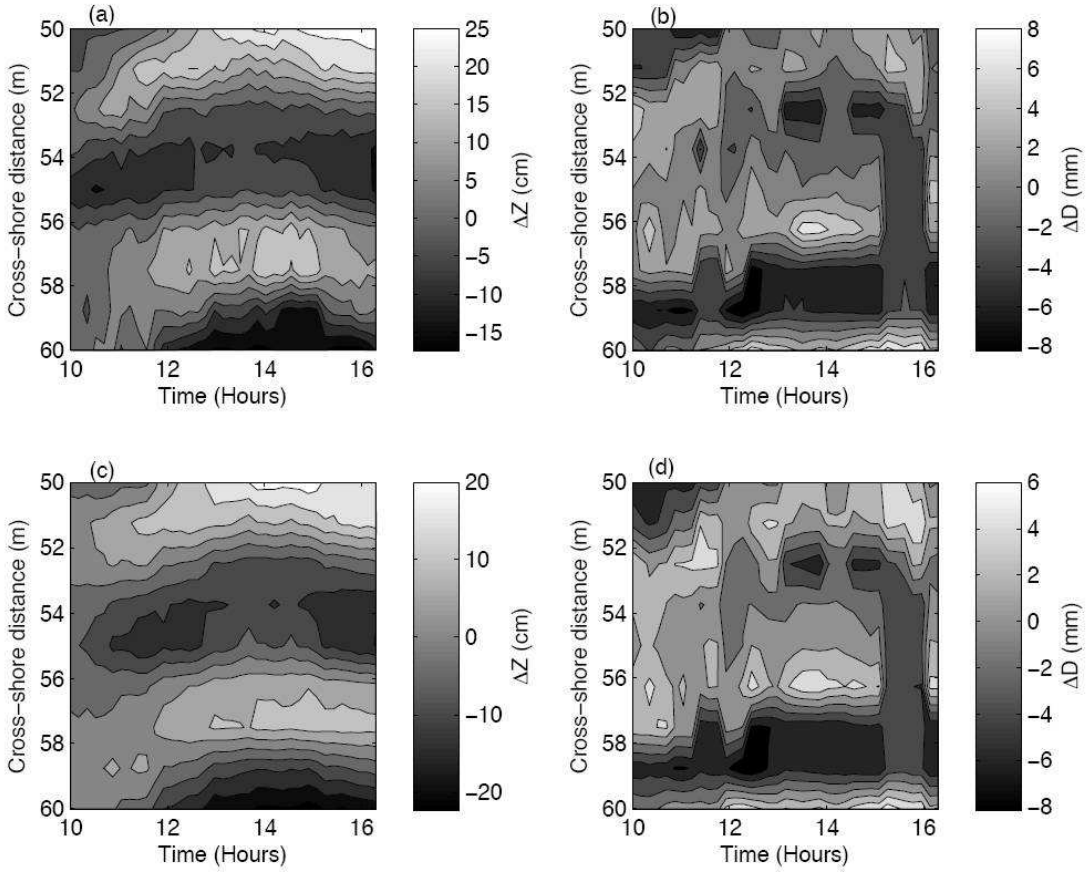

Fig. 5.8 *EOF analysis of morpho-sedimentological trends. (a) Cumulative change in bed elevation relative to initial profile Δz (cm); (b) cumulative change in sediment size relative to the sediment size standard deviation for every cross-shore position over the entire measurement period ΔD (mm); (c) EOF-Reconstruction of the Morphological data in (a), using the first 2 EOFs, which account for $\geq$90% variance; and (d) EOF-Reconstruction of the Sedimentological data in (b), using the first 4 EOFs, which account for $\geq$90% variance.*

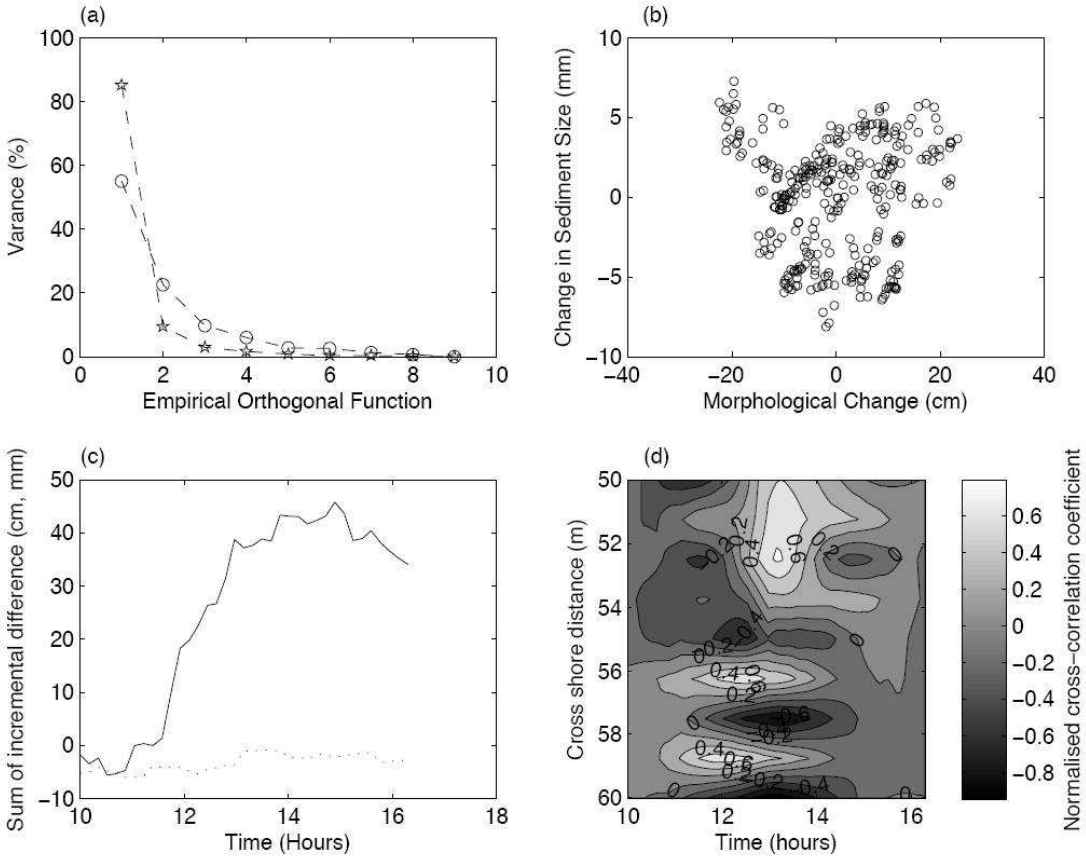

Fig. 5.9 *Morpho-sedimentary dynamics of the nearshore region. (a) Scree plot of percentage explained morphological (pentagons) and sedimentological (circles) variance associated with each empirical orthogonal function (EOF); (b) morphological and sedimentological change has an uncorrelated domain of co-variation; (c) the sum of the temporal derivative (solid line) of Δz (cm) and (dotted line) ΔD (mm); and (d) contour plot of morpho-sedimentary cross-correlation (cross-correlation coefficients normalised so that the auto-correlations at zero lag equal unity).*

described by two and four EOFs, respectively. It is possible to look for co-variability in the morph-sedimentary signal having first reconstructed the data to show the dominant trends. Overall for the whole beachface there is little correlation between the morphological and sedimentological signals (Figure 5.9). This is confirmed by the sum of the temporal derivatives of Δz (cm) and ΔD (mm), which display significantly different trends, relative to the start conditions, through time. Cross-correlating the morphological and sedimentological change data demonstrates a maximum correlation (r = 0.6) across the berm at high tide suggesting that as the berm accretes the sediments become coarser. A similar result is observed across the step-crest and at the base of the step during the mid-food tide, but in contrast, the sediment and morphological change are negatively correlated in the nearshore and step-face. The spatial dependence of sediment size may be seen in Figure 5.10 where the spatial location of absolute fining or coarsening relative to standard deviation is marked as white shading. Note the proximity to the developing berm and step features.

The narrow region of wave breaking on a gravel beach (and its morphological progenitor, the beach step) is an important one. The energy associated with this region is of primary importance to a given beach configuration and sediment pattern at any given time. The step and berm were found to be very responsive over individual tides. The step was consistently seen to migrate with the semi-diurnal tide. Whilst the morphological sampling resolution precluded the analysis of the dimensional analysis of the step on a wave-by-wave basis, what is clear is that it remains submerged; it forces wave breaking and it keeps a quasi-steady distance from the shoreline (but not the run-up maximum). The gross morphological changes which occur across the steep macrotidal gravel beachface are largely consistent with those reported in earlier findings, i.e. a berm develops through swash over-topping and asymmetry [Hine, 1979; Austin and Masselink, 2006*a*; Weir et al., 2006], whilst seaward of the run down limit, a large beach step evolves [Austin and Masselink, 2006*a*].

Morphological changes on the beachface and just seawards of the step are in proportion to step dimensions for a given set of (low-medium energy) wave-tide conditions, implying a source-sink relationship and sediment convergence. The whole of the active foreshore is thus involved in maintaining the position and characteristics of wave breaking, in a morphodynamic relationship. Berm formation requires energy and

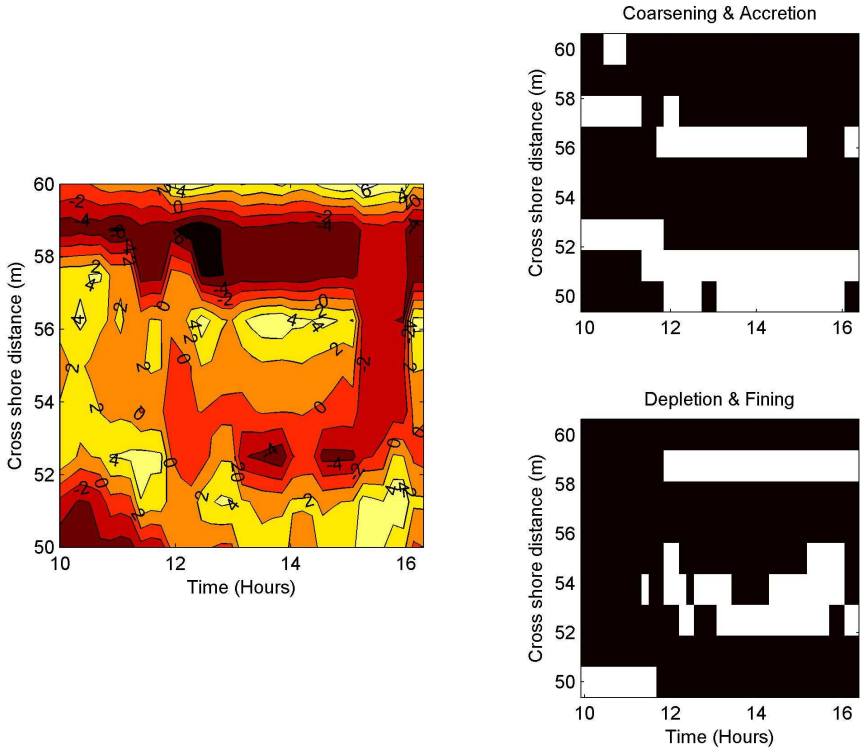

Fig. 5.10 *Sedimentological change (**left panel**), in mm, relative to mean size profile (lighter shading indicates coarsening); regions of morpho-sedimentary co-variation (**right panels**) - coexistence of relative sediment accretion and coarsening (top), and relative sediment depletion and fining (**bottom**).*

tidal stationarity over-and-above that required for step formation so in consequence, whilst a berm does not always develop, in contrast, a step always does. The step or berm may or may not migrate significantly over a single tidal cycle - this depends on the tidal translation distance. Where the berm does move, the toe of the berm remains at a fixed cross-shore position so the entire berm structure does not move onshore, but rather swash washes sediment over the crest which is re-established landwards [Austin and Masselink, 2006*a*]. Foreshore sediment conservation of mass is not always achieved - the step is a mechanism by which beachface building and depletion occurs, liberating and transporting material from different areas in the tidal frame. Indeed, here is little net morphological change when the step is not very active. A consequence of having such dynamic step and berm morphologies, over relatively short distances on these steep beaches, is that the swash and surf zones are linked to a high degree, exchanging a great deal of material and momentum.

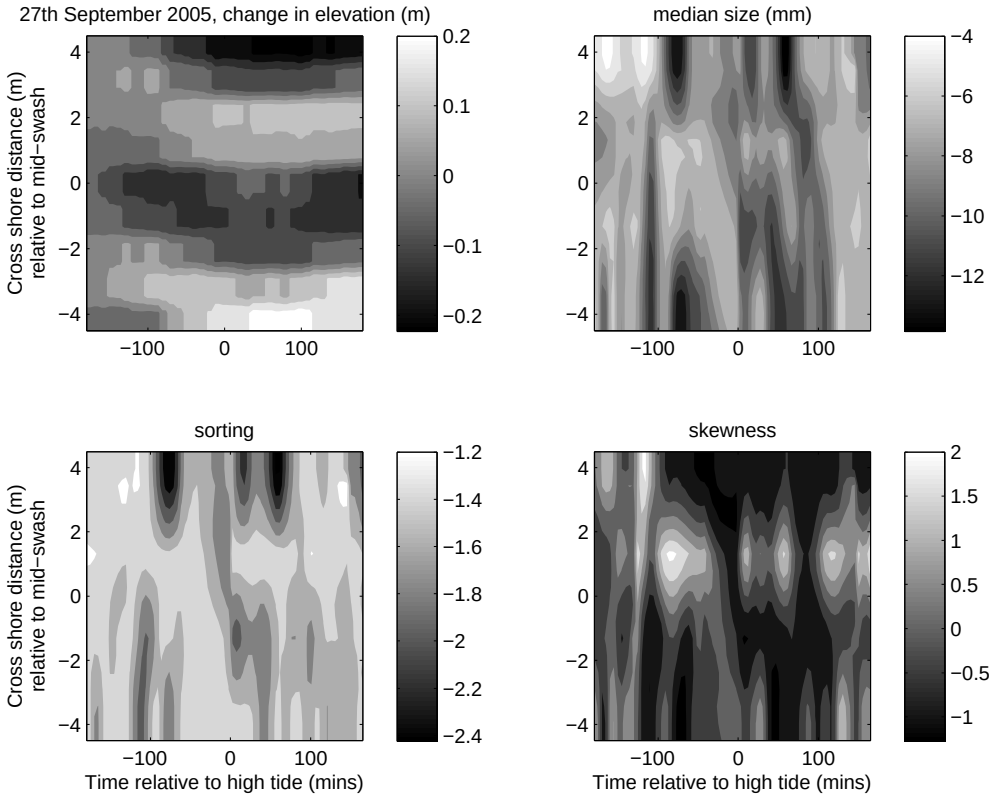

Fig. 5.11 *27/09/05.* ***Clockwise from top left****: morphological change (m) relative to initial, mid-swash, and time of high tide; median sediment size (mm) relative to standard deviation of size for that sampling time, mid-swash, and time of high tide; graphical skewness relative to standard deviation of size for that sampling time, mid-swash, and time of high tide; and graphical sorting relative to standard deviation of size for that sampling time, mid-swash, and time of high tide.*

Net berm growth appears to result from swash asymmetry [Duncan, 1964; Eliot and Clarke, 1988], whereas the step forms at the point of convergence between offshore transport in the mid- and lower-swash and onshore transport of sediment eroded from the nearshore. Under these conditions, the step is an ephemeral feature with a short relaxation time that forms during the flood phase of the tide and is destroyed during the ebb. Step face sediments are sourced from the nearshore region and transported onshore to converge with sediment sourced from the lower swash which builds up the step crestal region. During the ebb, the crestal region is eroded and its constituent sediment returned to the nearshore. The berm develops coincidentally to the step during the flood, but it has a relaxation time that is related to the spring-neap cycle and, unlike the step, persists on the beachface because it remains stranded above the shoreline as the tide ebbs. Therefore, the berm conserves its sediment over a single high tide whereas the step does not. The step and berm are effectively independent features forced by discordant timescales: the relaxation time of the berm is linked with spring-neap tidal cycle, whereas the relaxation time of step is linked with semi-diurnal tidal cycle, and relative tidal stationarity, and with the mid-foreshore remaining a morphological 'pivot point'. Therefore, there is hysteresis in volumetric response of step and nearshore, but not in volumetric response of berm and foreshore.

A summary of the morpho-sedimentary trends for each of the remaining four experiments may be seen in Figures 5.12 to 5.15. Different modes of behaviour in the morphological response are clearly observed depending on the hydrodynamic conditions of the survey day, such as the dimensions and migration distances of the step and berm, which are summarised in Table 5.2. Migration distance of the step is clearly associated with the tidal range, although the step dimensions do not seem to be correlated with breaking wave height. Similarly, the dimensions and migration rate of the berm appear to be poorly parameterised by the wave height and tidal range. This is probably because of the observed asymmetry with respect to tide, and the interplay between large run-up and large backwash. On those occasions where the swash period is small, berm building is aided by relatively weak backwashes, however under longer swash periods, strong backwashes tend to prevent significant berm building. Larger and more mobile berms are associated with relatively erosive foreshores (Figures 5.11 to 5.15, upper panels).

Spatial trends in sedimentology consistent across surveys are harder to discern, but

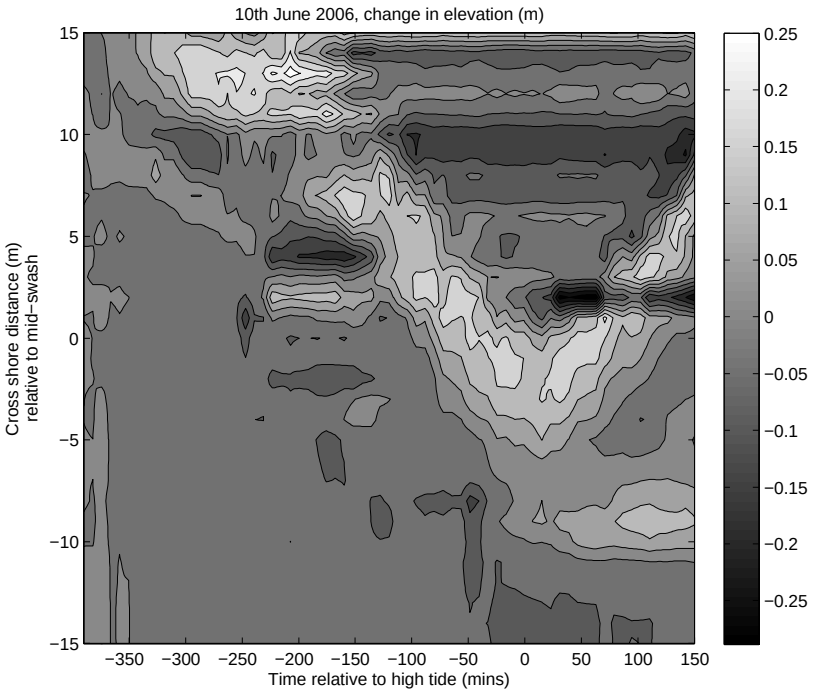

Fig. 5.12 *10/06/06. Morphological change (m) relative to initial, mid-swash, and time of high tide; median sediment size (mm) relative to standard deviation of size for that sampling time, mid-swash, and time of high tide.*

some broad generalisations may be made. The step and berm are generally the coarsest and most positively skewed of the beachface sediments. The step is generally poorly sorted but there are often phases where it becomes well sorted. The response times of the beachface sedimentology are much faster than those of the morphologies, and it is likely that a 10min sample resolution is insufficient to draw out more meaningful trends.

Tab. 5.2 *Summary of trends in dynamics of step and berm for each run, along with range in H_s and TR.*

Run	Step	Berm	H_s (m)	TR (m)
27/09/05	no migration (-180:180 HT); max 20cm	max 25cm berm; migration 2m	0.5-0.4	1.25
10/10/06	migration 20m (-390:150 HT); max 25cm	max 20cm berm; no migration	0.4-0.6	3.51
25/04/07	no migration (-180:170 HT); max 30cm	no berm	0.1-0.15	1.58
26/04/07	migration 5m (-290:180 HT); max 60cm	max 20cm berm; migration 5m	0.1-0.15	1.67
02/05/07	migration 20m (-300:80 HT); max 25cm	no berm	0.25-0.4	3.85

Bi-variation in sedimentary parameters do show coherence (see Table 5.3). Coarsening is associated with the development of step and berm features, and generally seawards to the breaker line (in agreement with Krumbein [1938]; Evans [1939]; Bagnold [1940]; Bascom [1951]; Miller and Ziegler [1958]). Fining is associated with the upper foreshore,

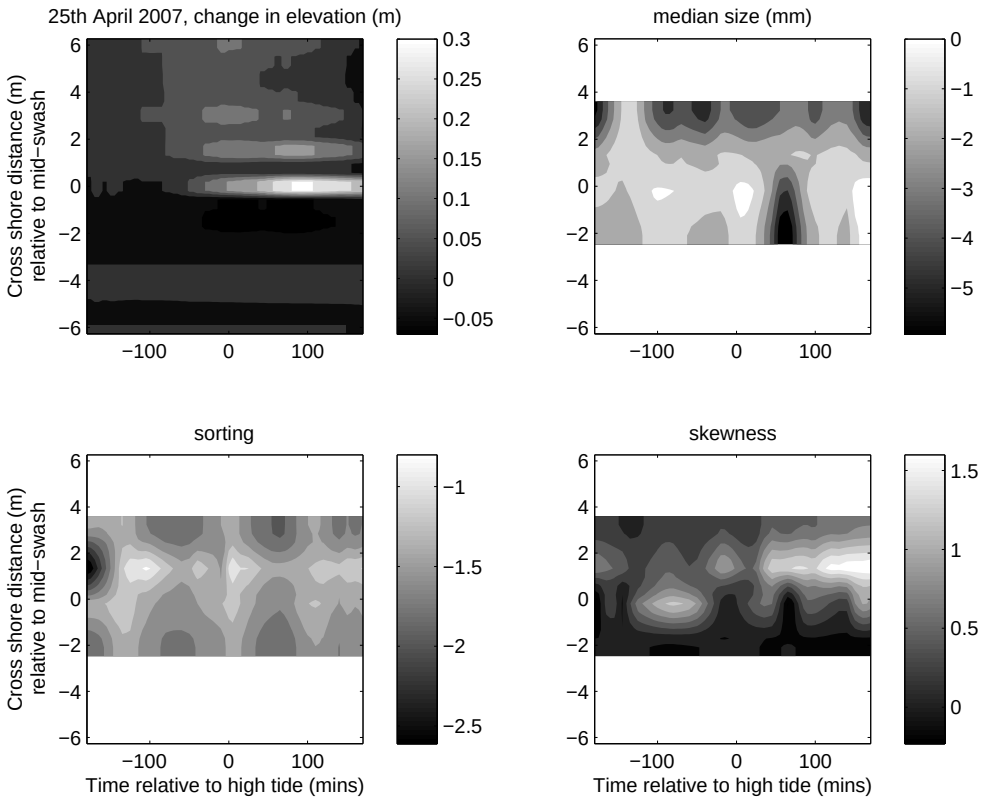

Fig. 5.13 *25/04/07.* ***Clockwise from top left****: morphological change (m) relative to initial, mid-swash, and time of high tide; median sediment size (mm) relative to standard deviation of size for that sampling time, mid-swash, and time of high tide; graphical skewness relative to standard deviation of size for that sampling time, mid-swash, and time of high tide; and graphical sorting relative to standard deviation of size for that sampling time, mid-swash, and time of high tide.*

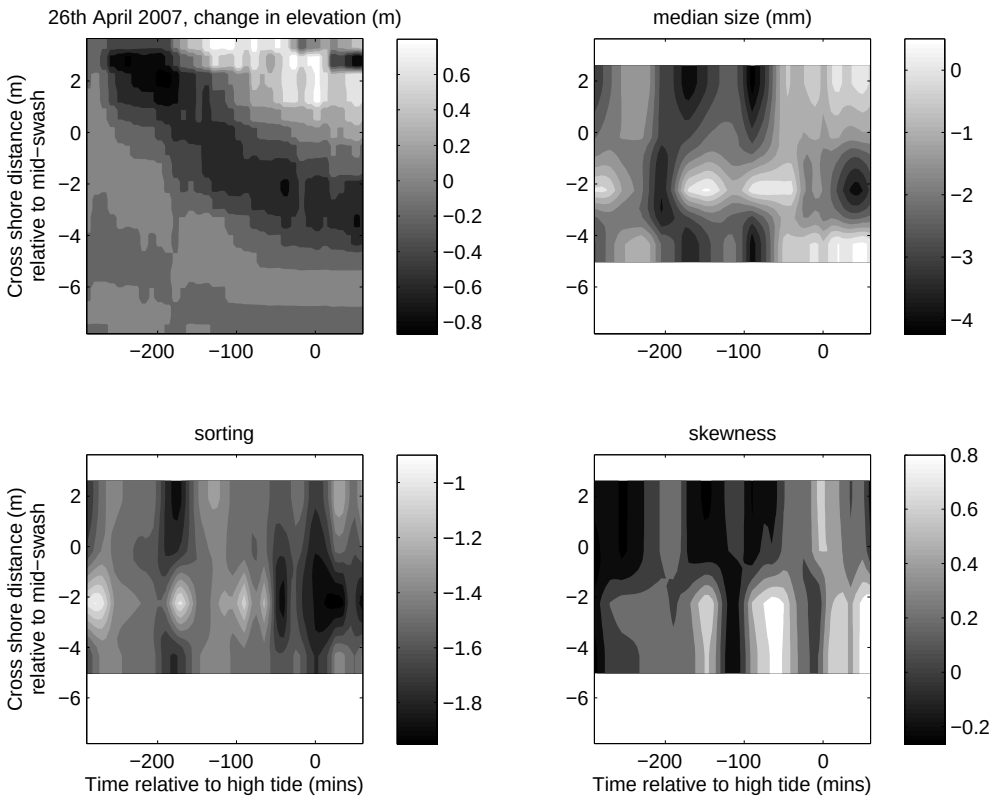

Fig. 5.14 *26/04/07.* ***Clockwise from top left****: morphological change (m) relative to initial, mid-swash, and time of high tide; median sediment size (mm) relative to standard deviation of size for that sampling time, mid-swash, and time of high tide; graphical skewness relative to standard deviation of size for that sampling time, mid-swash, and time of high tide; and graphical sorting relative to standard deviation of size for that sampling time, mid-swash, and time of high tide.*

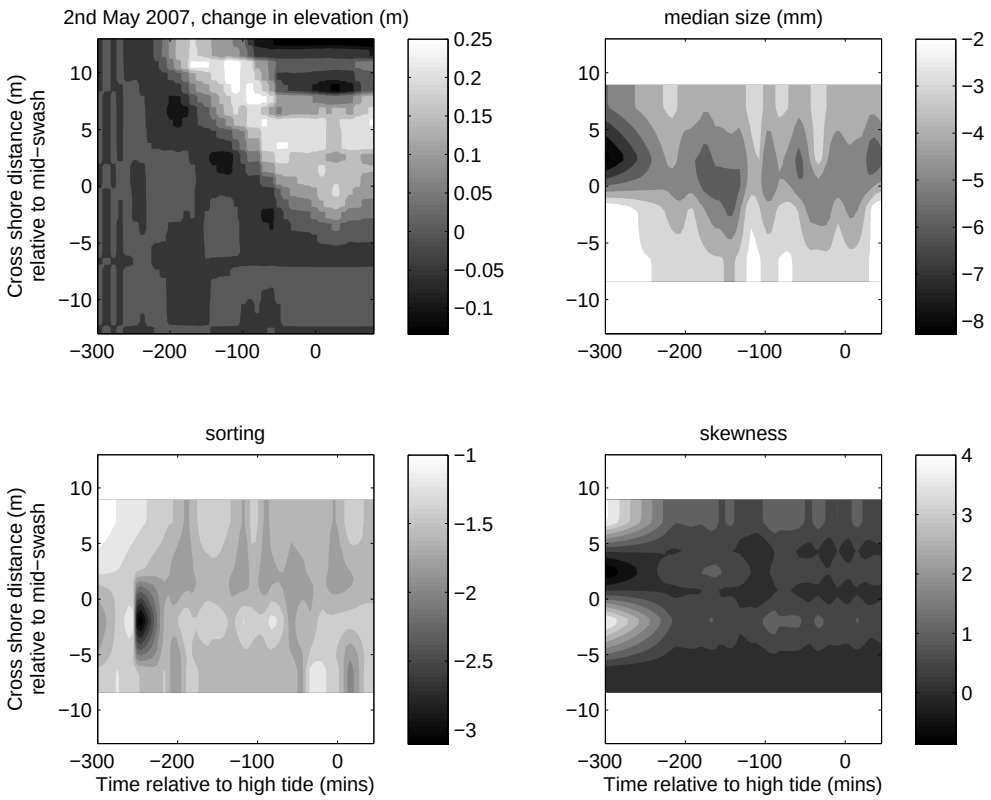

Fig. 5.15 *02/05/07.* ***Clockwise from top left****: morphological change (m) relative to initial, mid-swash, and time of high tide; median sediment size (mm) relative to standard deviation of size for that sampling time, mid-swash, and time of high tide; graphical skewness relative to standard deviation of size for that sampling time, mid-swash, and time of high tide; and graphical sorting relative to standard deviation of size for that sampling time, mid-swash, and time of high tide.*

co-incident with removal of material, and step crest which is coincident with the deposition of material. In a gross sense, each hydro-kinematic region thus has a distinct 'morpho-sedimentary domain', so it is possible to trace the gross trends of berm and step building-coarsening through time, and it may be seen that the mid-foreshore is a sedimentological as well as morphological pivot point. Despite the location of the step, it has remarkably stable and distinctive sedimentology: step sediments are characteristically coarser skewed, and more platykurtic, than the sediments of the foreshore and berm. It is thus possible to distinguish the step from the foreshore using bivariation in sedimentary moments (e.g. Figures 5.16 and 5.17).

Tab. 5.3 *Correlation coefficients for sedimentary and morpho-sedimentary bi-variate relationships.*

Run	Md/σ	Md/Sk	σ/Sk	Md/Δ z	σ/Δ z	Sk/Δ z
27/09/05	0.72	0.73	0.52	0.41	0.26	0.7
25/04/07	0.83	-0.21	-0.39	-0.32	0.019	0.24
26/04/07	0.82	0.21	-0.03	0.7	-0.24	0.39
02/05/07	0.86	-0.32	-0.32	0.15	-0.15	-0.82

Bivariate scatterplots of sedimentary parameters (Figure 5.17) reveal some significant correlations in the time series of the step face sediments that are not present in the swash sediments. Relationships were found between sediment parameters only for the step sediments - coarser sediments are more positively skewed (Figure 5.17), more poorly sorted (Figure 5.17), and more platykurtic (Figure 5.17). Perhaps the best parameter to discriminate step and swash sediments is kurtosis - step sediments of a given size are consistently more leptokurtic than swash sediments meaning that, even though overall swash sediments are slightly better sorted, the ratio between the spreads of the tails and centre of the distribution is greater and the step sediments are better sorted in the central part of the distribution.

5.3.2 *Sediment mobility*

Sediment transport just seaward of the breaker zone was found to be intermittent, and characterised by periods of relative mobility and relative inactivity. The Ω parameter was calculated for 402370 consecutive images, representing $\approx$4.5hrs of decompiled video data of the nearshore bed surface at Rig 2. Field observations indicated that the largest

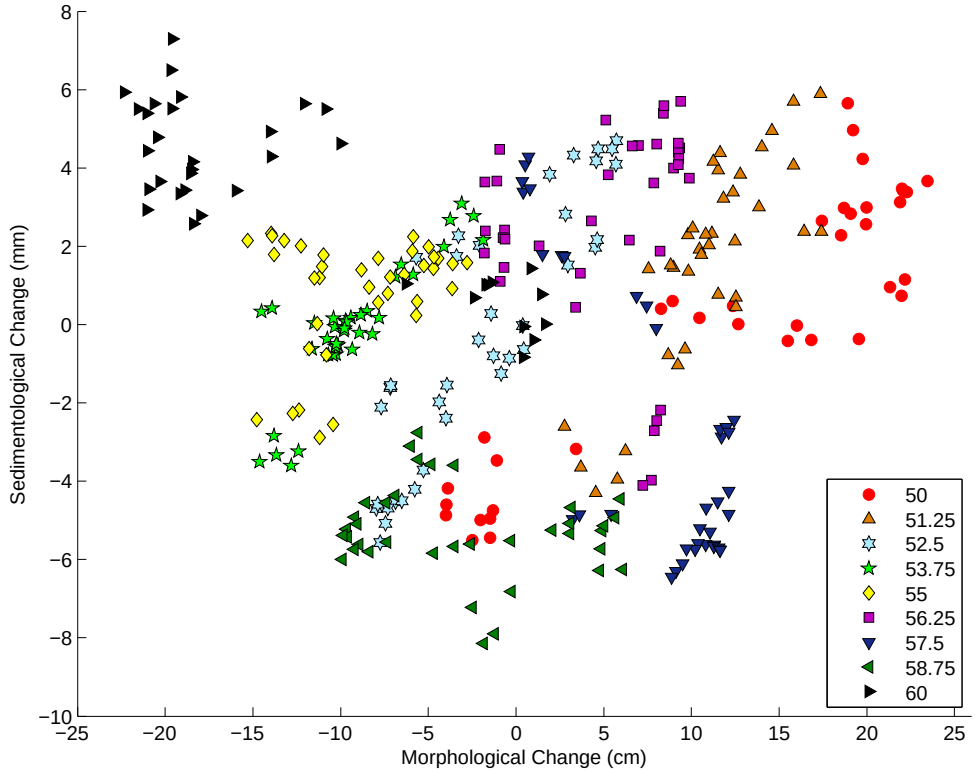

Fig. 5.16 *Morpho-sedimentary bi-variation grouped according to location. Data comes from the survey of 27/09/05: groupings refer to distance cross shore (increasing seawards). Each hydro-kinematic region occupies a different parameter space. Note that sediment size is relative to standard deviation of all sediment sizes.*

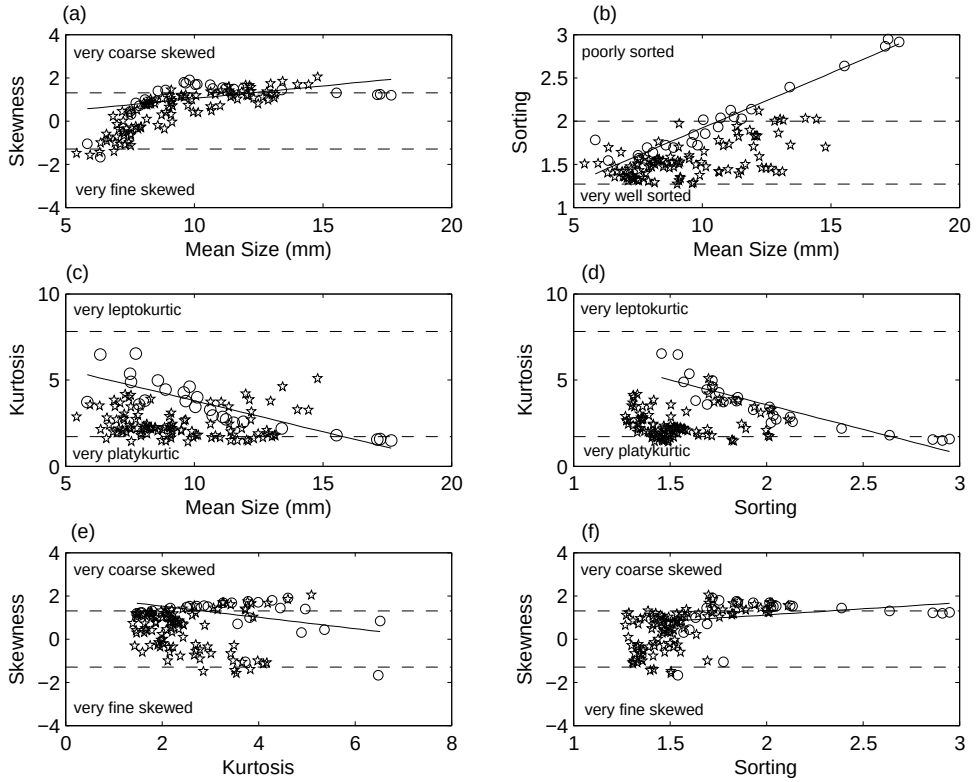

Fig. 5.17 *Bivariate scatterplots of geometric moments for swash/berm (stars) and step (circles) sediments. Solid lines show linear least squares fits through the step data; dashed lines show dependent variable classification boundaries (Folk and Ward, 1957).*

transport events occurred at frequencies greater than the incident wave period, suggesting the involvement of wave groups.

Upon visual inspection there was systematic bed motion response to neither velocity (u) direction nor magnitude; acceleration (a_u) direction nor magnitude. Indeed, bed motion induced by similar velocity or acceleration events was often very different in duration and magnitude. This was probably because 'bed motion' parameterised by Ω is not the same as volumetric sediment transport. Assuming instantaneous sediment transport response to nearshore fluid motions, the sign of Ω was scaled according to the instantaneous directional component of velocity and acceleration (i.e. positive onshore, negative offshore), to yield $\pm\Omega_u$ and $\pm\Omega_{a_u}$ respectively, and the following calculations were performed for each 5min segment of data:

$$\delta_a = \log\left(\frac{\sum|\Omega_{a_u}|}{\sum|-\Omega_{a_u}|}\right) \tag{5.16}$$

$$\delta_u = \log\left(\frac{\sum|\Omega_u|}{\sum|-\Omega_u|}\right) \tag{5.17}$$

providing a ratio of time-averaged onshore - offshore dimensionless sediment flux, assuming instantaneous response to fluid forcing. Figure 5.18 (left) shows these ratios over time, showing that in general values lie close to unity, however in general in can be seen that sediment flux which occurs when flows are accelerating offshore is greater than sediment flux which occurs when flows are accelerating onshore. Conversely, sediment flux is greater when velocity is directed onshore.

The role of wave groupiness was investigated by comparing time-series of cross-shore current velocity, the wave groupiness envelope and bed motion (Figure 5.19). The groupiness envelope was computed by lowpass-filtering the modulus of the cross-shore current record at 0.05Hz. Visual inspection of the time series indicates that the structure of the groupiness envelope is very similar to, but slightly lagged behind, that of the bed motion. The cross-correlation function between the groupiness envelope and the lowpass-filtered bed motion confirms the strong positive correlation, and quantifies the time lag as 5s. Closer observation of the time series of u and Ω suggests that strong backwashes at the start of the wave group initiate maximum bed mobilisation. The 5 s time lag exists because the maxima of the wave group envelope function is at the centre

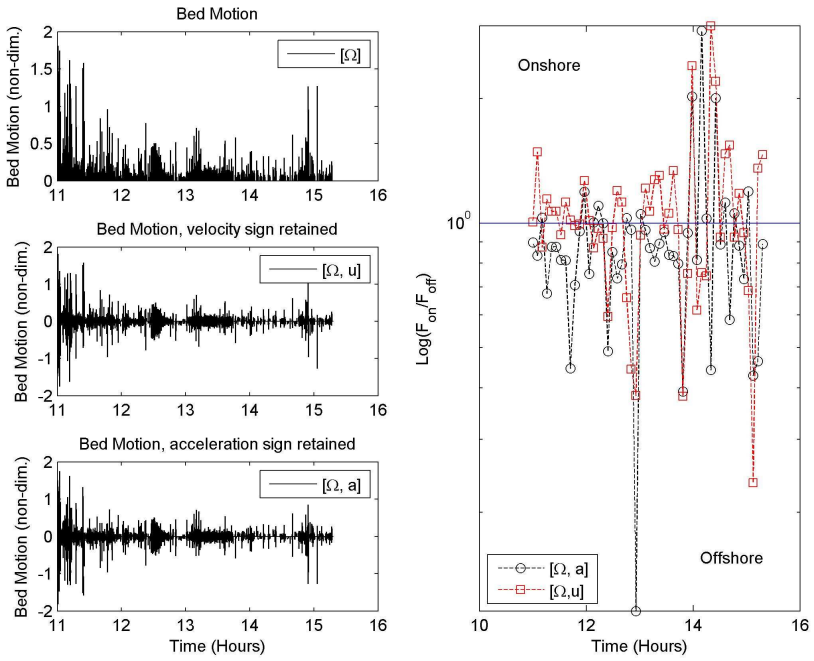

Fig. 5.18 *Magnitude-response diagram for Ω. The original time series of Ω is depicted in the upper left panel; the middle left panel shows Ω magnitude with the instantaneous directional component of velocity retained; and the lower left panel shows Ω magnitude with the instantaneous directional component of velocity acceleration retained. The right panel shows normalised bed motion magnitude (see text) for acceleration (black circles) and velocity (red squares).*

of the group, and therefore the cross-correlation ignores the effect of first few constituent waves of the group. This suggests that sediments respond strongest to sub-incident wave frequencies, which could mean that individual waves stir/destabilise sediments, and the largest wave(s) in a group carry out most of the transportation. Equally, it could indicate that the importance of the magnitude of the velocity event which transports most sediment is diminished, if the sequence of individual waves which are large enough to stir the bed is long enough. In which case, stress 'histories' may be more important in the movement of clasts than instantaneous bed stresses [Paphitis and Collins, 2005].

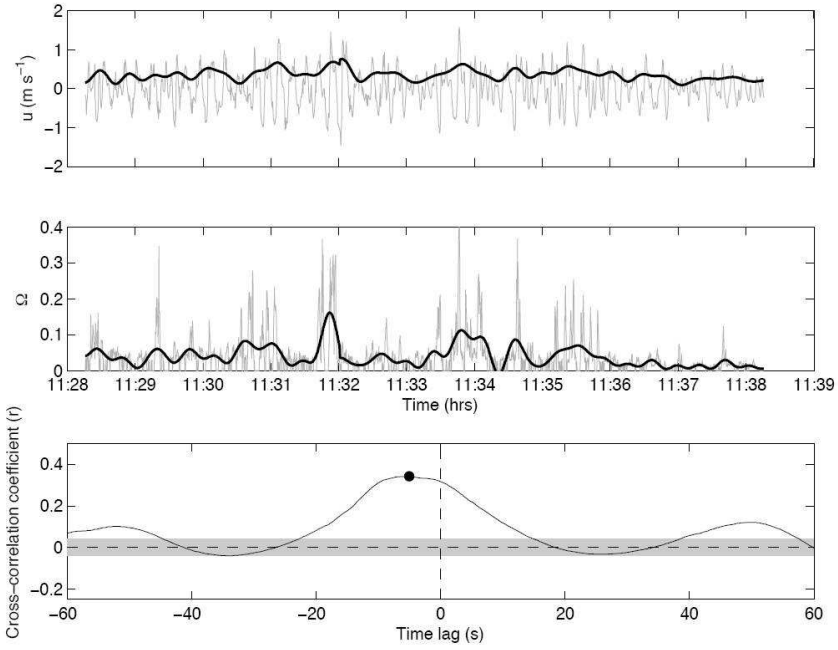

Fig. 5.19 *Time series of (**top**) cross-shore current velocity u (solid line) and envelope function of u (thick solid line); (**centre**) non-dimensional bed motion Ω (solid line) and lowpass-filtered Ω (thick solid line) and (**bottom**) cross-correlation between the groupiness envelope and the lowpass-filtered Ω. The solid circle indicates the maximum correlation coeffcient and the shaded region represents the 95% confidence limit calculated as $2/\sqrt{N}$, where N is the number of samples. The cut-off for the lowpass-filter was 0.05Hz.*

It is likely that the first waves in a group 'clear' the bed of a certain proportion of movable grains, until a threshold is reached where the conditions have been primed for the greatest amount of transport, after which the bed is relatively immobile. This implies a great deal of initial resistance to movement imposed by the micro-mechanical configurations of the bed (temporal and spatial distributions of grain-size, 'hiding' factors, relative flow protrusion, etc). These findings are in general agreement with previous work on marine gravel transport.

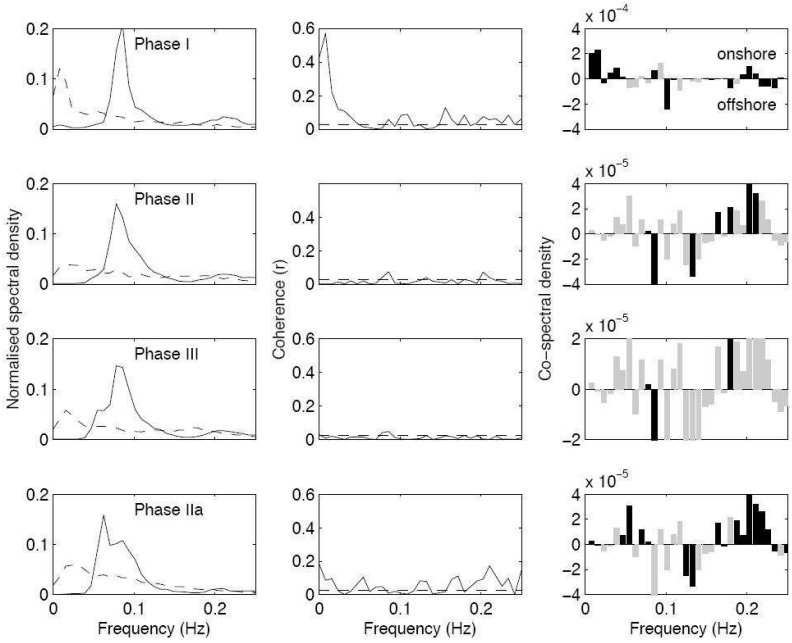

Fig. 5.20 *Spectral analysis of u and Ω during the four previously identified phases of morphological change.* ***Left panels*** *- normalised auto-spectra of u (solid line) and Ω (dashed line).* ***Centre panels*** *- coherence spectra (solid line) and 95% confidence limit (dashed line);* ***right panels*** *- co-spectra. Frequencies where u and Ω are significantly coherent are shown in black, grey bars indicate non-significant correlation. The normalised auto-spectra were computed by dividing the individual spectral estimates by the sum of the spectral estimates (i.e. total variance of the time series).*

Cross-spectral analysis was used to further explore the relationship between Ω and u (Figure 5.20). Auto-spectra of the cross-shore current and the bed motion are characterised by a strong peak at 0.08Hz and a secondary peak at 0.2Hz for the current, and a peak frequency of 0.03 Hz for the bed motion. These spectral peaks indicate a wave group period of 33s, and confirm the bi-modal wave field of 12.5s swell, and 5s wind waves. There is generally very poor correlation between Ω and u, except at the wave group frequency during Phase I of morphological change, and this is further reflected when the co-spectra are calculated between current velocity and sediment motion [Huntley and Hanes, 1987], which are often barely significant over the frequencies of interest. Using Ω as a proxy for sediment transport, the co-spectra quantify the magnitude and direction of the sediment flux at different frequencies in the same way as the co-spectrum between u and the suspended sediment concentration on a sandy beach. Low coherence between velocity and transport suggests transport is highly intermittent, highly variable at swell frequencies, and clearly a highly non-linear function of flow velocity. During Phase I, maximum bed motion coincides with the onshore phase of the wave-oscillatory currents at the wave group and windwave frequencies; there is some offshore transport at swell frequencies. Progressing into Phases II and III, where significant, transport is onshore due to wind waves and offshore due to swell. Here, transport at the wave group frequencies is largely insignifcant. Onshore transport continues at wind wave frequencies throughout Phase IIa with some onshore contribution from the swell.

A simple probablilistic model of bed mobility

In order to glean further information about the nature of bed motion, the data was analysed further using a probabilistic model in order to reconstruct an ensemble or 'typical' transport event. Dimensionless raw Ω was linearly rescaled to span the interval 0 –10, and rounded to the nearest integer in order to obtain a discrete record Ω_{rr} which maintained similar resolution. A transition probability matrix (TPM) —see Figure 5.21 —of the Ω_{rr} data was constructed (Figure 5.22), and using Markov Chain theory [Kemeney and Snell, 1960], analysed for its general distributional form and persistence characteristics.

With reference to the TPM for Ω_{rr} in Figure 5.22, the absence of transitional extremes

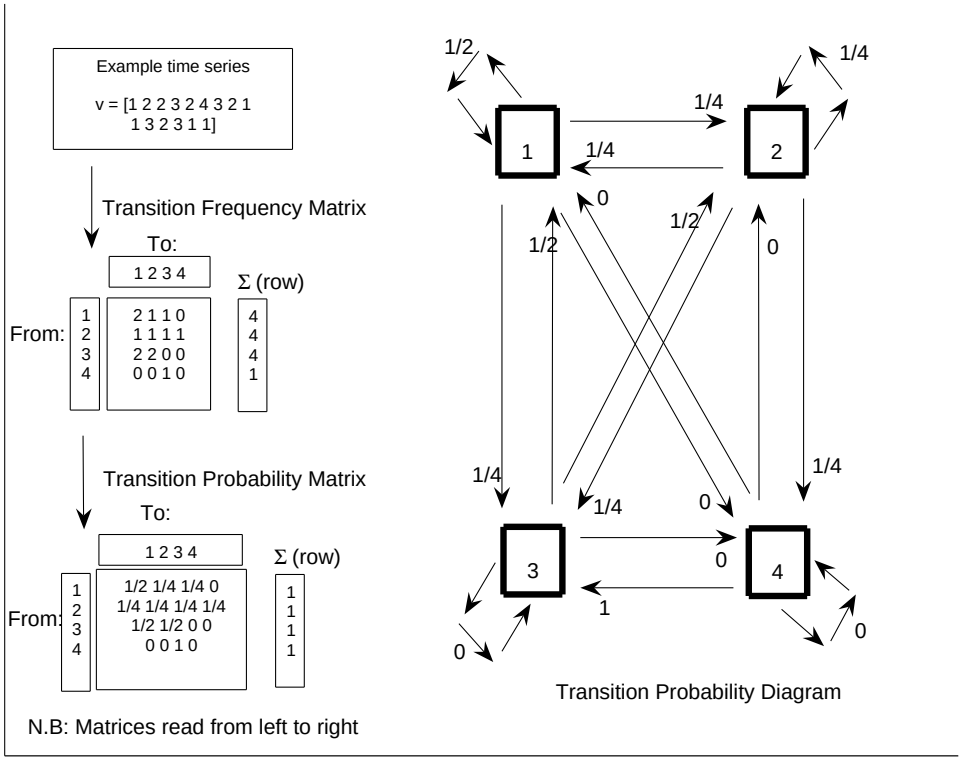

Fig. 5.21 *Example time series re–cast as a TFM and TPM. The TPM may be summarised diagrammatically as shown on the left of the figure.*

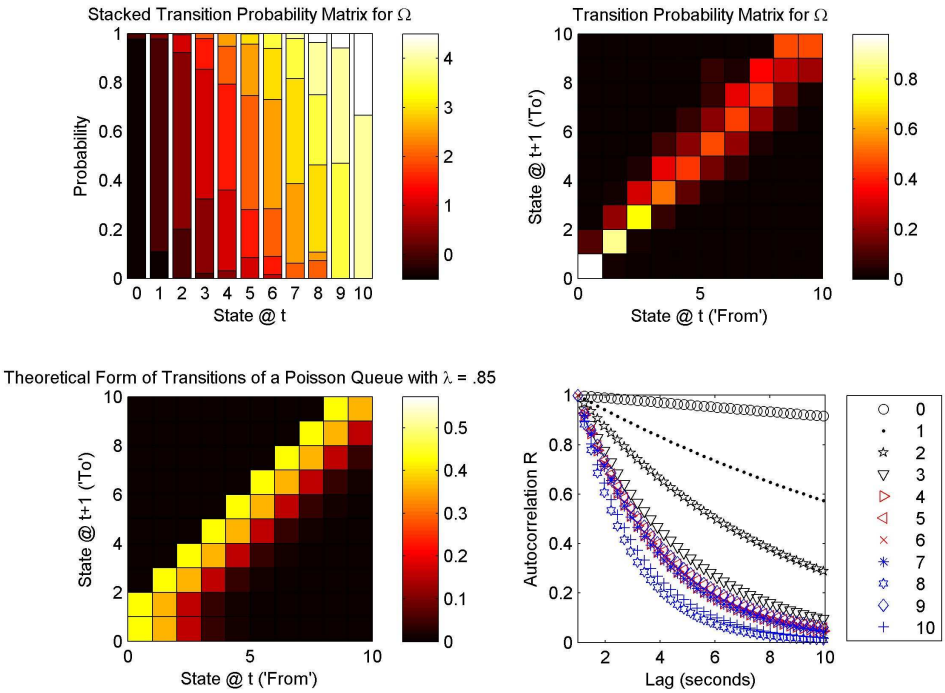

Fig. 5.22 *Sediment transport as a Markov chain: transition probability matrix for* Ω_{rr} *(**top panels**); autocorrelation functions,* R*, for* Ω_{rr} *states (**bottom panels**).*

validates the sample frequency at which the data was collected. The transition matrix shows that sediment transport 'events' are in general negatively skewed. For example, the transition probabilities are not symmetrical about the inertial left-right diagonal, and the probability for an event of increased magnitude to follow an event of given magnitude is larger than the vice-versa (i.e. incline tendencies). Specifically, values of average magnitude have a larger transitional spread; therefore the skew in the wave will not be drawn by the mode (event peak) or tails but by the falling limb. In order to reconstruct the ensemble event the remaining information required is the persistence characteristics of every magnitude. The rank autocorrelation function of a Markov chain is given by [Basawa, 1972]:

$$r = \frac{\sum_{x,y} xy\Theta_{xy} - \left(\sum_{x,y} x\Theta_{xy}\right)^2}{\sum_{x,y} x^2\Theta_{xy} - \left(\sum_{x,y} x\Theta_{xy}\right)^2} \tag{5.18}$$

where $\Theta_{xy} = \Pi^T \times P^T$ such that $\sum_{x,y} \Theta_{x,y} = 1$, and where T, x, y, P, and Π denote matrix transpose, row, column, transition matrix, and steady state probability vector, respectively. The steady state vector Π is found by solving the set of equations, in matrix notation:

$$\Pi = P\Pi \tag{5.19}$$

subject to $\sum \Pi = 1$. The autocorrelation functions for each magnitude are shown in Figure 5.22 (right panel), showing an almost linear decrease in persistence with increasing magnitude. What this means in a physical sense is that a typical sediment transport event resembles a negatively skewed wave which is composed of a series of steps of increasing shorter length. This general form complies with visual inspection of the data, and could be interpreted as the first waves in a group 'clearing' the bed of a certain proportion of movable grains, until a threshold is reached where the conditions have been primed for the greatest amount of transport, after which the bed is relatively immobile. This implies a great deal of initial resistance to movement imposed by the micro-mechanical configurations of the bed (temporal and spatial distributions of grain-size, 'hiding' factors, relative flow protrusion, etc).

A discrete 'queueing process' is a simple statistical model which tries to predict the dynamics of a stochastic process which is characterised by queue-like properties, in so

much as it is a governed by the rate of arrivals and departures of a finite and discrete number of entities (or 'customers') into and out of the queue [Gross and Harris, 1998]. In a discrete time-series, the 'queue' is the time interval of interest and the 'customers' are the entities within the queue which arrive, wait, and depart at some rate. The sediment transport time-series Ω_{rr} is suitable for consideration as a queueing process because it is long, discrete, and characterised by punctuated quiescence (or a series of instantaneous 'events' separated by relatively long periods of inactivity) and no temporal trend. In this situation the probability of an event (state) occurring in an interval of any length within the time-series is proportional to the length of that interval. The TPM for Ω_{rr} was characterised only by values on or immediately around the diagonals, which in the literature is known as a 'birth-death' process [Gross and Harris, 1998] where the transitions are restricted to neighbouring states. In this 'smooth transition' situation, the queue is characterised by individual (not bulk) arrivals of states, or in other words an orderly queue which is simply modelled.

The Poisson model has long been used to characterise such discrete time-series [Davis, 1986; Zaman, 2002] as 'birth-death' (simple) queueing processes. The Poisson distribution models a queue where, in a fixed period of time, the probability of arrival of a discrete event is independent of the period of time since the last event of identical magnitude [Griffith and Haining, 2006], controlled by a known rate of arrival (departure). The Poisson distribution and Markov chain are often utilised together in statistical modelling because they share certain assumptions in common, for example arrivals (of states) are random and independent events; all states may precede or be preceded by others (the assumption of chain irreducibility); and only one state can occupy the chain, or queue, at any one time (i.e. 'customers' are served one at a time). The use of probability models has some history in sediment transport research. In the seminal work on the subject, Einstein [1937] showed that gravel in rivers is transported in a series of discrete, serially independent step and rest 'events' which may be approximated by a probability distribution in the exponential family (e.g. Gamma, Poisson), a general observation which has aided individually-tailored research problems in fluvial geomorphology [Hassan et al., 1991; McNamara and Borden, 2002].

If we assume that the TPM encompasses the entire state space ($[N, N]$) of Ω_{rr} (i.e. if in a sufficiently long time-series we have observed all possible values of Ω_{rr}), the

probability that Ω_{rr}, as a random variable, equals a particular value, $\mathbf{y}$, within N may be given by the Poisson distribution [Griffith and Haining, 2006]:

$$p(\Omega_{rr} = \mathbf{y}) = \frac{\exp^{-\lambda_p} \lambda_p^{\mathbf{y}}}{\mathbf{y}!},\ \lambda_p \geq 0,\ \mathbf{y} = 0, 1, 2, \ldots, N+1 \tag{5.20}$$

with ('intensity') parameter λ_p as the 'rate of occurrence' [Griffith and Haining, 2006]. The probability that a transition will have occurred in a time interval equals 1 if the assumptions of the chain are adhered to, so a probability matrix of departure D_p for $N{=}x$ may be given as an identity matrix of dimensions $x+1 \times x+1$ with all elements set to zero except the entries (*(1,1)* and (*x,x-1*) which equal 1. For example, D_p for $x{=}4$ would be given by:

$$D_p = \begin{pmatrix} 1 & 0 & 0 & 0 & 0 \\ 1 & 0 & 0 & 0 & 0 \\ 0 & 1 & 0 & 0 & 0 \\ 0 & 0 & 1 & 0 & 0 \\ 0 & 0 & 0 & 1 & 0 \end{pmatrix}$$

A probability matrix of arrivals D_a, of dimensions $N+1 \times N+1$, and governed by a Poisson model, for $\mathbf{y} = 0, 1, 2, \ldots, N+1$ according to the elements $D_a(\mathbf{y}, \mathbf{y} : N+1) = p(\Omega_{rr} = \mathbf{y})$, and elements $A(y, N+1) = 1 - \Sigma(D_a(y, y : N+1))$ (so each row sums to 1). For the *x=4* example above, $p(\Omega_{rr} = \mathbf{y}) = [0.4493, 0.3595, 0.1493, 0.0383, 0.0077]$ for $\mathbf{y} = [0, 1, 2, 3, 4]$ and if $\lambda_p = 0.8$, therefore $_a$ is given by:

$$D_a = \begin{pmatrix} 0.4493 & 0.3595 & 0.1438 & 0.0383 & 0.0091 \\ 0 & 0.4493 & 0.3595 & 0.1438 & 0.0474 \\ 0 & 0 & 0.4493 & 0.3595 & 0.1912 \\ 0 & 0 & 0 & 0.4493 & 0.5507 \\ 0 & 0 & 0 & 0 & 1 \end{pmatrix}$$

In a Markov-Poisson model such as this, parameter λ_p which determines the shape of the distribution is interpreted as the average 'arrival rate' of a new element (state) into the queue. The estimated TPM is given by the product of D_p and D_a, and the mean

waiting time for an arriving entity (state) is given by $(i \times \Pi)$, where $i = [1, 2, \ldots, N]$.

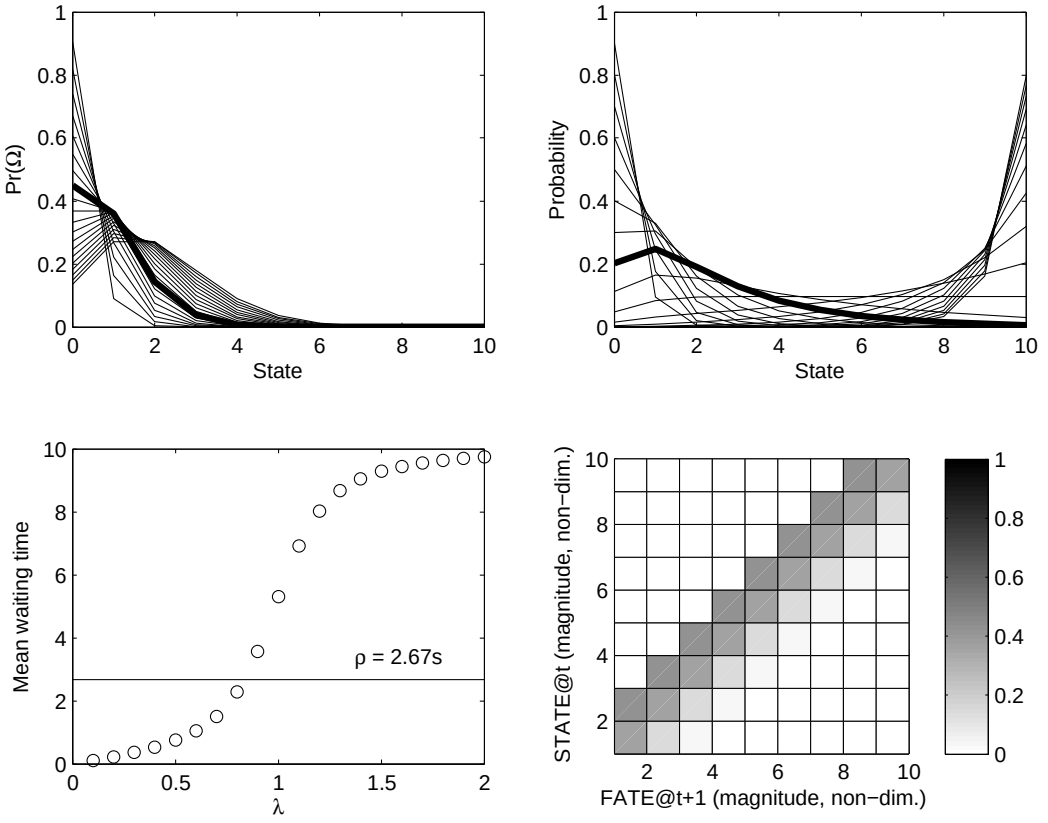

Fig. 5.23 *Poisson Model for Sediment Transport.* ***Top left****: Poisson distributions for a Discrete-State Markov chain with* $\lambda_p = 0.1 \rightarrow 2$ *(heavy line is* $\lambda_p = 0.85$*).* ***Top right****: Steady state distributions (*Π*) for the associated Markov-Poisson processes (heavy line is* $\lambda_p = 0.85$*).* ***Bottom right****: mean waiting times in the queue for* $\lambda_p = 0.1 \rightarrow 2$*. The damping ratio,* $\overline{\rho_p}$*, for sediment transport data* Ω_{rr} *is shown as a solid straight line.* ***Bottom left****: the modelled TPM of a Markov-Poisson process with* $\lambda_p = 0.85$ *and* $\overline{\rho_p} = 2.67$*.*

Some results of the model are shown in Figure 5.23. The damping ratio, given by the ratio of the first and second eigenvalues $\overline{rho_p} = \lambda_{p1} / |\lambda_{p2}|$ Caswell [see 2001] for Ω_{rr} equals 2.67s (shown as a solid line in Figure 5.23, bottom left), and the Markov-Poisson model outlined above when $\lambda_p \approx 0.85$, gives a mean waiting time 2.67 seconds. The 'damping ratio' may be considered as the rate of convergence to complete time-independence (p=0) for each individual state. The distribution $p(\Omega_{rr})$ for $\lambda_p = 0.85$ has been used to construct a TPM (Figure 5.23, bottom right) which closely approximates the TPM of Ω_{rr} (Figure 5.22). Of particular note is how closely the features of the actual (Figure 5.22) and modelled TPM (Figure 5.23) match, for example the larger values left of the diagonals relative to those to the right (in general terms, any given state is more likely to be preceded by smaller values than larger values). In

consequence, the steady state vector associated with this modelled TPM (heavy line in top right panel), gives the best approximation to the shape of the steady state probability vector (Π) of the TPM for Ω_{rr} in the range $\lambda = 0.1 \rightarrow 2$.

5.4 *Discussion*

The narrow region of wave breaking on a gravel beach (and its morphological progenitor, the beach step) is an important one. The energy associated with this region is of primary importance to a given beach configuration and sediment pattern at any given time. The step and berm were found to be very responsive over individual tides. The step was consistently seen to migrate with the semi-diurnal tide. Whilst the morphological sampling resolution precluded the analysis of the dimensional analysis of the step on a wave-by-wave basis, what is clear is that it remains submerged; it forces wave breaking; and it keeps a quasi-steady distance from the shoreline (but not the run-up maximum). The gross morphological changes which occur across the steep macrotidal gravel beachface are largely consistent with those reported in earlier findings: a berm develops through swash over-topping and asymmetry [Hine, 1979; Austin and Masselink, 2006*a*; Weir et al., 2006], whilst seaward of the run down limit, a large beach step evolves [Austin and Masselink, 2006*a*].

Referring to the measured morphological change, it is evident from the sediment volumes, that as the tide begins to flood, the beachface initially undergoes a phase of consolidation. This is succeeded by a period of rapid morphological change during the mid-flood when the step and berm develop, followed by a quiescent period over the high tide still-stand. The berm and step then exhibit contrasting morphological behaviour, whereby the berm is consolidated whilst the step returns to a similar state to that before tidal inundation. The gross morphological changes which occurred across the beachface during the present study are consistent with the other fndings, in particular those of Austin and Masselink [2006*a*], where both the spatial distribution and temporal phasing of the step and berm development are in excellent agreement. During the last three experimental runs of this study, the magnitude of the morphological changes were signifcantly smaller due to calm wave conditions, but the trends dissimilar.

During the first two experimental runs of the present study and that of Austin and

Masselink [2006*a*], the step and berm were principally accretionary features linked to the tidal stage; however, the step and berm display several dissimilarities that lead to the question of whether they exhibit co-dependent behaviour or are independent features. On occasion, the step built *in-situ*, with its crest remaining at approximately the same contour throughout the sampling period, whilst in contrast the berm crest migrated landwards by ≈1.5 m. The toe of the berm remained at a fixed cross-shore position so the entire berm structure did not move onshore, but rather swash washed sediment over the crest which was re-established landwards. However, during the last three experimental runs, the whole structure of the small berm migrated landwards. During the present study, there was a net increase in sediment volume across the beachface, and whilst the volume of sediment eroded from the nearshore and mid-swash was roughly balanced by accretion at the step, the volume of material incorporated into the berm did not correspond to the erosion; this material must either have come from seawards of the step or was recycled from the step which was subsequently recharged from offshore. Alternatively, sediment supply to the berm and step was both ample and equal, but differing hydrodynamic or hydraulic forcing caused different patterns of sedimentation.

Net berm growth results from swash asymmetry [Duncan, 1964; Eliot and Clarke, 1988], whereas the step forms at the point of convergence between on/off-shore transport in the mid- and lower-swash and onshore transport of sediment eroded from the nearshore. Under these conditions, the step is an ephemeral feature with a short relaxation time that forms during the flood phase of the tide and is destroyed during the ebb. Step face sediments are sourced from the nearshore region and transported onshore to converge with sediment sourced from the lower swash which builds up the step crestal region. During the ebb, the crestal region is eroded and its constituent sediment returned to the nearshore. The berm develops coincidentally to the step during the flood, however, it has a relaxation time that is related to the spring-neap cycle and, unlike the step, persists on the beachface because it remains stranded above the shoreline as the tide ebbs; therefore, the berm conserves its sediment over a single high tide whereas the step does not. Consequently there is hysteresis between the coupled mid-swash-step-nearshore region, but not between the un-coupled bermmid-swash or bermnearshore regions. Step dynamics are thus tidally modulated: they are consistently more pronounced at high tide compared to mid-tide and often absent at low tide, instead

replaced, under calm conditions, with a series of subtidal ripples with long wavelengths.

Morphological changes on the beachface and just seawards of the step are in proportion to step dimensions for a given set of (low-medium energy) wave-tide conditions, implying a source-sink relationship and sediment convergence. The whole of the active foreshore is thus involved in maintaining the position and characteristics of wave breaking, in a morphodynamic relationship. Berm formation requires energy and tidal stationarity over-and-above that required for step formation, so in consequence, whilst a berm does not always develop, in contrast, a step always does. Step or berm may or may not migrate significantly over a single tidal cycle - this depends on the tidal translation distance. Where the berm does move, the toe of the berm remains at a fixed cross-shore position so the entire berm structure does not move onshore, but rather swash washes sediment over the crest which is re-established to landwards [Austin and Masselink, 2006*a*]. Foreshore sediment conservation of mass is not always achieved - the step is a mechanism by which beachface building and depletion occurs, liberating and transporting material from different areas in the tidal frame. Indeed, here is little net morphological change when the step is not very active.

Part of the reason for the different relaxation times of the berm and the step may be that alongshore sediment transport processes partially control the amplitude of the berm relative to the foreshore, but not the amplitude of the step (at least not directly). This is because the gradients in alongshore sediment transport may not be sufficiently strong at the breakpoint, given the extent of the forward momentum of the (highly nonlinear) waves. It remains possible, however, that volumes contributed or removed by alongshore transport on a given cross-shore stretch of beach may contribute to the supply at the step.

One of the key points of interest during the experiments was why the rate morphological change suddenly accelerated at 11:30 with the ensuing step formation. Considering the degree of morphological change that occurred across the beachface over the high tide period, the hydrodynamic conditions remained remarkably consistent. At the initiation of the step, there was no coincident change in H_s or T_s, or the proportion of low-frequency motions as reported by Ivamy and Kench [2006]. The only change observed was in S, from negative to positive, suggesting a switch from onshore to onshore sediment transport if following an energetics approach [Bailard, 1981]; however,

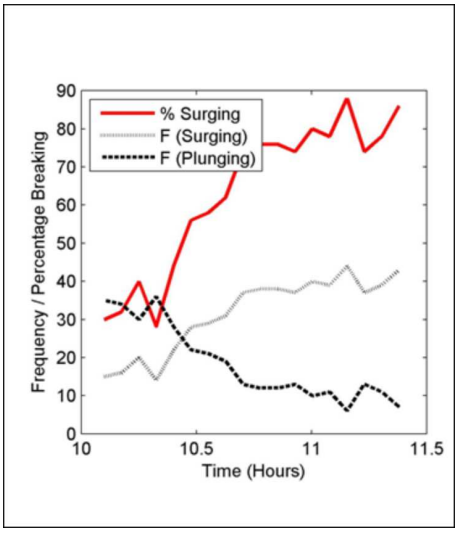

Fig. 5.24 *Example time-series of wave breaker type, visually assessed using a video record. This record is from 27th September 2005 experiment, around the time of step initiation.*

as Austin and Masselink [2006*a*] demonstrated, the direction of net sediment transport is not correlated to S across the nearshore at Slapton. Of potentially greater significance is the stationarity of the tide. The step is a region of sediment convergence between offshore transport in the lower-swash and onshore advection under the breaking waves. During periods of rapid tidal translation, there is insuffcient time for a step to form at the convergence point, which simply migrates with the breakpoint; however, once the TTR decreases approaching high tide, a point is reached whereby there is suffcient time (stationarity) to trigger step formation. Subsequently, positive feedback takes over and the reduction in water depth and increased beachface steepness forces wave breaking over the step, further increasing its height. A morphodynamic 'trigger' mechanism appeared to control step initiation, where a wave breaker transition occurs from plunging to surging. Breakers were classified 'wave-by-wave' visually using the subaerial video record (e.g Figure 5.24), and it was found that the agreement between visual observations and Iribarren number (ξ) was excellent. Here, any causative relationships dictate that timing is crucial, i.e. whether the step begins to build before or after the change in wave breaking. If the step forms before the change in breaker type from plunging to surging, then that would be the necessary increase in slope to affect ξ, yet if the wave breaker transition precedes step formation then it is more likely that tidal excursion over a concave slope is key. It was found that the latter case of tidal advection making conditions more reflective, was more likely. Thus, the surf scaling and similarity

parameters are suitable for quantifying this phenomenon. Any backwash vortex which may be present will also be amplifed by the positive feedback and will induce further sedimentation as described by Larson and Sunamura [1993]. The positive feedback is clearly illustrated by the rapid increase in the Irribarren number as waves are forced from breaking at the transition of plunging-surging to being firmly within the surging regime. During the falling tide, once the change in h and TTR increases above a certain limit, the seaward migration of the breakpoint breaks the cycle of positive feedback with the step, which then begins to be eroded by the backwash and smeared across the beachface. It is interesting to note that the step appears to be destroyed more rapidly during the falling tide than it is formed during the rising tide. This may be related to the asymmetry in $\delta h/\delta t$ observed in the semi-diurnal tidal curve and may also provide an explanation as to why the step is absent at low tide.

Changes in the sedimentology, unlike those of nearshore volumetric change, display no significant hysteresis. However, there are some interesting trends in the sediment size data which can be attributed to associated morphologies. The sediments are not as negatively skewed as is common with beach sediments [Masselink and Hughes, 2003], indicating the presence of a more mobile coarse fraction than is common on sand beaches, and corroborated by the general coarseness of the step and berm. The coarsening of the upper berm is consistent with observations from earlier work [Duncan, 1964; Masselink and Li, 2001], and while the four distinct phases of morphological change are not clearly reflected in the sedimentary signal, temporal changes in the sedimentology can be related to the morphological response across regions of the beachface. At the berm, step-crest and just seaward of the step, accretion (erosion) is linked to coarsening (fining) of the sediments. Conversely, across the step-face and part of the nearshore, the negative correlation between sediments and morphology indicates divergent behaviour; accretion is associated with fining and erosion with coarsening. The coarsening of the step sediments over high tide can be attributed to the preferential removal of fine sediments, seawards to the base of the step and landwards to the mid-swash. In contrast to Strahler [1966], who suggested that the coarse sediments accumulated at the step since they could more easily be transported over the finer sediments either side of the step, these findings indicate that the coarse sediments at the step constitute a lag deposit. Subsequently, during the falling tide, the retreating swash smears the fine mid-swash sediments over

the lower beachface. These findings contradict those of Masselink et al. [2007], that temporal changes in sedimentology were unrelated to the morphological response.

The coarsening of the upper berm is consistent with observations from earlier work [Duncan, 1964; Masselink and Li, 2001]. At the berm, step-crest and just seaward of the step, accretion (erosion) is linked to coarsening (fining) of the sediments. Conversely, across the step-face and part of the nearshore, the negative correlation between sediments and morphology indicates divergent behaviour; accretion is associated with fining and erosion with coarsening. In accordance with Strahler [1966], coarse sediments could accumulate at the step since they could more easily be transported over the finer sediments either side of the step, due to the sediment convergence which is thought to account for the formation of the step as a stable morphological form. Where the fining of the foreshore cannot be accounted for by this mechanism alone, additional fine material may be sourced from seawards to the base of the step, by-passing the step itself, or possibly cycled through the step. If the latter, this may also account for the wide variability in sorting and size at the step. There is, for example, not always persistence of coarse material on the step, since it is very sensitive to individual wave groups. To uncover the sedimentological dynamics of the step, the resolution employed by this study perhaps was not sufficient, i.e. a finer temporal sampling resolution is required, which necessitates remote sensing technologies. If the fine sediment generally by-passes the step, an advective and convective sediment transport mechanism is required, although this remains to be verified. In either case, the ('null point' - see chapter 2) sediment pattern/sorting model of Miller and Ziegler [1958], which treats shoal, breaker and swash zones separately, is neither conceptually nor empirically supported. Theories which account for step formation and maintenance need to take a holistic approach to the step with context to its evolving hinterland (Figure 5.25).

Temporal trends in sedimentary parameters were found to be generally unrelated to those of morphological change, however a degree of consistency in the spatial zonation of sedimentary parameters, when suitably averaged, suggest that negative feedback mechanisms are in place to retain a signature sedimentology on the beachface. These unknown mechanisms reinforce the spatially signatory structure of gravel beachface sedimentology despite changing wave and tide conditions; rates and magnitude of morphological change; and antecendent sedimentological conditions. The same remarks

of 'changing sea-state and tidal effect' not changing the 'underlying stability' of the gravel beachface sedimentology were made by Miller and Ziegler [1958]. Sediment trend models remained to be explored in this environment because under oscillatory flows, one would expect a pivot or 'pinch' in the spatial trend of size, sorting and skewness parameters around the lower-swash region (zone of divergence), which indeed there appears to be.

Sediment size distributions are found to vary on a time-scale comparable to the hydrodynamic forcing (wave time-scale), not the morphological changes, therefore improper sampling of the sedimentary signal may cause high-frequency components to be aliased with genuine low-frequency ones. Furthermore, only the top layer of the bed was sampled across the subaerial beachface and this may not have been representative of the active layer of the beachface as a whole since the presence of vertical variations in grain-size in beach sediment is well known in the form of laminae [Emery, 1978] and dual sedimentation units [Duncan, 1964]. However, the assertion that the step and berm are not morphodynamically co-dependent is mirrored by the surficial sedimentary record.

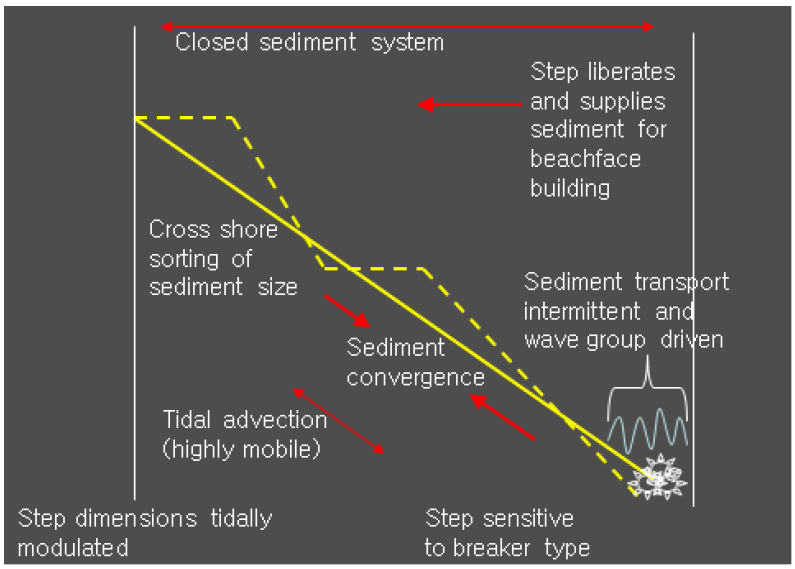

Fig. 5.25 *Summary schematic of some ideas discussed in this chapter related to the semi-diurnal dynamics of a gravel beachface.*

This study has attempted to measure instantaneous cross-shore sediment transport on a gravel beach using a novel video remote sensing method (Figure 5.25). Whilst suspended sediment transport can be measured with relative ease on sandy beaches with

optical and acoustic backscatter sensors, the quantification of the bedload and sheet flow modes of transport that prevail on gravel beaches is a much greater challenge. The implementation of the video-based bed monitoring system and the non-dimensional bed motion parameter Ω to provide a means to quantify the sediment transport through the change in bed texture. The results clearly demonstrate periodic transport due to the elevated flow velocities under wave group crests [Huntley and Hanes, 1987; Hanes, 1991], but the issue of similar magnitude velocity events causing differing bed responses causes problems when interpreting sediment fluxes. For example, in Figure 5.19, the flow velocity at 11:28–11:29 is comparable to that at 11:36–11:37, but Ω is twice as large during the former. The net result of this observation is poor coherence between Ω and u when the spectra are computed. On the whole, sediment transport is onshore at wind wave and wave group frequencies, but that due to swell is highly variable. This accounts for the net onshore-directed morphological change across the upper beachface (i.e. the conservation of berm sediments), but the lower beachface was approximately in equilibrium with the prevailing hydrodynamic conditions so this onshore transport must somehow be compensated by offshore transport. It is tentatively suggested that this occurs during the falling tide due to three mechanisms: (1) the tail end of the backwash increasingly acting upon the step crest and avalanching sediment down the step face; (2) the return of the wave breaker type towards the plunging-surging transition; and (3) the drainage of groundwater from the beachface during the falling tide [Austin and Masselink, 2006*a*].

The sediment transport events indicated by may not be linearly proportional to the instantaneous volumetric sediment flux and hence may be the reason why there are many occasions where the bed motions induced by two similar velocity events are very different. There are several possible mechanical explanations for the differing bed responses to velocity events of similar magnitude, but changes in bed roughness due to the wide variation of grain-sizes may be the main cause. It was frequently observed that changes in sediment size and distribution could occur on a wave-by-wave basis. It is therefore conceivable that an instantaneous change in the textural properties of the bed during one transport event may cause either positive or negative feedback upon the system by changing sediment transport thresholds. For example, if one transport event results in sediment coarsening through the removal of fines, this will cause an increase in

bed roughness through greater protrusion of the remaining larger grains into the boundary layer. This has at least three possible repercussions: (1) an increase in bed shear stress and turbulence leading to greater sediment mobility; (2) preferential transport of the largest grains due to their protrusion into the boundary layer; or (3) reduced mobility due to the larger entrainment thresholds of the bigger grains. Consequently, the following velocity event of similar magnitude may result in very different rates of bed motion. Therefore a better correlation may be obtained between and a shear stress parameter incorporating a variable bed roughness term, i.e. a Shields parameter containing a time-variant friction factor; however, this requires knowledge of the instantaneous grain-size/distribution.

5.5 *Summary*

(i) The gravel beach step and berm are accretionary features strongly linked to tidal stage, evolving with different relaxation times. Initiation of step morphology requires tidal stationarity and is perhaps triggered by a change wave breaker type from plunging to surging (although a morphodynamic relationship is also thought to exist between slope and breaker type).

(ii) Step dynamics are tidally modulated: they are consistently more pronounced at high tide compared to mid-tide, and often absent at low tide, instead replaced, under calm conditions, with a series of subtidal ripples with long wavelengths.

(iii) If the gravel beach step was forced by relative tidal stationarity, one would expect the step to have largest dimensions at both high and low tide, and to be smallest around mid-tide where tidal translation rate across the beachface is greatest. The fact that it is usually absent at low tide, and maximum in amplitude around high tide, suggests that the trigger for step growth and decay is some combination of factors forced by a threshold slope.

(iv) Berms may form and be pushed onshore with the tide as well as steps, but that the berm remains whilst the step does not (they have different relaxation times). Whilst the dynamics of the berm and step are related, the formation of the step is not dependent on the formation of the berm (although the reverse scenario remains an interesting research question).

(v) While the beachface at this timescale is not a closed sedimentary unit, what seems clear is that the step is a very important mechanism by which the upper beachface loses or gains material, by 'liberating' material either onshore or offshore depending on the hydrodynamic conditions. The zone of sediment transport is not restricted to the swash and surf zones, with exchanges of sediment extending into several metres of water depth, as shown by video observations.

(vi) The erosive phase of the tidal cycle persists longest in the lower swash zone. The dynamics of both the step and berm are asymmetrical with respect to tide. The latter is easier explained than the former in terms of the effects of groundwater.

(vii) Future simulations should shed some light on the role the step has to play, and indeed how much morphological change would be possible without the presence of the step. Theories which account for step formation and maintenance need to take a holistic approach to the step with context to its evolving hinterland.

(viii) The sedimentary record is very variable compared to the morphological record, and requires noise-reduction techniques such as EOFs to draw out the dominant modes of behaviour.

(ix) The step and beachface may be differentiated using sedimentary moments, and different morphological features such as the step have typical spatial sedimentary responses.

(x) A new technique to determine bed mobility from the shoaling/breaking zone has been devised, using output from an underwater video camera. At present, the technique cannot parameterise volumetric sediment transport, but in the future it may provide the basis for quantification of coarse sediment transport under waves in natural conditions.

(xi) Nearshore sediment transport may be related to sub-incident frequencies (wave groups) but appears not to be a linear function of either velocity magnitude or direction. Therefore, a better description of sediment transport requires instantaneous sediment size information, which has to be remotely sensed.

6 MORPHO-SEDIMENTARY DYNAMICS OVER THE SEMI-LUNAR TIDAL CYCLE

He had forty-two boxes, all carefully packed,
With his name painted clearly on each:
But, since he omitted to mention the fact,
They were all left behind on the beach.

Lewis Carroll (1832-1898). British poet. The Hunting of the Snark.

6.1 *Introduction and Data Collection*

Previous studies on gravel beaches at the time-scale of the spring-spring tidal cycle have either focused on aspects of morphological change, *or* sedimentological change, with respect to hydrodynamic forcing. There is little comparitive work on the simultaneous response of a relatively fine and relatively coarse gravel beach under similar hydrodynamic conditions. Our insight into gravel beach morpho-sedimentary dynamics over the present time-scale of interest would improve if such detailed measurements were taken.

Accordingly, the first survey campaign in the autumn of 2005 was designed to compare the morpho-sedimentary dynamics of a relatively coarse (central Slapton Sands) and relatively fine (Strete Gate) gravel beach, experiencing similar wave-tide conditions. The beach at Strete contains a cross sectional volume of 320m^3 from barrier crest to MLWS at -2m ODN, is convex in profile, and has a mean sediment size of $\approx$ 4mm. The beach at central Slapton contains a cross sectional volume of 86m^3, is more planar, and has a mean sediment size of $\approx$ 6mm. In this survey, beach profiles and surface samples were

taken over 26 consecutive low tides. Samples were taken every 0.5m across the active intertidal beachface (from previous high tide to low tide shoreline). Disturbance depths (the lowest detectable depth of sediment activation relative to the surface) and sub-surface sediments were recorded occasionally.

The data set consisted of beach profiles and sediment samples taken from the active intertidal area of Slapton, every low tide over a semi-lunar tidal cycle. The first consisted of profiles and surface samples taken every half-metre across the beachface in the central portion of Slapton during the autumn of 2005, over 26 consecutive tides. At the same time, the second consisted of profiles and surface samples taken every half-metre across the beachface in the northern portion of Slapton, called Strete, again over 26 consecutive tides. The central Slapton (hereafter, simply 'Slapton') and Strete sites are separated by some 2km, and differ in their mean sediment size which was ≈6mm and ≈4mm, respectively during the respective campaigns. Profiles were taken using a total station, which has a vertical accuracy of the order of millimetres. To ensure samples were taken at identical points along the profile each low tide, a rope marked every half-metre was extended from a consistent reference point. The third data set consisted of profiles, and samples taken at the surface, and sub-surface to the depth of disturbance over the previous tide (the maximum depth to which sediments were disturbed). The disturbance depths (hereafter, 'DOD') were measured using a rod and washer system described and used by Greenwood and Hale [1980]; Jackson and Nordstrom [1993]; and on the same beach as the present study by Austin and Masselink [2006*a*]. Profiles were again taken with a total station at a spacing of ≈ 1m, and the consistent location of the samples was ensured by the rods inserted into the beach for the DOD measurements. Both surface and sub-surface sediments were thus 'active' over the last semi-diurnal tidal cycle, although it was expected that their sedimentology would differ markedly, the latter on this steep reflective beach being associated with the passage of the step into and out of the frame over the previous tide [Jackson and Nordstrom, 1993]. In total, 1546 sediment samples were collected: 1220 in the first experiment, and 326 in the second.

The relationship between the morpho-sedimentary dynamic signature left at depth and that at the surface was the primary focus of the second survey data set drawn upon in this chapter. Relatively little is known about the size and sedimentology of the active layer on a gravel beach, in contrast with a lot of such work on sandy beaches [Jackson

and Nordstrom, 1993; Anfuso et al., 2000; Anfuso, 2005]. Correct determination of the disturbance depth alone is crucial for correct determination of volumes of sediment transport moved cross- and alongshore. The second survey campaign in the spring of 2007 focused on one site (Strete) in more detail. As well as beach profiles and surface sediment samples, depth of disturbance (hereafter, DOD) and sub-surface samples were taken over 24 consecutive tides. Samples were taken every metre across the active intertidal beachface (from previous high tide to low tide shoreline). Field hydrodynamic and morphological instrumentation and data acquisition for these campaigns are outlined in Chapter 4, as well as the analysis of the sediment samples, and the derivation of standard hydrodynamic and morphodynamic parameters.

6.2 *Data Analysis*

To uncover any potential 'triad' relationships between hydrodynamics, morphological and sedimentological change, a number of statistical techniques based on eigen-decomposition and correlation were employed. Autocorrelation ±95% confidence intervals are given by $\pm 2/\sqrt{N/2}$. Unless otherwise stated, the correlogram sequence is normalised so the autocorrelations at zero lag are 1. Significantly autocorrelated values are delimited by a Z-test score Z=1.96 at $\alpha = 0.05$, where

$$Z = r_\tau \sqrt{n - \tau + 3} \tag{6.1}$$

and where l, r_l, and N are lag, correlation at lag, and sample size respectively [Davis, 1986]. Significantly cross-correlated values are delimited by a **t**-test of $H_o : r = 0; H_1 : r \neq 0$ given by

$$\mathbf{t} = r_l \sqrt{\frac{N-2}{1-r_l^2}} \tag{6.2}$$

with N-2 degrees of freedom, tested at $\alpha = 0.05$ [Swan and Sandilands, 1995]. All quoted and plotted autocorrelations in this chapter are two-dimensional, and significances have been determined at α=0.05. The more sophisticated numerical methodologies employed on the data sets here —those designed to uncover dominant and simultaneously occurring patterns in the data, and those to statistically assign causal linkages (of a linear nature) —are detailed below.

6.2.1 *Empirical Orthogonal Function (EOF) Analysis*

The mathematical details of EOF analysis are detailed in chapter 5 are so are not reproduced here. The EOFs were used in an identical fashion, i.e. the morphological and sedimentological data sets analysed using EOFs consisted of matrices of observations over space (x, rows) organised in time (t, columns). Resulting eigenfunctions were therefore either temporal modes denoted $c_q(t)$, or spatial modes denoted $e_q(x)$ (following Miller and Dean [2007]). EOF analysis uncovers 'stationary' (non-propagating) patterns because it is based on simultaneous covariances. In this study it was noted that some EOF modes for morphological change and sediment size/sorting were better correlated at some lag (cross-correlated) than at zero lag. Further to an ordinary EOF analysis to uncover simulatenous covariance in morphological and sedimentological datasets, complex EOFs (CEOFs) were used to investigate relative phase information in both space in morphological change and sediment size and sorting. In the coastal literature, CEOFs have been used by Ruessink et al. [2000] to investigate the dynamics of bars on the Dutch coast by separating the two- and three-dimensional variability. CEOFs are able to extract non-stationary information, based on the notion that any waveform can be expressed using a complex representation:

$$x(t) = \wp \exp^{\mathbf{i}ft+w} \tag{6.3}$$

where $\wp$ is the wave amplitude, and f and w are its frequency and phase shift respectively. The data matrix is transformed into its complex form as [Ruessink et al., 2000]:

$$\ddot{Y}_c(x,t) = \Re y_c(x,t) + \Im y_c(x,t) \tag{6.4}$$

where the real ($\Re$) part is the original data and the imaginary ($\Im$) part is its Hilbert transform given by:

$$H(\hat{Y}_c) = \sum_{\omega} \ell(\omega) \cos \omega t - \wp(\omega) \sin \omega t \tag{6.5}$$

where $\wp$ and ℓ are the Fourier coefficients. Following Barnett [1983], the Hilbert transform represents a simple phase shift $\pi/2$ in time/space and is calculated using a FFT algorithm. The data is then transformed into:

$$\tilde{Y_c} = \mathbf{i} + \ddot{Y_c} \times H \tag{6.6}$$

where $\mathbf{i} = \sqrt{-1}$. The CEOFs are obtained from the covariance matrix of $\tilde{Y_c}$ [Horel, 1984], given by:

$$CV = 1/N \sum_{q=1}^{N} \tilde{Y_c} \tilde{Y_c}^{*T} \tag{6.7}$$

where * denotes complex conjugate. The CEOFs are then given as:

$$\hat{Y_c} = \mathbf{E}_c \lambda \mathbf{C}_c^T \tag{6.8}$$

where λ are the eigenvalues of CV; $\mathbf{E}_c$ are the spatial CEOFs ($c_{qc}(x)$), given by the matrix product of $\ddot{Y_c}^T$ and the eigenfunctions of R; and $\mathbf{C}_c$ are the temporal CEOFs ($e_{qc}(t)$), given by the product of $\mathbf{E}_c$ and $\ddot{Y_c}^T$. The spatial and temporal phase are defined by, respectively [Ruessink et al., 2000]:

$$\theta(x) = \arctan\left(\frac{\Im c_{qc}(x)}{\Re c_{qc}(x)}\right) \tag{6.9}$$

$$\psi(t) = \arctan\left(\frac{\Im e_{qc}(t)}{\Re e_{qc}(t)}\right) \tag{6.10}$$

For every EOF mode, various measures can be used for quantifying features in the data. The amplitude of $c_q(x)$ and $c_{qc}(x)$ represent the spatial varibility associated with that mode, and the spatial phase function $\theta(x)$ shows the relative phase of fluctuation at various locations. The spatial gradient of $\theta(x)$ provides local wavenumbers [Ruessink et al., 2000], the spatial analogue of frequency. The amplitude of $e_q(t)$, and the amplitude and phase of $e_{qc}(t)$ provide information on the temporal variability associated with each EOF mode, and the time derivative of $\psi(t)$ is a measure of frequency.

The EOF technique has been reviewed by Larson et al. [2003] for use on bathymetric data sets. For a more detailed mathematical description of the whole EOF family of techniques and their inter-relations, the reader is referred to Horel [1984] and Hannachi et al. [2007]. The use of CEOFs provides a more robust method of pattern identification in data sets because they are less sensitive to the spatial domain and time period, and the number of degrees of freedom.

6.2.2 *Canonical Correlation Analysis*

Uncovering any morpho-sedimentary-dynamic relationships is essentially a problem based on how much the three sets of variables correlate, or simulataneously vary. Note that correlation is usually a better measure of linear association than covariance [Davis, 1986]. The problem with correlation, however, is that it does not imply causation: where present, correlation between morphological change and beachface sedimentology exists, to an unknown degree, because they are both functions of a third set of variables: hydrodynamics.

Canonical correlation analysis (CCA) is a multivariate extension of correlation which assesses the relationship between two sets of variables (thus differing from multiple regression which can only assess the relationship between one dependent variables and set of independent variables). CCA is therefore appropriate for this study since not only will it enable identification of linear relationships between morphological and sedimentological variables, but also between either of these and a set of hydrodynamic forcing variables. In short, it is a potentially useful tool in uncovering the triad of relationships which may exist between hydrodynamics, morphological change and sedimentological change on a gravel beach. CCA can be used to investigate whether there are any patterns which occur simultaneously in two sets of data (variables), and assign a strength of correlation between them. CCA was used by Larson et al. [2000] to study the dynamics of beach profiles at Duck, North Carolina, in relation to hydrodynamic forcing. An additional advantage of CCA, and one also utilised by Larson et al. [2000], is that a certain number of EOF modes are commonly used as input variables so as to reduce the noise in the statistical model.

Two original data sets, Y_1 and Y_2, are transformed into new new data sets, Y_3 and Y_4, which are linear and maximally correlated combinations of the original:

$$Y_3 = \aleph^T Y_1 \tag{6.11}$$

$$Y_4 = \nabla^T Y_2 \tag{6.12}$$

where $\aleph$ and ∇ are arbitrary vectors, selected so correlations are maximised [Davis, 1986]. These vectors (or 'weights') for Y_2 are given by the solution to an eigenvalue

problem given by (modified from [Davis, 1986]):

$$(\Lambda - \lambda I_d)\nabla = 0 \tag{6.13}$$

where I_d is an identity matrix; λ are the eigenvalues; and $\Lambda = \left[(Y_1^T Y_1)^{-1}(Y_1^T Y_2)(Y_2^T Y_2)^{-1}(Y_2^T Y_1)\right]$. The equivalent canonical transform of Y_1 is found by:

$$\aleph = (Y_2^T Y_2)^{-1}(Y_1^T Y_2)\nabla/\sqrt{\lambda} \tag{6.14}$$

The canonical scores (modes) for Y_1 and Y_2 are obtained as, respectively (modified from [Davis, 1986]):

$$\amalg(x) = \amalg^T Y_1 \tag{6.15}$$

$$\amalg(y) = \amalg^T Y_2 \tag{6.16}$$

where $\amalg = CR_x^{-1} r_{pm} \varrho$, CR_x is the correlation matrix of Y_1; r_{pm} is the product-moment correlation of Y_1 and Y_2; and ϱ are the eigenfunctions of the covariance matrix of Y_1 and Y_2, CV, given by:

$$CV = CR_y^{-1} P^T CR_x^{-1} r_{pm}^T \tag{6.17}$$

where CR_y is the correlation matrix of Y_2. The canonical correlations are given $r_{CCA} = \sqrt{\lambda_{CCA}}$, where λ_{CCA} are the eigenvalues of CV.

6.3 *Hydrodynamic Conditions*

The hydrodynamic conditions for the autumn 2005 survey are summarised in Figure 6.1. Offshore measurements come from the WaveWatch III model, at the Start Point nodal point, as described in Chapter 7. The general picture was one of consistent south-westerly swell, becoming more broad-banded with a significant wind component after tide 10 (23^{rd} September). Nearshore wave heights for the first two tides were in the region of ≈0.2m, and between tides 4 and 20 increased steadily from ≈0.15 to ≈0.5m, then back down to ≈0.2m by tide 26 (1^{st} October).

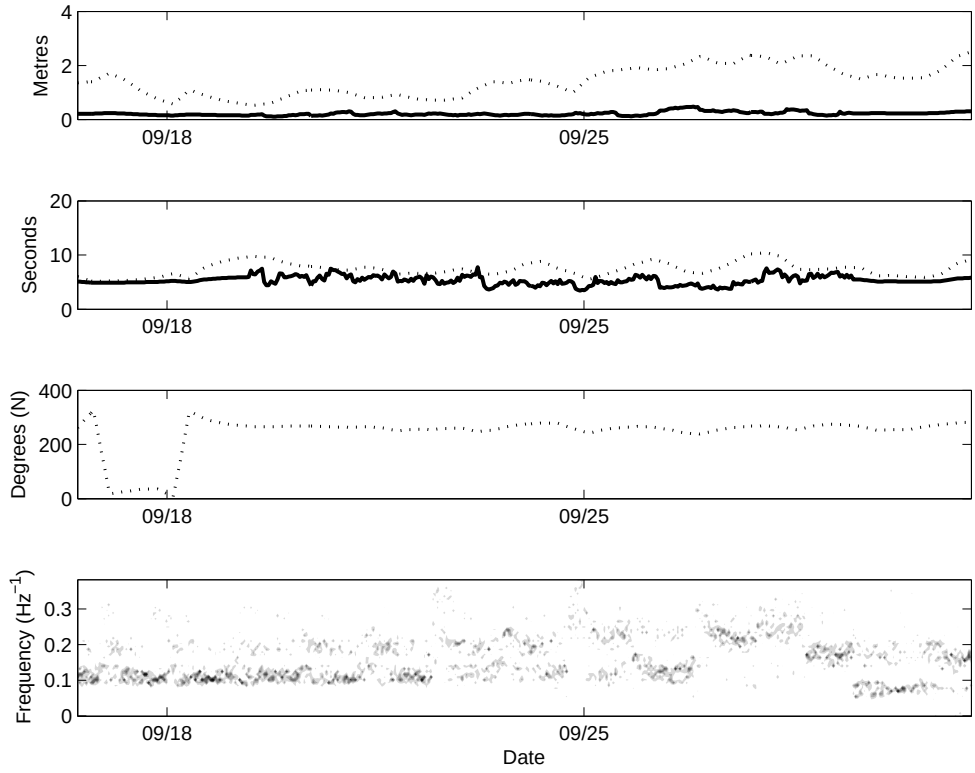

Fig. 6.1 *Hydrodynamic conditions for the Autumn 2005 field survey.* ***From top to bottom****: half-hourly H_s and H_o; T_s and T_o; Θ_w, and normalised wave spectral density (m Hz^{-1}). Dashed and solid horizontal lines indicate mean values for the offshore and nearshore records of wave height and period.*

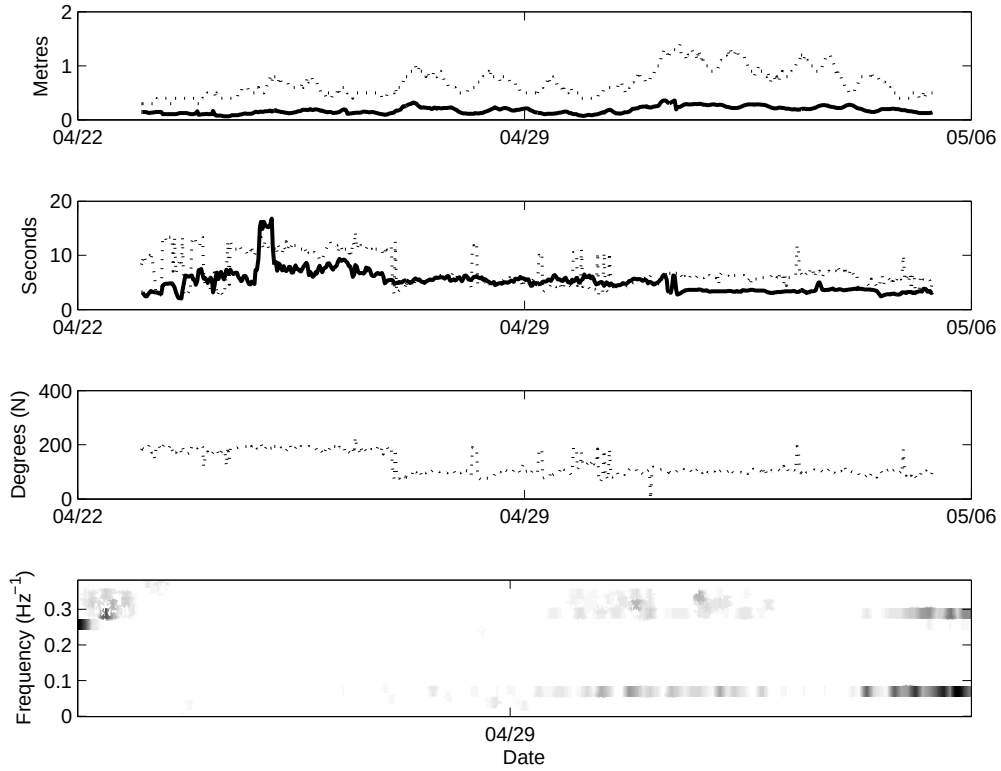

Fig. 6.2 *Hydrodynamic conditions for the Spring 2007 field survey.* ***From top to bottom****: half-hourly H_s and H_o; T_s and T_o; Θ_w, and normalised wave spectral density (m Hz^{-1}). Dashed and solid horizontal lines indicate mean values for the offshore and nearshore records of wave height and period. Nearshore data to the right of the dashed vertical line have had a linear transfer function applied from the offshore record.*

The hydrodynamic conditions for the spring 2007 survey are summarised in Figure 6.2. Due to technical difficulties, the last few days of the pressure record was unusable so a linear transfer function was created using the measured offshore and nearshore wave record to estimate the nearshore wave height, direction and period for the time covering the missing nearshore wave records. Offshore measurements come from the directional waverider buoy described in Chapter 7. During the spring 2007 survey, the general picture was one of low crested (≈0.2–0.3m nearshore, ≈0.4–0.7m offshore), south-westerly, narrow-banded swell at variable 8–15 second period between tides 1 and 9 (23^{rd}–27^{th} April), thereafter giving way to larger (0.4–0.5m nearshore, 0.8–1m offshore) and more easterly broader-banded sea at decreasing 8–4 second periods, with a subordinate swell component.

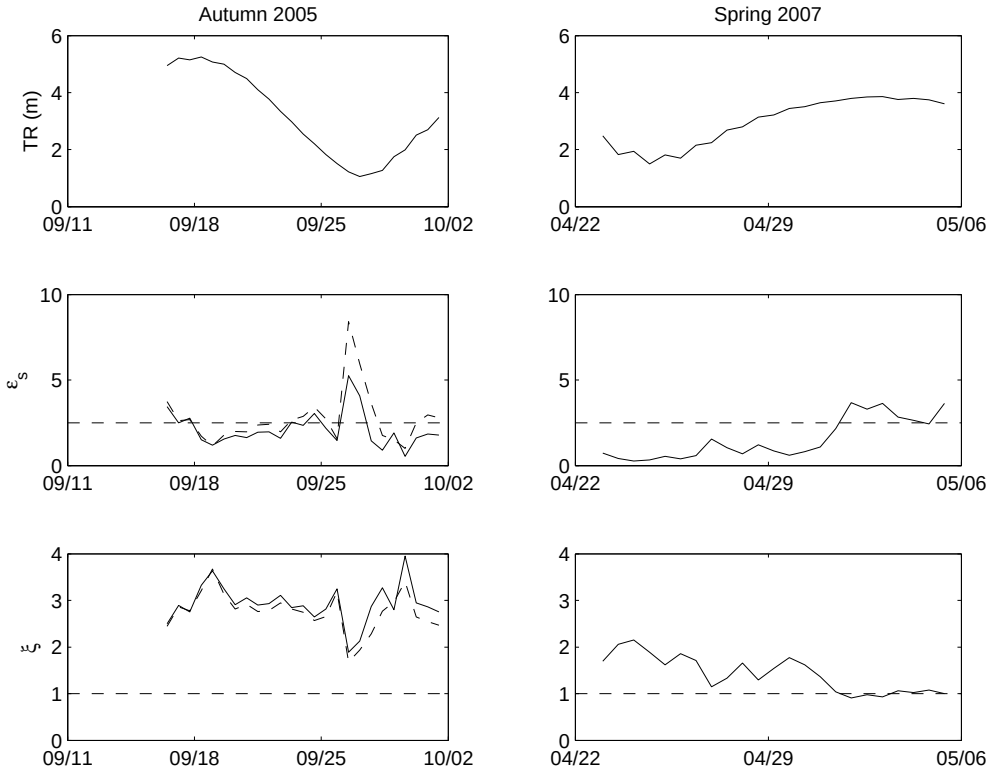

Fig. 6.3 ***From top to bottom****: tidal range, surf similarity, Iribarren number, groupiness function, spectral width. Varibles for the autumn 2005 and spring 2007 surveys are on the left and right panels, respectively. Left of the dashed line for the latter two variables in the spring 2007 survey there is no data available. The horizontal dashed line in ϵ_s delimits reflective and intermediate conditions, and the horizontal dashed line in ξ delimits surging and plunging breakers. Dot-dash lines in ϵ_s and ξ trace the response at Strete.*

With reference to Figure 6.3, there were a number of differences in the hydrodynamic and morphodynamic record for the respective survey campaigns. The major difference

was the lunar tidal phase: the autumn 2005 survey started just before spring tide, and finished on mid-cycle after neap, whereas the spring 2007 survey started mid-cycle after springs and finished just after the subsequent spring tide. Conditions for both surveys fluctuated between reflective and intermediate-reflective (ϵ_s), but ξ predicted surging breakers at all times, which became substantially more broad-banded (ϵ_w) during the spring 2007 survey.

6.4 *Morphological Change*

Beach profiles for the three data sets may be seen in Figure 6.4, as envelopes (top panels) and stacked successively in time (bottom panels). Note how much more obvious the berm building is more obvious at Slapton compared with Strete (the relatively fine end of the beach). Also note the extent of the disturbance depth envelope, marked by a dashed line on the top left sub-panel.

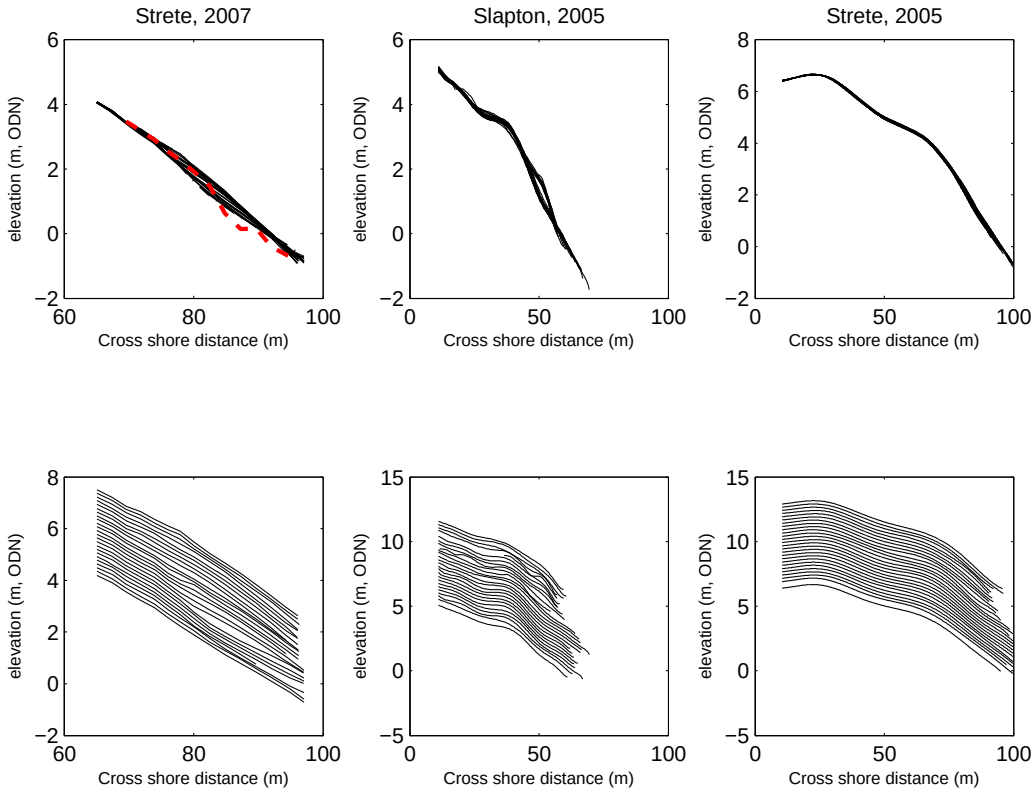

Fig. 6.4 *Beach profiles for the three data sets.* ***Top panels****: profiles for, left to right, Strete 2007; Slapton 2005; and Strete 2005.* ***Bottom panels****: profiles stacked in time (bottom to top). Dashed line on the top left panel indicates maximum depth of disturbance over the survey period over the intertidal profile.*

With reference to Figure 6.5, initial relative depletion at Slapton during the autumn 2005 survey over tides 1 and 2 preceded a period of quiescence for the next 13 tides, when little net sedimentation occurred. Between tides 15 and 20, sustained berm building (in two stages, between tides 16–18 and 20–21) coincided with an increase in wave height and a more broad-banded wave field around neap tide, followed by some net depletion over tides 22–24, and finally net accretion thereafter. Over the 26 tides there was net (positive) sedimentation over the intertidal profile. Periods of relative morphological quiescence, and the rate of morphological change over individual time steps (the first temporal derivative), are reflected nicely by the cross-shore averaged morphological change (per unit metre of beachface) and correlograms in Figure 6.5.

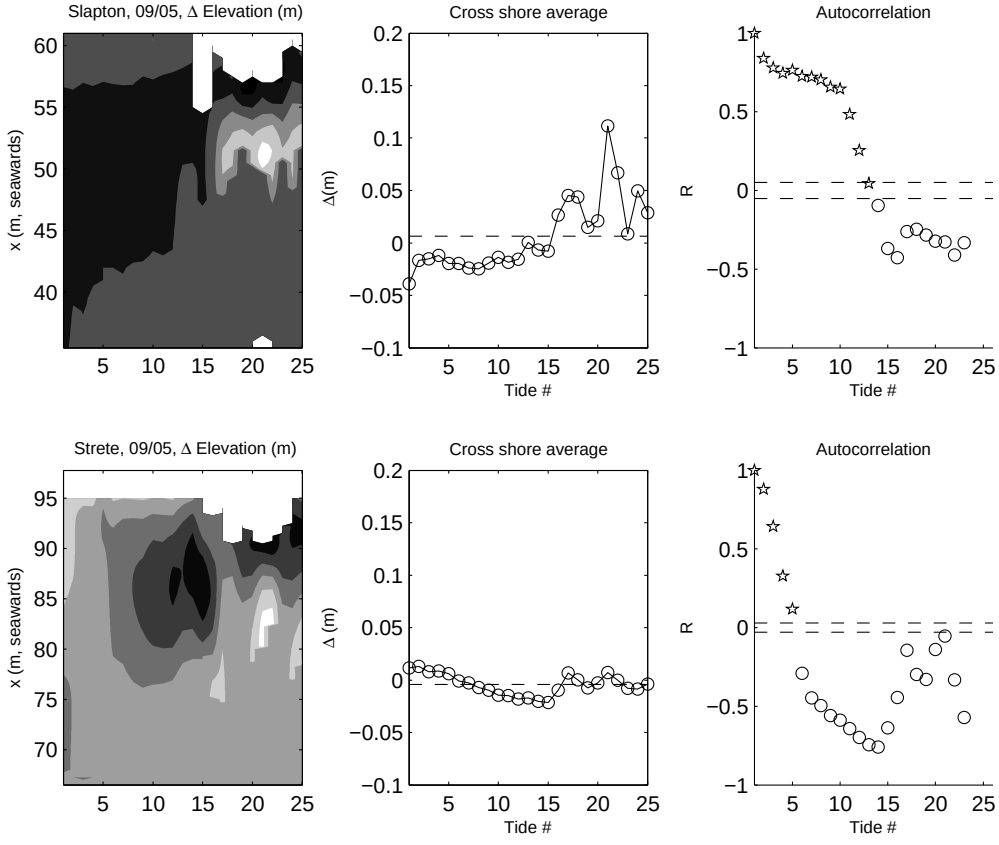

Fig. 6.5 *Morphological change, September 2005. Top: Slapton; Bottom: Strete.* ***From left to right****: elevation relative to initial (*Δm*) - contours incremented by* $2\times std(\Delta m)$*; cross-shore averaged* Δ *m, with averaged value marked as dashed line; two-dimensional autocorrelation of* Δ *m. Confidence intervals marked as dashed lines; significantly autocorrelated values as stars, and significantly un-autocorrelated values as circles.*

Steady depletion occurred at Strete during the autumn 2005 survey over tides 1 and 15. Like at Slapton, berm accretion occurred in two stages over tides 15–18 and again over 20–21. Thereafter, there was some relative depletion, although overall over the 26

tides there was no net sedimentation and the magnitudes of morphological change were small. Morphological change at both locations was dominated by the berm which developed over tide 15–16; however it seems that the mechanism of berm building differed subtly between the two sites, which is supported by several strands of evidence.

At Slapton, the new berm developed 10m seaward of the existing berm at the end of the spring → neap transition over tide 16, sourcing material from seawards of the new berm (where relative depletion was evident). At Strete, berm formation was detectable slightly earlier, at the beginning of the tidal wane on tide 15, and more likely through a mechanism identified by Austin and Masselink [2006*a*] as (cut and fill) 'regression', where the new berm developed as an extension of the existing berm without the extensive removal of material from lower in the profile. The mechanism of the berm formation at Slapton may be more descriptively termed (cut and fill) 'transgression', not being associated with either sediment draw-down from elevated regions in the intertidal zone, nor feature coalescence, but a fresh input of sediment sourced from lower in the intertidal frame.

During the spring 2007 survey, because of the smaller tidal range (Figure 6.3), the active intertidal area was slightly smaller. Again the morphological record (Figure 6.6) was dominated by berm building, and bore a great deal of resemblance to the morphological change at Strete during the autumn 2005 campaign, except that this time there was no pre-existing berm. The mechanism for berm building is again thought to be that of cut and fill transgression. The major difference between the two surveys in terms of morphological change was the timimg of depletion and subsequent berm building relative to the tidal cycle. Depletion during the 2005 surveys coincided with relatively small waves and a spring tide, whereas berm building occurred around neap tide under slightly more energetic conditions. During the 2007 survey, however, depletion occurred from mid-spring tide under calm waves, and berm building occurred from mid-spring tide under slightly more energetic and broad-banded conditions.

The DOD record (Figure 6.6) showed a clear spatial pattern, being consistently larger on the lower intertidal than the upper intertidal beach. This is thought to be so because of the shorewards and seawards migration of an active beach step with the semi-diurnal tidal cycle (see Chapter 5). However, the temporal trend was less simple. Indeed, there was very little association between the cross-shore average of DOD and either tidal

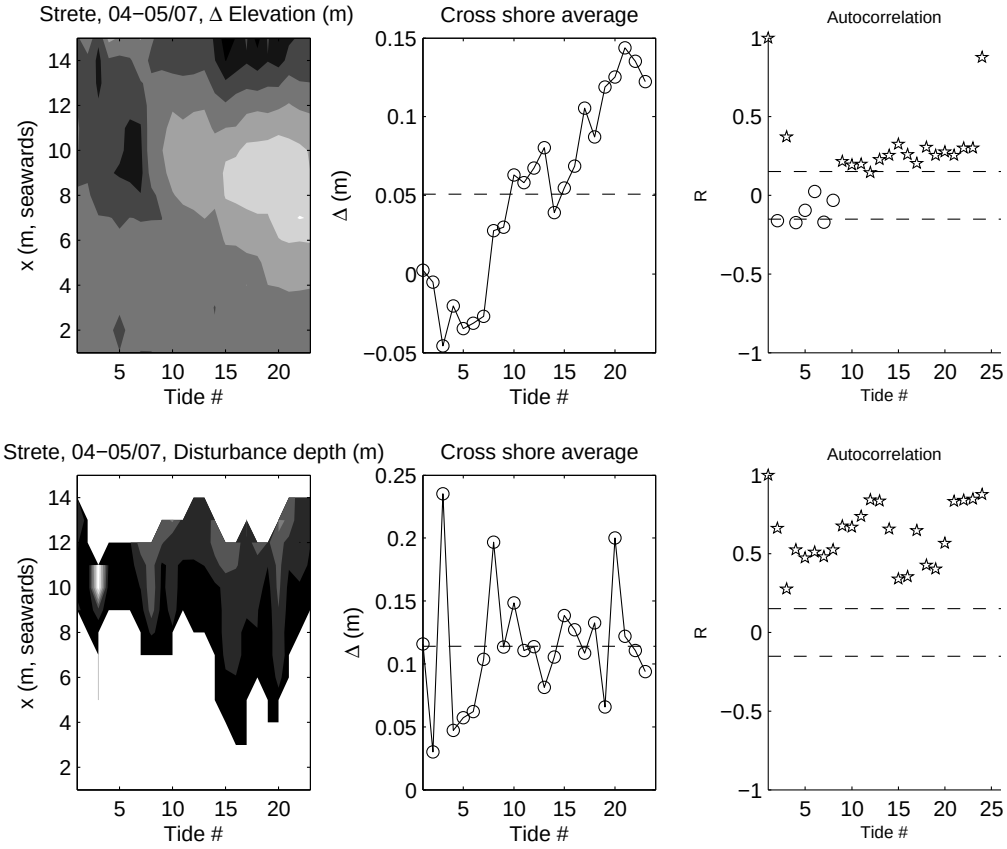

Fig. 6.6 *Morphological change, April-May 2007.* ***Top, from left to right****: depth of disturbance (m) - contours incremented by 2×std(DODm); cross-shore averaged depth of disturbance (m); and two-dimensional autocorrelation.* ***Bottom, from left to right****: morphological change relative to initial (Δm); cross-shore averaged Δ m, with averaged value marked as dashed line; two-dimensional autocorrelation of Δ m. Confidence intervals marked as dashed lines; significantly autocorrelated values as stars, and significantly un-autocorrelated values as circles.*

range, wave height/steepness or beachface reflectivity.

6.5 Sediment Dynamics

6.5.1 Sediment Size

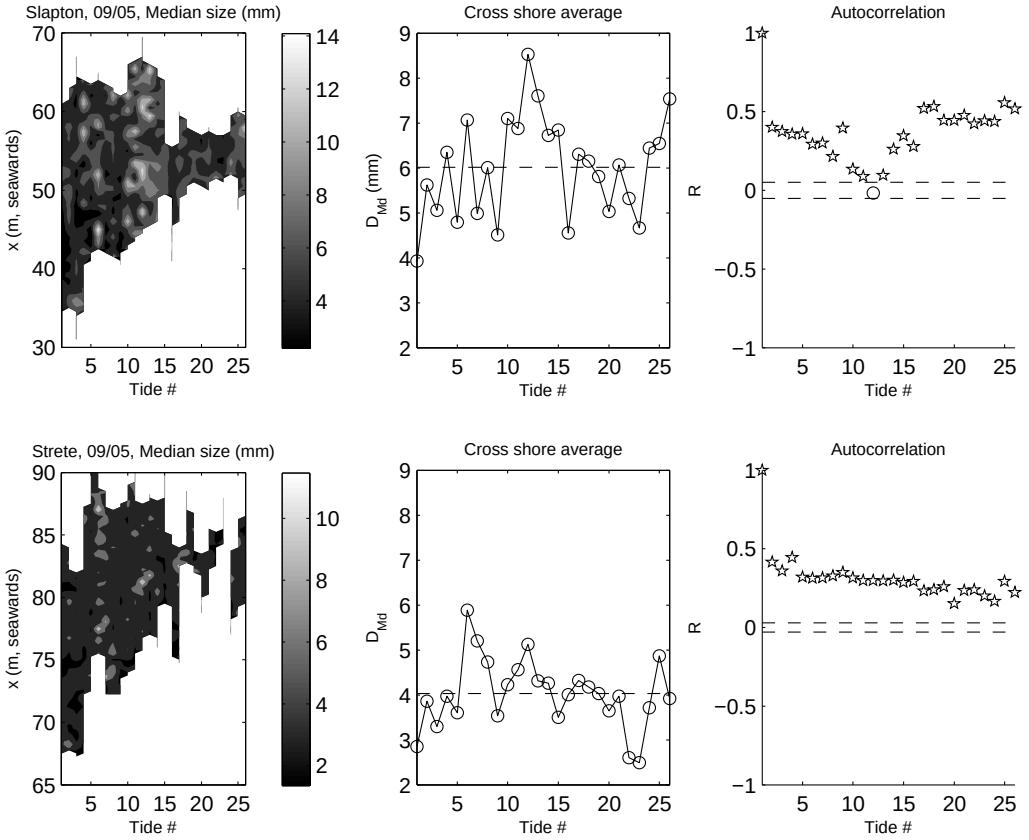

Fig. 6.7 *Change in sediment size, September 2005. Top: Slapton; Bottom: Strete.* ***From left to right****: sediment size (mm) - contours incremented by 2× std(D_{Md} mm); cross-shore averaged size (mm), with averaged value marked as dashed line; two-dimensional autocorrelation of size (mm). Confidence intervals marked as dashed lines; significantly autocorrelated values as stars, and significantly un-autocorrelated values as circles.*

Median surface sediment size for the autumn 2005 surveys is depicted in Figure 6.7, along with respective cross-shore averages over time, and autocorrelation profiles (correlograms). Sediment size fluctuated considerably about their respective temporal means (depicted by the dashed horizontal lines in the centre subpanels); however, they both remained significantly autocorrelated for almost the entire survey. Of note are a major coarsening event around tides 12–14 at Slapton and Strete, and a coarsening event at Strete on tide 6. In general there is some degree of coherence in this temporal sediment size signal at Slapton and Strete, although they are out of phase possibly as

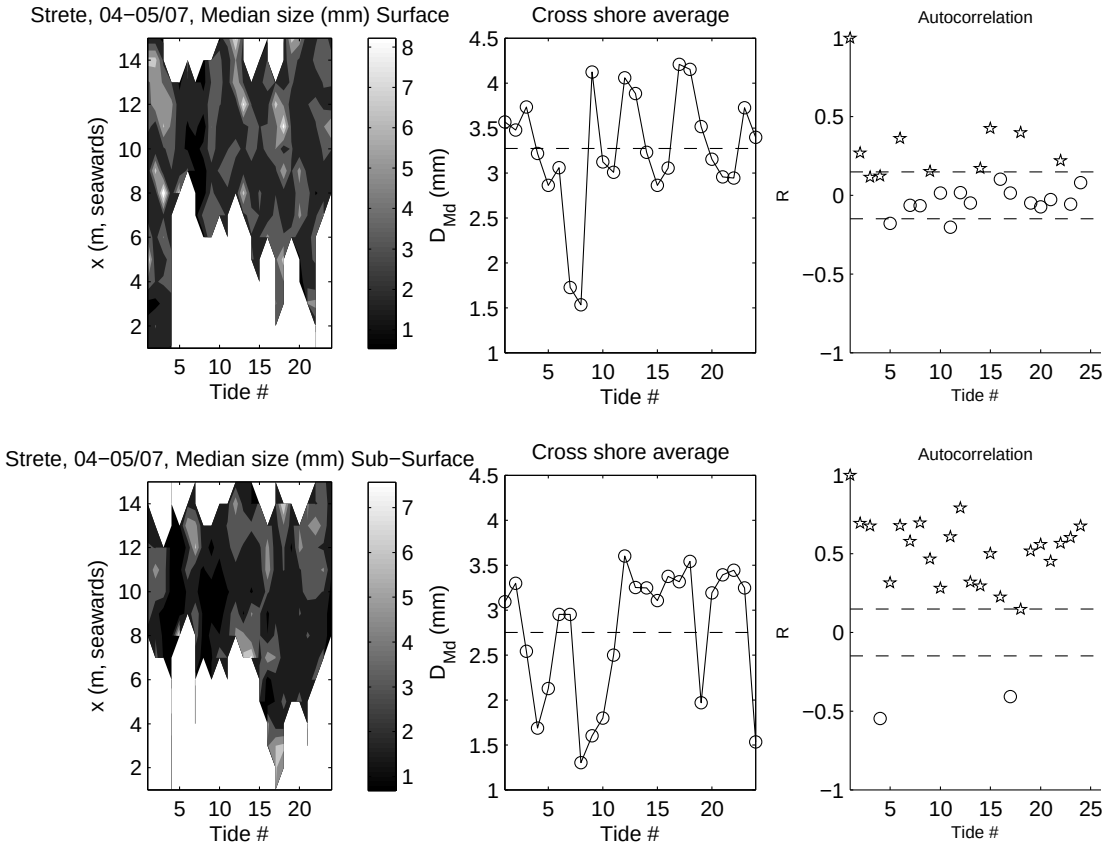

Fig. 6.8 *Change in sediment size, April-May 2007.* ***Top, from left to right****: sediment size (mm) - contours incremented by 2× std(D_{50} mm); cross-shore averaged size (mm); and two-dimensional autocorrelation.* ***Bottom, from left to right****: sediment size (mm); cross-shore averaged size, with averaged value marked as dashed line; two-dimensional autocorrelation of size. Confidence intervals marked as dashed lines; significantly autocorrelated values as stars, and significantly un-autocorrelated values as circles.*

much as they are in phase. The same is true for their respective spatial and temporal derivatives (not shown). It is clear that sediment size had a complicated space-time history during the surveys, and thus it is very difficult to assess visually any coherent patterns in the surficial sediment size and morphological change at respective locations

The surface and sub-surface sediment size records for the spring 2007 survey are the subject of Figure 6.8. On this evidence, there is perhaps more coherence between surface and sub-surface sediments in the same location than between surficial samples separated by over 2km. This was expected to some extent since the beach is usually graded alongshore, although not usually across the entire intertidal profile (Chapter 3). The sub-surface size record shows much clearer spatial segregation (coarsening seawards) than the surficial sediment size records from the other three data sets. Whereas the sub-surface size record is usually significantly positively autocorrelated, interestingly the same is not true for the surface size during the 2007 campaign. Again the temporal trend is highly variable, and once again it is difficult to visually discern any meaningful relationship with the associated morphological change. For sediment size records from both survey campaigns, it is equally difficult to resolve coherent and consistent patterns with the tide and wave records.

6.5.2 *Sediment Sorting and Skewness*

The space-time fields of geometric sorting (σ) for the autumn 2005 survey may be seen in Figure 6.9 for Slapton and Strete on top and bottom panels, respectively, along with temporal trends and correlograms. One might surmise Slapton as being varying moderately well sorted to moderately sorted. Strete is generally moderately well sorted, but displays spikes of moderately poorly sorted sediment (please refer to Chapter 4 for a classification guide on geometric sorting). Again the pattern in both space and time is very complicated, and it is rather difficult to glean any patterns which share similarity in both data sets. One thing that is apparent, however, is the similarity of the correlograms for sediment size (Figure 6.7) and sorting (Figure 6.9) for both sites. It would appear that the pattern in space of size and sorting is more similar for both sites, since the same coherence is not readily apparent in the temporal trends.

The corresponding field of sorting (surface and sub-surface) for the spring 2007 survey is the subject of Figure 6.10. Surface and sub-surface sorting appear to be spatially

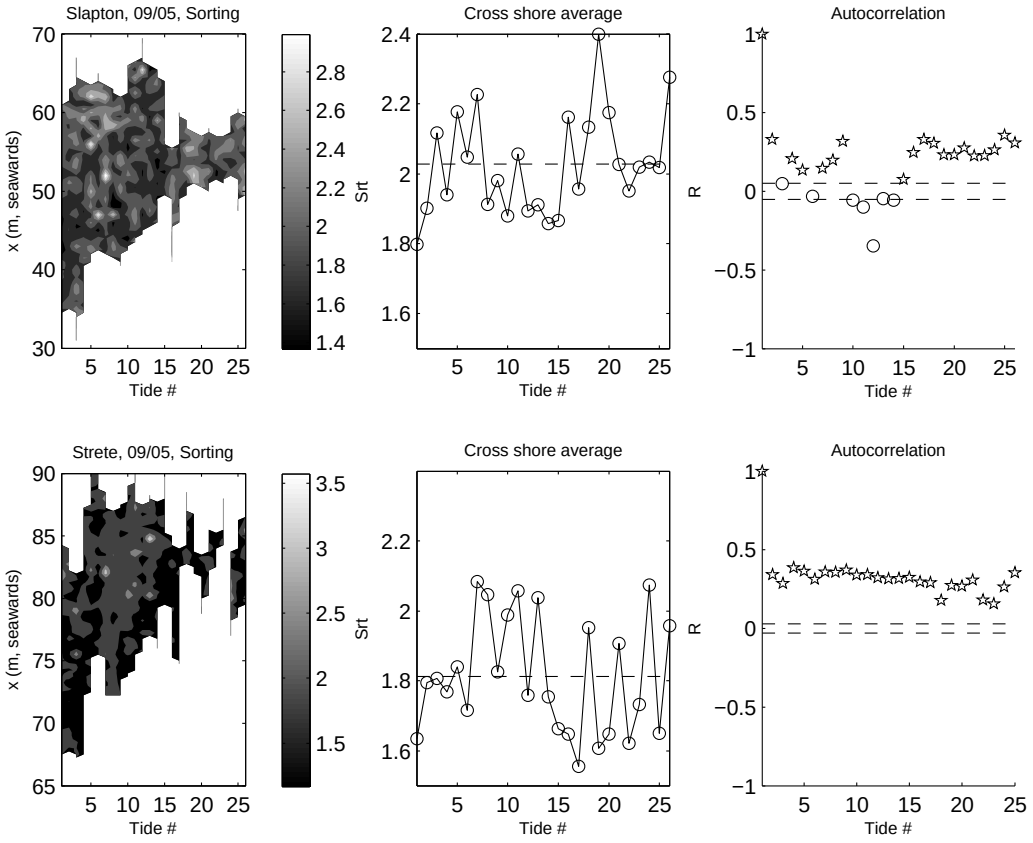

Fig. 6.9 *Change in sediment sorting, September 2005. Top: Slapton; Bottom: Strete.* ***From left to right****: sediment sorting - contours incremented by 2× std(σ); cross-shore averaged sorting, with averaged value marked as dashed line; two-dimensional autocorrelation of sorting. Confidence intervals marked as dashed lines; significantly autocorrelated values as stars, and significantly un-autocorrelated values as circles.*

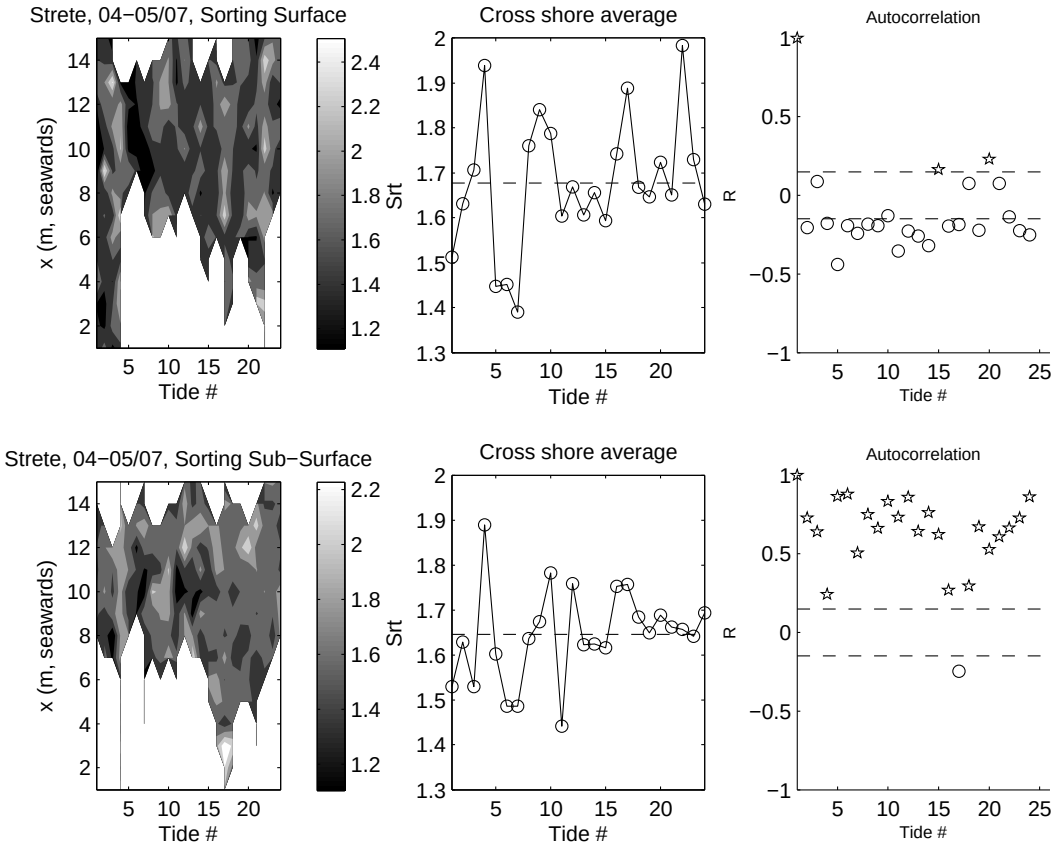

Fig. 6.10 *Change in sediment sorting, April-May 2007.* ***Top, from left to right****: sediment sorting - contours incremented by 2× std(σ); cross-shore averaged sorting; and two-dimensional autocorrelation.* ***Bottom, from left to right****: sediment sorting; cross-shore averaged sorting, with averaged value marked as dashed line; two-dimensional autocorrelation of sorting. Confidence intervals marked as dashed lines; significantly autocorrelated values as stars, and significantly un-autocorrelated values as circles.*

similar in general compared with surface and sub-surface size (Figure 6.8). For example, they have near identical ranges and mean values. As seen in Figure 6.8 for sub-surface sediment size, sub-surface sorting is significantly better autocorrelated than surface sorting. This is perhaps surprising considering that sub-surface samples were taken only from the maximum depth of disturbance upwards, so only actively sedimented samples are included. The reason appears to be genetically linked to the beach step, which is the likely mechanism for observed disturbance depths (Figure 6.6), especially on the lower intertidal beachface. The significant autocorrelations suggest that surface and sub-surface sediments are distinct subpopulations in terms of size and sorting. sub-surface sediments are likely to be lag deposits of the step which has passed out of the measurement area with the ebb tide. This implies not only that the step has distinct sedimentology, but that it remains more self-similar than sediments elsewhere on the profile through time and changing wave conditions, and irrespective of location on the intertidal profile. This bolsters the same argument made in Chapter 5, where direct measurements of step sedimentology were made as it migrated across the intertidal profile.

Sediment skewness for the autumn 2005 survey is shown in Figure 6.11. It is again spatially variable, with little consistent cross-shore zonation apparent. It remains fairly symmetrical through the survey campaign, and across space. The temporal patterns differ markedly between sites, however there is a large degree of similarity between the correlograms of each, indicating some shared underlying structure in space-time. The correlograms for the respective sites have a similar form to those for sediment size (Figure 6.7) and sorting (Figure 6.9), which is remarkable considering how complicated the respective space-time fields are. It suggests two things: firstly, that the three sedimentary parameters are responding to some, or some combination of, external forcing. Equally, it could imply that the two parameters are phase-locked to a third. That third could either be responding to morphodynamic forcing or itself could be involved in a morpho-sedimentary-dynamic feedback mechanism which is keeping combinations of the other two in check. Secondly, it suggests is that the two-dimensional autocorrelation of a space-time field of sedimentary parameters is an excellent tool for visualising dynamics in several parameters with the same time and space axes, although it is not alone enough to satisfactorily resolve the foregoing quandry.

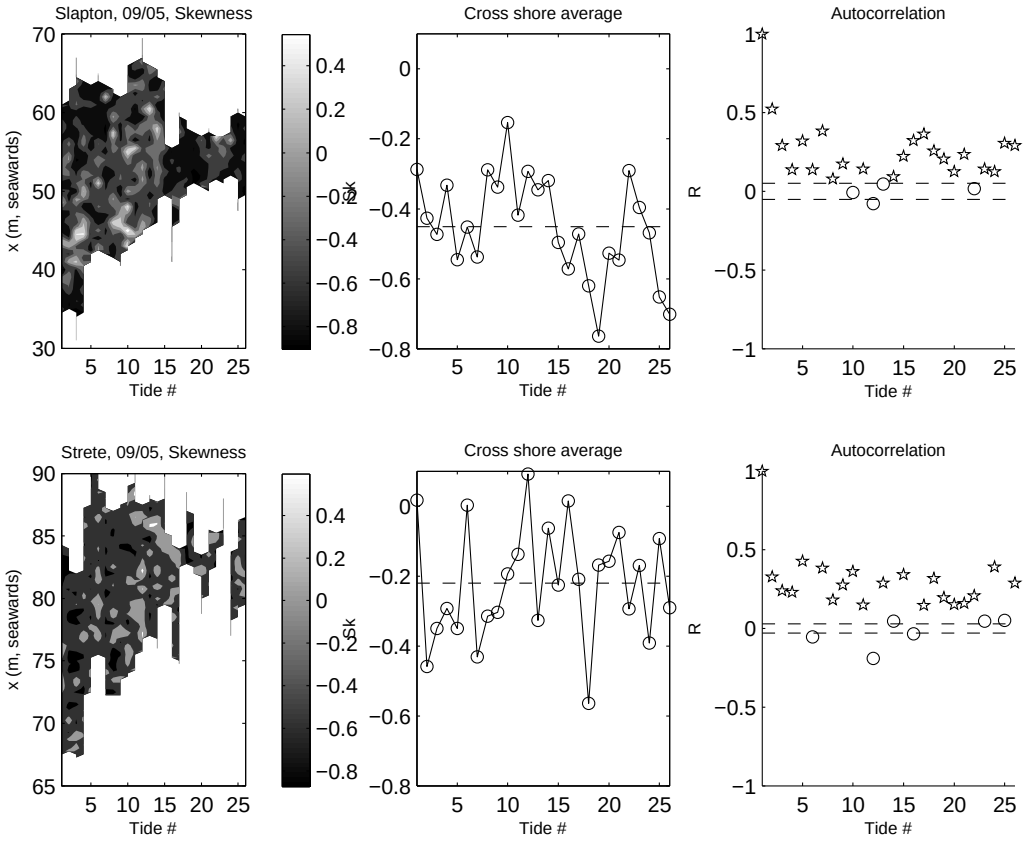

Fig. 6.11 *Change in sediment skewness, September 2005. Top: Slapton; Bottom: Strete.* ***From left to right****: sediment skewness - contours incremented by 2× std(Sk); cross-shore averaged skewness, with averaged value marked as dashed line; two-dimensional autocorrelation of skewness. Confidence intervals marked as dashed lines; significantly autocorrelated values as stars, and significantly un-autocorrelated values as circles.*

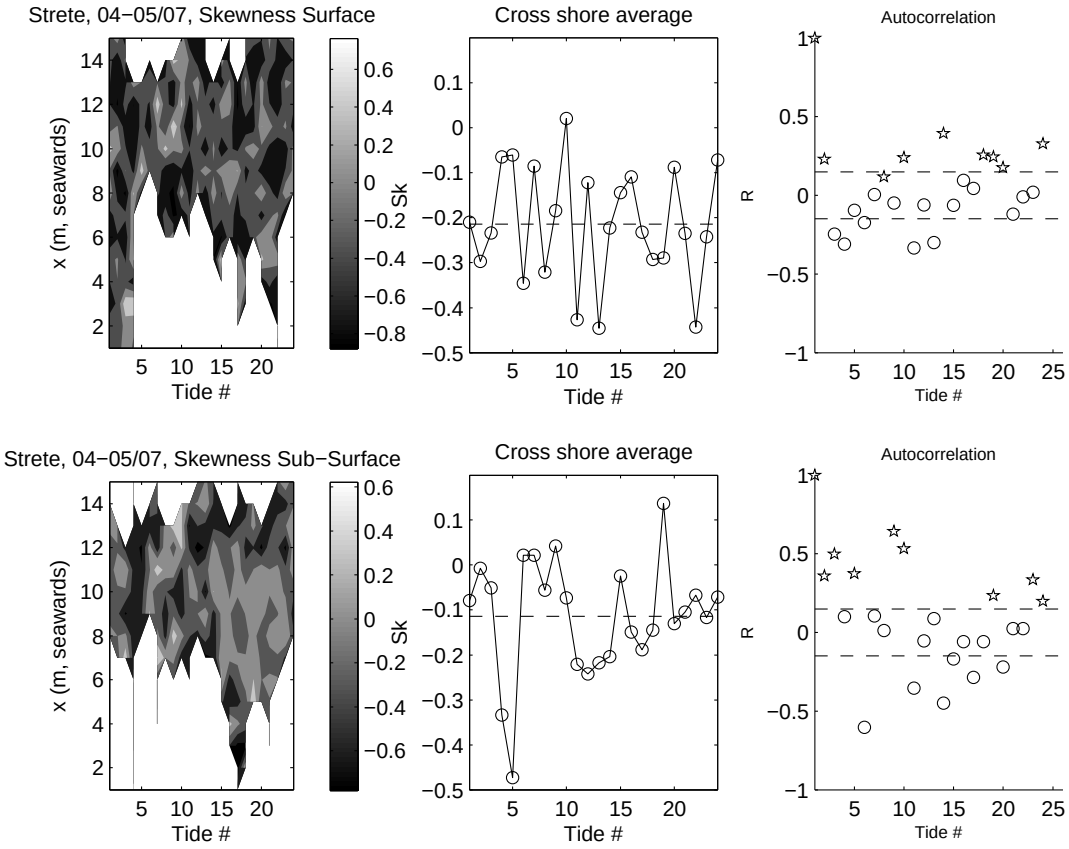

Fig. 6.12 *Change in sediment skewness, April-May 2007.* ***Top, from left to right****: sediment skewness - contours incremented by* $2\times std(Sk)$*; cross-shore averaged skewness; and two-dimensional autocorrelation.* ***Bottom, from left to right****: sediment skewness; cross-shore averaged skewness, with averaged value marked as dashed line; two-dimensional autocorrelation of skewness. Confidence intervals marked as dashed lines; significantly autocorrelated values as stars, and significantly un-autocorrelated values as circles.*

The corresponding space-time field of skewness (surface and sub-surface), along with respective cross-shore averages and correlograms, are the subject of Figure 6.12. One interesting comparison which can be made of the autumn 2005 and spring 2007 surveys is that the sedimentology of the former are generally more self-similar (in space-time) than the latter. This is particularly evident in skewness, which at depth does not share the self-similar expression in the correlogram as size and sorting. Returning to a previous discussion, one might conclude the step as having distinct sedimentology, and consistent with respect only to sediment size and sorting.

A summary of cross-shore trends in sediment size, sorting, and skewness may be seen in Figure 6.13. Surface sediments tend to coarsen; become more poorly sorted; and finer skewed, in the seawards direction. In contrast, sub-surface sediments become finer, better sorted, and more positively skewed across the intertidal profile seawards. The range of values is smallest at the seawards and landwards extremities, and largest at approximately mid-intertidal region.

6.5.3 *Correlation of Morphological Change and Sedimentology*

Morpho-sedimentary co-variation was addressed by correlating a number of variables. Pearson correlation coefficients suffer from the pull of outliers when sample sizes are small. Therefore in this study they were calculated using a bootstrapping scheme, whereby the data with N points was re-sampled a thousand times. Each re-sample comprised an arbitrary subsample of n points with replacement, and a correlation cofficient calculated for each. A mean of these thousand values was taken as the correlation coefficient.

Morphological change relative to initial is denoted Δz_1, and over individual time steps as Δz_i. Change in sediment size (D_s or D_{ss} for surface and sub-surface, repsectively) and sediment sorting (σ_s and σ_{ss} for surface and sub-surface, respectively) relative to initial and cross-shore average are suffixed by '1' and 'm', respectively. Changes over individual time steps are suffixed by 'i'. The analysis was limited to sediment size and sorting since the physical relevance of skewness and kurtosis is less assured. With reference to Table 6.1 (sediment size) and 6.2 (sorting), it was found that no significant correlations were found between any morphological and sedimentological parameter. Some correlations significantly different from zero were found between DOD and

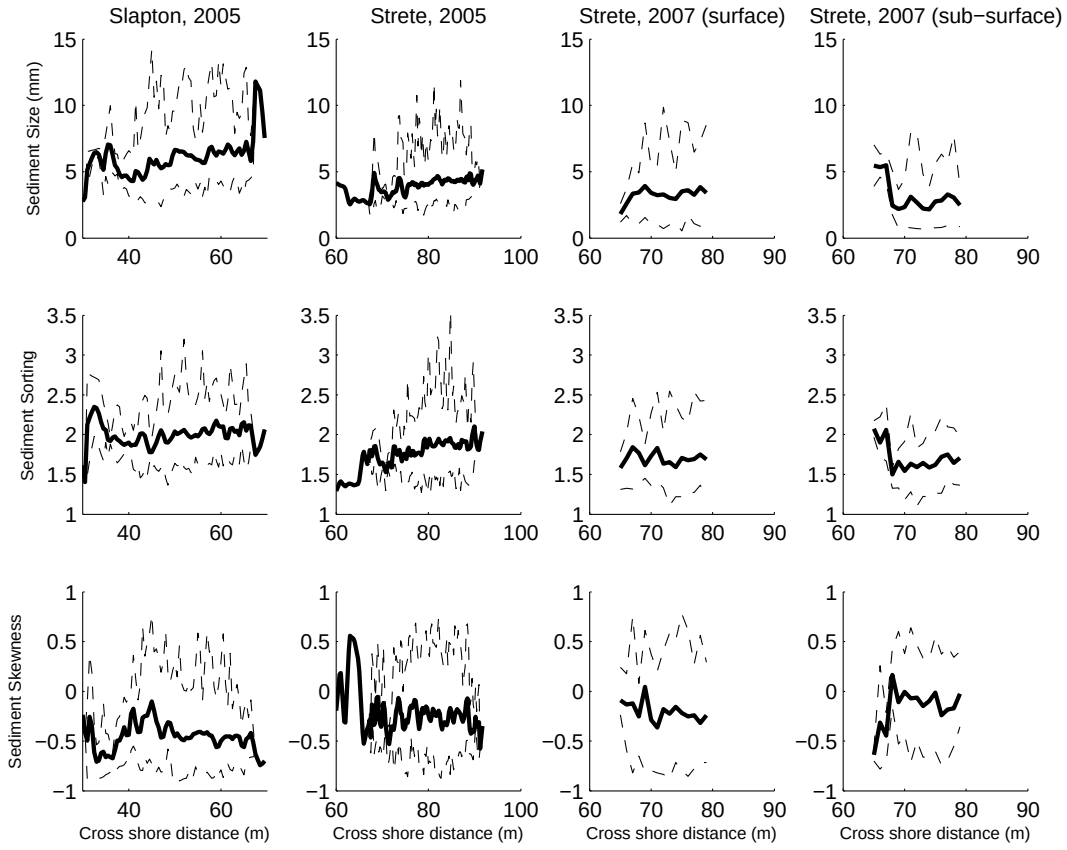

Fig. 6.13 *Summary of spatial trends in sedimentary parameters.* ***From left to right****: Slapton 2005, Strete 2005, Strete 2007 (surface) and Strete 2007 (sub-surface); and* ***from top to bottom****: size, sorting and skewness. Heavy black line represents mean, surrounded by maximums and minimums depicted as dashed lines.*

sedimentological parameters. The reason for this might be that the sub-surface samples are more reliable indicators of sedimentological change over the time-scale of interest (whereas it is more difficult to attach a time-scale to the sedimentation of the surface sediments). In addition, as Chapter 5 demonstrated, the sedimentology of the step is more consistent than the foreshore in terms of its relationship to the magnitude of morphological change, and hence hydrodynamic energy expenditure.

Tab. 6.1 *Summary of correlations between morphological and sediment size parameters (associations significantly different from zero are shaded).*

	D_s	ΔD_{si}	ΔD_{sm}	ΔD_{s1}	D_{ss}	ΔD_{ssi}	ΔD_{ssm}	ΔD_{ss1}
Slapton 2005 Δz_1	-0.049	-0.017	-0.094	-0.12	-	-	-	-
Strete 2005 Δz_1	-0.09	-0.03	-0.07	-0.093	-	-	-	-
Slapton 2005 Δz_i	0.152	0.07	0.008	0.084	-	-	-	-
Strete 2005 Δz_i	0.13	-0.09	-0.04	-0.011	-	-	-	-
Strete 2007 Δz_1	0.11	0.06	-0.029	0.19	0.15	0	-0.16	-0.13
Strete 2007 Δz_i	-0.01	0.07	-0.06	0.04	-0.007	-0.002	0.06	-0.12
Strete 2007 DOD	0.35	0.03	0.06	0.03	0.28	-0.09	-0.08	-0.17
Strete 2007 DOD	-0.04	0.09	0.07	0.003	0.02	-0.1	0.09	0.07

Tab. 6.2 *Summary of correlations between morphological and sorting parameters (associations significantly different from zero are shaded).*

	σ_s	$\Delta\sigma_{si}$	$\Delta\sigma_{sm}$	$\Delta\sigma_{s1}$	σ_{ss}	$\Delta\sigma_{ssi}$	$\Delta\sigma_{ssm}$	$\Delta\sigma_{ss1}$
Slapton 2005 Δz_1	-0.05	0.03	0.07	0.05	-	-	-	-
Strete 2005 Δz_1	-0.08	0.05	-0.08	-0.05	-	-	-	-
Slapton 2005 Δz_i	0.15	-0.03	-0.04	-0.007	-	-	-	-
Strete 2005 Δz_i	0.15	-0.02	-0.07	-0.12	-	-	-	-
Strete 2007 Δz_1	0.15	0.02	-0.07	0.23	0.24	-0.04	-0.13	-0.02
Strete 2007 Δz_i	0.09	0.03	-0.07	0.03	0.06	0.11	0.06	0.08
Strete 2007 DOD	0.4	-0.003	0.05	0.29	0.46	-0.02	0.03	0.31
Strete 2007 DOD	-0.04	0.27	-0.05	-0.01	-0.03	0.26	0.02	-0.04

6.6 *Morpho-sedimentary-dynamics*

Internal Variability of Sedimentology and Morphology

Despite the lack of correlation, a few significant associations were evident when parameters were cross-correlated, suggesting that sediments may have been responding to morphological change with a lag in time or space. These significant cross-correlations were consistent in neither parameter pair nor lag. EOFs were used to reveal the patterns in the data in order to establish whether or not there was any correlation in the

individual decomposed modes of the data sets, and to shed some light on the (perhaps spurious) cross-correlations. In particular, EOF analysis was used to reveal whether sediments responded in time or in space, or both, to morphological change. An additional useful consequence of EOF analysis is the number of modes required to account for most of the variation gives an indication on the stochasticity of the time-space data field, or its internal variance.

Ordinary and Complex EOF analysis was performed on the morphological (Δz_1, Δz_i), sediment size (D_s, D_{ss}, ΔD_{s1}, ΔD_{ss1}, ΔD_{si}, ΔD_{ssi}, ΔD_{sm}, ΔD_{ssm}), and sorting (σ_s, σ_{ss}, $\Delta\sigma_{s1}$, $\Delta\sigma_{ss1}$, $\Delta\sigma_{si}$, $\Delta\sigma_{ssi}$, $\Delta\sigma_{sm}$, $\Delta\sigma_{ssm}$) data matrices for the three survey campaigns (Slapton 2005, Strete 2005, and Strete 2007) organised as [x,t] for rows and columns, respectively, so a row contained a time series of one variable, being magnitude at that location.

Typical spectra (scree plots) of EOF modes are depicted in Figure 6.14. The number of EOF modes required to explain 90% of the variance in the respective data sets was consistently highest for sediment size variables and lowest for morphological change variables, indicating that sediment size has the most stochastic variation and the least inheritance. This is broadly compatible with the autocorrelation profiles for these variables in Figures 6.5, 6.6 (morphology), 6.7, 6.8 (sediment size), 6.9 and 6.10 (sorting). A summary of the number of modes required to account for 90% of the variance are shown in Tables 6.3, 6.4, and 6.5 for morphology, sediment size and sorting, respectively. Note that fewer CEOF modes are generally required to reconstruct the data compared with EOF modes, and that fewer modes are required for the Strete 2007 data sets because they are smaller.

Tab. 6.3 *Number of EOF modes required to account for 90% of variance, Morphology.*

	Δz_1	Δz_i	DOD	DOD_i
EOFs, Slapton 2005	4	5	-	-
EOFs, Strete 2005	3	4	-	-
EOFs, Strete 2007	2	4	3	3
CEOFs, Slapton 2005	2	4	-	-
CEOFs, Strete 2005	2	3	-	-
CEOFs, Strete 2007	1	3	2	2

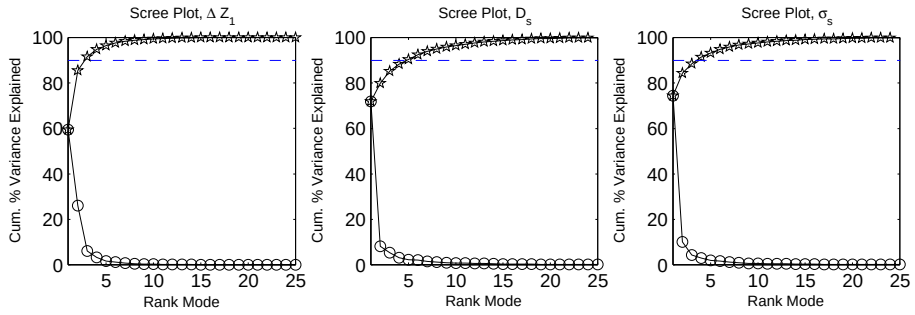

Fig. 6.14 *Typical scree plots for,* ***from left to right****, morphological change, surface sediment size and surface sediment sorting. Shown as variance associated with rank mode (circles) and cumulative variance (stars). Dashed line indicates 90% variance accounted for.*

Tab. 6.4 *Number of EOF modes required to account for 90% of variance, Sediment Size.*

	D_s	ΔD_{si}	ΔD_{sm}	ΔD_{s1}	D_{ss}	ΔD_{ssi}	ΔD_{ssm}	ΔD_{ss1}
EOFs, Slapton 2005	4	8	10	8	-	-	-	-
EOFs, Strete 2005	5	9	13	11	-	-	-	-
EOFs, Strete 2007	5	7	8	7	5	6	5	5
CEOFs, Slapton 2005	5	5	7	6	-	-	-	-
CEOFs, Strete 2005	5	8	10	8	-	-	-	-
CEOFs, Strete 2007	6	5	6	5	6	5	5	4

Tab. 6.5 *Number of EOF modes required to account for 90% of variance, Sorting.*

	σ_s	$\Delta\sigma_{si}$	$\Delta\sigma_{sm}$	$\Delta\sigma_{s1}$	σ_{ss}	$\Delta\sigma_{ssi}$	$\Delta\sigma_{ssm}$	$\Delta\sigma_{ss1}$
EOFs, Slapton 2005	3	9	11	10	-	-	-	-
EOFs, Strete 2005	4	9	11	9	-	-	-	-
EOFs, Strete 2007	2	6	8	6	3	6	7	5
CEOFs, Slapton 2005	3	7	8	7	-	-	-	-
CEOFs, Strete 2005	4	7	9	7	-	-	-	-
CEOFs, Strete 2007	4	5	6	5	3	5	4	4

6.6.1 *Spatial Structure of Morpho-Sedimentary Relationships*

Some spatial eigenfunctions are for morpho-sedimentary variables are plotted in Figure 6.15. The first indication of some association between morphological change and sedimentological change is seen in hysteresis when the first eigenmode of Δz_1 is plotted against those of D_s and σ_s. The same anticlockwise reponse is seen in all three data sets, so one might conclude it is a scale-invariant feature of morpho-sedimentary change. Some of these typical patterns are depicted in Figure 6.16. In a physical sense it means that sediment size co-varies with net sedimentation patterns: both sediment fining/ameliorated sorting and relative depletion occur seawards of the berm at the top of the intertidal profile to some point in the centre of the intertidal profile. From that point, coarsening/deteroriated sorting and relative accretion occurs seawards to the shoreline. In the autumn 2005 survey the hysteresis loop closed, whereas in the spring 2007 survey it did not. It is interesting to ponder whether the hysteresis would continue on a second cycle from the step (another major secondary morphological feature) seawards under the shoaling waves. The hysteresis uncovered by the primary EOFs is not readily detectable in the non-decomposed data sets, nor is it present in the subordinate modes. The variance associated with the data represented by such modes acts to mask this spatial coherence.

The following concerns the derivative of spatial phase, $\theta(x)$, calculated from the CEOF modes and measures of similarity over space (consistent through time). With reference to Figure 6.17, two large negative ramps (hiatuses) are apparent in approximately the same normalised intertidal position in the first CEOF modes (top row) at Slapton and Strete. These could be associated with lower and upper intertidal source regions, for example the first coincides approximately with the berm face and the second with the lower swash, both (on the evidence of Chapter 5) transitional zones where sediment passes through in large quantities. For the Strete 2007 record, the general trend in the first CEOF mode is for offshore propagation, except at ≈10m, which is the site of maximum depletion prior to berm building and subsequently the berm face. The phase associated with the 2nd CEOF modes in each survey (bottom panels of Figure 6.17) indicate an on-offshore propagation periodicity of ≈3m for Strete 2007, and ≈5m for the mid-low intertidal records at Slapton and Strete 2005. These features are difficult to

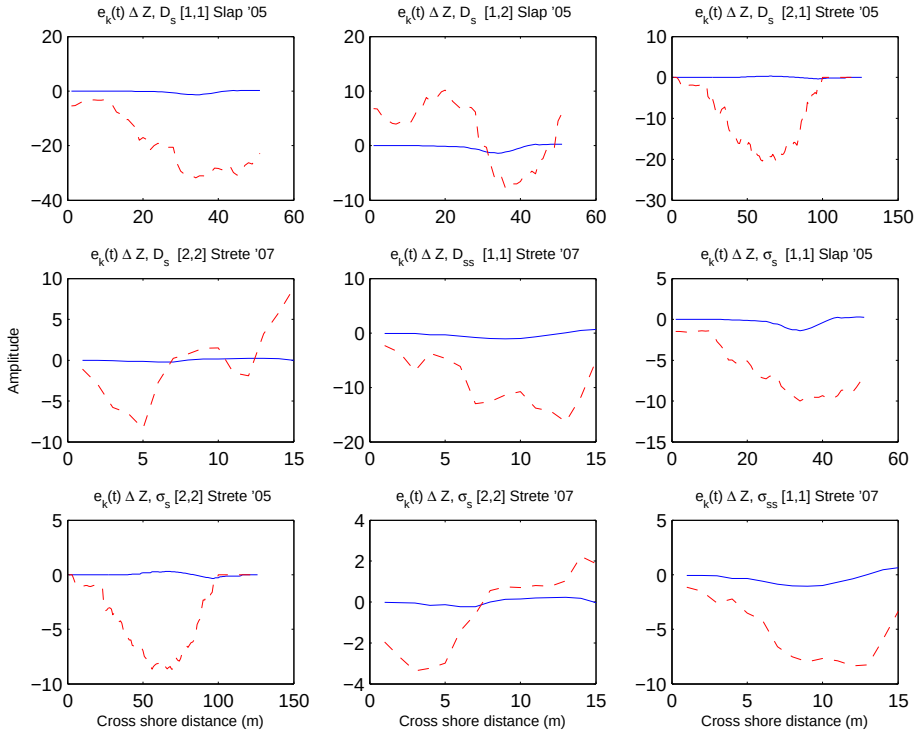

Fig. 6.15 *Some spatial eigenmodes plotted against cross-shore distance (in metres) for various morpho-sedimentary variables from the three data sets, the specifics denoted by the title of each subpanel.*

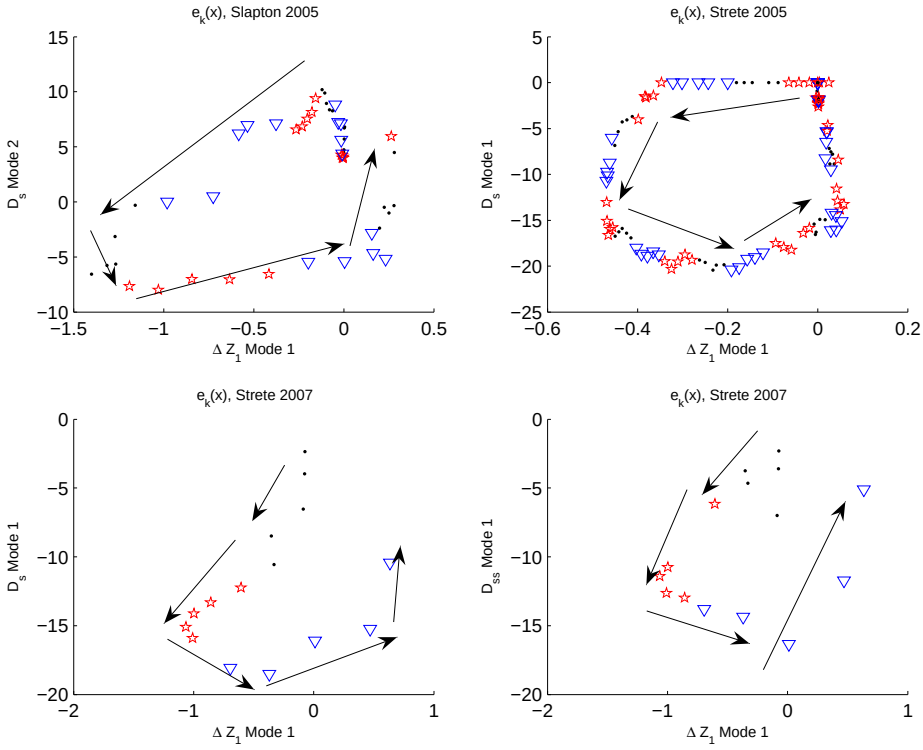

Fig. 6.16 *Typical hysteresis patterns in Δz_1 and sediment size uncovered by spatial EOFs.*

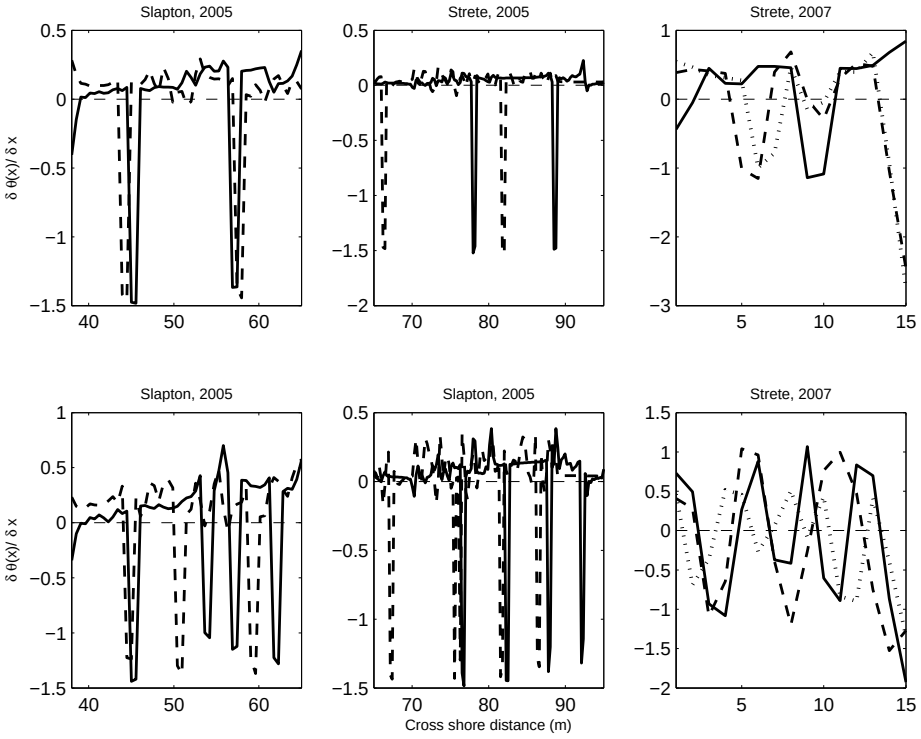

Fig. 6.17 *Spatial derivative of $\theta(x)$ for D_s (dashed line), D_{ss} (dotted line), and Δz_1 (solid line). First and second modes on top and bottom rows, respectively.*

interpret because they do not coincide with the phase pattern from the first CEOF (being associated with a mode orthogonal to the first).

Some patterns in the spatial derivative of $\theta(x)$ for the CEOFs of size and sorting were found, some of which were coherent with the corresponding patterns in the record for Δz_1 at respective locations. According to Figure 6.17, of particular note are the spikes associated with the 1st CEOF at Slapton 2005 being in identical places as those for Δz_1, but not coincident with respect to the 2nd complex eigenmode. The reverse is true, however, for the Strete 2005 record. The reason is because $\Delta z_1, c_k(x)$ is related to $D_s, c_k(x)2$ in the Slapton 2005 record, but to $D_s, c_k(x)1$ in the Strete 2005 record (Figure 6.16). The patterns for surface (dashed line) and sub-surface (dotted line) sediment size during the Strete 2007 survey fall in and out of concurrency with the Δz_1 spatial phase derivative pattern associated with the primary complex eigenmode, but that the relative records are in greater accordance for the 2nd CEOF.

6.6.2 *Temporal Structure of Morpho-Sedimentary Relationships*

Whereas significant correlations were not found between the non-decomposed data sets, significant associations in some of the temporal EOFs were found using CCA. Tables 6.6 and 6.7 house the canonical correlation coefficients and associated p-values for sediment size and sorting, respectively, relative to morphological change. Some of the stronger correlations between modes are shown in Figure 6.18. With reference to Table 6.6, several significant relationships were determined by CCA analysis between morphological and sediment size. Consistent relationships between data sets were found in the pairing of $[\Delta z_1, e_k(t)1]$ and $[D_s, e_k(t)1]$ at Slapton 2005 and Strete 2007, and the pairing of $[\Delta z_1, e_k(t)1]$ and $[D_s, e_k(t)2]$ at Slapton 2005 and Strete 2005. Likewise, Table 6.7 shows that a number of consistent significant relationships were determined by CCA analysis on the temporal eigenmodes of Δz_1 and σ_s/σ_{ss}. For example, the pairing of $[\Delta z_1, e_k(t)1]$ and $[\sigma_s, e_k(t)1]$ at Slapton 2005 and Strete 2007, and the pairing of $[\Delta z_1, e_k(t)1]$ and $[\sigma_s, e_k(t)2]$ at Slapton 2005 and Strete 2005. These are the same equivalent pairing for sediment size. In addition, significant relationships were found between the 1st mode of DOD and the first and second modes of both σ_s and σ_{ss}. Note that the imaginary CEOF component yielded very similar results, and are therefore not shown.

Far fewer significant correlations were found between Δz_1 and the matrices of D_s, D_{ss}, σ_s and σ_{ss} relative to initial and mean, and over individual time steps. Likewise, matrices of Δz_i found few significant correlations with sedimentary matrices (these results are therefore not shown). This implies that net sedimentation is associated with the absolute magnitude of sediment parameters rather than relative to those in local time and space. It also implies that sediments do not respond instantaneously to morphological change over individual tides (in addition, far fewer significant correlations were found between Δz_i and the sedimentary matrices, further indicating that individual sedimentation events do not show a parallel response in the sedimentary parameters). It explains the lack of correlation between the non-decomposed parameter sets. There is less inheritance in the sediments than the morphology: it is less of a product of what value it was before, supported by the steeper correlogram slopes for sediment size and sorting at lag, and by the consistently greater number of modes required to account for the variance in the data. It is therefore more likely, on this evidence, that the sediment

Tab. 6.6 *Canonical correlation coefficients (and p-values in parentheses) between dominant sediment size temporal modes (columns) and morphological temporal modes (rows). Significant correlations are shaded.*

Pair	Mode	1	2	3	4	5
Δz_1 $e_k(t)$ & D_s $e_k(t)$, Slapton '05	1	0.75 (0)	0.75 (0)	0.31 (0.16)	0.07 (0.76)	0.19 (0.38)
	2	0.03 (0.87)	0.33 (0.052)	0.25 (0.14)	0.39 (0.06)	0.05 (0.81)
	3	0.13 (0.49)	0.02 (0.91)	0.33 (0.052)	0.15 (0.43)	0.23 (0.25)
	4	0.13 (0.51)	0.45 (0.02)	0.22 (0.31)	0.05 (0.76)	0.05 (0.82)
Δz_1 $e_k(t)$ & D_s $e_k(t)$, Strete '05	1	0.14 (0.46)	0.43 (0.02)	0.41 (0.052)	0.12 (0.48)	0.036 (0.88)
	2	0.63 (0)	0.37 (0.04)	0.19 (0.35)	0.29 (0.17)	0.11 (0.55)
	3	0.18 (0.34)	0.25 (0.2)	0.31 (0.15)	0.01 (0.94)	0.08 (0.65)
Δz_1 $e_k(t)$ & D_s $e_k(t)$, Strete '07	1	0.41 (0.05)	0.01 (0.91)	0.23 (0.24)	0.59 (0)	0.21 (0.28)
	2	0.3 (0.15)	0.28 (0.14)	0.07 (0.67)	0.23 (0.34)	0.08 (0.7)
Δz_1 $e_k(t)$ & D_{ss} $e_k(t)$, Strete '07	1	0.56 (0)	0.21 (0.33)	0.06 (0.63)	0.1 (0.52)	0.42 (0.02)
	2	0.25 (0.27)	0.22 (0.25)	0.12 (0.52)	0.25 (0.23)	0.37 (0.1)
DOD $e_k(t)$ & D_s $e_k(t)$, Strete '07	1	0.27 (0.16)	0.38 (0.07)	0.17 (0.49)	0.39 (0.05)	0.06 (0.67)
	2	0.06 (0.71)	0.22 (0.42)	0.11 (0.47)	0.06 (0.71)	0.05 (0.84)
	3	0.21 (0.37)	0.2 (0.36)	0.1 (0.66)	0.04 (0.82)	0.11 (0.65)
DOD_i $e_k(t)$ & D_{ss} $e_k(t)$, Strete '07	1	0.12 (0.61)	0.66 (0)	0.1 (0.93)	0.11 (0.66)	0.13 (0.51)
	2	0.4 (0.06)	0.4 (0.09)	0.2 (0.35)	0.01 (0.96)	0.29 (0.22)
	3	0.02 (0.92)	0.01 (0.9)	0.22 (0.33)	0.15 (0.49)	0.28 (0.14)

Tab. 6.7 *Canonical correlation coefficients (and p-values in parentheses) between dominant sediment sorting temporal modes (columns) and morphological temporal modes (rows). Significant correlations are shaded.*

Pair	Mode	1	2	3	4
Δz_1 $e_k(t)$ & σ_s $e_k(t)$, Slapton '05	1	0.84 (0)	0.81 (0)	0.31 (0.09)	0.13 (0.58)
	2	0.18 (0.32)	0.26 (0.2)	0.32 (0.17)	0.14 (0.56)
	3	0.07 (0.74)	0.01 (0.93)	0.26 (0.15)	0.14 (0.51)
	4	0.4 (0.02)	0.51 (0.04)	0.23 (0.22)	0.01 (0.94)
Δz_1 $e_k(t)$ & σ_s $e_k(t)$, Strete '05	1	0.11 (0.58)	0.42 (0.04)	0.48 (0.01)	0.21 (0.28)
	2	0.69 (0)	0.42 (0.06)	0.16 (0.4)	0.39 (0.02)
	3	0.02 (0.9)	0.21 (0.21)	0.28 (0.22)	0.01 (0.97)
Δz_1 $e_k(t)$ & σ_s $e_k(t)$, Strete '07	1	0.39 (0.03)	0.007 (0.97)	0.46 (0.052)	0.31 (0.12)
	2	0.13 (0.48)	0.27 (0.15)	0.12 (0.66)	0.29 (0.11)
Δz_1 $e_k(t)$ & σ_{ss} $e_k(t)$, Strete '07	1	0.46 (0.02)	0.27 (0.23)	0.05 (0.85)	0.39 (0.07)
	2	0.03 (0.86)	0.24 (0.3)	0.04 (0.08)	0.19 (0.36)
DOD $e_k(t)$ & σ_s $e_k(t)$, Strete '07	1	0.49 (0.02)	0.41 (0.04)	0.07 (0.76)	0.31 (0.13)
	2	0.02 (0.93)	0.31 (0.16)	0.44 (0.042)	0.14 (0.46)
	3	0.17 (0.31)	0.28 (0.12)	0.26 (0.21)	0.32 (0.21)
DOD_i $e_k(t)$ & σ_{ss} $e_k(t)$, Strete '07	1	0.78 (0)	0.65 (0)	0.01 (0.92)	0.004 (0.98)
	2	0.34 (0.12)	0.4 (0.03)	0.11 (0.66)	0.32 (0.18)
	3	0.09 (0.64)	0.07 (0.73)	0.47 (0.01)	0.01 (0.97)

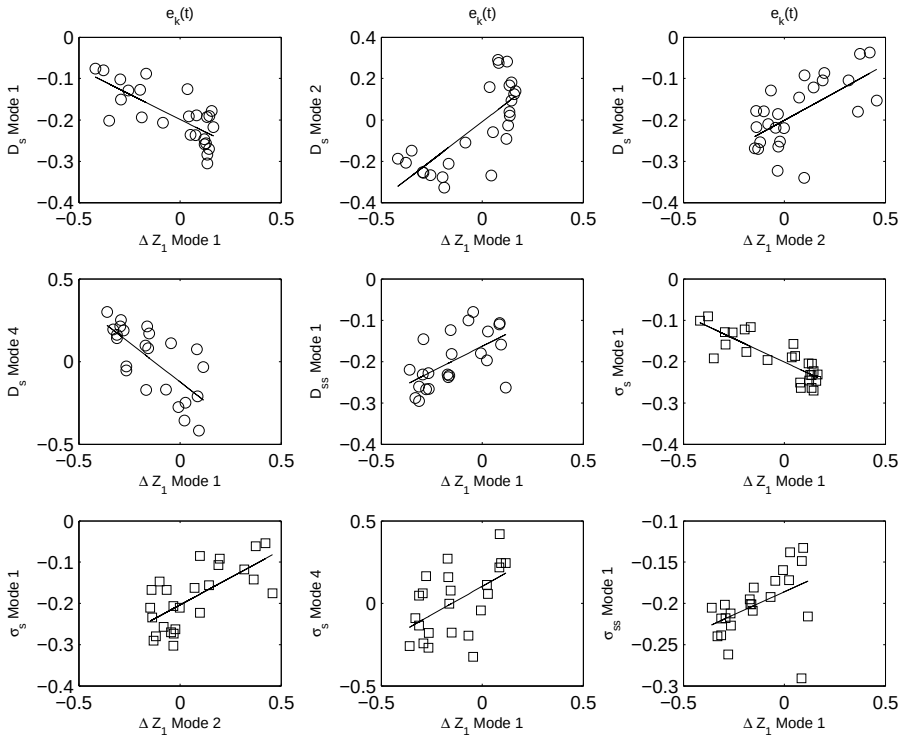

Fig. 6.18 *Some correlations in the temporal EOFs of morphological and sedimentological parameters (with linear least squares fits).*

parameters reflect the morphological change rather than vice-versa.

During the autumn 2005 survey, berm building (represented by $[\Delta z_1, e_k(t)1]$) at Slapton was reflected in both the temporal mean component of size and sorting ($[D_s, e_k(t)1; \sigma_s, e_k(t)1]$), and with the temporal fining/ameliorated sorting component ($[D_s, e_k(t)2; \sigma_s, e_k(t)2]$), as depicted in Figures 6.19 and 6.20, which also show that berm building at Strete ($[\Delta z_1, e_k(t)1]$, a mode which includes both prior relative depletion in the same cross-shore position as subsequent berm building), was reflected in the temporal coarsening/deteriorated sorting component of sediment size/sorting ($[D_s, e_k(t)2; \sigma_s, e_k(t)2]$). During the spring 2007 survey, morphological change separated into two eigenmodes representing the dynamics of, respectively, the lower and upper intertidal area ($[\Delta z_1, e_k(t)1]$ and $[\Delta z_1, e_k(t)2]$). The first was related to the first and fourth eigenmodes of D_s, and the first eigenmode of σ_s, representing the mean components of each.

The following concerns the derivative of temporal phase, $\psi(t)$, calculated from the CEOF modes, and analogous to relative frequency. Following Ruessink et al. [2000], a negative phase ramp of Δz_1 (solid lines in the panels of Figure 6.17), indicates a

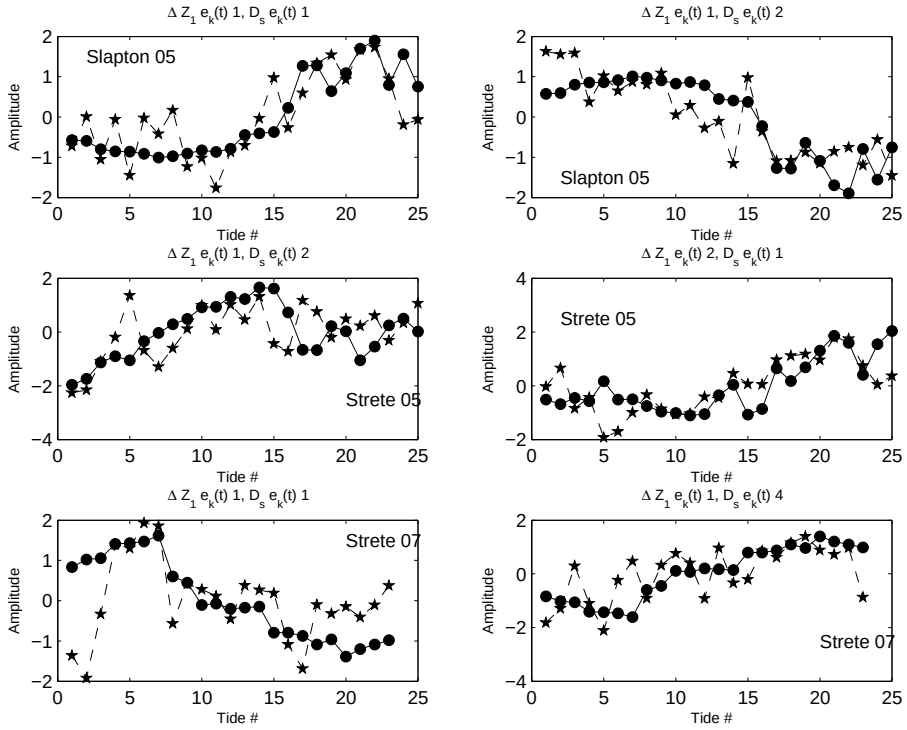

Fig. 6.19 *Temporal amplitudes of CCA modes for morphological change (circles) and sediment size (stars).* ***From top to bottom****: Slapton '05, Strete '05, and Strete '07.*

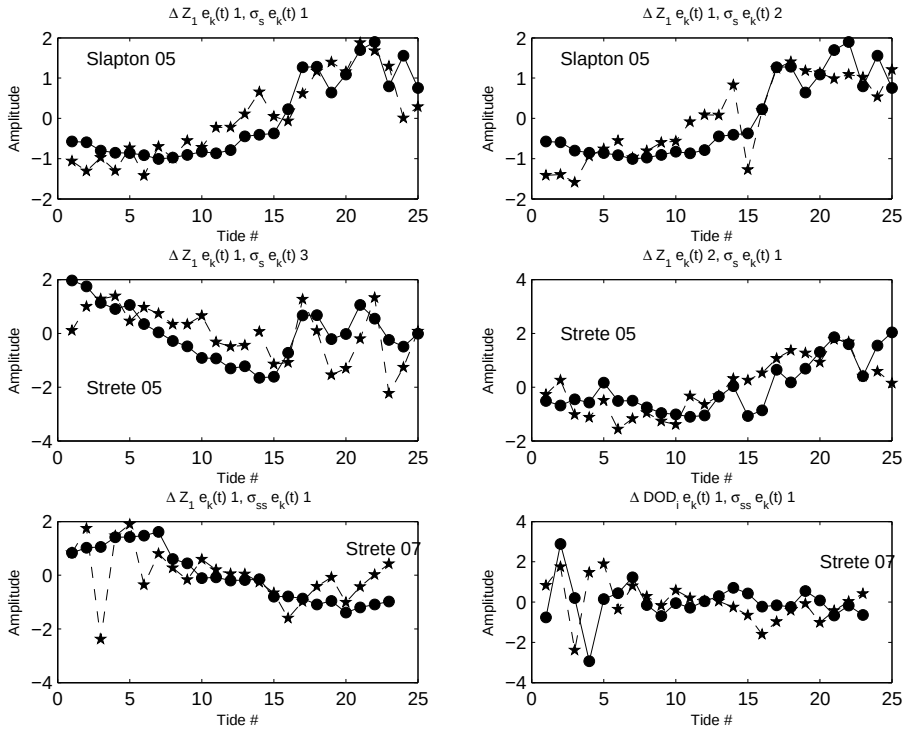

Fig. 6.20 *Temporal amplitudes of CCA modes for morphological change (circles) and sediment sorting (stars).* ***From top to bottom****: Slapton '05, Strete '05, and Strete '07.*

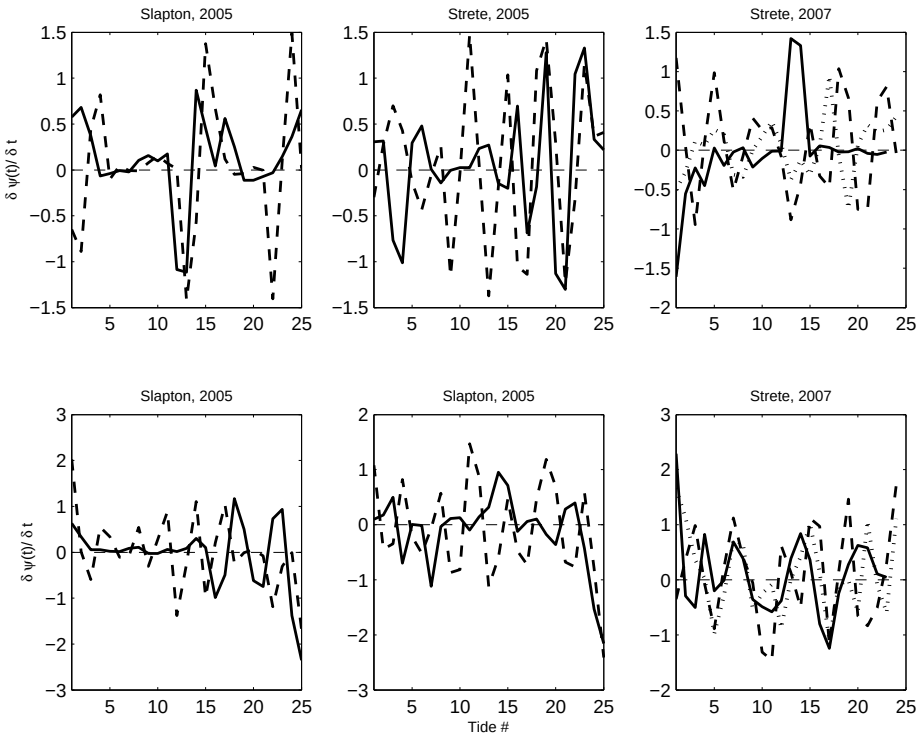

Fig. 6.21 *Temporal derivative of $\psi(t)$ for σ_s (dashed line), σ_{ss} (dotted line), and Δz_1 (solid line). First and second modes on top and bottom rows, respectively.*

propagating feature onshore (decreasing x coordinate), and a positive phase ramp indicates a propagating feature in the offshore direction (increasing x coordinate). These reflect (temporally-averaged) spatial nodes where on- and off-shore sedimentation occurred. For sediment size and sorting, positive and negative ramps indicate coarsening/fining or deteriorating/ameliorating sorting, respectively. The upper and lower panels of Figure 6.21 depict the records with respect to the first and second CEOFs for sorting, respectively, for Δz_1 (solid line), σ_s (dashed line) and σ_{ss} (dotted line). The same applies for sediment size, which is therefore not shown.

Similar patterns are evidence of synchroneity. For the Slapton 2005 data set, the first CEOF of Δz_1 and σ_s agree well, but the latter lags the former when berm building occurs, which indicates that morphological change associated with berm building (in this case intertidal advecting pulses of sedimentation) causes a response in the temporal mean component of size and sorting. The 2nd CEOF, representing the temporal fining/ameliorated sorting component, becomes more and more in phase with Δz_1 over the survey period. At Strete 2005, it is the 1st CEOF, representing the temporal coarsening/deteroriated sorting component, becomes more and more in phase with Δz_1

over the survey period. The indication is two-fold: that beachface sedimentology is 'slaved' [Werner, 1999] to morphological change rather than vice-versa; and that the relationships become more evident as secondary morphological features develop on the beachface. For the spring 2007 survey data set, much more coherence was found between the 2nd CEOFs for Δz_1 (associated with lower beachface change) and sedimentological variables than for the primary modes (associated with mean components), which is in agreement with the canonical correlations housed in Tables 6.6 and 6.7.

6.6.3 *Morpho-Sedimentary-Dynamic Relationships*

Morpho-sedimentary-dynamics implies cause and effect (and feedback processes); therefore we are concerned primarily in this section with the coherence found between morpho-sedimentary parameters in time rather than space. Having already demonstrated that sediment size and sorting are related to morphological change, it was decided to only include hydrodynamic variables to seek coherent responses in those significant morpho-sedimentary eigenmode pairs. The morpho-sedimentary eigenmode pairs with statistically significant correlation were taken and CCA analysis was performed on each with respect to a matrix of nine forcing variables, namely: semi-diurnal tidal range (TR, m); surf similarity parameter (ϵ_s, non-dim.); spectral width (ϵ_w, non-dim.); significant wave height (H_s, m); significant spectral wave period (T_s, s); mean wave direction ($\overline{\Theta_w}$, radians); Iribarren number (ξ, non-dim.), groupiness function (GF, non-dim.); and a vector of Gaussian white noise (A). With the exception of the white noise, which was included in order to check the morpho-sedimentary response was not random, the predictor matrix was thus populated with those which were deemed likely to force a linear change in the reponse variables. The CCA analysis was therefore designed to see what hydrodynamic parameter, if any, was forcing the response in the morpho-sedimentary pair which significantly co-varied. If no statistically significant results could be found, it implied that either the morpho-sedimentary response was due to a parameter not included in the model, or that the response was non-linear. This latter category would include a situation where a feedback mechanism was in place between the morpho-sedimentary variable and the hydrodynamics. Unfortunately such a situation would not be resolved with the linear techniques employed here; however, these results constitute the first objective demonstration that

both morphology and sedimentology co-varies in phase with hydrodynamic forcing on a gravel beach. The results are seen in Tables 6.8, 6.9, and 6.10 for Slapton 2005, Strete 2005, and Strete 2007, respectively: p-values have been bootstrapped so do not suffer from the pull of outliers, and significant values (at α=0.05) are shaded. Note that for the autumn 2005 data sets, tides 2 to 26 inclusive were used for the analysis, but for the spring 2007 data set only the measured nearshore record was used; therefore, only tides 2 to 19 were included in the analysis.

Tab. 6.8 *Canonical Correlation Analysis results for hydrodynamic forcing of significantly correlated morpho-sedimentary eigenmodes at Slapton, 2005. P-values are shown. Significant values shaded.*

Slapton	TR	ϵ_s	ϵ_w	H_s	T_s	$\overline{\Theta_w}$	ξ	GF	A
$[\Delta z_1, 1; D_s, 1]$	0	0.88	0.16	0	0.74	0.83	0.81	0.3	0.97
$[\Delta z_1, 1; D_s, 2]$	0	0.97	0.02	0	0.6	0.02	0.75	0.18	0.16
$[\Delta z_1, 4; D_s, 2]$	0	0.07	0.052	0	0.36	0.01	0.2	0.84	0.52
$[\Delta z_1, 1; \sigma_s, 1]$	0	0.83	0	0	0.8	0.1	0.81	0.16	0.94
$[\Delta z_1, 1; \sigma_s, 2]$	0	0.95	0.042	0	0.67	0.06	0.8	0.29	0.28
$[\Delta z_1, 4; \sigma_s, 1]$	0	0.052	0	0	0.58	0.07	0.41	0.07	1
$[\Delta z_1, 4; \sigma_s, 2]$	0	0.07	0.02	0	0.41	0.02	0.24	0.53	0.77

Tab. 6.9 *Canonical Correlation Analysis results for hydrodynamic forcing of significantly correlated morpho-sedimentary eigenmodes at Strete, 2005. P-values are shown. Significant values shaded.*

Strete	TR	ϵ_s	ϵ_w	H_s	T_s	$\overline{\Theta_w}$	ξ	GF	A
$[\Delta z_1, 1; D_s, 2]$	0.04	0.5	0.15	0.18	0.8	0	0.88	0.27	0.96
$[\Delta z_1, 2; D_s, 1]$	0	0.18	0.21	0	0.17	0.1	0.11	0.09	0.54
$[\Delta z_1, 2; D_s, 2]$	0.01	0.74	0.11	0.02	0.63	0	0.81	0	0.66
$[\Delta z_1, 1; \sigma_s, 2]$	0.03	0.47	0.1	0.07	0.88	0	0.84	0.25	0.92
$[\Delta z_1, 1; \sigma_s, 3]$	0	0.96	0.25	0.68	0.85	0.02	0.7	0.18	0.67
$[\Delta z_1, 2; \sigma_s, 1]$	0	0.28	0.13	0	0.01	0.32	0.24	0.0352	0.51
$[\Delta z_1, 2; \sigma_s, 2]$	0.02	0.66	0.1	0.04	0.7	0	0.66	0.01	0.63
$[\Delta z_1, 2; \sigma_s, 4]$	0.06	0.34	0.62	0.02	0.6	0.44	0.11	0.052	0.56

Some of the statistically significant temporal CCA amplitudes of morpho-sedimentary pair and hydrodynamic variable are seen in Figure 6.22. Note that the CCA amplitudes are standardised to ease comparison. The $[\Delta z_1, D_s]$ eigenpair and $[\Delta z_1, \sigma_s]$ are depicted as circles and stars, respectively, around a solid line representing a hydrodynamic parameter inputted in the predictor matrix. Taken as a whole, they represent further robust evidence that beachface change and sedimentology have some detectable cause.

Tab. 6.10 *Canonical Correlation Analysis results for hydrodynamic forcing of significantly correlated morpho-sedimentary eigenmodes at Strete, 2007 (first 18 tides). P-values are shown. Significant values shaded.*

Strete	TR	ϵ_s	ϵ_w	H_s	T_s	$\overline{\Theta_w}$	ξ	GF	A
$[\Delta z_1, 1; D_s, 1]$	0	0	0	0.66	0	0	0	0.03	0.18
$[\Delta z_1, 1; D_s, 4]$	0	0	0	0	0	0	0	0.35	0.94
$[DOD, 1; D_s, 4]$	0.04	0.11	0.03	0.19	0.09	0	0.06	0.38	0.83
$[\Delta z_1, 1; \sigma_s, 1]$	0	0	0	0.052	0	0	0.01	0.052	0.35
$[DOD, 1; \sigma_s, 1]$	0.51	0.35	0.49	0.45	0.77	0.41	0.74	0.13	0.25
$[DOD, 1; \sigma_s, 2]$	0.37	0.61	0.27	0.43	0.7	0.08	0.56	0.8	0.58
$[DOD, 2; \sigma_s, 3]$	0.27	0.69	0.18	0.56	0.08	0.25	0.34	0.15	0.74
$[\Delta z_1, 1; D_{ss}, 1]$	0	0	0	0.052	0	0	0	0.86	0.85
$[\Delta z_1, 1; D_{ss}, 5]$	0	0.01	0	0.01	0	0	0	0.62	0.22
$[DOD, 1; D_{ss}, 2]$	0.24	0	0.33	0.01	0.66	0.4	0.09	0.92	0.12
$[\Delta z_1, 1; \sigma_{ss}, 1]$	0	0.02	0	0.04	0	0	0	0.89	0.09
$[DOD, 1; \sigma_{ss}, 1]$	0.09	0.04	0.06	0.11	0.43	0.17	0.07	0.96	0.08
$[DOD, 1; \sigma_{ss}, 2]$	0.28	0	0.23	0.02	0.48	0.42	0.09	0.92	0.11
$[DOD, 2; \sigma_{ss}, 2]$	0.11	0	0.03	0.06	0.052	0.24	0.042	0.63	0.32
$[DOD, 3; \sigma_{ss}, 3]$	0.54	0.48	0.67	0.2	0.41	0.49	0.09	0.4	0.91

Berm building (represented by $\Delta z_1, e_k(t)1$) at Slapton was reflected in both the temporal mean component of size and sorting ($[D_s, e_k(t)1; \sigma_s, e_k(t)1]$), and with the temporal fining/ameliorated sorting component ($[D_s, e_k(t)2; \sigma_s, e_k(t)2]$, see also Figures 6.19 and 6.20). With reference to the left hand panels of Figure 6.22 and the corresponding shaded values in Table 6.8, these were both related strongly with the semi-lunar tidal cycle, with a secondary role played by significant wave height. The fining/ameliorated sorting - berm building relationship was further associated by some degree to spectral width, which showed relative peaks around the two berm building phases, and also with a change in wave direction from easterly (tides 1-5, associated with relative depletion) to south-westerly (thereafter, associated with relative accretion). The dependency on wave direction suggests advection of sediment from elsewhere, rather than just cross-shore re-distribution.

Berm building at Strete ($[\Delta z_1, 1]$, a mode which includes both prior relative depletion in the same cross-shore position as subsequent berm building) was reflected in both the temporal coarsening/deteriorated sorting component of sediment size/sorting ($[D_s, e_k(t)2; \sigma_s, e_k(t)2]$, see also Figures 6.19 and 6.20), but not in the respective mean components (unlike at Slapton). With reference to the centre panels of Figure 6.22 and the corresponding shaded values in Table 6.9 as a combined signal, this was found to be

related strongly to the tidal cycle, with secondary roles played by significant wave height and mean wave direction (as at Slapton). Unlike at Slapton during the same time frame, the mean morphological component ($[\Delta z_1 e_k(t)1; e_k(t)2]$) at Strete also had significant linear association with the secondary modes of size and sorting.

During the spring 2007 survey, morphological change separated into two eigenmodes representing the dynamics of, respectively, the lower and upper intertidal area ($[\Delta z_1, e_k(t)1; e_k(t)1]$ and $[\Delta z_1 e_k(t)1, e_k(t)2]$). The first was related to the first and fourth eigenmodes of D_s, and the first eigenmode of σ_s, representing the mean components of each. With reference to the right hand panels of Figure 6.22 and the upper section of Table 6.10, it was found that a number of signals dominated the lower beach (surface) morpho-sedimentary relationships ($[\Delta z_1, e_k(t)1; D_s, e_k(t)1]$ and $[\Delta z_1, e_k(t)1; \sigma_s, e_k(t)2]$), including *TR*, ϵ_s, ϵ_w, T_s, θ and ξ. The same is true of the corresponding sub-surface modes.

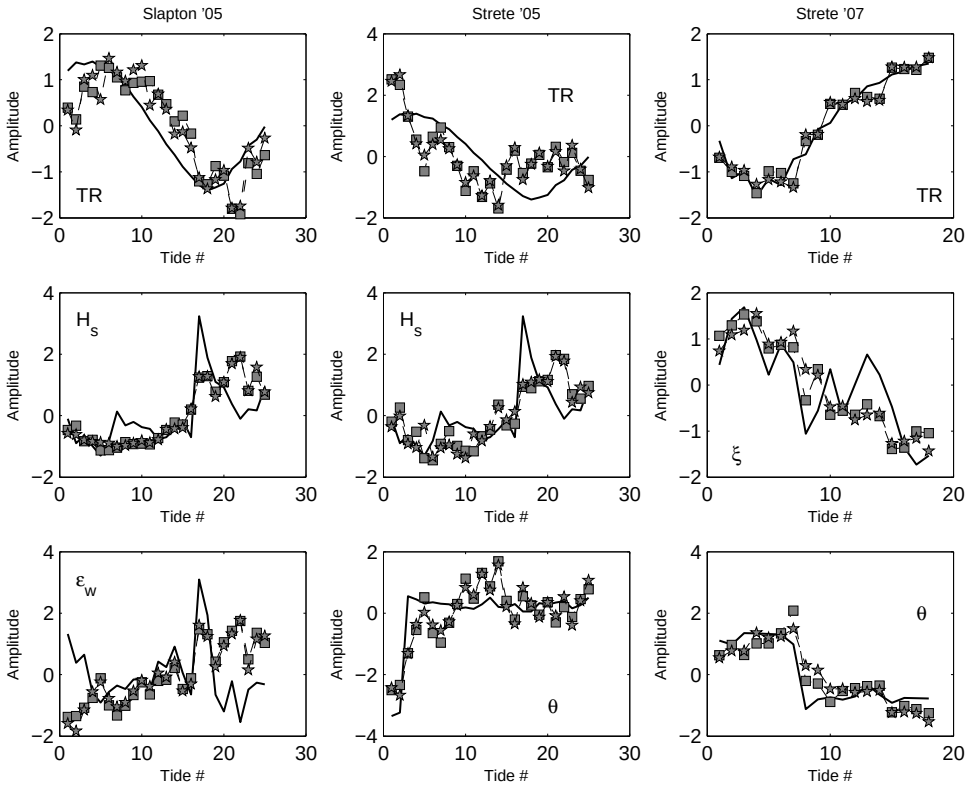

Fig. 6.22 *Temporal amplitudes of CCA modes for hydrodynamic parameter (solid line), and significantly correlated morpho-sedimentary eigenmodes ($\Delta z_1, D_s$ as circles and $\Delta z_1, \sigma_s$ as stars). The amplitudes have been standardised to aid comparisons. From left to right: Slapton '05, Strete '05, and Strete '07.*

6.7 *Summary*

(i) Morphological, sedimentological, and hydrodynamic data from two survey campaigns on a gravel beach over a semi-lunar tidal cycle have been collected and analysed. The aim of the research was to uncover relationships between the triad of variables.

(ii) Morphological change was consistently dominated by relative depletion high on the intertidal beachface, prior to 'cut and fill' berm building. This occurred in both field surveys despite the surveys straddling different phases of the spring-neap-spring tidal cycle.

(iii) Surface sediments tend to coarsen; become more poorly sorted; and finer skewed, in the seawards direction. In contrast, sub-surface sediments become finer, better sorted, and more positively skewed across the intertidal profile seawards.

(iv) Sediment size, sorting and skewness had very complicated space-time histories, and therefore it was difficult to visually assess coherent patterns between them, and likewise between each of them and morphological change.

(v) The two-dimensional correlogram was found to be a useful tool to glean consistent signals in the records for the sedimentological parameters. An inability of this tool and others, however, to adequately separate the complicated trace through time of the sedimentological parameters from the stochastic variation in space, disallowed any meaningful relationships between hydrodynamic variables to be discerned.

(vi) It was concluded from this initial analysis that both morphology and sedimentology was generally more similar at a given spatial location over time than it was for space for each individual time. The coherent response of variables alluded to in their respective correlograms also suggested that they were being forced by some common external forcing mechanism.

(vii) sub-surface sedimentology over the depth of disturbance indicated that the step, a morphological feature that had passed through the system consistently with the previous high tide, could be traced through the sediment characteristics.

(viii) Ordinary correlation, however, was not sufficient to yield significant relationships between morphological and sedimentological variables, in neither absolute values, over individual time steps, nor relative to initial or mean values.

(ix) EOF analysis was used to decompose the data sets into their consistuent modes, consistently showing that more EOF modes were required for median sediment size (D_{50}) than for either Δz or sediment sorting (σ), implying D_{50} has more stochastic variation and less inheritance.

(x) Strong hysteresis patterns were evident in the dominant spatial EOFs of a morphological parameter which reflected net sedimentation relative to the start of the survey campaigns (termed Δz_1), and surface sediment size and sorting spatial EOFs.

(xi) The spatial phase parameter calculated from the respective CEOFs (complex EOFs) confirmed that an association not apparent in the non-decomposed data sets was consistently present in the data associated with the most variance.

(xii) CCA analysis was used on the temporal EOFs in order to investigate the relationship between morphological and sedimentological change. It further confirmed that, whereas significant correlations could not be found between non-decomposed data sets, such relationships were statistically significant if the spatial and temporal information within the data was decomposed into orthogonal modes.

(xiii) Significant relationships were found only between the absolute values of sediment size and sorting and Δz_1, suggesting that sediments responded better to net sedimentation patterns rather than individual sedimentation events.

(xiv) Specifically, berm building was found to be reflected in the mean and trend components of size and sorting. In the Slapton 2005 data set, this trend in time was general fining and ameliorated sorting, and at Strete during the same time the trend was general coarsening and deteriorated sorting. In the spring 2007 data set, the EOF analysis separated the Δz_1 signal into upper and lower beach modes, and surface sedimentology was found to have association only with the latter.

(xv) CCA analysis was used to uncover coherent responses in those pairs of morpho-sedimentary EOFs that had statistically significant correlation.

(xvi) A predictor matrix of nine variables was used for each of the morpho-sedimentary data sets, consisting of time series from eight hydrodynamic/morphodynamic parameters, plus a vector of Gaussian white noise.

(xvii) The morpho-sedimentary eigenmode pairs were found to be strongly related to hydrodynamic forcing, which provided further evidence that morpho-sedimentary change (on gravel beaches over the timescale of interest) had some detectable cause. These forcings veried between data sets, but tidal range and wave height were consistently represented.

7 MORPHO- SEDIMENTARY DYNAMICS OVER ONE YEAR

They went to sea in a Sieve, they did,
In a Sieve they went to sea:
In spite of all their friends could say,
On a winter's morn, on a stormy day.

Edward Lear (1812-1888), British poet. The Jumblies.

7.1 *Introduction*

This chapter will present and explain the morphological and sedimentological changes at Slapton, sampled at identical spatial and temporal resolution, over one calendar year. The previous chapters have focused on beach variability at the time-scale of seconds to weeks, and length-scales of fractions of metres to tens of metres. These studies have improved the knowledge base for better-informed models of short term morphological and sedimentological change on gravel beaches. This chapter will develop and explain a sediment budget for Slapton, as well as document the co-evolution of beachface morphology and sedimentology of this gravel beach over a larger time and spatial scale. As such, it draws upon some data and themes first outlined in Chapter 3 since it relates to the longer term dynamics of the site.

Morphodynamic studies begin with experience, and seek to investigate the cause [Komar, 1998]. The association of monthly changes in beach profiles with seasonal variation in wave climate is a fundamental tenet of beach morphodynamics [Winant et al., 1975; Komar, 1998; Masselink and Hughes, 2003]. Beach profiling and wave recording, which are, in the modern sense, relatively simple to collect, must remain at

the central core to our understanding and prediction of beach change. Beach profiles reach equilibrium in the laboratory but do not in the field, and indeed few models accurately predict the behaviour of profile change. Without good beach profile data sets over a range of scales it will be equally impossible to develop accurate morphodynamic models for gravel beaches. Without sedimentological information at the same resolution as profile information, it will be impossible to model the sensitivity of profile change to changes in sedimentology.

Many early studies into beach behaviour were carried out on gravel beaches [King, 1972], and these studies collectively showed that profile change on gravel beaches will be greater than on sand beaches for a given set of hydrodynamic conditions [Bagnold, 1954; Emery, 1955], a theme whcih continues in more modern studies [Austin and Masselink, 2006*a*; Horn and Li, 2006]. Response times on gravel beaches are considered short. The 'summer-winter' seasonal model has been challenged on beaches, including those composed of gravel [e.g. Dingler, 1981; Carr et al., 1982]. Constructive wave action and berm building on coarse grained beaches, first elucidated by Lewis [1931] and later experimentally verified by others [Duncan, 1964; Masselink and Li, 2001; Austin and Masselink, 2006*a*; Weir et al., 2006], is discussed in greater detail in Chapter 2. Despite many of the early conceptual advances on beach behaviour being based on gravel beaches, models for profile change on gravel beaches [e.g. Powell, 1990] are poor, primarily because of the paucity of appropriate data sets, particularly in response to storms [Orford, 1977; Orford et al., 2003]. The industry standard model for gravel beach profile change, that of Powell [1990], is largely based on the geometric relationship between tidal elevation and freeboard, as well as some overly-simplistic relationships between sedimentation, sediment size and wave steepness. The crests of many of the gravel beaches in the UK are well above spring high tide level, for example the crest of Chesil beach at Portland lies 13.3m above normal high tide level [King, 1972], and similar super-elevations are found at Orfordness and Dungeness [Hey, 1966]. Slapton has a freeboard of only 3-4m above MHWS. Mechanisms for crest sedimentation have been proposed [Orford, 1977], but these conceptual models remain to be fully validated using measurements. No existing model is applicable to the problem of gravel beach overwash. Models for sand barrier overwash are primarily based on inundation conditions where the freeboard is not as great as on many gravel barriers, where overwash is caused by violent

wave breaking and associated run-up. As yet there are no numerical models based on the physics of sediment transport available for gravel beach profile response during storms. The sedimentological responses to storms on gravel shores are equally poorly understood [Hart and Plint, 1989].

The larger scale coastal behaviour (LSCB) of many sand beaches is dominated by the cyclical generation-migration-degeneration patterns in nearshore bar systems [Wijnberg and Terwindt, 1995; Plant et al., 1999; Ruessink et al., 2003]. Large measured morphological data sets are now available for sand beaches, for example at Duck, NC (USA) and along the Dutch coast. In addition, many Argus stations, at the time of writing, have been running for over a decade (for example Oregon in the USA, and Perranporth in the UK). Few morphological data sets are available to assess the LSCB of gravel beaches, which is partly why the seasonal response of gravel beaches has not been better parameterised. Studies into LSCB find better tangible outcomes when physical processes such as waves and tides are parameterised in simple relationships and then used to explain observed/measured beach changes, themselves succinctly and simply parameterised [deVriend, 1997; Horn, 2002b]. Such an approach is adopted here, acknowledging that developing a model on the basis of one year of data from one beach would be an ambitious undertaking, especially considering the lack of current insight we have of the relationship between sedimentation patterns and sedimentology on beaches.

7.2 *Field Site, Methods and Data*

7.2.1 *Hydrodynamics and Weather*

The three sources of hydrodynamic data used in this study are outlined in Chapter 3. For this study, both the hourly offshore wave data measured by WW III model, as well as the half-hourly inshore wave data measured by the Start Bay buoy, were used to characterise the hydrodynamic conditions forcing beach change. However, the latter record was only available since 5th April 2007. Linear regressions were performed between the measured inshore and measured/modelled offshore records (resampled/interpolated to the frequency of the wave buoy). The agreements are not good, as may be seen in the bottom two rows of Figure 7.1. There are many potential reasons for the scatter observed, including time-delay and resampling effects, and the

relative sheltering of the bay compared to the open coast. South-westerly waves are significantly refracted around Start Point and Skerries Bank, which attenuates and focusses wave energy according to spatial location within the Bay (see chapter 3). In addition, the parameters are not directly equivalent, having different sensitivities to wind and swell components. Hydrodynamic data outliers were removed prior to analysis. An outlier was defined to be a value that is at least three standard deviations away from the mean. Mean wave (and wind) directions were calculated respecting the circular nature of the data, as the four quadrant arctangent of the real and imaginary parts of the elements of the angular data series in radians. All correlations expressed have been bootstrapped 1000 times using a re-sampling algorithm, and a mean of those 1000 bootstrapped coefficients has been taken.

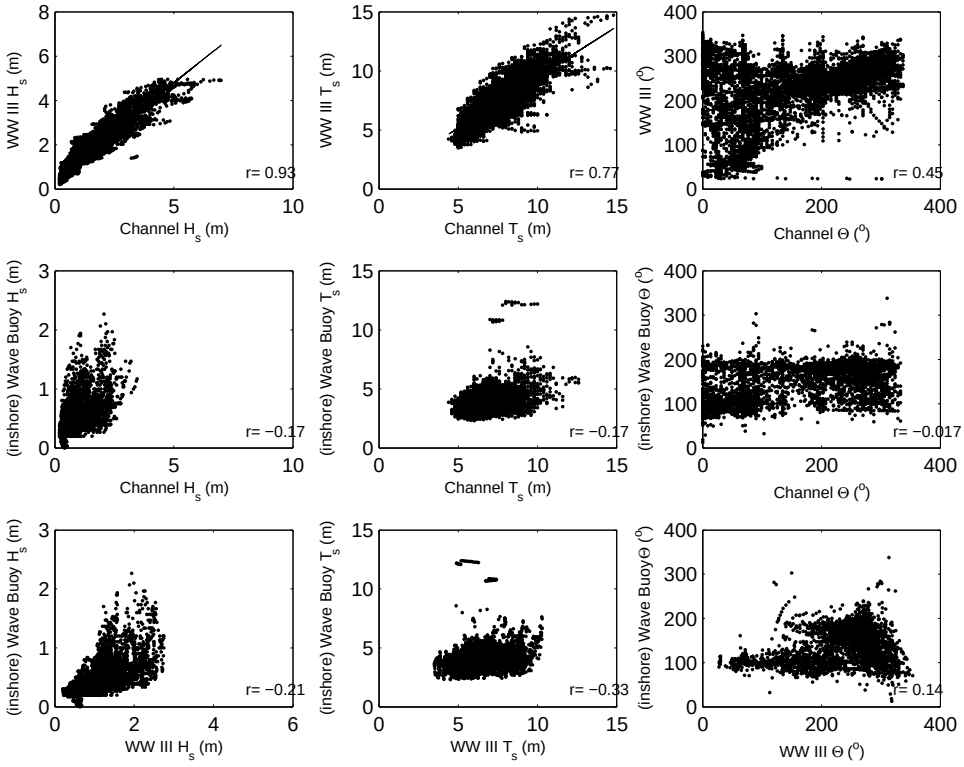

Fig. 7.1 ***Top row****: regression analyses between measured and modelled offshore wave parameters (top row, from left to right:* H_s*,* T_s*, and* Θ*) between October 2006 and October 2007.* ***Next two rows****: regression analyses between measured and modelled offshore and inshore wave parameters between April and October 2007 (*H_s*,* T_s*, and* Θ*).*

In addition to the weather data described in Chapter 3, a BaroTroll (Win Situ Inc.; Colorado, USA) was mounted at 32m ODN to measure and log air temperature and pressure every hour for the entire duration of the present survey period.

7.2.2 *Beach surveys*

The primary data set consists of regular beach profiles every 250m along a 3.25km stretch of Slapton Sands between Torcross and Strete. These profile lines (Figure 7.2) were surveyed using a Trimble 5800 series Real Time Kinematic Global Positionning (RTK-GPS) system [e.g. Haxel and Holman, 2004] every two weeks at spring low tide between 23rd October 2006 and 12th October 2007, the data set therefore consisting of a total of 24 surveys. Additional beach profiles were sporadically taken at the southern and northern extremes of the beach. Surveys were carried out not more than 2 hours before and 2 hours after low tide, from barrier crest to shoreline. Whilst the cross-shore extent of the surveys depended in some small measure on the survey time relative to low tide, as well as the storm set-up, good intertidal coverage was always attained. Each profile line, drawn at 115 degrees relative to magnetic north, was closely followed using an uploaded map into the RTK-GPS system's control screen. Errors created through survey track deviation along a fixed line were removed to generate more realistic along line distances. Pythagoras' theorem was used to find the errors in horizontal distance from the deviations in collected $[x_m, y_m]$ points relative to the reference 115 degree $[x, y]$ line using:

$$D_e = \sqrt{\left[(x - x_{md})^2 + (y - y_{md})^2\right]} \tag{7.1}$$

Using vectors of $[x_{md}, y_{md}]$ coordinates interpolated so as to be much finer in spatial resolution than the points collected in the field, to yield $[x_{mi}, y_{mi}]$. Finally the corrected $[x, y]$ positions were found as the values of $[x_{mi}, y_{mi}]$ indexed by the vector $\min(D_e)$. Additional checks on elevation values for each survey were made with reference to very accurate observed control points made on 13 permanent benchmarks spaced uniformly along the barrier crest. Vertical errors were typically between $\pm$2cm.

In addition to the topographic surveys, sediment samples were collected for every surveyed point in the cross-shore from the shoreline to a subjective estimate of approximate high water spring during the past fortnight (invariably this was the previous tide just a few hours before surveys began, so it was relatively easy to discern the limit of the 'fresh' sediment deposits using a strand line). The samples were collected and analysed using the digital photography techniques which are the subject of chapter

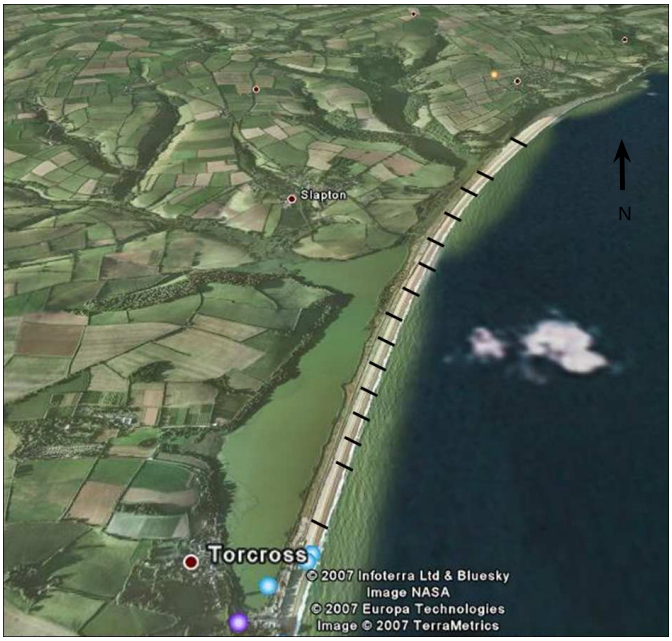

Fig. 7.2 *Aerial image of Slapton barrier, with the villages of Torcross and Slapton indicated. The profile lines surveyed regularly as part of this study are shown in black. Base image courtesy of Google Earth®.*

4. In this way thousands of sediment samples were collected, geo-referenced, and analysed for their median size, geometric sorting and skewness.

Additional alongshore sedimentological data sets were acquired in January, June, and November 2006, and February and May 2007. These consisted of sediment samples every 15m along the berm crest for the entire 4.5km length of the barrier. The samples were also collected and analysed using the digital photography techniques discussed in chapter 4, and collectively constitute thousands of samples. The results in this chapter draw upon a total of 6441 digitally imaged samples.

Data were processed in two ways. Firstly, as individual cross-shore profile lines, expressed in distance from a reference datum (permanent benchmark) on the back of the barrier at an approximately uniform distance from the barrier crest, linearly interpolated to 1m horizontal cross-shore distance accounting for changes in slope. Due to the 250m spacing of the survey lines, it was assumed that alongshore changes in profiles were less important than cross-shore changes. A well sorted gravel barrier beach like Slapton is perhaps one of the few cases where such an assumption is reasonable, and this is verified by measurements such as those plotted in Figure 7.3 which, on a given survey and for both the northern and southern ends of the beach, shows three beach profiles spaced

50m apart, display remarkable cross-shore uniformity over distances in excess of 150m.

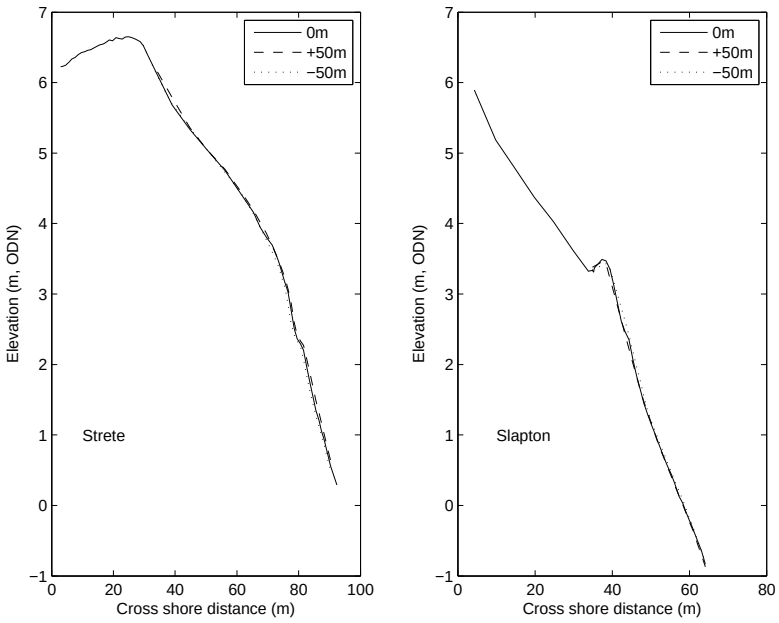

Fig. 7.3 *The relative alongshore uniformity of Slapton beach. Three cross-shore profiles spaced 50m apart (0,-50 and +50m), at Strete (towards the north,* ***left panel****) and Slapton (towards the south,* ***right panel****).*

Surface sedimentology varies to a much greater degree compared with profile elevation alongshore, as is illustrated by Figure 7.4, which shows the variability associated with a $36m^2$ section of beachface, sampled every 0.5m. This is because, on gravel beaches, as discussed in Chapter 2, surficial sediments tend to congregate into 'assemblages' or 'textural mosaics'. Observations such as these have prompted the present study to investigate whether there are morphological-sedimentological covariances, and whether the morphodynamics of a gravel beachface leaves a sedimentological fingerprint. It may seem perverse, therefore, that sediments were not surveyed at a greater resolution than elevations, in the knowledge of a greater stochasticity. However, sediments still tend to vary more in the cross-shore than alongshore, the larger length scale. In addition, there is a clear alongshore trend in the sedimentary parameters, about which small-scale sediments are stochastic fluctuations, and clearly a product of localised processes or even remnants of prior morphologies. The alongshore trends observed visually, and obtained quantitatively along individual cross-shore locations relative to the shoreline, were better matched by a linear interpolation routine than a routine based on a semivariogram, which used the extent of the spatial dependence in the sedimentary parameters. This

confirmed that, whilst assuming grain size does not change over the 250m is unreasonable, that one sediment sample's characteristics grade linearly to the next over this distance actually confirms visual observations and measurements made along a single cross-shore location alongshore, better than using a more sophisticated interpolation routine, which uses information on the spatial evolution of the sedimentary parameters. At this time and spatial scale, therefore, it was concluded that a more densely-resolved spatial grid for sediments compared to profiles would have been an unnecessary undertaking. Besides, and to turn the original potential counter-argument on its head, detection of morpho-sedimentary association at the same scale is a key element of this study.

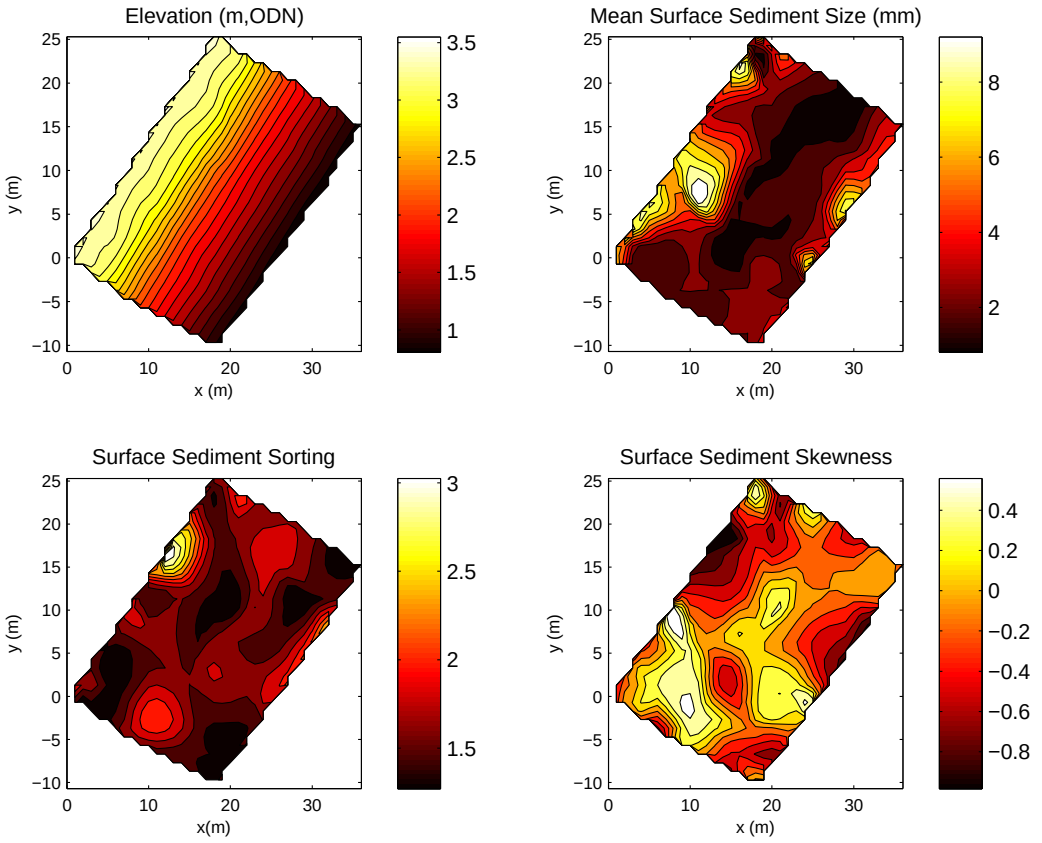

Fig. 7.4 *A 36m^2 planar section of intertidal gravel beach face, with no secondary morphological features (**top left**), displays a marked variation in sedimentary characteristics. On this occasion, mean surface sediment size (**top right**) varies between 1mm (0 ϕ) and 9.5mm (-3.25 ϕ); sorting (**bottom left**) between 1 and 3; and skewness (**bottom right**) between-0.9 and 0.5 (based on Folk and Ward [1957] logarithmic graphical measures).*

The second morpho-sedimentary data processing method by means of Digital Elevation Model (DEM) surfaces for visual assessment of spatial trends. Data gridding was acheived through standard Delaunay triangulation using the convex hull algorithm

detailed in Barber et al. [1996]. Since Slapton beach is approximately 45 times as long as it is wide, data gridding using Delaunay triangulation was hampered and potentially erroneous due to the due to the irregularity of the triangulation points. Therefore, the procedure was aided considerably by first removing the curvature from the coordinate system into a more rectangular grid. This reduced the coordinate system to a geometrically skewed (but fully-reversible) version with a ratio between length and width in the region 15:1. Slapton is approximately log-spiral in shape [Yasso, 1965], so the pre-processing procedure of Harley and Turner [2007] was used to first remove the log-spiral curvature through the 3D data sets. Using an origin in Start Bay located at [289106.0312 E, 42430.2637 N], the radial vector from the origin to a point of the curve , r_s, was found to be best approximated using an initial radius of r_o=7190.4853m, and an angle between r_s and r_o of-89.7195^o, with a RMS error fit of 31.5m. The Cartesian coordinates were thus transformed into a coordinate system relative to the curvature in planform of the beach, more akin to our notions of alongshore and cross-shore, as described in Harley and Turner [2007]. Interpolation down to a 1m grid was thus faster and more accurate.

The same profile lines were surveyed along varying widths, depending on the location of the shoreline at the time of the survey, itself dependent on the tidal state, wave set-up, and relative shoreline change in the intervening time between surveys. Figure 7.5 shows a schematic of the conventions used for volumetric calculations. Volumes (Q) were calculated as area of beach under the profile relative to -1m ODN, multiplied by per 1m strip alongshore, multiplied by the distance between survey lines. The -1m ODN level was chosen because that was a level consistently reached by the RTK-receiver operator. All beach widths and heights are expressed in metres: beach widths were recast from grid coordinates ([Eastings, Northings]) to distance from the permanent bench mark from which each survey emanated. In this way, the two end points of the profile were fixed, and the area of the cross-section was dependent only on the profile changes. In addition, a convexity index was calculated for each profile line, for each survey, following Sonu and Vanbeek [1971] and Caldwell and Williams [1985]. The more convex the beach, the greater subaerial volume is stored and the higher the ratio between beach volume (Q) and beach width (w). Note that in this instance the beach width is allowed to vary, and is not fixed at the-1m ODN level. A time-series of profile volume is not suitable

because each profile line is a different length. Changing Q/w values relative to initial for each survey line indicate the relative volumetric 'health' of each local beach section through time.

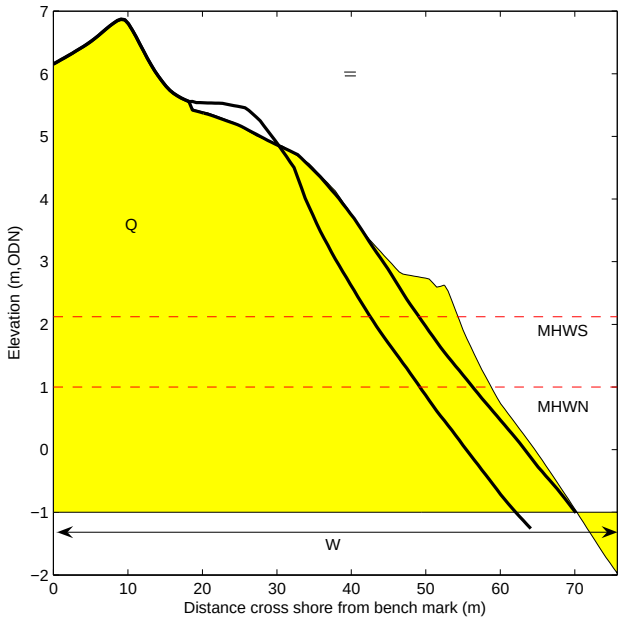

Fig. 7.5 *Schematic of the volumetric calculations made from beach profiles, by integrating under a beach profile to-1m ODN (dashed, also MHWN and MHWS indicated by dashed lines). The vertical scale of error is indicated by the parallel lines. The heavy lines show the same profile at different times.*

Cross-correlation confidence intervals were calculated as independent (not simultaneous) and asymptotic (because the data were not continuous), and the appropriate corrections for small sample sizes were applied where appropriate. The lower and upper confidence intervals at 95% were calculated as, respectively:

$$CI_L = \tanh(z_r - \mathbf{T}_{\alpha,\nu}^{-1}\hbar) \tag{7.2}$$

$$CI_U = \tanh(z_r + \mathbf{T}_{\alpha,\nu}^{-1}\hbar) \tag{7.3}$$

where $T_{\alpha,\nu}^{-1}$ is the inverse of Student's $\mathbf{T}$ cumulative distribution function at α=0.05 and ν=N-2 degrees of freedom; z_r is the $\mathbf{z}$-transform of Pearson's cross-correlation coefficient, with Hotelling's (1953) correction [Hotelling, 1974] for sample size, given by:

$$z_r = \sqrt{(N-1)}\left[0.5\log\left(\frac{1+r}{1-r}\right) - \frac{1.51\log(1+r/1-r)+r}{4(N-1)}\right] \tag{7.4}$$

and where $\hbar$ is the standard error of z_r, given by $1/\sqrt{\nu}$.

7.3 Results

7.3.1 Hydrodynamics and Meteorology

The available wave height, period and direction traces, from the WAVEWATCH III model and the Start Bay buoy (since April), are the subject of Figure 7.6. Inshore significant wave heights measured by the buoy between April and October 2007 are typically 34% smaller than the deep water model predictions. Similarly, significant wave periods are typically 56% shorter, and wave directions are much less variable. Wave heights are characteristically higher between November and March, and three periods of sustained storm conditions are evident, at the beginning of December, the beginning of January, and from the middle of February to the beginning of March. Each lasted approximately two weeks, and were composed of three storms apiece where offshore H_s exceeded 4m. There is nothing to distinguish these three stormy periods in terms of wave period or direction, which was consistently south-westerly (Figure 7.6). Offshore wave heights rarely exceeded 2m between March and October 2007, except for a period of energetic activity in July. Figure 7.7 contours the joint probability of wave height with direction and period, respectively. Note the consistency of swell wave direction, and that south-westerlies were associated with both greater wave heights and a greater range of wave heights.

Using the joint distributions of wave height and direction, directional wave energy estimates were obtained by summing energy over each direction. Energy density is proportional to the square of wave height, and is calculated as [Komar, 1998], where g is gravitational acceleration and ρ is the density of seawater:

$$\varepsilon = \frac{1}{8}\rho g H^2 \tag{7.5}$$

which is expressed as $\mathrm{N/m^2}$ and converted to Joules (1J = 1N/m = 1 watt/s) per unit time, assuming wave height does not change considerably between measurements. According to Airy wave theory, longshore energy flux, as wave power per unit length of wave, is given by:

$$P_l = ECn\cos\alpha\sin\alpha \tag{7.6}$$

where n:

$$n = \frac{1}{2}\left[1 + \frac{2kh}{\sinh(2kh)}\right] \tag{7.7}$$

which approximates 0.5 in deep water [Komar, 1998], and group celerity C is given by:

$$C = \frac{g}{2\pi}T \tag{7.8}$$

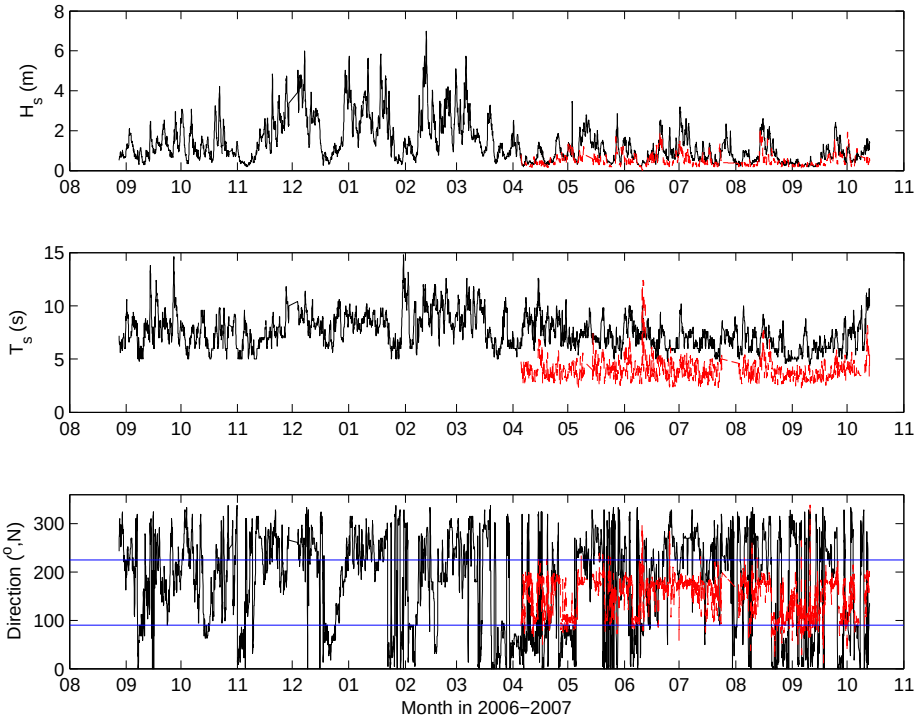

Fig. 7.6 *Hydrodynamic time-series.* ***From top to bottom****, black solid lines: H_s, T_s, and Θ_w between September 2006 and October 2007, modelled in deep water off Start Point using WaveWatch III. Red dashed lines: H_s, T_s, and Θ_w measured by a wave buoy in Start Bay between April and October 2007. The horizontal lines in the bottom sub-panel represent due east and due south-west, respectively.*

The use of deep water wave climate discounts the likely energy attenuation caused by refraction (especially of the southerlies and westerlies, around Skerries Bank and Start Point), and local effects such as offshore winds, wave interactions, etc. In addition, within Start Bay the difference in spread and azimuth in on- and off-shore wave direction will depend on prevailing wave direction. Therefore, the data from the Wavewatch III model was used in conjunction with an industry-standard wave propagation

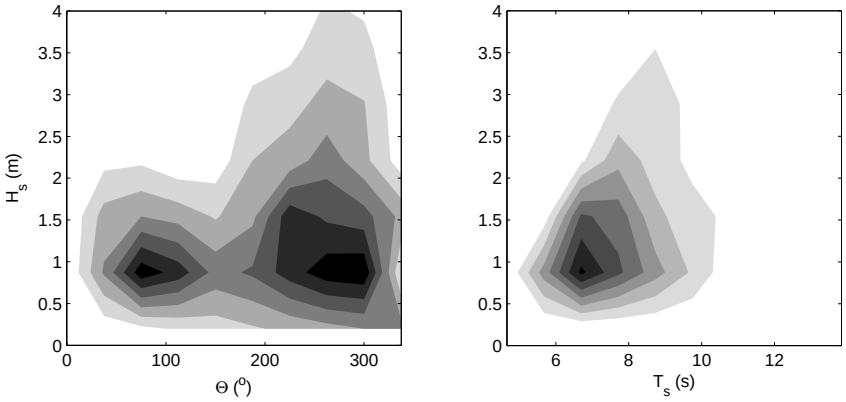

Fig. 7.7 *Joint empirical probability distributions for wave height with direction (**left**), and period (**right**) using the offshore WW3 model.*

(refraction/diffraction) hindcast model (SWAN; Simulating WAves Nearshore, version 40.72 developed by Delft Hydraulics). The measured inshore buoy data was incomplete (being available only from April 2007), and, in addition, did not measure wind speed and direction which is useful for characterising/modelling the local sea (wind-generated) wave climate. In this way, the refraction of waves around Start Point and Skerries Bank into Slapton could be realistically simulated for better quantification of the nearshore wave climate.

SWAN is a spectral phase-averaged model which incorporates both wind and swell wave components. Phase-averaged models compute the change in wave spectra over complex coastal bathymetry while maintaining computational effciency. It incorporates wave propagation, shoaling, refraction due to current and depth; white-capping, bottom friction and depth-induced breaking; wave-induced set-up; and a rudimentary treatment of diffraction [Holthuijsen et al., 1989; Ris, 1997]. The inputs (wave height, period and direction; wind speed and direction) are used to generate a JONSWAP spectrum with a cos2(θ) directional distribution centred around the local wind and wave directions. Bathymetric charts of Start Bay were obtained from Marine Digimap, and a simple regular computational and output grid was defined as shown in Figure 7.8.

SWAN provides many output quantities including one- and two-dimensional spectra, significant wave height and wave period, average wave direction and directional spreading, root-mean-square of the orbital near-bottom motion, cross- and along-shore force, etc, for a number of pre-specified positions. Simulations were rapid - typically 6-7 seconds per day or 45 minutes for a year of simulation. Spectral densities (either m^2/Hz in 1D or $m^2/Hz/Deg$ in 2D) were output in the frequency range $0.04 \leq \mathrm{f} \leq 1.00$ Hz. The model was run using the WW III model outputs for 00:00:00 every day between 01/10/2006 and 31/10/2007 using the friction factor of Madsen et al. [1988] - a drag coeffcient from the quadratic drag law based on Jonsson [1966]; the dissipation of wave energy due to whitecapping model of Hasselman [1974]; and the depth-induced wave breaking model of Battjes and Janssen [1978]. Some outputs for a location in the centre of the barrier at 2m are seen in Figures 7.9 to 7.13.

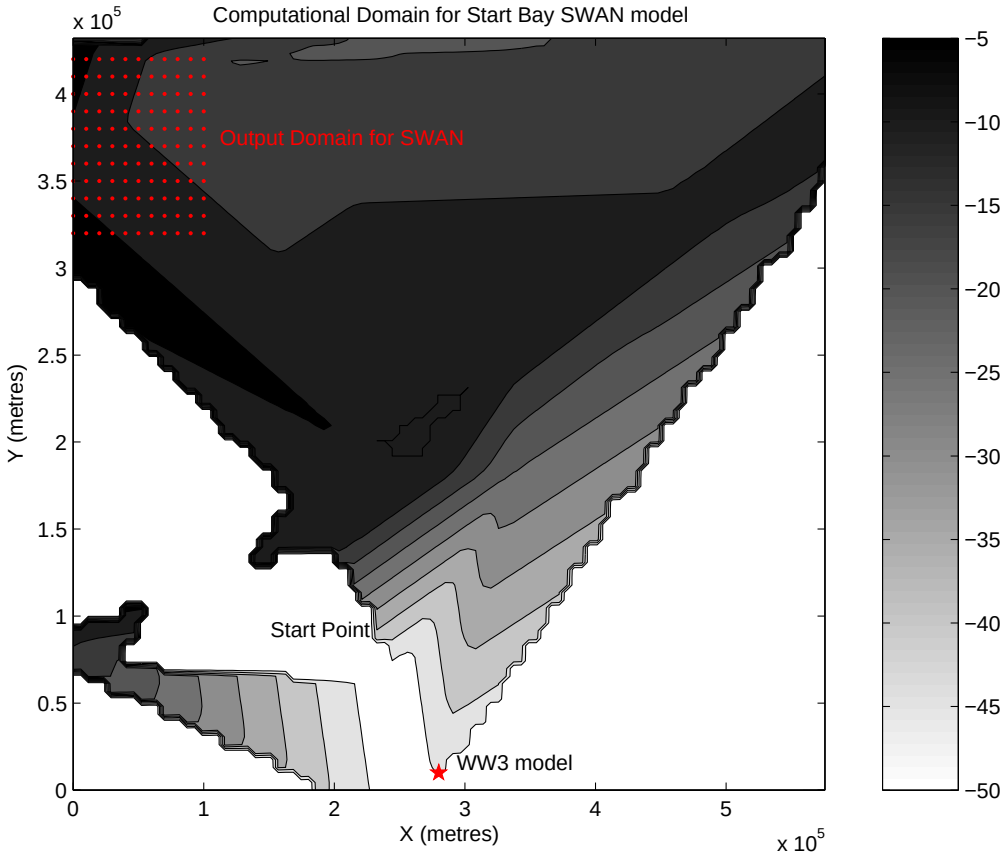

Fig. 7.8 *Input bathymetry and model domain for wave propagation in SWAN. All dimensions in metres.*

The longshore power (P_l, equation 7.6, Figure 7.12) stresses the difference in the energy transfer from waves to the beach between south-westerlies and northerlies/easterlies,

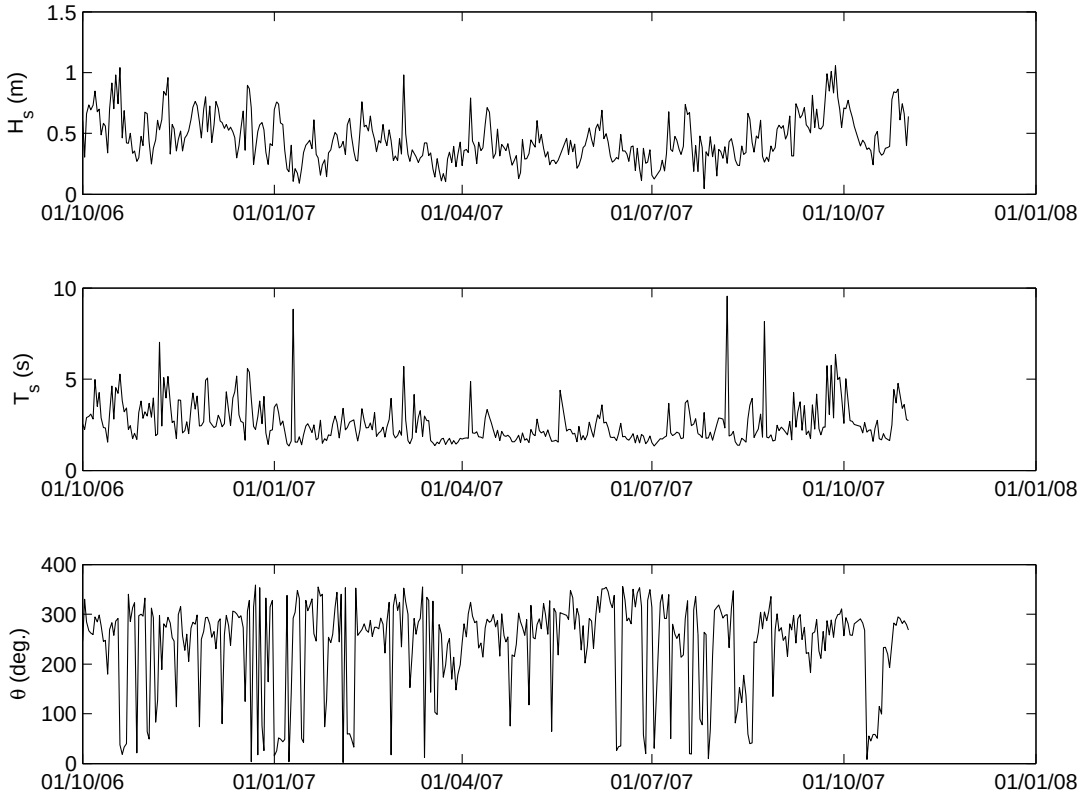

Fig. 7.9 *Modelled wave parameters in 2m water depth in approximately the centre of Slapton barrier. From top to bottom: significant wave height (m); spectral wave period (s); and mean wave direction (degrees).*

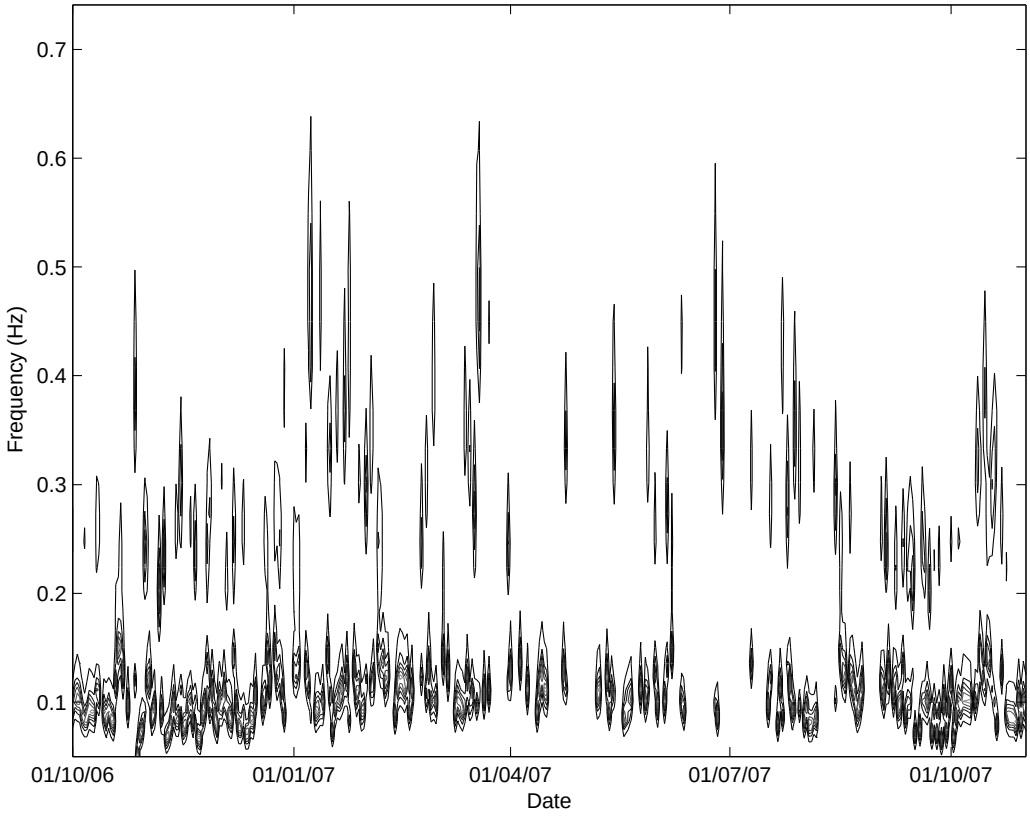

Fig. 7.10 *Spectral density of waves in 2m water depth in approximately the centre of Slapton barrier (m^2/Hz normalised by the total variance), as a function of frequency (Hz) and time.*

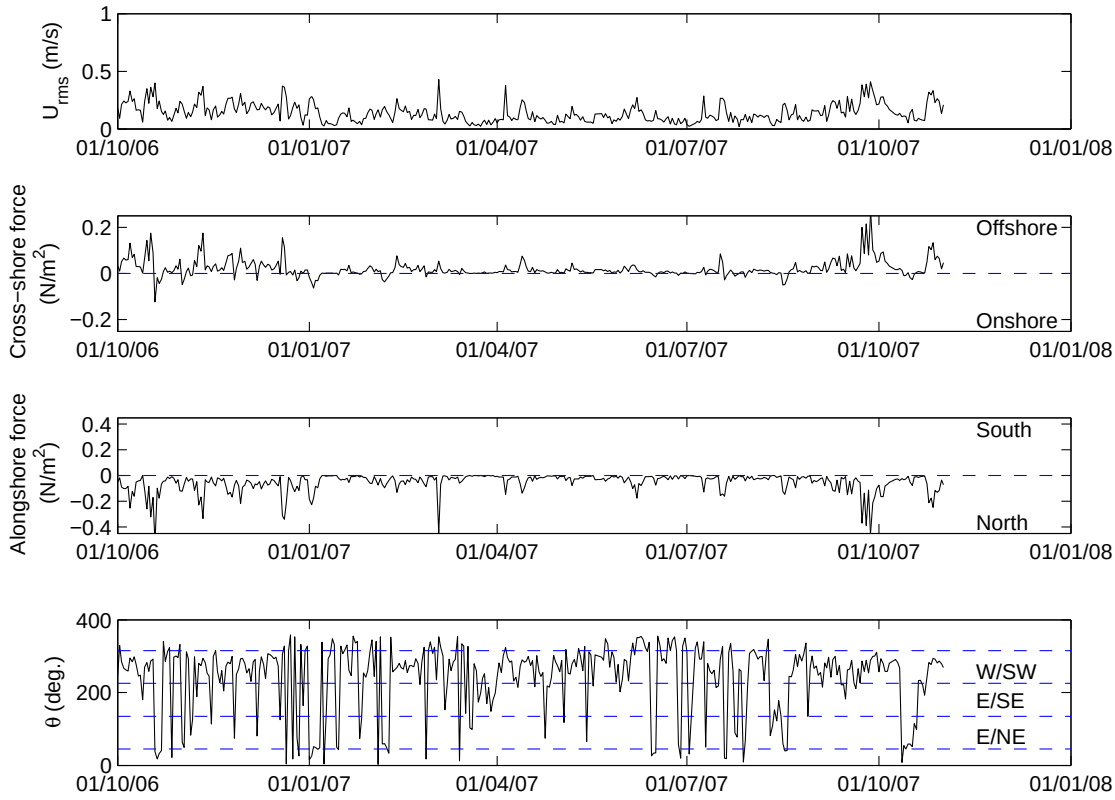

Fig. 7.11 *Modelled wave parameters in 2m water depth in approximately the centre of Slapton barrier. From top to bottom: the root-mean-squared value of the of the orbital velocity near the bottom (in m/s); mean cross-shore wave stress (N/m^2); mean along-shore wave stress (N/m^2); and wave direction (degrees, same as Figure 7.9, bottom panel, for reference)*

.

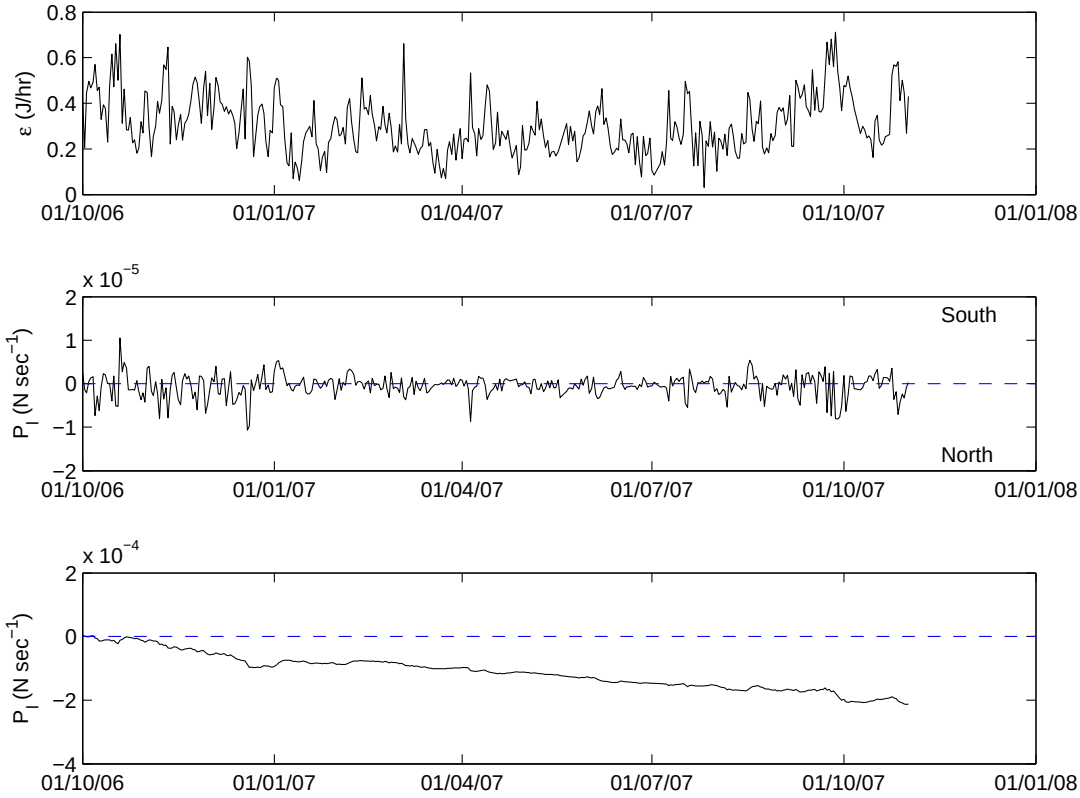

Fig. 7.12 *Nearshore wave energy over October 2006 - October 2007, derived from the SWAN model outputs in 2m water depth. Top: energy (J/hr), calculated using equation 7.5, taking into account the discrete nature of the model inputs/outputs; centre: alongshore energy flux (N/sec^{-1}), calculated using equation 7.6; and bottom: cumulative alongshore energy flux.*

which would imply more energy available for northerly sediment transport, as opposed to southerly. The longshore energy flux, as wave power per unit length of wave, equalled $4.71 \times 10^{-4} Nsec^{-1}$ for northwards flows and $2.58 \times 10^{-4} Nsec^{-1}$ for southwards flows (in the direction of Torcross). Similarly, a calculated 1.0448 N/m^2 cross-shore energy flux occurred in the onshore direction, opposed to a 9.1140 N/m^2 in the offshore direction. Some bivariation in various important parameters may be seen in Figure 7.13. In the bottom right panel, longshore energy flux is seen as a function of wave direction.

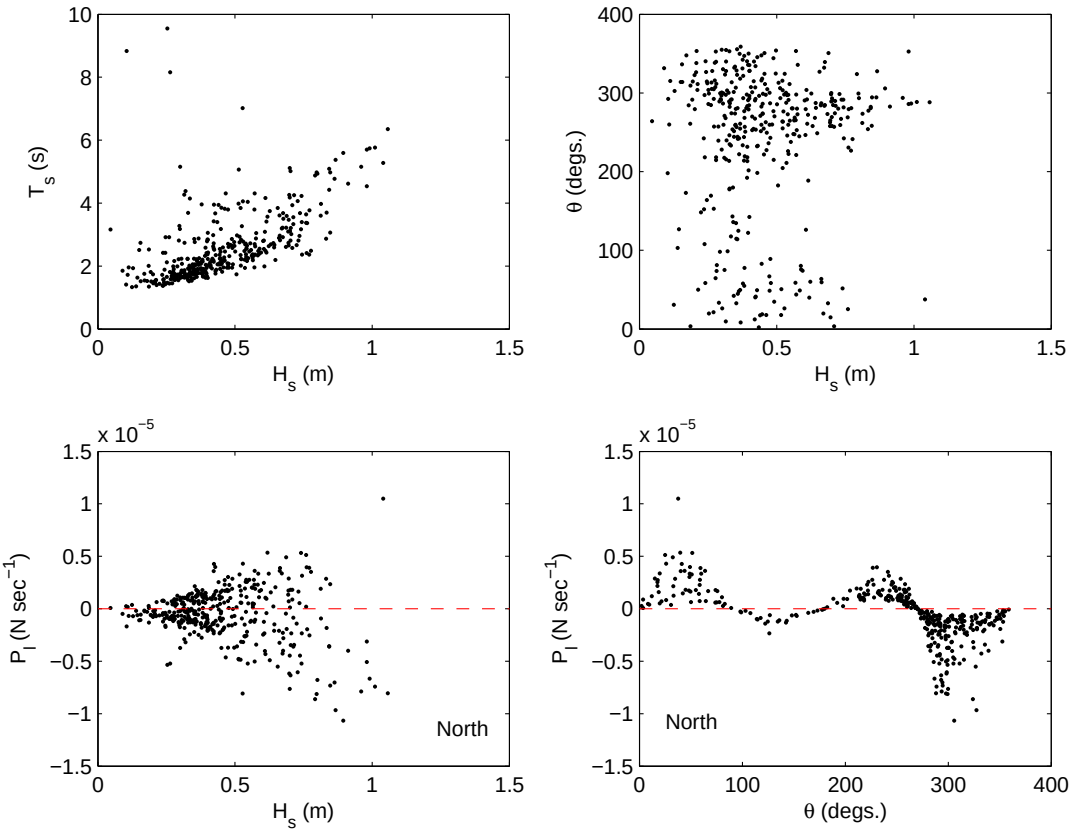

Fig. 7.13 *Bivariation in some model outputs, clockwise from top left: H_s versus T_s, H_s versus θ, H_s versus P_l, and θ versus P_l.*

The year 2006-07, whilst the highest on record, does conform with the general trend of rising temperatures since 1960. In terms of wind speed and direction, 2006-07 is very close to the average (Figure 7.14). It is possible to use significant wave generation theory (so-called *S-M-B* methods after Sverdrup, Munk and Bretschneider) to estimate mean offshore wave heights from the measured wind record. The wind stress factor, in ms^{-1}, is given by [Komar, 1998]:

$$u^* = 0.71 u_w^{1.23} \tag{7.9}$$

where u_w is measured wind speed in m/s (1 km/h = 0.2778 m/s). Deep water wave height is then found from the following relationship:

$$\frac{gH_s}{u^{*2}} = 1.6 \times 10^{-3} \left(\frac{g\Lambda_F}{u^{*2}} \right)^{1/2} \tag{7.10}$$

classifying direction using the measured wind record, assigning fetch (Λ_F) lengths of 6,796,414m (due south-west) and 367,209m (due east). Interestingly, wave heights have been larger and less consistent in recent years, despite a general decrease in wind stress, owing to a greater frequency of south-westerly winds. This illustrates the importance of wind direction and fetch lengths on waves affecting Slapton (Figure 7.14).

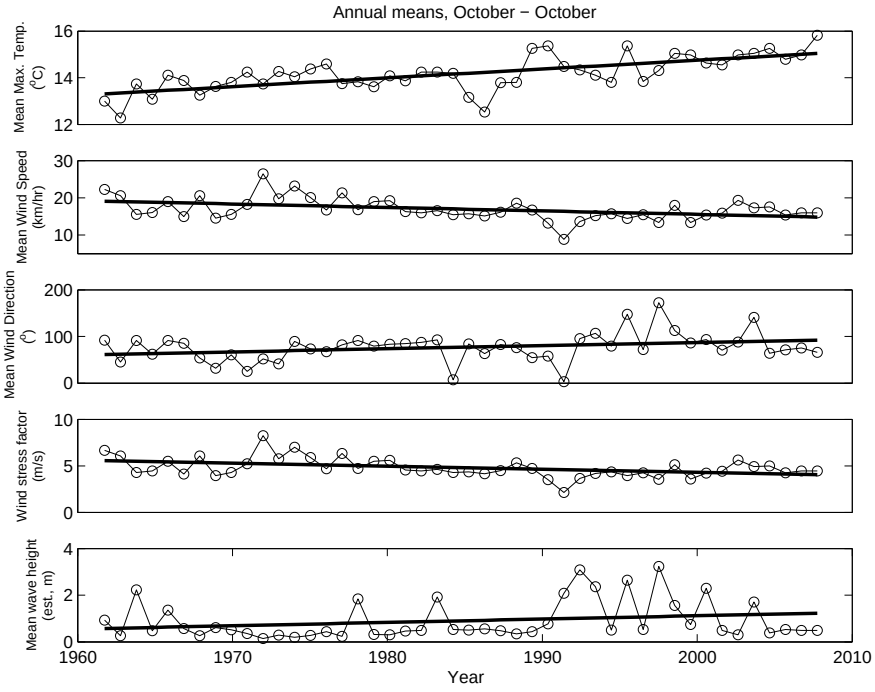

Fig. 7.14 *Trends in annual means, one year being October-October,* ***from top to bottom****, for maximum temperature; wind speed; wind direction; wind stress; and offshore wave height, from 1960–61 to the present year.*

7.3.2 *Beach profiles, and volumes.*

Typical sweep zones of profiles for the southern and northern ends of the barrier (Figure 7.15, top panels) indicate huge changes relative to a given mean profile. The envelope of variability was ±1m relative to the mean (Figure 7.15, bottom panels). Out of the

thirteen profiles regularly surveyed, the eleven most southerly had a greater difference between the mean and minimum elevation than the mean and maximum location for each 1m spaced increment in the cross-shore direction. For the remaining two (northerly) profiles the situation was reversed. This gave the first implication that the beach may have showed net depletion for much of its length, over the year. Between individual surveys, profile elevation changes would have maxima at approximately MHWN and minima above MHWS.

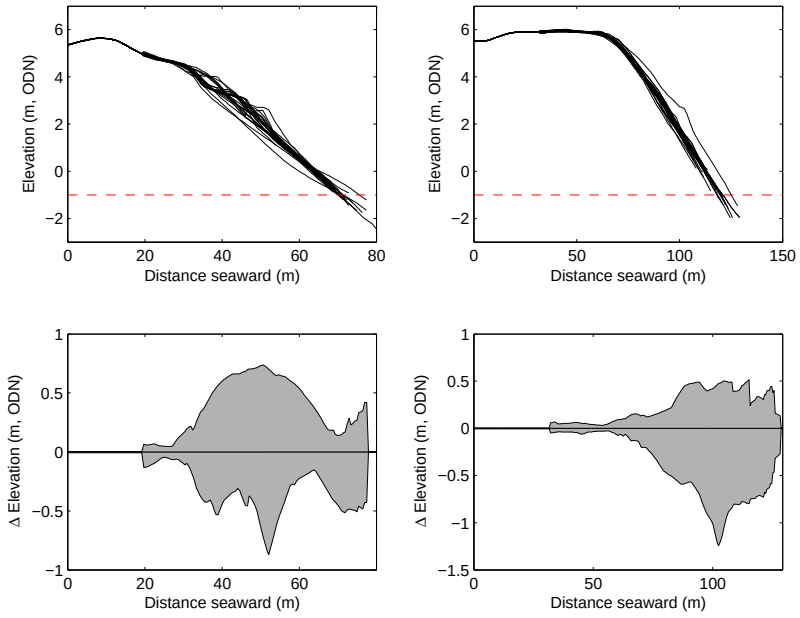

Fig. 7.15 *Profile sweep zone (**top panels**) and typical envelopes of variability around mean cross shore profiles (**bottom panels**). Left panels show a site at the southern end of the survey area, and right panels a site at the northern end.*

The beach was very responsive to changes in the wave climate, in the modes of behaviour were in broad agreement with previous researchers on this beach [Carr et al., 1982; Austin and Masselink, 2006*a*] and other similar coarse-grained beaches [Dingler, 1981; Maejima, 1982]. Figure 7.16 show some example responses of the barrier to constructive (left) and destructive (right) wave action. Considerable changes can occur during individual spring-spring tidal cycles, and this can take the form of both cut-back and sedimentation at barrier crest (overwash). With reference to Figure 7.16, these responses are not consistent alongshore-the northern end of the beach often showed different modes of behaviour to the central and southern (also seen in the fortnightly data presented in Chapter 6). Whereas accretionary periods consisted of localised

sedimentation, mainly as overwash, or more commonly, berm building (usually approximately around around the previous neap tide level), depletionary periods consisted of erosion across the entire profile. In general, the berm rarely lasted more than one spring-spring tidal cycle, although the beach remained in a depleted state for several weeks without suffering extensive further losses, in some locations. On occasion, the volumetric losses incurred on the seaward and landward sides of the berm approximately equalled the volumetric gain caused by the berm's presence. More often, however, sediments were not conserved, suggesting alongshore transport, or offshore transport outside the measurement area. During an overwashing event, volumetric gains incurred at the crest were not matched by (greater) losses further down the profile, so the beach would steepen, and these storm surge events would show net depletion.

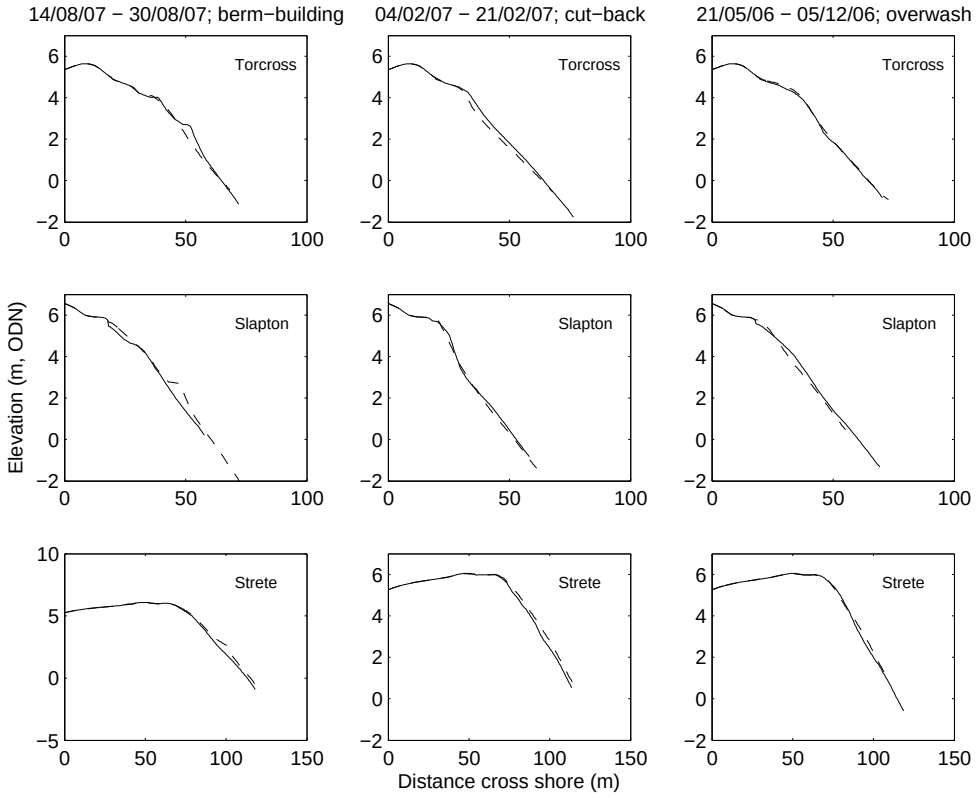

Fig. 7.16 *Profile changes along the barrier.* ***From left to right****: example cut-back between 4th and 21st February 2007; berm building between 14th and 30th August 2007; and changing profile shapes over the year (solid line-November 2006; dotted line-October 2007). Three locations have again been chosen to illustrate the alongshore variability of the changes: in the southern (****top row****), central (****middle row****), and northern (****bottom row****) locations along the barrier.*

The morphological response through the year is examined in a little more detail in Figure 7.17 and 7.18 which collectively show the spatial and temporal scales and

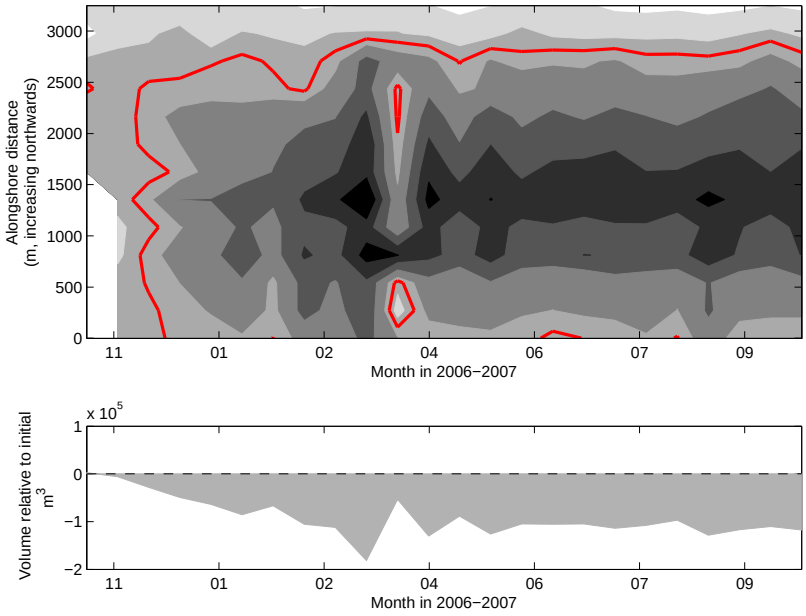

Fig. 7.17 ***Top panel****: volumetric change as a function of time and alongshore distance. Dark shading represents depletion relative to initial, and light shading represents relative accretion. Values range between-1.0155 to 0.266* m^3/m^2 *beachface.* ***Bottom panel****: whole beach mean volumetric change relative to initial, as a function of time, again in* m^3/m *beachface.*

dimensions of beach morphological change. The upper panel of Figure 7.17 contours volumetric change over time, relative to the volume for each respective alongshore location at the start of the surveying campaign in October 2006. Dark areas show relative depletion, and lighter areas show accretion, and the zero contour representing the demarcation between net gains/losses, has been highlighted to show the locations and times of relative net depletion and accretion. It is evident that, whereas net gains have been made by the beach to the north, and little change to the south, in the centre of the beach, approximately in line with, and just north of, Slapton village, significant volumetric losses have been incurred. As is apparent in the bottom panel of Figure 7.17, which charts the volumetric change relative to initial per unit squared metre of beach, net losses in beach material have were sustained in this section of Slapton barrier between October 2006 and October 2007, approximately $0.4m^3$ per m^2 beachface. A similar spatial response as the upper panel of Figure 7.17 may be seen in both panels of Figure 7.18. Here, the upper panel shows the difference in 0m ODN contour position between 6th November 2006 (dashed line) and 12th October 2007 (solid line): the losses are apparent for almost the entire length of the beach, but especially in the central

portion. Note that this is in evidence for every contour value below MHWN (see Chapter 3). The bottom panel of Figure 7.18 also shows the mean net volumetric discrepancies in space, over the whole year, where only the last two profiles to the north have shown a net surplus.

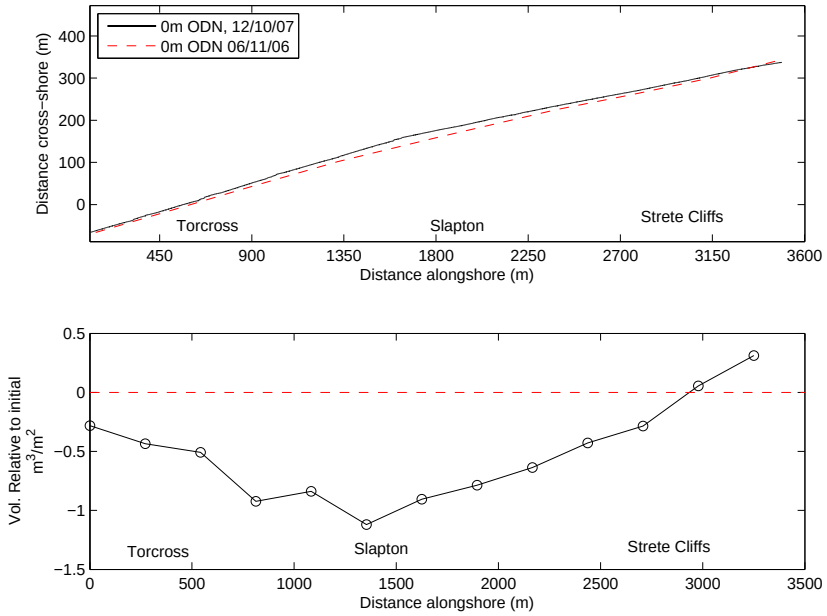

Fig. 7.18 ***Top panel****: evidence of central cut-back and rotation towards the north. Dashed line is the 0m contour on 6th November 2006, and the solid line is the same contour on 12th October 2007.* ***Bottom panel****: net volumetric change alongshore (m^3/m^2) over the measurement period, showing clear differences in the beach depending on location.*

The spatial trends are extended northwards and southwards in the (less regularly profiled) record at the extremes of the beach, pointing to an overall northwards 'rotation' (or embayment-deepening) in the plan shape of the beach in response to what is likely to be some considerable alongshore transport. The gross volumetric changes along the entire length of the barrier, which includes 3250m surveyed every 2 weeks, and the remaining 1250m surveyed approximately every 4 to 6 weeks, have been estimated and is graphed in Figure 7.19. The overall the sediment budget for the entire beach is not in deficit, even though for a large proportion it is, because of the huge gains made to the extreme north of the beach. The surplus is an estimated 10189 m^3, or 2.7$\times$ 10^4 metric tonnes of sediment. Approximate maximum error margins have been calculated as $\pm$6376 m^3, calculated as beach area (318380m^2) multiplied by volumetric error estimate of $\pm$0.02m^3 per metre beach (itself based upon an up to $\pm$2 cm maximum vertical error).

The 'rotational pivot' point is just south of the middle of the barrier, near the war

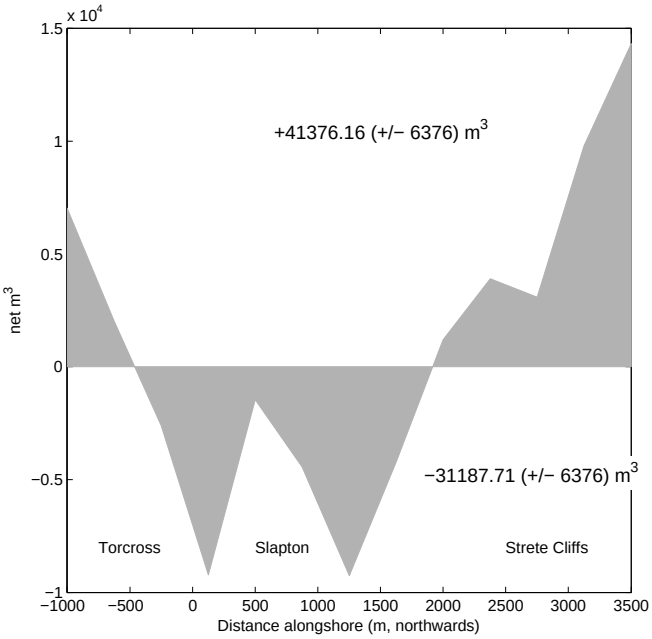

Fig. 7.19 *A sediment budget for Slapton for October 2006-October 2007, expressed in units of cubic metres, as a function of distance alongshore. Figures represent total net gains and losses, therefore the beach as a whole is in surplus by approximately 10,000 m^3. Note that the $\pm$ values indicate those for the whole beach sediment budget, not the individual accretionary or erosionary elements.*

memorial in between the Higher and Lower Leys; and the losses to the south of this point do not match the gains to the north. Due to this alongshore volumetric discrepancy, either some material has been gained from offshore in this region, or from southerly transport around the headland at Strete, or alternatively this material has passed through unaccounted for, through either insufficiently-frequent or (spatially) finely-resolved surveying. This sediment budget does not support the assertion that Slapton is a closed sedimentary system. It also emphasises the importance of taking the entire beach into account-most gains have been made at the ends of the beach.

In order to address the likelihood of considerable northerly alongshore transport during the survey period, and because of the possible frequency-dependence in the data just mentioned, the profile record was analysed in the time-domain using cross-correlation. The input parameter was a time-series of the convexity index (outlined in the methods section of this chapter (Q/w)), relative to convexity index of the beach line at the start of the profiling campaign. Time-series of Q/w, relative to initial, and for each cross-shore profile, were subjected to a cross-correlation analysis similar to Howd and Holman [1987], whereby the time-series for the central cross-shore line was

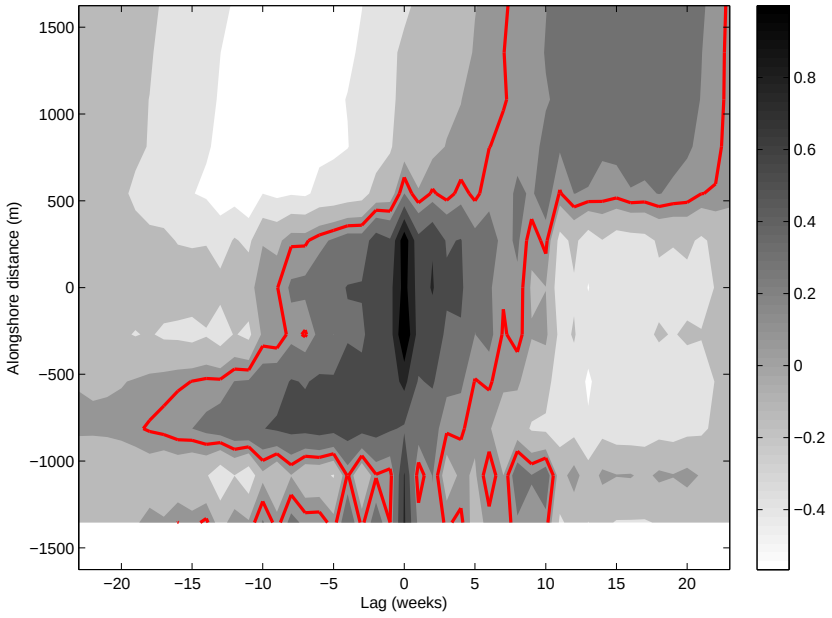

Fig. 7.20 *Contour map of cross-correlation coefficients between the time-series of the ratio of volume to width at the central cross-shore profile line (at 0m), and the ratio of volume to width at each of the rest of the profiles, as a function of time lag (in weeks). See text for explanation.*

cross-correlated with each of the others in turn. Figure 7.20 maps the cross-correlation coefficients as a function of alongshore distance and time. High correlations (darker shading) at negative lags indicate events at that alongshore location preceded those at the reference line in the centre of the beach. Alongshore progression of material would therefore be characterised by relative darker shading in either diagonal of the map in Figure 7.20, in this case showing propagation of sediment to the north: extending contours of high correlations (dark shading) from the bottom left to the top right, showing the progression of material from the south (bottom) to the north (top) in time (left to right). The zero contour in Figure 7.20, representing the inflection in correlation coefficient, has been highlighted to ease interpretation.

Following Sonu and James [1973], profiles were classified according to their geometry, and an analysis of transition was carried out. For each profile, each value in the time-series of Q/w greater than one standard deviation of all Q/w were classified as 'convex-upward' or 'C'. Each value in the time-series of Q/w less than than minus one standard deviation of all Q/w were classified as 'concave-upward' or 'A', and the rest as 'linear' or 'B'. The classified profiles are summarised in Table 7.1, which shows a reasonable amount of coherence alongshore between adjacent profiles on a given survey,

confirming the two-dimensionality of the beach.

Tab. 7.1 *Classification of surveyed profiles based on their subaerial geometry ('C' refers to convex, 'A' to concave, and 'B' to linear-see text). Profile numbers increase towarsd the north.*

Survey↓/Profile→	5	6	7	8	9	10	11	12	13	14	15	16	17
1	C	C	C	C	C	C	C	C	C	B	B	C	B
2	C	B	C	C	C	C	C	C	C	B	B	B	A
3	B	B	C	C	C	C	C	B	B	B	B	B	A
4	B	B	B	C	C	B	C	B	B	B	B	B	B
5	B	B	A	B	B	B	B	B	B	B	B	B	B
6	B	A	A	A	A	A	B	B	B	B	B	B	B
7	B	B	B	C	B	B	A	B	B	B	B	B	B
8	A	A	A	A	A	A	A	B	A	B	B	B	C
9	A	A	A	A	A	A	A	B	A	B	B	B	C
10	A	A	A	A	A	A	A	A	A	A	A	B	A
11	B	C	C	A	C	C	C	C	C	C	B	B	A
12	B	B	B	A	A	A	A	A	A	A	B	B	B
13	B	B	B	B	B	A	B	B	B	B	B	B	C
14	B	B	A	A	A	A	A	A	A	B	B	B	B
15	B	B	B	B	B	B	B	B	B	B	B	B	B
16	B	B	B	B	A	B	A	B	B	B	B	B	B
17	B	B	C	B	B	B	B	B	B	B	B	B	B
18	B	B	B	B	B	B	B	B	B	B	B	B	B
19	B	B	B	C	B	B	C	B	B	B	B	B	B
20	B	B	B	C	C	C	C	B	C	B	B	B	B
21	A	A	A	A	B	B	C	B	B	B	B	B	B
22	B	B	B	C	C	C	B	B	B	B	B	B	B
23	B	B	C	C	C	C	C	B	C	B	B	B	A
24	B	B	B	C	C	C	C	B	C	B	B	B	B

Transitional probabilities were calculated fom the 13 regularly-surveyed profiles over individual time steps, for each transitional type (from C-C through to A-A). The results were contoured as a function of alongshore distance (Figure 7.21). In general, self-self transition (C-C, B-B, or A-A) was most common, indicating a degree of inheritance in the profile geometry. Transitions into C (B-C and A-C) were less likely than transitions into A (C-B and A-B), indicating that the beach spent more time, out of its 'linear' state, relatively concave rather than relatively convex (Figure 7.21). Thus the profile shape classification reflected the generally declining beach volumes, and negative sediment budget, for this survey stretch (0-3250m alongshore). Self-self linear transitions (B-B) were more common at the northern and southern extremes of the beach, and less common in the central portion, further confirming the relative instability of this central region of the barrier.

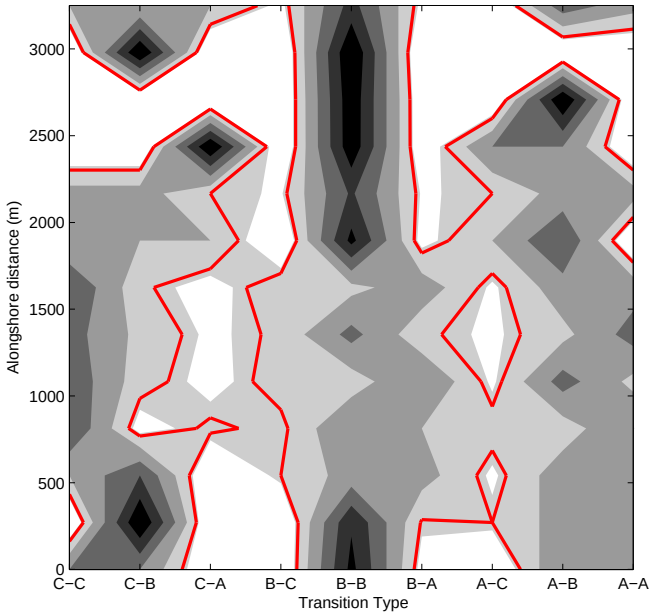

Fig. 7.21 *Contour map of probabilities associated with transitions from profiles classified as convex (C), concave (A), or linear (B), as a function of alongshore distance. Darker shading indicates greater likelihood of transition over one time step. Heavy red line indicates the 0.2 contour. See text for explanation.*

7.3.3 *Sedimentology*

Chapter 6 showed that the sedimentology of Slapton over a spring-spring tidal cycle was variable to a large degree, and changes in sedimentary parameters associated with given wave and tide levels were predictable to a lesser degree than profile change. The bi-weekly sampling resolution meant that it is difficult to know whether the observed profile and sedimentology was as much a function of the previous receding tide, or a cumulative function of the whole two weeks (the sedimentology perhaps more so than the morphologies, since sediments have to be redistributed for morphological change to occur, there is inherently less inertia in individual patches of sediments). Nevertheless, due to the length of the record, cross-and along-shore averages should be able to tease out the temporal and spatial structures associated with morpho-sedimentary change.

Synthesising visual observations made by myself and previous workers on Slapton (particularly N.Binney, A.Davies, G.Masselink, *pers. comm*), plus measurements made between 2002 and 2004 [Austin, 2005], suggested that the temporal variability of grain size at Slapton is very large, and that the central region of the barrier had become progressively finer through recent time. Figure 7.22 suggests that not only was the entire beach much finer than normal, the beach often lost its distinct alongshore grading. This

varies, but the gradient in sediment size per metre is O(10^{-3}) millimetres, meaning a 1000m distance alongshore will grade by approximately 1mm. The fining associated with general volumetric losses indicates that the material being removed from a large section of the beach was, preferentially, coarser material. That considerable northerly alongshore sediment transport occurred over the winter and spring of 2006-07 is supported by the general coarsening to the north and fining to the south. One limitation of the present sedimentological data set is that it is only surficial. However, whilst sub-surface sedimentology would have potentially uncovered some of the finer details behind some observed sedimentological changes, over the scale of interest where some considerable bed elevation changes were observed, one is able to reconstruct likely sediment sizes at depth from previous surfaces in a generally depositional part of the beach. Retrodiction of approximate past sub-surface sedimentologies is equally possible on an erosional stretch by, at any time, observing present surface sedimentologies. Muir Wood [1970]'s hypothesis that the strength of the alongshore gradient in size is a particularly notable sign of a stable or healthy beach is qualitatively verified here.

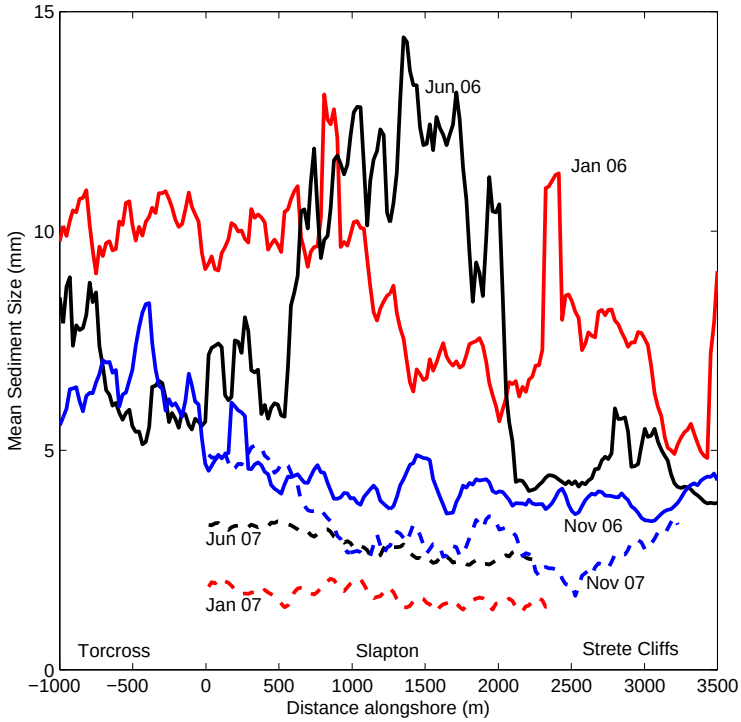

Fig. 7.22 *Changes in alongshore sediment size between January 2006 and November 2007. Solid lines indicate the surveys for 2006, and dashed lines for 2007.*

Alongshore trends in the mean, maxima, and minima of sedimentary parameters

averaged in the cross-shore direction, and through time (Figure 7.23) show that, in general, and in a departure from recent trends, there is a weak positive correlation between alongshore distance (northwards) and sediment size. Sediment size reaches a peak at North Slapton: this is the location where the envelope of profile variability is greatest, and later will be shown to have suffered the most volumetric losses during the survey campaign. The same trends are mirrored in the grain size minima, but not the maxima. This supports the notion that the variation in the minima is systematic and reflects the mean, whereas the maximum grain size at any given time or location is more difficult to predict, i.e. it is inherently more variable, perhaps due to the existence of a very mobile coarse sedimentary population with a shorter residence time than that of the rest of the beach (a notion which resonates with the principle of 'overpassing'- see Chapter 2). The general fine skew of the beach sediments indicates the presence of a relatively mobile coarse fraction. That coarser beach material is more mobile than fine on beaches also echo statements made by previous authors King [e.g. 1972]; Carter and Orford [e.g. 1988]. Note, however, that this is contrary to Gleason et al. [1975] who measured alongshore sediment transport on beaches in Start Bay, including Slapton, and found an inverse relationship between sediment size and transport distance, implying smaller fractions were more mobile. Their study was, however, over a larger spatial area, and they drew trends from beach to beach in Start Bay, with different background populations in terms of size and sorting.

There is a strong inverse correlation between sediment sorting and alongshore distance (northwards), and a strong positive association between skewness and alongshore distance. This is also reflected in respective minima and maxima, although on this occasion there is more variation in maxima of sorting and skewness relative to the mean (in the cross shore direction the opposite was the case - Figure 7.25). Over the survey period, therefore, the beach, in general, becomes finer, better sorted and more positively skewed (although remaining negatively skewed) northwards. The extent to which morphological and sedimentological parameters varied about their respective means changed alongshore. Figure 7.24 depicts the standard deviations for elevation, sediment size, sorting, and skewness. The beach is generally more variable in the centre than at either end, most obviously so for profile elevation. Importantly, the sample numbers are large, and the standard deviations are much smaller than the respective means, so the

trends may be interpreted with confidence.

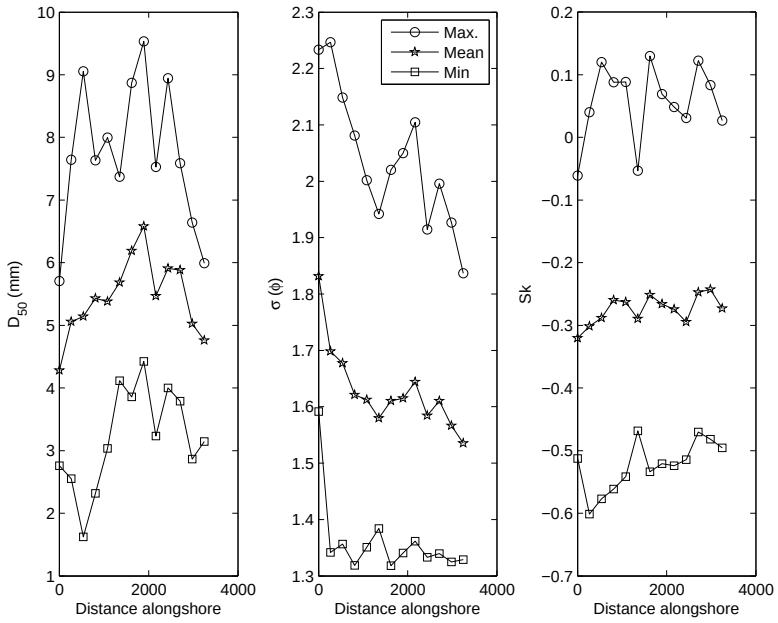

Fig. 7.23 *Alongshore trends in max. (circles), mean (stars), and min. (squares), of sediment size (left), sorting (middle), and skewness (right).*

A number of interesting themes are present which apply alongshore (i.e. they are not dependent on the background 'coarseness' of the local beach profile). For example, there is consistently more variation in the minima of sorting and skewness than the maxima. The same can be said for morphologies, principally because of the occasional presence of berms. This is, however, not generally the case for sediment size. Another interesting trend is that the supratidal and upper intertidal beachface is more poorly sorted where morphological change is at its minimum, but it is not necessarily coarser or finer, nor fine-or coarse-skewed to a greater degree. Mean cross shore profiles for median sediment size, sorting and skewness correlate much better with each other than minimum and maximum cross-shore profiles in the same parameters, because the mean reflects the trend in the cross-shore disitribution, whereas the minima and maxima are stochastic variations about the mean. Figure 7.25 depicts typical cross-shore mean profiles for sediment size, sorting and skewness, with associated envelopes, for the same locations. There is quite a range of values for both sorting and skewness, perhaps more than would be expected for a 'well sorted' gravel beach [McLean and Kirk, 1969; Gleason et al., 1975]. Although variable, the beach sediments are almost always negatively skewed, which is agreement with the majority of previous studies on beach sediments [Masselink

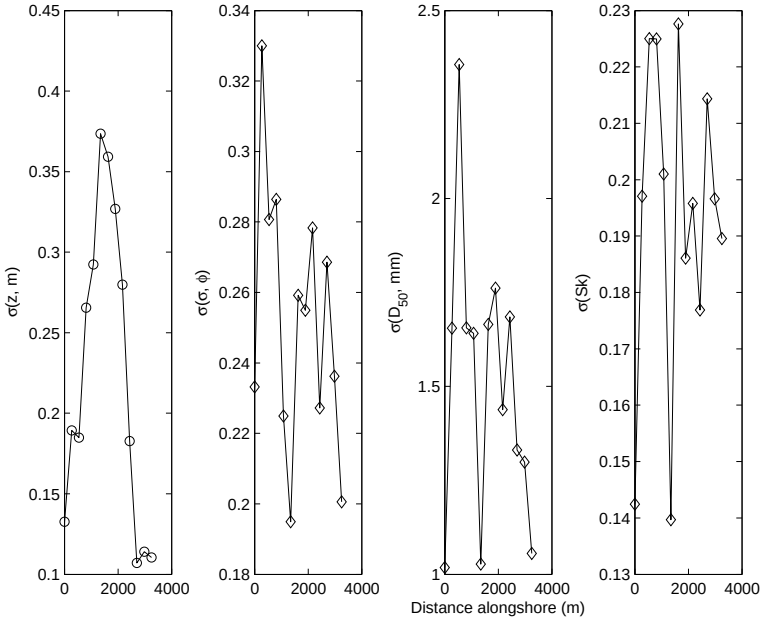

Fig. 7.24 *Alongshore trends in standard deviation of,* ***from left to right****, profile elevation, median sediment size, sorting, and skewness.*

and Hughes, 2003]. On sandy beaches, this negative skewness is thought to be due to the presence of shell fragments, and because of the non-normaility of sediments in suspension [Kennedy et al., 1981]. On gravel beaches, however, the explanation for negative skewness may equally require a mechanism to remove the coarser tail from samples, which might be supplied through overpassing processes operating in the alongshore direction, or the association of the coarse material, in a self-limitating system for coarse fractions, with particular beach features such as overwash, berms and steps. It is equally likely that the source of the skewness comes from sampling the surface, i.e. one sedimentary subpopulation: Sallenger [1981] and Masselink et al. [2008] showed that the laminae of beach sediments are always skewed, and that as laminae are combined the skewness disappears.

The temporal trends in morpho-sedimentary parameters (Figure 7.26) show steady declines in beach volumes and sediment skewness, and a general increase in sediment size and sorting. As expected from the work of the previous chapter, sediment size has the greatest temporal variability and beach volume has the least. The major event of note in the volumetric record is the erosional period of late March-early April. This event is also reflected in the sedimentological record, where a general coarsening and a worsening of sorting is observed. Interestingly, however, this erosive period does not make much

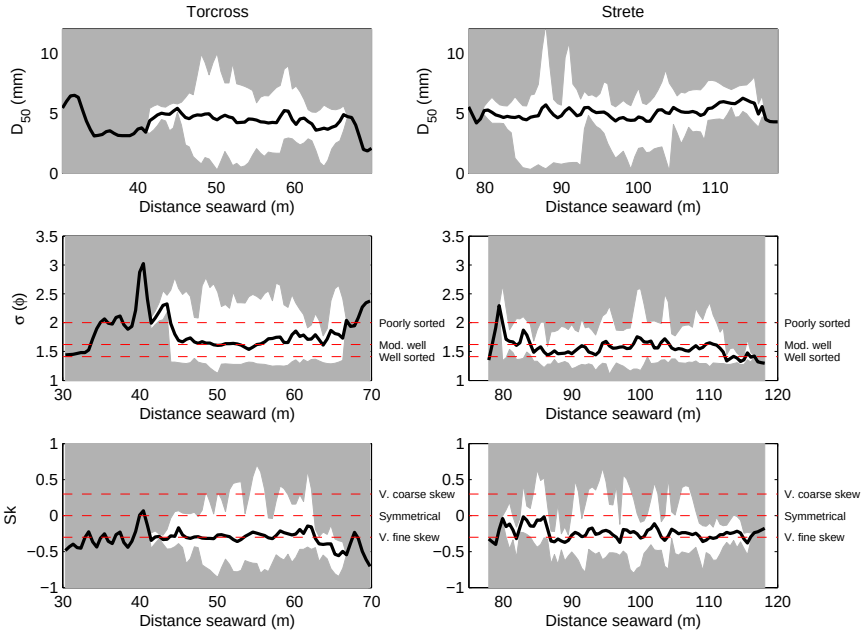

Fig. 7.25 *Typical envelopes of variability around mean cross shore profiles for sediment size (**top**), sorting (**middle**) and skewness (**bottom**). Left panels show a site at the southern end of the survey area, and right panels a site at the northern end.*

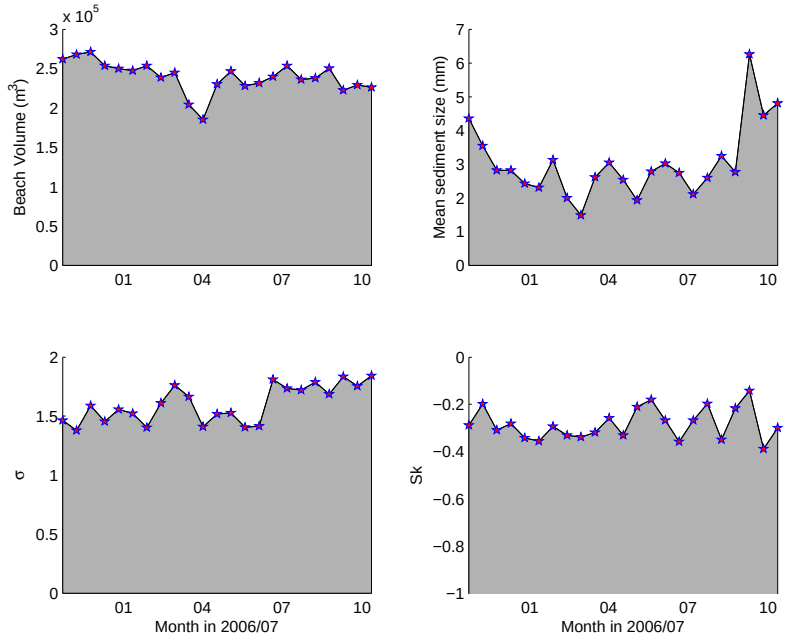

Fig. 7.26 *Time-series of beach volumes (**top left**); mean median sediment size (**top right**); mean geometric sorting (**bottom left**); and mean geometric skewness (**bottom right**).*

difference to the trend in skewness, which is more variable in the summer months than in the winter and spring. Sorting, in contrast, is less variable in summer, and sediment size appears to be equally variable throughout the year, with coarsening events almost in phase with erosive events.

Fig. 7.27 *Slapton 2006–2007.* ***Top left****: looking south to Torcross; a very fine and well-sorted beach, with a coarser, more poorly-sorted storm beach deposit.* ***Top right****: looking north from Slapton; a fine, well-sorted beachface with clearly-defined swash mark.* ***Bottom left****: following a series of large waves, an unusually fine central Slapton is affected by significant groundwater seepage, probably caused by high water levels in the backbarrier lagoon.* ***Bottom right****: large waves encroach upon a rather flat central Slapton profile, causing significant scarping.*

The sedimentological response of Slapton to morphological change over the study year was interesting, and sometimes unexpected. There were a number of interesting (3D) features in the sedimentology even when the morphology of the beach (distinctly 2D) was behaving in a predictable manner. There were also observations not revealed by the resolution of the sampling scheme. On a couple of occasions following storms the intertidal profile was left very coarse at the top of the beach and uniformly fine lower on the profile (Figures 7.27 and 7.28, top left). This is a classic 'storm beach' response, but

interestingly it only manifest in the southern section of the beach. In the north, there was not the available coarse material for this phenomenon to occur. Perhaps surprisingly for a gravel beach, swash mark is a common occurrence on Slapton (Figure 7.27, top right) when the profile is relatively flat and has suffered recent depletion. The swash mark is always coarser than the background material. Large pebbles were observed to overpass the finer background material, travelling up the profile and accumulating near the strand line as a longshore-coherent band of material (Figure 7.28, bottom panels). More common, however, especially during the winter months, was a rather uniform cross-shore and alongshore general coarsening or fining of the beach, clearly in response to prevailing wave/tide conditions (Figure 7.27, bottom right). Rilling and bifurcations below the groundwater exit point (Figure 7.27, bottom left) were commonly observed across the beachface at low tide, and this discharge may be significant from the point of view of the morphodynamics of the beach. This process appears to be aided by the vertical stratification of the bed, most noticeable when coarse material was overlain by fines (Figure 7.28, top right).

7.4 *Discussion*

In general terms, longshore grading by grain-size may be attributable by parallel variations in wave energy. Under this hypothesis, the difference in energy focussed on the southern end of the barrier in 2006 relative to the northern end would have to have been greater than in 2007. This implies relative sheltering for Strete and relative exposure for Torcross in 2006 but not 2007. However, it has already been noted that the difference in wave power associated with certain directions was greater in 2007 than the 4 year average (Figure **??**), so in fact Torcross may have been, in gross terms, more exposed in 2007. The coarsest section of beach was the centre of the barrier, where the greatest morphological and shoreline change occurred. The general fining of the beach in 2007 could not be attributed to selective rates of transport, because the fining occurred along the whole barrier. The grading observed in a 'typical' year, such as 2006, may be generally explained by the interplay between a directionally-bimodal waves, associated with different energy levels, as has been suggested for Chesil Beach in Dorset [summarised by Bird, 1996]. However, what is interesting about 2007 is that the the

Fig. 7.28 *Slapton 2006–2007.* ***Top left****: looking south to Torcross; storms leave the beach very fine and flat. The seawall, out of shot to the extreme south, is undermined by large shoreline recession and erosion.* ***Top right****: a saturated and very fine surface layer conceals the coarse sediments underneath, through which significant volumes of groundwater are seeping.* ***Bottom left****: looking south from Strete; bands of coarse material begin to push back onshore.* ***Bottom right****: looking north from Strete Gate; a typical coarse band of sediments at the high tide strand line.*

difference in energy levels associated with the two dominant wave directions was greater than in a normal year, and the grading broke down. The lack of the gradient in grain-size alongshore in 2007 relative to 2006 (Figure 7.22) is perhaps more attributable to the selective removal of the coarser grain-sizes from the beach, either offshore or alongshore (out of the Slapton barrier system), or alongshore and buried. Grading is enhanced where there is more coarser material available in the southern section. Grading is diminished when longshore transport volumes are high. The finer fractions appear to be defaulted alongshore. In the absence of detailed measurements in adjacent beaches, offshore, or at depth, one can only speculate as to where the coarse material had gone.

Using the data from the present study, the volume of net annual longshore sediment transport for the area between survey lines was calculated as the temporal gradient of volumetric changes, with respect to each cross-shore distance, summed, then integrated alongshore. The results are shown as a heavy black line in the upper panel of Figure 7.29, along with the results of a similar study carried out by Chadwick et al. [2005], who modelled the alongshore sediment transport rates between 1999 and 2002 using the longshore sediment transport equation of Van Wellen et al. [2000]. Their simulation used a spectral wave model (MIKE 21) to transform offshore waves, as predicted by a Met. Office wave hincasting model, to inshore locations. Positive values indicate net northerly annual sediment transport (in m^3), towards Strete, and negative values indicate net southerly transport towards Torcross. Note that while the analysis of Chadwick et al. [2005] for each year was for January-December inclusive, the calculated volumes marked '2007' in Figure 7.29 are in fact October 2006 —October 2007. The time-periods are therefore the same in length, but not phase. There are a number of notable features here. Firstly, and most importantly, the transport direction corroborates the profile and cross-correlation analyses in the previous section. However, the magnitudes are much smaller than those quoted by Chadwick et al. [2005], a possible discrepancy due to inadequacies in the sediment transport equation used, or the hindcasted and refracted modelled wave data. There is little indication that the years 1999—2002 would have yielded significantly higher values for alongshore sediment transport, and indeed such values would require a considerable and rather unrealistic change to the geometry of the active beachface. There are further potential reasons, for example Chadwick et al. [2005] assumed that the system is closed at the headlands. In addition, the influence of

on-offshore transport is not taken into account by the model, but is by the calculations using the beach volumes, thus the estimates from the sediment transport formulae might be regarded as a sediment transport potential not taking into account on-offshore sediment flux or possible leakage from the system.

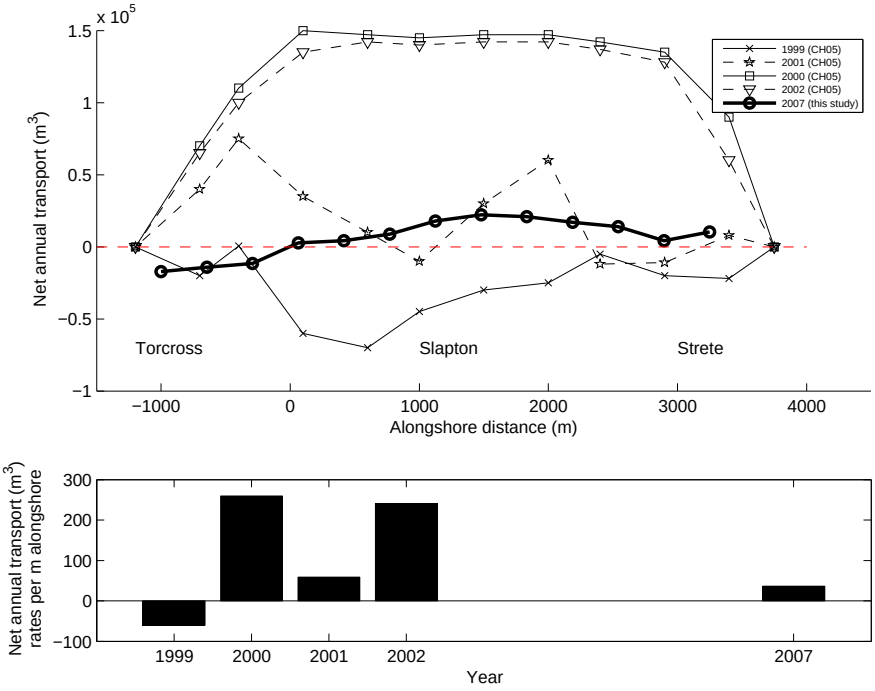

Fig. 7.29 *Predicted net annual longshore transport rates for Slapton Barrier, synthesising measured data from this study (heavy solid black line with circles), and modelled data from four recent years published in a previous study (Chadwick et al. [2005], labelled CH05).*

For the 2006-2007 profile data set, the changes in shoreline (again defined as 1m ODN, approximate position of MHWN) relative to initial are graphed in Figure 7.30. Similar spatial trends are in evidence, with shorelines towards Torcross remaining quasi-constant; those northwards at Strete advancing; and in the central barrier large cut-backs observed (as is also evident in Figures 7.17 and 7.18). It appears that 2006—2007, in terms of the integrity of the central barrier, was similar to that of 1988—1991 (approximately 10m recession), but not as severe as 1992—1993 where recessions in excess of 20m were recorded (Figure 3.7). The vulnerability of the central section of barrier is a constant theme, remarked upon by Orford [2001]; Pethick [2001] and Chadwick et al. [2005] in their respective studies. Given the changing direction of net sediment flux from year to year (Figure 7.29), the large fluctuations in shoreline in the central region of the barrier are likely to be because of the large throughput of material in this region, which acts as a hinge point in the inter-annual rotation evident from the

shoreline records at the northern and southern extremities of the beach. Another feature of note is that the 10m advance recorded at Strete is unusually large, some 2m greater than in any previous year between 1972 and 2003, as determined from the FSC data set.

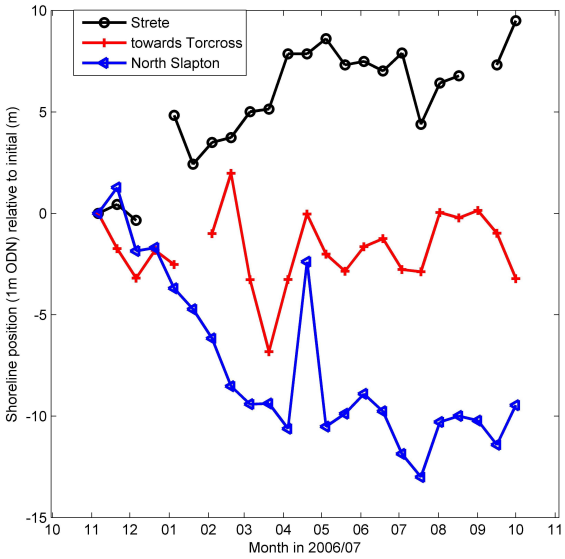

Fig. 7.30 *Changes in the shoreline position (again taken as 1m ODN) relative to 23rd October 2007, for three alongshore positions, over the 2006–2007 survey record. Shorelines have advanced some 10m at Strete, and recessed some 10m in the centre of the barrier ('North Slapton').*

Figures 3.6 and 3.7 in Chapter 3 show longer term trends which support the findings of the present study. The bahaviour of the apparent 'rotation' of the beach towards Strete is interesting because, unlike most previous studies into beach rotation [Dingler and Reiss, 2002; Ranasinghe et al., 2004], at Slapton the process appears to be assymetrical. In other words the shoreline advances being made at Strete are not at the expense of the southerly section (Torcross), but the middle section of the beach.

One final data set is available to provide context and comparison to the present study. Seventeen profiles, spaced 300m apart, were surveyed at Slapton by Carr et al. [1982], monthly between September 1971 and September 1972 (except November 1971 and May-July 1972). This study confirmed the two-dimensionality of the beach: profiles spaced alongshore tended to respond in the same way in a given month, which was also found in the present study. Significantly, they found that net volumes of sediment were identical between winter and summer periods, made possible since accretional events

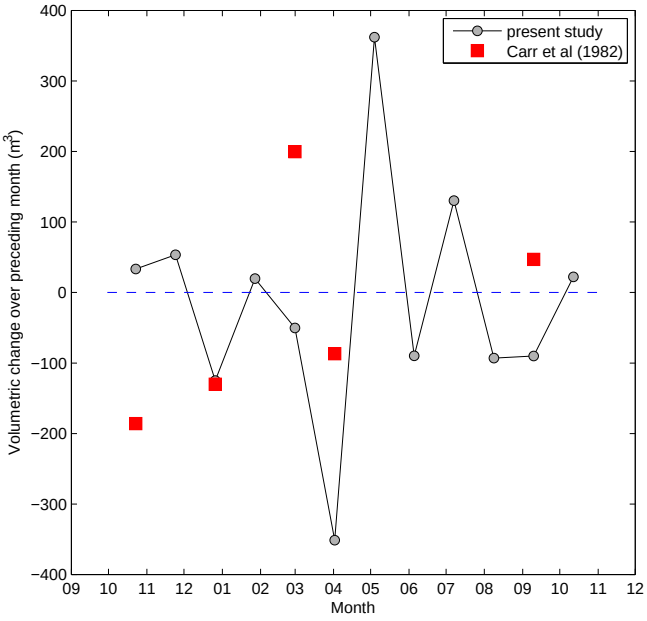

Fig. 7.31 *Volumetric changes at Slapton, over individual months. The solid line represents the present study. The red squares come from data published in Carr et al., (1982), for a comparable data set collected over 1971-1972.*

were fewer in number but lasted longer in the winter. Some results from Carr et al. [1982] are reproduced in Figure 7.31. With only five data points available from the Carr et al. [1982] study, it is difficult to discern whether or not a similar response is in evidence season to season. With the exception of January, net volumes are dissimilar, and in three cases out of five, opposite in sign. However, what is important for the present purpose is that the magnitudes plot within the envelope of variability for the 2006-2007 data set, and whilst the range of the 2006-2007 data is greater, the observed changes are not significantly different. Besides, there is nothing to say that the range might have increased for the 1971-72 data set would have increased if more data were available.

Figure 7.32 details the relationships between some variables, suitably averaged, over the study period. The relationship between beach volume and sedimentary parameters was poor (Figure 7.32, upper panels). The relationship between morpho-sedimentary variables and hydrodynamics were better (Figure 7.32, lower panels), with the exception of wave direction. All significant correlations were inverse. These findings are in general agreement with a similar study made by Gleason et al. [1975], who found stronger correlations between wave height and surface size than with wave direction. Better agreements may have been made between inshore hydrodynamics and

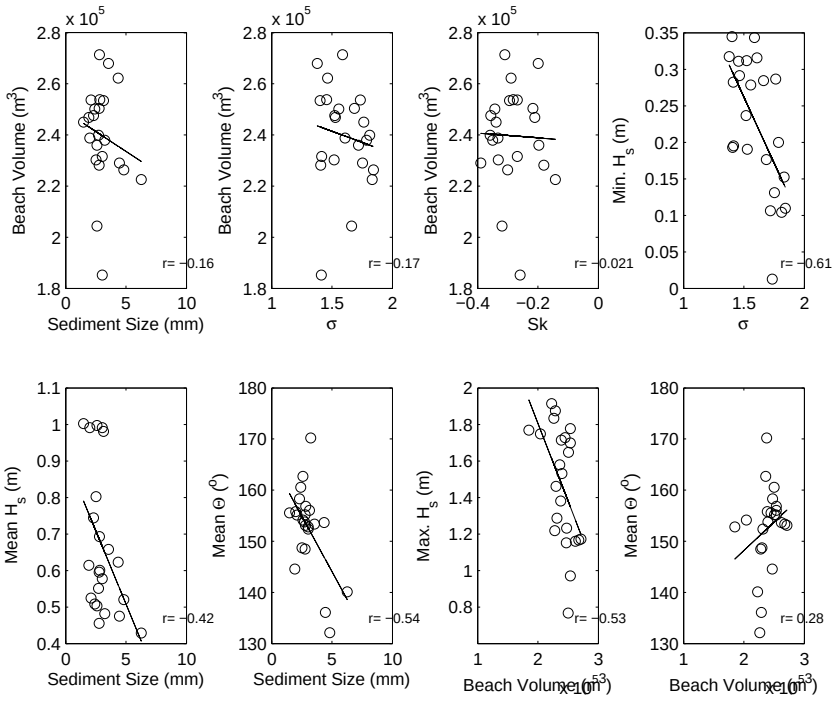

Fig. 7.32 ***Top panels****: relationships between, from left to right, beach volume and D_{50}; sorting, and skewness; and relationshop between sorting and H_s, each for every 2 week period.* ***Bottom panels****: relationships between, from left to right, D_{50} and H_s; D_{50} and $\overline{\Theta_w}$; beach volume and max. H_s; and beach volume and $\overline{\Theta_w}$, each for every 2 week period.*

morpho-sedimentary parameters. In addition, measures of central tendency may not be appropriate, since morpho-sedimentary parameters may better respond to more subtle changes in the distribution or chronology of the wave field. For example, in a strongly bimodal wave field, mean direction is not a true characterisation. The lack of correlation between beach volume and mean wave direction may also be attributable to the spatial divergence of volumetric losses (i.e. they were not uniform alongshore). Cross-correlation analysis revealed that associations were not necessarily improved at lag, possibly because hydrodynamic parameters had to be averaged over two-week periods between surveys. Indeed, this averaging may have significantly obscured the range and relative duration of wave energies, which might be crucial to the morpho-sedimentary response of the beach. The relative cross-shore location of morphological or sedimentological change may have also been significant, which may partly depend on changing tidal spring-spring ranges.

The lack of association between the morphological and sedimentological parameters is perhaps more surprising. However, there are a number of potential factors in operation which may obscure any co-variation, for example; the beach is naturally graded, and over the study period a change in the direction of that grading was evident. The relationship

between morphological and sedimentological change may have therefore been obscured by the beach sedimentology relaxing to a new equillibrium. Sub-surface sedimentology may better reflect obscured morphological changes. Groundwater variations are also likely to be a major influence. An additional factor in the poor associations observed by ordinary correlation may have been time lags in the cause and effect. Finally, the processes of sedimentation were different, over time and through space. Over relatively long time-scales, the beach cannot so easily be assumed a closed sedimentary system, both in terms of sediment volumes and sediment attributes. When sedimentary subpopulations are removed offshore or alongshore, or buried, sediment supply becomes a limiting factor on the sedimentology of that location.

7.5 *Summary*

(i) The morpho-sedimentary dynamics of Slapton have been documented over one calendar year, using a data set of regular fortnightly beach profiles and sediment sampling taken between October 2006 and October 2007;

(ii) Net profile and volumetric changes over the study period showed northerly alongshore drift of material, sourced primarily from the central region of the barrier, whilst net changes from toward the sourthern end of the beach at Torcross were negligible, except near the headland. The barrier therefore underwent net northerly indentation during the year, although the volumes lost from south of the rotational point did not match those gained to the north. It is likely that this additional material was either sourced from offshore or alongshore beyond the headlands, implying that Slapton is not a closed sedimentary system;

(iii) The asymmetrical behaviour of the indentation, however, differed from bay beach rotation observed in many other areas of the world;

(iv) A sediment budget revealed that, taken as a whole, the barrier was in net surplus of $\approx$ 10,000 m^3, which does not support the claim that the barrier is a closed sedimentary system. Strete appears to be an efficient sediment trap, but the magnitudes of inputs from either side of the headlands at Strete and Torcross are unknown, as are the exchanges on-offshore;

(v) Most of the changes in beach morphology can be attributed to persistent south-westerly waves over the winter and early spring when the waves were highest, driving net northerly sediment transport. Easterly waves have not been sufficiently frequent nor large to maintain equilibrium in beach volumes alongshore;

(vi) The frequency of dominant south-westerly years are likely to have increased since 1990, which has implications for the energy transferred to the beach. This is because, for Slapton, the discrepancy between fetch lengths between the two most dominant wave directions make direction more important than wind stress in wave generation. Several years in succession similar to 2006-07 would have serious implications for the central barrier;

(vii) However, it remains the case that the magnitude of changes in a given cross-shore profile can be greater over one extreme event than the net changes over a whole year. Spatial gradients in sedimentation can quickly and efficiently recover beach volumes;

(viii) Cross-correlation analysis on the volumetric record in the centre of the beach with those to the north and to the south clearly showed the dominant direction of material transport;

(ix) A comparison of measured and previously published modelled alongshore sediment rates suggested that these models should be regarded as sediment transport potentials, assuming no net on-offshore exchange of material, and a closed sedimentary system;

(x) The enormous variations in intertidal sediment size, sorting and skewness obscured any consistent cross-shore or along-shore trends in these parameters, although there was consistently more variation in the minima than the maxima when averaged alongshore;

(xi) The beach was almost always negatively skewed, regardless of morphological changes, and the beach was generally more poorly sorted when morphological change was at a minimum. Sediment size was greatest where net morphological change was greatest, and coarsening was generally in phase with erosive events. Sorting was much more variable in the winter, whereas skewness was significantly more variable in the summer;

(xii) In the alongshore direction, the variation maximum grain-size of a given location is more difficult to predict than the minimum, when the mean size is known. The opposite is the case for the cross-shore direction. It was suggested that the coarser fractions are more mobile than the finer sediments, with a shorter residence time;

(xiii) The variability of morpho-sedimentary parameters decreased as a function of distance alongshore;

(xiv) Changes in sediment size, especially the seemingly relatively long-term fining of the beach, are more difficult to explain, but appear to be phase-decoupled from, and distinctly non-linearly related to, morphological change.

(xv) In a gross sense, however, the beach was coarsest where most net shoreline losses occurred, qualitatively supporting the relationship between energy and sediment size. The volumetric stability/health of the beach may be qualitatively evaluated using the gradient of the alongshore sediment size.

(xvi) More sedimentological data sets of comparable resolution and length, including sub-surface as well as surface, are required to better understand the nature and importance of sedimentological change on beaches.

8 SEDIMENT TREND MODELS TO INFER NET SEDIMENTATION ON A GRAVEL BEACH

What could be cuter
Than to feed to a computer
With wrong information
But naïve expectation
To obtain with precision
A Napoleonic decision?

Major Alexander P. de Seversky,

quoted in J.C. Davis, "Statistics and Data Analysis in Geology" (1986).

8.1 *Introduction*

There are models which purport to predict universal sedimentation patterns (erosion and deposition) which are based on grain-size parameters alone. They fall under two broad classes: (1) models which, from a time-series of certain parameters from grain-size distributions, predict (retrodict) the recent net sedimentation history where that sample came from, i.e. relative erosion or deposition at a certain time compared to the previous time [e.g. Barndorff Nielsen and Christiansen, 1988; Martz and Li, 1997]; and (2) models which, from a spatial distribution of certain parameters from grain-size distributions, predict recent net sediment transport pathways [e.g. McLaren and Bowles, 1985; Gao and Collins, 1992]. Both are based solely on the statistics of sediment samples, i.e. no physical terms are required. The basic assumption of both classes of model is that there is information on recent sedimentation patterns within time- and spatial-series of sedimentary parameters. For this assumption to hold true, morphological change and

sedimentological change would be required to co-vary, and that this co-variation is predictable and universal. If these classes of model were verified, their impact would be significant because, whilst it is unrealistic to expect a complete understanding of recent sedimentation in a given environment could be gained from sediment statistics alone, gaps of knowledge or measurement in process studies could be approximated cheaply and with large spatial coverage. In turn, relationships between sedimentation and sediment distribution could better inform a new generation of morphodynamic process models on beaches with grain-size as a free rather than constant parameter (Chapter 2).

Barndorff Nielsen and Christiansen [1988] describe a physical-mathematical model from first principles called the 'hyperbolic shape triangle model', for the sedimentary imprint of erosion and deposition under fluid flows. To the authors knowledge the model has thus far not been used to infer sedimentation dynamics on beaches. The model has a number of attractions, the primary one being that it is generalised and simple to implement, which makes it testable in the field. As will be elaborated upon in the next section, it is based on the co-variation between two parameters, and as such is part of a long tradition of sub-environmental discrimination on beaches using bivariation in sedimentary parameters [Nordstrom, 1977; Friedman, 1979]. The advantage of the bivariate parameter space of the hyperbolic shape triangle model over traditional approaches, is that the parameters used are invariant under changes in location and scale, whereas those of a log-normal model are not. An advantage the model of Barndorff Nielsen and Christiansen [1988] has over sediment trend vector models is that it is based on the hyperbolic distribution of particle sizes. In most previously published research on the log-hyperbolic model for size distributions, the consensus is that it does provide a better fit [Hartmann and Christiansen, 1988; Fieller et al., 1992; Lund Hansen and Oehmig, 1992; Scott and Haschenburger, 2005; Masselink et al., 2008], being a more general model controlled by four parameters. That the shape triangle model is based on the log-hyperbolic distribution is, at the same time, a disadvantage over conventional sediment trend models because of the difficulties associated with fitting the distribution, especially to irregular size-distributions [Fieller et al., 1992]. What is controversial is whether it is neccessary to have such a complicated model for grain-size distributions, and what additional information on the processes of sedimentation it can give [Wyrwoll and Smyth, 1985; Masselink et al., 2008]. It is this latter point which is tested to some

extent in this contribution.

Grain-size distributions in sedimentary environments are affected by selective entrainment, transport, and deposition. Many researchers have used sediment characteristics to identify sediment sources, transport modes, and transport directions [Visher, 1969; Swift, 1970; Stubblefield et al., 1977; Bartholoma and Flemming, 2007]. McLaren [1981] started a new direction in this type of research, using spatial changes in three grain-size parameters (mean, sorting, and skewness) to infer sediment transport directions (McLaren and Bowles 1985), and this approach has been used by several researchers to infer likely net sediment transport pathways. Currently, there are several versions available [McLaren and Bowles, 1985; Gao and Collins, 1992; Le Roux, 1994*a*, *b*; Asselman, 1999; Le Roux et al., 2002; Lucio et al., 2006; Poizot et al., 2006], and the relative advantages and disadvantages of each technique is the subject of a recent review [Le Roux and Rojas, 2007]. Based on a set of 'universal' premises that grain-size distributions change along a sediment transport gradient, collectively they have been applied to a wide range of sedimentary environments [Masselink, 1992; Asselman, 1999; Van DerWal, 2000; Cheng et al., 2004]. Their use is widespread but still controversial [Flemming, 1988; Masselink, 1992; Guillen and Jimenez, 1995; Masselink et al., 2008], and as far as the author is aware, have not yet been applied to a gravel beach.

8.2 *Test of the Hyperbolic Shape Triangle Model to Infer Net Sedimentation*

8.2.1 *The hyperbolic shape triangle sedimentation model*

The log-hyperbolic distribution and its shape triangle

Barndorff Nielsen [1977] recognised that grain distribution characteristics were better approximated by a log-hyperbolic probability density function (a hyperbola controlled by four parameters μ_{LH}, δ_{LH}, ϕ_{LH}, γ_{LH}), rather than the traditional normal model (a parabola controlled by two parameters μ_{LH}, σ, and which is a limiting case of the log-hyperbolic distribution). The hyperbolic function was introduced to the sedimentological community by Bagnold and Barndorff Nielsen [1980*b*] and is given by:

$$p(x;\mu_{LH},\delta_{LH},\phi_{LH},\gamma_{LH}) = \alpha_{LH}(\delta_{LH},\phi_{LH},\gamma_{LH})\exp^{-1/2(\phi_{LH}h_{\pm}\gamma_{LH}h_{+})} \qquad (8.1)$$

where Y is observed variate (this case, grain-size), and parameter μ_{LH} gives location

(Bagnold's (1940) peak diameter), δ_{LH} provides scale (equivalent to Folk and Ward's (1957) standard deviation), and ϕ_{LH} $(\alpha_{LH} + \beta_{LH})$ and γ_{LH} $(\alpha_{LH} - \beta_{LH})$ give the slopes of the left and right tails, respectively:

$$h = \sqrt{\delta_{LH}^2 + (Y - \mu_{LH})^2} \pm (Y - \mu_{LH}) \tag{8.2}$$

$$\alpha_{LH}(\delta_{LH}, \phi_{LH}, \gamma_{LH}) = \frac{\sqrt{(\phi_{LH}\gamma_{LH})}}{\left[\delta_{LH}(\phi_{LH} + \gamma_{LH})K_1\delta_{LH}\sqrt{(\phi_{LH}\gamma_{LH})}\right]} \tag{8.3}$$

where K_1 is a Bessel function of the third kind, index 1. It is common to plot grain-size distributions as double logarithms, therefore we are interested in the log-hyperbolic density function, which is given by:

$$\log p(Y) = -\alpha_{LH}\sqrt{\delta_{LH}^2 + (Y - \mu_{LH})^2} + \beta_{LH}(Y - \mu_{LH}) + \diamond \tag{8.4}$$

where $\diamond$ is determined as a function of $[\alpha_{LH}, \beta_{LH}, \delta_{LH}]$ subject to the constraint that the integral of $p(Y)$ equals 1 [Bagnold and Barndorff Nielsen, 1980*b*]. Barndorff Nielsen [1977] showed that $\diamond$ satisfies:

$$e^{-\diamond} = \left(\phi_{LH}^{-1} + \gamma_{LH}^{-1}\right)\delta_{LH}\sqrt{\phi_{LH}\gamma_{LH}K_1}\left(\delta_{LH}\sqrt{\phi_{LH}\gamma_{LH}}\right) \tag{8.5}$$

Log-hyperbolic symmetry (skewness) and peakedness (kurtosis) are given by, respectively:

$$\chi_{LH} = \left(\frac{\phi_{LH} - \gamma_{LH}}{\phi_{LH} + \gamma_{LH}}\right)\xi_{LH} \tag{8.6}$$

$$\xi_{LH} = \left(1 + \delta_{LH}\sqrt{(\phi_{LH}\gamma_{LH})}\right)^{-1/2} \tag{8.7}$$

and are, importantly, invariant under transformations of scale and location.

An additional useful property of the sedimentation model of Barndorff Nielsen and Christiansen [1988] is that its parameters may be visualised using the 'hyperbolic shape triangle', which is the domain of variation between ξ_{LH} and χ_{LH} (Figure 8.1). Log-normal distributions have non-heavy tails and rounded peaks at the mode, and plot near $\xi_{LH} = 0$; log skew-Laplace distributions [Fieller et al., 1984] have heavy tails and sharp peaks near the mode, and plot near $\xi_{LH} = 1$; and log-hyperbolic distributions have

heavy tails and more rounded peaks near the mode, and plot near $\xi_{LH} = 0.5$ [Hartmann and Christiansen, 1992]. Individual sediments may be visually classified in their scale and location invariant forms, which may be additionally useful in process-based studies where the sedimentary signature of morphological change requires more elucidation. The hyperbolic model has been used on beach sediments by, among others, Hartmann and Christiansen [1992]; Lund Hansen and Oehmig [1992]; Sutherland and Lee [1994]; Bartholdy et al. [2007]; and Masselink et al. [2008].

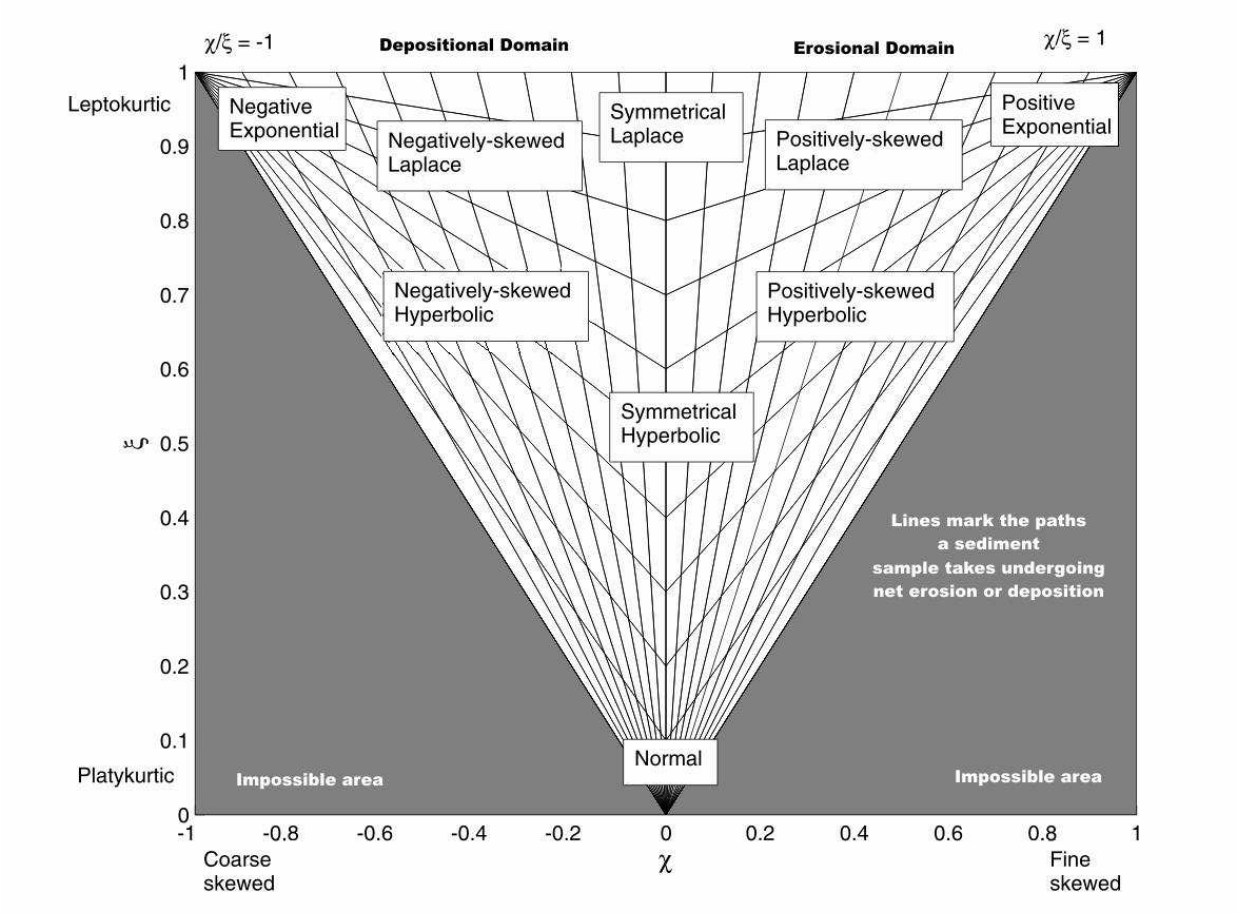

Fig. 8.1 *The hyperbolic shape triangle of Barndorff-Nielsen and Christiansen (1988). The white and grey areas represent the possible and impossible areas, respectively, of the domain of variation between [ξ_{LH}, χ_{LH}]. Some limiting cases of the log-hyperbolic distribution are shown in their double-log form, including the normal, exponential and Laplace distributions.*

The sedimentation model of Barndorff Nielsen and Christiansen [1988]

The assumptions and constructs of the model are important to the present discussion so are reproduced in this section with some detail, from Barndorff Nielsen and Christiansen [1988] and Bagnold and Barndorff Nielsen [1980*b*]. A median size exists, by definition,

because the probability of removal (or otherwise absence) for grains smaller and larger than it, is higher. One may postulate, for example, that smaller grains are more mobile and have a greater probability of being removed or carried away out of the sampling field, or that larger grains are less mobile and have a greater tendency of being buried or otherwise not being moved into the sampling field. It has long been known that the log of the number of particles larger and smaller than the median size plot against the log of size as straight lines of slope -*m* and *m*, respectively [Bagnold, 1940], which can be described as a hyperbola [Bader, 1970; Bagnold and Barndorff Nielsen, 1980*b*].

With reference to Figure 8.2, the model of Barndorff Nielsen and Christiansen [1988] expresses the probability density function (PDF) of size $\mathbf{s}$ as *p(**s**)* and the PDF after a time of net sedimentation (Figure 8.2, top left) as $\perp p(\mathbf{s})\pi(\mathbf{s})$ (Figure 8.2, top right), where $\pi(\mathbf{s})$ is the proportion of size $\mathbf{s}$ relative to that previously, and where $\perp$ is a norming constant which ensures $\int p(\mathbf{s})\pi(\mathbf{s})=1$. Barndorff Nielsen and Christiansen [1988] consider $\pi(\mathbf{s})$, which may be alternatively expressed as the probability that size $\mathbf{s}$ is not removed and which therefore may be negative, to be some increasing function of *d*, indeed some power of $\mathbf{s}$, which they express as 'power-law erosion' expressed as $\pi(\mathbf{s}) = \perp_0 \mathbf{s}^{\epsilon}$ for $\perp_0=1$ and ϵ greater than zero (deposition if ϵ is less than zero). Curves for ϵ erosion and deposition are seen in Figure 8.2, bottom left, as solid and dashed lines, respectively, for $\perp_0=1$ (the integral constant at initial conditions) and $\epsilon=\pm 0.52$. For logarithmic size ($\mathbf{s}$) and density classes it may be expressed as $\perp p(\mathbf{s}) \exp^{\epsilon(\mathbf{S})}$.

The assumption that the probability of the proportion of grains of a given size after an erosive period (relative to the proportion of those grains at the beginning of that period) is proportional to some power of that given size has some physical plausibility since it has been demonstrated that thresholds of entrainment are governed by powers of velocity [Bridge, 1981; Bailard, 1981]. It also implies that non-hyperbolically distributed sediment will inevitably become hyperbolically-distributed as a function of selective sorting, which also has some empirical backing [Engelund and Fredsoe, 1976; Deigaard and Fredsoe, 1978].

If ξ_{LH} is re-written as:

$$\xi_{LH} = \left(1 + \delta_{LH}\alpha_{LH}\sqrt{[1-(\chi_{LH}/\xi_{LH})^2]}\right)^{-1/2} \tag{8.8}$$

since any pair of $[\chi_{LH}, \xi_{LH}]$ have $\delta_{LH}\alpha_{LH}$ in common, Barndorff Nielsen and Christiansen [1988] show that two samples separated in time undergoing net ϵ-erosion/deposition are related by:

$$\chi_{LH}^2 = \xi_{LH}^2 - (\delta_{LH}\alpha_{LH})^{-2}(\xi_{LH} - \xi_{LH}^{-1})^2 \tag{8.9}$$

which are the 'hammock' ϵ erosion/deposition curves which plot left to right in Figure 8.1.

The model thus far assumes firstly that sediment samples are log-hyperbolically distributed; secondly, that deposition is simply erosion in reverse; and thirdly that erosion/deposition is not influenced by the proportion of sizes on the bed, i.e. the relative differences in sizes between particles (χ_{LH} and ξ_{LH} are location/size and scale/sorting invariant). The third assumption was addressed by Barndorff Nielsen and Christiansen [1988] with the development of 'pure' or κ-erosion/deposition, which is designed to account for feedbacks induced by changes in the (mixed) grain-size composition on the resulting sedimentation process.

As suggested by Figure 8.2, bottom right, adding another term to ϵ, here called κ, would result in modifying the size distribution after an interval of ϵ-erosion/deposition to better account for the relative contribution of the fine and coarse tails. Barndorff Nielsen and Christiansen [1988] show that a suitable value for κ is given by the ratio of slope parameters ϕ_{LH} and γ_{LH}, or the ratio of fine and coarse particles. For ϵ values greater than zero, the combined effects of ϵ-and κ-erosion/deposition correspond to $\chi_{LH} = \rho_{LH}\xi_{LH}$ and $\xi_{LH} = \left(1\delta_{LH}\alpha_{LH0}\exp^{-(\kappa\epsilon)\rho_{LH}}\sqrt{(1-\rho^2)}\right)^{-1/2}$, for $-1 \leq \rho_{LH} \leq 1 = \chi_{LH}/\xi_{LH}$ and where α_{LH0} is the value of α_{LH} corresponding to $\chi_{LH} = 0$.

It follows that μ_{LH} and δ_{LH} would remain constant under ϵ-and κ-erosion/deposition, but ν (typical log grain-size) would change with time by:

$$\nu = \mu_{LH} + \delta_{LH}\rho_{LH}\sqrt{(1-\rho^2)} \tag{8.10}$$

It further follows that sorting (τ_{LH}) changes as a function of time and ρ_{LH} as:

$$\tau_{LH} = \delta_{LH}^{-1/2}\alpha_{LH}{}_o^{1/2}\exp^{-1/2(\kappa/\epsilon)\rho_{LH}}(1-\rho_{LH}^2)^{3/4} \tag{8.11}$$

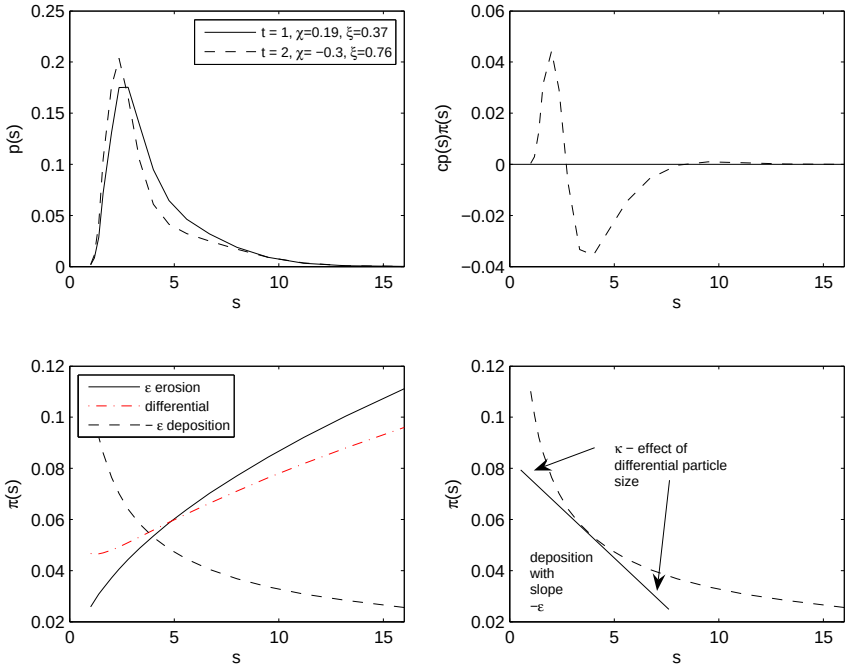

Fig. 8.2 *The erosion/deposition model of Barndorff Nielsen and Christiansen [1988]. Two distributions separated by* Δ *t (**top left**) are related by a function which conserves probability mass (**top right**). Erosion and deposition are characterised by some power of sediment size (**bottom left**), here depicted for* $\epsilon = 0.52$ *and* $\perp_0 = 1$ *by solid and dashed lines, respectively (the difference between the two is shown by the dash-dot line). Another form of erosion/deposition is required to model the potential influence created by mixtures of sizes (**bottom right**).*

Combined, this means that sediments tend to coarsen ($\nu_{LH} \rightarrow \infty$) and become more poorly sorted ($\tau \rightarrow 0$) as ρ decreases towards -1 (i.e. under ϵ deposition). For a given choice of the functions ϵ and κ, the variation of ν_{LH}, τ_{LH}, ρ_{LH} and ξ_{LH} can be studied and compared to measured size distributions. This provides four criteria with which to test the hyperbolic shape model. Firstly, sediments in an area of known depletion over at any t should have $[\chi_{LH}, \xi_{LH}]$ positions to the right of those at *t-1*, and sediments in an area of known accretion at any t should have $[\chi_{LH}, \xi_{LH}]$ positions to the left of those at *t-1*, along the delimiting curves of ϵ-erosion/deposition. Secondly, sediments in an area of known depletion over Δt should have $[\chi_{LH}, \xi_{LH}]$ positions in an upward part of the triangle relative to those at t, and sediments in an area of known accretion at any t should have $[\chi_{LH}, \xi_{LH}]$ positions in a downward part of the triangle of those at *t-1*, along the delimiting curves of κ-erosion/deposition. Note that it is the relative positions over time that are important, as exemplified in Figure 8.3 for hypothetical changes to a sediment sample over five time steps. Thirdly, and as a collorary to the model, depositional sediments should coarsen, and erosional sediments should fine, and finally, depositional sediments should become more poorly sorted, and erosional sediments should become better sorted.

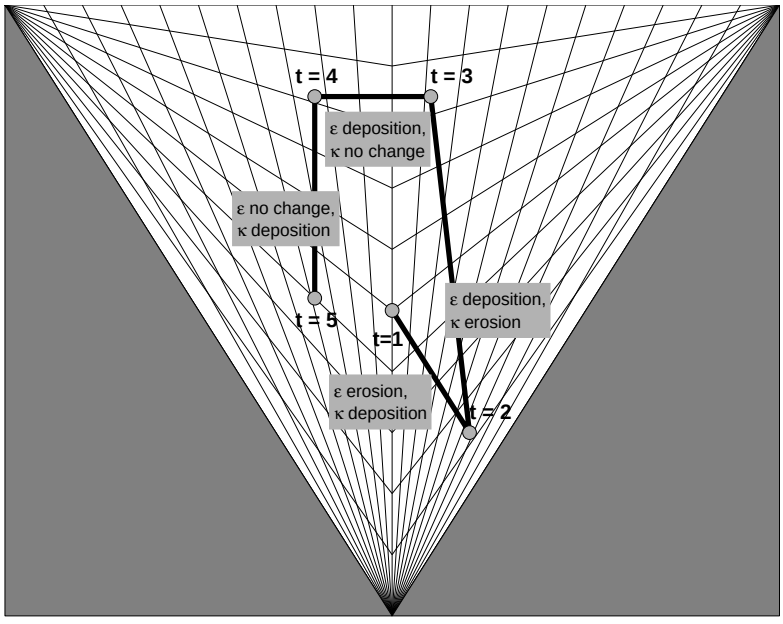

Fig. 8.3 *Example sequence of events in the erosion/deposition model of Barndorff Nielsen and Christiansen [1988], as it maps into the hyperbolic shape triangle.*

If we define the changing $[\chi_{LH}, \xi_{LH}]$ positions over a time step Δt as $\epsilon = \chi_{LHt} - \chi_{LHt-1}$ and $\kappa = \xi_{LHt} - \xi_{LHt-1}$ we are able to explore the utility of the model for beach sedimentation. In addition, if the model and its assumptions were verified, it would suggest the resultant vector of the ϵ and κ, $\vec{R}_{\epsilon,\kappa}$ would indicate the relative dominance of fluid-controlled ('power-law') erosion/deposition and grain-controlled ('pure') erosion/deposition.

8.2.2 *Methods*

All samples were dry sieved at $\phi/4$. The *ShefSize* program [Robson et al., 1997] was used to fit the log normal and log-hyperbolic models to the measured (non-truncated) sieved distributions. In addition, graphical geometric moments [Blott and Pye, 2001] were obtained for each of the samples (median size, sorting, skewness and kurtosis). Graphical (after Folk and Ward [1957], so-called F&W) measures have been used rather than moments, which are sensitive to irregularities in the tails [Bartholdy et al., 2007]. Truncation is therefore often a necessary pre-operation using moments, however this effectively limits the amount of distributional information, and besides, the comparisons made here are with a log-hyperbolic model which by definition is designed to be able to cope with 'heavy' tails. In addition, most sedimentological research on beaches have used F&W statistics. When grain proportions are taken by sieving, the number of single particles is unknown and this lack of sample size negates the use of conventional measures of goodness-of-fit such as chi-squared. The 'quasi sample size' statistic of Fieller et al. [1992] is adopted here:

$$N_{crit} = \frac{\chi_{LH}{}^2_{\mathbf{t}:0.95}}{\sum_1^N r_i - p_i(\Theta_\in)^2/p_i(\Theta_\in)} \tag{8.12}$$

where $\mathbf{t}$=N-$\in$-1, k is the number of size classes and $\in$ is the number of parameters estimated by model $\Theta_\in$. This measure accounts for model parsimony (degrees of freedom as a conditional factor in the numerator) and a lack of sample size, and is interpreted as the critical sample size required to detect a lack of model fit at the 5% level [Fieller et al., 1992]. The higher *Ncrit*, the better the distributional fit.

The hyperbolic model has not been widely adopted by most sedimentologists [Hartmann, 2007], and consequently its parameters lack a consensus over their respective

physical meanings. As stated previously, χ_{LH} and ξ_{LH} are scale-and location-invariant skewness and kurtosis, but are not directly equivalent to skewness and kurtosis obtained by traditional means (i.e. moments). As a measure with which to independently assess the shape triangle model, a classification method similar to the hyperbolic shape triangle was sought. It was found that the hyperbolic shape triangle is in fact an extension of a rather older idea that the in field of skewness against kurtosis, there are mathematically impossible and possible areas, and in the statistical literature it is known as a Rhind diagram, after Rhind [1909], or Pearson plane, after Pearson [1901]. Like the hyperbolic shape triangle, the location of a point within the possible areas indicate the distributions appearance [Leroy, 1981]. The non-orthogonality of skewness and kurtosis limits the utility of the Rhind diagram (because it severly warps the field), so the delta variate of Craig [1936] is employed, given by:

$$\delta_t = \frac{2Kt - 3Sk^2 - 6}{Kt + 3} \tag{8.13}$$

A 'Craig diagram' [Leroy, 1981] is the parameter space of δ_t and skewness (Sk). Figure 8.4 shows a Craig diagram Leroy [modified from 1981] which expresses δ_t against skewness, onto which kurtosis maps as continuous lines on this unwarped field with no impossible areas. The utility of this classification is that unusual distribution shapes such as 'U-shaped' (bimodal) and 'J-shaped' (highly skewed) are depicted, and it is based on moments alone (which are easily computed and understood) without accepting the specific axioms of probability density functions.

Associations were tested in this study using correlation coefficients under a bootstrapping scheme, where the mean of 1000 bootstrapped coefficients was taken. Partial correlation was used to assess the correlation of morphological change with ϵ and κ sedimentation while controlling for a third variable. The partial correlation coefficient of variables Y_1 and Y_2, given the variable Y_3, is given by [Fisher, 1924]:

$$r_{Y_1Y_2.Y_3} = \frac{[r_{Y_1Y_2} - (r_{Y_1Y_3} \times r_{Y_2Y_3})]}{\sqrt{(1 - r^2_{Y_1Y_3}) \times \sqrt{(1 - r^2_{Y_2Y_3})}}} \tag{8.14}$$

If there is no difference between the correlation coefficient $r_{Y_1Y_2}$ and the partial correlation coefficient $r_{Y_1Y_2.Y_3}$, then the variable Y_3 doesn't have an effect on the correlation. If $r_{Y_1Y_2.Y_3}$ is smaller than the original correlation, variable Y_3 is said to affect

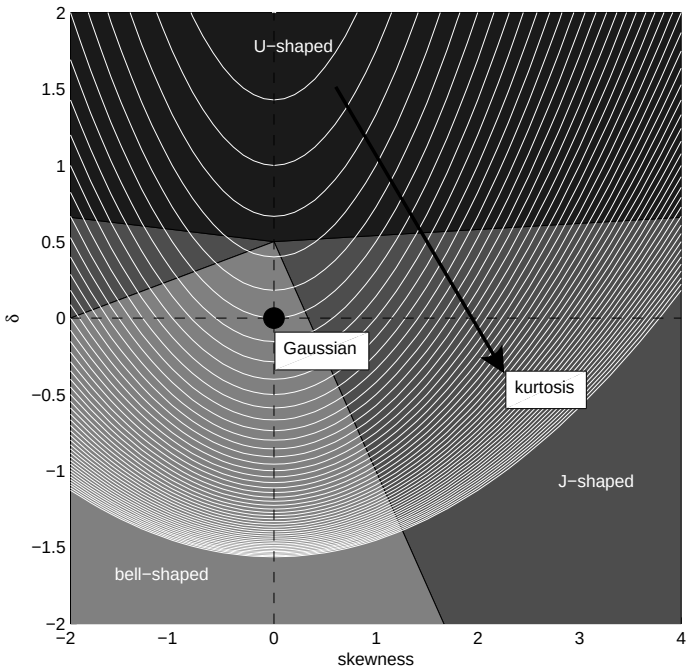

Fig. 8.4 *The domain of co-variation between δ_t and skewness, with contours of kurtosis. The fields of positive and negative 'J-shaped', bell-shaped and 'U-shaped' distributions are shown. The Gaussian distribution scales as [0,0], and the rectangular as [0,0.5], on an infinite field of distribution forms [after Leroy, 1981]*

.

or 'interfere' with the correlation between Y_1 and Y_2.

8.2.3 *Results*

The hyperbolic shape triangle and Craig diagram as classification tools

The sedimentation model of Barndorff Nielsen and Christiansen [1988] was tested on the intertidal zone of active sedimentation on a macrotidal gravel beach. The data set consisted of the three sets of beach profiles and sediment samples which are detailed in Chapter 6. These were collected over between 24 and 26 consecutive low tides, at between 0.5 and 1m cross shore spacing. In this study the size distributions almost always had heavy tails, and the log-hyperbolic model consistently provided a better fit to the sediment samples sieved at $\phi/4$, based on N_{crit} values, compared with the log-normal model. This is in accordance with previous authors in sandy [Hartmann and Christiansen, 1988; Masselink et al., 2008] and gravelly [Scott and Haschenburger, 2005] environments.

The sediment samples for each of the three data sets (hereafter referred to as Slapton

'05, Strete '05, and Strete '07) were plotted on the hyperbolic shape triangle and the Craig diagram, and may be seen in Figures 8.5, 8.6, 8.8 (surface) and 8.8 (sub-surface), respectively. For all data sets, the hyperbolic shape triangle is shown in scatter form and contoured form (following the methodology and Hartmann and Christiansen, 1992) as well as the Craig diagram. For the spring 2007 survey, both the surface and sub-surface samples are depicted.

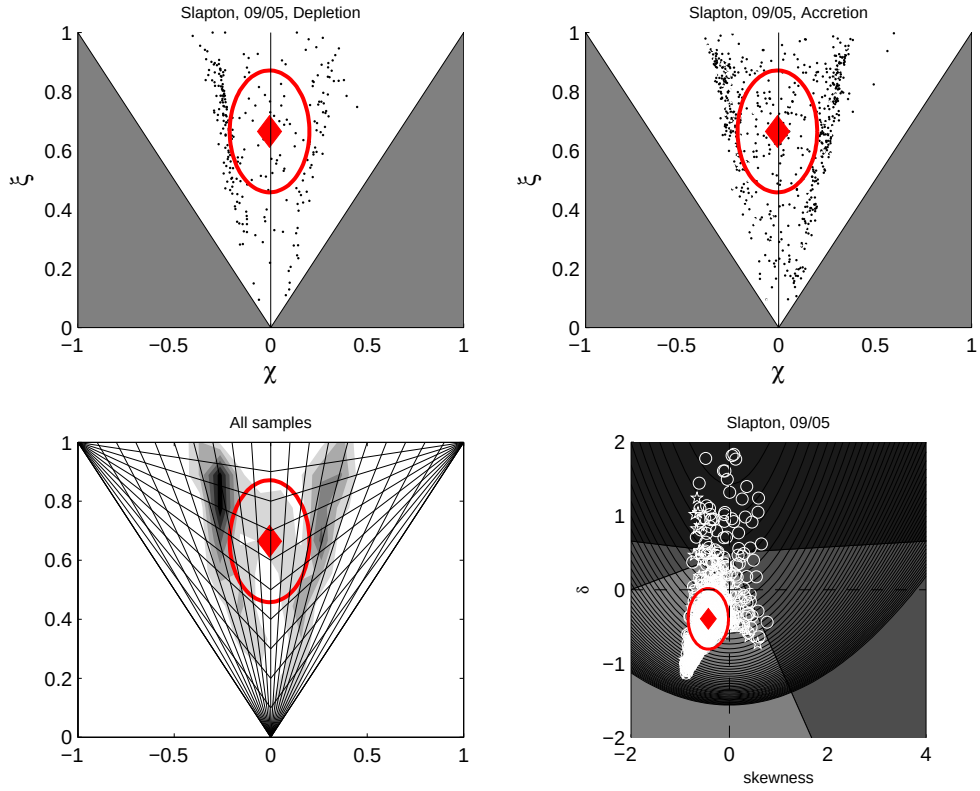

Fig. 8.5 *Slapton September 2005 sediment sample classification. The small circles in the top and bottom left panels depict samples from a patch which had been relativly depleted relative to initial, and stars depict samples from an area relatively accreted. The large diamond in the top left panel shows the centroid* $[\chi_{LH}, \xi_{LH}]$ *position, wrapped by a circle with a diameter equal to the standard deviation of the deviations of the data around that centroid. The hyperbolic shape triangle couplets in the top right panel have been contoured according to the method of Hartmann and Christiansen [1992].*

A number of things are apparent from these plots. The first is that the shape triangle is a poor predictor of net sedimentation relative to initial profile: according to the shape triangle model, circles should plot on the right hand side of the shape triangle, and stars to the left. On no occasion were these trends evident. The second is that the beach sediments from all surveys plot in a consistent domain, slightly either side of χ_{LH}=0, and along almost the entire range of ξ_{LH}. It might be said that these samples share consistently higher variability in ξ_{LH} than they do in χ_{LH}. The third thing of note is

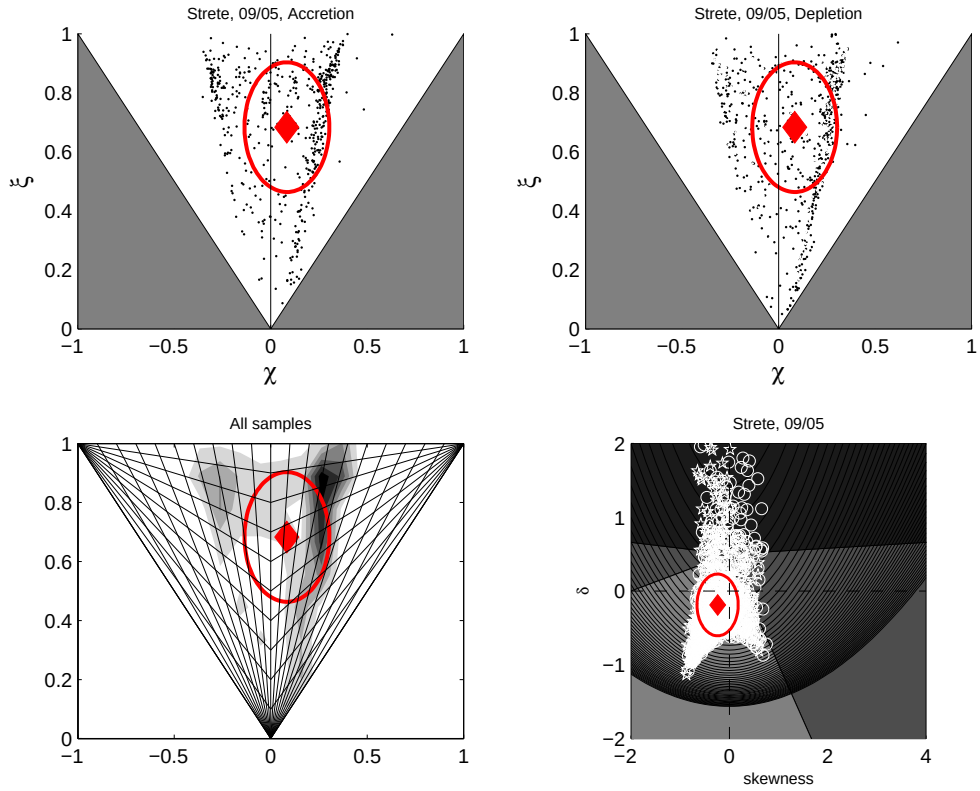

Fig. 8.6 *Strete September 2005 sediment sample classification. The small circles in the top and bottom left panels depict samples from a patch which had been relativly depleted relative to initial, and stars depict samples from an area relatively accreted. The large diamond in the top left panel shows the centroid* $[\chi_{LH}, \xi_{LH}]$ *position, wrapped by a circle with a diameter equal to the standard deviation of the deviations of the data around that centroid. The hyperbolic shape triangle couplets in the top right panel have been contoured according to the method of Hartmann and Christiansen [1992].*

that mean $[\chi_{LH}, \xi_{LH}]$ positions in the triangle for the surface samples are consistently within the hyperbolic domain, around ξ_{LH}=0.5, whereas more sub-surface samples plot nearer 0, suggesting they are more normally distributed. The final thing of note is that the Craig diagram supports these general findings: the majority of samples plot in the 'bell shaped' domain (where hyperbolically-distributed samples would also plot); the bimodal nature of these sediments with respect to skewness is also apparent (in the 'forking' of the cloud of samples); and also that the sub-surface samples plot closer to [0,0] than the surface samples, indicating they are more normally distributed. In general, it may be seen that log-hyperbolically distributed samples plot between δ_t=0 and δ_t=-1, and thus the Craig diagram could potentially be used as pre-indication of whether the log-hyperbolic model would provide a better fit to measured size-frequency distributions of beach gravels.

Whilst the samples were fairly symmetrical, on all occasions samples were found to span the full range of kurtosis, which in the hyperbolic triangle is a broad measure of distributional type (normal at ξ_{LH}=0, hyperbolic between ξ_{LH}=0.1 and 0.9, and skew-Laplacian at ξ_{LH}=1). This is in marked contrast to previous studies which found that different sedimentary environments plotted in separate areas of the shape triangle, thus aiding environmental discrimination [Hartmann and Christiansen, 1988, 1992; Sutherland and Lee, 1994]. It is, however, in accordance with Masselink et al. [2008] who found that not only did their beach sand samples occupy a relatively large domain within the model, but that the shape triangle mis-classified the sediment samples according to their sedimentation history. Thus, the results from this study, in conjunction with the findings of Masselink et al. [2008] on their sand beach, suggest that intertidal beach sediments occupy a large range of distributional forms perhaps compared with other environments such as sand dunes [Hartmann and Christiansen, 1988, 1992]. This distributional heterogeneity is also reflected well in the Craig diagram.

The hyperbolic shape triangle as model for recent net sedimentation

This section presents the results for the test of the shape triangle model over individual tides. The absolute $[\chi_{LH},\xi_{LH}]$ positions were plotted, and the changing cross-shore averaged $[\chi_{LH},\xi_{LH}]$ positions over each time (individual semi-diurnal tidal cycles) were analysed relative to the previous tide by use of the ϵ and κ parameters. The results for

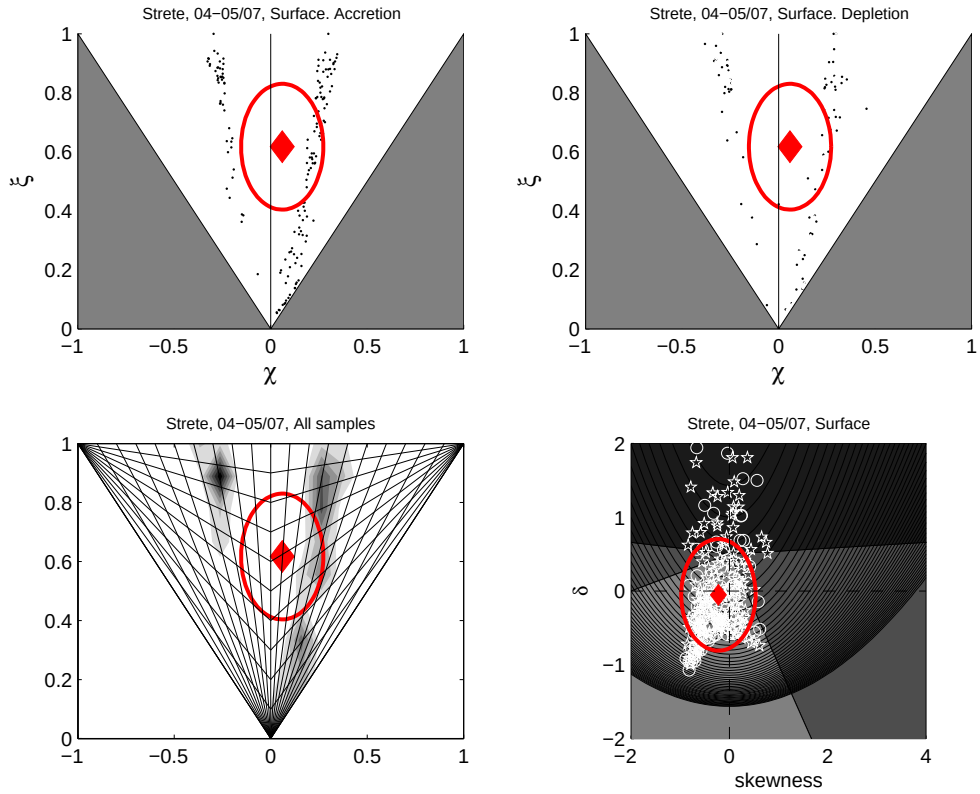

Fig. 8.7 *Strete, April-May 2007 sediment sample classification: surface. The symbols in the top left panel depict samples from a patch which had been relativly accreted relative to initial, and the symbols in the top right panel depict samples from an area relatively accreted. The large diamonds here show the centroid* $[\chi_{LH}, \xi_{LH}]$ *position, wrapped by a circle with a diameter equal to the standard deviation of the deviations of the data around that centroid. The hyperbolic shape triangle couplets in the bottom left panel has been contoured according to the method of Hartmann and Christiansen [1992]. The bottom right panel shows the sediments classified on a Craig diagram.*

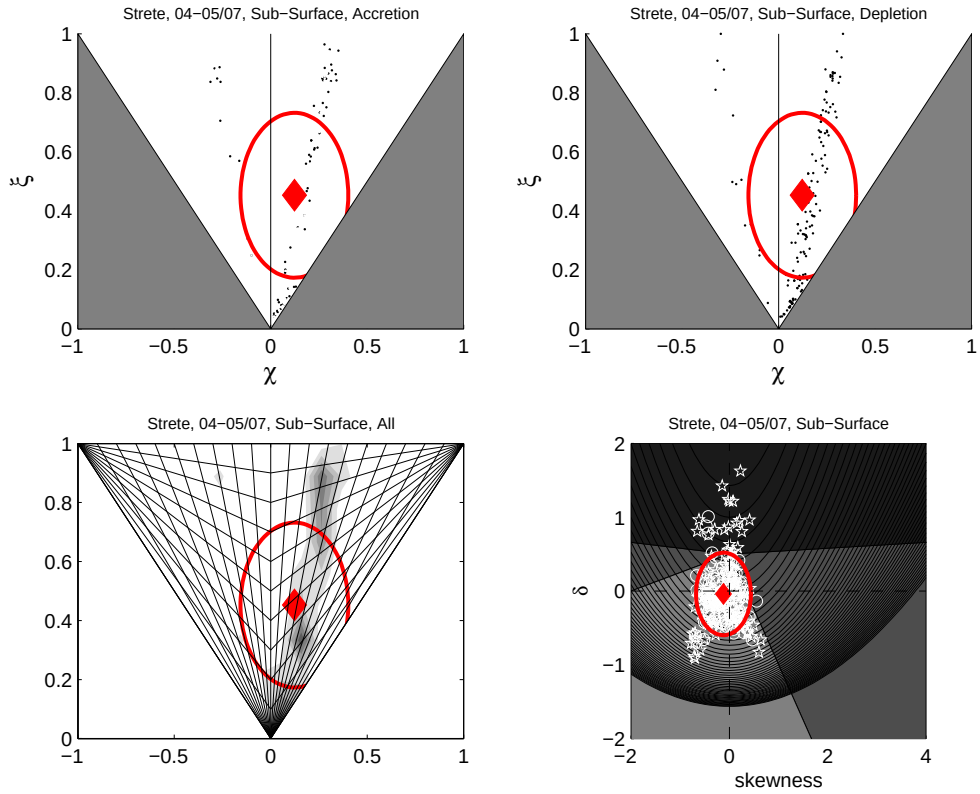

Fig. 8.8 *Strete, April-May 2007 sediment sample classification: sub-surface. The symbols in the top left panel depict samples from a patch which had been relativly accreted relative to initial, and the symbols in the top right panel depict samples from an area relatively accreted. The large diamonds here show the centroid* $[\chi_{LH}, \xi_{LH}]$ *position, wrapped by a circle with a diameter equal to the standard deviation of the deviations of the data around that centroid. The hyperbolic shape triangle couplets in the bottom left panel has been contoured according to the method of Hartmann and Christiansen [1992]. The bottom right panel shows the sediments classified on a Craig diagram.*

the autumn 2005 data sets may be seen in Figures 8.9 (tides 1–9), 8.10 (tides 10–18), and 8.11 (tides 19–26). The large circles and squares indicate mean [χ_{LH},ξ_{LH}] position for the given set of samples over each tide (the centroid in the cloud of those samples). The solid and dashed cross-hairs on each sub-panel indicate the mean [χ_{LH},ξ_{LH}] position on the previous tide, for Slapton and Strete samples, respectively. On each sub-panel, three values for each site are scribed in the corners of the shape triangle's impossible areas: ϵ ($\chi_{LHt} - \chi_{LHt-1}$), κ ($\xi_{LHt} - \xi_{LHt-1}$), and Δz (mean elevation change in metres over the tide). The results are summarised in Table 8.1 for the Slapton data set, and Table 8.2 for the Strete data set, where the rows contain the correlation coefficients between Δz and model parameters, squared correlation coefficients and **t**-values (2 tailed **t**-test at α=0.05). This has been done for the data sets as a whole (in the upper halves of the tables), and for the tides where absolute net sedimentation was greater than 5 cm (in the lower halves of the tables). As well as $-\epsilon$ and κ, the three measures of statistical association are shown for the resultant of ϵ and κ, plus median size (Md) and sorting (σ).

An identical analysis was performed on the spring 2007 data sets, the results of which may be seen in Figures 8.12 and 8.13, and in Table 8.3. Here, circles and squares refer to surface and sub-surface samples, respectively.

Tab. 8.1 *Table of correlations between Δz_i and epsilon, κ, $\vec{R_{\epsilon,\kappa}}$, median size (Md) and geometric sorting (σ) for the Slapton 2005 survey, surface samples. Rows indicate correlation coefficient (r), R^2, and **t** value (values which indicate significant difference from zero are shaded, critical value shown in parentheses). The upper portion of the table houses values for all tides, and the lower for those only when morphological change over a given tide was $\geq \pm 5$ cm.*

Slapton 2005 $\Delta z_i (n = 25)$	ϵ $\xi_{LHt} - \xi_{LHt-1}$	κ $\chi_{LHt} - \chi_{LHt-1}$	$\vec{R_{\epsilon,\kappa}}$ $\epsilon + \kappa$	Md	σ
r	0.62	-0.163	-0.53	-0.34	0.43
R^2	0.39	0.02	0.27	0.11	0.18
t (3.104)	23.21	3.85	16.78	8.87	12.08
$\Delta z_i > \pm$5cm (n=19)					
r	0.76	-0.19	-0.59	-0.36	0.51
R^2	0.57	0.03	0.35	0.13	0.26
t (3.22)	30.74	3.40	15.71	7.17	12.04

With reference to Figures 8.9 to 8.13 inclusive, the position of [χ_{LH},ξ_{LH}] relative to it on the previous tide was quite variable. Indeed, little systematic direction of travel of the mean [χ_{LH},ξ_{LH}] position through the phase space over time was discernible. What is clear is that the 'absolute' position of [χ_{LH},ξ_{LH}] does not reflect well the actual amount

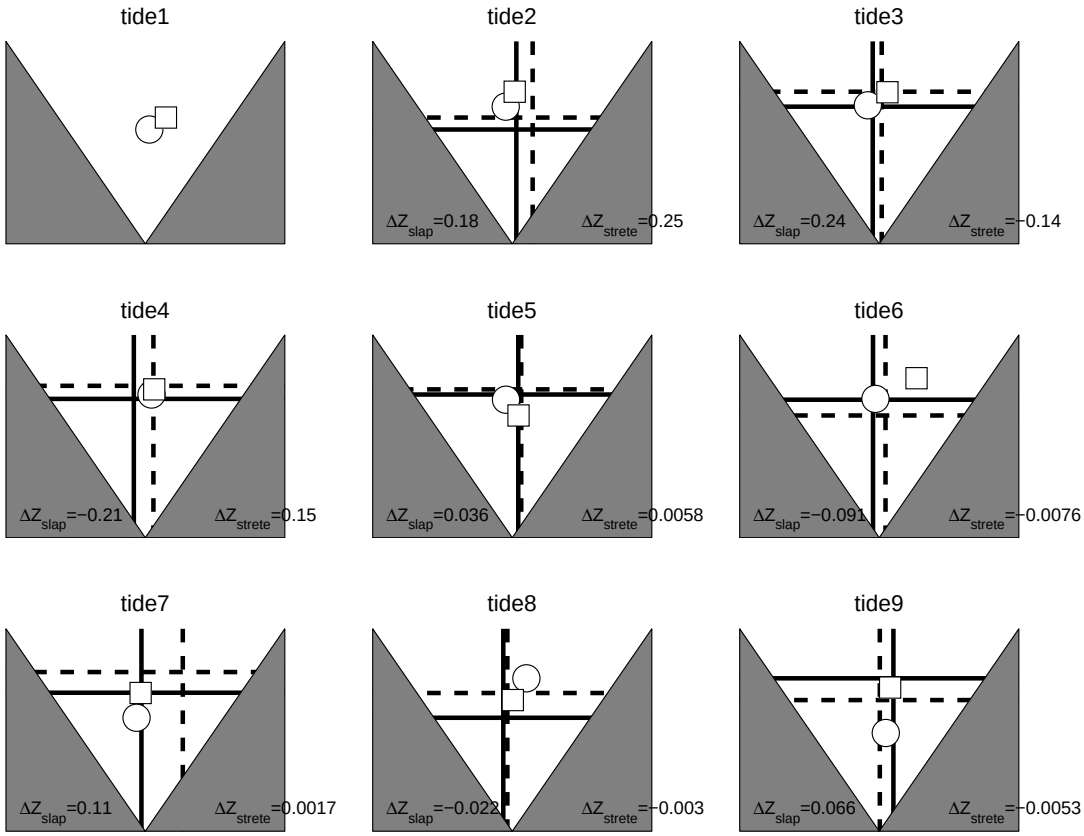

Fig. 8.9 *Hyperbolic domain for Slapton and Strete September 2005 sediment samples, tides 1–9. Mean positions for that tide are marked by large circles and squares, and the mean positions for the previous tide by solid and dashed cross-hairs, for Slapton and Strete sediments respectively. Mean morphological change over that tide is denoted* Δz_{slap} *and* Δz_{strete} *for Slapton and Strete, respectively.*

Tab. 8.2 *Table of correlations between* Δz_i *and* ϵ, κ, $\vec{R_{\epsilon,\kappa}}$, *median size (Md) and geometric sorting* (σ) *for the Slapton 2005 survey, surface samples. Rows indicate correlation coefficient* (r), R^2, *and* $\mathbf{t}$ *value (values which indicate significant difference from zero are shaded, critical value shown in parentheses). The upper portion of the table houses values for all tides, and the lower for those only when morphological change over a given tide was* $\geq \pm 5$ *cm.*

Strete 2005 $\Delta z_i (n = 25)$	ϵ $\xi_{LHt} - \xi_{LHt-1}$	κ $\chi_{LHt} - \chi_{LHt-1}$	$\vec{R_{\epsilon,\kappa}}$ $\epsilon + \kappa$	Md	σ
r	0.53	-0.12	-0.39	-0.04	0.38
R^2	0.28	0.01	0.15	0.002	0.14
t (3.104)	17.00	2.80	10.77	1.11	10.24
$\Delta z_i > \pm 5$cm (n=15)					
r	0.73	-0.11	-0.50	-0.03	0.47
R^2	0.54	0.013	0.25	0.001	0.22
t (3.372)	21.05	1.52	8.67	0.51	7.94

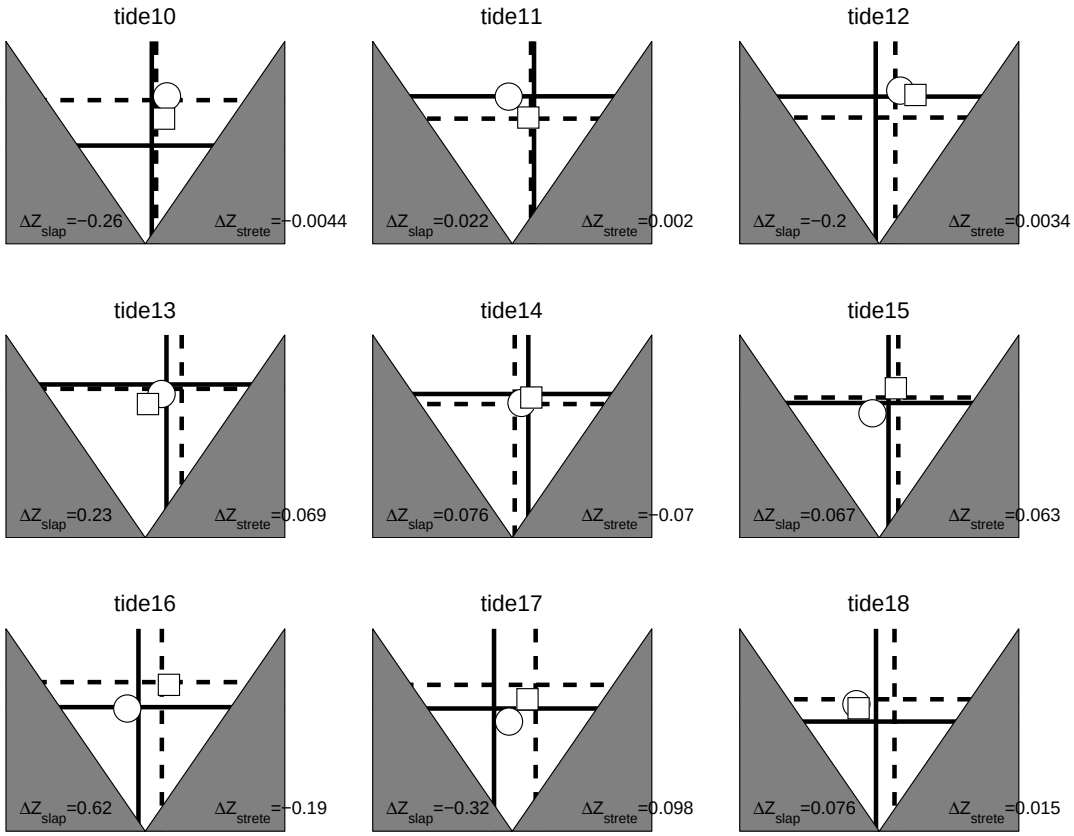

Fig. 8.10 *Hyperbolic domain for Slapton and Strete September 2005 sediment samples, tides 10–18. Mean positions for that tide are marked by large circles and squares, and the mean positions for the previous tide by solid and dashed cross-hairs, for Slapton and Strete sediments respectively. Mean morphological change over that tide is denoted* Δz_{slap} *and* Δz_{strete} *for Slapton and Strete, respectively.*

Tab. 8.3 *Table of correlations between* Δz_i *and* r_ϵ, r_κ, $\vec{R_{\epsilon,\kappa}}$, *median size (Md) and geometric sorting (*σ*) for the Strete 2007 survey, surface samples. Rows indicate correlation coefficient (r),* R^2, *and* **t** *value (values which indicate significant difference from zero are shaded, critical value shown in parentheses). The upper portion of the table houses values for all tides, and the lower for those only when morphological change over a given tide was* $\geq \pm 5$ *cm.*

Strete 2007 surface $\Delta z_i (n = 23)$	r_ϵ $\xi_{LHt} - \xi_{LHt-1}$	r_κ $\chi_{LHt} - \chi_{LHt-1}$	$\vec{R_{\epsilon,\kappa}}$ $r_\epsilon + r_\kappa$	Md	σ
r	0.54	0.07	-0.29	0.34	0.27
R^2	0.29	0.005	0.08	0.12	0.07
t (3.13)	16.32	1.61	6.67	8.35	6.22
$\Delta z_i > \pm 5$cm (n=21)					
r	0.57	0.029	-0.31	0.32	0.28
R^2	0.32	0.0008	0.10	0.10	0.07
t (3.17)	17.82	0.62	7.42	7.75	6.43

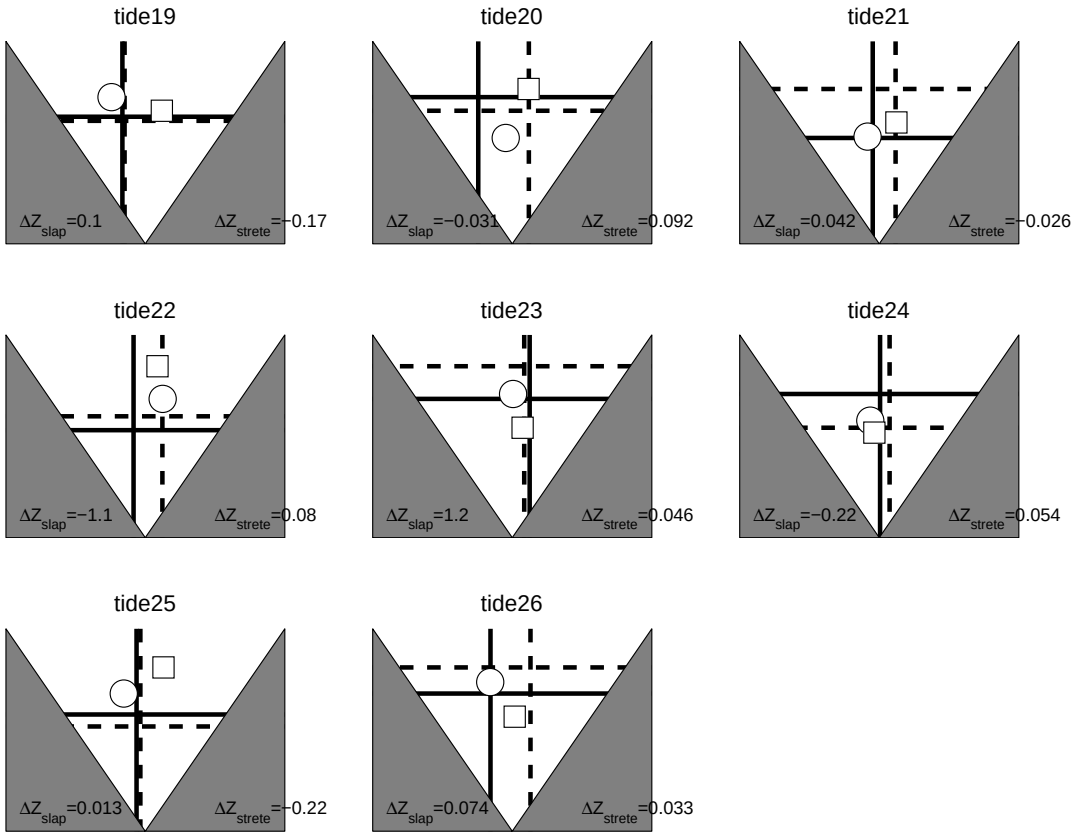

Fig. 8.11 *Hyperbolic domain for Slapton and Strete September 2005 sediment samples, tides 19–26.Mean positions for that tide are marked by large circles and squares, and the mean positions for the previous tide by solid and dashed cross-hairs, for Slapton and Strete sediments respectively. Mean morphological change over that tide is denoted* Δz_{slap} *and* Δz_{strete} *for Slapton and Strete, respectively.*

Tab. 8.4 *Table of correlations between* Δz_i *and* r_ϵ, r_κ, $\vec{R_{\epsilon,\kappa}}$, *median size (Md) and geometric sorting (*σ*) for the Strete 2007 survey, sub-surface samples. Rows indicate correlation coefficient (r),* R^2, *and* $\mathbf{t}$ *value (values which indicate significant difference from zero are shaded, critical value shown in parentheses). The upper portion of the table houses values for all tides, and the lower for those only when morphological change over a given tide was* $\geq \pm 5$ *cm.*

Strete 2007 sub-surface $\Delta z_i (n = 23)$	r_ϵ $\xi_{LHt} - \xi_{LHt-1}$	r_κ $\chi_{LHt} - \chi_{LHt-1}$	$\vec{R_{\epsilon,\kappa}}$ $r_\epsilon + r_\kappa$	Md	σ
r	0.048	-0.038	-0.05	0.29	0.10
R^2	0.002	0.001	0.002	0.08	0.011
$\mathbf{t}$ (3.13)	1.01	0.81	1.09	6.75	2.29
$\Delta z_i > \pm$5cm (n=21)					
r	0.06	-0.03	-0.05	0.31	0.14
R^2	0.004	0.001	0.003	0.09	0.01
$\mathbf{t}$ (3.17)	1.23	0.74	1.11	6.62	2.71

Tab. 8.5 *Table of correlations between DOD and r_ϵ, r_κ, $\vec{R_{\epsilon,\kappa}}$, median size (Md) and geometric sorting (σ) for the Strete 2007 survey, surface samples. Rows indicate correlation coefficient (r), R^2, and* **t** *value (values which indicate significant difference from zero are shaded, critical value shown in parentheses). The upper portion of the table houses values for all tides, and the lower for those only when morphological change over a given tide was $\geq \pm 5$ cm.*

Strete 2007 surface DOD (n=23)	r_ϵ $\xi_{LHt} - \xi_{LHt-1}$	r_κ $\chi_{LHt} - \chi_{LHt-1}$	$\vec{R_{\epsilon,\kappa}}$ $r_\epsilon + r_\kappa$	Md	σ
r	0.198	0.30	0.11	0.27	0.26
R^2	0.03	0.09	0.01	0.07	0.07
t (3.13)	4.33	7.05	2.55	6.37	6.06
Strete 2007 sub-surface					
r	0.04	-0.03	-0.05	0.29	0.10
R^2	0.002	0.001	0.002	0.08	0.01
t (3.13)	1.01	0.81	1.09	6.75	2.29

of net sedimentation (Δz) over a given tide, for either case of ϵ or κ sedimentation. However, scrutiny of these diagrams does suggest that the position of [χ_{LH},ξ_{LH}] at any given time-step relative to [χ_{LH},ξ_{LH}] on the previous time-step does seem to reflect ϵ sedimentation better. These observations are confirmed by the correlation results in Tables 8.1 to 8.3, inclusive, which show at least two clear trends across the data sets. The first is that $-\epsilon$ for the surface samples is the best associated with Δz, with correlation coefficients of between 0.53 and 0.62, and second best associated with $\vec{R_{\epsilon,\kappa}}$, with correlation coefficients of between -0.29 and -0.53 (minus because minus values of ϵ indicate accretion). In general, correlations between Δz and κ, *Md*, and σ are poor. The second key result is that correlations consistently improve when only 'significant' net changes occur, delimited by ±5cm morphological change. In contrast, Table 8.4, which contains the results for the sub-surface samples, does not portray the same relationships, indicating that the sub-surface and surface samples respond very differently to the parameters (although only one sub-surface data set was used, compared to three surface sample data set). Sub-surface sample parameters are equally un-responsive to changes in the DOD record, as shown in Table 8.5.

With reference to Table 8.6, a partial correlation analysis revealed that variation of κ did not have an effect on the correlations observed between Δz and $-\epsilon$. Thus it can be confirmed in this study that the ϵ and κ parameters respond to two different morpho-sedimentary processes. In contrast, sample sorting was found to have an

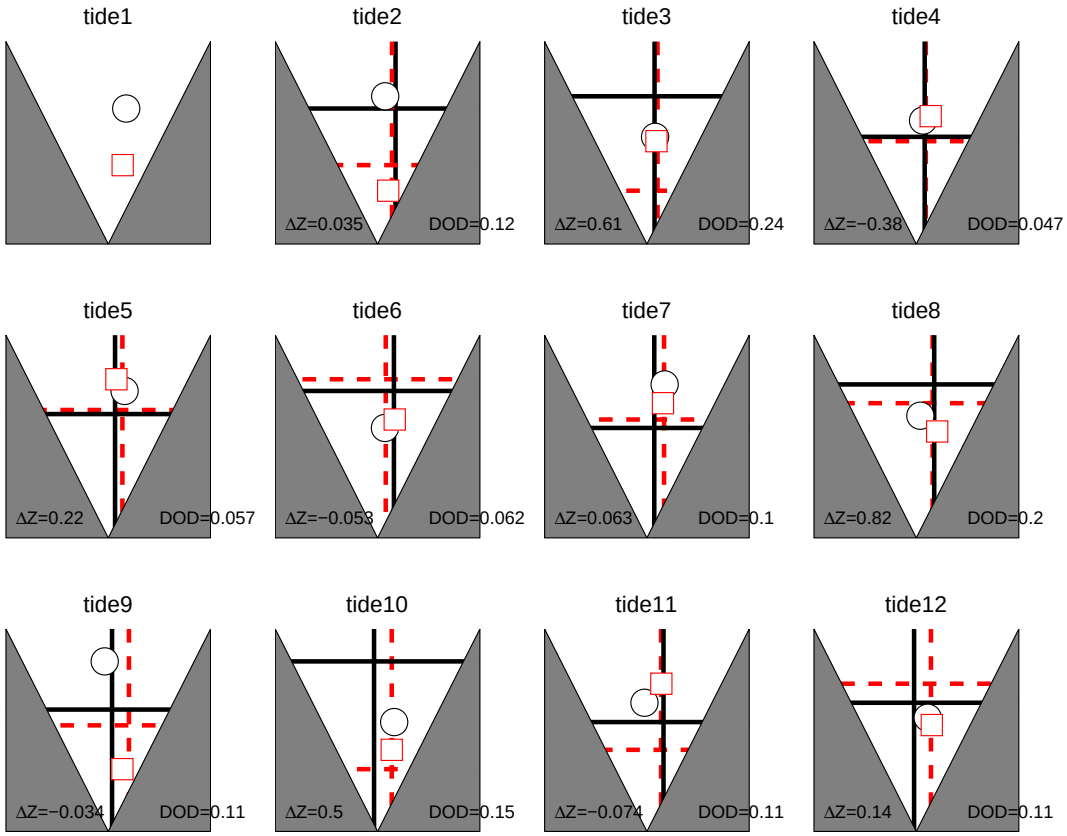

Fig. 8.12 *Hyperbolic domain for surface and sub-surface April-May 2007 sediment samples, tides 1–12. Mean positions for that tide are marked by large circles and squares, and the mean positions for the previous tide by solid and dashed cross-hairs, for surface and sub-surface sediments respectively. Mean morphological change over that tide is denoted.*

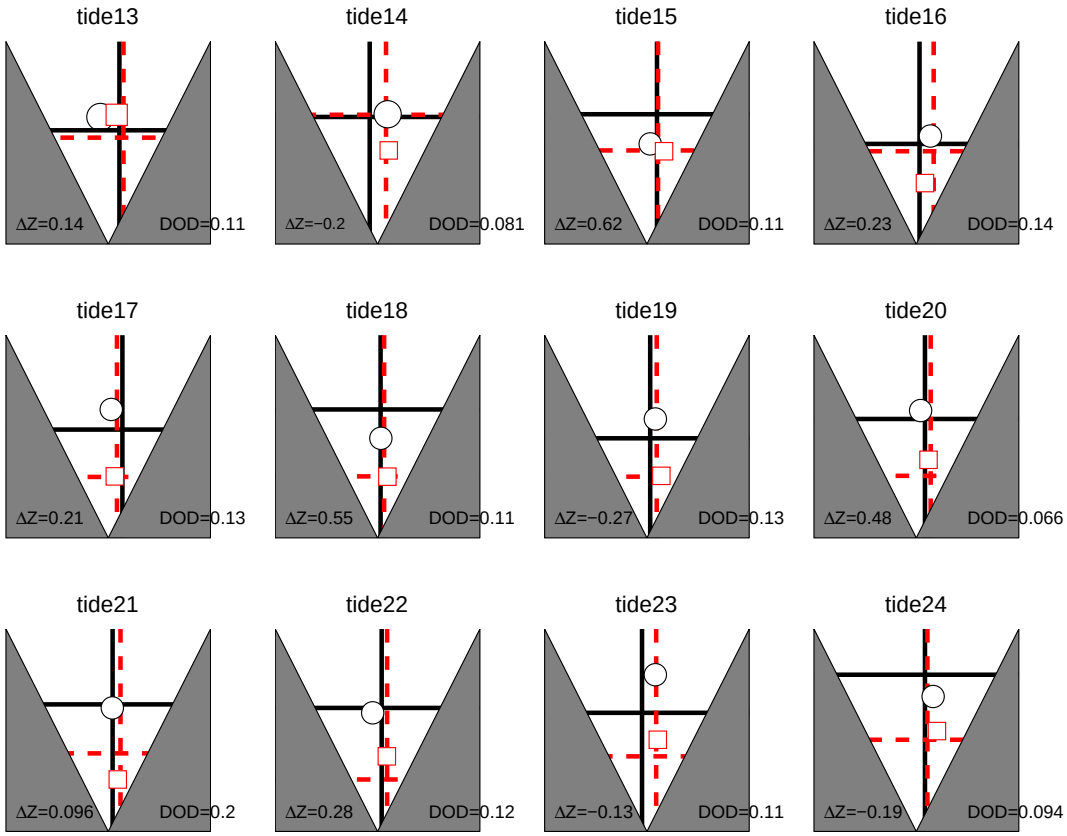

Fig. 8.13 *Hyperbolic domain for surface and sub-surface April-May 2007 sediment samples, tides 13–24. Mean positions for that tide are marked by large circles and squares, and the mean positions for the previous tide by solid and dashed cross-hairs, for surface and sub-surface sediments respectively. Mean morphological change over that tide is denoted.*

interfering influence on the original correlations for the autumn 2005 data sets, on occasion where Δz and σ were better correlated.

Tab. 8.6 *Correlation coefficients, and partial correlation coefficients controlling κ, Md and σ, for Δz and $-\epsilon$. Shaded values indicate partial correlations $\leq$ .05 the original correlation, suggesting an interference by that variable in the original correlation ($r_{\Delta z,\epsilon}$).*

	Slapton '05 all	Slapton '05 ± 5cm	Strete '05 all	Strete '05 ± 5cm	Strete '07 all (surf.)	Strete '07 ± 5cm (surf.)
$r_{\Delta z,-\epsilon}$	0.62	0.76	0.53	0.53	0.54	0.57
$r_{\Delta z,-\epsilon}.\kappa$	0.62	0.76	0.52	0.52	0.54	0.58
$r_{\Delta z,-\epsilon}.Md$	0.56	0.72	0.53	0.53	0.52	0.56
$r_{\Delta z,-\epsilon}.\sigma$	0.49	0.64	0.41	0.42	0.52	0.55

8.3 Sediment Trend Analysis

8.3.1 Methods

Sediment trend analysis has been performed using the fortnightly-sampled sediment size and profile data set, which is the subject of Chapter 7, adopted for application to the problem of discerning sedimentation patterns from grain-size measurements. The raw (non-gridded) grain-size parameters have been used along with their associated coordinates in [Eastings,Northings], so the distance between points in the cross-shore (1-2m) are much smaller than the distance between points in the alongshore (250m). The data set was deemed suitable because, from the volumetric record taken every two weeks over the year October 2006-October 2007, clear net drift directions were able to be determined. In addition, the grain-size data was high resolution in both space and time. It could be reasonably assumed that the observed changes in net sedimentation across space between individual surveys, taken at a regular fortnightly interval, had taken place at some time during that time interval, and also that the majority of sediment transported into or out of any point within the study would have been sourced from another point within the study area. The study site is graded alongshore and cross-shore, and this changes through time at such a frequency that there were no deposits samples that wouldn't have been transported within the intervening time interval between surveys. Indeed, only known intertidal areas were sampled (see Chapter 7 for more information on the data and sampling framework). All sediment parameters in this section were derived from the image method detailed in Chapter 4, which

reported that, whilst the mean size and sorting parameters obtained closely match those obtained from sieving, the skewness parameter was not as accurate. The particular method to determine the grain-size parameters is not too important for sediment trend analysis, as the relative values between sampling points are more important than the absolute values [Le Roux et al., 2002; Le Roux and Rojas, 2007]. We therefore expect the parameters to work reasonably well for sediment trend modelling, becaused the digital image method predicts the sign and the relative changes of the skewness well.

Slapton is generally a graded barrier (see chapter 3). For example, Figure 8.14 depicts data from a typical alongshore survey of sediment size, showing decreasing trends northwards in sediment size, sorting and skewness, which would correspond to the trend vector type 1 as defined by Le Roux [1994*b*]; Gao and Collins [1992] (or 'A' by McLaren and Bowles [1985]), and qualitatively supports net northerly transport, as was the case prior to sampling. However, as chapter 7 documents, the grading is not always present when the beach has under gone net erosion. This chapter looks at whether sediment trend analysis performs well as a tool for predicting net sedimentation over fortnightly periods, i.e. its use as a *dynamic* model, which is still in some doubt [Masselink et al., 2008].

The technical details of sediment trend modelling have been reviewed extensively elsewhere [McLaren and Bowles, 1985; Gao, 1996; Le Roux et al., 2002; Le Roux and Rojas, 2007; McLaren et al., 2007]. The method proposed by Gao and Collins [1992], henceforth referred to as the GSTA model (grain-size Trend Analysis), is the most suitable method for the marine environment and is adopted here to be directly comparable with previous studies (being available as a commercial product/service, the model of McLaren and Bowles [1985] appears more widely used, but one of the main assumptions of the approach is that the sediment transport is by uni-directional currents). The McLaren and Bowles [1985] model uses only two sampling stations at a time, whereas the Gao and Collins [1992] model uses all samples within a (pre-defined) 'characteristic distance', or sedimentary 'sphere of influence'. According to the GSTA model of Gao and Collins [1992], in the direction of sediment transport, sediments may become either finer, better sorted and more negatively skewed (*FB-*; Case 1) or coarser, better sorted and more positively skewed (*CB+*; Case 2). These two sediment trends are also considered in the GSTA models of McLaren and Bowles [1985] and Le Roux (1994),

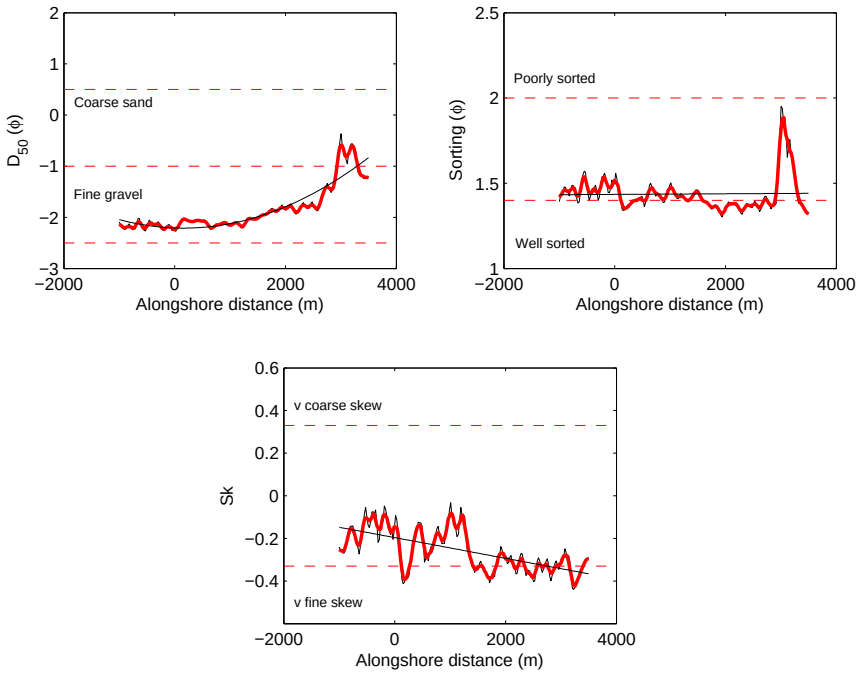

Fig. 8.14 *Alongshore trends in sediment size, May 2007, taken every 25m along the high tide berm, against alonsghore distance (m).* ***Clockwise, from top left****: geometric mean sediment size (ϕ), sorting (ϕ) and skewness (non-dim.). For each, the heavy black line is the raw data; the heavy red line is the 4-point (100m) moving average; and the light black line is the least squares trend.*

where they are referred to as Case B and C, and Type 1 and 2, respectively. The GSTA method compares the sediment characteristics (size, sorting and skewness) of adjacent sample points in a spatial grid, vectors of unit length are drawn between two points if they conform to the 'rules' of the GSTA model (i.e., *FB-* or *CB+*; cf., Gao [1996]). These vectors are calculated from parameters of each sample with its nearest neighbours in any direction lying within a characteristic distance, D_{cr}, which in this study is equal to the maximum sampling interval, 250 m. Summing the vectors at each sample point produces a single vector with unit length, which should reflect the net trends in sediment transport (i.e., the trend vector). Summing the vectors at each data station produces a single vector for this site $\vec{R}(x, y)$:

$$\vec{R}(x, y) = \sum \vec{r}(x, y)_i \tag{8.15}$$

where $\vec{r}(x, y)$ is the trend vector for station i. Gao and Collins [1991] mathematically described how two more sediment trends might occur (*FB+* and *CB-*), a concept continued in the work of Le Roux et al. [2002]. The method has been evaluated by

Le Roux et al. [2002], who states that it is generally preferable to the McLaren-Bowles method since it is more objective; two-dimensional; and less sensitive to irregularities in the sampling configuration. The Gao and Collins [1992] method applies a spatial filter to the vector field to remove noise, however both Asselman [1999] and Le Roux et al. [2002] strongly recommend against it for averaging may lead to spurious results and a loss of information, so following Masselink et al. [2008], the averaging procedure has not been carried out here.

Following Masselink et al. [2008], on the basis that, since collectively Gao and Collins [1991] and Le Roux [1994*a*] mathematically make a case for four trend cases (FB-, FB+, CB-, CB+), an alternative sediment trend model can therefore be formulated solely based on the sediment sorting [McLaren et al., 2007]. Sediment trend vectors are drawn from the spatial gradient in sorting values (multiplied by -1, since we are looking for an improvement in sorting). In other words, the direction and length of the trend vectors at each of the sample locations are proportional to the first derivative of sorting $(\delta\sigma/\delta x, \delta\sigma/\delta y)$, and the contributions of size and skewness are ignored. This model was referred to as the "sorting model" by Masselink et al. [2008].

The trend vectors obtained from the GSTA analysis were tested for statistical significance using the Rayleigh test for non-uniformity, given by [Fisher, 1993] a $\mathbf{Z}$-score defined as:

$$\mathbf{Z} = N \times \overline{R}_l^2 \tag{8.16}$$

where $\overline{R}_l = |R_u| / N$ is the mean resultant length, and N is the sample number, and where R_u is:

$$R_u = \emptyset^T \exp(1\mathbf{i} \times \angle) \tag{8.17}$$

where $\emptyset^T$ is a transposed vector of weights (optional), $\mathbf{i} = \sqrt{-1}$ and $\angle$ is the series of angles. The probability that $\mathbf{Z}$ is due to chance is given by:

$$p = \exp(\mathbf{Z}) \times \frac{1 + (2\mathbf{Z} - \mathbf{Z}^2)}{4N - (24\mathbf{Z} - 132\mathbf{Z}^2 + 76\mathbf{Z}^3 - 9\mathbf{Z}^4)/288N^2} \tag{8.18}$$

The test is two-tailed: if the value of Z is not significant, we conclude that the observed vector pattern cannot be distinguished from a pattern generated by a random

process [Davis, 1986]. Circular mean is given by the four quadrant arctangent of the real and imaginary parts of R_u, and circular variance is given by $1 - \overline{R}_l$. The circular correlation coefficient; a $\mathbf{t}$ test of significance; and the probability that $\mathbf{t}_\angle$ is due to chance, are given by, respectively [Jammalamadaka and Sengupta, 2001]:

$$r_\angle = \frac{\sum \left[\sin(\angle_1 - \overline{\angle_1}) \sin(\angle_2 - \overline{\angle_2})\right]}{\sqrt{\sum \left[\sin(\angle_1 - \overline{\angle_1})^2 \sin(\angle_2 - \overline{\angle_2})^2\right]}} \tag{8.19}$$

$$\mathbf{t}_\angle = r_\angle \sqrt{\frac{N \frac{\sin(\angle_1 - \overline{\angle_1})^2}{N} \frac{\sin(\angle_2 - \overline{\angle_2})^2}{N}}{\left[\sin(\angle_1 - \overline{\angle_1}) \ \sin(\angle_2 - \overline{\angle_2})\right]^2}} \tag{8.20}$$

$$p = 2\left(1 - \mathbf{N}_{\alpha,\nu}|\mathbf{t}_\angle|\right); \tag{8.21}$$

where $\mathbf{N}_{\alpha,\nu}$ is the normal cumulative distribution function at α=0.05 and ν=N-2 degrees of freedom [Jammalamadaka and Sengupta, 2001].

8.3.2 *Results*

Some results of the GSTA analysis may be seen in Figures 8.15 and 8.17, for various times during the year 2006-2007. Mean trend vectors have been drawn from each mid sample station to illustrate the general trends in the data. The results of the sediment sorting model analysis may be seen in Figures 8.16 and 8.18, for the same survey periods. The maps are aligned to north, so Strete is at the top of the figure panels, Torcross at the bottom, and offshore to the right. Trends across space for any given survey are relatively easy to discern for example in Figure 8.15, the 06/11/06 trend vectors indicate onshore sediment transport for a large proportion of the barrier's length, and the 20/12/06 vectors indicate predominant offshore sediment transport.

The GSTA results in full are tabulated in Table 8.7. Against survey date, the net sediment transport directions, as determined from the beach volumetric record (refer to chapter 7), are shown as compass directions: N for alongshore northerly (towards Strete), S for alongshore southerly (towards Torcross), W for onshore, and E for offshore. Note that whereas the N-S sediment transport component between individual surveys is easily determined from the profile record, the E-W component is not so easily determined. Here, estimates have been made based on the sign of the first differential in the volumetric record when the alongshore volumes have been accounted for, i.e. any

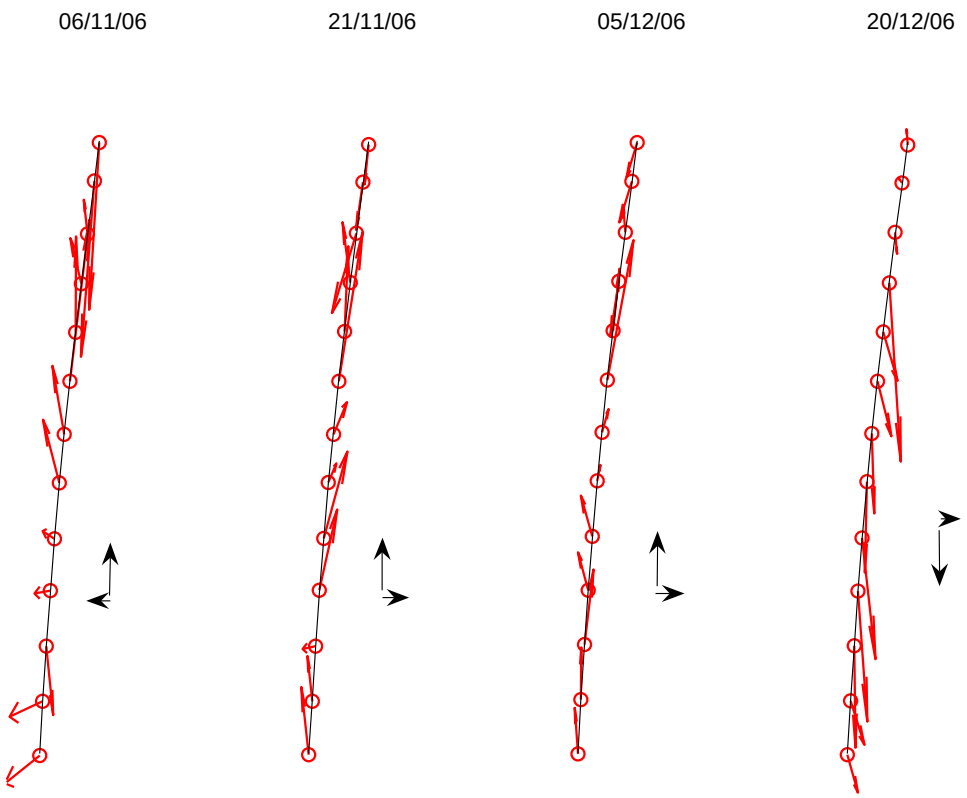

Fig. 8.15 *Resultant trend vectors drawn for each cross-shore sediment sampling station, from the central sediment sample station. Example data shown for winter 2006. Dark arrows show the inferred sediment transport from the profile data set.*

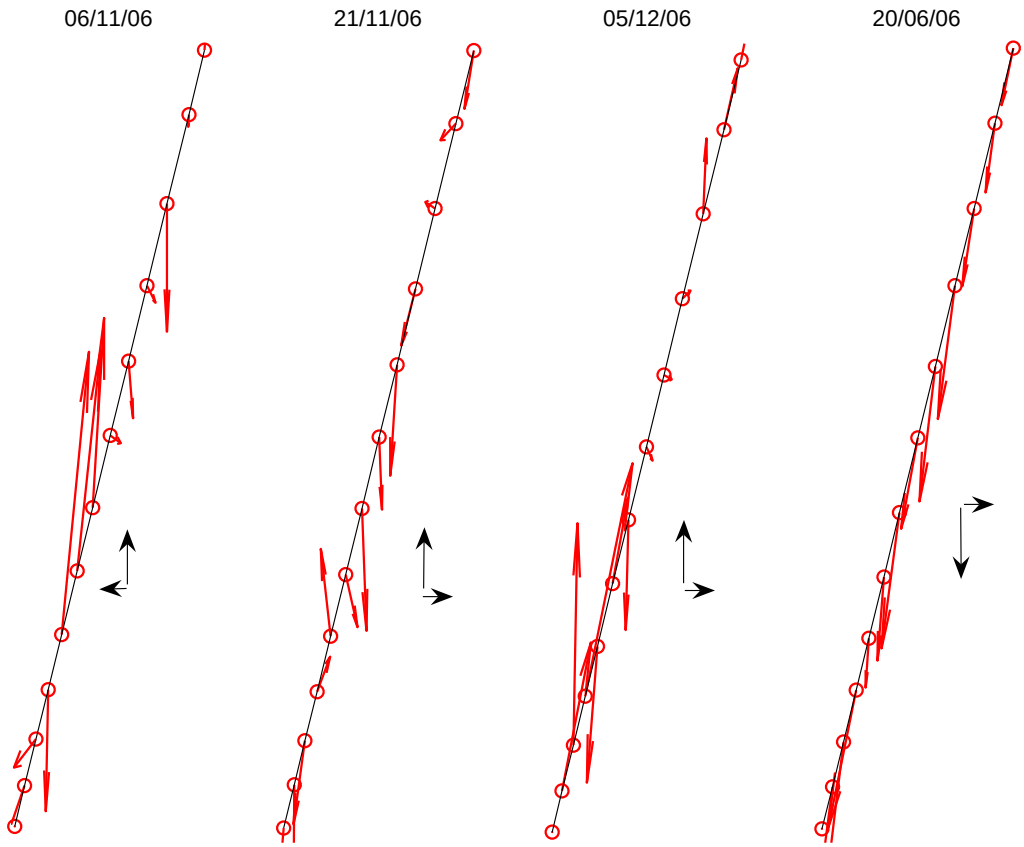

Fig. 8.16 *Resultant vectors drawn for each cross-shore sediment sampling station, from the central sediment sample station, using only information on relative sorting. Example data shown for winter 2006. Dark arrows show the inferred sediment transport from the profile data set.*

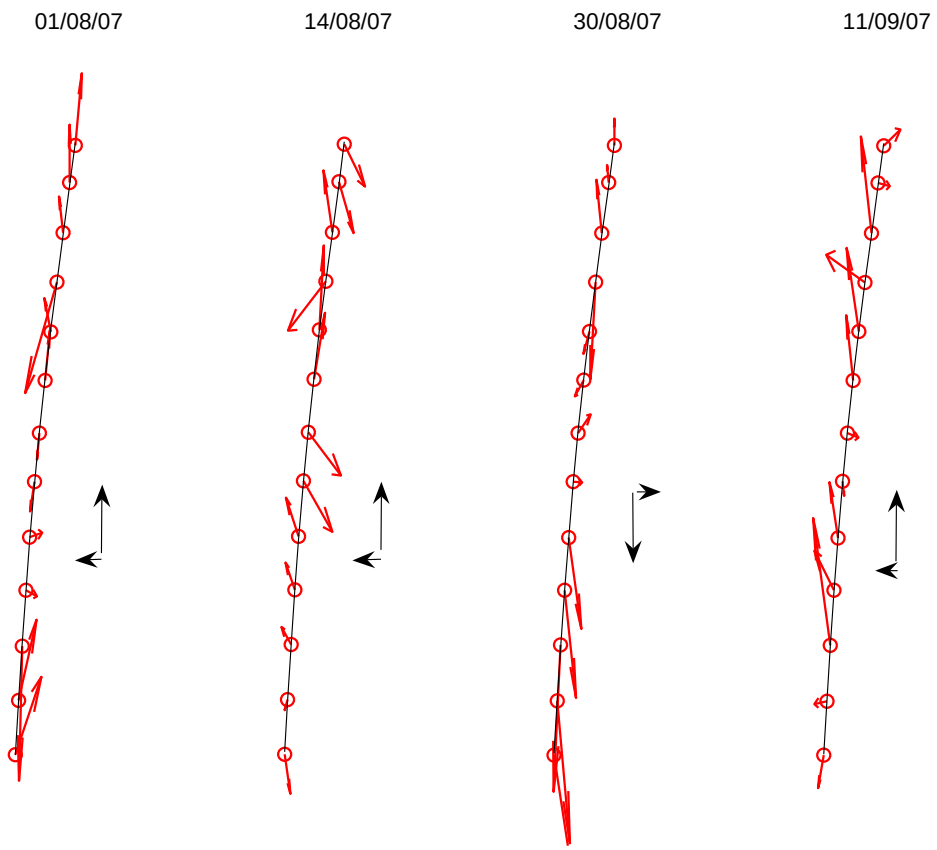

Fig. 8.17 *Resultant trend vectors drawn for each cross-shore sediment sampling station, from the central sediment sample station. Example data shown for late summer/autumn 2007. Dark arrows show the inferred sediment transport from the profile data set.*

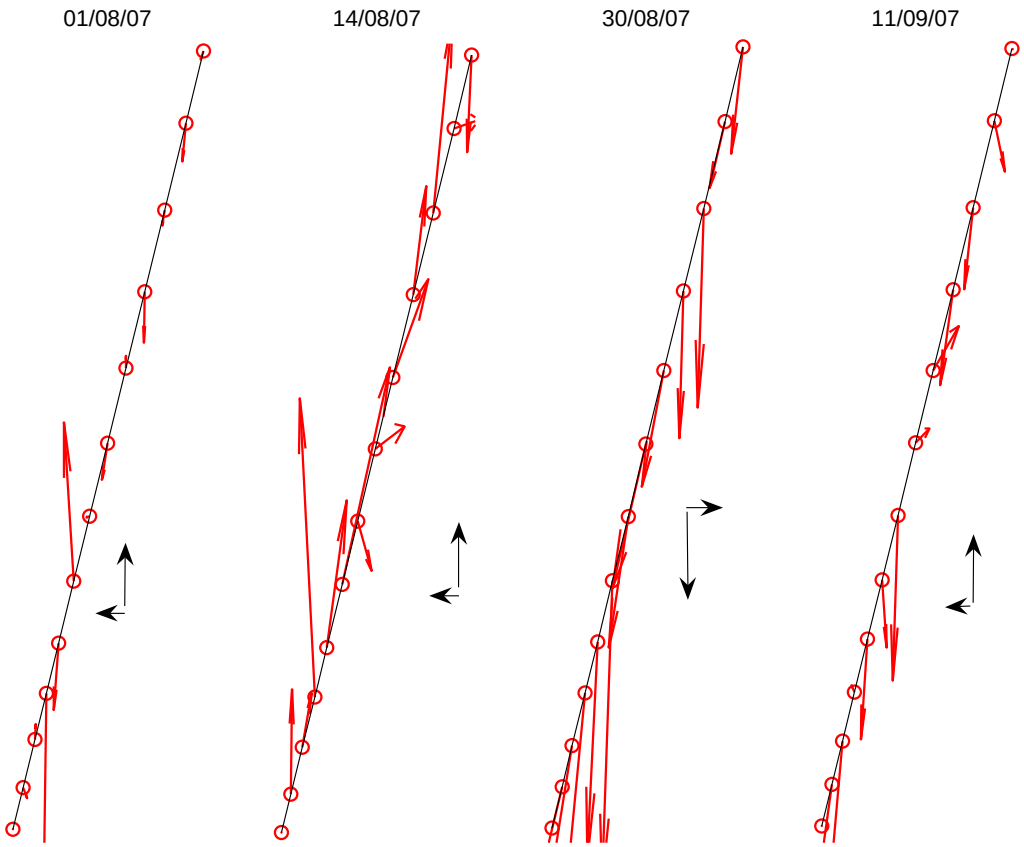

Fig. 8.18 *Resultant vectors drawn for each cross-shore sediment sampling station, from the central sediment sample station, using only information on relative sorting. Example data shown for late summer/autumn 2007. Dark arrows show the inferred sediment transport from the profile data set.*

remaining deficits or surpluses in the fortnightly sediment budget. The next two columns of Table 8.7 show the angular variance and the resultant vector length for the vector field generated from the GSTA analysis on the data from each survey. Angular variance $\rightarrow 1$ indicates a highly variable vector field, therefore a small resultant vector length. The number of vectors in each quadrant have been tallied with respect to the circular nature of the data, and are expressed as a percentage in the next four columns of Table 8.7. The final two columns house the **Z** test value for each vector field, and whether or not the data were random, as determined from the p value at α=0.05. Eight out of the twenty-four data sets tested generated a non-random distribution of vectorial trends, therefore these results only, reproduced in Table 8.8, are the subject of further discussion.

Tab. 8.7 *Results from GSTA, from left to right: survey date; net transport direction; circular variance; mean resultant vector length; %N; %S; %E; %W (as predicted by GSTA); Rayleigh **Z**-score for non-uniformity; Random/Non-random*

Survey	Net Trans.	Ang. Var.	Res. Length	%N	%S	%E	%W	Z score	Random?
06/11/2006	N+W	0.5001	0.4999	30.77	15.38	46.15	7.69	3.2489	N
21/11/2006	N+E	0.6905	0.3095	15.38	23.08	7.69	53.85	1.2454	Y
05/12/2006	N+E	0.5289	0.4711	30.77	7.69	46.15	15.38	2.8849	Y
20/12/2006	S+E	0.345	0.655	38.46	23.08	30.77	7.69	5.5782	N
04/01/2007	N+E	0.7056	0.2944	23.08	23.08	23.08	30.77	1.127	Y
21/01/2007	S+E	0.4279	0.5721	30.77	30.77	30.77	7.69	4.2546	N
04/02/2007	N+W	0.5329	0.4671	30.77	30.77	7.69	30.77	2.8366	Y
20/02/2007	S+E	0.7028	0.2972	7.69	30.77	38.46	23.08	1.1485	Y
06/03/2007	N+W	0.1863	0.8137	30.77	23.08	15.38	30.77	8.6069	N
19/03/2007	S+E	0.3837	0.6163	30.77	7.69	38.46	23.08	4.9384	N
03/04/2007	N+E	0.4168	0.5832	7.69	23.08	30.77	38.46	4.421	N
18/04/2007	S+W	0.6944	0.3056	38.46	46.15	7.69	7.69	1.2142	Y
01/05/2007	N+W	0.1192	0.8808	23.08	23.08	23.08	30.77	10.0862	N
19/05/2007	S+E	0.5571	0.4429	30.77	23.08	23.08	23.08	2.5504	Y
01/06/2007	N+W	0.5485	0.4515	53.85	23.08	15.38	7.69	2.6501	Y
14/06/2007	N+W	0.7018	0.2982	7.69	53.85	15.38	23.08	1.1559	Y
02/07/2007	N+W	0.6701	0.3299	15.38	23.08	30.77	30.77	1.4145	Y
14/07/2007	S+E	0.3456	0.6544	23.08	38.46	15.38	23.08	5.5668	N
01/08/2007	N+W	0.8058	0.1942	23.08	30.77	15.38	30.77	0.4902	Y
14/08/2007	N+W	0.946	0.054	46.15	23.08	23.08	7.69	0.0379	Y
30/08/2007	S+E	0.7279	0.2721	15.38	38.46	23.08	23.08	0.9623	Y
11/09/2007	N+W	0.6798	0.3202	15.38	30.77	15.38	38.46	1.3333	Y
30/09/2007	N+W	0.6823	0.3177	23.08	23.08	23.08	30.77	1.3118	Y
12/10/2007	N+W	0.7468	0.2532	30.77	15.38	23.08	30.77	0.8331	Y

The statistically significant results are re-tabulated in Table 8.8, where the percentages of trend vectors have been shaded with the dominant net transport directions as inferred from the profile record. In general it must be concluded that the GSTA technique failed

Tab. 8.8 *Statistically significant results from GSTA, from left to right: survey date; net transport direction; %N; %S; %E; %W (as predicted by GSTA). Shading corresponds to the directions implied by the field survey profile data.*

Survey	Net Trans.	%N	%S	%E	%W
06/11/2006	N+W	30.77	15.38	46.15	7.69
20/12/2006	S+E	38.46	23.08	30.77	7.69
21/01/2007	S+E	30.77	30.77	30.77	7.69
06/03/2007	N+W	30.77	23.08	15.38	30.77
19/03/2007	S+E	30.77	7.69	38.46	23.08
03/04/2007	N+E	7.69	23.08	30.77	38.46
01/05/2007	N+W	23.08	23.08	23.08	30.77
14/07/2007	S+E	23.08	38.46	15.38	23.08

to classify the net transport direction in any systematic manner. Only one third of the vector fields through the year showed a statistically trend (Table 8.7), and out of the these, only two showed good or reasonable agreement with observed sedimentation patterns (Table 8.8). Further, a circular correlation between mean transport direction (as determined by GSTA) and mean wave direction yielded r=0.2740, which with a **t** value of 1.3 was statistically insignificant at p=0.19.

The sorting trend vectors results in full are tabulated in Table 8.9. Using this approach, fifteen out of the twenty-four data sets tested generated a non-random distribution of vectorial trends. Comparing the sum percentage of vectors in the two dominant transport directions for each survey period, out of these fifteen statistically significant vector fields, twelve collectively accounted for $\geq 50\%$ of the vectors, and out of these, six of these accounted for $\geq 66\%$. Thus the sorting vector model out-performed the GSTA model both in terms of randomness, and in the proportion of correct identifications for the sediment transport pathways.

8.4 Discussion

The log-hyperbolic model enjoyed a consistently good fit to the sieved samples, and the shape triangle proved to be a helpful classifier of distributional shape. In addition, the cloud of samples plotted on a Craig diagram (which plots ordinary skewness against another parameter which is dependent on both skewness and kurtosis) was found to display similar attributes to the hyperbolic shape triangle, suggesting that further work could (empirically or theoretically) reveal the relationship between the two, perhaps

Tab. 8.9 *Results from trend analysis based only on sorting, from left to right: survey date; net transport direction; circular variance; mean resultant vector length; %N; %S; %E; %W (as predicted by GSTA); Rayleigh **Z**-score for non-uniformity; Random/Non-random*

Survey	Net Trans.	Ang. Var.	Res. Length	%N	%S	%E	%W	Z score	Random?
06/11/2006	N+W	0.52	0.47	8.3	41.6	33.3	16.6	2.68	Y
21/11/2006	N+E	0.70	0.29	30.76	38.46	15.38	15.38	1.12	Y
05/12/2006	N+E	0.39	0.60	25	25	8.3	41.6	4.34	N
20/12/2006	S+E	0.03	0.96	33.3	33.3	16.6	16.6	11.23	N
04/01/2007	N+E	0.12	0.87	33.3	8.3	16.6	41.6	9.20	N
21/01/2007	S+E	0.41	0.58	25	25	50	0	4.0741	N
04/02/2007	N+W	0.36	0.63	25	16.6	41.6	16.6	4.79	N
20/02/2007	S+E	0.78	0.21	33.3	25	25	16.6	0.53	Y
06/03/2007	N+W	0.30	0.69	25	16.6	16.6	41.6	5.72	N
19/03/2007	S+E	0.17	0.82	25	16.6	25	33.3	8.24	N
03/04/2007	N+E	0.22	0.77	41.66	33.3	8.3	16.6	7.13	N
18/04/2007	S+W	0.19	0.80	25	25	16.6	33.3	7.86	N
01/05/2007	N+W	0.67	0.32	58.3	16.6	16.6	8.3	1.24	Y
19/05/2007	S+E	0.40	0.59	25	33.3	16.6	25	4.22	N
01/06/2007	N+W	0.57	0.42	0	16.6	50	33.3	2.18	Y
14/06/2007	N+W	0.44	0.55	0	23.07	30.76	46.15	4.06	N
02/07/2007	N+W	0.14	0.85	58.3	8.3	8.3	25	8.71	N
14/07/2007	S+E	0.73	0.26	33.3	8.3	50	8.3	0.82	Y
01/08/2007	N+W	0.70	0.29	25	25	16.6	33.3	1.07	Y
14/08/2007	N+W	0.22	0.77	25	25	8.3	41.6	7.14	N
30/08/2007	S+E	0.02	0.97	16.6	41.6	25	16.6	11.45	N
11/09/2007	N+W	0.04	0.95	8.3	33.3	16.6	41.6	10.86	N
30/09/2007	N+W	0.81	0.18	46.15	0	23.07	30.76	0.42	Y
12/10/2007	N+W	0.67	0.32	16.6	25	50	8.3	1.27	Y

circumnavigating the need for the un-parsimonious log-hyperbolic model for use in sedimentary classification. Sedimentology has a large body of work based on graphical measures [Bartholdy et al., 2007] for a number of different types of sedimentary environments, so it would seem counter-productive to resort to models with more parameters for individual or sets of samples where ordinary graphical measures would do. The Craig diagram has not enjoyed widespread popularity amongst sedimentologists for classification purposes, and it would appear it could warrant further employment, however it will not in isolation reveal any further information on *why* distribution shapes change with relation to hydrodynamic and morphodynamic forcing on beaches. Such a situation could in theory be realised if a model for the changing distributional shape of sediment samples could be empirically (and consistently) related to observed changes in sedimentation. The only existing model to the authors knowledge that is based on skewness and kurtosis (albeit scale and location invariant forms which do not linearly relate to those obtained by other means), is that of Barndorff Nielsen and Christiansen [1988], and this study represents the first to examine in detail the model's utility to the problem of detecting net sedimentation change from sedimentary parameters.

However, the shape triangle model has been shown to be a rather ambiguous predictor of the net sedimentation patterns of a gravel beach over individual tides, with the results obtained producing more questions than they do answers. For example, it is unclear why the ϵ parameter correlates reasonably well with Δz, consistently over three separate data sets for surface samples, but not for sub-surface samples. Equally, it is not clear why the κ parameter, in contrast, was found to have poor association, suggesting 'pure' or 'grain-dominated' sedimentation is of subordinate importance to 'power-law' or 'fluid-dominated' sedimentation. The results suggest that net positive sedimentation has a negative ratio of χ_{LH}/ξ_{LH}, and a net negative sedimentation has a positive ratio of χ_{LH}/ξ_{LH}, but that net sedimentation did not have a detectable influence on distributional shape, quantified for a given value of χ_{LH} by ξ_{LH}. This result is particularly intriguing, although it is not clear what exactly 'fluid-dominated' sedimentation should come to mean, since there was a consistent response in the relationship between ϵ sedimentation and morphological change irrespective of changing wave and tide conditions. It would appear 'sedimentation-dominated-sedimentation' would thus appear to be a more appropriate name, although the feedbacks involved are

not readily and independently verified.

The lack of accord between net morphological change and disturbance depths over individual tides with $-\epsilon$ trends in the sub-surface sedimentology (Tables 8.4 and 8.5) suggests that a very different process is in operation on the sub-surface sedimentology compared with the surface. It is likely that the disturbance depths are controlled by the migration of an active beach step, which is echoed by researchers on steep sand beaches [Jackson and Nordstrom, 1993; Anfuso, 2005]. It is unlikely for such a simplistic model to be able to reflect the passage of such a dynamic and rapidly migrating feature for two main reasons. Firstly, because net morphological change over the tide does not quantify well the dynamics of a feature which can pass into and out of the system, but leave no net morphological trace. Secondly, because the sedimentology of the beach step is distinct from the beachface, and possibly out of 'sedimentological equillibrium' [Bauer and Allen, 1995]. The complication of mixing pre-surface sedimentology and the specific sedimentology of a propagating morphological feature was perhaps far beyond the remit of the net sedimentation model. What is more difficult to explain is why, if $-\epsilon$ sedimentation of the surface samples reflected the morphological change rather well, the equivalent parameters were not reflected in the sub-surface samples relative to the DOD record. The disturbance depth was taken as the depth to which waves and currents disturb the bed, in this case over single semi-diurnal tidal cycles, determined on each relative to the previous bed level. Therefore, as Masselink et al. [2007] pointed out, any net erosion over that tidal cycle truncates the measured DOD, and it is perhaps this which accounts for the observed discrepancies.

Slapton is a graded barrier, but during 2006-2007 when the data used for this section was sampled, significant changes in that gradient, and even reversals, were common (Chapter 7). The test here was the utility of grain-size trend models to predict sedimentation patterns in a system so dynamic as a gravel beach, sampled fortnightly. Figure 8.14 showed snapshot of the alongshore trends in sedimentology in May 2007, suggesting a northerly transport FB- situation (type 1). However, subsequent detailed application of the technique showed that the model was unable to systematically predict the likely movement of sediments at the time-scale of interest. An underlying assumption in sediment trend modelling is that the probability of transport must increase monotonically as grain-size decreases [McLaren et al., 2007]. In very general terms, then,

since net northerly transport would implicate sediment sourced from the south, the south would be generally coarser than the north, and indeed that is generally true at Slapton. Beyond this macroscopic interpretation, however, application of the Gao and Collins [1992] technique to predict net sedimentation patterns between individual fortnightly surveys was not successful (Tables 8.7 and 8.8), and it is interesting to postulate why that might have been the case.

It could be argued that sediment trend analysis was not designed for the study site or substrate. Successful applications of the GSTA method have generally been on large-scale coastal systems, mainly estuaries. However since gradients in parameters such as size and sorting were frequently much stronger with distance, the suitability of the scale of the study site (4.5km) is perhaps not a key factor in the failure of the models. The Gao and Collins [1992] method was chosen over the McLaren and Bowles [1985] method because the former is supposed to be better suited to bi-directional current and sediment transport situations.

The likely reason for failures of sediment trend modelling in this instance are unlikely to be methodological: the model works on relative rather than absolute changes in grain-size distributions, so the methods employed to obtain the grain parameters, as long as they are consistent, should not affect the model's outputs. Similarly, modifications have been suggested to the way the characteristic distance is determined, the space over which sediment parameters can be mutually-affecting, some logical [Le Roux, 1994*a*], others statistical [Lucio et al., 2006; Poizot et al., 2006]. Whilst improvements in this area are likely to improve the models from a theoretical point of view, they are unlikely to have made a significant difference to the results obtained in this study. The 'radial' method of Le Roux [1994*a*], for example, is unsuitable when the ratio of the sample distance in the alongshore and cross-shore is so high. As discussed in Chapter 7, geostatistical models such as employed Lucio et al. [2006] and Poizot et al. [2006] would not have improved the vector calculations because the spatial independence in the data was so small (variogram sills were reached almost immediately). Since one would model sediment transport, in a serious application, based on the strength of the non-dimensional vector output from the model, in effect the model's outputs should be treated as largely qualitative, designed to substantiate claims and fill knowledge gaps as part of a multi-faceted study. Since the utility is largely qualitative, the basic premises

behind the approach must be correct, otherwise there is little use for this class of modelling.

The question of whether gravel-sized sediment is suitable for sediment trend analysis is perhaps much more pertinent. GSTA may not suitable for gravel sized sediment, however any reason for that would not likely be methodological, since the techniques use only relative differences between the grain-size parameters. Sediment trend techniques require that the sediment sample is adequately described by statistical moments of its distribution, and whilst one cannot state with certainty that was the case, the use of sedimentary parameters have been shown in previous chapters to be useful in sedimentary discrimination. It is more likely, therefore, any failure of GSTA simply because the substrate used was gravel, would be because of the fundamental transport behaviour of gravel in the nearshore.

In the GSTA model, the two rules tested share an improvement in sorting in common, whereas coarsening/fining can co-vary with more negative/positive skewness. The relationship between transport direction and sorting is therefore a 'universal', and the connection between transport direction and either size or skewness varies. While it is well established that in the direction of sediment transport, the sediment sorting improves due to selective sorting [Krumbein, 1938; Inman, 1949], on gravel beaches the probability of coarse grains being deposited from sediment in transport is not necessarily greater than fine grains, as is demonstrated by the principle of overpassing (see chapter 2). GSTA assumes that the probability for deposition is greater for coarser grains than for fine grains, and this assumption is too simplistic for a gravel beach, where the opposite is often the case. The first case tested by the GSTA model (FB-) is interpreted as being a low energy regime, because the sediments are fining (there is insufficient energy to carry coarser sediments, which therefore travel shorter distances). Detailed data in neither chapter 5 nor 6 would generally support such an assertion, or at least this is not systematic. Intuitively, and averaged over a longer term, one might find a case for this general statement. However, the second case (CB+) is termed the 'high energy' case because sediments coarsen in the direction of transport. This situation allows coarse grains to be transported while finer grains are left behind. A plausible physical explanation is that 'armouring' or 'overpassing' or both, has occurred at the source location, more efficiently trapping the underlying layers of finer material.

Beach researchers are less consensual with regards to the changes in the size and skewness than they are over sorting. For example, beach sediments have been observed to both become finer [Self, 1977] and coarser [McCave, 1978] in the direction of predominant transport. Individual landforms on the study site in question have been shown in previous chapters to be associated with particular sedimentologies, but linking sedimentation patterns with surface (and sub-surface) sedimentology has proved difficult. Skewness has been used to effectively discriminate between depositional environments (for example the use of bi-variate diagrams of sorting versus skewness to discriminate beach, river and dune deposits has been explored repeatedly, [Stewart, 1958; Friedman and Sanders, 1978; Friedman, 1979], yet shows little sensitivity to transport direction at the sedimentary sub-population level. The difficulties discussed by McLaren et al. [2007], Le Roux and Rojas [2007], and others, are largely methodological, discussing sample spacing, preparation, analysis almost as if they were of equal importance to the physical processes underlying the assumptions in the model. There has remains very little published work which has directly, and experimentally, addressed the validity of the basic tenets of the models' approach.

McLaren and Bowles [1985] and Gao and Collins [1992] only consider cases *FB-* and *CB+* for sediment trend analysis; however, net sediment transport pathways are not the only factor involved in generating spatial patterns in sediment characteristics. For example, the variation in sediment transport pathways may have a much greater role. In addition, sediment mixing by waves has shown to be significant on Slapton, especially through the passage of dynamic features such as the step and berm. Groundwater is another key, but yet largely unexplored, consideration on the nature of sediment assemblages on gravel beaches. Sub-surface sediment data presented in Chapter 6 showed that sediments buried at depth could be substantially different from surficial sediments. In fact on occasion sediments can vary more over centimetres at depth, than tens of metres over the surface. Consequently, net sediment transport may actually be of subordinate importance when compared to other factors. On the evidence of data presented here and in chapters 5, 6 and 7, the rules of the GSTA model are probably too simplistic for application on a gravel beach.

The GSTA approach assigns equal importance to size, sorting and skewness parameters in determining the likely transport vector field. In the nearshore, perhaps,

there has not been enough research on sediment transport from the viewpoint of changes in grain-size distributions to know whether this assumption is unreasonable, however what is known is that there is a non-linear relationship between the three parameters in a grain-size distribution Jones [1971]; Flemming [2004]; Bartholdy et al. [2007]. The better results obtained by trend vectors based on sorting alone would suggest that sorting should have a dominant weighting in trend vector models, since placing equal importance on size and skewness tends to lead to more incorrect predictions.

8.5 *Summary*

(i) The closest equivalent classification system to the log-hyperbolic shape triangle which uses ordinary sample moments, the Craig Diagram [Leroy, 1981], was found to be a potentially useful pre-indicator of log-hyperbolic model fit.

(ii) The majority of samples were classified on a Craig diagram as 'bell shaped', and represented slight deviations from Gaussian. It was suggested that log-hyperbolically distributed samples plot between δ_t=0 and δ_t=-1, and thus the Craig diagram could be used as pre-indication of whether the (rather less parsimonious, numerically less stable and difficult to code Jensen [1988]) log-hyperbolic model would provide a better fit to measured size-frequency distributions of beach gravels.

(iii) The distributional forms classified by the Craig diagram possibly map directly onto the parameter space of the hyperbolic model, opening the future possibility that directly determining χ_{LH} and ξ_{LH} by fitting log-hyperbolic distributions to data could be circumnavigated. However, much more work would be needed to verify and explore this.

(iv) The use of the hyperbolic shape triangle as a predictor of recent net sedimentation on a gravel beach when used with surface samples (but, interestingly, not sub-surface samples) was found to be promising in some respects, but ambiguous in others.

(v) Correlations between mean morphological change and shift in mean χ_{LH} position over individual tides (termed r_ϵ, representing Barndorrf-Nielsen and Christiansen's (1988) ϵ, or 'fluid controlled' erosion/deposition) were between 0.53 and 0.62 for all tides, and between 0.57 and 0.76 for tides where net mean morphological change over individual tides was $\geq \pm$ 5cm.

(vi) However, mean morphological change and shift in mean ξ_{LH} position over individual tides (termed r_κ, representing Barndorrf-Nielsen and Christiansen's (1988) κ, or 'grain controlled' erosion/deposition), did not correlate well.

(vii) The systematic predictions made about how mean size and sorting would behave

under net ϵ and κ erosion/deposition were unverified. This aspect of the model is probably too simplistic for a nearshore environment.

(viii) A partial correlation analysis revealed that variation of κ did not have an effect on the correlations observed between Δz and $-\epsilon$. Thus it can be confirmed in this study that the ϵ and κ parameters respond to two different morpho-sedimentary processes, as stated in the model.

(ix) The fact that ϵ erosion/deposition correlated well for surface samples but not sub-surface samples was an interesting finding. It was concluded that in this instance the sub-surface samples were perhaps a compound function of antecendent surface sedimentology and the passage of the beach step, a secondary morphological feature which passed through the measurement area with each semi-diurnal tide. The complication of mixing pre-surface sedimentology and the specific sedimentology of a propagating morphological feature was perhaps far beyond the remit of the net sedimentation model.

(x) The findings suggest that variations in skewness are more useful in discerning morphological change than kurtosis, in either graphical or location/scale-invariant forms, but that the bi-variation of these two parameters may still deserve further exploratory research in a range of environments.

(xi) The sediment trend model was applied with less success, and this work adds to a growing literature which has called into question the utility of the technique [Flemming, 1988; Masselink, 1992; Guillen and Jimenez, 1995; Masselink et al., 2008]. This is perhaps because the rules upon which the model is based are too simplistic for application on a gravel beach.

(xii) Trend vectors based on sorting alone, however, out-perform a traditional sediment trend vector approach. This implies that sorting should have greater weighting in the GSTA model.

(xiii) Kurtosis is rarely used in process-based sedimentological studies, especially on beaches, because of ambiguity surrounding its physical relevance. Consequently, no sediment trend model includes kurtosis as an indicator of spatial sediment transport gradient. A recent study by Bartholdy et al. [2007], however, has

suggested that the kurtosis parameter of the log-hyperbolic distribution, ξ_{LH}, is much less sensitive than kurtosis as derived by the moments method to small and insignificant changes in the size-distribution, and therefore may warrant inclusion into sediment trend modelling. The apparent success here of a model based on the bi-variation of kurtosis and skewness would support Bartholdy et al. [2007]'s findings.

9 DISCUSSION & SYNTHESIS

You'll never find your gold on a sandy beach.

Jim Steinman (1947 —), from 'Two Out Of Three Ain't Bad', sung by Meatloaf.

9.1 *Introduction*

Coastal morphodynamics can no longer be understood and explained as a unified and cohesive whole, even by specialists. This is in part because the subject warrants ever more detailed treatments: the need for deterministic explanation forces researchers to specialize within sub-disciplines of increasingly narrow focus to obtain satisfactory insights. Every generation of coastal geomorphologists has to look at the fundamental research questions of their discipline in the light not only of fresh and expanding scholarship, but of contemporary societal preoccupations. This study on gravel beaches has been carried out very much within this context; immediately before and during the course of the study, several research articles have appeared on coarse particle transport under waves and oscillatory currents, gravel beach groundwater dynamics and morphological change. Contributions have been received by leading international journals from engineers and mathematicians, as well as geomorphologists/geologists and oceanographers, in nearly equal number. They are mining a largely untapped seam of scholarship not only because it is academically challenging and interesting, but also because of a real societal need for our understanding of coarse-grain coastal depositional landforms to improve (related to beach nourishment, sea-level rise, and sedimentation prediction for logistic and military purposes - see Chapters 1 and 2). As a scientist, it is

important not to be over-impressed by the volume of material published in certain narrow fields, where new material and enthusiasm over ideas and techniques may result in an intensification of detailed knowledge without disclosing much of general interest. It was felt that in the field of gravel beach morphodynamics, researchers to date had overseen the importance of the beach's sedimentology, and thus work was undertaken to start to redress this fact.

There was another, at present more esoteric, motivation for this study: within-beach trends in grain-size are often hard to discern, thus the sedimentology of secondary morphological features, and the spatial differentiation of sedimentary properties on beaches, remains poorly understood. Consequently, little is known about how the sedimentology of beachfaces respond to changing sedimentation patterns through time, and indeed whether it is even possible to detect phase-locked responses in morphological and sedimentological change on beaches over short time-scales. It is often assumed that changes in sediment size and sorting (etc) are merely the product of morphological change or net sedimentation. Accordingly, beachface sedimentology is granted little or no role as a forcing agent in beachface morphodynamics, known to be dominated by strong feedbacks between hydrodynamic forcing and morphological change. A number of recent researchers, however, have postulated that significant changes in sediment properties in response to morphological change may not only be detectable, but indeed may even have some morphodynamic role [e.g. Nicholson et al., 2003*b*; Gallagher and McMahan, 2006]. Such ideas on gravel beaches are even older [Carter and Orford, 1984; Sherman et al., 1993], and were summarised in Chapter 2 under the idiom 'morpho-sedimentary-dynamics'. Until now it has never, been demonstrated convincingly that both, or either, temporal and spatial variations in sediment size are strongly related to morphological change. The gravel beach foreshore served as an ideal setting to examine this relationship, which traditionally receives poor coverage in morphodynamic experiments.

The thesis objectives were outlined in Chapter 1. One of the principal aims of the investigation was to develop a conceptual framework which allowed for the possibility that sedimentological characteristics have additive and/or independent controls on morphodynamics (Chapter 2). To do this, the current understanding and possible future directions of gravel beach morphodynamics and sediment dynamics had to be

comprehensively reviewed. The study was empirically-based, and drew on data-driven (geo-statistical/phenomenological) models (Chapter 1) to uncover any relationships between morphodynamics and sediment dynamics. Both gravel beach sedimentological and morphological changes are ultimately forced by hydrodynamic conditions, so data-driven models should not alias hydrodynamic forcing. Previous efforts in this area therefore would have interpolated sediment and morphological data has to be to the frequency of the hydrodynamic data. However, by doing so the basic question could not be answered, therefore this study required information on both morphological and sedimentological change at a comparable resolution and sample frequency. In order to do this, the development of methodologies which enable the quantification of sediment characteristics from digital images of the bed (Chapter 4) was crucial, thus a lot of time was devoted to methodological advances in this area, as well as proper validation and sensitivity procedures. Morphological change and sediment dynamics on a gravel beach were investigated at three broad scales, each of which are detailed in separate chapters (5 to 7). The final objective was to establish a link between beachface sediments and morphological change. Whilst this has already been a consistent theme throughout the thesis, individual chapters have discussed the relationship only in terms of the temporal and spatial scale relevant to the chapter. In this chapter, an attempt is made to integrate observations of the relationship between morphological and sedimentological change over all scales studied, as well as discuss the potential implications of them.

9.2 *Sedimentology and net sedimentation patterns*

Sediment size has been invoked to partially explain the development of gravel beach features such as the berm [Masselink and Li, 2001; Austin and Masselink, 2006*a*], and cusps [Sherman et al., 1993]. The observed persistence of coarse sediments at the step [Miller and Ziegler, 1958; Bauer and Allen, 1995] would also suggest that sediment size has morphodynamic implications in the region of wave breaking. Indeed, previous studies have suggested that sediment size and morphological change have a co-variability which may reinforce individual distinct morphological features, and sediment transport characteristics through those features, through feedback processes [Sherman et al., 1993; Tolman, 1994; Rubin and Topping, 2001]. However, it is unclear from previous beach

morphodynamic studies whether morphological change (or net sedimentation pattern) leaves a sedimentological imprint. Liu and Zarillo [1993] and Masselink et al. [2007] found no such relationship on sand beaches, whilst Medina et al. [1994] and Bartholdy et al. [2002, 2005] did claim such an association. This uncertainty is in spite of the common practice of inferring gradients in sediment transport directions from the spatial arrangement of grain-size statistics [McLaren and Bowles, 1985; Gao and Collins, 1992].

There is disagreement between those authors who believe that changes in grain-size do not remain correlated through time [Davis, 1985; Liu and Zarillo, 1993; Masselink et al., 2007], and those that believe there to be a temporal correlation or 'persistence' in sedimentary data [Losada et al., 1992]. The intermediate case is that morphological change results in a spatial variability in grain-size which displays temporal persistence, but that these are stochastic variations about a 'master' (or time-averaged) grain-size distribution [Medina et al., 1994; Guillen and Palanques, 1996]. The latter two cases potentially allow grain-size characteristics to have a morphodynamic role, in order to partially explain morphological change.

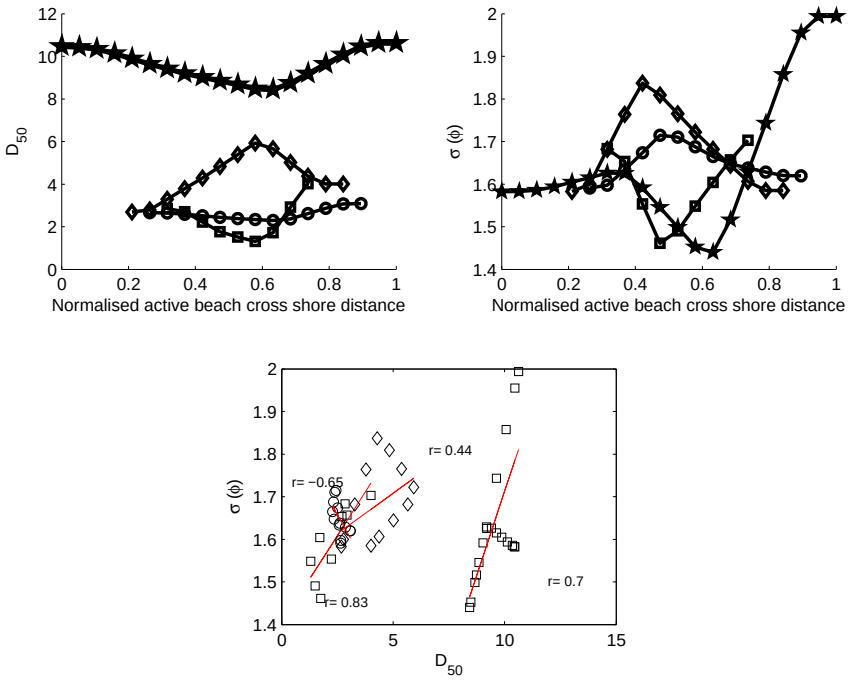

Fig. 9.1 *Sediment size (**upper right**) and sediment sorting (**upper left**) as a function of normalised active beach cross shore distance (increasing seawards). Data from the surveys taken over individual tidal cycles. On upper panels, solid lines show the mean of data per normalised cross-shore location, increasing seawards. **Bottom panel**: the relationship between mean cross-shore sorting and mean cross-shore size.*

According to Figure 9.1, spatial trends can be obtained at relatively short timescales. The trends are not consistent between surveys (sediment size, for example, was finest in the mid-foreshore on three occasions, but coarsest during the other survey - Figure 9.1, top left), but the relationship between the spatial trend in mean size and the spatial trend in mean sorting is usually good (Figure 9.1, bottom). However, clear trends are apparent in neither sediment size nor sorting, over the time-scale of one year (surveyed every fortnight, Figure 9.2) or over one sprng-spring tidal cycle (surveyed every low tide, Figure 9.3). Trends are not apparent as a function of absolute cross-shore distance either (not shown). Other studies based on very large number of samples have also found a surprising lack of cross-shore trends on gravel beaches [e.g. Gleason et al., 1975; Jennings and Shulmeister, 2002] and mixed-sand-gravel beaches [e.g. McLean, 1970]. The 'master' grain-size distribution for Slapton (time-averaged - see Figures 9.2 and 9.3) shows very little spatial structure, in marked contrast to similar curves found for sandy environments [e.g. Medina et al., 1994; Guillen and Hoekstra, 1997]. Since Slapton is macrotidal, the sediment size must be viewed as a function of normalised active beach location (zero and one being the landward and seaward limits, respectively, of the intertidal profile on the survey day).

On the available evidence, therefore, not only is the variation in grain-size considerable on Slapton (the standard deviation is often close to the mean), but it isn't even a stochastic fluctuation about a 'master' grain-size distribution which shows any clear spatial structure. Guillen and Hoekstra [1997] and Li et al. [2006] termed the temporally-averaged grain-size distribution the 'equilibrium' curve (to be determined using ≥ 1 year data), and it was interpreted as varying as a function of average hydrodynamic conditions at each location. They believed that this signature can be used to predict the cross-shore redistributions that would be the result of a beach nourishment. The same equilibrium curve has not been found at Slapton, for mean size or any percentile of the distribution [e.g. Medina et al., 1994], possibly because the tide smooths any spatial trends, or perhaps because the beach is as dependent on alongshore as cross-shore sediment transport processes. Both could explain why trends are more readily discerned over shorter time periods.

The tendencies for increasing grain-size up the beach face in the landward direction reported by some authors [e.g. Bascom, 1951; Shepard, 1963; McLean and Kirk, 1969;

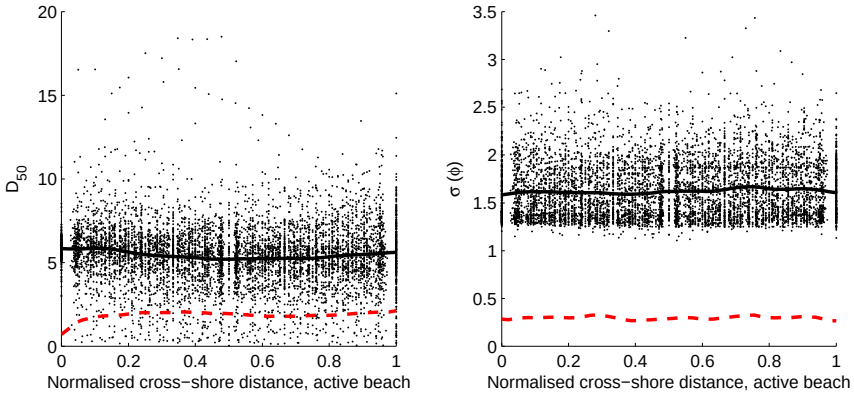

Fig. 9.2 *Sediment size (D_{50}, **left panel**) and sorting (σ, **right panel**) as a function of normalised active beach cross shore distance (increasing seawards). Data from the fortnightly surveys taken over one year. Solid and dashed lines show the mean and standard deviation, respectively, of data per normalised cross-shore location.*

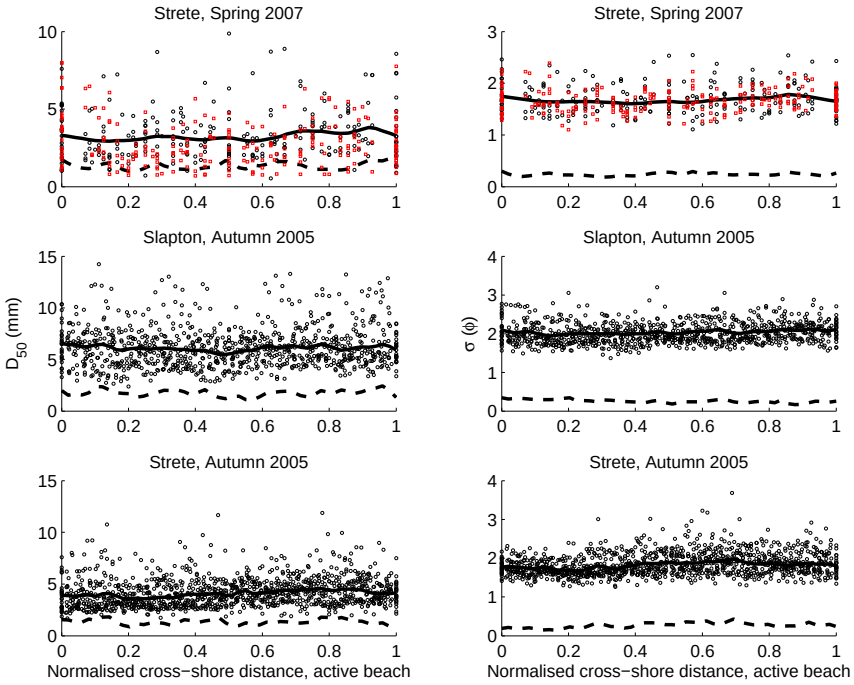

Fig. 9.3 *Sediment size (**left panels**) and sediment sorting (**right panels**) as a function of normalised active beach cross shore distance (increasing seawards). Data from the twice-daily surveys taken over two spring-spring tidal cycles. On upper panels, circles represent surface samples, and squares represent sub-surface samples. Solid and dashed lines show the mean and standard deviation, respectively, of data per normalised cross-shore location.*

Horn, 1992] have not been found in this study. Instead, the cross-shore profile of sediment was highly variable, so much so that it is difficult to say what the typical cross-shore profile of sediment size should be. Researchers have always assumed they can, theoretically or at least heuristically, account for spatial trends and changes in grain-size sorting. Models for grain sorting tend to be of the 'equilibrium' type, i.e. that every grain-size has a cross-shore location where it is in equilibrium with the conditions there. Miller and Ziegler [1958] developed a model for grain-size sorting on a sand beach which assumed that the smallest particles are entrained longest, therefore travel the furthest, leaving a lag deposit seawards to the breakers of increasing sediment size. As has already been discussed, the assumption that the finest travel furthest may also be violated on gravel beaches, which perhaps partially accounts for the general failure of the sediment trend modelling in Chapter 8.

Notably, the difference between the mean and standard deviation, as expressed as a percentage of the mean (coefficient of variation - note that the mean and standard deviation have the same units so a comparison between D_{50} and ϕ is valid) is always much smaller for sorting than that for sediment size. Sorting is perhaps a more useful parameter than size for identifying recent trends in sedimentation, borne out by the EOF analysis in Chapter 6, and perhaps in the ability to use the spatial gradients in sorting to find reasonable association with directional trends in sediment transport (Chapter 8). The idea that sorting may be a better indicator of morphodynamic processes echoes the sentiments of Bagnold [1954] and Bagnold and Barndorff Nielsen [1980*a*], who stated that it is the relative abundance of particles in different size fractions that is more important in sedimentation.

The relationship between beachface morphodynamics, sedimentology and wave 'energy' is scale-dependent. The greatest degree of morphological change on a gravel beach over a relatively large scale is not necessarily found where the most energy occurs, just like on sand beaches [e.g. Masselink et al., 2007]. For example, in Chapter 7, the most amount of energy on Slapton over the study year should have been at Torcross at the southern end, under the influence of the predominantly south-westerly waves [Holmes, 1975]. However, the greatest amount of both change and erosion was in the centre of the beach, because of the dominance in alongshore transport processes over this time-scale. Equally, on a shorter time-scale, the secondary morphological features are

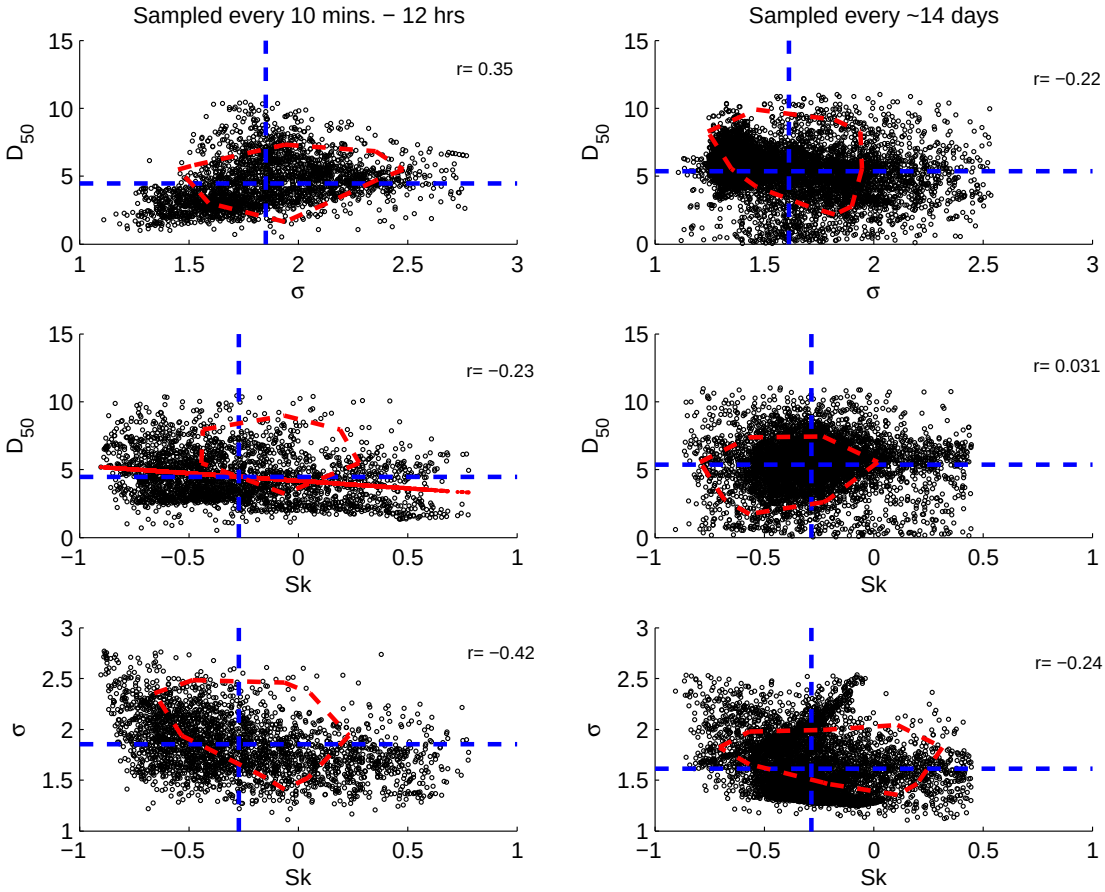

Fig. 9.4 *Relationship between sedimentary parameters.* ***Left panels****: all samples collected at a frequency of minutes to hours.* ***right panels****: all samples collected at a frequency of 2 weeks. The r-value quoted is an ordinary (linear) correlation coefficient. The dashed horizontal and vertical lines represent the mean values. The area within the contoured dashed lines represents the parameter space where at least 20% of observations plot, based on the joint probability distribution.*

not necessarily associated with the greatest amount of energy. Cusps and berms, for example, being associated with times and spaces, respectively, of relatively low energy; and steps being associated with greater wave energy. Mean size is expected to increase commensurately with energy [e.g. Bascom, 1951; Ingle, 1966; King, 1972], although not always [e.g. Engstrom, 1974]. The sedimentology of Slapton is similarly ambiguous with regards to energy: the coarsest section of the beach during 2006-07 was the one associated with greatest net depletion. The coarsest regions of the beach during the short-term experiments (Chapter 5) were the step and berm. During the fortnightly campaigns (Chapter 6), the beach either fined under relatively large waves (as in the Strete 2007 data set), or coarsened (e.g Slapton 2005 data set).

The difference between the relationships found between size and sorting over relatively short (Figure 9.4, top left) and relatively long (Figure 9.4, top right) time-scales is probably due to the fact that the shorter-term measurements include both breaker zone and intertidal sediments, thus including sediments from the step which has been shown to be quite a distinct sedimentary environment (Chapter 5). Interestingly, the relationship between sorting and skewness, overall the strongest, is similar irrespective of scale (Figure 9.4, bottom panels).

This study has shown that the relationship between morphology, or morphological change, and sedimentology, perhaps has a relationship that cannot be expressed by averages. It has also gone some way to show, based on a number of very large data sets, that if there is any morpho-sedimentary co-variation on gravel beaches such as Slapton, it is distinctly non-linear in character. Surficial sediment size has been shown to be a highly stochastic variable. In the past, researchers have attributed the large degree of sedimentary variability they have observed to either anthropogenic influences [e.g. Guillen and Palanques, 1996], or because of the variable influence of sediment supply [e.g. Engstrom, 1974; Jennings and Shulmeister, 2002]. On Slapton the absence of a 'supply' issue, *sensu stricto*, may be substituted by alongshore redistributions of material.

This sedimentary variation may impose another layer of nonlinearity to cross-shore-dominated beach morphodynamics in the short-term. Alternatively, it may be an emergent property of the morphodynamic system. It may or may not have practical importance to morphodynamic models of beach change. On the one hand then, because of the variability of surficial grain-size on Slapton (naturally a relatively well

sorted gravel beach - see Chapter 3), the sampling resolution, at all scales studied, may have built up a picture which is a gross parody of the real case. This might imply that even the number of samples taken may not have been enough to characterise the beach, or in other words, aliasing has occurred. The principle of diminishing returns may also apply, in that there comes a point where taking more samples does not give the sampler a commensurate increase in knowledge. Indeed, it would be valid to say that s/he just widens his/her error bars. However, without taking so many samples, how would one know how capricious the surficial sediment size is? That consistent patterns in time and space did not arise does show the stochasticity of surficial sedimentology, and in itself may be an important demonstration. For example, it does yield a robust average and associated variation around the mean, which is useful for modelling (see this chapter's final section).

Hardly any sedimentological paper has dealt with the topic of errors in sediment sampling and aliasing, partly because the data sets required are not extensive enough. This topic has recently been highlighted by Hartmann [2007] as being crucial for further work, but he makes the important point that in order to know how many samples are required for a given area and environment, a certain relationship between the population of grains and the processes in operation upon them must be assumed *a priori*. The same point was made by Ferguson and Paola [1997] in reference to sampling of fluvial gravels, and it is not easily circumnavigated.

Chapter 7 compared modelled net annual longshore sediment rates at Slapton between 1999 and 2002 [Chadwick et al., 2005] with rates derived from the measured profile record. The modelled rates tended to be greater than the 'measured' rates by up to several orders of magnitude. The failure of the model in this instance were perhaps due to an inappropriate characterisation of grain-size, but it is more likely in this case that the failures were due to not calibrating the model, or inappropriate characterisation of the physics of coarse-grain transport, or due to a compound modelling problem, thus propagation of errors. One might argue, on the grounds of regression to the mean, that a constant grain-size is more appropriate when it has been shown that grain-size is so stochastic. The problems arise when you get that mean wrong and, in many ways unfortunately, the more samples you take the better that characterisation is going to be. However, a constant grain-size is not better than a perfect characterisation of grain-size

at all spatial and temporal scales when sediment transport is a non-linear function of sediment size. Models should be inproved to incorporate such information.

That surface sediment size is such a stochastic parameter which appears to poorly preserve a record of recent hydro- or morphodynamic processes, might be a 'mixed-blessing' for coastal managers who seek a representative grain-size for beach nourishment projects. Beach nourishment is important and on the increase, especially for coarse-grained shorelines [Komar, 2007]. The anticipated demand of England and Wales for the period 1995 to 2015 was estimated at 209M m^3 of gravel and 224M m^3 of sand [Hanson et al., 2002]. A crucial part of the design process is to determine suitability of beach fill material - which sediment do we dredge, how much to we dump, and how frequently [Stauble, 2007; Finkl et al., 2007]? Models are required which will both predict the likely volumes of borrow material required for the desired level of storm protection, and the suitability of the borrow material (i.e. how stable it will be in a given environment). The suitability of the borrow material depends strongly on its sedimentology, i.e. the collective properties of the sediment such as size (median size, but also the grain-size distribution) and sorting, density, etc. This is primarily because sediment transport processes are selective. The little information on natural variability of sedimentological properties of beaches, against which the characterisation of native beach sediment can be made to inform the suitability of borrow material, is currently, and understandably, perceived as being problematic [Horn and Walton, 2007].

However, this study, drawing on more than 8000 sediment samples over a range of time and spatial scales, has shown that the natural variability is enormous. In brief, there are non-linear and inconsistent relationships between sedimentary parameters; there is no spatial structure in sedimentary parameters when time-averaged; and there is little consistent temporal response when averaged over space, with respect to morphological change and hydrodynamic forcing. It may mean that, on beaches similar to the study site, assessing the suitability of the borrow material in relation to the indigenous material may be an impossible task without modelling the likely temporal changes in sedimentology, at present beyond the state of the art. Alternatively, it may mean that the sensitivity of the transport of beach sediment to its various sedimentological characteristics may be of subordinate importance to gravel beach fills compared with artificial sand beach replenishment. Since the sedimentology naturally varies so much, it

may be argued that relatively poor matches may be subsumed into the system, and detection of adverse changes as a result of the artificial material would be difficult, being within the envelope of natural variability. Whichever viewpoint is found to be correct in the fullness of time in the context of coarse-grain beach recharge, this study has gone some way to both increase the potential accuracy and reduce the margin for error in finding a stable beach fill material.

9.3 *Sediment size and beach gradient*

There are few sites and studies which have enough sediment samples to determine a 'master' grain-size. However, the relationship between the spatial variation in sediment size (some measure of central tendency) and beach slope is well documented, both in the field [Krumbein, 1938; Inman, 1953; Davis, 1985] and simulated in the laboratory [Bagnold, 1940]. This association is apparent on beaches of all sedimentary composition [Bascom, 1951; Shepard, 1963; McLean and Kirk, 1969; Horn, 1992; Hegge, 1994]. Indeed, the relationship between median sediment size and beachface slope is considered a fundamental principle of beach morphodynamics [Bascom, 1951; Sunamura, 1984; Komar, 1998], and in one study [Bagnold, 1940] it was found that slope of the foreshore depended only on the size of beach material.

The relationships between median sediment size and active intertidal beachface gradient (the gradient of the beachface from strand to shoreline on a given survey) are shown in Figures 9.5 and 9.6, for the fortnightly (Chapter 7) and twice-daily (Chapter 6) data sets, respectively. The fortnightly data set is shown both as the mean median sediment size versus gradient per profile (13) per survey (24): Figure 9.5 (left) shows that there is not a clear relationship. The same is true of smaller spatial subunits, e.g. lower foreshore and upper foreshore (not shown). This means that, at this time/spatial scale, the slope of the beach cannot impart information on its sediment size. Likewise, if you go to the beach on any given day and take a representative sample of the foreshore, it will give you little information about the beachface slope. A clearer relationship was found when the record from each profile line was averaged over time, to yield a size-slope relationship for each alongshore location (Figure 9.5, right). The association was positive, in accordance with the literature and, although not strong, was close to the

curve published by Shepard [1963] for coarse beaches, which indicates that Slapton is not an unusual gravel beach when sufficient averaging takes place. It is possible that a range of grain-sizes can give similar slopes, since the curve in the right panel of Figure 9.5 is fairly flat, and the range of slopes encountered in the left panel is only 3–4^o. The data also suggest that at time-scales shorter than one year, beach slopes are not in equilibrium with the sediment size. It is by no means a well-founded assumption that slope is the dependent variable, as depicted in Figure 9.5, however noting that grain-size the more stochastic parameter of the two it might be reasonably assumed that the change in slope over time is associated with a set of forcing conditions including size, but only at some lag.

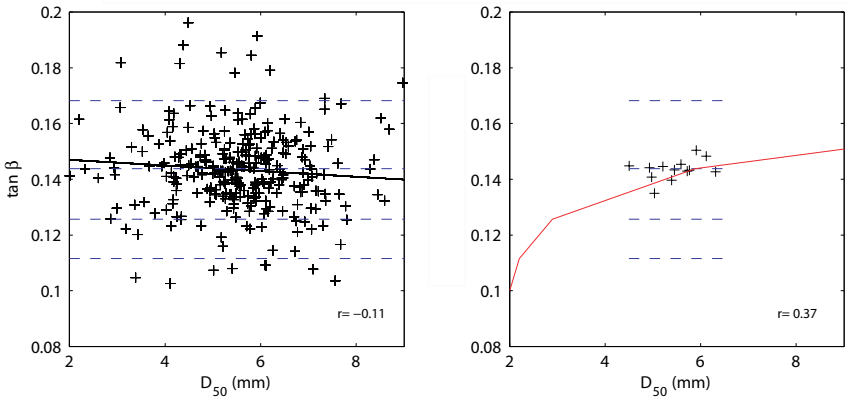

Fig. 9.5 *The relationship between sediment size and slope. Data from the fortnightly surveys (Chapter 7). Left panel plots individual cross-shore profile gradients versus mean median sediment size. Right panel plots this data from each cross-shore profile, averaged through time. Solid line on right panel shows the relationship obtained by Shepard [1963].*

The temporal structure of the correlations between median size and intertidal gradient were explored, by taking the (24-point) time-series of mean median size and slope, each cross-shore, of each regular survey line, and computing the correlation between them. The time-series were then divided into three, and the correlations for each segment were again computed. The results, in Table 9.1, show that more correlations significantly different from zero (shaded values) are found when the time-series is broken down into

smaller periods. The statistically significant associations during the first eight surveys, over the winter of 2006-07, showed a generally positive relationship between size and slope. The second, over the spring, were mainly negative. The third, over the summer and early autumn, were again negative. Fifteen out of fifty-two correlations were significant, and the majority of these came from the 2nd set of eight surveys.

Tab. 9.1 *Correlations between intertidal gradient and median sediment size*

km	0	.25	.5	.75	1	1.25	1.5	1.75	2	2.25	2.5	2.75	3
all	0.04	0.11	-0.26	-0.17	-0.19	-0.17	0.10	-0.25	-0.049	-0.46	-0.21	-0.10	0.038
1st eight	0.22	-0.058	0.04	0.27	0.38	-0.73	0.23	0.46	-0.077	0.33	0.47	-0.33	-0.21
2nd eight	0.42	0.50	-0.36	-0.15	-0.22	-0.41	0.19	-0.73	-0.45	-0.58	-0.32	-0.05	0.28
3rd eight	-0.11	0.33	-0.28	-0.52	-0.24	-0.15	-0.12	-0.069	-0.09	-0.54	-0.22	-0.11	-0.66

An identical analysis was carried out between sediment sorting and gradient, as seen in Table 9.2. Again, the statistically significant relationships have been shaded, and it is clear that, like with sediment size, better relationships are obtained when the year-long time-series is segmented into three distinct epochs. Sixteen out of fifty-two correlations were significant, and unlike sediment size, the majority came from the first and third set of surveys. Generally, therefore, when there was a significant association between sediment size and slope, there wasn't between sediment sorting and slope, and vice-versa. The statistically significant associations during the first eight surveys, over the winter of 2006-07, showed a generally negative relationship between sorting and slope. The second, over the spring, were mainly positive. The third, over the summer and early autumn, were again positive.

Tab. 9.2 *Correlations between intertidal gradient and median sorting*

km	0	.25	.5	.75	1	1.25	1.5	1.75	2	2.25	2.5	2.75	3
all	-0.058	-0.10	-0.13	-0.004	-0.059	0.047	-0.34	-0.159	-0.064	0.13	-0.045	0.14	-0.43
1st eight	-0.37	-0.27	-0.58	-0.23	-0.24	-0.074	-0.77	-0.62	-0.32	-0.62	-0.66	-0.14	-0.48
2nd eight	-0.36	-0.31	-0.27	-0.15	0.19	-0.003	0.13	-0.068	0.48	0.53	0.29	0.47	-0.34
3rd eight	-0.03	-0.15	0.49	0.50	-0.51	0.70	0.02	0.58	0.10	0.53	0.36	0.34	0.31

A partial correlation analysis of sediment size and slope, accounting for sediment sorting, was performed and the results are shown in Table 9.3. Twenty-three out of fifty-two correlations showed partial dependence, as defined by a reduction in correlation

by at least 0.05 (shaded). Ten out of the original fifteen statistically significant size-slope associations showed partial dependence on sorting, which corroborates the findings of McLean and Kirk [1969] regarding the influence of sorting on size-slope relationships.

Tab. 9.3 *Partial correlations between intertidal gradient median size, with the influence of median sorting*

km	0	.25	.5	.75	1	1.25	1.5	1.75	2	2.25	2.5	2.75	3
all	0.03	0.10	-0.32	-0.18	-0.21	-0.17	-0.11	-0.26	-0.06	-0.47	-0.22	-0.073	-0.13
1st eight	0.19	-0.10	-0.09	0.17	0.33	-0.73	-0.46	0.05	-0.09	0.54	0.81	-0.70	0.05
2nd eight	0.22	0.44	-0.71	-0.24	-0.14	-0.49	0.45	-0.85	-0.33	-0.60	-0.16	-0.15	0.20
3rd eight	-0.24	0.44	-0.22	-0.54	-0.29	-0.25	-0.12	-0.04	-0.11	-0.64	-0.27	0.0005	-0.61

The consistent theme thus far is that size-slope relationships are stronger at shorter time-scales, and this was further verified by a correlation analysis performed on the twice-daily survey data set. Figure 9.6 plots each of the four data sets which are the subject of Chapter 6. The difference between sub-surface and surface mean median sediment size and intertidal gradient was negligible. In general, the coarser the beachface the stronger the relationship between size and slope, although the relationship could be either positive (e.g. the Strete 2007 data sets), or negative (the Slapton 2005 data set).

That associations can be found between size and slope at a relatively large spatial and temporal scale (Figure 9.5, right) and at a relatively small spatial scale and temporal sampling frequency (Figure 9.6), but not readily at an intermediate sampling frequency (every two weeks, Figure 9.5 left panel), is interesting. It may be that, at a sample frequency of every spring low tide Slapton, as two-dimensional and convex in profile as any gravel beach, is dominated by net changes in alongshore sediment transport. This may account for the general breakdown in typical size-slope relationships at this time-scale. At shorter sampling frequencies, the measured profile is likely to dominated by cross-shore sediment tranport but net alongshore sedimentation may be small. Similarly, when data is averaged through time the influence of alongshore sediment redistributions may be negligible (note, however, that it may be responsible for the scatter observed at both time-scales).

Note that this is not the first study to find a negative association between sediment size and intertidal slope, but on sand beaches these can ordinarily be attributed to either very low energy or lacustrine environments [e.g. Engstrom, 1974; Cunningham and Fox,

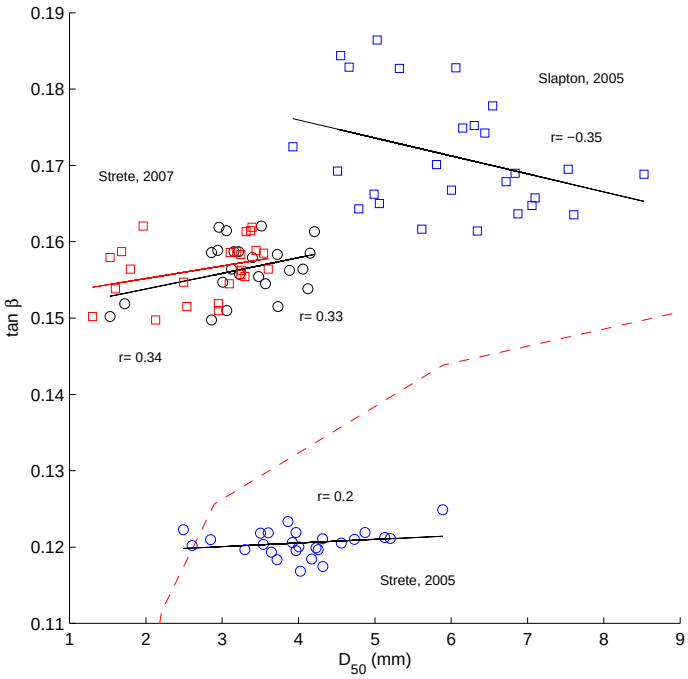

Fig. 9.6 *The relationship between mean median sediment size and slope. Data from the twice-daily profiles (Chapter 6). The circles and squares for the 'Strete 2007' data set represent surface and sub-surface samples, respectively. Dashed line shows the relationship obtained by Shepard [1963].*

1974] or the presence of heavy minerals in significant quantities [Dubois, 1972]. Perhaps more pertinent to this study is that the same conclusions were reached by Jennings and Shulmeister [2002], which is one of the few studies to systematically review and compare coarse-grain beaches in this respect. They found that, based on 42 gravel and mixed-sand-gravel beaches studied, there was no statistically significant relationship between beach slope and grain-size in either the swash zone, or an average of the intertidal profile. However, when only the pure gravel beaches were taken into account, they did find a significant positive association, and based on fewer surveys and samples, and a smaller range of sizes, than presented here.

The unusual response at Slapton may be because the foreshore doesn't systematically become flatter when eroding and steeper when building up. Often, the reverse is the case because net positive sedimentation not associated with berm building has a tendency to be uniform over the intertidal profile, or even increase seawards. Likewise, under erosive conditions, cut-back lower on the profile (sometimes with accretion at the top of the profile) tends to accentuate slopes. Longshore transport, which primarily occurs in the swash zone of coarse beaches [Van Wellen et al., 2000], may be of greater importance to

the maintenance of the distinct two-dimensionality found on pure gravel beaches such as Slapton at an intermediate time-scale (between 12 hours and 12 months). Since longshore transport primarily occurs in the swash, tidal range, translation rate and wave set-up will have dominant roles to play. Alongshore transport serves to either supply or remove material to the cross-shore profile of interest, but in such a way as the removal takes place uniformly across the profile. Sherman and Nordstrom [1985] term this process 'swash grazing', but whereas on sand beaches this can lead to scarping and steep slopes, on gravel beaches, because of the strength of individual backwashes under the influence of steeper slopes, it leads to more spatially-uniform sedimentation patterns (thereby controlling the slope). Thus, in the short-term, cross-shore transport processes are thought to account for the existence and cross-shore location of secondary morphological features such as the berm and step, but alongshore sediment transport processes may be responsible for the gross sediment supply, and thus the slope of the foreshore at time-scales greater than one tidal period.

An alternative hypothesis for the breakdown of the size-slope relationship in this study concerns the near-surface stratigraphy. A given cross-shore profile may be steep but fine because its core is primarily composed of coarse material, and the surface fines sampled are just a veneer. Chapter 6 showed how sediment size on the surface was not necessarily a reflection of that at depth. Variable sediment size with depth may also modify the hydraulic properties of the beach. The sub-surface, generally more positively skewed than the surface, may even be on average coarser than the surface, and thereby may have a greater tendency to faster convey water acting under seawards-directed hydraulic gradients (especially in lagoon-backed barriers such as Slapton). At present the effects of these barrier-scale variations in groundwater on foreshore profiles is largely unknown [Isla and Bujalesky, 2005].

9.4 *Spatial differentiation of sediment properties, and sediment transport gradients*

Fluid forces on beaches drive sediment transport gradients which result in different spatial sedimentation rates, and hence morphological change. Since thresholds for sediment entrainment vary as a function of particle size, and possibly by the ratio of

particle size to bed roughness [Wiberg and Smith, 1987; Williams and Caldwell, 1988; Rubin and Topping, 2001], it has been commonly assumed that the detailed features of a sediment size-frequency distribution may be used to infer information about the relative fluid forces acting upon the sediment. The hope is that a better understanding of the changes which occur in size distributions in one location (and relatively over space) during cycles of erosion, transport and deposition, would shed more light on the underlying processes of sediment transport (our current understanding of which is largely empirically based). That systematic grain-size and sorting patterns are associated with secondary morphological features such as berms [Masselink and Li, 2001; Austin and Masselink, 2006*a*], steps [Bauer and Allen, 1995], ripples [Doucette, 2002; Gallagher et al., 2003], and cusps [Longuet Higgins and Parkin, 1962; Sherman et al., 1993], is therefore tantalising, and suggests that the processes which drive changes in net sedimentation may be reflected in the sedimentology, if only the correct tools could be found to find such an association.

One would expect net morphological change to be reflected in the sedimentology of a beachface if finite and constant gross volumes are assumed, i.e. under relatively short time-scales, where recently displaced sediments in areas of net sedimentation gains are equal and opposing in number to those recently displaced from areas of net sedimentation losses. Two additional requirements are that probability mass over the size range of the sediment population is preserved, and the spatial gradient in sedimentation parameters across the locality where net sedimentation is zero was negligible prior to the resulting morphological change. Spatial sorting by size or other properties which was in perfect accordance with spatial net sedimentation patterns would manifest if source areas supplied only grains of a certain type to sink areas, thus the gradient in that sediment property or suite of sedimentary parameters, termed 'grading', would perfectly reflect the sediment transport gradient.

On beaches, spatial patterns in net sedimentation can be variable as a result of sediment convergence and divergence, and where sediment transport gradients operate in every direction, and over multiple scales [Masselink et al., 2008]. Thus the idealised situation outlined above is compounded by sediment transport gradients operating at the same scale but in different directions, for example under wave-induced transport, and under current-induced transport. As a result, research into the sedimentological reflection

of morphological change over time is contradictory. Some authors have reported that it is difficult to detect and predict morpho-sedimentary relationships on beaches over short (sub-lunar tidal cycle) time-scales [Stubblefield et al., 1977; Horn, 1992; Liu and Zarillo, 1993; Masselink et al., 2007], whilst others have found such a relationship [Guillen and Hoekstra, 1997; Medina et al., 1994]. It should not assumed that such relationships exist without proper verification, as in a recent paper [Li et al., 2006].

The results from the sediment trend analyses found that the sediment trend model of Gao and Collins [1992] failed to predict observed sediment transport directions. However, a model based purely on the improvment in sorting worked better. This is probably because sediment size can become either coarser in the direction of net transport, for example by the overpassing of coarser grains due to relative boundary layer protrusion [Carr, 1969], the prefential removal of fines elsewhere [Greenwood and Xu, 2001; Masselink et al., 2007], or through percolation losses [Masselink and Li, 2001]; or finer in the direction of net transport due to size-threshold winnowing or because of the input of fines from elsewhere, for example from inherited turbulence [Greenwood and Davidson Arnott, 1972; Jackson et al., 2004]. Indeed, sand beaches have been shown to both coarsen [e.g. Guillen and Palanques, 1996] and fine [e.g. Winkelmolen and Veenstra, 1980] as a result of storms. In short, there are no rules with respect to size common to all types of beach. Sorting, on the other hand, does tend to improve in the direction of transport.

In some respects the problem is finding the smallest scale at which systematic changes in beachface sedimentology reflect those of sedimentation and hydrodynamic forcing, where the natural variation of grain-size parameters is usually much greater than either. In general, the conclusions of Nordstrom [1977] and Masselink et al. [2007] still apply: the differences amongst beaches with respect to surface sedimentology are never as conspicuous as one might logically deduce.

The distribution of grain-sizes on a gravel beach may not be representative for some specific mean or steady hydrodynamic conditions. This may be because there is no time-integrated response to hydrodynamic and sediment transport processes affecting the sediment properties, or because the sediments are inadequately parameterised to reflect the hydrodynamic and/or sediment transport climate. Equally, it could be that the environment on a macrotidal gravel beach is too changeable, or that there is a

certain amount of 'memory' in the sedimentary system which induces reponse at some lag. What is clear is that, where so many size fractions are available, and they are interacting in some complex way through non-linear and even 'granular-controlled' sediment transport processes, the fundamental laws governing the sorting patterns obtained are imperfectly known.

9.5 *Future Work and Implications for Modelling*

Complex patterns have been observed in the sedimentology of a gravel beach at a number of scales. The internal variation of various sedimentological parameters has been shown to be (perhaps surprisingly) high and relationship between sedimentological and morphodynamics is highly three-dimensional, dissipative, and non-linear. Currently, there are no models able to replicate their development, although a first approximation would require something to be said about the relationship between the 'triad' of sediment patchiness, hydrodynamic forcing, and morphological change. This study resolved to document the spatial and temporal patterns in sedimentary parameters at a number of over-lapping scales, in order to elucidate the nature of the variability and change, which should find utility informing future models of sedimentological change. Data-driven (statistical, possibly site-specific) models, such as CCA, EOFs, and parametric-probabilistic models, were used in order to uncover associations between the triad. Whilst the sedimentary time-series were always noisy and highly variable, the results alluded to the fact that underneath a lot of randomness there was an associative signal, thus the sedimentology of a gravel beach may be, admittedly perhaps some way in the future, modelled deterministically. Further work in this area should include a move towards more generic, process-driven models.

Many short-medium term morphological models in widespread usage for beaches solve the so-called 'initial value problem', which treat waves as random and morphological developments as being sensitive to initial bed configurations and as some function of the previous state. Currently, the approximations and assumptions for parameterising sediment transport and morphological change under such a framework are poorly resolved compared to those for the hydrodynamic field. Equipped with the insight revealed by the present study (i.e. the inherent non-linearity and lack of auto-regression

in the sediment dynamics), the modeller of gravel beach sedimentation and sedimentology may not decide to adopt such an approach, arguing that another layer of complexity (the sediment dynamics) may produce non-linkable set of sub-processes. Setting a 'boundary-layer problem' and modelling morphological and sedimentary change as a function of random external forcing rather than given some estimate of current conditions, may in the first instance be of greater utility to coastal management. The implication is that that modelling inter-beach sedimentological variability may be able to predict the inevitability of an event but not its timing. The modellers' decision is intimately linked with scale.

10 CONCLUSIONS

... No-one promised this when I was a kid ...
Kicking pebbles on a beach,
When time couldn't reach me

Ocean Colour Scene. "Charlie Brown Says".

10.1 *Summary of Findings*

In assessing the present state of scholarly interest in gravel beach morphodynamics, Chapter 2 argued that on gravel beaches, sedimentological changes in space and time could be as pronounced and important as morphological changes. It was argued that in order to further our understanding of gravel beaches, sedimentological data would need to be collected and analysed at a temporal resolution similar to that of the hydrodynamics.

To help quantify and substantiate this conceptual framework, there was a pressing need to develop innovative automatic sediment sizing techniques based on digital images of sediments. This alone would allow the collection and analysis of high-resolution sediment data. Chapter 4 expanded upon the 'digital grain-size' methods proposed by Rubin [2004] and Rubin et al. [2006] for use on sand sized sediment, for use on larger sediment sizes (coarse sand to pebbles). Importantly then, sizing from images is now possible in the full range from fine sands to very coarse gravels. A number of new techniques were introduced for automated grain-size estimates from digital images of sediment, which will broaden the applicability and accuracy of the technique. The principles behind all techniques were theoretically explored. A new method was

introduced to obtain better estimates of the entire distribution from the statistical information contained within an image of sediment, and despite the theoretical difficulties in comparing GSDs (grain-size Distributions) obtained from two-dimensional images with GSDs obtained from sieving, the results were very encouraging.

A total of 8805 sediment samples were collected during three years for this doctoral thesis, of which 6850 were imaged using a digital camera and analysed using a 'hybrid' of two of the methods elaborated upon in Chapter 4. The kernel density approach developed there better approximated the GSD from images. In addition, 1955 (including those use to calibrate the imaging technique) were manually sampled and sieved. The manual sieving and data handling took an estimated 122 working days (8 hours each) in total, or $\frac{1}{3}$ year, thus the samples digitally imaged saved an estimated 428 working days (or just under 1 $\frac{1}{4}$ years).

The morpho-sedimentary variation of the study site over individual semi-diurnal tidal cycles was the subject of Chapter 5. A number of experiments which looked at the evolving beachface over a number of hours were carried out. It was found that the gravel beach step and berm are accretionary features strongly linked to tidal stage, i.e. shoreline position, evolving with different relaxation times. Initiation of step morphology requires tidal stationarity and is perhaps triggered by a change wave breaker type from plunging to surging. The step and beachface may be differentiated using sedimentary moments, and different morphological features such as the step, broadly have typical spatial sedimentary responses. Step dynamics are tidally modulated: they are consistently more pronounced at high tide compared to mid-tide due to stationarity, and often absent at low tide, instead replaced, under calm conditions, with a series of subtidal ripples with long wavelengths. It was concluded that the importance of the step in gravel beach development must not be downplayed: it appears to be a very important mechanism by which the upper beachface loses or gains material, by 'liberating' material either onshore or offshore depending on the hydrodynamic conditions. The erosive phase of the tidal cycle persists longest in the lower swash zone, and the dynamics of both the step and berm are asymmetrical with respect to tide. The latter is easier explained than the former in terms of the effects of groundwater. Morphodynamic profile models of gravel beaches need to be able to replicate the behaviour of the step, whilst preserving its relationship to the berm, and also its unique sedimentary characteristics which may

be key to understanding the dynamics of the step, and thus the dynamics of the whole intertidal zone. A new technique to determine bed mobility from the nearshore of a gravel beach, using underwater video cameras, was devised. Nearshore sediment transport was tentatively suggested as being related to sub-incident frequencies (wave groups), but appeared to be a linear function of neither velocity magnitude nor direction. Therefore, a better description of sediment transport may require instantaneous sediment size information, which has to be remotely sensed. Better parameterisation of 'bed motion' is also required. Critical thresholds for sediment transport were often exceeded in the shoaling zone, therefore sediment transport on a gravel beach is not restricted to the swash and breaking zones.

Chapter 6 focussed on the morpho-sedimentary-dynamics of the gravel beachface at Slapton over the time-scale of a spring-spring tidal cycle, and over a spatial scale of one or two cross-shore profiles sampled every 0.5-1m. Detailed measurements of profile and sediment dynamics were obtained. Surface and sub-surface sediment samples, beach profiles, and disturbance depths were taken from the intertidal zone on consecutive low tides over half-lunar tidal cycles, along with wave and tide measurements. Results from two separate field surveys (autumn 2005, and spring 2007) were presented, representing 26 and 24 consecutive low tides, respectively. Morphological change was consistently dominated by relative depletion high on the intertidal beachface, prior to 'cut and fill' berm building. It was found that disturbance depths were not proportional to slope [Anfuso, 2005] or breaking wave height [Jackson and Nordstrom, 1993; Anfuso et al., 2000; Anfuso, 2005] (as on sand beaches), but rather step dimensions, which are less a factor of wave height than tidal stationarity. This stationarity is, however, related to beach slope. No aspect of morphology/morphological change could be found to have a statistically significant association with sedimentology/sedimentological change.

A combination of Canonical Correlation Analysis (CCA) and Empirical Orthogonal Function (EOF) analysis was used to identify a number of consistent relationships in morphological and sedimentological variables not readily apparent using ordinary correlations. EOF analysis showed that sediment size was consistently more variable than sorting. Beachface morphology and sedimentology are more similar at a given spatial location over time than over space (cross-shore) at any individual time. In other words, temporal variability in any location is much less than the instantaneous spatial

variability. sub-surface sedimentology over the depth of disturbance indicates that the step can be traced through the sediment characteristics. Strong hysteresis over space was present in the EOF modes associated with the most variance in the data sets, for both sediment size and sorting. Statistically significant relationships were found between the temporal modes of (absolute) size/sorting and net sedimentation associated with the largest variance in the non-decomposed respective data sets. Finally, significant relationships were found between a suite of measured hydrodynamic time-series (including wave, tide and morphodynamic parameters) and pairs of significantly correlated morpho-sedimentary eigenmodes. The techniques used were thus able to objectively demonstrate linear association between morphological and sedimentological change on a gravel beachface over a semi-lunar tidal cycle; and also that simultaneous changes in each could be linearly correlated to hydrodynamic forcing, especially wave height and tidal range.

Whilst the available evidence implied that morphological change co-varied with sedimentological change, it was only with the use of relatively advanced statistical models, and it was not possible to demonstrate cause and effect (for example by consistent cross-correlations at lag or phase relationships). The results imply that median sediment size and geometric sorting are suitable parameters for detecting morpho-sedimentary relationships, but also that relatively sophisticated techniques are required to satisfactorily detect them. These techniques are purely statistical, so cannot be expressed in any physically-meaningful units. Whilst adequate for the objectives of the present study, as an exercise of exploratory data analysis providing evidence for a concept (morpho-sedimentary dynamics), it does limit its utility beyond, for example in physical-numerical modelling.

Morpho-sedimentary variations at Slapton were documented over one calendar year, using a data set of regular fortnightly beach profiles and sediment samples. The barrier underwent net northerly ‘rotation’ during the year, however the asymmetrical behaviour of the rotation differed from bay beach rotation observed in many other areas of the world, and perhaps should be more correctly termed ‘embayment deepening’. The volumes lost from south of the rotational point did not match those gained to the north, implying that the site is not a closed sedimentary system as some researchers previously suggested. This work highlighted the importance of alongshore sediment transport

processes, even on this supposedly 'swash-aligned' beach. A comparison of measured and previously published modelled alongshore sediment rates suggested that these models, currently the best available for coarse beaches, should be regarded as sediment transport (maximum) potentials, assuming no net on-offshore exchange of material, and a closed sedimentary system. The beach was almost always negatively skewed, regardless of morphological changes, and the beach was generally more poorly sorted when morphological change was at a minimum. At the broadest level, sediment size was greatest where net morphological change was greatest, providing broad support for the energy-sediment size relationship found by previous researchers. Sorting was much more variable in the winter, whereas skewness was significantly more variable in the summer. Changes in sediment size, especially the seemingly relatively long-term fining of the beach, were more difficult to explain, but appeared to be phase-decoupled from, and distinctly non-linearly related to, morphological change. The hypothesis of Muir Wood [1970] —that the strength of the alongshore gradient in size is a sign of a volumetrically-stable beach —is verified by the present study.

In the absence of process models which would seem likely to explain or replicate the observed patterns of behaviour, and in light of the fact that few if any previous studies had morphological and sedimentological information at identical sampling resolution, Chapter 8 looked at a particular class of models for use in the nearshore which may have been able to predict observed sedimentation patterns from the statistics of grain-size data. The implication was that, if the models succeded in replicating observed patterns of behaviour, despite the apparent stochasticity of sedimentary variables and the complicated nature of change, it would support the basic assumptions behind the models. In turn, this might provide a starting point for modelling the relationship between gravel beach morphodynamics and sedimentology.

The 'hyperbolic shape triangle' sedimentation model of Barndorff Nielsen and Christiansen [1988], which is based on the bivariate plot of log-hyperbolic skewness (χ) and kurtosis (ξ), was tested on the intertidal zone of active sedimentation. A large field data set was used to test the shape triangle's ability to both classify and retrodict sediment samples according to their sedimentation history. When parameters were suitably averaged, the model was found to be a reasonable predictor of recent mean net sedimentation on a gravel beach when used with surface samples, and over individual

tides. In all other scenarios the model failed to correctly assign the sedimentation history of the samples, as determined from beach profiles. Correlations between mean morphological change and shift in mean χ position over individual tides (termed r_ϵ, representing Barndorrf-Nielsen and Christiansen's [1988] ϵ, or 'fluid controlled' erosion/deposition) were reasonable, and improved when net mean morphological change over individual tides was $\geq \pm$ 5cm. However, mean morphological change and shift in mean ξ position over individual tides (termed r_κ, representing Barndorrf-Nielsen and Christiansen's [1988] κ, or 'grain controlled' erosion/deposition), did not correlate well. In addition, the systematic predictions made about how mean size and sorting would behave under net ϵ and κ erosion/deposition were unverified. The closest equivalent classification system to the log hyperbolic shape triangle which uses ordinary sample moments, the Craig Diagram [Leroy, 1981], was found to be a potentially useful pre-indicator of log-hyperbolic model fit. Finally, it was tentatively suggested that the distributional forms classified by the Craig diagram map directly onto the parameter space of the hyperbolic model, opening the future possibility that directly determining χ and ξ by fitting log-hyperbolic distributions to data could be circumnavigated.

Chapter 8 also tested use of the spatial distribution of sedimentary parameters to derive likely sediment transport pathways. Researchers on beaches have had mixed levels of success with these techniques [Masselink, 1992; Pedreros et al., 1996; Masselink et al., 2008]. The sediment trend model of Gao and Collins [1992] was applied without success, therefore this work added to a growing literature which has called into question the utility of the technique [Flemming, 1988; Masselink, 1992; Guillen and Jimenez, 1995; Masselink et al., 2008]. This is perhaps because the rules upon which the model is based are too simplistic for application on a gravel beach. However, trend vectors based on sorting alone, out-performed a traditional sediment trend vector approach, which implies that if sorting had a greater weighting in the GSTA model, it might find better accord with observed sedimentation patterns.

Finally chapter 9, by integrating the three scales studied and based on a number of very large data sets, showed that the relationship between morphology, or morphological change, and sedimentology, perhaps has a relationship that cannot be expressed by averages, and it is distinctly non-linear in character. Surficial sediment size has been shown to be a highly stochastic variable. Two important findings are that surface

sampling appears to be inappropriate to characterise sedimentological change at time-scales greater than a semi-diurnal tidal cycle, and that sub-surface sampling on the intertidal zone on diurnal and semi-lunar time-scales may be useful in assessing the dynamics of the step, itself a potentially important mechanism for onshore and offshore net volumetric transport. In the light of this information, a general discussion was presented on errors in sediment sampling and aliasing, and the implications for coarse-grain transport and morphological modelling. The observed failure of the positive size-slope relationship, and of sediment trend modelling, was also discussed. Sediment modelling approaches are fundamentally limited by the fact that in order to know how many samples are required for a given area and environment, a certain relationship between the population of grains and the processes in operation upon them must be assumed *a priori*, and this relationship is currently very poorly elucidated.

10.2 *Concluding Comments*

In accordance with many previous studies on sand beaches, temporal grain-size changes are largely unrelated to seasonal changes in wave climate and morphologies [e.g. Davis, 1985; Liu and Zarillo, 1993; Guillen and Palanques, 1996]. Unlike these studies, however, it was found that grain-size varies in time to a greater extent than over space. Even with large numbers of samples, there is a lot of noise in sedimentary data, although sorting is much less noisy than size and so may prove more useful in further studies. There has been enough evidence presented in this thesis to show that sedimentological changes are related in a non-linear fashion to hydrodynamic forcing, but whether or not sedimentological changes are forcing or responding to morphological change, especially on a short time-scale, is still not clear.

Hartmann [2007] identified four major branches of sediment dynamics research, and the present study falls into two of those categories. The first, which he termed "Process Oriented Population Statistics" (POPS) is the study of sedimentary systems where sediments, forces and morphology can all be measured directly. Since such work has relatively small spatial and temporal coverage, it should aim for as fine resolution as possible. The second, termed "Sediment Dispersal and Trend Analysis" (SEDITRANS), uses surface sediment samples to mutually connect locations, thus identify dominant

dispersal processes and directions. A POPS analysis has traditionally been carried out to identify a number of connected sedimentary sub-populations. This study used some of these ideas and techniques to investigate whether there are any such sub-environments on a gravel beach. It was found that techniques based on bi-variation of sedimentary parameters were not useful in their classic sense, but the use of different parametric models and/or dimensionless scaling may have further utility. Sedimentary analysis with respect to any aspect of morphological or hydrodynamic change, using linear techniques and traditional parameterisations, proved less fruitful, and in this respect a POPS approach largely failed. More advanced statistical techniques, however, were able to demonstate relationships between hydro- and morphodynamic variables and sedimentary parameters. A SEDITRANS approach over a larger scale and longer term was found also to be flawed, however substantial improvements were made by simplifying the 'rules' of the basic model.

It has been shown that traditional methods of process identification and classification, for example the statistics of linear association, using parameterisations based on central tendency or variance, failed to reveal satisfactory insight between gravel beach morphodynamics and sediment dynamics. This failure is likely to be due to many potential factors. For example, surface sampling may be inappropriate, and the measurements may not have had the required accuracy and/or precision to characterise the changes. However, the techniques used to measure the hydrodynamics and morphological change are standard, and their inaccuracies are well known. Whilst it is acknowledged that some of the measurements techniques used to characterise the sedimentology were novel, they were rigorously tested before application. Note that all particle size measurements are prone to substantial errors due to the sampling and mechanical measurements in the laboratory, which are themselves a 'stochastic process' [Winkelmolen, 1982]. The look-up cataloguing procedure used in this study has at least two methodological advantages over all others: the first is that the samples have not been removed from their natural context, thus not destroying the spatial arrangement of grains; and the second is that the photographic technique provides equivalent and comparable measures of grain-size across a variety of sediment types.

It is more likely that more inaccuracies were introduced to the study due to inappropriate sampling frameworks and experimental designs rather than accuracy in

the field methods. The measurements may not have been made at the required spatial/temporal coverage and/or resolution to characterise the changes. However, spatial trends in grain-size, sorting or skewness actually diminish progressively the larger the length over which one averages, which suggests that the resolution of measurements was suitable for the spatial coverage of individual components of the study. Further, it has been shown that important findings can be obtained if sampled with such resolution, for example that bi-variation of sediment parameters find strongest association between skewness and sorting, irrespective of scale. In addition, that size-slope relationships are stronger at shorter time-scales, but can be positive or negative, and sorting has an influence on the relationship between size and slope. A key finding of this work is that morphodynamic relationships preserved in sedimentary spatial trends may be better found in grain sorting rather than grain-size.

There may be no *linear* association between morphological change and sedimentological change, therefore traditional descriptive and basic inferential statistics may be inappropriate tools. Sources of non-linearity may include time and spatial lags at all scales, as well as forcing the morphological-sedimentological system out of equilibrium at any given scale. This information may not even be obtained by sampling sediments, because the assumption there is that the processes of beach change leave some signature preserved in the nuances of the distributional form, which only requires the correct statistical technique(s) to tease out. In this respect, the fact that this study found that more sophisticated analytical techniques and models perform better, is encouraging. For example, dimensional- and 'noise'- reduction (such as EOFs), or parametric models with more free parameters (such as the hyperbolic shape triangle), revealed associations using ordinary parameterisations, implying there is detectable covariance underlying a lot of stochastic system noise. It implies that the parameterisations and measurement techniques do not necessarily need to change, only the way in which we collect and analyse the data. Chapter 5 demonstrated that 'bed motion' in the region of near-breaking could be modelled as a first-order Markov process. What this broadly implies is that its behaviour is non-deterministic, in that the state it is in at present does not fully determine its next state. Even though each particle is moving in a deterministic path, hence predictable using classical physics, is the motion of a collection of them computationally and practically unpredictable? It will be a better characterisation of the

direct and emergent properties of the sedimentology of the nearshore which will determine, in the long term, the answer to this question.

To the authors' knowledge, this study has drawn upon measurements which are more finely resolved than any previous study on gravel beach morphodynamics, and has aided coastal management and engineering practices in three broad ways. Firstly, it has documented and quantified the spatio-temporal variability of morpho-sedimentary change on a gravel beach; its intra- and inter-variability, and its scale-dependency. This information is likely to increase the accuracy and reduce the margin of error in a number of applications, including sediment transport modelling, and beach recharge. Secondly, it has provided a number of conceptual frameworks within which to study gravel beach morpho-sedimentary dynamics at a more generic level than was previously attempted. Finally, potentially innovative solutions have been forwarded, such as digital grain-size mapping, and the use of dimensional-decomposition techniques on noisy sediment data.

Finally, the possibility still remains that there is no association between morphological change and sedimentological change. However, in terms of the contribution of sediment dynamics to the morphodynamics of the beach, it may not matter because the Morpho-Sedimentary Dynamic (MSD) hypothesis and co-variation in sedimentology and morphology are not necessarily the same thing. That the present study found that, at all scales studies, there is at best a weak correlation between sedimentology/sedimentological change and morphology/morphological change, does not strictly bear much relevance on MSD because the influence of sedimentology on morphodynamics may be obscured by the readiness with which we see morphologies evolve. As an example, this study verified the general notion that the coarsest zone of the beachface is the turbulent area of wave breaking, an observation which has been made on tideless [Fox et al., 1966] and tidal [Bascom, 1951; Inman, 1953; Miller and Ziegler, 1958] sand beaches, and gravel beaches [Krumbein and Griffith, 1938; Jennings and Shulmeister, 2002]. One might conclude that hydrodynamics concentrate the coarsest sediments, and advect the fines (equilibrium/null-point argument). However, this study also showed that the area of most dynamic morphological change was in the region of wave breaking. A morphodynamic interpretation would be that the morphologies and hydrodynamics are co-evolving: waves and currents transport sediment which builds steep slopes, which force wave breaking and maintain steep slopes, etc. As

a result, the coarse particles remain and the fines are removed. An MSD approach would advocate the possibility that there is some contribution to the turbulence caused by the coarseness of the particles, or that there is some contribution by the sedimentology to the slope, or that there was some contribution made by the sedimentology of the beachface to the initial conditions required to start the morphodynamic feedback loops. MSD is about keeping that possibility open until it has been proved beyond reasonable scientific doubt, i.e. knowing, in the words of Werner and Kocurek [1997] in the context of wave ripples, whether or not 'the tail is wagging the dog'. Whilst expressing and quantifying the inherent uncertainties in the gravel beach system may be difficult, what is clear is that a constant grain-size is not better than a perfect characterisation of grain-size at all spatial and temporal scales when sediment transport is a non-linear function of sediment size. Models should be improved to incorporate such information.

REFERENCES

Acton, J. and Dyer, C. [1975], 'Mapping the tidal currents near the Skerries bank', *Proceedings of the Royal Society of London, Series A* **131**(1), 63 – 68.

Allan, J. C., Hart, R. and Tranquili, J. V. [2006], 'The use of Passive Integrated Transponder (PIT) tags to trace cobble transport in a mixed sand - and - gravel beach on the high - energy Oregon coast, USA', *Marine Geology* **232**(1 - 2), 63 – 86.

Anfuso, G. [2005], 'Sediment - activation depth values for gentle and steep beaches', *Marine Geology* **220**(1 - 4), 101 – 112.

Anfuso, G., Gracia, F. J., Andres, J., Sanchez, F., Del Rio, L. and Lopez Aguayo, F. [2000], 'Depth of disturbance in mesotidal beaches during a single tidal cycle', *Journal of Coastal Research* **16**(2), 446 – 457.

Anthony, E. J. [2002], 'Long - term marine bedload segregation, and sandy versus gravelly Holocene shorelines in the eastern English Channel', *Marine Geology* **187**(3 - 4), 221 – 234.

Arber, M. [1940], 'The outline of south west England in relation to wave attack', *Nature* **146**, 27 – 28.

Arnold Bos, A., Malkasse, J. P. and Kervern, G. [2005], Towards a model - free denoising of underwater optical images, *in* 'Institute of Electrical and Electronics Engineers Conference on Oceans (Europe)', Brest, France.

Asselman, N. [1999], 'Grain size trends used to assess the effective discharge for floodplain sedimentation, River Waal, the Netherlands.', *Journal of Sedimentary Research* **69**, 51 – 61.

Aubrey, D. and Ross, R. [1985], 'The quantitative description of beach cycles', *Marine Geology* **69**, 155 – 170.

Austin, M. J. [2005], *Swash, groundwater and sediment transport processes on a gravel beach*, PhD thesis, Loughborough University.

Austin, M. J. and Masselink, G. [2006*a*], 'Observations of morphological change and sediment transport on a steep gravel beach', *Marine Geology* **229**(1 - 2), 59 – 77.

Austin, M. J. and Masselink, G. [2006*b*], 'Swash - groundwater interaction on a steep gravel beach', *Continental Shelf Research* **26**(20), 2503 – 2519.

Austin, M. J., Masselink, G., O'Hare, T. and Russell, P. E. [2007], 'Relaxation time effects of wave ripples on tidal beaches.', *Geophysical Research Letters* **34**, L16606, doi:10.1029/2007GL030696.

Bader, H. [1970], 'Hyperbolic distribution of particle sizes', *Journal of Geophysical Research* **75**(15), 2822 – 2830.

Bagnold, R. [1940], 'Beach formation; some model - experiments in a wave tank', *Proceedings of the Institute of Hydraulic Engineers* pp. 27 – 52.

Bagnold, R. [1954], 'Experiments on a gravity - free dispersion of large solid spheres in a Newtonian fluid under shear.', *Proceedings of the Royal Society, London. Series A* **225**, 49 – 63.

Bagnold, R. A. and Barndorff Nielsen, O. [1980*a*], 'The pattern of natural size distributions', *Sedimentology* **27**(2), 199 – 207.

Bagnold, R. and Barndorff Nielsen, O. [1980*b*], 'The pattern of natural size distributions', *Sedimentology* **27**, 199 – 207.

Bailard, J. A. [1981], 'An energetics total load sediment transport model for a plane sloping beach', *Journal of Geophysical Research - Oceans and Atmospheres* **86**(NC11), 938 – 954.

Baldock, T. E., Baird, A. J., Horn, D. P. and Mason, T. [2001], 'Measurements and modeling of swash - induced pressure gradients in the surface layers of a sand beach', *Journal of Geophysical Research - Oceans* **106**(C2), 2653 – 2666.

Baldock, T. E. and Holmes, P. [1999], 'Simulation and prediction of swash oscillations on a steep beach', *Coastal Engineering* **36**(3), 219 – 242.

Baldock, T. E. and Hughes, M. G. [2006], 'Field observations of instantaneous water slopes and horizontal pressure gradients in the swash - zone', *Continental Shelf Research* **26**(5), 574 – 588.

Baldock, T. E., Tomkins, M. R., Nielsen, P. and Hughes, M. G. [2004], 'Settling velocity of sediments at high concentrations', *Coastal Engineering* **51**(1), 91 – 100.

Baldock, T., Holmes, P. and Horn, D. [1997], 'Low frequency swash motion induced by wave grouping', *Coastal Engineering* **32**, 866 – 874.

Barber, C., Dobkin, D. and Huhdanpaa, H. [1996], 'The quickhull algorithm for convex hulls', *ACM Transactions on Mathematical Software* **22**, 469 – 483.

Barnard, P., Rubin, D., Harney, J. and Mustain, N. [2007], 'Field test comparison of an autocorrelation technique for determining grain size using a digital beachball' camera versus traditional methods', *Sedimentary Geology* **201**, 180 – 195.

Barndorff Nielsen, O. [1977], 'Exponentially decreasing distributions for the logarithm of particle size', *Proceedings of the Royal Society, London. Series A* **353**, 401 – 419.

Barndorff Nielsen, O. E. and Christiansen, C. [1988], 'Erosion, deposition and size distributions of sand', *Proceedings of the Royal Society of London Series A - Mathematical Physical and Engineering Sciences* **417**(1853), 335 – 352.

Barne, J., Robson, C., Kazowska, S., Doody, J., Davidson, N. and Buck, A., eds [1996], *Region 10 South - west England: Seaton to Roseland Peninsula*, Coasts and seas of the United Kingdom, Joint Nature Conservation Committee, Peterborough.

Barnett, T. P. [1983], 'Interaction of the monsoon and pacific trade - wind system at interannual time scales .1. the equatorial zone', *Monthly Weather Review* **111**(4), 756 – 773.

Bartholdy, J., Bartholoma, A. and Flemming, B. W. [2002], 'Grain - size control of large compound flow - transverse bedforms in a tidal inlet of the Danish Wadden Sea', *Marine Geology* **188**(3 - 4), 391 – 413.

Bartholdy, J., Christiansen, C. and Pedersen, J. [2007], 'Comparing spatial grain - size trends inferred from textural parameters using percentile statistical parameters and those based on the log - hyperbolic method', *Sedimentary Geology* **202**, 436 – 452.

Bartholdy, J., Flemming, B. W., Bartholoma, A. and Ernstsen, V. B. [2005], 'Flow and grain size control of depth - independent simple subaqueous dunes', *Journal of Geophysical Research - Earth Surface* **110**(F4).

Bartholoma, A. and Flemming, B. [2007], 'Progressive grain - size sorting along an intertidal energy gradient', *Sedimentary Geology* **202**, 464 – 472.

Bartlett, M. [1992], 'Comparison of methods for measuring fractal dimensions', *Australian Physics and Engineering Science in Medicine* **14**, 146 – 152.

Basawa, I. [1972], 'Estimation of the autocorrelation coefficient in simple markov chains.', *Biometrika* **59**, 85 – 89.

Bascom, W. [1951], 'The relationship between sand size and beach face slope', *Transactions of the American Geophysical Union* **32**, 866 – 874.

Battjes, J. [1974], Surf similarity, *in* 'Proceedings of the 14th International Conference on Coastal Engineering', American Society of Coastal Engineering, Copenhagen.

Battjes, J. and Janssen, P. [1978], 'Energy loss and set - up due to breaking of random waves', *Proceedings of the 16th International Conference on Coastal Engineering* pp. 59 – 587.

Bauer, B. O. and Allen, J. R. [1995], 'Beach steps - an evolutionary perspective', *Marine Geology* **123**(3 - 4), 143 – 166.

Bird, E. C. F. [1996], 'Lateral grading of beach sediments: A commentary', *Journal of Coastal Research* **12**(3), 774 – 785.

Blackman, R. and Tukey, J. [1958], *The measurement of power spectra from the point of view of communications engineering*, Dover Publications, New York.

Blondeaux, P. [2001], 'Mechanics of coastal forms', *Annual Review of Fluid Mechanics* **33**, 339 – 370.

Blott, S. J. and Pye, K. [2001], 'GRADISTAT: A grain size distribution and statistics package for the analysis of unconsolidated sediments', *Earth Surface Processes and Landforms* **26**(11), 1237 – 1248.

Bluck, B. [1967], 'Sedimentation of beach gravels: examples from South Wales', *Journal of Sedimentary Petrology* **37**(1), 128 – 156.

Bluck, B. J. [1999], 'Clast assembling, bed - forms and structure in gravel beaches', *Transactions of the Royal Society of Edinburgh - Earth Sciences* **89**, 291 – 323. Part 4.

Botev, Z. [2006], A novel nonparametric density estimator, *in* 'Postgraduate Seminar Series, Mathematics (School of Physical Sciences)', The University of Queensland.

Bowen, A. [1980], 'Simple models of nearshore sedimentation: beach profiles and longshore bars', *Geological Survey of Canada Paper* **80 - 100**, 1 – 11.

Bowman, A. and Azzalini, A. [1997], *Applied smoothing techniques for data analysis*, Oxford Statistical Science Series, Clarendon Press, Oxford.

Box, G. and Jenkins, F. [1976], *Time series analysis: forecasting and control.*, 2nd edn, Holden - Day, California.

Box, G. and Pierce, D. [1970], 'Distribution of residual autocorrelations in autoregressive - integrated moving average time series models', *Journal of the American Statistical Association* **65**, 1509 – 1526.

Bradbury, A. [2001], *Strategic monitoring of the coastal zone: towards a regional approach*, Technical report, Report to SCOPAC, South Downs Coastal Group, South East Coastal Group and Environment Agency.

Brampton, A. and Goldberg, D. [1991], Mathematical model of groyned shingle beaches, *in* '*Coastal Sediments* 1991, American Society of Civil Engineers', pp. 1842 – 1855.

Bridge, J. S. [1981], 'Hydraulic interpretation of grain - size distributions using a physical model for bedload transport', *Journal of Sedimentary Petrology* **51**(4), 1109 – 1124.

Brockwell, P. and Davis, R. [n.d.], *Time Series: Theory and Methods*, 2nd edn, Springer Verlang, New York.

Burt, T. [1993], *A field guide to the geomorphology of the Slapton region*, Field Studies Council.

Burt, T. and Horton, B. [2001], 'The natural history of the Slapton Ley national nature reserve XXIII: the climate of Slapton Ley', *Field Studies* **10**, 93 – 114.

Burt, T. P. [1994], 'Long - term study of the natural environment - perceptive science or mindless monitoring?', *Progress in Physical Geography* **18**(4), 475 – 496.

Butler, J. B., Lane, S. N. and Chandler, J. H. [2001], 'Automated extraction of grain - size data from gravel surfaces using digital image processing', *Journal of Hydraulic Research* **39**(5), 519 – 529.

Butt, T. and Russell, P. [2000], 'Hydrodynamics and cross - shore sediment transport in the swash - zone of natural beaches: A review', *Journal of Coastal Research* **16**(2), 255 – 268.

Butt, T., Russell, P., Puleo, J., Miles, J. and Masselink, G. [2004], 'The influence of bore turbulence on sediment transport in the swash and inner surf zones', *Continental Shelf Research* **24**(7 - 8), 757 – 771.

Butt, T., Russell, P. and Turner, I. [2001], 'The influence of swash infiltration - exfiltration on beach face sediment transport: onshore or offshore?', *Coastal Engineering* **42**(1), 35 – 52.

Caldwell, N. E. and Williams, A. T. [1985], 'The role of beach profile configuration in the discrimination between differing depositional - environments affecting coarse clastic beaches', *Journal of Coastal Research* **1**(2), 129 – 139.

Carr, A. [1969], 'Size grading along a pebble beach; Chesil Beach, England', *Journal of Sedimentary Research* **39**, 297311.

Carr, A. [1974], Differential movement of coarse clastic particles, *in* 'Procedings of 14th International Coastal Engineering Conference', pp. 851 – 870.

Carr, A. P. [1971], 'Experiments on longshore transport and sorting pebbles - Chesil Beach, England', *Journal of Sedimentary Petrology* **41**(4), 1084 – 1104.

Carr, A. P., Blackley, M. W. L. and King, H. L. [1982], 'Spatial and seasonal aspects of beach stability', *Earth Surface Processes and Landforms* **7**(3), 267 – 282.

Carter, R. [1998], *Coastal environments : an introduction to the physical, ecological, and cultural systems of coastlines*, Academic Press, London.

Carter, R. and Orford, J. [1993], 'The morphodynamics of coarse clastic beaches and barriers: a short term and long term perspective', *Journal of Coastal Research* **SI 15**, 158179.

Carter, R. W. G. and Orford, J. D. [1984], 'Coarse clastic barrier beaches - a discussion of the distinctive dynamic and morphosedimentary characteristics', *Marine Geology* **60**(1 - 4), 377 – 389.

Carter, R. W. G. and Orford, J. D. [1988], 'Conceptual - model of coarse clastic barrier formation from multiple sediment sources', *Geographical Review* **78**(2), 221 – 239.

Cartwright, D. and LonguetHiggins, M. [1956], 'The statistical distribution of the maxima of a random function', *Proceedings of the Royal Society of London. Series A, Mathematical and Physical Sciences'* **237**, 212 – 232.

Caswell, H. [2001], *Matrix population models: construction, analysis, and interpretation*, Sinauer Associates Inc., Sunderland, Mass.

Chadwick, A., Karunarathna, H., Gehrels, W., Massey, A., O'Brien, D. and Dales, D. [2005], 'A new analysis of the Slapton barrier beach system, UK', *Maritime Engineering* **158**, 147161.

Chaudhuri, B. and Sarkar, N. [1995], 'Texture segmentation using fractal dimension', *Institute of Electrical and Electronics Engineers Transactions in Pattern Analysis and Machine Intelligence* **17**, 72 – 77.

Chell, K. [2002], 'Coastline in decay', *Geography Review* **18**, 32 – 36.

Cheng, P., Gao, S. and Bokuniewicz, H. [2004], 'Net sediment transport patterns over the Bohai Strait based on grain size analysis.', *Estuarine, Coastal and Shelf Science* **60**, 203 – 212.

Chica Olmo, M. and Abarca Hernandez, F. [2000], 'Computing geostatistical image texture for remotely sensed data classification', *Computers and Geosciences* **26**(4), 373 – 383.

Clarke, D. J., Eliot, I. G. and Frew, J. R. [1984], 'Variation in subaerial beach sediment volume on a small sandy beach over a monthly lunar tidal cycle', *Marine Geology* **58**(3 - 4), 319 – 344.

Clarke, S. and Damgaard, J. [2002], Applications of a numerical model of swash zone on gravel beaches, *in* 'Coastal Engineering 2002', pp. 1028 – 1036.

Clarke, S., Dodd, N. and Damgaard, J. [2004], 'Modelling flow in and above a porous beach', *Journal of Waterway Port Coastal and Ocean Engineering - ASCE* **130**(5), 223 – 233.

Clifton, H. [1969], 'Beach lamination: nature and origin', *Marine Geology* **7**, 553 – 559.

Coco, G., Burnet, T. K., Werner, B. T. and Elgar, S. [2004], 'The role of tides in beach cusp development', *Journal of Geophysical Research - Oceans* **109**(C4).

Coco, G., Huntley, D. A. and O'Hare, T. J. [2001], 'Regularity and randomness in the formation of beach cusps', *Marine Geology* **178**(1 - 4), 1 – 9.

Coco, G., O'Hare, T. J. and Huntley, D. A. [1999], 'Beach cusps: A comparison of data and theories for their formation', *Journal of Coastal Research* **15**(3), 741 – 749.

Cooper, J. A. G., Jackson, D. W. T., Navas, F., McKenna, J. and Malvarez, G. [2004], 'Identifying storm impacts on an embayed, high - energy coastline: examples from Western Ireland', *Marine Geology* **210**(1 - 4), 261 – 280. Sp. Iss. SI.

Cooper, J. A. G. and Pilkey, O. H. [2004], 'Alternatives to the mathematical modeling of beaches', *Journal of Coastal Research* **20**(3), 641 – 644.

Cornaglia, P. [1877], 'On beaches', *in Horn, D.P. (1992)* .

Cowell, P., Hanslow, D. and Meleo, J. [1999], The shoreface, *in* A. D. Short, ed., 'Handbook of beach and shoreface morphodynamics', Wiley, Chichester, pp. 39 – 72.

Cowell, P. and Thom, B. [1994], *Morphodynamics of Coastal Evolution*, In: Carter, R.W.G. and Woodroffe, C.D., Coastal evolution: late Quaternary shoreline morphodynamics.

Craig, C. C. [1936], 'On the frequency function of xy', *Annals of Mathematical Statistics* **7**, 1 – 15.

Cunningham, R. and Fox, W. [1974], 'Coastal processes and depositional patterns on Cape Ann, Massechusetts', *Journal of Sedimentary Petrology* **44**, 522 – 531.

Davidson, M. A., Russell, P. E., Huntley, D. A. and Hardisty, J. [1993], 'Tidal asymmetry in suspended sand transport on a macrotidal intermediate beach', *Marine Geology* **110**(3 - 4), 333 – 353.

Davis, J. [1986], *Statistics and Data Analysis in Geology*, 2nd edn, John Wiley, New York.

Davis, R. A. [1985], *Beach and nearshore zone*, *in* R. Davis, ed., 'Coastal Sedimentary Environments', Springer, New York., p. 50.

Deigaard, R. and Fredsoe, J. [1978], 'Longitudinal grain sorting by current in alluvial streams', *Nordic Hydrology* **9**(1), 7 – 16.

deVriend, H. [1997], Prediction of aggregated - scale coastal evolution, *in* 'Coastal Dynamics 1997', pp. 644 – 653.

Dingler, J. [1981], 'Stability of a very coarse grained beach at Carmel, California', *Marine Geology* **44**, 241 – 252.

Dingler, J. and Reiss, T. [2002], 'Changes to Monterey Bay beaches from the end of the 198283 El Nino through the 199798 El Nino', *Marine Geology* **181**, 265283.

Dobkins, J. and Folk, R. [1970], 'Shape development on Tahiti - Nui', *Journal of Sedimentary Research* **40**(4), 1167 – 1203.

Dodd, N., Blondeaux, P., Calvete, D., De Swart, H. E., Falques, A., Hulscher, S., Rozynski, G. and Vittori, G. [2003], 'Understanding coastal morphodynamics using stability methods', *Journal of Coastal Research* **19**(4), 849 – 866.

Doucette, J. S. [2002], 'Geometry and grain - size sorting of ripples on low - energy sandy beaches: field observations and model predictions', *Sedimentology* **49**(3), 483 – 503.

Drake, T. G. and Calantoni, J. [2001], 'Discrete particle model for sheet flow sediment transport in the nearshore', *Journal of Geophysical Research - Oceans* **106**(C9), 19859 – 19868.

Dubois, R. [1972], 'Inverse relation between foreshore slope and mean grain size as a function of the heavy mineral content', *Geological Society of America Bulletin* **83**, 871 – 876.

Duncan, J. [1964], 'The effects of water table and tidal cycle on swash - backwash sediment distribution and beach profile development', *Marine Geology* **2**, 186 – 197.

Einstein, H. [1937], *Bedload transport as a probability problem*, PhD thesis, Eidenoess. tech. Hochsch. (English translation by W.W. Sayre, in Sedimentation, edited by H.W. Shen, Appendix C, H.W. Shen, Fort Collins, Colo., 1972).

Elfrink, B. and Baldock, T. [2002], 'Hydrodynamics and sediment transport in the swash zone: a review and perspectives', *Coastal Engineering* **45**(3 - 4), 149 – 167.

Elgar, S. and Guza, R. [1985], 'Observations of bispectra of shoaling surface gravity waves', *Journal of Fluid Mechanics* **161**, 425 – 448.

Eliot, I. G. and Clarke, D. [1988], 'Semi - diurnal variation in beachface aggradation and degradation', *Marine Geology* **79**, 1 – 22.

Emery, K. [1955], 'Grain size of marine gravels', *Journal of Geology* **63**, 39 – 49.

Emery, K. [1978], 'Grain - size in laminae of beach sand', *Journal of Sedimentary Petrology* **48**, 1203 – 1212.

Engelund, F. and Fredsoe, J. [1976], 'Sediment transport model for straight alluvial channels', *Nordic Hydrology* **7**(5), 293 – 306.

Engstrom, W. [1974], 'Beach foreshore sedimentology and morphology in the Apostle Islands of Northern Wisconsin', *Journal of Sedimentary Petrology* **44**, 190 – 206.

Eriksen, N. [1970], 'Measurement of tide induced change to water table profiles in coarse and fine sand beaches along Pegasus Bay, Canterbury', *Earth Science Journal* **4**(1), 24 – 31.

Erikson, L., Larson, M. and Hanson, H. [2005], 'Prediction of swash motion and run - up including the effects of swash interaction', *Coastal Engineering* **52**(3), 285 – 302.

Evans, O. [1939], 'Sorting and transportation of material in the swash and backwash', *Journal of Sedimentary Petrology* **9**(1), 28 – 31.

Felton, E. A., Crook, K. A. W. and Keating, B. H. [2000], 'The Hulopoe Gravel, Lanai, Hawaii: new sedimentological data and their bearing on the 'giant wave' (mega - tsunami) emplacement hypothesis', *Pure and Applied Geophysics* **157**(6 - 8), 1257 – 1284.

Ferentinos, G. and Collins, M. [1980], 'Effects of shoreline irregularities on a rectilinear tidal current and their significance in sedimentation processes', *Journal of Sedimentary Petrology* **50**(4), 1081 – 1094.

Ferguson, R. I. and Paola, C. [1997], 'Blas and precision of percentiles of bulk grain size distributions', *Earth Surface Processes and Landforms* **22**(11), 1061 – 1077.

Fieller, N., Gilbertson, D. and Olbricht, W. [1984], 'A new method for environmental analysis of particle size distribution data from shoreline sediments', *Nature* **311**, 648 – 651.

Fieller, N. R. J., Flenley, E. C. and Olbricht, W. [1992], 'Statistics of particle - size data', *Applied Statistics: Journal of the Royal Statistical Society Series C* **41**(1), 127 – 146.

Finkl, C., Andrews, J. and Benedet, L. [2007], Presence of beach - compatible sediments in offshore borrows: new challenges and trade - offs in developing codifications, *in* '*Coastal Sediments* 2007, American Society of Civil Engineers', Vol. 3, ASCE, New Orleans.

Fisher, N. [1993], *Statistical Analysis of Circular Data*, Cambridge University Press, Cambridge.

Fisher, R. [1924], 'The distribution of the partial correlation coefficient', *Metron* **3**, 329 – 332.

Flemming, B. [1988], *Process and pattern of sediment mixing in a microtidal coastal lagoon along the west coast of South Africa.*, Tide - Influenced Sedimentary Environments and Facies, D. Reidel, Dordrecht.

Flemming, B. [2004], Factors affecting the shape of particle frequency distributions and associated textural parameters, *in* 'From particle size to sediment dynamics', Int. Workshop, Delmenhorst, Germany (Delmenhorst).

Flemming, N. [1964], 'Tank experiments on the sorting of beach material during cusp formation', *Journal of Sedimentary Petrology* **34**, 112 – 122.

Folk, R. and Ward, W. [1957], 'Brazos River, Brazil: a study of the significance of grain size parameters', *Journal of Sedimentary Petrology* **27**, 3 – 26.

Fox, W., Ladd, J. and Martin, M. [1966], 'A profile of the four movement measures perpendicular to a shore line, South Haven, Michigan', *Journal of Sedimentary Petrology* **9**, 28 – 31.

Friedman, G. M. [1979], 'Differences in size distributions of populations of particles among sands of various origins - addendum to IAS presidential - address', *Sedimentology* **26**(6), 859 – 861.

Friedman, G. and Sanders, J. [1978], *Principles of Sedimentology*, John Wiley, New York.

Fuller, R. M. and Randall, R. E. [1988], 'The Orford Shingles, Suffolk, UK - classic conflicts in coastline management', *Biological Conservation* **46**(2), 95 – 114.

Gale, S. J. and Hoare, P. G. [1992], 'Bulk sampling of coarse clastic sediments for particle - size analysis', *Earth Surface Processes and Landforms* **17**(7), 729 – 733.

Gallagher, E. L., Thornton, E. B. and Stanton, T. P. [2003], 'Sand bed roughness in the nearshore', *Journal of Geophysical Research - Oceans* **108**(C2).

Gallagher, E. and McMahan, J. [2006], Spatial and temporal variability of grain size and small scale morphology, *in* '30th International Conference on Coastal Engineering', ASCE, San Diego.

Gao, S. [1996], 'A FORTRAN program for grain - size trend analysis to define net sediment transport pathways', *Computers and Geosciences* **22**(4), 449 – 452.

Gao, S. and Collins, M. [1991], 'A critique of the McLaren method for defining sediment transport paths - discussion', *Journal of Sedimentary Petrology* **61**(1), 143 – 146.

Gao, S. and Collins, M. [1992], 'Net sediment transport patterns inferred from grain - size trends, based upon definition of transport vectors', *Sedimentary Geology* **81**(1 - 2), 47 – 60.

Gehrels, W. [2006], 'Sea level rise and coastal subsidence in Southwest England', *Reproductions of the Transactions of the Devon Association for the Advancement of Science* **138**, 25 – 42.

Gleason, R., Blackley, M. and Carr, A. [1975], 'Beach stability and particle size distribution, Start Bay', *Proceedings of the Royal Society of London, Series A* **131**(1), 83 – 101.

Graham, D. J., Rice, S. P. and Reid, I. [2005], 'A transferable method for the automated grain sizing of river gravels', *Water Resources Research* **41**(7).

Grant, U. [1948], 'Influence of the water table on beach aggradation and degradation', *Journal of Marine Research* **7**(3), 655 – 660.

Grazzini, J., Turiel, A., Yahia, H. and Herlin, I. [2007], 'A multifractal approach for extracting relevant textural areas in satellite meteorological images', *Environmental Modelling and Software* **22**(3), 323 – 334.

Greenwood, B. and Davidson Arnott, G. [1972], 'Textural variation in sub - environments of shallow - water wave zone, Kouchibouguac Bay, New - Brunswick', *Canadian Journal of Earth Sciences* **9**(6), 679 –.

Greenwood, B. and Hale, P. [1980], Depth of activity, sediment flux, and morphological change in a barred nearshore environment, *in* S. McCann, ed., 'The Coastline of Canada', Geological Survey of Canada, pp. 89 – 109.

Greenwood, B. and Xu, Z. [2001], 'Size fractionation by suspension transport: a large scale flume experiment with shoaling waves', *Marine Geology* **176**(1 - 4), 157 – 174.

Griffith, D. and Haining, R. [2006], 'Beyond mule kicks: the Poisson distribution in geographical analysis.', *Geographical Analysis* **38**, 123 – 139.

Gringarten, E. and Deutsch, C. [2001], 'Variogram interpretation and modeling', *Mathematical Geology* **33**, 507 – 534.

Gross, D. and Harris, C. [1998], *Fundamentals of Queueing Theory.*, Wiley.

Guillen, J. and Hoekstra, P. [1997], 'Sediment distribution in the nearshore zone: Grain size evolution in response to shoreface nourishment (Island of Terschelling, The Netherlands)', *Estuarine Coastal and Shelf Science* **45**(5), 639 – 652.

Guillen, J. and Jimenez, J. [1995], 'Processes behind the longshore variation of the sediment grain size in the ebro delta coast', *Journal of Coastal Research* **11**, 205 – 218.

Guillen, J. and Palanques, A. [1996], 'Short and medium term grain size changes in deltaic beaches (Ebro Delta, NW Mediterranean)', *Sedimentary Geology* **101**, 55 – 67.

Guza, R. T. and Inman, D. L. [1975], 'Edge waves and beach cusps', *Journal of Geophysical Research - Oceans and Atmospheres* **80**(21), 2997 – 3012.

Hails, J., Kelland, N. and Lees, B. [1975], 'Submarine geology, sediment distribution, Quaternary history of Start Bay, Devon', *Proceedings of the Royal Society of London, Series A* **131**(1), 3 – 49.

Hails, J. R. [1975], 'Offshore morphology and sediment distribution, Start Bay, Devon', *Philosophical Transactions of the Royal Society of London Series a - Mathematical Physical and Engineering Sciences* **279**(1288), 221 – 230.

Hails, J. R. [1975b], 'Some aspects of the quaternary history of Start Bay, Devon', *Field Studies* **4**, 207 – 222.

Halcrow Group, S. [2002], 'Futurecoast (http://www.defra.gov.uk/environ/fcd/futurecoast.htm)'.

Hamza, A., Escamilla, L., P.L., Aroza, J. and Roldan, R. [1999], 'Removing noise and preserving details with relaxed median filters', *Journal of Mathematical Imaging and Vision* **11**, 161 – 177.

Hanes, D. M. [1991], 'Suspension of sand due to wave groups', *Journal of Geophysical Research - Oceans* **96**, 8911 – 8915.

Hannachi, A., Jolliffe, I. and Stephenson, D. [2007], 'Empirical orthogonal functions and related techniques in atmospheric science: a review', *International Journal of Climatology* **27**, 1119 – 1152.

Hanson, H., Brampton, A., Capobianco, M., Dette, H., Hamm, L., Laustrup, C., Lechuga, A. and Spanhoff, R. [2002], 'Beach nourishment projects, practices, and objectives - a european overview', *Coastal Engineering* **42**, 81 – 111.

Hardisty, J., Hart, S., Rouse, H. L. and Blythe, C. [1996], 'Theoretical analysis of wave - induced gravel movements', *Earth Surface Processes and Landforms* **21**(1), 93 – 102.

Harley, M. and Turner, I. [2007], 'A simple data transformation technique for pre - processing survey data at embayed beaches', *Coastal Engineering* **55**, 63 – 68.

Hart, B. and Plint, A. [1989], 'Gravelly shoreface deposits: a comparison of modern and ancient facies sequences', *Sedimentology* **36**, 551 – 557.

Hartmann, D. [2007], 'From reality to model: Operationalism and the value chain of particle - size analysis of natural sediments', *Sedimentary Geology* **202**, 383 – 401.

Hartmann, D. and Christiansen, C. [1988], 'Settling - velocity distributions and sorting processes on a longitudinal - dune - a case - study', *Earth Surface Processes and Landforms* **13**(7), 649 – 656.

Hartmann, D. and Christiansen, C. [1992], 'The hyperbolic shape triangle as a tool for discriminating populations of sediment samples of closely connected origin', *Sedimentology* **39**(4), 697 – 708.

Hartstein, N. D. and Dickinson, W. W. [2006], 'Wave energy and clast transport in eastern Tasman Bay, New Zealand', *Earth Surface Processes and Landforms* **31**(6), 703 – 714.

Hassan, M., Church, M. and Schick, A. [1991], 'Distance of movement of coarse particles in gravel bed streams', *Water Resources Research* **27**(503 - 511).

Hasselman, K. [1974], 'On the spectral dissipation of ocean waves due to whitecapping', *Boundary - Layer Meteorology* **6**, 107 – 127.

Haxel, J. and Holman, R. [2004], 'The sediment response of a dissipative beach to variations in wave climate', *Marine Geology* **206**, 73 – 99.

Heathershaw, A. and Thorne, P. [1985], 'Sea bed noises reveal role of turbulent bursting phenomena in sediment transport by tidal currents', *Nature* **31**, 339 – 342.

Hegge, B. J. [1994], *Low energy sandy beaches of southwestern Australia: two dimensional morphology and dynamics*, PhD thesis, University of Western Australia.

Hegge, B. J. and Masselink, G. [1996], 'Spectral analysis of geomorphic time series: Auto - spectrum', *Earth Surface Processes and Landforms* **21**(11), 1021 – 1040.

Hey, R. [1966], 'Sections in the beach plain deposits of Dungeness, Kent.', *Geological Magazine* **104**, 361 – 370.

Hine, A. C. [1979], 'Mechanisms for berm development and resulting beach growth along a barrier spit complex', *Sedimentology* **26**, 333351.

Hoefel, F. and Elgar, S. [2003], 'Wave - induced sediment transport and sandbar migration', *Science* **299**(5614), 1885 – 1887.

Holland, K., Puleo, J. and Konney, T. [2001], 'Quantification of swash flows using video - based particle image velocimetry', *Coastal Engineering* **44**, 65 – 77.

Holland, K. T. and Puleo, J. A. [2001], 'Variable swash motions associated with foreshore profile change', *Journal of Geophysical Research - Oceans* **106**(C3), 4613 – 4623.

Holman, R. A. and Bowen, A. J. [1982], 'Bars, bumps, and holes - models for the generation of complex beach topography', *Journal of Geophysical Research - Oceans and Atmospheres* **87**(NC1), 457 – 468.

Holmes, P. [1975], 'Wave conditions in Start Bay', *Journal of the Geological Society (London)* **131**, 57 – 62.

Holmes, P., Horn, D., Blewett, J., Blanco, B., Peel Yates, T. and Shanehsaz zadeh, A. [2002], Hydraulic gradients and bed level changes in the swash zone on sand and gravel beaches, *in* '28th International Conference on Coastal Engineering', ACSE, New York., Cardiff.

Holthuijsen, L., Booij, N. and Herbers, T. [1989], 'A prediction model for stationary, short - crested waves in shallow water with ambient currents', *Coastal Engineering* **13**, 23 – 54.

Horel, J. D. [1984], 'Complex principal component analysis - theory and examples', *Journal of Climate and Applied Meteorology* **23**(12), 1660 – 1673.

Horn, D. [2002b], 'Mesoscale beach processes', *Progress in Physical Geography* **26**(2), 271 – 289.

Horn, D. and Li, L. [2006], 'Measurement and modelling of gravel beach groundwater response to wave run - up: Effects on beach profile changes', *Journal of Coastal Research* **22**(5), 1241 – 1249.

Horn, D., Li, L. and Holmes, P. [2003], Measurement and modelling of gravel beach groundwater response to wave run - up, *in* '*Coastal Sediments* 2003, American Society of Civil Engineers', ASCE, New York.

Horn, D. P. [1992], 'A review and experimental assessment of equilibrium grain - size and the ideal wave - graded profile', *Marine Geology* **108**(2), 161 – 174.

Horn, D. P. [2002], 'Beach groundwater dynamics', *Geomorphology* **48**(1 - 3), 121 – 146. Sp. Iss. SI.

Horn, D. and Walton, S. [2007], 'Spatial and temporal variations of sediment size on a mixed sand and gravel beach', *Sedimentary Geology* **202**, 509 – 528.

Hotelling [1974], 'Hotelling,h 1895 - 1973', *American Statistician* **28**(2), 71 – 73.

Houser, C. and Greenwood, B. [2005], 'Hydrodynamics and sediment transport within the inner surf zone of a lacustrine multiple - barred nearshore', *Marine Geology* **218**(1 - 4), 37 – 63.

Howd, P. and Holman, R. [1987], 'A simple model of beach foreshore response to long period waves', *Marine Geology* **78**, 11 – 22.

Hughes, M. G. [1992], 'Application of a nonlinear shallow - water theory to swash following bore collapse on a sandy beach', *Journal of Coastal Research* **8**(3), 562 – 578.

Hughes, M. G. [1995], 'Friction factors for wave uprush', *Journal of Coastal Research* **11**(4), 1089 – 1098.

Hughes, M. G. and Baldock, T. E. [2004], 'Eulerian flow velocities in the swash zone: Field data and model predictions', *Journal of Geophysical Research - Oceans* **109**(C8).

Hughes, M. G. and Cowell, P. J. [1987], 'Adjustment of reflective beaches to waves', *Journal of Coastal Research* **3**(2), 153 – 167.

Hughes, M. G., Masselink, G. and Brander, R. W. [1997], 'Flow velocity and sediment transport in the swash zone of a steep beach', *Marine Geology* **138**(1 - 2), 91 – 103.

Hunt, J. [1979], 'Direct solution of the wave dispersion equation', *Journal of Waterways, Ports, Coastal Oceans Divison* **105**, 457 – 459.

Huntley, D. and Bowen, A. [1975a], 'Field observation of edge waves and their effect on beach material', *Journal of the Geological Society (London)* **131**, 69 – 81.

Huntley, D. and Hanes, D. [1987], Direct measurement of suspended sediment transport, *in* '*Coastal Sediments* 1987, American Society of Civil Engineers', ASCE, pp. 723 – 737.

HydraulicsResearch [1991], *Beesands sea defences: hydraulic model studies*, Technical Report EX2400, Report to NRA (South West).

Illenberger, W. K. [1991], 'Pebble shape (and size)', *Journal of Sedimentary Petrology* **61**(5), 756 – 767.

Ingle, J. [1966], *The movement of beach sand*, Elsevier, Amsterdam, pp 221.

Inman, D., Ewing, G. and Corliss, J. [1966], 'Coastal sand dunes of Guerro Negro, Baja California, Mexico', *Bulletin of the Geological Society of America* **77**, 787802.

Inman, D. L. [1949], 'Sorting of sediments in the light of fluid mechanics', *Journal of Sedimentary Petrology* **19**(2), 51 – 70.

Inman, D. L. [1953], 'Areal and seasonal variations in beach and nearshore sediments at La Jolla, California', *U.S. Army Corps of Engineering Beach Erosion Technical Board Memo.* **Technical Report 39, pp.134**.

Inman, D. L. and Guza, R. T. [1982], 'The origin of swash cusps on beaches', *Marine Geology* **49**(1 - 2), 133 – 148.

IPCC [2007], *Intergovernmental Panel on Climate Change - Climate Change 2001 - The Scientific Basis*, Cambridge University Press.

Isla, F. I. [1993], 'Overpassing and armoring phenomena on gravel beaches', *Marine Geology* **110**(3 - 4), 369 – 376.

Isla, F. I. and Bujalesky, G. G. [2000], 'Cannibalisation of Holocene gravel beach - ridge plains, northern Tierra del Fuego, Argentina', *Marine Geology* **170**(1 - 2), 105 – 122.

Isla, F. I. and Bujalesky, G. G. [2005], 'Groundwater dynamics on macrotidal gravel beaches of Tierra del Fuego, Argentina', *Journal of Coastal Research* **21**(1), 65 – 72.

Ivamy, M. C. and Kench, P. S. [2006], 'Hydrodynamics and morphological adjustment of a mixed sand and gravel beach, Torere, Bay of Plenty, New Zealand', *Marine Geology* **228**(1 - 4), 137 – 152.

Jackson, N. L., Masselink, G. and Nordstrom, K. F. [2004], 'The role of bore collapse and local shear stresses on the spatial distribution of sediment load in the uprush of an intermediate - state beach', *Marine Geology* **203**(1 - 2), 109 – 118.

Jackson, N. L. and Nordstrom, K. F. [1993], 'Depth of activation of sediment by plunging breakers on a steep sand beach', *Marine Geology* **115**(1 - 2), 143 – 151.

Jammalamadaka, S. R. and Sengupta, A. [2001], *Topics in Circular Statistics (Series on Multivariate Analysis)*, World Scientific, London, pp 348.

Jennings, R. and Shulmeister, J. [2002], 'A field based classification scheme for gravel beaches', *Marine Geology* **186**(3 - 4), 211 – 228.

Jensen, J. [1988], 'Maximum - likelihood estimation of the log - hyperbolic parameters from grouped observations', *Computers and Geosciences* **14**(3), 389 – 408.

Job, D., ed. [1993], *The Start Bay barrier beach system*, Vol. FSC Occasional Publication 27 of *A field guide to the geomorphology of the Slapton region*, Field Studies Council (Slapton Ley Field Studies Centre).

Johnston, M. R. [2001], 'Nelson Boulder Bank, New Zealand', *New Zealand Journal of Geology and Geophysics* **44**(1), 79 – 88.

Jones, A. [1971], 'A textural study of marine sediments in a portion of Cardigan Bay (Wales)', *Journal of Sedimentary Petrology* **41**, 505 – 516.

Jonsson, I. [1966], 'Wave boundary layers and friction factors', *Proceedings of the 10th International Conference on Coastal Engineering* pp. 127 – 148.

Kay, S. [1998], *Modern Spectral estimation: Theory and Application.*, Prentice Hall, New Jersey.

Kelland, N. and Hails, J. [1972], 'Bedrock morphology and structures within overlying sediments, Start Bay, southwest England, determined by continuous seismic profiling, side - scan sonar and core sampling', *Marine Geology* **13**(2), M19 – M26.

Kemeney, J. and Snell, J. [1960], *Finite Markov Chains.*, Van Nostrand, Princeton (New Jersey).

Kemp, P. [1975], Wave asymmetry in the nearshore zone and breaker area, *in* J. Hails and A. Carr, eds, 'Nearshore Sediment Dynamics and Sedimentation', Wiley, London, p. 4767.

Kennedy, S., Ehrlich, R. and Kana, T. [1981], 'The non - normal distribution of intermittent suspension sediments below breaking waves', *Journal of Sedimentary Petrology* **51**(4), 1103 – 1108.

Kent, M., Moyeed, R. A., Reid, C. L., Pakeman, R. and Weaver, R. [2006], 'Geostatistics, spatial rate of change analysis and boundary detection in plant ecology and biogeography', *Progress in Physical Geography* **30**(2), 201 – 231.

Kidson, C., Carr, A. and Smith, D. [1958], 'Further experiments using radioactive methods to detect the movement of shingle over the sea bed and alongshore', *The Geographical Journal* **124**, 209 – 218.

King, C. [1972], *Beaches and Coasts*, 2nd edn, Edward Arnold, London, pp 403.

King, C. A. M. [1970], 'Feedback relationships in geomorphology', *Geografiska Annaler. Series A, Physical Geography* **52**(3 - 4), 147 – 159.

Kirk, R. [1980], 'Mixed sand and gravel beaches: morphology, processes and sediments', *Progress in Physical Geography* **4**, 189 – 210.

Klein, A., Benedet, L. and Schumacher, D. H. [2002], 'Short - term beach rotation processes in distinct headland bay beach systems', *Journal of Coastal Research* **18**(3), 442 – 458.

Komar, P. [1998], *Beach processes and sedimentation*, Prentice Hall, New Jersey.

Komar, P. [2007], The design of stable and aesthetic beach fills: learning from nature., *in* '*Coastal Sediments* 2007, American Society of Civil Engineers', pp. 420 – 433.

Kovesi, P. [1999], Phase preserving de - noising of images, *in* 'The Australian Pattern Recognition Society Conference, Digital Image Computing Techniques and Applications 1999 (DICTA99)', pp. 47 – 67.

Krumbein, W. C. [1938], 'Local areal variations of beach sands', *Geological Society of America Bulliton* **49**, 653658.

Krumbein, W. C. and Griffith, J. [1938], 'Beach environment in Little Sister Bay, Wisconsin', *Geological Society of America Bulletin* **49**, 629 – 652.

Krumbein, W. and Monk, G. [1943], 'Permeability as a function of the size parameters of unconsolidated sand', *Transactions of the American Institute of Mineral and Metallic Engineers. In: Bear, J. (Ed.), 1972. Dynamics of Fluids in Porous Media. Elsevier, New York. 764 pp.* .

Kuenen, P. [1948], 'The formation of beach cusps', *Journal of Geology* **56**, 34 – 40.

Kulkarni, C. D., Levoy, F., Monfort, O. and Miles, J. [2004], 'Morphological variations of a mixed sediment beachface (Teignmouth, UK)', *Continental Shelf Research* **24**(11), 1203 – 1218.

Lara, J., Losada, I. and Cowen, E. [2002], Large scale turbulence structures over an immobile gravel - bed inside the surf zone, *in* 'Proceedings of Coastal Engineering', ASCE, New York, pp. 1050 – 1061.

Lark, R. M. [1996], 'Geostatistical description of texture on an aerial photograph for discriminating classes of land cover', *International Journal of Remote Sensing* **17**(11), 2115 – 2133.

Larson, M., Capobianco, M. and Hanson, H. [2000], 'Relationship between beach profiles and waves at Duck, North Carolina, determined by canonical correlation analysis', *Marine Geology* **163**, 275 – 288.

Larson, M., Capobianco, M., Jansen, H., Rozynski, G., Southgate, H., Stive, M., Wijnberg, K. and Hulscher, S. [2003], 'Analysis and modeling of field data on coastal morphological evolution over yearly and decadal time scales. Part 1: background and linear techniques', *Journal of Coastal Research* **19**(4), 760 – 775.

Larson, M. and Sunamura, T. [1993], 'Laboratory experiment on flow characteristics at a beach step', *Journal of Sedimentary Petrology* **63**(3), 495 – 500.

Latham, J., Hoad, J. and Newton, M. [1998], Abrasion of a series of tracer materials on a gravel beach, Slapton Sands, Devon, UK., *in* 'Advances in aggregates and armourstone evaluation', Vol. Engineering Geology Special Publication 13, Geological Society, London, pp. 121 – 135.

Lawrence, J., Karunarathna, H., Chadwick, A. and Fleming, C. [2002], Cross - shore sediment transport on mixed and coarse grain sized beaches: modeling and measurements, *in* 'Procedings of Coastal Engineering 2002.', ASCE, New York, pp. 2565 – 2577.

Lawson, C. and Hanson, R. [1974], *Solving Least Squares Problems*, PrenticeHall.

Le Roux, J. P. [1994*a*], 'An alternative approach to the identification of net sediment transport paths based on grain - size trends', *Sedimentary Geology* **94**(1 - 2), 97 – 107.

Le Roux, J. P. [1994*b*], 'A spreadsheet template for determining sediment transport vectors from grain - size parameters', *Computers and Geosciences* **20**(3), 433 – 440.

Le Roux, J. P. [2002], 'Shape entropy and settling velocity of natural grains', *Journal of Sedimentary Research* **72**(3), 363 – 366.

Le Roux, J. P., O'Brien, R. D., Rios, F. and Cisternas, M. [2002], 'Analysis of sediment transport paths using grain - size parameters', *Computers and Geosciences* **28**(5), 717 – 721.

Le Roux, J. P. and Rojas, E. [2007], 'Sediment transport patterns determined from grain size parameters: Overview and state of the art', *Sedimentary Geology* **in press**, doi:10.1016/j.sedgeo.2007.03.014.

Lee, K. et al. [2007], 'The effect of groundwater on topographic changes in a gravel beach', *Ocean Engineering* **34**(3 - 4), 605 – 615.

Lee, M. and others. [2007], 'Number of tracers required for the measurement of longshore transport distance on a shingle beach', *Marine Geology* **240**, 57 – 63.

Leroy, S. [1981], 'Grain size and moment measures: a new look at Karl Pearson's ideas on distribution', *Journal of Sedimentary Petrology* **51**(2), 0625 – 0630.

Lewis, W. [1931], 'The effect of wave incidence on the configutaion of a shingle beach', *Geographical Journal* **78**, 129 – 148.

Li, F., Dyt, C. and Griffiths, C. [2006], 'Multigrain sedimentation/erosion model based on cross - shore equilibrium sediment distribution: application to nourishment design', *Estuarine, Coastal and Shelf Science* **67**, 664 – 672.

List, J. H. [1991], 'Wave groupiness variations in the nearshore', *Coastal Engineering* **15**(5 - 6), 475 – 496.

Liu, J., Huang, J. S., Hsu, R. and Chyan, J. M. [2000], 'The coastal depositional system of a small mountainous river: a perspective from grain size distributions', *Marine Geology* **165**, 63 – 86.

Liu, J. T. and Zarillo, G. A. [1993], 'Simulation of grain - size abundances on a barred upper shoreface', *Marine Geology* **109**(3 - 4), 237 – 251.

Ljung, G. and Box, G. [1978], 'On a measure of lack of fit in time - series models', *Biometrika* **65**, 297 – 303.

Longo, S., Petti, M. and Losada, I. J. [2002], 'Turbulence in the swash and surf zones: a review', *Coastal Engineering* **45**(3 - 4), 129 – 147.

Longuet Higgins, M. and Parkin, D. [1962], 'Sea waves and beach cusps', *Geographical Journal* **128**, 194 – 201.

Lorang, M. S. [2000], 'Predicting threshold entrainment mass for a boulder beach', *Journal of Coastal Research* **16**(2), 432 – 445.

Lorang, M. S. [2002], 'Predicting the crest height of a gravel beach', *Geomorphology* **48**(1 - 3), 87 – 101. Special Issue.

Losada, M. A., Medina, R., Vidal, C. and Losada, I. [1992], Temporal and spatial cross - shore distributions of sediment at 'El Puntal' spit, Santander, Spain, *in* '23rd International Conference on Coastal Engineering (ICCE)', ACSE, p. 22512264.

Lucio, P. S., Bodevan, E. C., Dupont, H. S. and Ribeiro, L. V. [2006], 'Directional kriging: A proposal to determine sediment transport', *Journal of Coastal Research* **22**(6), 1340 – 1348.

Lund Hansen, L. and Oehmig, R. [1992], 'Comparing sieve and sedimentation analysis of beach lake and eolian sediments using log - hyperbolic parameters', *Marine Geology* **107**, 139 – 147.

Madsen, O., Poon, Y. and Graber, H. [1988], 'Spectral wave attenuation by bottom friction: experiments.', *Proceedings of the 21st International Conference on Coastal Engineering* pp. 492 – 504.

Maejima, W. [1982], 'Texture and stratification of gravelly beach sediments, Enju beach, Kii peninsula, Japan.', *Journal of Geosciences, Osaka City University* **25**(Art. 3), 35 – 51.

Mandelbrot, B. [1983], *The Fractal Geometry of Nature*, W.H. Freeman and Co., New York, pp 480.

Marcotte, D. [1996], 'Fast variogram computation with FFT', *Computers and Geosciences* **22**(10), 1175 – 1186.

Martz, L. W. and Li, L. [1997], 'Grain - size analysis of surface material under wind erosion using the effective surface concept', *Earth Surface Processes and Landforms* **22**(1), 19 – 29.

Mase, H. [1988], 'Spectral characteristics of random wave run - up', *Coastal Engineering* **12**(2), 175 – 189.

Mase, H. [1995], 'Frequency down - shift of swash oscillations compared to incident waves', *Journal of Hydraulic Research* **33**(3), 397 – 411.

Mason, T. and Coates, T. T. [2001], 'Sediment transport processes on mixed beaches: A review for shoreline management', *Journal of Coastal Research* **17**(3), 645 – 657.

Massari, F. and Parea, G. C. [1988], 'Progradational gravel beach sequences in a moderate - energy to high - energy, microtidal marine - environment', *Sedimentology* **35**(6), 881 – 913.

Masselink, G. [1992], 'Longshore variation of grain - size distribution along the coast of the Rhone Delta, Southern France - a test of the McLaren model', *Journal of Coastal Research* **8**(2), 286 – 291.

Masselink, G., Hegge, B. J. and Pattiaratchi, C. B. [1997], 'Beach cusp morphodynamics', *Earth Surface Processes and Landforms* **22**(12), 1139 – 1155.

Masselink, G. and Hughes, M. G. [2003], *Introduction to Coastal Processes and Geomorphology*, Hodder - Arnold, London.

Masselink, G. and Li, L. [2001], 'The role of swash infiltration in determining the beachface gradient: a numerical study', *Marine Geology* **176**(1 - 4), 139 – 156.

Masselink, G. and Pattiaratchi, C. [1998*a*], 'Morphodynamic impact of sea breeze activity on a beach with beach cusp morphology', *Journal of Coastal Research* **14**(2), 393 – 406.

Masselink, G. and Pattiaratchi, C. B. [1998*b*], 'Morphological evolution of beach cusps and associated swash circulation patterns', *Marine Geology* **146**(1 - 4), 93 – 113.

Masselink, G. and Puleo, J. A. [2006], 'Swash - zone morphodynamics', *Continental Shelf Research* **26**(5), 661 – 680.

Masselink, G., Russell, P., Coco, G. and Huntley, D. [2004], 'Test of edge wave forcing during formation of rhythmic beach morphology', *Journal of Geophysical Research - Oceans* **109**(C6).

Masselink, G. and Short, A. D. [1993], 'The effect of tide range on beach morphodynamics and morphology - a conceptual beach model', *Journal of Coastal Research* **9**(3), 785 – 800.

Masselink, G. et al. [2007], 'Short - term morphological change and sediment dynamics in the intertidal zone of a macrotidal beach', *Sedimentology* **54**(1), 39 – 53.

Masselink, G. et al. [2008], 'Sediment trend models fail to reproduce small scale sediment transport patterns on an intertidal beach', *Sedimentology* **55**, 667 – 688.

Matsunaga, N. and Honji, H. [1980], 'The backwash vortex', *Journal of Fluid Mechanics* **99**, 813 – 815.

Matsunaga, N. and Honji, H. [1983], 'The steady and unsteady backwash vortices', *Journal of Fluid Mechanics* **135**, 189 – 197.

McCave, I. [1978], 'Grain size trends and transport along beaches: example from eastern England', *Marine Geology* **28**, M43 – M51.

McLaren, P. [1981], 'An interpretation of trends in grain - size measures', *Journal of Sedimentary Petrology* **51**(2), 611 – 624.

McLaren, P. and Bowles, D. [1985], 'The effects of sediment transport on grain - size distributions', *Journal of Sedimentary Petrology* **55**(4), 457 – 470.

McLaren, P., Hill, S. and Bowles, D. [2007], 'Deriving transport pathways in a sediment trend analysis (sta)', *Sedimentary Geology* **202**, 489 – 498.

McLean, R. [1970], 'Variations in grain - size and sorting on two Kaikoura beaches', *New Zealand Journal of Marine and Frehwater Research* **4**, 141 – 164.

McLean, R. and Kirk, R. [1969], 'Relationships between grain size, size sorting, and foreshore slope on mixed sand shingle beaches', *New Zealand Journal of Geology and Geophysics* **12**, 138 – 155.

McManus, J. [1975], 'Quartile deviation - median diameter analysis of surface and core sediments from Start Bay', *Proceedings of the Royal Society of London, Series A* **131**(1), 51 – 56.

McNamara, J. and Borden, C. [2002], 'Observations on the movement of coarse gravel using implanted motionsensing radio transmitters', *Hydrological Processes* **18**, 18711884.

Medina, R., Losada, M. A., Losada, I. J. and Vidal, C. [1994], 'Temporal and spatial relationship between sediment grain - size and beach profile', *Marine Geology* **118**(3 - 4), 195 – 206.

Miles, J. R. and Russell, P. E. [2004], 'Dynamics of a reflective beach with a low tide terrace', *Continental Shelf Research* **24**(11), 1219 – 1247.

Miller, J. K. and Dean, R. G. [2007], 'Shoreline variability via empirical orthogonal function analysis. Part 1: temporal and spatial characteristics', *Coastal Engineering* **54**(2), 111 – 131.

Miller, R. and Ziegler, J. [1958], 'A model relating dynamics and sediment pattern in equilibrium in the region of shoaling waves, breaker zone, foreshore', *Journal of Geology* **66**, 417 – 441.

Morey, C. [1976], 'The natural history of Slapton Ley nature reserve, IX: the morphology and history of the lake basins', *Field Studies* **4**(353 - 368).

Morey, C. [1983], 'The evolution of a barrier - lagoon system - a case study from Start Bay', *Proceedings of the Ussher Society* **5**(454 - 459).

Moss, A. [1962], 'The physical nature of common sandy and pebbly deposits: Part I', *American Journal of Science* **260**, 337 – 373.

Moss, A. [1963], 'The physical nature of common sandy and pebbly deposits: Part II', *American Journal of Science* **261**, 197 – 243.

Mottershead, D. [1986], *Classic landforms of the South Devon coast*, Geographical Association, Sheffield.

Mottershead, D. N. [1983], 'Rapid bedrock weathering by coastal salt spray, South Devon', *Journal of the Geological Society* **140**, 321 – 321.

Mottershead, D. N. [1989], 'Rates and patterns of bedrock denudation by coastal salt spray weathering - a 7 - year record', *Earth Surface Processes and Landforms* **14**(5), 383 – 398.

Mottershead, D. N. [1998], 'Coastal weathering of greenschist in dated structures, South Devon, UK', *Quarterly Journal of Engineering Geology* **31**, 343 – 346.

Mottershead, D. N. [2000], 'Weathering of coastal defensive structures in southwest England: A 500 year stone durability trial', *Earth Surface Processes and Landforms* **25**(10), 1143 – 1159.

Muir Wood, A. [1970], Characteristics of shingle beaches: the solution to some practical problems, *in* '12th coastal engineering conference', American Association of Civil Engineers, pp. 1059 – 1075.

Mustain, N., Griggs, G. and Barnard, P. [2007], A rapid compatibility analysis of potential offshore sand sources for beaches of the Santa Barbara littoral cell., *in* '*Coastal Sediments* 2007, American Society of Civil Engineers', Vol. 3, ASCE, New Orleans, pp. 2501 – 2514.

Nicholls, R. and Webber, N. [1988], Characteristics of shingle beaches with reference to Christchurch Bay, S. England, *in* 'Proceedings of the 21st Conference on Coastal Engineering', American Society for Civil Engineers.

Nicholson, J., Pan, S. and O'Connor, B. A. [2003*a*], Effect of sediment grading on morphodynamics, *in* A. S. R. A. Davis and P. Howd, eds, 'Coastal Sediment '03', ASCE, pp. CD – Rom, 8 pages.

Nicholson, J., Pan, S. and O'Connor, B. A. [2003*b*], Effect of sediment grading on morphodynamics, *in* A. S. R. A. Davis and P. Howd, eds, 'Coastal Sediment '03', ASCE, pp. CD – Rom, 8 pages.

Nielsen, P. [2002], 'Shear stress and sediment transport calculations for swash zone modelling', *Coastal Engineering* **45**(1), 53 – 60.

Nolan, T. J., Kirk, R. M. and Shulmeister, J. [1999], 'Beach cusp morphology on sand and mixed sand and gravel beaches, South Island, New Zealand', *Marine Geology* **157**(3 - 4), 185 – 198.

Nordstrom, K. F. [1977], 'Use of grain - size statistics to distinguish between high - energy and moderate - energy beach environments', *Journal of Sedimentary Petrology* **47**(3), 1287 – 1294.

Nordstrom, K. and Jackson, N. [1990], 'Migration of swash zone, step and microtopographic features during tidal cycles on an estuarine beach, Delaware Bay, New Jersey, USA.', *Marine Geology* **92**, 147 – 154.

Novak, I. D. [1972], 'Swash - zone competency of gravel - size sediment', *Marine Geology* **13**(5), 335 – 345.

Oak, H. L. [1984], 'The boulder beach: A fundamentally distinct sedimentary assemblage', *Annals of the Association of American Geographers* **74**(1), 74 – 82.

Orford, J. [2001], *Slapton Sands: implications of rock armouring*, Technical report, Report to English Nature.

Orford, J., Carter, R., Forbes, D. and Taylor, R. [1988], 'Overwash occurrence consequent on morphodynamic changes following lagoon outlet closure on a coarse clastic barrier', *Earth Surface Processes and Landforms* **13**(1), 27 – 35.

Orford, J. D. [1975], 'Discrimination of particle zonation on a pebble beach', *Sedimentology* **22**(3), 441 – 463.

Orford, J. D. [1977], 'Proposed mechanism for storm beach sedimentation', *Earth Surface Processes and Landforms* **2**(4), 381 – 400.

Orford, J. D., Forbes, D. L. and Jennings, S. C. [2002], 'Organisational controls, typologies and time scales of paraglacial gravel - dominated coastal systems', *Geomorphology* **48**(1 - 3), 51 – 85. Special Issue.

Orford, J., Jennings, S. and Pethick, J. [2003], Extreme storm effect on gravel - dominated barriers, *in* R. Davis, ed., '*Coastal Sediments* 2003, American Society of Civil Engineers'.

Outcalt, S. I. and Melton, M. A. [1992], 'Geomorphic application of the Hausdorff - Besicovich dimension', *Earth Surface Processes and Landforms* **17**(8), 775 – 787.

Palmer, H. [1834], 'Observations on the motion of shingle beaches', *Philosophical Transactions of the Royal Society of London* **124**, 567 – 576.

Paphitis, D. and Collins, M. B. [2005], 'Sand grain threshold, in relation to bed 'stress history': an experimental study', *Sedimentology* **52**(4), 827 – 838.

Pearson, K. [1901], 'Mathematical contributions to the theory of evolution, X: Supplement to a memoir on skew variation', *Philosophical Transactions of the Royal Society of London, Series A* **197**, 443459.

Pedreros, R., Howa, H. L. and Michel, D. [1996], 'Application of grain size trend analysis for the determination of sediment transport pathways in intertidal areas', *Marine Geology* **135**(1 - 4), 35 – 49.

Pedrozo Acuna, A., Simmonds, D. J., Otta, A. K. and Chadwick, A. J. [2006], 'On the cross - shore profile change of gravel beaches', *Coastal Engineering* **53**(4), 335 – 347.

Peregrine, D. [1966], 'Calculations of the development of an undular bore', *Journal of Fluid Mechanics* **25**, 321 – 330.

Peregrine, D. H. and Williams, S. M. [2001], 'Swash overtopping a truncated plane beach', *Journal of Fluid Mechanics* **440**, 391 – 399.

Pethick, J. [2001], *Slapton Sands: Proposed road alignment. Assessment of geomorphological impacts in relation to management of the road*, Technical report, Report to English Nature.

Petrov, V. A. [1989], 'Gravel differentiation on a beach', *Okeanologiya* **29**(2), 279 – 284.

Phillips, J. D. [1992], 'Nonlinear dynamic - systems in geomorphology - revolution or evolution?', *Geomorphology* **5**(3 - 5), 219 – 229.

Plant, N. G., Holman, R. A., Freilich, M. H. and Birkemeier, W. A. [1999], 'A simple model for interannual sandbar behavior', *Journal of Geophysical Research - Oceans* **104**(C7), 15755 – 15776.

Poizot, E., Mear, Y., Thomas, M. and Garnaud, S. [2006], 'The application of geostatistics in defining the characteristic distance for grain size trend analysis', *Computers and Geosciences* **32**(3), 360 – 370.

Pontee, N. I., Pye, K. and Blott, S. J. [2004], 'Morphodynamic behaviour and sedimentary variation of mixed sand and gravel beaches, Suffolk, UK', *Journal of Coastal Research* **20**(1), 256 – 276.

PosfordDuvivier [1998], *Shoreline Management Plan (Non-Technical Summary)*, Technical report, Report to Lyme Bay and South Devon Coastline Group.

Powell, K. [1988], The dynamic response of shingle beaches to random waves, *in* 'Proceedings of the 21st Conference on Coastal Engineering', American Society of Civil Engineers, pp. 1763 – 1773.

Powell, K. [1990], *Predicting Short Term Profile Response for Shingle Beaches*, Hydraulics Research Station.

Priestly, M. [1994], *Spectral Analysis and Time Series.*, Academic Press, London, pp 890.

Pritchard, D. and Hogg, A. J. [2005], 'On the transport of suspended sediment by a swash event on a plane beach', *Coastal Engineering* **52**(1), 1 – 23.

PSML [2006], 'Permanent Service for Mean Sea-Level 2006 Annual Report, (http://www.pol.ac.uk/psmsl/reports/anrep06.pdf)'.

Puleo, J. A. and Holland, K. T. [2001], 'Estimating swash zone friction coefficients on a sandy beach', *Coastal Engineering* **43**(1), 25 – 40.

Radhakrishnan, P. and Dinesh, S. [2006], 'An alternative approach to characterize time series data: Case study on Malaysian rainfall data', *Chaos Solitons and Fractals* **27**(2), 511 – 518.

Ranasinghe, R., McLoughlin, R., Short, A. and Symonds, G. [2004], 'The Southern Oscillation Index, wave climate, and beach rotation', *Marine Geology* **204**(3 - 4), 273 – 287.

Ratsey, S. [1975], 'The climate at Slapton Ley', *Field Studies* **4**, 191 – 206.

Rhind, A. [1909], 'Tables to facilitate the computation of the probable errors of the chief constants of skew frequency distributions', *Biometrika* **7**, 127147.

Richmond, B. and Morton, R. [2007], Coral gravel storm ridges: examples from the tropical Pacific and Caribbean, *in* '*Coastal Sediments* 2007, American Society of Civil Engineers', ASCE, New York, New Orleans.

Ris, R. [1997], 'Spectral modelling of wind waves in coastal areas', *Communications on Hydraulic and Geotechnical Engineering, Delft.* **97 - 4**, 23 – 54.

Rittenhouse, G. [1943], 'Transportation and deposition of heavy minerals', *Bulletin of the Geological Society of America* **57**, 651 – 674.

Robinson, A. [1961], 'The hydrography of Start Bay, and its relationship to beach changes at Hallsands', *Geographical Journal* **127**(1), 63 – 77.

Robson, D., Fieller, N. and Stillman, E. [1997], 'ShefSize (computer program), Department of Probability and Statistics, University of Sheffield, Sheffield, UK.'.

Rubin, D. M. [2004], 'A simple autocorrelation algorithm for determining grain size from digital images of sediment', *Journal of Sedimentary Research* **74**(1), 160 – 165.

Rubin, D. M. and Topping, D. J. [2001], 'Quantifying the relative importance of flow regulation and grain size regulation of suspended sediment transport α and tracking changes in grain size of bed sediment β.', *Water Resources Research* **37**(1), 133 – 146.

Rubin, D., Topping, D., Wright, S. and Melis, T. [2006], Incorporating bed sediment grain size in predictions of suspended - sediment concentration; three approaches tested using 20,000 bed - sediment grain - size measurements from the Colorado River in Grand Canyon, *in* '[abs.]. American Geophysical Union Fall 28 Meeting', San Francisco, California.

Ruessink, B. G., van Enckevort, I. M. J., Kingston, K. S. and Davidson, M. A. [2000], 'Analysis of observed two - and three - dimensional nearshore bar behaviour', *Marine Geology* **169**(1 - 2), 161 – 183.

Ruessink, B. G., Wijnberg, K. M., Holman, R. A., Kuriyama, Y. and van Enckevort, I. M. J. [2003], 'Intersite comparison of interannual nearshore bar behavior', *Journal of Geophysical Research - Oceans* **108**(C8).

Ruggiero, P., Adams, P. and Warrick, J. [2007], Mixed sediment beach processes: Kachemak Bay, Alaska, *in* '*Coastal Sediments* 2007, American Society of Civil Engineers', Vol. 1, ASCE, New Orleans, pp. 463 – 476.

Sallenger, A. [1981], 'Swash mark and grain flow', *Journal of Sedimentary Petrology* **51**(1), 0261 – 0264.

Sallenger, A. H. [1979], 'Beach - cusp formation', *Marine Geology* **29**(1 - 4), 23 – 37.

Sallenger, A. and Richmond, B. [1984], 'High frequency sediment - level oscillations in the swash zone', *Marine Geology* **60**, 155 – 164.

Sanders, D. [2000], 'Rocky shore - gravelly beach transition, and storm/ post - storm changes of a Holocene gravelly beach (Kos Island, Aegean Sea): stratigraphic significance', *Facies* **42**, 44 – 47.

Savage, S. B. [1984], 'The mechanics of rapid granular flows', *Advances in Applied Mechanics* **24**, 289 – 366.

SCOPAC [2007], 'Standing conference on problems associated with the coastline'.

Scott, D. J. and Haschenburger, J. K. [2005], 'Using the hyperbolic distribution to estimate the precision of size distribution percentiles of fluvial gravels', *Computers and Geosciences* **31**(10), 1224 – 1233.

ScottWilson [2004], Slapton Coastal Zone Management. Main study volume 4: Executive summary, Technical report, Report to Slapton Line Partnership.

Self, R. [1977], 'Longshore variation in beach sands, Nautla area, Veracruz, Mexico', *Journal of Sedimentary Petrology* **47**, 1437 – 1443.

Seminara, G. [1998], 'Stability and morphodynamics', *Meccanica* **33**(1), 59 – 99.

Shanehsazzadeh, A. and Holmes, P. [2007], 'Field investigation on the results of non - linear shallow water equations in the swash zone', *Coastal Engineering* **54**, 835 – 855.

Sheather, S. and Jones, M. [1991], 'A reliable data - based bandwidth selection method for kernel density estimation', *Journal of the Royal Statistical Society B* **53**, 683690.

Shen, M. and Meyer, R. [1963], 'Climb of a bore on a beach (part 3: run - up).', *Journal of Fluid Mechanics* **16**, 108125.

Shepard, F. [1963], *Submarine Geology*, Harper and Row, New York.

Sherman, D. J. [1991], 'Gravel beaches', *Research and Exploration* **7**(4), 442 – 452.

Sherman, D. J. and Nordstrom, K. F. [1985], 'Beach scarps', *Zeitschrift Fur Geomorphologie* **29**(2), 139 – 152.

Sherman, D. J., Orford, J. D. and Carter, R. W. G. [1993], 'Development of cusp - related, gravel size and shape facies at Malin Head, Ireland', *Sedimentology* **40**(6), 1139 – 1152.

Short, A. D. [1984], 'Temporal change in beach type resulting from a change in grain - size', *Search* **15**(7 - 8), 228 – 230.

Sime, L. C. and Ferguson, R. I. [2003], 'Information on grain sizes in gravel - bed rivers by automated image analysis', *Journal of Sedimentary Research* **73**(4), 630 – 636.

Smith, T., Marks, W., Lange, G., Sheriff, W. and Neale, C. [1990], 'A fractal analysis of cell images', *Journal of Neuroscience Methods* **27**, 173 – 180.

Sonu, C. J. and Vanbeek, J. L. [1971], 'Systematic beach changes on Outer Banks, North Carolina', *Journal of Geology* **79**(4), 416 – 425.

Sonu, C. and James, W. [1973], 'A Markov model for beach profile change', *Journal of Geophysical Research* **78**(3), 1462 – 1471.

Stauble, D. [2007], Assessing beach fill compatibility through project performance evaluation, *in* '*Coastal Sediments* 2007, American Society of Civil Engineers', Vol. 3, ASCE, New Orleans.

Stewart, H. [1958], 'Sedimentary reflections on depositional environments in San Migue Lagoon, Baja, California, Mexico', *Bulletins of the American Association of Petrologists and Petrologists and Geologists* **42**, 2567 – 2618.

Stive, M., Reniers, A., Terrile, E. and Verhagen, H. [2005], Coarse particles threshold of motion under shoaling waves, *in* 'Coastal Dynamics 05', American Association of Civil Engineers, Barcelona.

Strahler, A. [1966], 'Tidal cycle of changes in an equilibrium beach, Sandy Hook, New Jersey', *Journal of Geology* **74**(247 - 268).

Stubblefield, W. L., Permenter, R. W. and Swift, D. J. P. [1977], 'Time and space variation in surficial sediments of New - York - Bight Apex', *Estuarine and Coastal Marine Science* **5**(5), 597.

Sunamura, T. [1984], 'Quantitative predictions of beach - face slopes', *Geological Society of America Bulletin* **95**(2), 242 – 245.

Sunamura, T. and Aoki, H. [2000], 'A field experiment of cusp formation on a coarse clastic beach using a suspended video - camera system', *Earth Surface Processes and Landforms* **25**(3), 329 – 333.

Sutherland, R. and Lee, C. T. [1994], 'Application of the log - hyperbolic distribution to Hawai'ian beach sands', *Journal of Coastal Research* **10**(2), 251 – 262.

Swan, A. and Sandilands, M. [1995], *Introduction to Geological Data Analysis*, Blackwell Science, Oxford.

Swift, D. [1970], 'Quaternary shelves and the return to grade', *Marine Geology* **8**, 5 – 30.

Takeda, I. and Sunamara, T. [1983], 'A wave flume experiment of beach steps', *Annual Report of the Institute of Geoscience, University of Tsukuba* **9**, 45 – 48.

Terwindt, J. and Battjes, J. [1990], Research on large scale coastal behaviour, *in* 'Coastal Engineering 1990', pp. 1975 – 1983.

Terwindt, J. and Wijnberg, K. [1991], Thoughts on large scale coastal behaviour, *in* '*Coastal Sediments* 1991, American Society of Civil Engineers', pp. 1476 – 1487.

Thorne, P. D. [1986], 'An intercomparison between visual and acoustic detection of seabed gravel movement', *Marine Geology* **72**(1 - 2), 11 – 31.

Tolman, H. [1994], 'Wind waves and movable - bed bottom friction', *Journal of Physical Oceanography* **24**, 994 – 1009.

Tolman, H. [2002g], 'User manual and system documentation of WAVEWATCH - III version 2.22', *NOAA / NWS / NCEP / MMAB Technical Note 222, 133 pp.* .

Tolman, H. L. [1991], 'A third - generation model for wind waves on slowly varying, unsteady and inhomogeneous depths and currents', *Journal of Physical Oceanography* **21**, 782 – 797.

Tuceryan, M. and Jain, A. [1998], Texture analysis, *in* C. Chen, L. Pau and P. Wand, eds, 'The Handbook of Pattern Recognition and Computer Vision', 2nd edn, World Scientific Publishing Co., pp. 207 – 248.

Turner, I. L. and Masselink, G. [1998], 'Swash infiltration - exfiltration and sediment transport', *Journal of Geophysical Research - Oceans* **103**(C13), 30813 – 30824.

Van DerWal, D. [2000], 'Grain - size - selective aeolian sand transport on a nourished beach', *Journal of Coastal Research* **16**, 896908.

Van Wellen, E., Chadwick, A. J. and Mason, T. [2000], 'A review and assessment of longshore sediment transport equations for coarse - grained beaches', *Coastal Engineering* **40**(3), 243 – 275.

Visher, G. [1969], 'Grain size distributions and depositional processes', *Journal of Sedimentary Petrology* **39**(3), 1074 – 1106.

Voss, R. [1988], Fractals in nature, *in* H. Peitgen and D. Saupe, eds, 'The Science of Fractal Images', Springer - Verlag, New York.

Voulgaris, G., Workman, M. and Collins, M. B. [1999], 'Measurement techniques of shingle transport in the nearshore zone', *Journal of Coastal Research* **15**(4), 1030 – 1039.

Waddell, E. [1976], Swash groundwater beach profile interactions., *in* E. R. Davis Jr., R.A., ed., 'Beach and Nearshore Sedimentation', Vol. 24, Society of Economic Paleontologists and Mineralogists Special Publication, Tulsa, OK, pp. 115 – 125.

Weir, F. M., Hughes, M. G. and Baldock, T. E. [2006], 'Beach face and berm morphodynamics fronting a coastal lagoon', *Geomorphology* **82**(3 - 4), 331 – 346.

Werner, B. T. [1999], 'Complexity in natural landform patterns', *Science* **284**(5411), 102 – 104.

Werner, B. T. and Fink, T. M. [1993], 'Beach cusps as self - organized patterns', *Science* **260**(5110), 968 – 971.

Werner, B. T. and Kocurek, G. [1997], 'Bed - form dynamics: does the tail wag the dog?', *Geology* **25**, 771 – 774.

Whalley, W. B. and Orford, J. D. [1989], 'The use of fractals and pseudofractals in the analysis of two - dimensional outlines - review and further exploration', *Computers and Geosciences* **15**(2), 185 – 197.

Wiberg, P. L. and Smith, J. D. [1987], 'Calculations of the critical shear - stress for motion of uniform and heterogeneous sediments', *Water Resources Research* **23**(8), 1471 – 1480.

Wijnberg, K. and Terwindt, J. [1995], 'Extracting decadal morphological behaviour from high resolution, long term bathymeric surveys along the Holland coast using eigenfunction analysis', *Marine Geology* **126**, 301 – 330.

Williams, A. T. [1973], 'Problem of beach cusp development', *Journal of Sedimentary Petrology* **43**(3), 857 – 866.

Williams, A. T. and Caldwell, N. E. [1988], 'Particle - size and shape in pebble - beach sedimentation', *Marine Geology* **82**(3 - 4), 199 – 215.

Williams, J. [1990], 'Video observations of marine gravel transport', *Geo - Marine Letters* **10**, 1432 – 1157.

Wilson, K. C. [1987], 'Analysis of bed - load motion at high shear - stress', *Journal of Hydraulic Engineering - American Association of Civil Engineers* **113**(1), 97 – 103.

Winant, C., Inman, D. and Nordstrom, C. [1975], 'Description of seasonal beach changes using empirical eigenfunctions', *Journal of Geophysical Research* **80**(15), 1979 – 1986.

Winkelmolen, A. M. [1982], 'Critical remarks on grain parameters, with special emphasis on shape', *Sedimentology* **29**(2), 255 – 265.

Winkelmolen, A. M. and Veenstra, H. [1980], 'The effect of a storm surge on nearshore sediments in the Ameland - Schiermonnikoog area (North Netherlands)', *Geology Mijnbouw* **59**, 97 – 111.

Wright, L. D., Chappell, J., Thom, B. G., Bradshaw, M. P. and Cowell, P. [1979], 'Morphodynamics of reflective and dissipative beach and inshore systems - southeastern Australia', *Marine Geology* **32**(1 - 2), 105 – 140.

Wright, L. and Short, A. [1984], 'Morphodynamic variability of surf zone and beaches: a synthesis', *Marine Geology* **56**(93 - 118).

Wright, L. and Thom, B. [1977], 'Coastal depositional landforms: a morphodynamic approach', *Progress in Physical Geography* **1**, 412 – 459.

Wyrwoll, K. H. and Smyth, G. K. [1985], 'On using the log - hyperbolic distribution to describe the textural characteristics of eolian sediments', *Journal of Sedimentary Petrology* **55**(4), 471 – 478.

Yasso, W. [1965], 'Plan geometry of headland bay beaches', *Journal of Geology* **73**, 702 – 714.

Zaman, Z. [2002], 'Coach Markov pulls goalie Poisson.', *Chance* **14**, 31 – 35.

Zenkovich, V. [1967], *Processes of coastal development*, Oliver and Boyd, Edinburgh, pp 738.

Zenkovich, V. P. and Schwartz, M. L. [1987], 'Protecting the Black - Sea Georgian - SSR gravel coast', *Journal of Coastal Research* **3**(2), 201 – 209.